frontiers | Research Topics

Cancer cell metabolism and drug targets

Edited by
Hai-long Piao, Fei Han, Donglai Wang, Yongbin Xu and Jongchan Kim

Published in
Frontiers in Pharmacology
Frontiers in Oncology

ISSN 1664-8714
ISBN 978-2-8325-3928-6
DOI 10.3389/978-2-8325-3928-6

About Frontiers

Frontiers is more than just an open access publisher of scholarly articles: it is a pioneering approach to the world of academia, radically improving the way scholarly research is managed. The grand vision of Frontiers is a world where all people have an equal opportunity to seek, share and generate knowledge. Frontiers provides immediate and permanent online open access to all its publications, but this alone is not enough to realize our grand goals.

Frontiers journal series

The Frontiers journal series is a multi-tier and interdisciplinary set of open-access, online journals, promising a paradigm shift from the current review, selection and dissemination processes in academic publishing. All Frontiers journals are driven by researchers for researchers; therefore, they constitute a service to the scholarly community. At the same time, the *Frontiers journal series* operates on a revolutionary invention, the tiered publishing system, initially addressing specific communities of scholars, and gradually climbing up to broader public understanding, thus serving the interests of the lay society, too.

Dedication to quality

Each Frontiers article is a landmark of the highest quality, thanks to genuinely collaborative interactions between authors and review editors, who include some of the world's best academicians. Research must be certified by peers before entering a stream of knowledge that may eventually reach the public - and shape society; therefore, Frontiers only applies the most rigorous and unbiased reviews. Frontiers revolutionizes research publishing by freely delivering the most outstanding research, evaluated with no bias from both the academic and social point of view. By applying the most advanced information technologies, Frontiers is catapulting scholarly publishing into a new generation.

What are Frontiers Research Topics?

Frontiers Research Topics are very popular trademarks of the *Frontiers journals series*: they are collections of at least ten articles, all centered on a particular subject. With their unique mix of varied contributions from Original Research to Review Articles, Frontiers Research Topics unify the most influential researchers, the latest key findings and historical advances in a hot research area.

Find out more on how to host your own Frontiers Research Topic or contribute to one as an author by contacting the Frontiers editorial office: frontiersin.org/about/contact

Cancer cell metabolism and drug targets

Topic editors

Hai-long Piao — Dalian Institute of Chemical Physics, Chinese Academy of Sciences (CAS), China

Fei Han — Shenyang Pharmaceutical University, China

Donglai Wang — Chinese Academy of Medical Sciences and Peking Union Medical College, China

Yongbin Xu — Dalian Minzu University, China

Jongchan Kim — Sogang University, Republic of Korea

Citation

Piao, H.-L., Han, F., Wang, D., Xu, Y., Kim, J., eds. (2023). *Cancer cell metabolism and drug targets*. Lausanne: Frontiers Media SA. doi: 10.3389/978-2-8325-3928-6

Table of contents

frontiers | Frontiers in Oncology

TYPE Mini Review
PUBLISHED 16 September 2022
DOI 10.3389/fonc.2022.1008361

OPEN ACCESS

EDITED BY
Donglai Wang,
Chinese Academy of Medical Sciences and Peking Union Medical College, China

REVIEWED BY
Jian-Fei Pei,
Chinese Academy of Medical Sciences and Peking Union Medical College, China
Bo Chu,
Shandong University, China

*CORRESPONDENCE
Mingliang Xiang
mingliangxiang@163.com
Bin Ye
aydyebin@126.com

†These authors have contributed equally to this work

SPECIALTY SECTION
This article was submitted to Pharmacology of Anti-Cancer Drugs, a section of the journal Frontiers in Oncology

RECEIVED 31 July 2022
ACCEPTED 31 August 2022
PUBLISHED 16 September 2022

CITATION
Miao X, Wang B, Chen K, Ding R, Wu J, Pan Y, Ji P, Ye B and Xiang M (2022) Perspectives of lipid metabolism reprogramming in head and neck squamous cell carcinoma: An overview.
Front. Oncol. 12:1008361.
doi: 10.3389/fonc.2022.1008361

Perspectives of lipid metabolism reprogramming in head and neck squamous cell carcinoma: An overview

Xiangwan Miao[1,2,3†], Beilei Wang[1,2,3†], Kaili Chen[1,2,3], Rui Ding[1,2,3], Jichang Wu[1,2,3], Yi Pan[1,2,3], Peilin Ji[1,2,3], Bin Ye[1,2,3*] and Mingliang Xiang[1,2,3*]

[1]Department of Otolaryngology & Head and Neck Surgery, Ruijin Hospital, Shanghai Jiao Tong University School of Medicine, Shanghai, China, [2]Shanghai Key Laboratory of Translational Medicine on Ear and Nose Diseases, Shanghai, China, [3]Ear Institute, Shanghai Jiao Tong University School of Medicine, Shanghai, China

Recent studies showed that lipid metabolism reprogramming contributes to tumorigenicity and malignancy by interfering energy production, membrane formation, and signal transduction in cancers. HNSCCs are highly reliant on aerobic glycolysis and glutamine metabolism. However, the mechanisms underlying lipid metabolism reprogramming in HNSCCs remains obscure. The present review summarizes and discusses the "vital" cellular signaling roles of the lipid metabolism reprogramming in HNSCCs. We also address the differences between HNSCCs regions caused by anatomical heterogeneity. We enumerate these recent findings into our current understanding of lipid metabolism reprogramming in HNSCCs and introduce the new and exciting therapeutic implications of targeting the lipid metabolism.

KEYWORDS

lipid metabolism reprogramming, lipid catabolism, lipid synthesis, lipid uptake, HNSCCs

Introduction

Over 850,000 people are diagnosed with head and neck squamous cell carcinomas (HNSCCs) worldwide, and 440,000 people die of it (1, 2). Although human papillomavirus (HPV)-positive HNSCCs patients have better outcomes with overall survival (OS) rate of 70% (3, 4), patients with stage III–IV disease still suffer from local invasion and therapeutic failure, with a poor prognosis and OS of approximately 40% at 5 years (5). The treatment for HNSCCs is individualized, with either surgery or combined with radiotherapy, chemotherapy, target therapy or immunotherapy, as indicated by the pathological or clinical features and anatomical regions (6). Extensive tissue resection,

reconstruction, and side effects of radiotherapy and chemotherapy seriously affect the life quality and survival rate of HNSCCs patients, primarily due to impaired swallowing, speaking and breathing functions (7). Because of inadequate nutrient intake, half of the HNSCCs patients are malnourished and about 80% of them lose weight during treatment (8, 9), whereas some lose up to 20% of body weight (10). After exposure to treatments, several metabolic changes occur because of wound repairing and immune response (7), accompanied with other existed metabolism reprogramming in tumors (11).

It's well known that HNSCCs are highly reliant on glucose metabolism, known as Warburg effect (12, 13). However, nutritional limitation of the total calorie intake in HNSCCs patients promote cancer cell proliferation (14, 15), indicating that not only glucose metabolism, but also other metabolic processes, such as glutamine and lipid metabolism, are vital. As a newly discovered cancer characteristic (16), studies have found that lipid metabolism is reprogrammed in cancers, too (17). Lipid metabolism could support survival, proliferation, invasion, and metastasis in cancer cells by contributing to membrane formation, energy production and signal transduction, and even mediate drug resistance (18, 19). Due to the rapid proliferation rates and high metabolic energy requirements, cancer cells have tremendous demand of lipids (20, 21). Moreover, a variety of intermediate substrates produced by glucose and glutamine metabolism could participate in lipid metabolism, forming a "shortcut" cycling (22). Thus, lipid metabolism reprogramming plays a "vital" role in HNSCCs.

However, it should be noted that the anatomical HNSCCs regions, especially in the neck and supraclavicular regions, mainly contain brown adipose tissue and beige adipose cells (23), which promote energy consumption and help improve the glucose and lipid metabolic disorders (24). And this could partially explain the marked heterogeneity among different head and neck regions (25), especially nasopharyngeal carcinoma (NPC). In NPC, the most common manifestation is cervical lymph node metastasis, which is riches in brown adipose tissue (23). Distant metastasis occurs in about 20% of NPC cases, and half of them are bone/bone marrow metastasis (26), a region where adipocytes predominate (27). Latest studies found that activated brown adipose tissue can reduce glucose around cancers and inhibit cancer growth (28). Because of these differences in adipose tissue distribution, the mechanisms underlying lipid metabolism in different HNSCCs, and other solid carcinomas may vary.

Up to date, most studies were working on the key enzymes involved in lipid uptake and synthesis in HNSCCs, and the upregulation of these enzymes indicates the therapeutic potentials of lipid uptake and synthesis inhibitors in HNSCCs. In this review, we summarize the current studies working on lipid metabolism enzymes and signal transduction molecules and introduce the advancements for lipid metabolism disruption in HNSCCs. Lipids are composed of fat (triglyceride, TG) and lipoid (phospholipid, cholesterol, and cholesterol esters) and both are involved in lipid uptake, synthesis, storage, and catabolism (20). Thus, this review introduces the reprogramming of lipid metabolism in HNSCCs by FA and cholesterol, which are the main substrate for fat and lipoid.

Lipid uptake in HNSCCs

Cholesterol uptake

Cholesterol, which plays a crucial role in membrane structure, is absorbed by intestinal enterocytes (29) and used to synthesize very low-density lipoprotein (VLDL) in the liver (30). VLDL is released into the blood and processed into low-density lipoprotein (LDL), which is taken up by low-density lipoprotein receptors (LDLR) on peripheral cells (31). Nicotine in tobacco can induce an increase in LDLR expression in oral epithelial cells, while smoking is an important risk factor for HNSCCS (32). But the blood cholesterol and LDL levels are significantly decreased in oral carcinoma patients (33, 34). These results indicate that HNSCCs require more cholesterol and LDL than normal cells. Daker et al. also found that Epstein-Barr virus encoded RNA (EBERs) up-regulated LDLR and FA synthase (FASN) in NPC cells (35). Besides, experiments on head and neck cancer (HNC) cell lines revealed that the expression of CD36 and LOX-1, another two LDL membrane receptors, were significantly upregulated after exposure to oxidized LDL (oxLDL) (36), which also suggested that the uptake of cholesterol increased in HNSCCSs. However, lipid metabolism varies according to different tumor microenvironment (TME) and progression stages (37, 38). When oxLDL upregulated CD36 in HNC cell lines, the migration of cancer cells were reduced after oxLDL exposure (36). Thus, the regulation of LDL receptors needs further exploration in order to guide the administration of cholesterol uptake inhibitor. The mechanisms underlying cholesterol efflux proteins, such as LXR or ABCA1, in HNSCCs are still lacking, which worth more attention since they affect the total concentration of cholesterol inside the cells, too.

FA uptake

FA is another essential molecule involved in lipid biosynthesis and serves as a substrate for energy production metabolism. Mammals produce only a few endogenous FAs, which carry a double bond at δ 9 in the hydrocarbon chain. Other necessary FAs, especially polyunsaturated FAs, need to be obtained from food (20, 39). FA are taken up by simple diffusion through the lipid bilayer or by FA transporters on the membrane (22). The currently known FA transporters include differentiated cluster 36 (CD36, also known as FA translocation enzyme), FA

transporter family (FATPs, also known as SLC27), and FA binding proteins on the plasma membrane (also known as FABPs). Abnormal elevation of these three proteins occurs in a variety of cancers (20, 40). Among them, CD36 has been studied most comprehensively in HNSCCs. In oral squamous cell carcinoma (SCC), CD36 upregulation promotes tumor metastasis, while its inhibition leads to complete remission or elimination of lymph node and lung metastases in *in vivo* oral carcinoma models (40). These findings suggest the therapeutical use of CD36 inhibitors in advanced HNSCCs patients. What's more, CD36 inhibitors could reduce the growth of oral SCC cells and inhibited lipid droplet (LD) formation, tumor progression, and metastasis (41–43). And it is important to know that our daily dietary intake may affect the expression of CD36 as Pascual et al. found that dietary palmitic acid (PA) activated CD36 in oropharyngeal carcinoma and stimulated metastasis of cancer cells, which was promoted by a specialized proregenerative extracellular matrix secreted from cancer-associated Schwann cells (44). Thus, nutritional interventions should be considered together with lipid metabolism inhibitors for cancer treatment. Similar to CD36, Rauch et al. found that FABP protein expression was significantly increased in HNSCCs compared to normal tissues (45). Then, Ohyama et al. further found abnormal expressions of FABP4 and FABP5 in tongue carcinoma, whereas only FABP5 was expressed in normal tongue epithelial cells, which showed a higher expression level in injured and cancer tissues (46). Although few studies have evaluated the role of FA transporter family in HNSCCs, these studies revealed that HNSCCs require more FAs than normal cells. However, the killing efficiency of the FA uptake inhibitors should be researched more specifically, along with the optimal duration of use, usefulness and efficiency of nutritional interventions, and long-term side effects.

Lipid synthesis and storage in HNSCCs

Citric acid, produced by the citric acid cycle or glutamine metabolism, is the starting molecule involved in intracellular lipid synthesis. ATP-citric acid lyase (ACLY) converts citric acid to acetyl-CoA and oxaloacetate, which are used to synthesize different lipids in the cells (Figure 1). Although there is no direct evidence of ACLY expression in HNSCCs, Zheng et al. found that the long non-coding RNA TINCR could bind to ACLY and protect it from degradation in NPC, which maintained the total acetyl-CoA level in cells (47). In addition, Sur et al. reported that bitter gourd extract could significantly reduce the expression of ACLY, acetyl-CoA carboxylase (ACC), and FASN genes in oral carcinoma, and promote cell apoptosis (48). These results suggest that the ACLY expression is increased in HNSCCs, which may contribute to the survival of cancer cells and ACLY inhibition may be used as a new anticancer treatment in HNSCCs.

Cholesterol synthesis

Cholesterol biosynthesis begins with the conversion of two molecules of acetyl-CoA to acetoacetyl-CoA by acetyl-CoA

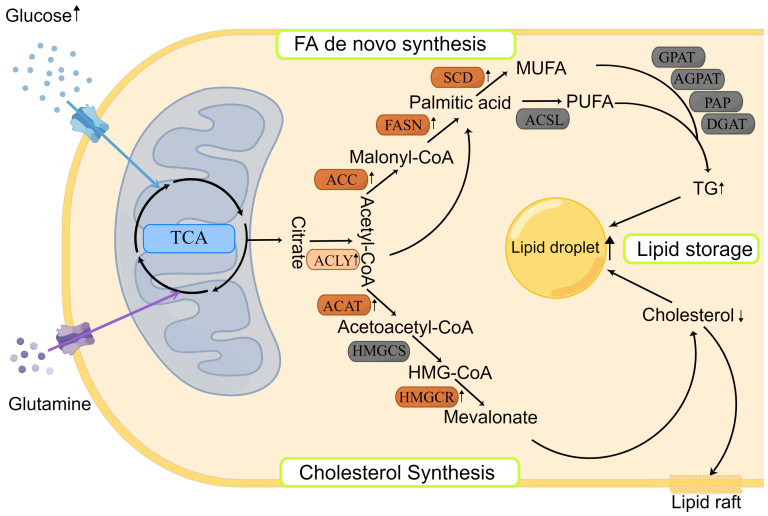

FIGURE 1
Lipid synthesis and storage in HNSCCs. Lipid synthesis begins with citric acid, produced from the TCA cycle, which is used to synthesize different lipids in the cytoplasm. There are two main pathways involved: FA *de novo* synthesis and cholesterol synthesis. The produced lipids are stored as LDs. Most enzymes involved in lipid synthesis are upregulated in HNSCCs.

acetyltransferase (ACAT). Subsequently, a third acetyl-CoA molecule is synthesized into HMG-CoA by HMG-CoA synthase (HMGCS). HMG-COA reductase (HMGCR) is the next rate-limiting step in cholesterol synthesis and produces mevalonate (Figure 1). Mevalonate can be modified to produce different cholesterols with various physiological functions, such as lipid raft in cell membrane (29). Using genetic variation assessment, Gormley et al. reported that there was limited evidence regarding LDL reduction by HMGCR, Niemann-Pick type C1-like 1 (NPC1L1), CETP, or other circulating lipid trait genes on the risk of oral or oropharyngeal carcinoma (49). However, ACAT1 was reported to be associated with poor prognosis of oral SCC (50). This may be explained by the lack of consideration of cholesterol efflux in the previous study, which affects the total quantity of cholesterol inside the cancer cells. Although previous findings related to cholesterol synthesis are controversial and there are limited reports about the expression and prognostic role of cholesterol synthesis-related enzymes in HNSCCs, statins, which are the cholesterol-lowering drugs that act by HMGCR inhibition (51), could induce apoptosis of cancer cells by consuming non-steroidal mevalanoic acid metabolites in HNSCCs (52). Furthermore, statins could enhance the effects of cisplatin with concomitant use and potentiate the efficacy of immunotherapy in HNSCCs (53). These results highlight the potential therapeutic use of statins in HNSCCs, which should be further studied to clarify the mechanisms behind.

FA *de novo* synthesis

FA *de novo* synthesis begins with the conversion of acetyl-CoA to malonyl-CoA by ACC. Then, acetyl-CoA and malonyl-CoA are catalyzed by FASN to form palmitate, which is further modified by elongase of very long chain fatty acids (ELOVL) enzymes to elongate the length of FA chains. Finally, polysaturated FAs, such as palmitic acid, are desaturated to produce unsaturated FAs by stearoyl-CoA desaturase (SCD) and/or other fatty acyl-CoA desaturases (Figure 1). The expression of various rate-limiting enzymes involved in FA *de novo* synthesis was increased in HNSCCs. In HNSCCs with lymph node metastasis, highly phosphorylated ACC expression was found to be associated with poor survival outcomes (54). And ACC2 serves as a vital prognostic indicator and potential therapeutic target in HNSCCs (55). As another key rate-limiting enzyme in FA synthesis, FASN expression was found to be increased in HNSCCs, too. Epstein-Barr virus could promote FASN expression in NPC cells (35, 56) and FASN transcription was increased in cisplatin-resistant SCCs and played a role in cisplatin resistance (57). Furthermore, FASN siRNA inhibited the growth of *in vivo* oral SCC and lymph node metastasis (58), and FASN inhibitors increased the sensitivity to radiotherapy (59). The aforementioned results suggest that inhibition of FA synthesis would be a novel and exciting treatment for HNSCCs. Clinical trials evaluating the efficiency of the FASN inhibitors are currently ongoing on variety of cancers, including oral cancers (NCT02223247) (www.clinicaltrails.gov). Besides, SCD inhibitors could hinder cancer cell proliferation and invasion in oral carcinoma (60, 61), but need more in-depth and long-term studies.

Total lipid synthesis and storage

After synthesis, FAs bind to different backbones to produce different classes of fat in the body, such as phospholipids and TGs with glycerol is the most common backbone, except phospholipids. FAs produce TGs through several enzymes, including Gly3P phosphate acyltransferase (GPAT), 1-acyl-sn-Gly3P acyltransferase (AGPAT), PA phosphatase (PAP), and DAG acyltransferase (DGAT). TGs are then encapsulated in LDs, which is the main storage form of lipids (Figure 1). LD accumulation serves as a phenotype for metastasis initiation, energy storage, and regulatory mechanism of reactive oxygen species in carcinomas (62). HNSCCs show increased LD accumulation, too (63, 64). However, the distribution and mechanism of key enzymes and molecules, such as lipins, in HNSCCs have not been reported previously, and merit further exploration.

Lipid catabolism in HNSCCs

Lipolysis

In response to the requirements of rapid growth and invasion, intracellular lipolytic enzyme activity is also increased (65). In mitochondria, long chain FAs are transformed into acetyl-CoA through lipid catabolism (20), thereby providing ATP and substrates for lipid synthesis (66). The initial step of lipolysis is the hydrolysis of TG into diacylglycerol (DAG) by lipases. Two main lipases are involved in this process, namely, hormone-sensitive lipase (HSL) and fatty triglyceride lipase (ATGL, also known as phospholipase A2, PNPLA2, or PLA2). Rather than TG, HSL hydrolyzes DAG to monoacylglycerol (MAG), while ATGL almost completely hydrolyzes TGs to release DAG (67, 68). DAG is derived from TGs *via* ATGL, and DAG is hydrolyzed by HSL to 2-MAG. Then, 2-MAG is hydrolyzed by MAG lipase (MGL) to free FAs and glycerol, which is then secreted extracellularly (22) (Figure 2).

In 2012, Tripathi et al. found that, along with the Warburg effect, the phosphatidylcholin/lysophosphatidylcholine and phosphatidylcholine/glycerophosphatidylcholine ratios were significantly increased and the activity of ATGL in HNSCCs (oral, tongue, and larynx) was enhanced (69). However, Zhou

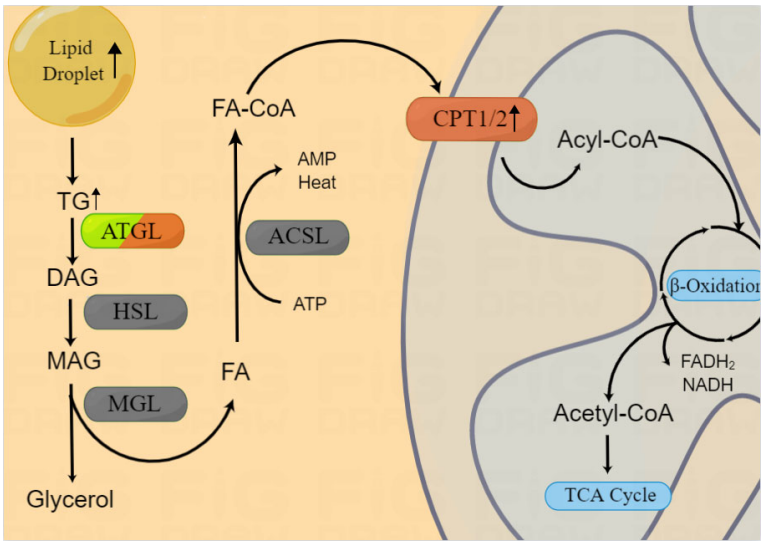

FIGURE 2
Lipid catabolism in HNSCCs. Enzymes involved in lipid catabolism are shown in the figure. After release from the LD, triacylglycerol is broken into FA-CoA by lipolysis-related enzymes and catabolized by FAO to produce energy and substrates for the mitochondrial TCA cycle. β-oxidization are reported to be upregulated in HNSCCs, however, the expression of ATGL in HNSCCs is still controversial.

et al. found that in NPC, ATGL expression was inhibited, lipolysis was reduced, and LD accumulation was increased (63). In addition, they found that low ATGL expression was associated with poor prognosis of patients and ATGL inhibition was regulated by Epstein-Barr virus-encoded membrane latent protein 2A (LMP2A). LMP2A not only promoted lipid accumulation by inhibiting ATGL, but also enhanced migration *in vitro* (64). Thus, the expression and mechanisms of ATGL varied according to the anatomical regions of HNSCCs. As we mentioned above, this gene heterogeneity may be related with the different adipose tissue distribution and lipid metabolism in HNSCCs.

FA catabolism

In addition to being a metabolic intermediate in lipid anabolism, FAs are an important energy source. FAs are catabolized by fatty acid oxidation (FAO), also known as β oxidation. FA-CoA was transformed into FA-carnitine by carnitine palmityl transferase (CPT) and transported from the cytosol across the outer mitochondrial membrane. Within the mitochondria, FAs are repeatedly cleaved to produce acetyl-CoA, which is recycled into the citric acid cycle to produce the reductive equivalent of oxidative phosphorylation (Figure 2). Du et al. found that increased CPT1A-mediated FAO was significantly associated with radiotherapy resistance in NPC (70), suggesting the potential use of combination treatment of FAO inhibitors and radiotherapy. However, the mechanism underlying the role of CPT1/2 in other HNSCCs as well as its other functions require further evaluation.

Regulation pathways of lipid metabolism reprogramming in HNSCCs

In addition to the key lipid metabolic steps mentioned previously, there are also many important signaling pathways involved in lipid metabolism regulation, such as PI3K/AKT, mTOR, and AMPK pathways, which have been discussed previously and are not included in this review (22, 71). In addition to the above pathways, there is a star lipid regulation pathway, which is involved in the regulation of synthesis of multiple lipids, namely, INSIG/SCAP/SREBPs, and requires further attention. The INSIG/SCAP/SREBPs complex is located on the endoplasmic reticulum but does not have any regulatory activity. After cholesterol or glucose stimulates INSIG, the SCAP/SREBPs complex is transported to the Golgi and cleaved into the activated form. Then, SREBP-1c is released into the cell nucleus and regulates the downstream genes as a transcriptional factor. SREBPs has three main forms, namely, SREBP1a, SREBP1c, and SREBP2. SREBP1 mainly regulates the expression of FA synthesis genes and LDLR, while SREBP2 preferentially regulates the expression of cholesterol biosynthesis genes (20). In NPC, SREBP1 activation mediated lipid synthesis and promoted tumor proliferation and progression (72). However, the distributions, expression levels, and specific

mechanisms of INSIG/SCAP/SREBPs in different HNSCCs are still unclear.

Effects of high-risk factors on lipid metabolism reprogramming in HNSCCs tumor microenvironment

Tobacco and alcohol

Compared with non-smoker who never drank, those who drank and smoked every day had a 14-fold higher risk for head and neck squamous cell carcinoma (73). Alcohol consumption alone increases the risk for head and neck squamous cell carcinoma (74, 75). Ethanol is oxidized into acetaldehyde after absorption, which forms various proteins and DNA adducts that promote DNA repair failure, lipid peroxidation and metabolism (76). In HNSCCs, there is a significant positive dose-response relationship between prediagnosis alcohol intake and worse OS, especially associated with the fast ADH1B and the slow/nonfunctional ALDH2 genotype combination (77), two dehydrogenase for alcohol and aldehyde. Chronic alcohol exposure decreases the DNA binding ability of PPARα, a nuclear hormone receptor involved in mitochondrial β-oxidation regulation (78, 79), and impairs cholesterol synthesis (80, 81), which may promote cancer progression, and may also occur in head and neck epithelial cells. Another risk factor that HNSCCs patients are frequently exposed to is tobacco. Difference in lipidome signatures can be found between smokers and non-smokers across a number of lipid species (82, 83). Compared with unexposed, active or passive smokers have higher LDL (84–87) and lower HDL (88). Nicotine in tobacco can induce up-regulation of LDLR expression in oral epithelial cells (32). However, the serum levels of total lipids, cholesterol and HDL in patients with oral cancer are significantly reduced, while triglycerides and VLDL are increased (33, 34). Above results support that lipid metabolism reprogramming has a significant relationship with HNSCCs development, although the specific mechanisms of alcohol and tobacco regulation is still unclear.

Virus infection

As a part of the upper aerodigestive tract, HNSCCs are often affected by viral or bacterial microbes, such as HPV and EBV. Viruses require lipid-mediated endocytosis to enter the cell and HPV proteins L1 and L2 could activate lipid-raft mediated endocytosis to increase its infection (89). The HPV16 E5 protein even can change the lipid composition in cells to help establishing an immune suppressed TME that favors HPV long-term infection (90). HPV16 E6 and E7 could up-regulate lipid synthesis by activating PI3K/AKT/mTOR (91) and SREBPs lipid synthesis signaling pathways (92–94). HPV-positive HNSCCs patients had higher levels of gene expression in TCA cycle, oxidative phosphorylation and β-oxidation, compared with HPV-negative patients (95). However, due to the different adipose tissue distribution, the lipid metabolism regulated by HPV may also varied in different cancers. For example, although HPV is involved in the regulation of cell metabolism in both cervical cancer and HNSCCs, its functions varied. In HPV-associated HNSCCs, it mainly promotes oxidative phosphorylation to obtain energy (96, 97), while in cervical cancer, HPV E6 protein up-regulates lipolysis and down-regulates oxidative phosphorylation (98).

Another well-known virus risk factor in HNSCCs is Epstein-Barr virus, which is also involved in lipid metabolism reprogramming in HNSCCs TME. EBV encoded LMP1 has been reported to regulate glycolysis and lipogenesis in NPC (56, 99, 100). EBV-mediated reprogramming of lipid biosynthesis promotes B-cell activation and differentiation surrounding TME (101, 102), which help shaping a tumor favored TME. At the same time, EBV can also release inflammatory factors, such as IL6, IL-10 and leptin, which promote fat consumption (103–105) and help cancer cells to evade immune surveillance (106). Therefore, virus associated HNSCCs show differences in lipid metabolism compared with non-infectious HNSCCs, which worth more study in the future.

Dietary interventions

Dietary interventions alter the metabolic substrates concentrations in the TME, which will reprogram the cancer cell metabolism and induce cancer development and progression (107–111). Caloric restriction inhibits the growth of pancreatic cancers and helps limit cancer progression (112). However, the total calory intake restriction intervention does not improve the survival prognosis in HNSCCs, but improves the cancer cells proliferation (14, 15). Whether a hypoglycemic diet will inhibit cancer growth may be determined by the mismatch between the fatty acid desaturation degree and the available specific fatty acid types in the cancer (112). Therefore, the role of lipid metabolism in HNSCCs deserves further investigation.

Ferroptosis is an iron-mediated lipid peroxidation that causes non-apoptotic cell death, which is associated with cancer development and therapy response. Inhibition of GPX4, an important ferroptosis regulation molecule, can sensitize drug-resistant cancer cells in HNSCCs (113). During ferroptosis, polyunsaturated fatty acids (PUFAs) are most susceptible to peroxidation, which can cause the destruction of the lipid bilayer and affect membrane function (114). In oral cancer, glutathione can regulate lipid oxidation by binding to PTGS2 which promotes ferroptosis (115). What's more, high fat-soluble vitamins, such as Vitamin D is associated with lower

risk of cancer (116). Thus essential nutrients such as glutathione (GSH), fat-soluble vitamins A, D and K, which help remove ROS (98) and regulate lipid peroxidation and ferroptosis (117), have potential anticancer application in HNSCCs by promoting ferroptosis.

In addition to essential nutrients, there are many exogenous lipid nutrients with potential cancer killing effects in HNSCCs. Reports have shown that docosahexaenoic acid, a ω-3 fatty acid, can induce the degradation of HPV E6/E7 oncoprotein and promote apoptosis (118). Ergosterol Peroxide extracted from mushroom can increase radiotherapy sensitization in cervical cancer cells (119). Salvianolic acid B extracted from salvia miltiorrhiza, which could can also inhibit the malignant transformation of oral premalignant lesion (120), which has been reported had the protective effect on metabolic homeostasis by regulating PPARγ, FASN, SCD1 and CD36 (121). These results suggest that exogenous unsaturated fatty acids and lipid nutrients extracted from plants may have therapeutical potential in HNSCCs.

Regulation of lipid metabolism in HNSCCs by cancer associated cells in TME

Apart from cancer cells, cancer-associated cells in the TME also play an important role in the occurrence and development in cancers. Among them, the one that has been studied the most is cancer-associated fibroblasts (CAFs), which can be derived from normal fibroblasts around cancers, mesenchymal stem cells and cancer cells undergoing EMT transformation (27). It interacts with cancer cells and other components in the TME which help forming a tumor-supporting TME (122–124). HPV-negative oropharyngeal cancer cells can stimulate normal fibroblasts to produce HGF and IL-6 (125), and senescent CAFs will secrete more IL-6, COX2 and PGE2 (126). And then, IL-6 further promotes cancer cell invasion, lipid depletion and immunosuppression (103–106). Although there is evidence that CAFs in HNSCCs exhibit similar metabolic characteristics with cancer cells (127, 128), studies on lipid metabolism in CAFs are still lacking. What's more, Pascual et al. found that dietary PA could induce the cancer associated Schwann cells to secrete a specialized extracellular matrix to promote metastasis (44). All these results support that cancer associated cells help reprogramming the lipid metabolism in HNSCCs TME.

Adipocytes also can differentiate into CAFs (27). Cancer cells could regulate lipid metabolism of adipocytes to produce cancer-associated adipocytes, which are morphologically and functionally different from normal adipocytes (129). Cancer-associated adipocytes then further release fatty acids, mitogens and proinflammatory adipokines to promote the occurrence and development of cancers (130–134). Adipokines such as leptin and adiponectin are lower in HNSCCs patients (135–138), whereas visfatin and chemerinze are higher (28, 139).However, adipocytes distribution in different regions of HNSCCs varies, which may be the reason for the distinct metabolism CAFs subtypes in HNSCCs (128, 140). All these evidences support that cancer associated adipocytes and CAFs play a vital role in lipid metabolism in HNSCCs, but needs more exploration.

Summary and future prospects

The mask of lipid metabolic reprogramming in HNSCCs is gradually being revealed. Previous studies reported that a variety of lipid metabolic enzymes are upregulated in HNSCCs, but heterogeneous was also existed according to different TME and anatomical regions. Cancer cells are constantly reprogramming their lipid metabolisms in response to the TME and/or metastasis/colonization needs in HNSCCs. In this article, we summarized the previous research on lipid metabolism reprogramming in HNSCCs. However, as shown in Table 1, only few lipid metabolism enzymes have been researched and there are still a lot of vacancy in this area which need further

TABLE 1 Expression of key lipid metabolism enzymes in HNSCCs.

Lipid metabolism type		Enzymes	Expression	Subsites	References
Lipid transportation	Cholesterol uptake	LDLR	Overexpression	Oral epithelial	(32)
				Nasopharyngeal carcinoma	(35)
		CD36	Overexpression	Head and neck carcinoma	(36)
		LOX-1	Overexpression		
	FA uptake	CD36	Overexpression	Oral squamous cell carcinoma	(40)
				Oropharyngeal carcinoma	(44)
		FABPs	Overexpression	Head and neck carcinoma	(45)
				Tongue carcinoma	(46)
Lipid anabolism		ACLY	Overexpression	Nasopharyngeal carcinoma	(47)

(Continued)

TABLE 1 Continued

Lipid metabolism type		Enzymes	Expression	Subsites	References
				Oral carcinoma	(48)
	Cholesterol synthesis	ACAT1	Overexpression	Oral carcinoma	(50)
		HMGCR	Overexpression	Head and neck carcinoma	(51)
				Head and neck carcinoma	(52)
				Head and neck carcinoma	(53)
	FA *de novo* synthesis	FASN	Overexpression	Nasopharyngeal carcinoma	(35)
				Nasopharyngeal carcinoma	(56)
				Nasopharyngeal carcinoma	(57)
				Oral carcinoma	(58)
				Head and neck carcinoma	(59)
		ACCs	Overexpression	Head and neck carcinoma	(54)
				Head and neck carcinoma	(55)
		SCD	Overexpression	Oral carcinoma	(60)
				Oral carcinoma	(61)
Lipid catabolism	Lipolysis	ATGL	Overexpression	Head and neck carcinoma	(69)
			Low expression	Nasopharyngeal carcinoma	(63)
	FA catabolism	CPT1	Overexpression	Nasopharyngeal carcinoma	(70)

exploration in the future. Importantly, HNSCCs comprise a diverse group of cancers that affect the upper aerodigestive tract. The differences in reprogramming of lipid metabolism under different TMEs in HNSCCs require additional studies. Lipid metabolism reprogramming not only shows extensive interaction with other metabolic mechanisms, but also has various crosstalk with surrounding cells, cytokines, growth factors, and even nutrient molecules within the malignant cancer cells. Therefore, the role of lipid metabolism reprogramming in HNSCCs needs additional studies, including, but not limited to, its effects on the immune microenvironment and angiogenesis. Further understanding of the lipid metabolism reprogramming mechanisms, key rate-limiting enzyme functions, and regulatory pathways in HNSCCs may help to develop the potential use of lipid metabolism pathways as targets for anti-tumor therapy, as well as the use of dietary/nutritional interventions to improve the prognosis and life quality of HNSCCs patients.

Author contributions

Conceptualization, XM, BY, and MX; methodology, YP; software, KC and PJ; validation, XM, BW, and BY; investigation, RD; resources, JW; data curation, XM and BW; writing—original draft preparation, XM; writing—review and editing, BY; visualization, BW; supervision, MX; project administration, MX; funding acquisition, XM, BY, and MX. All authors have read and agreed to the published version of the manuscript.

Funding

The study was supported by grants from the Cultivation Project of the Major Research Plan of the National Natural Science Foundation of China (grant No. 91949119), National Natural Science Foundation of China (No.82101209 and No.82101212), Science and Technology Commission of Shanghai Municipality (grant No.21ZR1440200), the Shanghai Sailing Program (20YF1426400, 19YF1430300), and Ruijin Youth NSFC Cultivation Fund.

Acknowledgments

Figures were generated by using Figdraw (www.figdraw.com).

Conflict of interest

The authors declare that the research was conducted in the absence of any commercial or financial relationships that could be construed as a potential conflict of interest.

Publisher's note

References

1. Siegel RL, Miller KD, Jemal A. Cancer statistics, 2020. *CA: Cancer J Clin* (2020) 70:7–30. doi: 10.3322/caac.21590

2. Sung H, Ferlay J, Siegel RL, Laversanne M, Soerjomataram I, Jemal A, et al. Global cancer statistics 2020: GLOBOCAN estimates of incidence and mortality worldwide for 36 cancers in 185 countries. *CA: Cancer J Clin* (2021) 71:209–49. doi: 10.3322/caac.21660

3. Ang KK, Harris J, Wheeler R, Weber R, Rosenthal DI, Nguyen-Tan PF, et al. Human papillomavirus and survival of patients with oropharyngeal cancer. *New Engl J Med* (2010) 363:24–35. doi: 10.1056/NEJMoa0912217

4. Nguyen-Tan PF, Zhang Q, Ang KK, Weber RS, Rosenthal DI, Soulieres D, et al. Randomized phase III trial to test accelerated versus standard fractionation in combination with concurrent cisplatin for head and neck carcinomas in the radiation therapy oncology group 0129 trial: long-term report of efficacy and toxicity. *J Clin oncol: Off J Am Soc Clin Oncol* (2014) 32:3858–66. doi: 10.1200/JCO.2014.55.3925

5. Cohen N, Fedewa S, Chen AY. Epidemiology and demographics of the head and neck cancer population. *Oral Maxillofac Surg Clinics North America* (2018) 30:381–95. doi: 10.1016/j.coms.2018.06.001

6. David G, Pfister SS, Douglas A, Birkeland A, Brizel D, Busse P, et al. *National comprehensive cancer network. head and neck cancers version 2.* (2022). p. ed2022. Available at: http://www.nccn.org/professionals/physician_gls/pdf/head-and-neck.pdf

7. Muller-Richter U, Betz C, Hartmann S, Brands RC. Nutrition management for head and neck cancer patients improves clinical outcome and survival. *Nutr Res* (2017) 48:1–8. doi: 10.1016/j.nutres.2017.08.007

8. Orell-Kotikangas H, Osterlund P, Makitie O, Saarilahti K, Ravasco P, Schwab U, et al. Cachexia at diagnosis is associated with poor survival in head and neck cancer patients. *Acta Otolaryngol* (2017) 137:778–85. doi: 10.1080/00016489.2016.1277263

9. Gorenc M, Kozjek NR, Strojan P. Malnutrition and cachexia in patients with head and neck cancer treated with (chemo)radiotherapy. *Rep Pract Oncol radiother: J Greatpoland Cancer Center Poznan Polish Soc Radiat Oncol* (2015) 20:249–58. doi: 10.1016/j.rpor.2015.03.001

10. Ehrsson YT, Langius-Eklof A, Laurell G. Nutritional surveillance and weight loss in head and neck cancer patients. *Supportive Care cancer: Off J Multinational Assoc Supportive Care Cancer* (2012) 20:757–65. doi: 10.1007/s00520-011-1146-4

11. Faubert B, Solmonson A, DeBerardinis RJ. Metabolic reprogramming and cancer progression. *Sci* (2020) 368(6487):1–10. doi: 10.1126/science.aaw5473.

12. Bozzetti F, Stanga Z. Does nutrition for cancer patients feed the tumour? a clinical perspective. *Crit Rev Oncology/Hematol* (2020) 153:103061. doi: 10.1016/j.critrevonc.2020.103061

13. Brizel DM, Schroeder T, Scher RL, Walenta S, Clough RW, Dewhirst MW, et al. Elevated tumor lactate concentrations predict for an increased risk of metastases in head-and-neck cancer. *Int J Radiat Oncol Biol Phys* (2001) 51:349–53. doi: 10.1016/S0360-3016(01)01630-3

14. Edstrom S, Westin T, Delle U, Lundholm K. Cell cycle distribution and ornithine decarboxylase activity in head and neck cancer in response to enteral nutrition. *Eur J Cancer Clin Oncol* (1989) 25:227–32. doi: 10.1016/0277-5379(89)90013-8

15. Baron PL, Lawrence WJr., Chan WM, White FK, Banks WLJr. Effects of parenteral nutrition on cell cycle kinetics of head and neck cancer. *Arch Surg* (1986) 121:1282–6. doi: 10.1001/archsurg.1986.01400110072012

16. Hanahan D, Weinberg RA. Hallmarks of cancer: the next generation. *Cell* (2011) 144:646–74. doi: 10.1016/j.cell.2011.02.013

17. Ocana MC, Martinez-Poveda B, Quesada AR, Medina MA. Glucose favors lipid anabolic metabolism in the invasive breast cancer cell line MDA-MB-231. *Biol* (2020) 9(1):1–12. doi: 10.3390/biology9010016

18. Chen X, Chen S, Yu D. Metabolic reprogramming of chemoresistant cancer cells and the potential significance of metabolic regulation in the reversal of cancer chemoresistance. *Metabolites* (2020) 10(7):1–15. doi: 10.3390/metabo10070289

19. Germain N, Dhayer M, Boileau M, Fovez Q, Kluza J, Marchetti P. Lipid metabolism and resistance to anticancer treatment. *Biol* (2020) 9(12):1–21. doi: 10.3390/biology9120474

20. Bian X, Liu R, Meng Y, Xing D, Xu D, Lu Z. Lipid metabolism and cancer. *J Exp Med* (2021) 218(1):1–17. doi: 10.1084/jem.20201606

21. Rohrig F, Schulze A. The multifaceted roles of fatty acid synthesis in cancer. *Nat Rev Cancer* (2016) 16:732–49. doi: 10.1038/nrc.2016.89

22. Prentki M, Madiraju SR. Glycerolipid metabolism and signaling in health and disease. *Endocr Rev* (2008) 29:647–76. doi: 10.1210/er.2008-0007

23. Zhang F, Hao G, Shao M, Nham K, An Y, Wang Q, et al. An adipose tissue atlas: An image-guided identification of human-like BAT and beige depots in rodents. *Cell Metab* (2018) 27:252–62 e3. doi: 10.1016/j.cmet.2017.12.004

24. White JD, Dewal RS, Stanford KI. The beneficial effects of brown adipose tissue transplantation. *Mol Aspects Med* (2019) 68:74–81. doi: 10.1016/j.mam.2019.06.004

25. Chow LQM. Head and neck cancer. *New Engl J Med* (2020) 382:60–72. doi: 10.1056/NEJMra1715715

26. Bensouda Y, Kaikani W, Ahbeddou N, Rahhali R, Jabri M, Mrabti H, et al. Treatment for metastatic nasopharyngeal carcinoma. *Eur Ann otorhinolaryngol Head Neck Diseases* (2011) 128:79–85. doi: 10.1016/j.anorl.2010.10.003

27. Liu SC, Tsang NM, Lee PJ, Sui YH, Huang CH, Liu TT. Epstein-Barr Virus induces adipocyte dedifferentiation to modulate the tumor microenvironment. *Cancer Res* (2021) 81:3283–94. doi: 10.1158/0008-5472.CAN-20-3121

28. Wang N, Wang QJ, Feng YY, Shang W, Cai M. Overexpression of chemerin was associated with tumor angiogenesis and poor clinical outcome in squamous cell carcinoma of the oral tongue. *Clin Oral Investigations* (2014) 18:997–1004. doi: 10.1007/s00784-013-1046-8

29. Broadfield LA, Pane AA, Talebi A, Swinnen JV, Fendt SM. Lipid metabolism in cancer: New perspectives and emerging mechanisms. *Dev Cell* (2021) 56:1363–93. doi: 10.1016/j.devcel.2021.04.013

30. Ko CW, Qu J, Black DD, Tso P. Regulation of intestinal lipid metabolism: current concepts and relevance to disease. *Nat Rev Gastroenterol hepatol* (2020) 17:169–83. doi: 10.1038/s41575-019-0250-7

31. Goldstein JL, Brown MS. The LDL receptor. *Arteriosclerosis thrombosis Vasc Biol* (2009) 29:431–8. doi: 10.1161/ATVBAHA.108.179564

32. Ito S, Gojoubori T, Tsunoda K, Yamaguchi Y, Asano M, Goke E, et al. Nicotine-induced expression of low-density lipoprotein receptor in oral epithelial cells. *PloS One* (2013) 8:e82563. doi: 10.1371/journal.pone.0082563

33. Srinivas GV, Namala S, Ananthaneni A, Puneeth HK, Devi BS. Evaluation and correlation of serum lipid profile in oral and gastrointestinal cancer patients. *J Int Oral Health: JIOH* (2013) 5:72–7. doi: 10.1084/jem.20201606

34. Chawda JG, Jain SS, Patel HR, Chaduvula N, Patel K. The relationship between serum lipid levels and the risk of oral cancer. *Indian J Med paediatric oncol: Off J Indian Soc Med Paediatric Oncol* (2011) 32:34–7. doi: 10.4103/0971-5851.81888

35. Daker M, Bhuvanendran S, Ahmad M, Takada K, Khoo AS. Deregulation of lipid metabolism pathway genes in nasopharyngeal carcinoma cells. *Mol Med Rep* (2013) 7:731–41. doi: 10.3892/mmr.2012.1253

36. Kindt N, Journe F, Carlier S, Trelcat A, Scalia A, Saussez S. Effect of oxidized low-density lipoprotein on head and neck squamous cell carcinomas. *Biomedicines* (2021) 9(5):1–11. doi: 10.3390/biomedicines9050513

37. Corbet C, Pinto A, Martherus R, Santiago de Jesus JP, Polet F, Feron O. Acidosis drives the reprogramming of fatty acid metabolism in cancer cells through changes in mitochondrial and histone acetylation. *Cell Metab* (2016) 24:311–23. doi: 10.1016/j.cmet.2016.07.003

38. Wang MD, Wu H, Huang S, Zhang HL, Qin CJ, Zhao LH, et al. HBx regulates fatty acid oxidation to promote hepatocellular carcinoma survival during metabolic stress. *Oncotarget* (2016) 7:6711–26. doi: 10.18632/oncotarget.6817

39. Nakamura MT, Nara TY. Structure, function, and dietary regulation of delta6, delta5, and delta9 desaturases. *Annu Rev Nutr* (2004) 24:345–76. doi: 10.1146/annurev.nutr.24.121803.063211

40. Pascual G, Avgustinova A, Mejetta S, Martin M, Castellanos A, Attolini CS, et al. Targeting metastasis-initiating cells through the fatty acid receptor CD36. *Nature* (2017) 541:41–5. doi: 10.1038/nature20791

41. Jiang M, Wu N, Xu B, Chu Y, Li X, Su S, et al. Fatty acid-induced CD36 expression *via* O-GlcNAcylation drives gastric cancer metastasis. *Theranostics* (2019) 9:5359–73. doi: 10.7150/thno.34024

42. Pan J, Fan Z, Wang Z, Dai Q, Xiang Z, Yuan F, et al. CD36 mediates palmitate acid-induced metastasis of gastric cancer *via* AKT/GSK-3beta/beta-catenin pathway. *J Exp Clin Cancer Research: CR.* (2019) 38:52. doi: 10.1186/s13046-019-1049-7

43. Corbet C, Bastien E, Santiago de Jesus JP, Dierge E, Martherus R, Vander Linden C, et al. TGFbeta2-induced formation of lipid droplets supports acidosis-driven EMT and the metastatic spreading of cancer cells. *Nat Commun* (2020) 11:454. doi: 10.1038/s41467-019-14262-3

44. Pascual G, Dominguez D, Elosua-Bayes M, Beckedorff F, Laudanna C, Bigas C, et al. Dietary palmitic acid promotes a prometastatic memory *via* schwann cells. *Nature* (2021) 599:485–90. doi: 10.1038/s41586-021-04075-0

45. Rauch J, Ahlemann M, Schaffrik M, Mack B, Ertongur S, Andratschke M, et al. Allogenic antibody-mediated identification of head and neck cancer antigens. *Biochem Biophys Res Commun* (2004) 323:156–62. doi: 10.1016/j.bbrc.2004.08.071

46. Ohyama Y, Kawamoto Y, Chiba T, Kikuchi K, Sakashita H, Imai K. Differential expression of fatty acid-binding proteins and pathological implications in the progression of tongue carcinoma. *Mol Clin Oncol* (2014) 2:19–25. doi: 10.3892/mco.2013.198

47. Zheng ZQ, Li ZX, Guan JL, Liu X, Li JY, Chen Y, et al. Long noncoding RNA TINCR-mediated regulation of acetyl-CoA metabolism promotes nasopharyngeal carcinoma progression and chemoresistance. *Cancer Res* (2020) 80:5174–88. doi: 10.1158/0008-5472.CAN-19-3626

48. Sur S, Nakanishi H, Flaveny C, Ippolito JE, McHowat J, Ford DA, et al. Inhibition of the key metabolic pathways, glycolysis and lipogenesis, of oral cancer by bitter melon extract. *Cell Commun Signaling: CCS* (2019) 17:131. doi: 10.1186/s12964-019-0447-y

49. Gormley M, Yarmolinsky J, Dudding T, Burrows K, Martin RM, Thomas S, et al. Using genetic variants to evaluate the causal effect of cholesterol lowering on head and neck cancer risk: A mendelian randomization study. *PloS Genet* (2021) 17:e1009525. doi: 10.1371/journal.pgen.1009525

50. Zhang L, Zhao S, Liu Y, Lv F, Geng X. Identification and validation of transcription factor-driven enhancers of genes related to lipid metabolism in metastatic oral squamous cell carcinomas. *BMC Oral Health* (2022) 22:126. doi: 10.1186/s12903-022-02157-7

51. Ahmadi M, Amiri S, Pecic S, Machaj F, Rosik J, Los MJ, et al. Pleiotropic effects of statins: A focus on cancer. *Biochim Biophys Acta Mol basis disease* (2020) 1866:165968. doi: 10.1016/j.bbadis.2020.165968

52. Dimitroulakos J, Marhin WH, Tokunaga J, Irish J, Gullane P, Penn LZ, et al. Microarray and biochemical analysis of lovastatin-induced apoptosis of squamous cell carcinomas. *Neoplasia* (2002) 4:337–46. doi: 10.1038/sj.neo.7900247

53. Kwon M, Nam GH, Jung H, Kim SA, Kim S, Choi Y, et al. Statin in combination with cisplatin makes favorable tumor-immune microenvironment for immunotherapy of head and neck squamous cell carcinoma. *Cancer Letters* (2021) 522:198–210. doi: 10.1016/j.canlet.2021.09.029

54. Su YW, Lin YH, Pai MH, Lo AC, Lee YC, Fang IC, et al. Association between phosphorylated AMP-activated protein kinase and acetyl-CoA carboxylase expression and outcome in patients with squamous cell carcinoma of the head and neck. *PloS One* (2014) 9:e96183. doi: 10.1371/journal.pone.0096183

55. Li K, Zhang C, Chen L, Wang P, Fang Y, Zhu J, et al. The role of acetyl-coA carboxylase2 in head and neck squamous cell carcinoma. *PeerJ* (2019) 7:e7037. doi: 10.7717/peerj.7037

56. Lo AK, Lung RW, Dawson CW, Young LS, Ko CW, Yeung WW, et al. Activation of sterol regulatory element-binding protein 1 (SREBP1)-mediated lipogenesis by the Epstein-Barr virus-encoded latent membrane protein 1 (LMP1) promotes cell proliferation and progression of nasopharyngeal carcinoma. *J pathol* (2018) 246:180–90. doi: 10.1002/path.5130

57. Huang Y, Bell LN, Okamura J, Kim MS, Mohney RP, Guerrero-Preston R, et al. Phospho-DeltaNp63alpha/SREBF1 protein interactions: bridging cell metabolism and cisplatin chemoresistance. *Cell Cycle* (2012) 11:3810–27. doi: 10.4161/cc.22022

58. Boelcke WP, Teixeira IF, Aquino IG, Mazzaro AR, Cuadra-Zelaya FJM, de Souza AP, et al. Pharmacological fatty acid synthase inhibitors differently affect the malignant phenotype of oral cancer cells. *Arch Oral Biol* (2022) 135:105343. doi: 10.1016/j.archoralbio.2021.105343

59. Mims J, Bansal N, Bharadwaj MS, Chen X, Molina AJ, Tsang AW, et al. Energy metabolism in a matched model of radiation resistance for head and neck squamous cell cancer. *Radiat Res* (2015) 183:291–304. doi: 10.1667/RR13828.1

60. Jain P, Nattakom M, Holowka D, Wang DH, Thomas Brenna J, Ku AT, et al. Runx1 role in epithelial and cancer cell proliferation implicates lipid metabolism and Scd1 and Soat1 activity. *Stem Cells* (2018) 36:1603–16. doi: 10.1002/stem.2868

61. Nanjappa V, Renuse S, Sathe GJ, Raja R, Syed N, Radhakrishnan A, et al. Chronic exposure to chewing tobacco selects for overexpression of stearoyl-CoA desaturase in normal oral keratinocytes. *Cancer Biol Ther* (2015) 16:1593–603. doi: 10.1080/15384047.2015.1078022

62. Cruz ALS, Barreto EA, Fazolini NPB, Viola JPB, Bozza PT. Lipid droplets: platforms with multiple functions in cancer hallmarks. *Cell Death disease* (2020) 11:105. doi: 10.1038/s41419-020-2297-3

63. Zhou X, Wei J, Chen F, Xiao X, Huang T, He Q, et al. Epigenetic downregulation of the ISG15-conjugating enzyme UbcH8 impairs lipolysis and correlates with poor prognosis in nasopharyngeal carcinoma. *Oncotarget* (2015) 6:41077–91. doi: 10.18632/oncotarget.6218

64. Zheng S, Matskova L, Zhou X, Xiao X, Huang G, Zhang Z, et al. Downregulation of adipose triglyceride lipase by EB viral-encoded LMP2A links lipid accumulation to increased migration in nasopharyngeal carcinoma. *Mol Oncol* (2020) 14:3234–52. doi: 10.1002/1878-0261.12824

65. Luo X, Cheng C, Tan Z, Li N, Tang M, Yang L, et al. Emerging roles of lipid metabolism in cancer metastasis. *Mol cancer* (2017) 16:76. doi: 10.1186/s12943-017-0646-3

66. Caro P, Kishan AU, Norberg E, Stanley IA, Chapuy B, Ficarro SB, et al. Metabolic signatures uncover distinct targets in molecular subsets of diffuse large b cell lymphoma. *Cancer Cell* (2012) 22:547–60. doi: 10.1016/j.ccr.2012.08.014

67. Zechner R, Strauss JG, Haemmerle G, Lass A, Zimmermann R. Lipolysis: pathway under construction. *Curr Opin lipidol* (2005) 16:333–40. doi: 10.1097/01.mol.0000169354.20395.1c

68. Mairal A, Langin D, Arner P, Hoffstedt J. Human adipose triglyceride lipase (PNPLA2) is not regulated by obesity and exhibits low *in vitro* triglyceride hydrolase activity. *Diabetologia* (2006) 49:1629–36. doi: 10.1007/s00125-006-0272-x

69. Tripathi P, Kamarajan P, Somashekar BS, MacKinnon N, Chinnaiyan AM, Kapila YL, et al. Delineating metabolic signatures of head and neck squamous cell carcinoma: phospholipase A2, a potential therapeutic target. *Int J Biochem Cell Biol* (2012) 44:1852–61. doi: 10.1016/j.biocel.2012.06.025

70. Du Q, Tan Z, Shi F, Tang M, Xie L, Zhao L, et al. PGC1alpha/CEBPB/CPT1A axis promotes radiation resistance of nasopharyngeal carcinoma through activating fatty acid oxidation. *Cancer sci* (2019) 110:2050–62. doi: 10.1111/cas.14011

71. Koundouros N, Poulogiannis G. Reprogramming of fatty acid metabolism in cancer. *Br J cancer* (2020) 122:4–22. doi: 10.1038/s41416-019-0650-z

72. Liu F, Wei J, Hao Y, Lan J, Li W, Weng J, et al. Long intergenic non-protein coding RNA 02570 promotes nasopharyngeal carcinoma progression by adsorbing microRNA miR-4649-3p thereby upregulating both sterol regulatory element binding protein 1, and fatty acid synthase. *Bioengineered* (2021) 12:7119–30. doi: 10.1080/21655979.2021.1979317

73. Hashibe M, Brennan P, Chuang SC, Boccia S, Castellsague X, Chen C, et al. Interaction between tobacco and alcohol use and the risk of head and neck cancer: pooled analysis in the international head and neck cancer epidemiology consortium. *Cancer epidemiol Biomarkers prevention: Publ Am Assoc Cancer Research cosponsored by Am Soc Prev Oncol* (2009) 18:541–50. doi: 10.1158/1055-9965.EPI-08-0347

74. Di Credico G, Polesel J, Dal Maso L, Pauli F, Torelli N, Luce D, et al. Alcohol drinking and head and neck cancer risk: the joint effect of intensity and duration. *Br J cancer* (2020) 123:1456–63. doi: 10.1038/s41416-020-01031-z

75. Koo HY, Han K, Shin DW, Yoo JE, Cho MH, Jeon KH, et al. Alcohol drinking pattern and risk of head and neck cancer: A nationwide cohort study. *Int J Environ Res Public Health* (2021) 18(21):1–14. doi: 10.3390/ijerph182111204

76. Ganne-Carrie N, Nahon P. Hepatocellular carcinoma in the setting of alcohol-related liver disease. *J hepatol* (2019) 70:284–93. doi: 10.1016/j.jhep.2018.10.008

77. Lee WT, Hsiao JR, Ou CY, Huang CC, Chang CC, Tsai ST, et al. The influence of prediagnosis alcohol consumption and the polymorphisms of ethanol-metabolizing genes on the survival of head and neck cancer patients. *Cancer epidemiol Biomarkers prevention: Publ Am Assoc Cancer Research cosponsored by Am Soc Prev Oncol* (2019) 28:248–57. doi: 10.1158/1055-9965.EPI-18-0425

78. Fischer M, You M, Matsumoto M, Crabb DW. Peroxisome proliferator-activated receptor alpha (PPARalpha) agonist treatment reverses PPARalpha dysfunction and abnormalities in hepatic lipid metabolism in ethanol-fed mice. *J Biol Chem* (2003) 278:27997–8004. doi: 10.1074/jbc.M302140200

79. Salaspuro MP, Shaw S, Jayatilleke E, Ross WA, Lieber CS. Attenuation of the ethanol-induced hepatic redox change after chronic alcohol consumption in baboons: metabolic consequences *in vivo* and *in vitro*. *Hepatology* (1981) 1:33–8. doi: 10.1002/hep.1840010106

80. Tomita K, Azuma T, Kitamura N, Nishida J, Tamiya G, Oka A, et al. Pioglitazone prevents alcohol-induced fatty liver in rats through up-regulation of c-met. *Gastroenterology* (2004) 126:873–85. doi: 10.1053/j.gastro.2003.12.008

81. Li Q, Zhong W, Qiu Y, Kang X, Sun X, Tan X, et al. Preservation of hepatocyte nuclear factor-4alpha contributes to the beneficial effect of dietary medium chain triglyceride on alcohol-induced hepatic lipid dyshomeostasis in rats. *Alcoholism Clin Exp Res* (2013) 37:587–98. doi: 10.1111/acer.12013

82. Middlekauff HR, William KJ, Su B, Haptonstall K, Araujo JA, Wu X, et al. Changes in lipid composition associated with electronic cigarette use. *J Trans Med* (2020) 18:379. doi: 10.1186/s12967-020-02557-9

83. Chelland Campbell S, Moffatt RJ, Stamford BA. Smoking and smoking cessation – the relationship between cardiovascular disease and lipoprotein metabolism: a review. *Atherosclerosis* (2008) 201:225–35. doi: 10.1016/j.atherosclerosis.2008.04.046

84. Azizi F, Raiszadeh F, Salehi P, Rahmani M, Emami H, Ghanbarian A, et al. Determinants of serum HDL-c level in a Tehran urban population: the Tehran lipid and glucose study. *Nutrition metabolism Cardiovasc diseases: NMCD* (2002) 12:80–9.

85. Mizoue T, Ueda R, Hino Y, Yoshimura T. Workplace exposure to environmental tobacco smoke and high density lipoprotein cholesterol among

nonsmokers. *Am J Epidemiol* (1999) 150:1068–72. doi: 10.1093/oxfordjournals.aje.a009930

86. Merianos AL, Jandarov RA, Khoury JC, Mahabee-Gittens EM. Tobacco smoke exposure association with lipid profiles and adiposity among U.S. adolescents. *J Adolesc health: Off Publ Soc Adolesc Med* (2018) 62:463–70. doi: 10.1016/j.jadohealth.2017.10.001

87. Zakhar J, Amrock SM, Weitzman M. Passive and active tobacco exposure and children's lipid profiles. *Nicotine tobacco research: Off J Soc Res Nicotine Tobacco* (2016) 18:982–7. doi: 10.1093/ntr/ntv158

88. Steenland K, Sieber K, Etzel RA, Pechacek T, Maurer K. Exposure to environmental tobacco smoke and risk factors for heart disease among never smokers in the third national health and nutrition examination survey. *Am J Epidemiol* (1998) 147:932–9. doi: 10.1093/oxfordjournals.aje.a009383

89. Bousarghin L, Touze A, Sizaret PY, Coursaget P. Human papillomavirus types 16, 31, and 58 use different endocytosis pathways to enter cells. *J virol* (2003) 77:3846–50. doi: 10.1128/JVI.77.6.3846-3850.2003

90. Bravo IG, Crusius K, Alonso A. The E5 protein of the human papillomavirus type 16 modulates composition and dynamics of membrane lipids in keratinocytes. *Arch virol* (2005) 150:231–46. doi: 10.1007/s00705-004-0420-x

91. Zhang L, Wu J, Ling MT, Zhao L, Zhao KN. The role of the PI3K/Akt/mTOR signalling pathway in human cancers induced by infection with human papillomaviruses. *Mol Cancer* (2015) 14:87. doi: 10.1186/s12943-015-0361-x

92. Cheng C, Geng F, Cheng X, Guo D. Lipid metabolism reprogramming and its potential targets in cancer. *Cancer Commun* (2018) 38:27. doi: 10.1186/s40880-018-0301-4

93. Chopjitt P, Pientong C, Bumrungthai S, Kongyingyoes B, Ekalaksananan T. Activities of E6 protein of human papillomavirus 16 Asian variant on miR-21 up-regulation and expression of human immune response genes. *Asian Pacific J Cancer prevention: APJCP* (2015) 16:3961–8. doi: 10.7314/APJCP.2015.16.9.3961

94. Ni K, Wang D, Xu H, Mei F, Wu C, Liu Z, et al. miR-21 promotes non-small cell lung cancer cells growth by regulating fatty acid metabolism. *Cancer Cell Int* (2019) 19:219. doi: 10.1186/s12935-019-0941-8

95. Prusinkiewicz MA, Gameiro SF, Ghasemi F, Dodge MJ, Zeng PYF, Maekebay H, et al. Survival-associated metabolic genes in human papillomavirus-positive head and neck cancers. *Cancers* (2020) 12(1):1–17. doi: 10.3390/cancers12010253

96. Martinez-Ramirez I, Carrillo-Garcia A, Contreras-Paredes A, Ortiz-Sanchez E, Cruz-Gregorio A, Lizano M. Regulation of cellular metabolism by high-risk human papillomaviruses. *Int J Mol Sci* (2018) 19(7):1–17. doi: 10.3390/ijms19071839

97. Cruz-Gregorio A, Martinez-Ramirez I, Pedraza-Chaverri J, Lizano M. Reprogramming of energy metabolism in response to radiotherapy in head and neck squamous cell carcinoma. *Cancers* (2019) 11(2):1–17. doi: 10.3390/cancers11020182

98. Cruz-Gregorio A, Aranda-Rivera AK, Ortega-Lozano AJ, Pedraza-Chaverri J, Mendoza-Hoffmann F. Lipid metabolism and oxidative stress in HPV-related cancers. *Free Radical Biol Med* (2021) 172:226–36. doi: 10.1016/j.freeradbiomed.2021.06.009

99. Cai TT, Ye SB, Liu YN, He J, Chen QY, Mai HQ, et al. LMP1-mediated glycolysis induces myeloid-derived suppressor cell expansion in nasopharyngeal carcinoma. *PloS pathog* (2017) 13:e1006503. doi: 10.1371/journal.ppat.1006503

100. Xiao L, Hu ZY, Dong X, Tan Z, Li W, Tang M, et al. Targeting Epstein-Barr virus oncoprotein LMP1-mediated glycolysis sensitizes nasopharyngeal carcinoma to radiation therapy. *Oncogene* (2014) 33:4568–78. doi: 10.1038/onc.2014.32

101. Petras G, Adam MM. Phases of the serological response in pseudomonas aeruginosa infections. *Acta microbiol Hungarica* (1987) 34:147–57.

102. Wang LW, Wang Z, Ersing I, Nobre L, Guo R, Jiang S, et al. Epstein-Barr Virus subverts mevalonate and fatty acid pathways to promote infected b-cell proliferation and survival. *PloS Pathog* (2019) 15:e1008030. doi: 10.1371/journal.ppat.1008030

103. Arora GK, Gupta A, Narayanan S, Guo T, Iyengar P, Infante RE. Cachexia-associated adipose loss induced by tumor-secreted leukemia inhibitory factor is counterbalanced by decreased leptin. *JCI Insight* (2018) 3(14):1–18. doi: 10.1172/jci.insight.121221

104. Strassmann G, Fong M, Kenney JS, Jacob CO. Evidence for the involvement of interleukin 6 in experimental cancer cachexia. *J Clin Invest* (1992) 89:1681–4. doi: 10.1172/JCI115767

105. Flint TR, Janowitz T, Connell CM, Roberts EW, Denton AE, Coll AP, et al. Tumor-induced IL-6 reprograms host metabolism to suppress anti-tumor immunity. *Cell Metab* (2016) 24:672–84. doi: 10.1016/j.cmet.2016.10.010

106. Middeldorp JM, Pegtel DM. Multiple roles of LMP1 in Epstein-Barr virus induced immune escape. *Semin Cancer Biol* (2008) 18:388–96. doi: 10.1016/j.semcancer.2008.10.004

107. Lien EC, Vander Heiden MG. A framework for examining how diet impacts tumour metabolism. *Nat Rev Cancer* (2019) 19:651–61. doi: 10.1038/s41568-019-0198-5

108. Sullivan MR, Mattaini KR, Dennstedt EA, Nguyen AA, Sivanand S, Reilly MF, et al. Increased serine synthesis provides an advantage for tumors arising in tissues where serine levels are limiting. *Cell Metab* (2019) 29:1410–21 e4. doi: 10.1016/j.cmet.2019.02.015

109. Sullivan MR, Danai LV, Lewis CA, Chan SH, Gui DY, Kunchok T, et al. Quantification of microenvironmental metabolites in murine cancers reveals determinants of tumor nutrient availability. *eLife* (2019) 8:1–27. doi: 10.7554/eLife.44235

110. Maddocks ODK, Athineos D, Cheung EC, Lee P, Zhang T, van den Broek NJF, et al. Modulating the therapeutic response of tumours to dietary serine and glycine starvation. *Nature* (2017) 544:372–6. doi: 10.1038/nature22056

111. Gao X, Sanderson SM, Dai Z, Reid MA, Cooper DE, Lu M, et al. Dietary methionine influences therapy in mouse cancer models and alters human metabolism. *Nature* (2019) 572:397–401. doi: 10.1038/s41586-019-1437-3

112. Lien EC, Westermark AM, Zhang Y, Yuan C, Li Z, Lau AN, et al. Low glycaemic diets alter lipid metabolism to influence tumour growth. *Nature* (2021) 599:302–7. doi: 10.1038/s41586-021-04049-2

113. Shin D, Kim EH, Lee J, Roh JL. Nrf2 inhibition reverses resistance to GPX4 inhibitor-induced ferroptosis in head and neck cancer. *Free Radical Biol Med* (2018) 129:454–62. doi: 10.1016/j.freeradbiomed.2018.10.426

114. Chen X, Kang R, Kroemer G, Tang D. Broadening horizons: the role of ferroptosis in cancer. *Nat Rev Clin Oncol* (2021) 18:280–96. doi: 10.1038/s41571-020-00462-0

115. Huang C, Zhan L. Network pharmacology identifies therapeutic targets and the mechanisms of glutathione action in ferroptosis occurring in oral cancer. *Front Pharmacol* (2022) 13:851540. doi: 10.3389/fphar.2022.851540

116. Budhathoki S, Hidaka A, Yamaji T, Sawada N, Tanaka-Mizuno S, Kuchiba A, et al. Plasma 25-hydroxyvitamin d concentration and subsequent risk of total and site specific cancers in Japanese population: large case-cohort study within Japan public health center-based prospective study cohort. *Bmj* (2018) 360:k671. doi: 10.1136/bmj.k671

117. Mishima E, Ito J, Wu Z, Nakamura T, Wahida A, Doll S, et al. A non-canonical vitamin K cycle is a potent ferroptosis suppressor. *Nature* (2022) 608 (7924):778–83. doi: 10.1038/s41586-022-05022-3

118. Jing K, Shin S, Jeong S, Kim S, Song KS, Park JH, et al. Docosahexaenoic acid induces the degradation of HPV E6/E7 oncoproteins by activating the ubiquitin-proteasome system. *Cell Death disease* (2014) 5:e1524. doi: 10.1038/cddis.2014.477

119. Meza-Menchaca T, Poblete-Naredo I, Albores-Medina A, Pedraza-Chaverri J, Quiroz-Figueroa FR, Cruz-Gregorio A, et al. Ergosterol peroxide isolated from oyster medicinal mushroom, pleurotus ostreatus (Agaricomycetes), potentially induces radiosensitivity in cervical cancer. *Int J med mushrooms* (2020) 22:1109–19. doi: 10.1615/IntJMedMushrooms.2020036673

120. Zhou ZT, Yang Y, Ge JP. The preventive effect of salvianolic acid b on malignant transformation of DMBA-induced oral premalignant lesion in hamsters. *Carcinogenesis* (2006) 27:826–32. doi: 10.1093/carcin/bgi271

121. Meng LC, Zheng JY, Qiu YH, Zheng L, Zheng JY, Liu YQ, et al. Salvianolic acid b ameliorates non-alcoholic fatty liver disease by inhibiting hepatic lipid accumulation and NLRP3 inflammasome in ob/ob mice. *Int immunopharmacol* (2022) 111:109099. doi: 10.1016/j.intimp.2022.109099

122. Buchsbaum RJ, Oh SY. Breast cancer-associated fibroblasts: Where we are and where we need to go. *Cancers* (2016) 8(2):1–19. doi: 10.3390/cancers8020019

123. Sun DY, Wu JQ, He ZH, He MF, Sun HB. Cancer-associated fibroblast regulate proliferation and migration of prostate cancer cells through TGF-beta signaling pathway. *Life Sci* (2019) 235:116791. doi: 10.1016/j.lfs.2019.116791

124. Ham IH, Lee D, Hur H. Role of cancer-associated fibroblast in gastric cancer progression and resistance to treatments. *J Oncol* (2019) 2019:6270784. doi: 10.1155/2019/6270784

125. Bolt R, Foran B, Murdoch C, Lambert DW, Thomas S, Hunter KD. HPV-negative, but not HPV-positive, oropharyngeal carcinomas induce fibroblasts to support tumour invasion through micro-environmental release of HGF and IL-6. *Carcinogenesis* (2018) 39:170–9. doi: 10.1093/carcin/bgx130

126. Kabir TD, Leigh RJ, Tasena H, Mellone M, Coletta RD, Parkinson EK, et al. A miR-335/COX-2/PTEN axis regulates the secretory phenotype of senescent cancer-associated fibroblasts. *Aging* (2016) 8:1608–35. doi: 10.18632/aging.100987

127. Jiang E, Xu Z, Wang M, Yan T, Huang C, Zhou X, et al. Tumoral microvesicle-activated glycometabolic reprogramming in fibroblasts promotes the progression of oral squamous cell carcinoma. *FASEB journal: Off Publ Fed Am Societies Exp Biol* (2019) 33:5690–703. doi: 10.1096/fj.201802226R

128. Zhang Z, Gao Z, Rajthala S, Sapkota D, Dongre H, Parajuli H, et al. Metabolic reprogramming of normal oral fibroblasts correlated with increased

glycolytic metabolism of oral squamous cell carcinoma and precedes their activation into carcinoma associated fibroblasts. *Cell Mol Life Sci: CMLS* (2020) 77:1115–33. doi: 10.1007/s00018-019-03209-y

129. Cristancho AG, Lazar MA. Forming functional fat: a growing understanding of adipocyte differentiation. *Nat Rev Mol Cell Biol* (2011) 12:722–34. doi: 10.1038/nrm3198

130. Dirat B, Bochet L, Dabek M, Daviaud D, Dauvillier S, Majed B, et al. Cancer-associated adipocytes exhibit an activated phenotype and contribute to breast cancer invasion. *Cancer Res* (2011) 71:2455–65. doi: 10.1158/0008-5472.CAN-10-3323

131. James RF, Lake SP, Chamberlain J, Thirdborough S, Bassett PD, Mistry N, et al. Gamma irradiation of isolated rat islets pretransplantation produces indefinite allograft survival in cyclosporine-treated recipients. *Transplantation* (1989) 47:929–33. doi: 10.1097/00007890-198906000-00001

132. Park EJ, Lee JH, Yu GY, He G, Ali SR, Holzer RG, et al. Dietary and genetic obesity promote liver inflammation and tumorigenesis by enhancing IL-6 and TNF expression. *Cell* (2010) 140:197–208. doi: 10.1016/j.cell.2009.12.052

133. Park J, Euhus DM, Scherer PE. Paracrine and endocrine effects of adipose tissue on cancer development and progression. *Endocr Rev* (2011) 32:550–70. doi: 10.1210/er.2010-0030

134. Gilbert CA, Slingerland JM. Cytokines, obesity, and cancer: new insights on mechanisms linking obesity to cancer risk and progression. *Annu Rev Med* (2013) 64:45–57. doi: 10.1146/annurev-med-121211-091527

135. Young MRI, Levingston C, Johnson SD. Cytokine and adipokine levels in patients with premalignant oral lesions or in patients with oral cancer who did or did not receive 1 alpha,25-dihydroxyvitamin d-3 treatment upon cancer diagnosis. *Cancers* (2015) 7:1109–24. doi: 10.3390/cancers7030827

136. Gharote HP, Mody RN. Estimation of serum leptin in oral squamous cell carcinoma. *J Oral Pathol med: Off Publ Int Assoc Oral Pathol Am Acad Oral Pathol* (2010) 39:69–73. doi: 10.1111/j.1600-0714.2009.00808.x

137. Lo HC, Yang CS, Tsai LJ. Simultaneous measurements of serum insulin-like growth factor-I and leptin reflect the postoperative nutrition status of oral tumor patients. *Nutrition* (2003) 19:327–31. doi: 10.1016/S0899-9007(02)01012-2

138. Guo XH, Wang JY, Gao Y, Gao M, Yu GY, Xiang RL, et al. Decreased adiponectin level is associated with aggressive phenotype of tongue squamous cell carcinoma. *Cancer sci* (2013) 104:206–13. doi: 10.1111/cas.12077

139. Yu-Duan T, Chao-Ping W, Chih-Yu C, Li-Wen L, Tsun-Mei L, Chia-Chang H, et al. Elevated plasma level of visfatin/pre-b cell colony-enhancing factor in male oral squamous cell carcinoma patients. *Med oral patol Oral y cirugia bucal* (2013) 18:e180–6. doi: 10.4317/medoral.18574

140. Kumar D, New J, Vishwakarma V, Joshi R, Enders J, Lin F, et al. Cancer-associated fibroblasts drive glycolysis in a targetable signaling loop implicated in head and neck squamous cell carcinoma progression. *Cancer Res* (2018) 78:3769–82. doi: 10.1158/0008-5472.CAN-17-1076

10.3389/fonc.2022.1008361

Glossary

ABCA1	ATP Binding Cassette Subfamily A Member 1
ACAT	acetyl-CoA acetyltransferase
ACC	acetyl-CoA carboxylase
ACLY	ATP-citric acid lyase
AGPAT	1-acyl-sn-Gly3P acyltransferase
ATGL	adipose triglyceride lipase
CD36	differentiated cluster 36
CETP	Cholesteryl Ester Transfer Protein
CPT	carnitine palmityl transferase
DAG	diacylglycerol
DGAT	DAG acyltransferase
EBERs	Epstein Barr virus encoded RNA
ELOVL	elongase of very long chain fatty acids
FA	fatty acid
FABPs	FA binding proteins
FA CoA	fatty acyl coenzyme A
FAO	fatty acid oxidation
FASN	fatty acid synthase
FDG-PET	fluorodeoxyglucose-positron emission tomography
GPAT	Gly3P phosphate acyltransferase
HMGCR	HMG-COA reductase
HMGCS	HMG-CoA synthase
HNSCC	Head and neck squamous cell carcinomas
HPV	human papilloma virus
HSL	hormone-sensitive lipase
LD	lipid droplets
LDL	low-density lipoprotein
LDLR	low-density lipoprotein receptors
LMP2A	membrane latent protein 2A
LXR	liver X receptor
MAG	monoacylglycerol
MGL	MAG lipase
NPC	nasopharyngeal carcinoma
NPC1L1	Niemann-Pick type C1-like 1
OS	overall survival
PA	palmitic acid
PAP	PA phosphatase
SCD	stearoyl-CoA desaturase
SUV	standard uptake values
TG	triacylglycerol
TME	tumor microenvironment
VLDL	very low-density lipoprotein

frontiers | Frontiers in Pharmacology

TYPE Original Research
PUBLISHED 26 September 2022
DOI 10.3389/fphar.2022.1007006

OPEN ACCESS

EDITED BY
Hai-long Piao,
Dalian Institute of Chemical Physics (CAS), China

REVIEWED BY
Jian Gao,
Xuzhou Medical University, China
Huai-Qiang Ju,
Sun Yat-sen University, China

*CORRESPONDENCE
Yangfan Qi,
yangfanqi@dmu.edu.cn
Wenjing Zhang,
zhangwj@dmu.edu.cn
Yang Wang,
yangwang@dmu.edu.cn

†These authors have contributed equally to this work

SPECIALTY SECTION
This article was submitted to Pharmacology of Anti-Cancer Drugs, a section of the journal Frontiers in Pharmacology

RECEIVED 29 July 2022
ACCEPTED 30 August 2022
PUBLISHED 26 September 2022

CITATION
Bai L, Sun S, Su W, Chen C, Lv Y, Zhang J, Zhao J, Li M, Qi Y, Zhang W and Wang Y (2022), Melatonin inhibits HCC progression through regulating the alternative splicing of NEMO. *Front. Pharmacol.* 13:1007006. doi: 10.3389/fphar.2022.1007006

Melatonin inhibits HCC progression through regulating the alternative splicing of NEMO

Lu Bai[1†], Siwen Sun[2†], Wenmei Su[3†], Chaoqun Chen[1], Yuesheng Lv[2], Jinrui Zhang[1], Jinyao Zhao[1], Man Li[2], Yangfan Qi[1]*, Wenjing Zhang[1]* and Yang Wang[1,3]*

[1]Institute of Cancer Stem Cell, Dalian Medical University, Dalian, China, [2]Department of Oncology, The Second Affiliated Hospital of Dalian Medical University, Dalian, China, [3]Department of Pulmonary Oncology, Affiliated Hospital of Guangdong Medical University, Zhanjiang, China

Hepatocellular carcinoma (HCC) is one of the most common primary cancers with limited therapeutic options. Melatonin, a neuroendocrine hormone produced primarily by the pineal gland, demonstrates an anti-cancer effect on a myriad of cancers including HCC. However, whether melatonin could suppress tumor growth through regulating RNA alternative splicing remains largely unknown. Here we demonstrated that melatonin could inhibit the growth of HCC. Mechanistically, melatonin induced transcriptional alterations of genes, which are involved in DNA replication, DNA metabolic process, DNA repair, response to wounding, steroid metabolic process, and extracellular matrix functions. Importantly, melatonin controlled numerous cancer-related RNA alternative splicing events, regulating mitotic cell cycle, microtubule-based process, kinase activity, DNA metabolic process, GTPase regulator activity functions. The regulatory effect of melatonin on alternative splicing is partially mediated by melatonin receptor MT1. Specifically, melatonin regulates the splicing of *IKBKG* (NEMO), an essential modulator of NF-κB. In brief, melatonin increased the production of the long isoform of NEMO-L with exon 5 inclusion, thereby inhibiting the growth of HepG2 cells. Collectively, our study provides a novel mechanism of melatonin in regulating RNA alternative splicing, and offers a new perspective for melatonin in the inhibition of cancer progression.

KEYWORDS

melatonin, HCC, NEMO, alternative splicing, MT1

Introduction

Liver cancer is the sixth most common cancer, and the third leading cause of cancer death all over the world (Sung et al., 2021). HCC accounts for about 80% of liver cancers, which has poor prognosis and is the major cause of liver cancer-related mortality (Yang et al., 2019). The current treatment strategies for HCC includes surgical resection, chemotherapy, hormonal therapy, liver transplantation and

percutaneous local ablation. Due to the absence of specific symptoms in early stages and the lack of diagnostic markers, more than 70% of patients with HCC are often diagnosed in an advanced stage (Llovet et al., 2016; Montella et al., 2016; Liu and Qin, 2019). The multiple-target tyrosine kinase inhibitor sorafenib is one of the most effective drugs for the advanced HCC (Yang et al., 2019). However, only about 30% of patients can benefit from sorafenib treatment, which might lead to drug resistance and side effects as well. HCC is a heterogeneous tumor, containing alterations of multiple signaling pathway. The complex patho-physiology of HCC urgently drives the discovery of new treatment or combination therapy (Huang et al., 2020; Tang et al., 2020).

Melatonin (N-acetyl-5-methoxytryptamine), a neuroendocrine hormone produced primarily by the pineal gland, has various functions, including regulating circadian rhythm and antioxidant. Melatonin can activate melatonin receptor MT1, MT2, MT3, and ROZ/ROR to function in a receptor-mediated manner. Meanwhile, melatonin can also be soluble into water and lipid environments, thus easily diffusing through cell membranes and penetrating cellular compartments to work through non-receptor-mediated mechanisms (Mao et al., 2010; Liu et al., 2016; Asghari et al., 2017; Ferlazzo et al., 2020). Melatonin exerts oncostatic functions in numerous human malignancies, containing breast cancer, ovarian cancer, prostate cancer, skin cancer, and liver cancer, etc. (Zhao et al., 2019). Melatonin could suppress cancer progression through regulating cancer cell proliferation, migration, invasion, angiogenesis, apoptosis and cell cycle (Fernandez-Palanca et al., 2021). In particular, as a natural compound, melatonin intriguingly plays antithetical roles in normal cells and cancer cells. For example, melatonin increases the activity of SIRT1 and inhibits apoptosis by reducing the expression of Ac-FOXO1A, Ac-TP53, or Ac-BAX in normal cells. Conversely, SIRT1 is highly activated in cancer cells, and melatonin blocks SIRT1, thereby inhibiting cell proliferation and exerting a tumor suppressing effect (Mayo et al., 2017). However, due to the clinical complexity, the anticancer mechanisms of melatonin in cancer therapeutics are still largely less understood.

Alternative splicing (AS) is a crucial post-transcriptional mechanism to regulate gene expression patterns that allows a single gene to code for multiple transcript isoforms, thereby increasing the diversity and complexity of the transcriptome (Yuan et al., 2017; Hu et al., 2020). Alternative splicing plays an important role in tumorigenesis and cancer progression. Aberrant splicing could induce the production of noncanonical and cancer-specific mRNA transcripts, causing the inactivation of tumor suppressors or the activation of oncogenes (Chen et al., 2019). These RNA variants could be translated into distinct protein isoforms, and might be involved in different tumor biological functions, such as proliferation, apoptosis, angiogenesis, metabolism, stemness, drug-resistance and metastasis (Bonnal et al., 2020; Sciarrillo et al., 2020). Importantly, abnormal RNA alternative splicing can promote the development of HCC. For example, BIN1 generates a short isoform (BIN1-S, which lacks exon 12a) that exerts a tumor suppressing effect by inhibiting the binding of c-Myc to target gene promoter in the normal liver. However, upregulated NONO helps the oncogenic splicing switch of BIN1 from BIN1-S to BIN1-L (a long isoform, which contains exon 12) to promote carcinogenesis in HCC (Hu et al., 2020). Therefore, the study of molecular mechanisms of alternative splicing might provide novel therapeutics for liver cancer. However, whether alternative splicing is involved in melatonin-mediated inhibition of tumor progression is still largely unknown.

Here, we reported that melatonin can exert antitumor effects by regulating cancer-related splicing events in HCC. To systematically identify melatonin-regulated splicing events, we performed mRNA-seq analysis on HepG2 cells with melatonin treatment for 24 h and 48 h. Importantly, in addition to the regulation of gene expression, melatonin also modulated the occurrence of a wide range of splicing events. Briefly, we identified 391 overlapped differentially expressed genes and 335 overlapped AS events after melatonin treatment for 24 h and 48 h in HepG2. Our results showed that exon skipping is the predominant type of melatonin-induced alternative splicing events, and we identified the alternative splicing switches of *IKBKG*, *LPIN1*, *ITGA6*, *TERF1*, *KIF23*, *SIN3B*, which might regulate the mitotic cell cycle, kinase activity, GTPase regulator activity, cellular response to DNA damage stimulus, and histone modification functions. The regulatory effect of melatonin on alternative splicing is partly mediated by MT1. Moreover, melatonin could exert tumor suppressing effect by up-regulating the expression of the long isoform of *IKBKG*. Taken together, our study systematically identified melatonin-mediated alternative splicing events, which might provide a new avenue to interpret the tumor suppressing function of melatonin in HCC.

Materials and methods

Cell culture and reagents

Human HCC HepG2 cell line and Hep3B cell line were obtained from the American Type Culture Collection. HepG2 cell line and Hep3B cell line were maintained at standard culture conditions (37°C, 5% CO_2) in MEM medium with 10% FBS (BI), Sodium Pyruvate (macgene, CC007), Nonessential Amino Acids Solution (macgene, CC25025).

HEK-293T cells were maintained at standard culture conditions (37°C, 5% CO_2) in DMEM medium with 10% FBS. NCI-H1299 cells were maintained at standard culture conditions (37°C, 5% CO_2) in 1640 medium with 10% FBS. A549 cells were maintained at standard culture conditions (37°C, 5% CO_2) in F12K medium with 10% FBS. Melatonin was purchased from Selleck (S1204).

Plasmid constructions and generation of stable cell lines

To generate the mammalian expression plasmids pCDH-Flag-NEMO-L and pCDH-Flag-NEMO-S, human NEMO-L and NEMO-S cDNA were amplified by PCR and then cloned into lentivirus vector pCDH-CMV-MCS-EF1-Puro with N-terminal Flag tag with restriction enzymes Nhe I and Not I. shRNAs targeting MT1 were cloned into the pLKO.1. To stably overexpress NEMO-L/S or knockdown MT1 in HepG2 cells, lentiviral particles were produced by transient transfection of HEK-293T cells with pCDH-Flag-NEMO-L or pCDH-Flag-NEMO-S or pCDH-empty or plko.1-empty or plko.1-shMT1 vectors. Media contains lentivirus were used to infect HepG2 cells, followed by 4 μg/ml puromycin (Solarbio, P8230) selection for 5 days. The expression of transgenes was confirmed by western blots, semi-quantitative RT-PCR or RT-qPCR before further analysis.

Western blot

Cells were washed twice with cold 1 × PBS and then lysed by RIPA lysis buffer containing 1 mM PMSF and 1 mM Cocktail. Cells were scraped off and collected into EP tubes, and centrifuged at 12,000 rpm for 15 min to remove cell debris. Equal amount of total protein was separated by 10% SDS-PAGE and transferred to nitrocellulose membrane, which were blocked with 5% fat-free milk and incubated with primary antibody at 4°C overnight. The following antibodies were used: Anti-Flag (Sigma, F1804), anti-GAPDH (Proteintech, 60004-1-Ig) and anti-NEMO (Proteintech, 18474-1-AP). After PBS washes, the membrane was incubated with secondary antibodies for 1 h at room temperature. Finally, bound antibodies were visualized with the ECL enhanced chemiluminescence regent Kit (NCM Biotech).

RT-qPCR and semi-quantitative RT-PCR

Total RNAs were extracted from cells treated with or without melatonin using TRIzol reagent (Invitrogen) according to the manufacturer's instructions. Genomic DNAs were removed and total RNA (2 μg) was reverse transcribed by the Thermo Scientific RevertAid First Strand cDNA Synthesis Kit (with DNase I). We performed RT-qPCR used MonAmp™ Taqman qPCR Mix (Monad) according to the manufacturer's instructions. The expression level of targets was normalized to the endogenous expression of *GAPDH*. The cDNA was also used as the template for semi-quantitative RT-PCR. Products were separated on 3% agarose gels, and imaged were captured using a CCD camera (Tanon 2500R). The primers listed in Supplementary Table S1.

RNA-seq analysis

HepG2 cells were treated with melatonin 1 mM or DMSO for 24 h and 48 h, and then extracted total RNAs using TRIzol and cleaned using RNAeasy Kit (Qiagen). The DNA was removed from total RNAs by digesting in column with RNase free DNase according to manufacturer's instructions. Polyadenylated RNA were purified from total RNA by using Illumina TruSeq Total RNA Sample Prep kits. For discover splicing junctions, we mapped the paired-end sequences to human genome (hg38) using Map Splice 2.0.1.6 (default parameters). The level of gene expression was analyzed by the mapped reads with Cufflinks. We analyzed the changes of splicing isoforms using MISO package with annotation of all known alternative splicing events, and the results filtered according to the PSI values.

We preformed gene ontology analysis and KEGG analysis using metascape.org to search for enriched functions and pathways. The functionally correlated network of melatonin-regulated genes was analyzed by STRING database.

IC50 measurement and growth curve assay

CCK8 assay was used to detect the IC50. Cells were seeded into 96-well plates (4000 cells/well) to culture overnight and then treated with different concentrations (0, 0.5, 1, 1.5, 2.5, 5, 7.5, 10 mM) of melatonin for 72 h. Then 10 μL/well CCK8 was added, allowing cells to continuously culture at 37°C for 2 h. Absorbance at 450 nm was measured using an ELISA reader (DNM-9602, Perlong). Dose-response curves were plotted to determine half maximal IC50 of melatonin using the GraphPad Prism. For growth curve assay, cells were seeded into 96-well plates (1000 cells/well) and cell viability was measured using CCK8 assay. Cell growth curves were determined by absorbance at 450 nm.

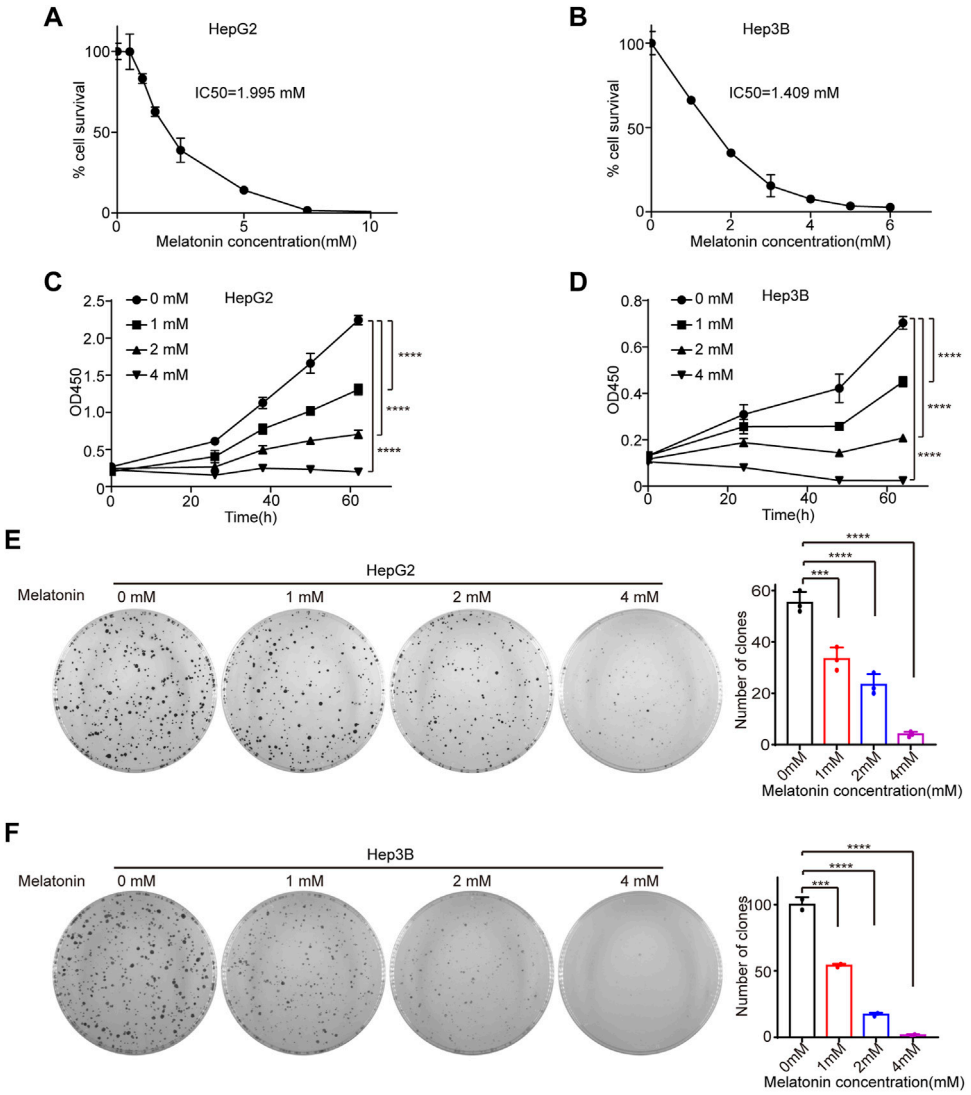

FIGURE 1
Melatonin inhibits cell proliferation. **(A)** HepG2 cells were treated with gradient concentrations of 0, 0.5, 1, 1.5, 2.5, 5, 7.5, 10 mM melatonin for 72 h, and cell viability was measured by CCK8 assay. **(B)** Hep3B cells were treated with gradient concentration of 0, 1, 2, 3, 4, 5, 6 mM melatonin for 72 h, and cell viability was measured by CCK8 assay. IC50 were calculated using GraphPad Prism. **(C,D)** The cell viability of HepG2 cells and Hep3B cells treated with gradient concentration of 0, 1, 2, 4 mM melatonin for 62 h, was measured by CCK8 assay at intervals, with *p* values calculated by two-way ANOVA. **(E,F)** The proliferation of HepG2 cells and Hep3B cells treated with gradient concentration of 0, 1, 2, 4 mM melatonin was examined with colony formation assay. Images of the whole plate are shown. The mean ± SD of relative colony numbers was plotted and *p* values calculated by one-way ANOVA.

Colony formation

Cells were seeded in 60-mm dishes (1500 cells per dish) and incubated at 37°C, 5% CO_2 in humidified incubator for 15 days. Each treatment was carried out in triplicate. Colonies were fixed with 4% PFA and stained with crystal violet.

Liver cancer tissue specimens

We collected fresh liver cancer tissues and adjacent normal tissues from patients with pathologically and clinically confirmed liver cancer. All human tumor tissues were obtained with written informed consent from patients or their guardians prior to participation in the study.

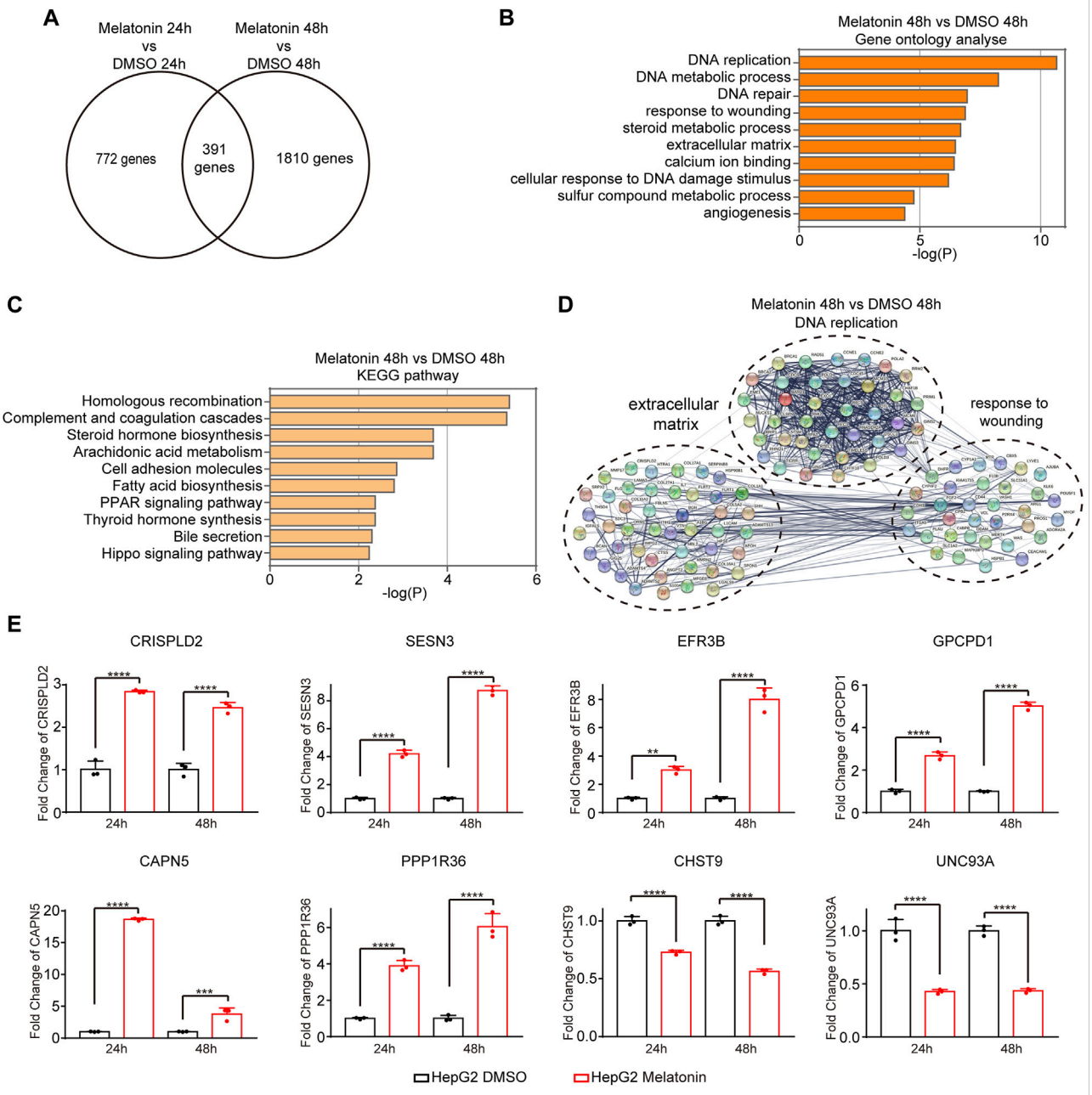

FIGURE 2
Analysis of gene expression changes induced by melatonin. **(A)** Venn diagram showed the overlapping genes differentially expressed in HepG2 cells treated with melatonin for 24 h and 48 h **(B)** Gene ontology analyses of gene expression events induced by melatonin treatment for 48 h. Fisher exact *p* values were plotted for each category. **(C)** KEGG pathway analyses of gene expression events induced by melatonin treatment for 48 h. **(D)** Functional association network of melatonin-induced gene expression changes. Genes in panel B were analyzed using the STRING database, and subgroups are marked according to their functions. **(E)** The identified gene expression changes were validated by RT-qPCR. The mean ± SD of relative fold changes was plotted (n = 3) with p values calculated by one-way ANOVA.

The Institutional Review Board of the Dalian Medical University approved use of the tumor specimens in this study. All of tissue specimens were immediately frozen in liquid nitrogen and kept at −80°C until the extraction of RNA.

Statistical analysis

Data was presented as mean ± SD. Statistical significance was determined by unpaired t test, one-way ANOVA or two-way ANOVA. Statistical analyses were performed using GraphPad

Prism 7 (NS, not significant; *$p < 0.05$, **$p < 0.01$, ***$p < 0.001$, ****$p < 0.0001$).

Results

Melatonin inhibits HCC cell proliferation

To explore the role of melatonin in HCC, HepG2 and Hep3B cells were treated with different concentrations of melatonin for 72 h and cell viability was determined by cell counting kit-8 (CCK8). The half maximal inhibitory concentration (IC50) of melatonin in HepG2 and Hep3B cells were 1.995 mM and 1.409 mM, respectively (Figures 1A,B). Importantly, melatonin inhibits cell proliferation in a dose-dependent manner in HCC HepG2 and Hep3B cells as judged by CCK8 and colony formation assay (Figures 1C–F). The treatment of 1 mM of melatonin showed a significant inhibition of cell growth, whereas higher concentrations (2 and 4 mM) demonstrated a much stronger inhibitory effect in HepG2 and Hep3B cells (Figures 1C–F). Altogether, melatonin can inhibit the growth of HCC cells in a dose-dependent manner.

Analysis of gene expression changes induced by melatonin

To further explore the molecular mechanism of melatonin-induced cell growth inhibitory, we performed high-throughput mRNA sequencing (mRNA-seq) with HepG2 cells treated with 1 mM melatonin for 24 h and 48 h separately. We identified 1163 genes and 2201 genes with significant expression change after 24 h and 48 h treatment with melatonin respectively as compared to controls ($p < 0.05$). Among which, 391 overlapping genes were differentially expressed in HepG2 cells treated with melatonin for 24 h and 48 h (Figure 2A). These genes are closely associated with DNA replication, DNA metabolic process, response to wounding, steroid metabolic process, extracellular matrix, calcium ion binding, cellular response to DNA damage stimulus, sulfur compound metabolic process and angiogenesis as judged by gene ontology analysis (Figure 2B, and Supplementary Figure S1A). In addition, those genes are enriched in homologous recombination, complement and coagulation cascades, steroid hormone biosynthesis, arachidonic acid metabolism, cell adhesion molecules, fatty acid biosynthesis, and PPAR signaling pathway as judged by KEGG analysis (Figure 2C, and Supplementary Figure S1B). Most of melatonin treatment for 48 h induced genes were functionally connected into a well linked interaction network that contains genes associated with DNA replication, response to wounding and extracellular matrix, as judged by the Search Tool for the Retrieval of Interacting Genes/Proteins (STRING) (Figure 2D). Meanwhile, many of those genes induced by melatonin treatment for 24 h were functionally correlated into a network that includes genes correlated with steroid metabolic process, response to wounding and extracellular matrix (Supplementary Figure S1C). Several target genes-induced by melatonin were randomly selected to further validate with quantitative real-time RT-PCR (RT-qPCR) in HepG2 cells treated with 1 mM melatonin for 24 h and 48 h, and the changes were consistent with the results obtained from mRNA-seq (Figure 2E). Among these genes, *CRISPLD2* and *SESN3* are involved in extracellular matrix. *EFR3B* and *GPCPD1* participate in regulating phospholipid metabolic process function. Taken together, melatonin can regulate the expression of cancer-related genes.

Analysis of alternative splicing events induced by melatonin

In order to explore the effect of melatonin on AS, we systematically analyzed mRNA-seq data to identify differentially changed AS events. We respectively identified 1670 and 2838 AS events with a significant change of percent-spliced-in (PSI) values (the change of PSI >0.15) after 24 h and 48 h treatment with melatonin compared to controls. 335 overlapping AS events were differentially expressed in HepG2 cells treated with melatonin for 24 h and 48 h (Figure 3A). Figure 3B shows the read tracks of one example. We found that melatonin can modulate various types of AS, including skipped exon (SE), alternative 5′ ss exon (A5E), alternative 3′ ss exon (A3E), retained intron (RI) and mutually exclusive exons (MXE) (Figure 3C and Supplementary Figure S2A). Subsequent analysis indicated that most of the SE events were positively regulated by melatonin (increased PSI value) while most of the RI events were negatively controlled (decreased PSI value) (Figure 3D and Supplementary Figure S2B).

We analyzed cellular functions of melatonin-induced AS events using gene ontology and found that these genes are associated with mitotic cell cycle, microtubule-based process, kinase activity, DNA metabolic process, GTPase regulator activity, cellular response to DNA damage stimulus, histone modification, spindle, DNA repair and cell division as judged by gene ontology analysis (Figure 3E and Supplementary Figure S2C). Meanwhile, the AS events are abundantly enriched in PPAR signaling pathway, nucleotide metabolism, homologous recombination, peroxisome and other pathways as judged by KEGG analysis (Figure 3F and Supplementary Figure S2D). In addition, we performed

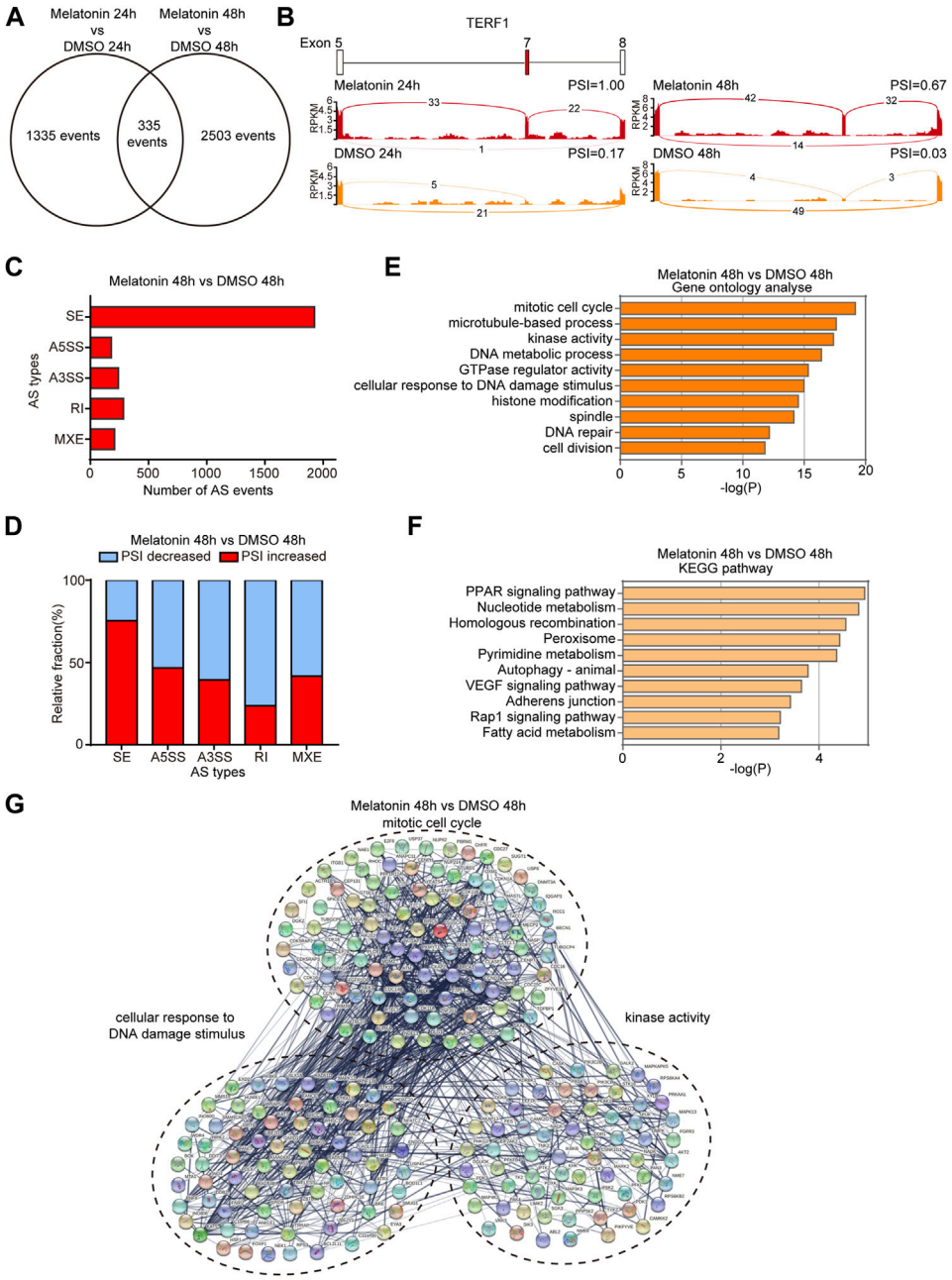

FIGURE 3
Analysis of alternative splicing events induced by melatonin. **(A)** Venn diagram showed the overlapping AS events differentially expressed in HepG2 cells treated with melatonin for 24 h and 48 h. **(B)** Example of alternative splicing affected by melatonin. Alternative splicing of *TERF1* was chosen to represent an increase of PSI, and numbers of exon junction reads were indicated. **(C)** Quantification of the different AS events affected by melatonin treatment for 48 h. **(D)** The relative fraction of each AS event positively or negatively induced by melatonin treatment for 48 h. **(E)** Gene ontology analyses of AS events regulated by melatonin treatment for 48 h. Fisher exact *p* values were plotted for each category. **(F)** Pathways were analyzed by KEGG pathway database for melatonin treatment 48 h induced AS events. **(G)** Functional association network of melatonin-induced AS events using the STRING database.

STRING analysis and found that many melatonin-regulated AS events were functionally connected into well linked interaction networks that contains genes associated with mitotic cell cycle, cellular response to DNA damage stimulus and kinase activity (Figures 3G, Supplementary Figure S2E). Taken together, these results suggest that the biological processes affected by melatonin are related to tumorigenesis and cancer progression.

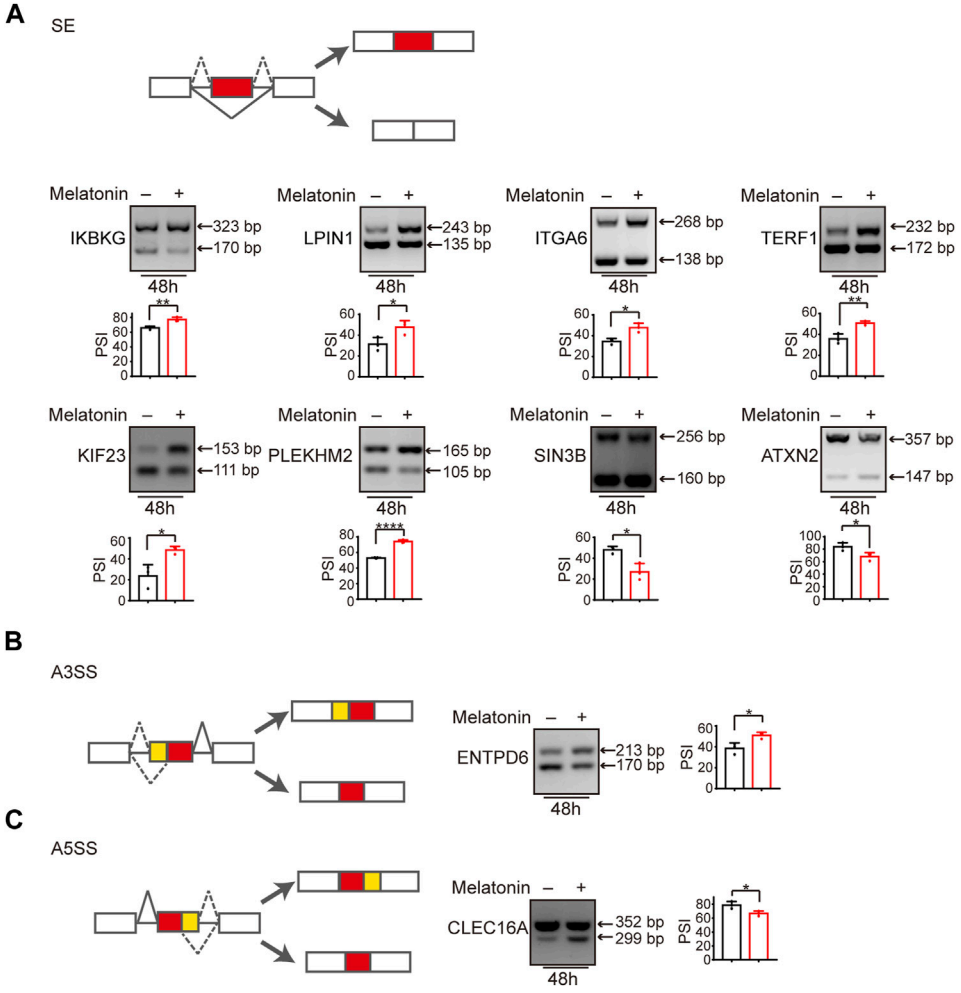

FIGURE 4
Alternative splicing switch induced by melatonin. **(A)** Exons skipping in *IKBKG*, *LPIN1*, *ITGA6*, *TERF1*, *KIF23*, *PLEKHM2*, *SIN3B*, and *ATXN2* were examined by semi-quantitative RT-PCR in HepG2 cells treated with 1 mM melatonin for 48 h. The mean ± SD of PSIs from three experiments were plotted and *p* values calculated by unpaired *t* test. **(B,C)** Alternative 3′ splice sites usage of *ENTPD6* and alternative 5′ splice sites usage of *CLEC16A* were examined by semi-quantitative RT-PCR in HepG2 cells treated with 1 mM melatonin for 48 h. The mean ± SD of PSIs from three experiments were plotted and *p* values calculated by unpaired *t* test.

Alternative splicing switches induced by melatonin

We subsequently validated mRNA-seq results by measuring the splicing change of randomly chosen targets in HepG2 and Hep3B cells treated with melatonin by the semi-quantitative RT-PCR assay. Consistent with the results from mRNA-seq analysis, melatonin promoted exon 5 splicing of *IKBKG* (inhibitor of nuclear factor kappa-B kinase subunit gamma). Similarly, melatonin also stimulated the inclusion of exon 6 of *LPIN1* (phosphatidic acid phosphatase 1), exon 25 of *ITGA6* (Integrin alpha-6), exon 7 of *TERF1* (telomeric repeat-binding factor 1), exon 8 of *KIF23* (mitotic kinesin-like protein 1) and exon 7 of *PLEKHM2* (Pleckstrin homology domain-containing family M member 2). Meanwhile, melatonin could induce the skipping of exon 10 of *SIN3B* (histone deacetylase complex subunit) and exon 10 of *ATXN2* (spinocerebellar ataxia type 2 protein) (Figure 4A and Supplementary Figures S3,S4). In addition, other types of splicing events induced by melatonin were also validated. Briefly, melatonin promoted the upstream 3′ ss usage of *ENTPD6* (ectonucleoside triphosphate diphosphohydrolase 6) and inhibited the distal 5′ ss usage of *CLEC16A* (c-type lectin domain family 16 member A) (Figures 4B,C). Among these genes, *IKBKG* encodes nuclear factor κB essential modulator (NEMO), which acts as a tumor repressor in HCC. Moreover, NEMO protects the liver against chronic inflammation, progression of nonalcoholic steatohepatitis, and hepatocarcinogenesis

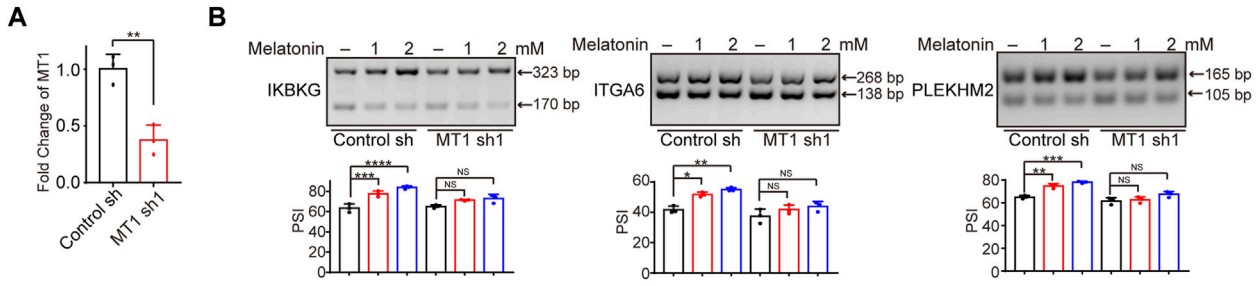

FIGURE 5
The regulatory effect of melatonin on alternative splicing is dependent on MT1. **(A)** The MT1 expression was validated by RT-qPCR. **(B)** Exons skipping of *IKBKG*, *ITGA6*, and *PLEKHM2* were examined by semi-quantitative RT-PCR in control and MT1-konckdown HepG2 cells treated with 1mM and 2 mM melatonin for 24 h. The mean ± SD of PSIs from three experiments were plotted and *p* values calculated by one-way ANOVA.

(Luedde et al., 2007; Kondylis et al., 2017). *LPIN1* could regulate nuclear remodeling, mediating the effect of mTORC1 on SREBP pathway (Peterson et al., 2011). *SIN3B* is a transcription suppressor, which interacts with MXI1 to repress MYC responsive genes, thereby antagonizing MYC oncogenic activities (Alland et al., 1997). *SIN3B* also regulates cell cycle progression by repressing the expression of cell cycle inhibitor genes (Bowman et al., 2014). Taken together, melatonin could regulate a variety of splicing events in HCC.

The regulatory effect of melatonin on alternative splicing is partially dependent on MT1

Previous study reported that melatonin exerted anti-tumor effect through interacting with melatonin receptors MT1 or MT2 (Mao et al., 2010; Liu et al., 2016; Asghari et al., 2017; Ferlazzo et al., 2020). Therefore, we investigated whether the regulation of alternative splicing by melatonin is dependent on melatonin receptors. Since MT2 is not expressed in HepG2 cells (Carbajo-Pescador et al., 2009; Carbajo-Pescador et al., 2011), we constructed HepG2 cells with MT1 stable depletion, and verified the knockdown efficiency by RT-qPCR (Figure 5A). Subsequently, we treated MT1-depleted and control HCC cells with different concentrations of melatonin for 24 h, and examined splicing switches using semi-quantitative RT-PCR. Importantly, we found that melatonin-induced splicing switches are at least partially dependent on the status of MT1. We revealed that melatonin promoted the production of the long-isoforms of *IKBKG*, *ITGA6*, and *PLEKHM2* in a dose-dependent manner, while the regulatory effect of melatonin was significantly attenuated in MT1-depleted HepG2 cells (Figure 5B). Overall, the regulatory effect of melatonin on alternative splicing in HCC cells is at least partly modulated by MT1.

IKBKG splicing switch participated in melatonin-induced HCC inhibition

We have demonstrated that melatonin promoted the inclusion of exon 5 of *IKBKG*, resulting in an increase of full length of *IKBKG* (Figure 6A). In addition to liver cancer, we examined the splicing change of *IKBKG* upon melatonin treatment in NCI-H1299 and A549 lung cancer cells, and human embryonic kidney HEK-293T cells. We found that melatonin could affect the splicing of *IKBKG* in multiple cell lines (Supplementary Figure S5A). Importantly, *IKBKG* encoding protein NEMO/IKK-γ, together with IKK-α and IKK-β to form IKK complex, thereby regulating the activity of NF-κB. Previously, NEMO was identified as a tumor suppressor in liver by conditional hepatocyte-specific deletion of NEMO in mice (Luedde et al., 2007; Seki and Brenner, 2007; Kondylis et al., 2015; Mossanen et al., 2019). Moreover, NEMO expression was down-regulated in HCC as compared to their surrounding non-neoplastic liver tissues (Aigelsreiter et al., 2012). Therefore, we further performed western blot assay and validated that melatonin could increase the protein level of long isoform of NEMO (Supplementary Figure S5B). Next, we sought to investigate the role of the long isoform (NEMO-L) and the short isoform (NEMO-S) of *IKBKG* in HCC progression. NEMO-L isoform is the full-length transcript, whereas NEMO-S isoform lacks the exon 5 that encodes the domain associating with TANK (Figure 6B). In order to explore the effects of two NEMO isoforms on cell proliferation, we stably overexpressed NEMO-L or NEMO-S in HepG2 cells respectively. The expression of NEMO-L and NEMO-S were verified at both RNA and protein levels using semi-quantitative RT-PCR and western blot assays (Figures 6C,D). We found that HepG2 cells expressing NEMO-L grew much slower as compared to control cells, as well as HepG2 cells expressing NEMO-S as judged by CCK8 and colony formation assays (Figures 6E,F). These results suggested that NEMO-L, the full-length

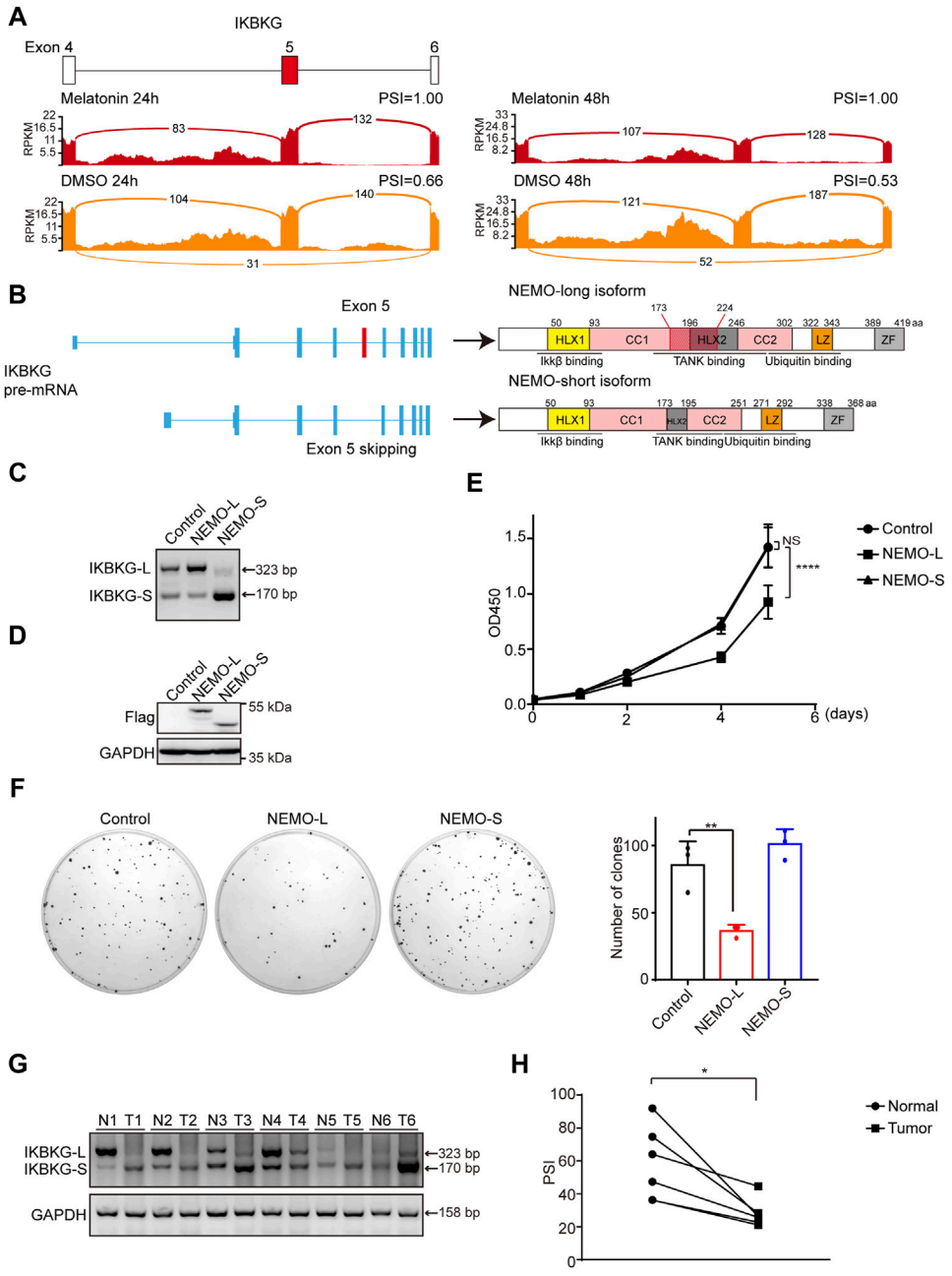

FIGURE 6
NEMO-L inhibits cell proliferation. **(A)** Alternative exon of *IKBKG* affected by melatonin. Numbers of exon junction reads and PSI were indicated. **(B)** Schematics of human *IKBKG* (NEMO) pre-mRNA and protein. NEMO-long isoform included the exon 5, while NEMO-short isoform skipped the exon 5. **(C,D)** HepG2 cells with stable expression of Flag-tagged NEMO-L or NEMO-S were constructed. RNA levels of *IKBKG* were examined by semi-quantitative RT-PCR **(C)**. Protein levels of exogenous NEMO were confirmed by western blot analysis using anti-Flag antibodies **(D)**. **(E)** Cell proliferation of HepG2 cells stably expressing NEMO-L or NEMO-S were analyzed by CCK8 assay at intervals, with *p* values calculated by two-way ANOVA. **(F)** Colony formation assays of HepG2 cells stably expressing NEMO-L or NEMO-S. Images of the whole plate are shown. The mean ± SD of relative colony numbers was plotted ($n = 3$) and *p* values calculated by one-way ANOVA. **(G,H)** Alternative splicing of *IKBKG* were measured in six paired liver cancer tissues and adjacent normal tissues by semi-quantitative RT-PCR. PSI values were plotted. * Indicated $p < 0.05$.

isoform, could inhibit HCC cell proliferation. Due to lack of exon 5, NEMO-S lost the ability to suppress HCC cell proliferation.

To further investigate the clinical significance of *IKBKG* splicing in cancer patients, we examined the relative levels of two *IKBKG* isoforms in six pairs of liver cancer samples and

adjacent normal tissues. Relative mRNA levels of *IKBKG*-L were significantly decreased in six liver cancer samples compared with paired normal tissues (Figures 6G,H), indicating that despite the apparent heterogeneity of different tumor samples, the expression of *IKBKG*-L is generally reduced. Taken together, our results indicate that melatonin suppresses HCC progression through mediating *IKBKG* splicing.

Discussion

Melatonin is a natural indole amine that is mainly produced by the pineal gland in human body. Melatonin has various functions, including the regulation of antioxidant and circadian rhythm. Numerous studies have shown that melatonin has significant anti-tumor activity in multiple cancers, including HCC, breast cancer, colorectal cancer, non-small lung cancer, and melanoma. Moreover, the tumor suppressing effect of melatonin is achieved by regulating various physiological functions, such as tumor proliferation, angiogenesis, metastasis, apoptosis, metabolism and immune escape (Talib, 2018; Talib et al., 2021). For example, melatonin and peroxisome proliferator-activated receptors (PPARγ) agonists synergistically induce apoptosis in breast cancer cells (Korkmaz et al., 2009). Melatonin inhibits proliferation of lung cancer cells by enhancing mitochondrial energy metabolism and reversed the Warburg effect (Chen et al., 2021). In addition, melatonin suppresses the migration and invasion of HCC cells by reducing the expression of VEGF and HIF1α (Colombo et al., 2016). Accumulating evidence suggests that melatonin has great potential in cancer therapy.

Alternative splicing of pre-mRNA is recognized as a key driver of proteomic diversity in human, by which a single gene can produce multiple isoforms with different or even opposite functions. For example, the long isoform of Bcl-x (Bcl-xL) plays an anti-apoptotic role, while its short isoform Bcl-xS functions as a pro-apoptotic factor (Wang et al., 2014). Alternative splicing can be deregulated in cancer, leading to the generation of aberrant splicing variants. These aberrant splicing variants can regulate tumorigenesis and cancer progression (Wang and Aifantis, 2020; Kitamura and Nimura, 2021). Accumulating evidence suggests that aberrant splicing variants confer therapeutic drug resistance in cancer (Sciarrillo et al., 2020). In our study, we demonstrated that melatonin exerts antitumor effects by regulating alternative splicing of many cancer-related genes. Specifically, melatonin could shift the splicing of *IKBKG* to increase the production of NEMO long isoform, thereby inhibiting cancer cell proliferation. This might be because that the full-length isoform of NEMO prevents RIPK1 activation and subsequent apoptosis by NF-κB-dependent or -independent functions, suppressing HCC progression (Kondylis et al., 2017). NEMO-S, the short isoform with the skipping of exon 5, impairs the TANK binding domain and cannot inhibit cancer cell proliferation. Our study provides a novel mechanism for melatonin to suppress cancer progression by regulating the alternative splicing of cancer-related genes.

In addition to the regulation of NEMO splicing, melatonin might also inhibit cancer progression through modulating the splicing of some other cancer-related genes. Using mRNA-seq analysis, we found that melatonin can regulate some splicing events related to mitotic cell cycle, kinase activity, DNA metabolic process, and GTPase regulator activity functions. For example, melatonin can regulate the splicing of *LPIN1* and *KIF23*, whose function is related to mitotic cell cycle. Taken together, melatonin may offer new opportunities for cancer therapeutics by regulating RNA alternative splicing.

Data availability statement

The datasets presented in this study can be found in online repositories. The names of the repository/repositories and accession numbers can be found below: https://www.ncbi.nlm.nih.gov/geo/, GSE210034.

Ethics statement

The studies involving human participants were reviewed and approved by The Institutional Review Board of the Dalian Medical University. The patients/participants provided their written informed consent to participate in this study.

Author contributions

YW, WZ, and YQ conceived the project and designed the experiments. LB, SS, WS, YL, JZ, and JZ designed and performed most of the experiments, whereas CC and ML performed data analysis. WZ and YQ provided funds. YW and WZ wrote the manuscript.

Funding

This work was supported by the National Natural Science Foundation of China (81872247 to WZ, 8210113819 to YQ); Dalian High Level Talents Renovation Supporting Program (2019RQ097 to WZ).

Conflict of interest

The authors declare that the research was conducted in the absence of any commercial or financial relationships that could be construed as a potential conflict of interest.

Publisher's note

All claims expressed in this article are solely those of the authors and do not necessarily represent those of their affiliated organizations, or those of the publisher, the editors and the reviewers. Any product that may be evaluated in this article, or claim that may be made by its manufacturer, is not guaranteed or endorsed by the publisher.

Supplementary material

The Supplementary Material for this article can be found online at: https://www.frontiersin.org/articles/10.3389/fphar.2022.1007006/full#supplementary-material

References

Aigelsreiter, A., Haybaeck, J., Schauer, S., Kiesslich, T., Bettermann, K., Griessbacher, A., et al. (2012). NEMO expression in human hepatocellular carcinoma and its association with clinical outcome. *Hum. Pathol.* 43, 1012–1019. doi:10.1016/j.humpath.2011.08.009

Alland, L., Muhle, R., Hou, H., Jr., Potes, J., Chin, L., Schreiber-Agus, N., et al. (1997). Role for N-CoR and histone deacetylase in Sin3-mediated transcriptional repression. *Nature* 387, 49–55. doi:10.1038/387049a0

Asghari, M. H., Moloudizargari, M., Bahadar, H., and Abdollahi, M. (2017). A review of the protective effect of melatonin in pesticide-induced toxicity. *Expert Opin. Drug Metab. Toxicol.* 13, 545–554. doi:10.1080/17425255.2016.1214712

Bonnal, S. C., Lopez-Oreja, I., and Valcarcel, J. (2020). Roles and mechanisms of alternative splicing in cancer - implications for care. *Nat. Rev. Clin. Oncol.* 17, 457–474. doi:10.1038/s41571-020-0350-x

Bowman, C. J., Ayer, D. E., and Dynlacht, B. D. (2014). Foxk proteins repress the initiation of starvation-induced atrophy and autophagy programs. *Nat. Cell Biol.* 16, 1202–1214. doi:10.1038/ncb3062

Carbajo-Pescador, S., Garcia-Palomo, A., Martin-Renedo, J., Piva, M., Gonzalez-Gallego, J., and Mauriz, J. L. (2011). Melatonin modulation of intracellular signaling pathways in hepatocarcinoma HepG2 cell line: Role of the MT1 receptor. *J. Pineal Res.* 51, 463–471. doi:10.1111/j.1600-079X.2011.00910.x

Carbajo-Pescador, S., Martin-Renedo, J., Garcia-Palomo, A., Tunon, M. J., Mauriz, J. L., and Gonzalez-Gallego, J. (2009). Changes in the expression of melatonin receptors induced by melatonin treatment in hepatocarcinoma HepG2 cells. *J. Pineal Res.* 47, 330–338. doi:10.1111/j.1600-079X.2009.00719.x

Chen, H., Gao, F., He, M., Ding, X. F., Wong, A. M., Sze, S. C., et al. (2019). Long-read RNA sequencing identifies alternative splice variants in hepatocellular carcinoma and tumor-specific isoforms. *Hepatology* 70, 1011–1025. doi:10.1002/hep.30500

Chen, X., Hao, B., Li, D., Reiter, R. J., Bai, Y., Abay, B., et al. (2021). Melatonin inhibits lung cancer development by reversing the Warburg effect via stimulating the SIRT3/PDH axis. *J. Pineal Res.* 71, e12755. doi:10.1111/jpi.12755

Colombo, J., Maciel, J. M., Ferreira, L. C., Rf, D. A. S., and Zuccari, D. A. (2016). Effects of melatonin on HIF-1α and VEGF expression and on the invasive properties of hepatocarcinoma cells. *Oncol. Lett.* 12, 231–237. doi:10.3892/ol.2016.4605

Ferlazzo, N., Andolina, G., Cannata, A., Costanzo, M. G., Rizzo, V., Curro, M., et al. (2020). Is melatonin the cornucopia of the 21st century? *Antioxidants (Basel)* 9, E1088. doi:10.3390/antiox9111088

Fernandez-Palanca, P., Mendez-Blanco, C., Fondevila, F., Tunon, M. J., Reiter, R. J., Mauriz, J. L., et al. (2021). Melatonin as an antitumor agent against liver cancer: An updated systematic review. *Antioxidants (Basel)* 10, 103. doi:10.3390/antiox10010103

Hu, Z., Dong, L., Li, S., Li, Z., Qiao, Y., Li, Y., et al. (2020). Splicing regulator p54(nrb)/Non-POU domain-containing octamer-binding protein enhances carcinogenesis through oncogenic isoform switch of MYC box-dependent interacting protein 1 in hepatocellular carcinoma. *Hepatology* 72, 548–568. doi:10.1002/hep.31062

Huang, A., Yang, X. R., Chung, W. Y., Dennison, A. R., and Zhou, J. (2020). Targeted therapy for hepatocellular carcinoma. *Signal Transduct. Target. Ther.* 5, 146. doi:10.1038/s41392-020-00264-x

Kitamura, K., and Nimura, K. (2021). Regulation of RNA splicing: Aberrant splicing regulation and therapeutic targets in cancer. *Cells*, 2021 923. doi:10.3390/cells10040923

Kondylis, V., Kumari, S., Vlantis, K., and Pasparakis, M. (2017). The interplay of IKK, NF-κB and RIPK1 signaling in the regulation of cell death, tissue homeostasis and inflammation. *Immunol. Rev.* 277, 113–127. doi:10.1111/imr.12550

Kondylis, V., Polykratis, A., Ehlken, H., Ochoa-Callejero, L., Straub, B. K., Krishna-Subramanian, S., et al. (2015). NEMO prevents steatohepatitis and hepatocellular carcinoma by inhibiting RIPK1 kinase activity-mediated hepatocyte apoptosis. *Cancer Cell* 28, 582–598. doi:10.1016/j.ccell.2015.10.001

Korkmaz, A., Tamura, H., Manchester, L. C., Ogden, G. B., Tan, D. X., and Reiter, R. J. (2009). Combination of melatonin and a peroxisome proliferator-activated receptor-gamma agonist induces apoptosis in a breast cancer cell line. *J. Pineal Res.* 46, 115–116. doi:10.1111/j.1600-079X.2008.00635.x

Liu, J., Clough, S. J., Hutchinson, A. J., Adamah-Biassi, E. B., Popovska-Gorevski, M., and Dubocovich, M. L. (2016). MT1 and MT2 melatonin receptors: A therapeutic perspective. *Annu. Rev. Pharmacol. Toxicol.* 56, 361–383. doi:10.1146/annurev-pharmtox-010814-124742

Liu, X., and Qin, S. (2019). Immune checkpoint inhibitors in hepatocellular carcinoma: Opportunities and challenges. *Oncologist* 24, S3–S10. doi:10.1634/theoncologist.2019-IO-S1-s01

Llovet, J. M., Zucman-Rossi, J., Pikarsky, E., Sangro, B., Schwartz, M., Sherman, M., et al. (2016). Hepatocellular carcinoma. *Nat. Rev. Dis. Prim.* 2, 16018. doi:10.1038/nrdp.2016.18

Luedde, T., Beraza, N., Kotsikoris, V., van Loo, G., Nenci, A., De Vos, R., et al. (2007). Deletion of NEMO/IKKgamma in liver parenchymal cells causes steatohepatitis and hepatocellular carcinoma. *Cancer Cell* 11, 119–132. doi:10.1016/j.ccr.2006.12.016

Mao, L., Cheng, Q., Guardiola-Lemaitre, B., Schuster-Klein, C., Dong, C., Lai, L., et al. (2010). *In vitro* and *in vivo* antitumor activity of melatonin receptor agonists. *J. Pineal Res.* 49, 210–221. doi:10.1111/j.1600-079X.2010.00781.x

Mayo, J. C., Sainz, R. M., Gonzalez Menendez, P., Cepas, V., Tan, D. X., and Reiter, R. J. (2017). Melatonin and sirtuins: A "not-so unexpected" relationship. *J. Pineal Res.* 62, e12391. doi:10.1111/jpi.12391

Montella, L., Palmieri, G., Addeo, R., and Del Prete, S. (2016). Hepatocellular carcinoma: Will novel targeted drugs really impact the next future? *World J. Gastroenterol.* 22, 6114–6126. doi:10.3748/wjg.v22.i27.6114

Mossanen, J. C., Kohlhepp, M., Wehr, A., Krenkel, O., Liepelt, A., Roeth, A. A., et al. (2019). CXCR6 inhibits hepatocarcinogenesis by promoting natural killer T- and CD4(+) T-cell-dependent control of senescence. *Gastroenterology* 156, 1877–1889. doi:10.1053/j.gastro.2019.01.247

Peterson, T. R., Sengupta, S. S., Harris, T. E., Carmack, A. E., Kang, S. A., Balderas, E., et al. (2011). mTOR complex 1 regulates lipin 1 localization to control the SREBP pathway. *Cell* 146, 408–420. doi:10.1016/j.cell.2011.06.034

Sciarrillo, R., Wojtuszkiewicz, A., Assaraf, Y. G., Jansen, G., Kaspers, G. J. L., Giovannetti, E., et al. (2020). The role of alternative splicing in cancer: From oncogenesis to drug resistance. *Drug resist. updat.* 53, 100728. doi:10.1016/j.drup.2020.100728

Seki, E., and Brenner, D. A. (2007). The role of NF-kappaB in hepatocarcinogenesis: Promoter or suppressor? *J. Hepatol.* 47, 307–309. doi:10.1016/j.jhep.2007.05.006

Sung, H., Ferlay, J., Siegel, R. L., Laversanne, M., Soerjomataram, I., Jemal, A., et al. (2021). Global cancer statistics 2020: GLOBOCAN estimates of incidence and mortality worldwide for 36 cancers in 185 countries. *Ca. A Cancer J. Clin.* 71, 209–249. doi:10.3322/caac.21660

Talib, W. H., Alsayed, A. R., Abuawad, A., Daoud, S., and Mahmod, A. I. (2021). Melatonin in cancer treatment: Current knowledge and future opportunities. *Molecules* 26, 2506. doi:10.3390/molecules26092506

Talib, W. H. (2018). Melatonin and cancer hallmarks. *Molecules* 2018, E518. doi:10.3390/molecules23030518

Tang, W., Chen, Z., Zhang, W., Cheng, Y., Zhang, B., Wu, F., et al. (2020). The mechanisms of sorafenib resistance in hepatocellular carcinoma: Theoretical basis and therapeutic aspects. *Signal Transduct. Target. Ther.* 5, 87. doi:10.1038/s41392-020-0187-x

Wang, E., and Aifantis, I. (2020). RNA splicing and cancer. *Trends Cancer* 6, 631–644. doi:10.1016/j.trecan.2020.04.011

Wang, Y., Chen, D., Qian, H., Tsai, Y. S., Shao, S., Liu, Q., et al. (2014). The splicing factor RBM4 controls apoptosis, proliferation, and migration to suppress tumor progression. *Cancer Cell* 26, 374–389. doi:10.1016/j.ccr.2014.07.010

Yang, J. D., Hainaut, P., Gores, G. J., Amadou, A., Plymoth, A., and Roberts, L. R. (2019). A global view of hepatocellular carcinoma: Trends, risk, prevention and management. *Nat. Rev. Gastroenterol. Hepatol.* 16, 589–604. doi:10.1038/s41575-019-0186-y

Yuan, J. H., Liu, X. N., Wang, T. T., Pan, W., Tao, Q. F., Zhou, W. P., et al. (2017). The MBNL3 splicing factor promotes hepatocellular carcinoma by increasing PXN expression through the alternative splicing of lncRNA-PXN-AS1. *Nat. Cell Biol.* 19, 820–832. doi:10.1038/ncb3538

Zhao, D., Yu, Y., Shen, Y., Liu, Q., Zhao, Z., Sharma, R., et al. (2019). Melatonin Synthesis and function: Evolutionary history in animals and plants. *Front. Endocrinol.* 10, 249. doi:10.3389/fendo.2019.00249

frontiers | Frontiers in Pharmacology

TYPE Original Research
PUBLISHED 01 November 2022
DOI 10.3389/fphar.2022.1039416

OPEN ACCESS

EDITED BY
Hai-long Piao,
Dalian Institute of Chemical Physics, Chinese Academy of Sciences (CAS), China

REVIEWED BY
Fergal Kelleher,
Trinity College Dublin, Ireland
Sankar Jagadeeshan,
Ben-Gurion University of the Negev, Israel

*CORRESPONDENCE
Pei Hu,
hubei01_pumch@163.com

†PRESENT ADDRESS
Pei Hu,
Linking Truth Techenology, Beijing, China

SPECIALTY SECTION
This article was submitted to Pharmacology of Anti-Cancer Drugs, a section of the journal Frontiers in Pharmacology

RECEIVED 08 September 2022
ACCEPTED 19 October 2022
PUBLISHED 01 November 2022

CITATION
Zhao Q, Wang T, Wang H, Cui C, Zhong W, Fu D, Xi W, Si L, Guo J, Cheng Y, Tian H and Hu P (2022), Phase I pharmacokinetic study of an oral, small-molecule MEK inhibitor tunlametinib in patients with advanced NRAS mutant melanoma.
Front. Pharmacol. 13:1039416.
doi: 10.3389/fphar.2022.1039416

Phase I pharmacokinetic study of an oral, small-molecule MEK inhibitor tunlametinib in patients with advanced NRAS mutant melanoma

Qian Zhao[1], Teng Wang[1], Huanhuan Wang[1], Cheng Cui[1], Wen Zhong[1], Diyi Fu[1], Wanlin Xi[1], Lu Si[2], Jun Guo[2], Ying Cheng[3], Hongqi Tian[3] and Pei Hu[1*†]

[1]Clinical Pharmacology Research Center, Peking Union Medical College Hospital, Chinese Academy of Medical Sciences & Peking Union Medical College, State Key Laboratory of Complex Severe and Rare Diseases, NMPA Key Laboratory for Clinical Research and Evaluation of Drug, Beijing Key Laboratory of Clinical PK and PD Investigation for Innovative Drugs, Beijing, China, [2]Key Laboratory of Carcinogenesis and Translational Research (Ministry of Education), Department of Renal Cancer and Melanoma, Peking University Cancer Hospital and Research Institute, Beijing, China, [3]Shanghai KeChow Pharma, Inc., Shanghai, China

Background: Malignant melanoma is an aggressive disease. Tunlametinib (HL-085) is a potent, selective, and orally bioavailable MEK1/2 inhibitor. The objective of this study was to determine the pharmacokinetics (PK) of tunlametinib and its main metabolite M8 in patients with *NRAS*-mutant melanoma following a single dose and multiple doses in a phase I safety and PK study.

Methods: A multiple-center phase I study was performed in patients with melanoma including dose-escalation phase and dose-expansion phase. PK following a single oral dose and multiple doses of 0.5–18 mg twice daily was assessed.

Results: A total of 30 participants were included in the dose escalation phase and then 11 patients were included in the dose-expansion phase (12 mg twice daily). Tunlametinib plasma concentration rapidly increased after dosing, with a T_{max} of 0.5–1 h. Mean elimination half-life ($t_{1/2}$) was dose-independent and had a range from 21.84 to 34.41 h. Mean apparent clearance (CL/F) and distribution volume (V/F) were 28.44–51.93 L/h and 1199.36–2009.26 L, respectively. The average accumulation ratios of AUC and C_{max} after the multiple administration of tunlametinib were 1.64–2.73 and 0.82–2.49, respectively. Tunlametinib was rapidly transformed into the main metabolite M8 and M8 reached the peak concentration about 1 h after administration. Mean $t_{1/2}$ of M8 was 6.1–33.54 h. The body exposure of M8 in plasma was 36%–67% of that of tunlametinib. There were general dose-proportional increases in maximum concentration (C_{max}) and area under the curve (AUC) of tunlametinib and M8 both in the single dose phase and in the multiple doses phase.

Conclusion: Tunlametinib was absorbed rapidly and eliminated at a medium speed after drug withdrawal. Pharmacokinetic body exposure increased in general dose-proportional manner from 0.5 mg up to 18 mg. Slight accumulation was found after multiple oral doses. The pharmacokinetics of tunlametinib and its metabolite suggest that twice daily dosing is appropriate for tunlametinib.

KEYWORDS

melanoma, NRAS mutation, mek inhibitor, pharmacokinetics, tunlametinib

Background

Melanoma is a malignance of melanocytes and an aggressive disease, which was recognized as the most dangerous type of skin cancer (Schadendorf et al., 2018). The five world regions with the greatest melanoma incidence and mortality rates were Australia, North America, Eastern Europe, and Western Europe and Central Europe (Karimkhani et al., 2017). The incidence of melanoma is keeping a worldwide increase. Incidence in Europe is about 25 cases per 100,000 population, while in Australia it reaches a rate of 60 new cases per 100,000 (Podlipnik et al., 2020; Conforti and Zalaudek, 2021). Total melanoma incidence was higher in male than female in US individuals (limited to white race), Canada, Australia, and New Zealand. Meanwhile, and male had higher rates of melanoma of the head and neck and trunk than female (Olsen et al., 2020). The age-standardized incidence rate of melanoma has increased from 0.4 per 100,000 in 1990 to 0.9 per 100,000 in 2017 in China (Wu et al., 2020). The median survival was about 1 year for advanced metastatic melanoma (Tsao et al., 2004). For 40 years, few effective systemic treatments to melanoma are available. The standard-of-care treatments included dacarbazine chemotherapy and immunotherapy with the cytokine IL-2/PD-1/PD-L1/CTLA-4. In the past 10 years, new targeted therapy has changed the treatment option for patients with metastatic melanoma (Luke et al., 2017; Schadendorf et al., 2018; Davis et al., 2019; Jenkins and Fisher, 2021).

Activating mutations in the MAPK signaling cascade was an important pathway that has the highest oncogenic and therapeutic relevance for melanoma (Carlino et al., 2015). Common mutations in the MAPK pathway include *BRAF*, *NRAS*, *HRAS*, *KRAS* and *NF1* (Schadendorf et al., 2015; Randic et al., 2021). BRAF signaling is dependent on downstream activation of MEK1/2 (Solit et al., 2006). Thus, several MEK inhibitors have been developed for melanoma treatment alone or in combination (Del Vecchio et al., 2015; Robert et al., 2015; Ascierto et al., 2016; Dummer et al., 2017). MEK inhibitors trametinib, cobimetinib and binimetinib have been approved for BRAF V600 melanoma by the Food and Drug Administration (Kakadia et al., 2018). However, no MEK inhibitor was approved for melanoma patients with *NRAS* mutation worldwide.

Tunlametinib (also known as HL-085) is a selective inhibitor of MEK1 and MEK2 with a half-maximum inhibitory concentration (IC_{50}) of 1.9–10 nmol/L (Cheng and Tian, 2017). Tunlametinib inhibited proliferation of RAS/RAF-mutated cell lines at nanomoles concentrations (unpublished investigator brochure, Shanghai KeChow Pharma.). Pharmacokinetic profiling results indicated a mean effective half life ($t_{1/2}$) of 3.55–4.62 and 3.99–9.37 h in rats and beagle dogs after single oral dosing of tunlametinib. CYP2C9 was the main metabolic enzyme of tunlametinib. The main metabolite M8 is inactive. >60% of ^{14}C-tunlametinib were excreted from feces in rats (unpublished investigator brochure, Shanghai KeChow Pharma.). Tunlametinib may be a potential treatment option for *NRAS*-mutant melanoma.

Tunlametinib was recently assessed in first-in-human trial: a single ascending-dose and a multiple ascending-dose phase I study in patients with advanced NRAS-mutated melanoma patients, which evaluated the safety, tolerability, and pharmacokinetics of tunlametinib in melanoma patients. Presented here are the pharmacokinetic data from this phase I study.

Methods

Study design and patients

This study was an open, single-arm, dose-escalation/dose-expansion phase I trial including two parts: a dose-escalation phase (Part 1) and an expansion phase (Part 2). The Part 1 dose-escalation phase adopted a standard 3 + 3 design to evaluate the pharmacokinetic characters of tunlametinib, and to identify the dose-limiting toxicity (DLT), maximum-tolerated dose (MTD), recommended Phase II dose (RP2D). According to a 3 + 3 design, at least three patients were treated at each dose level. In the Part 2 dose-expansion phase, patients were administered at the RP2D to further evaluate the tolerability, safety, and efficacy of tunlametinib. The design of this study was presented in the Supplementary Figure S1.

TABLE 1 Demographics characteristics of participants treated with tunlametinib.

Characteristics	0.5 mg (n = 3)	1 mg (n = 3)	2 mg (n = 3)	3 mg (n = 3)	4 mg (n = 3)	6 mg (n = 3)	9 mg (n = 3)	12 mg (n = 14)*	15 mg (n = 3)	18 mg (n = 3)	Total (n = 41)
Age (years)	55.0 (36–63)	54.0 (43–62)	46.0 (43–52)	50.0 (39–55)	62.0 (45–69)	58.0 (44–68)	58.0 (56–59)	56.5 (41–67)	57.0 (34–58)	59.0 (56–63)	56.0 (34–69)
Sex-no. (%)											
Female	2 (66.7%)	1 (33.3%)	1 (33.3%)	1 (33.3%)	2 (66.7%)	1 (33.3%)	1 (33.3%)	7 (500%)	3 (100%)	1 (33.3%)	20 (48.8%)
Male	1 (33.3%)	2 (66.7%)	2 (66.7%)	2 (66.7%)	1 (33.3%)	2 (66.7%)	2 (66.7%)	7 (50.0%)	0	2 (66.7%)	21 (51.2%)
Height (cm)	160.00 (154.0–172.0)	166.00 (148.0–167.0)	165.00 (160.0–172.0)	173.00 (154.0–180.0)	161.00 (150.0–170.0)	167.00 (159.0–175.0)	165.00 (158.0–171.0)	164.00 (158.0–175.0)	160.00 (153.0–163.0)	158.00 (157.0–159.0)	163.00 (148.0–180.0)
Weight (kg)	56.00 (48.0–72.0)	69.00 (62.0–85.0)	72.00 (62.0–84.0)	67.00 (55.0–75.0)	61.00 (60.0–78.0)	68.00 (67.4–87.0)	56.00 (49.0–88.0)	65.75 (46.0–98.0)	64.00 (54.0–75.0)	66.30 (59.0–71.5)	67.00 (46.0–98.0)
BMI (kg/m^2)	21.88 (20.24–24.34)	28.31 (25.04–30.48)	24.34 (22.77–32.81)	23.15 (22.39–23.19)	26.67 (23.53–26.99)	26.90 (24.17–28.41)	20.57 (19.63–30.09)	23.56 (18.43–36.00)	25.00 (20.32–32.04)	26.90 (23.34–28.64)	24.17 (18.43–36.00)

Data was presented as median and range (min, max) unless otherwise specific indicated.
BMI: body mass index.
*12 mg cohort include 3 patients in dose-escalation phase and 11 patients in dose-expansion phase.

Data for pharmacokinetics are reported here while other data will be reported separately. The study protocol was approved by local Ethics Review Committee and registered at clinicaltrials.gov (NCT03973151). All patients provided written informed consent. Studies were conducted in accordance with Declaration of Helsinki, Good Clinical Practice and applicable laws and regulations.

Eligible patients were aged 18–70 years with histologically or cytologically confirmed unresectable stage III or IV melanoma harboring *NRAS* mutations. Tumor biopsy was adequate for genetic testing of NRAS mutations. Patients were also required an Eastern Cooperative Oncology Group (ECOG) performance score of one or less; with measurable lesions per Response Evaluation Criteria in Solid Tumors (RECIST) version 1.1; life expectancy of >3 months and adequate hematologic, renal, and hepatic function.

Patients were excluded if they had active central nervous system disease except for patients with stable brain disease for ≥3 months following stereotactic brain radiotherapy or surgery; inability to swallow or any small intestinal resection that would preclude adequate absorption of the study drug; uncontrolled concomitant or infectious diseases; history of retinal disease; prior treatment with a specific MEK inhibitor; or known allergy to the study drug or its analogs. Strong inducers or inhibitors of CYP isozyme had to be discontinued ≥1 week before study treatment.

Procedures

This dose-escalation study experienced 10 dose-levels, including 0.5, 1, 2, 3, 4, 6, 9, 12, 15, and 18 mg, and all the patients were administered tunlametinib capsule twice daily except in the PK lead-in period. In dose-escalation phase, a 7-day pharmacokinetic lead-in period was designed for each patient before entering treatment cycles. During the PK lead-in period, all the patients were administered only one dose. In dose-expansion phase, patients were given the recommended phase II dose (12 mg BID) without lead-in period.

To assess the pharmacokinetic profile of tunlametinib and its main metabolite M8 (inactive metabolite), serial venous blood samples were collected after overnight fasting on day -7 (single dose, lead-in period) and day 28 (multiple doses).

In the lead-in period, blood samples were drawn pre-dose (0 h) and at 1, 2, 3, 4, 8, 12, 24, 48, 72, 96, 120, and 144 h after tunlametinib administration in the dose cohorts of 0.5 and 1 mg; This was optimized to pre-dose and at 0.25, 0.5, 1, 2, 4, 8, 12, 24, 48, 72, 96, 120, and 144 h after dosing for the following dose cohorts. On day 28, total seven time points of blood were collected pre-dose and 1, 2, 3, 4, 8, and 12 h post dose in the 0.5 mg cohort; and this was changed into total 8 time points including pre-dose and 0.25, 0.5, 1, 2, 3, 4, 8, and 12 h post dose in the other doses cohorts.

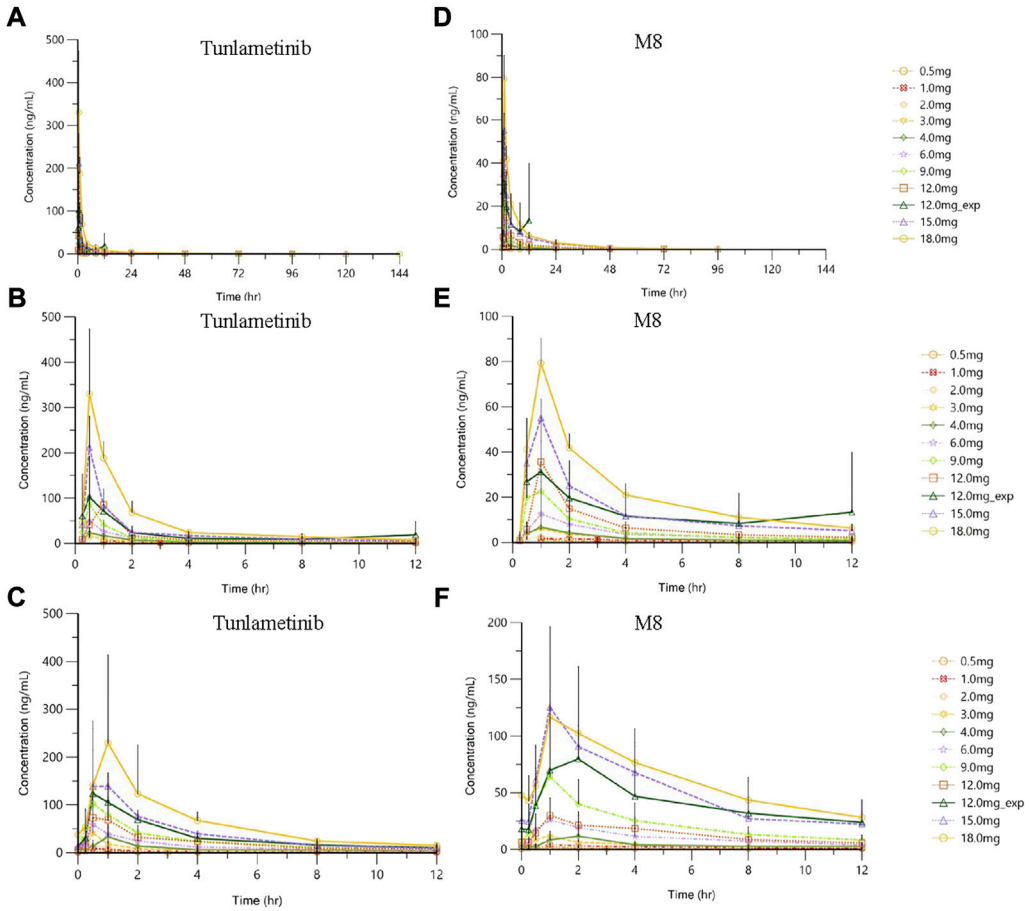

FIGURE 1
| Plasma concentration (mean ± SD)-time profiles of tunlametinib and M8 after orally administrated with 0.5–18 mg (*n* = 41) tunlametinib capsules. **(A)** single dose (0–144 h, tunlametinib); **(B)** single dose (0–12 h, tunlametinib); **(C)** multiple dose (tunlametinib); **(D)** single dose (0–144 h, M8); **(E)** single dose (0–12 h, M8); **(F)** multiple dose (M8).

In the dose-expansion phase, total 8 time points of blood were taken at pre-dose and at 0.25, 0.5, 1, 2, 4, 8, and 12 h post dose on both day 1 and day 28 of cycle 1.

Sparse sampling was also collected on days 8, 15, and 22 of cycle one at pre-dose in both dose-escalation and dose-expansion phases.

Sample processing and bioanalysis methods

Blood samples were collected into vacutainer tubes with EDTA-K_2 anticoagulation. Immediately after collection, the blood-containing tubes were centrifuged at 1500 g at 4°C for 10 min. All the plasma samples were stored in a freezer at −80°C until subsequent bioanalytical analysis.

Plasma samples were assayed for tunlametinib and M8 concentrations at Peking Union Medical College Hospital using a validated ultra-performance liquid chromatography-tandem mass spectrometry method. Samples were prepared by using a solid phase extraction method. The quantification range for tunlametinib and M8 in plasma were 0.1–100 ng ml^{-1} [0.3, 8, and 80 ng ml^{-1} for quality controls (QCs)]. Stable isotope labeled tunlametinib (D_4-tunlametinib) and M8 (D_3-M8) were used as an internal standard, respectively. The lower limit of quantitation of tunlametinib and M8 in plasma were 0.1 ng·mL^{-1}. The accuracy of the QC samples used during sample analysis ranged from -1.5% to 4.9% [relative standard deviation (RSD)% ≤ 13.2%] for tunlametinib and from -2.1% to 3.3% (RSD% ≤ 16.1%) for M8. All samples were analyzed within established storage stability periods.

Study outcomes

The parameters assessed during the study were maximum observed plasma concentration (C_{max}), time to C_{max} (T_{max}), area

TABLE 2 Summary of pharmacokinetic parameters of tunlametinib and M8.

			Dose-escalation phase										Expansion phase
	Parameter	Unit	0.5 mg (*n* = 3)	1.0 mg (*n* = 3)	2.0 mg (*n* = 3)	3.0 mg (*n* = 3)	4.0 mg (*n* = 3)	6.0 mg (*n* = 3)	9.0 mg (*n* = 3)	12.0 mg (*n* = 3)	15.0 mg (*n* = 3)	18.0 mg (*n* = 3)	12.0 mg (*n* = 11)
HL-085													
Single dose	AUC_{0-12h}	h*ng/mL	5.69 ± 0.93	17.25 ± 7.03	23.34 ± 6.85	37.20 ± 10.83	53.91 ± 12.05	84.61 ± 40.93	114.33 ± 43.22	147.6 ± 17.70	273.89 ± 21.81	488.89 ± 50.59	228.96 ± 77.81
	AUC_{inf}	h*ng/mL	/	42.76 ± 33.97	43.62 ± 9.57	73.49 ± 30.65	89.5 ± 25.29	144.48 ± 57.73	183.72 ± 33.90	232.69 ± 23.17	398.85 ± 34.57	635.74 ± 53.55	/
	$AUC_{\_\%Extrap}$	%	25.74 ± 4.06	17.05 ± 4.93	10.94 ± 3.66	6.86 ± 3.25	6.03 ± 1.61	6.18 ± 2.41	3.10 ± 0.97	2.61 ± 0.96	1.33 ± 0.36	0.83 ± 0.27	26.83 ± 27.56
	C_{max}	ng/mL	2.24 ± 0.99	6.98 ± 4.03	15.70 ± 2.39	19.60 ± 6.28	27.60 ± 4.75	54.07 ± 31.98	95.27 ± 85.79	85.63 ± 24.15	211.67 ± 68.82	349.33 ± 111.13	142.83 ± 88.63
	C_{last}	ng/mL	0.15 ± 0.06	0.15 ± 0.06	0.14 ± 0.03	0.12 ± 0.01	0.18 ± 0.07	0.19 ± 0.02	0.17 ± 0.03	0.16 ± 0.03	0.18 ± 0.05	0.14 ± 0.03	17.87 ± 27.52
	T_{max}[a]	H	0.98 (0.98.1.00)	0.92 (0.92.1.00)	0.50 (0.50.1.00)	0.50 (0.48.0.98)	0.50 (0.50.1.00)	0.50 (0.48.2.00)	0.52 (0.50.1.00)	1.00 (0.98.1.00)	0.50 (0.50.0.50)	0.52 (0.50.0.97)	0.53 (0.23.11.65)
	MRT	H	6.48 ± 2.88	19.26 ± 10.86	14.42 ± 1.69	18.02 ± 5.64	13.66 ± 3.73	15.41 ± 2.92	14.25 ± 4.57	14.99 ± 5.03	12.85 ± 4.51	10.54 ± 2.44	/
	$T_{1/2}$	H	/	34.41 ± 16.18	24.14 ± 3.15	28.2 ± 10.61	21.84 ± 5.66	30.79 ± 4.82	23.04 ± 5.52	26.18 ± 5.56	24.28 ± 10.33	29.13 ± 3.57	/
	CL/F	L/h	/	34.17 ± 27.15	47.32 ± 10.13	45.46 ± 17.04	47.43 ± 14.71	45.90 ± 16.74	50.10 ± 9.10	51.93 ± 5.47	37.81 ± 3.45	28.44 ± 2.28	/
	V_z/F	L	/	1379.52 ± 550.08	1617.46 ± 141.04	1772.99 ± 788.61	1422.54 ± 200.07	2009.26 ± 651.60	1708.45 ± 655.99	1942.20 ± 311.42	1292.35 ± 470.57	1199.36 ± 214.11	/
Multiple dose	AUC_{τ}	h*ng/mL	12.67 ± 3.02	31.56 ± 14.23	45.76 ± 12.31	76.42 ± 25.03	96.09 ± 47.77	163.95 ± 57.14	294.37 ± 114.84	266.55 ± 35.62	446.70 ± 73.76	906.33 ± 74.43	391.16 ± 97.85
	C_{avg}	ng/mL	1.06 ± 0.25	2.63 ± 1.19	3.81 ± 1.03	6.37 ± 2.09	8.01 ± 3.98	13.66 ± 4.76	24.53 ± 9.57	22.21 ± 2.97	37.23 ± 6.15	75.53 ± 6.20	32.60 ± 8.15
	C_{max}	ng/mL	2.52 ± 0.80	11.11 ± 9.57	14.50 ± 0.85	40.97 ± 25.44	33.23 ± 19.42	58.90 ± 37.74	109.40 ± 73.5	77.90 ± 46.49	186.33 ± 95.00	238.37 ± 168.72	140.57 ± 71.53
	C_{min}	ng/mL	0.74 ± 0.24	1.51 ± 0.66	2.44 ± 0.06	2.87 ± 0.60	3.29 ± 3.11	4.40 ± 0.60	6.22 ± 1.25	5.95 ± 2.01	12.05 ± 2.95	14.23 ± 4.23	10.12 ± 4.93
	Fluctuation%	%	166.40 ± 21.09	332.28 ± 204.62	331.62 ± 113.12	583.46 ± 268.56	391.32 ± 114.01	391.19 ± 174.17	384.33 ± 140.35	448.51 ± 181.90	450.60 ± 172.16	418.85 ± 33.95	435.72 ± 216.88
	T_{max}[a]	h	0.98 (0.97.0.98)	0.97 (0.52.1.02)	0.73 (0.50.0.97)	0.50 (0.48.0.50)	0.98 (0.95.1.00)	0.52 (0.50.1.00)	1.00 (0.50.1.02)	0.50 (0.50.2.08)	0.98 (0.53.1.00)	1.00 (0.98.4.02)	1.00 (0.48.2.03)
	R_1	-	1.44 ± 1.09	1.47 ± 0.61	0.93 ± 0.25	2.49 ± 2.27	1.28 ± 0.93	1.23 ± 0.54	1.73 ± 1.63	0.99 ± 0.63	0.97 ± 0.67	0.82 ± 0.78	0.94 ± 0.29
	R_2	-	2.32 ± 0.83	1.81 ± 0.18	2.42 ± 1.02	2.05 ± 0.36	1.83 ± 0.96	2.02 ± 0.46	2.73 ± 1.22	1.84 ± 0.55	1.64 ± 0.36	1.75 ± 0.09	1.59 ± 0.19
	R_3	-	/	0.69 ± 0.20	1.22 ± 0.49	1.08 ± 0.30	1.14 ± 0.66	1.15 ± 0.14	1.61 ± 0.61	1.08 ± 0.13	1.12 ± 0.10	1.39 ± 0.03	/

(Continued on following page)

10.3389/fphar.2022.1039416

TABLE 2 (*Continued*) Summary of pharmacokinetic parameters of tunlametinib and M8.

			Dose-escalation phase										Expansion phase
	Parameter	Unit	0.5 mg (*n* = 3)	1.0 mg (*n* = 3)	2.0 mg (*n* = 3)	3.0 mg (*n* = 3)	4.0 mg (*n* = 3)	6.0 mg (*n* = 3)	9.0 mg (*n* = 3)	12.0 mg (*n* = 3)	15.0 mg (*n* = 3)	18.0 mg (*n* = 3)	12.0 mg (*n* = 11)
M8													
Single dose	AUC_{0-12h}	h*ng/mL	4.23 ± 1.22	9.76 ± 6.21	7.50 ± 2.22	22.28 ± 11.53	22.82 ± 20.69	43.64 ± 31.68	60.91 ± 46.38	83.93 ± 30.01	161.99 ± 27.4	245.33 ± 16.17	120.43 ± 90.82
	AUC_{inf}	h*ng/mL	/	29.93 ± 27.99	9.76 ± 2.12	39.23 ± 25.87	33.00 ± 32.06	69.06 ± 46.60	89.19 ± 46.82	124.91 ± 28.5	261.27 ± 36.23	366.9 ± 48.25	/
	$AUC_{\_\%Extrap}$	%	26.39 ± 5.74	16.28 ± 6.21	17.65 ± 6.63	7.71 ± 5.84	8.70 ± 4.08	7.48 ± 7.13	5.49 ± 3.12	3.19 ± 2.24	1.40 ± 0.29	2.31 ± 1.02	19.55 ± 11.66
	C_{max}	ng/mL	1.19 ± 0.33	2.03 ± 0.36	2.73 ± 0.81	6.84 ± 1.86	6.70 ± 5.06	15.24 ± 11.68	23.54 ± 23.87	35.63 ± 20.53	55.10 ± 8.31	79.37 ± 10.74	42.22 ± 25.87
	C_{last}	ng/mL	0.13 ± 0.03	0.15 ± 0.08	0.20 ± 0.05	0.13 ± 0.03	0.17 ± 0.08	0.17 ± 0.03	0.21 ± 0.07	0.15 ± 0.08	0.20 ± 0.06	0.18 ± 0.02	12.36 ± 25.29
	T_{max}[a]	h	1.00 (0.98.1.93)	0.92 (0.92.2.92)	0.97 (0.50.1.00)	0.98 (0.48.1.03)	0.97 (0.95.1.00)	1.00 (0.95.2.00)	0.98 (0.50.1.00)	1.00 (0.98.1.00)	1.00 (1.00.1.03)	1.00 (0.97.1.00)	1.00 (0.50.11.65)
	MRT	h	6.81 ± 2.45	13.85 ± 10.67	6.12 ± 2.01	12.14 ± 6.72	7.31 ± 2.49	10.55 ± 5.01	10.66 ± 3.52	12.04 ± 3.47	13.94 ± 2.32	12.70 ± 2.72	/
	$T_{1/2}$	h	/	21.32 ± 13.74	6.10 ± 2.66	14.36 ± 5.22	9.89 ± 2.36	13.10 ± 3.87	12.79 ± 1.69	17.31 ± 2.74	15.75 ± 2.37	33.54 ± 11.84	/
	$MPratio_{\_AUC0-12h}$	-	0.88 ± 00.36	0.67 ± 0.30	0.36 ± 0.01	0.65 ± 0.16	0.49 ± 0.43	0.55 ± 0.23	0.55 ± 0.22	0.65 ± 0.23	0.67 ± 0.06	0.57 ± 0.05	0.58 ± 0.31
	$MPratio_{\_AUCinf}$	-	/	0.73 ± 0.16	0.25 ± 0.02	0.57 ± 0.15	0.42 ± 0.38	0.50 ± 0.23	0.53 ± 0.18	0.62 ± 0.21	0.75 ± 0.08	0.66 ± 0.07	/
	$MPratio_{\_Cmax}$	-	0.76 ± 0.53	0.42 ± 0.25	0.20 ± 0.07	0.40 ± 0.02	0.28 ± 0.22	0.39 ± 0.26	0.26 ± 0.04	0.46 ± 0.18	0.31 ± 0.07	0.27 ± 0.06	0.44 ± 0.38
Multiple dose	AUC_{τ}	h*ng/mL	8.90 ± 4.17	22.01 ± 10.25	16.45 ± 6.06	46.35 ± 18.22	58.79 ± NaN	123.87 ± 77.48	265.25 ± 154.14	132.32 ± 3.18	576.15 ± 96.75	864.79 ± 228.01	592.28 ± 499.53
	C_{avg}	ng/mL	0.74 ± 0.35	1.83 ± 0.85	1.37 ± 0.51	3.86 ± 1.52	4.9 ± NaN	10.32 ± 6.46	22.1 ± 12.85	11.03 ± 0.27	48.01 ± 8.06	72.07 ± 19.00	49.36 ± 41.63
	C_{max}	ng/mL	2.02 ± 0.72	4.04 ± 0.88	4.24 ± 0.78	11.89 ± 4.12	11.66 ± 7.46	26.8 ± 18.87	64.63 ± 48.38	33.93 ± 11.94	125.33 ± 14.36	128.57 ± 64.55	96.31 ± 78.85
	C_{min}	ng/mL	0.42 ± 0.23	0.98 ± 0.50	0.78 ± 0.25	1.37 ± 0.58	1.17 ± 1.12	3.49 ± 2.21	6.55 ± 2.78	6.28 ± 2.74	23.03 ± 3.04	28.07 ± 4.80	15.95 ± 17.3
	Fluctuation%	%	234.38 ± 62.35	187.42 ± 67.37	263.39 ± 58.61	282.46 ± 53.13	152.68 ± NaN	244.76 ± 95.39	237.43 ± 76.46	279.10 ± 165.31	219.23 ± 63.51	185.78 ± 9.34	244.48 ± 77.38
	T_{max}[a]	h	0.98 (0.97,0.98)	1.00 (0.97,1.02)	0.98 (0.97,1.00)	1.00 (0.98,1.03)	1.90 (1.90,2.00)	1.07 (1.00,2.00)	1.03 (1.02,1.95)	1.00 (1.00,2.08)	0.98 (0.98,1.00)	1.92 (1.00,4.02)	1.02 (0.95,3.95)
	R_1	-	1.68 ± 0.19	2.01 ± 0.38	1.88 ± 0.43	1.94 ± 1.14	1.84 ± 0.20	1.81 ± 0.11	3.25 ± 1.78	1.14 ± 0.61	2.32 ± 0.50	1.65 ± 0.83	2.04 ± 0.75
	R_2	-	2.04 ± 0.67	2.44 ± 0.84	2.76 ± 1.55	2.77 ± 2.02	5.16 ± NaN	2.96 ± 0.41	4.74 ± 2.09	2.01 ± 0.51	3.57 ± 0.39	3.51 ± 1.19	2.67 ± 0.13
	R_3	-	/	0.93 ± 0.39	2.51 ± NaN	1.80 ± 1.46	3.76 ± NaN	1.86 ± 0.16	2.89 ± 0.99	1.22 ± 0.06	2.22 ± 0.37	2.52 ± 1.09	-
	$MPratio_{\_AUC\tau}$	-	0.76 ± 0.23	0.83 ± 0.24	0.40 ± 0.04	0.80 ± 0.53	0.20 ± 0.35	0.79 ± 0.30	1.00 ± 0.53	0.57 ± 0.06	1.51 ± 0.46	1.10 ± 0.38	1.26 ± 1.08
	$MPratio_{\_Cmax}$	-	0.91 ± 0.10	0.61 ± 0.35	0.33 ± 0.08	0.38 ± 0.18	0.61 ± 0.64	0.52 ± 0.17	0.73 ± 0.55	0.67 ± 0.52	0.88 ± 0.33	0.84 ± 0.48	0.88 ± 0.85

a:T_{max} reported as median (range).

Blood samples were not collected after 12 h in the expansion cohort or $AUC_{\_\%Extrap}$>20%, so the parameters which related to elimination phase could not be calculated.

Abbreviations: $AUC_{0-12\ h}$ = Area under the concentration-time curve from 0 to 12 h after dosing, AUC_{inf}, Area under the plasma concentration-time curve from the time of dosing extrapolated to infinity, AUC_{τ}, Area under the concentration-time curve during a dosing interval at steady-state. $AUC_{\_\%Extrap}$ = Extrapolated area percentage calculated by $AUC_{t\text{-}inf}/AUC_{inf}$. C_{avg} = Average concentration, C_{max} = Maximum concentration. C_{last} = The last concentration which can be measured. C_{min} = Minimum concentration, CL/F = Apparent clearance, Fluctuation% = Percentage of concentration fluctuation, MPratio = Ratio of metabolite M8 to tunlametinib, R_1 = Accumulation ratio calculated by C_{max} (day28)/C_{max} (PK, lead-in period or day 1), R_2 = Accumulation ratio calculatedby AUC_{τ} (day28)/$AUC_{0-12\ h}$ (PK, lead-in period or day 1), R_3 = Accumulation ratio calculatedby AUC_{τ} (day28)/AUC_{inf} (PK, lead-in period or day 1), $T_{1/2}$ = Terminal half-life, T_{max} = Time taken to reach maximum concentration, V_z/F = apparent distribution volume.

10.3389/fphar.2022.1039416

TABLE 3 Linear evaluation of plasma pharmacokinetic parameters after single and multiple oral administration of 0.5–18 mg tunlametinib capsule in patients.

Occasion	Analyte	PK parameters	Point estimate of beta	90% CI of beta	Beta criteria
Single dose	Tunlametinib	$AUC_{0\text{-}12h}$	1.116	(1.023,1.210)	(0.938,1.062)
		AUC_{inf}	1.003	(0.870,1.136)	(0.938,1.062)
		C_{max}	1.282	(1.150,1.414)	(0.938,1.062)
	M8	$AUC_{0\text{-}12h}$	1.086	(0.923,1.249)	(0.938,1.062)
		AUC_{inf}	1.148	(0.873,1.424)	(0.938,1.062)
		C_{max}	1.167	(1.019,1.315)	(0.938,1.062)
Multiple dose	Tunlametinib	AUC_{τ}	1.077	(0.968,1.187)	(0.938,1.062)
		C_{max}	1.113	(0.936,1.289)	(0.938,1.062)
	M8	AUC_{τ}	1.203	(1.023,1.383)	(0.938,1.062)
		C_{max}	1.150	(0.990,1.310)	(0.938,1.062)

under the plasma concentration-time curve from the time of dosing extrapolated to infinity (AUC_{inf}), area under the concentration-time curve during a dosing interval at steady-state (AUC_{τ}), terminal elimination half-life ($t_{1/2}$), apparent clearance (CL/F), apparent volume of distribution during the terminal elimination phase (V_z/F), accumulation ratio calculated from $AUC_{\tau\ (day28)}$ and $AUC_{0-12\ h\ (PK\ lead\text{-}in\ period\ or\ day\ 1)}$.

Statistical analysis

The pharmacokinetic analysis set (PKAS) were used for the analysis of all pharmacokinetic data. The PKAS included all participants who took at least one dose of tunlametinib and had at least one collecting sample point parameter.

Plasma concentration-time data were analyzed and the PK parameters were calculated *via* non-compartmental analysis method using WinNonlin (version 8.3, Pharsight Corporation, United States). C_{max} and T_{max} were determined directly from experimental observations. AUC_{τ} was calculated using the linear trapezoidal method (linear up and log down). The first order rate constant (λ_z) of decline in tunlametinib and M8 plasma concentrations in the terminal phase of the plasma concentration-time curve was estimated using linear regression. The $t_{1/2}$ was estimated from $\ln 2/\lambda_z$. AUC_{inf} was calculated using the following equation: $AUC_{0\text{-}t} + AUC_{Ex}$, where $AUC_{0\text{-}t}$ was the area under the concentration-time curve from time zero (pre-dose) to the time of the last quantifiable concentration, and AUC_{Ex} was the observed concentration at last sampling time divided by λ_z. CL/F was calculated as the dose divided by AUC_{inf}, and V_z/F was estimated by dividing the apparent CL by λ_z. The accumulation ratio for tunlametinib and M8 at steady state was determined by dividing the AUC_{τ} (or C_{max}) on day 28 by the $AUC_{0-12\ h}$ (or C_{max}) on PK lead-in period. PK parameters of tunlametinib and M8 were summarized using descriptive statistics, including mean, coefficient of variation, median, minimum, maximum, and geometric mean, where applicable.

Dose-exposure relationship after single- and multiple-dose administration of tunlametinib capsule was evaluated. Dose proportionality using AUC_{inf} and C_{max} over the administered dose range was determined by using a power model: log (parameter) = $\alpha + \beta$ log(dose) where α was the intercept and β was the slope. $\beta = 1 + Ln\theta/Lnr$, where r was the ratio of high dose divided by low dose (for 0.5–18 mg dose range, r = 36), θ was the acceptance limit (lower limit θ_L = 0.80, upper limit θ_H = 1.25). $\theta_L < r^{\beta-1} < \theta_H$, dose proportionality was assessed based on whether the 90% CI constructed for the estimate of $r^{\beta-1}$ was within the acceptance interval (0.80–1.25), that is to say, whether the 90% CI of β was within the acceptance interval (0.938.1.062).

Results

Demographics

A total of 30 participants were included in the dose escalation phase and then 11 patients were included in the dose-expansion phase (12 mg twice daily). The demographic characteristics of 41 patients are summarized in Table 1. The range of age was from 34 to 69 years and males and females accounted for 51.2% and 48.8%, respectively. Overall median body mass index (BMI) was in the 18.43–36.00 kg/m^2 range.

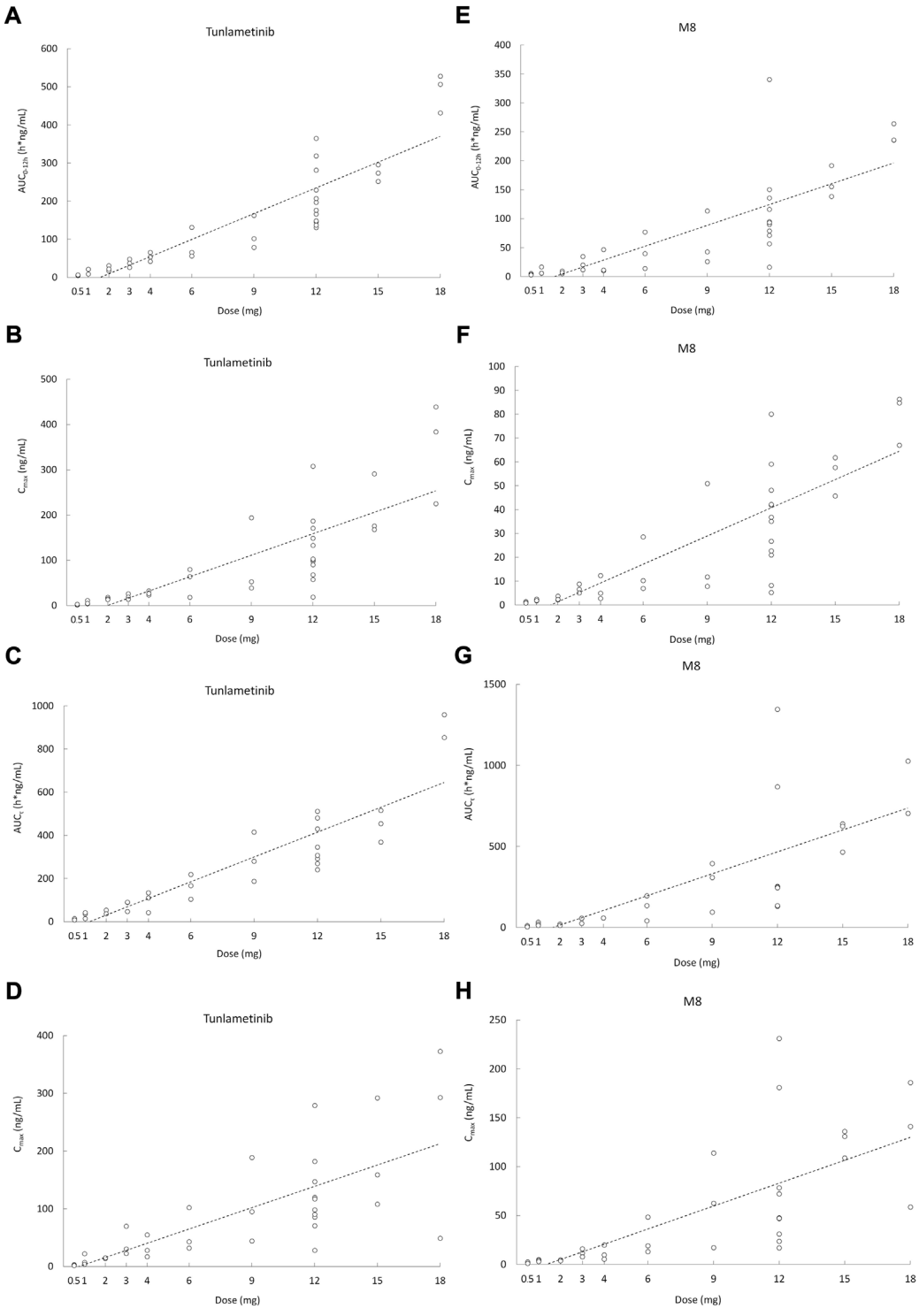

FIGURE 2
Scatter plot of AUC and C_{max} versus dose after orally administrated with 0.5–18 mg (n = 41) tunlametinib capsules. **(A)** single dose ($AUC_{0-12\ h}$, tunlametinib); **(B)** single dose (C_{max}, tunlametinib); **(C)** multiple dose (AUC_{τ}, tunlametinib); **(D)** multiple dose (C_{max}, tunlametinib); **(E)** single dose ($AUC_{0-12\ h}$, M8); **(F)** single dose (C_{max}, M8); **(G)** multiple dose (AUC_{τ}, M8); **(H)** multiple dose (C_{max}, M8).

Single-dose pharmacokinetics

Tunlametinib and M8 plasma concentration increased and reached to the peak concentration fast after tunlametinib administration, and then declined slowly. The concentration-time curve of tunlametinib and M8 was shown in Figure 1. Pharmacokinetics parameters of tunlametinib and M8 were shown in the Table 2.

Tunlametinib was rapidly absorbed, typically attaining T_{max} within 0.50–1 h after dosing. After C_{max} was reached, concentrations of tunlametinib declined in a biphasic manner, with a $t_{1/2}$ of 21.84–34.41 h regardless of dose level investigated. The coefficient of variation of $t_{1/2}$ of tunlametinib was low (13.03%–47.03%). The median CL/F was within the range of 28.44–51.93 L/h. The V_z/F was high across all dose levels (median V_z/F was within the range of 1199.36–2009.26 L). AUC_{0-t} was higher than 80% of AUC_{inf} for each dose level except to 0.5 mg dose group. Both the average C_{max} and AUC_{inf} of tunlametinib increased with increasing dose level in an approximately dose-proportional manner in the tunlametinib 0.5–18 mg dose range with a minimum of 2.24 ng/ml and 7.03 h*ng/ml (0.5 mg) and a maximum of 349.33 ng/ml and 635.74 h*ng/ml (18 mg) for C_{max} and AUC (Table 2). In the power model analysis, the β point estimates (90% CIs) of AUC_{inf} and C_{max} after single dose of tunlametinib were 1.003 (0.870–1.136) and 1.282 (1.150–1.414), respectively (Table 3). Dose proportionality for the systemic exposure parameters of tunlametinib could not be concluded because the 90% CIs for β estimates were not completely fell within the pre-specified interval of 0.938–1.062.

Similarly, the main metabolite M8 was produced rapidly. Median T_{max} range of M8 was 0.97–1 h for the 0.5–18 mg twice daily tunlametinib doses. The average $t_{1/2}$ range of M8 was 6.10–33.54 h and no dose dependency was observed for terminal half-life was detected throughout the study. The body exposure of metabolite M8 (based on AUC_{inf}) was 25%–75% of that of tunlametinib (Table 2). Both C_{max} and AUC_{inf} of M8 appeared to generally increase in a dose-proportional manner in the tunlametinib 0.5–15 mg dose range (Figure 1). In the power model analysis, the β point estimates (90% CIs) of AUC_{inf} and C_{max} after single dose of tunlametinib were 1.148 (0.873–1.424) and 1.167 (1.019–1.315), respectively (Table 3; Figure 2). Dose proportionality for the systemic exposure parameters of M8 could not be concluded because the 90% CIs for β estimates were not completely fell within the pre-specified interval of 0.938–1.062.

Multiple doses pharmacokinetics

Data from the dose-escalation phase and dose-expansion phase were pooled for multiple doses analysis according to twice daily dose level. The pharmacokinetic profiles of tunlametinib and M8 after the single dose and multiple doses of tunlametinib were similar. The concentration-time curve of tunlametinib and M8 was shown in Figure 1.

Median T_{max} range of tunlametinib was 0.50–1 h for the 0.5–18 mg twice daily tunlametinib doses. The mean accumulation ratio range of tunlametinib was 1.83–2.73, indicating minimal accumulation. Coefficient of variation of AUC_{τ} of tunlametinib was low (8.21%–47.52%) in the 0.5–18 mg range. The coefficient for variation for the C_{max} range of tunlametinib was 5.85%–70.08% (Table 2). Both C_{max} and AUC_{tau} of tunlametinib appeared to generally increase in dose-proportional manner in the tunlametinib 0.5–18 mg dose range (Table 3; Figure 1). In the power model analysis, the β point estimates (90% CIs) of AUC_{τ} and C_{max} after multiple doses of tunlametinib were 1.077 (0.968–1.187) and 1.113 (0.936–1.289), respectively (Table 3). Dose proportionality for the systemic exposure parameters of tunlametinib could not be concluded because the 90% CIs for β estimates were not completely contained within the pre-specified interval of 0.938–1.062. Dose proportionality was not proved, which might be related to the limited number of subjects.

Median T_{max} range of M8 was 0.98–1.92 h for the 0.5–18 mg twice daily tunlametinib doses. The mean accumulation ratio range of M8 was 2.04–5.16 (Table 2). Both C_{max} and AUC_{tau} of M8 appeared to increase in dose-proportional manner in the tunlametinib 0.5–18 mg dose range (Table 1; Figure 1). But in the power model analysis, dose proportionality for the systemic exposure parameters of M8 could not be concluded because the 90% CIs for β estimates were not completely contained within the pre-specified interval of 0.938–1.062 (Table 3; Figure 2).

Discussion

Tunlametinib capsule was absorbed rapidly after administration, and the peak time of tunlametinib plasma in most subjects was within 1 h after administration. During the collection of PK blood samples in the 0.5 mg dose group, blood samples within 1 h after administration were not collected, so that the first sampling time (1 h after administration) of all subjects in this dose group was the peak time of tunlametinib and M8. Therefore, starting from the 1 mg dose group, the blood collection time points of 0.25 and 0.5 h after administration were added in each dose group. At the same time, in order to reduce the total amount of blood collection, the blood collection 3 h after administration was removed.

According to the allometric scaling model based on preclinical data, the predicted effective half-life ($t_{1/2}$) of human is approximately 10 h. In addition, to secure the safety of patients such as dose related skin toxicity

observed in pre-clinical studies, twice daily administration was selected to reduce the peak concentration of tunlametinib and minimize the potential adverse reactions during the first-in-human trial. Based on the current clinical research results, it is also proved that twice daily administration can achieve good safety and the tunlametinib exposure accumulation ration from Day 28 to Day 1 is low (1.83–2.73), supporting the BID administration. No dose-limiting toxicity (DLT) was reported during dose escalation and maximum tolerated dose (MTD) was not reached with tunlametinib doses up to 18 mg twice daily. Dose-proportional appears to increase in tunlametinib exposure. At the recommended phase II dose, the exposure profile of the tunlametinib showed low interpatient variability.

The single-dose of tunlametinib pharmacokinetics recorded rapid absorption of tunlametinib (for all doses 0.5–18 mg; median T_{max} range 0.5–1 h), which was shorter than other MEK inhibitors such as trametinib (1.0–2.08 h) (Infante et al., 2012), binimetinib (1.00–3.00 h) (Bendell et al., 2017), selumetinib (1.0–3 h) (Adjei et al., 2008) and cobimetinib (2.4–3 h) (Rosen et al., 2016). Tunlametinib could be rapidly transformed into M8 after dosing. The T_{max} of M8 was a bit longer than that of tunlametinib (≤1 h vs. 0.98–1.92 h) after multiple doses while T_{max} was similar for M8 and tunlametinib after single administration.

The decline in concentrations of tunlametinib in a biphasic manner regardless of the dose level investigated. The reason for this phenomenon may be that the absorbed tunlametinib is distributed to the tissues at a faster speed and then cleared from the body at a slower speed. The pharmacokinetic data from the multiple doses (tunlametinib in the dose range of 0.5–18 mg) were consistent with the data from the single-dose of tunlametinib. There were general dose-proportional increases in C_{max} and AUC of tunlametinib and its main metabolite M8 in the single-dose and multiple doses of tunlametinib. Rats and dogs also demonstrated proportional increase in C_{max} and AUC with increasing tunlametinib doses (unpublished data). The degree of accumulation in AUC_{τ} for tunlametinib was not obvious with one- to two-fold after multiple doses which were lower than M8 (approximately 2–5 folds). There was low interpatient variability for C_{max} and AUC of tunlametinib for most of dose cohorts including 12 mg cohort at which dose recommend phase II dose was determined (detail data will be reported elsewhere). No food effect study was performed in this study but was performed in an independent study. The pharmacokinetics profile supports twice-daily dosing of tunlametinib. In our study, the dose escalation range of tunlametinib was 0.5–18 mg, while the range was 0.125–4 mg (Infante et al., 2012) for trametinib, 10–100 mg for cobimetinib (U.S. Food and Drug Administration Center For Drug Evaluation And Research, 2015), 30–80 mg for binimetinib (Bendell et al., 2017). Consistent with the approved MEK inhibitors, tunlametinib exhibited linear PK around the therapy dose. The pharmacokinetics monitoring in each dose in the dose escalation phase contributes to the RP2D selection and the general linear PK results provide an important instruction to dose selection in clinical use. Along with the KRAS inhibitor sotorasib (Skoulidis et al., 2021), the proof-of-concept of tunlametininb as a therapeutic approach towards NRAS mutant melanoma may broaden the once challenging area of RAS mutant cancer.

In the current study, a few limitations should be noted. Firstly, blood collecting points were not designed after 12 h in the expansion cohort, therefore, we could not calculate the parameters which related to elimination phase after multiple doses of tunlametinib, such as CL/F and V_z/F. Secondly, limited number of participants may contribute the large interpatient variability of some parameters.

Conclusions

This phase I study showed that tunlametinib is rapidly absorbed and eliminated at a medium speed after drug withdrawal. The pharmacokinetics of tunlametinib and its metabolite suggest that twice daily dosing is appropriate for tunlametinib. The results of these phase I studies support the feasibility of further investigation of the efficacy and safety of tunlametinib in melanoma. A phase II study to assess the safety and efficacy of tunlametinib (NCT05217303) was ongoing.

Data availability statement

The original contributions presented in the study are included in the article/Supplementary Material, further inquiries can be directed to the corresponding author.

Ethics statement

This study was approved by the Ethics Committee of Peking Union Medical College Hospital (Approval number: KS2017069). The patients provided their written informed consent to participate in this study.

Author contributions

PH and QZ wrote manuscript, designed experiments, performed data analysis and interpreted results. TW performed data analysis and sample testing. HW, CC, DF, and WX performed sample testing. WZ performed statistical analysis. LS and JG are responsible for subject dosing and clinical trial operations. YC and HT designed the trial.

Funding

This study received funding from National High Level Hospital Clinical Research Funding (No. 2022-PUMCH-A-144), Jinqiao Project of Beijing Association of Science and Technology (No. ZZ19005), and the Drug Development and Application of Chinese Pharmacological Society (No. 2019DL001).

Acknowledgments

The authors would like to thank staff in the study team and all study volunteers.

Conflicts of interest

YC and HT where employed by Shanghai KeChow Pharma, Inc.

The remaining authors declare that the research was conducted in the absence of any commercial or financial relationships that could be construed as a potential conflict of interest.

Publisher's note

All claims expressed in this article are solely those of the authors and do not necessarily represent those of their affiliated organizations, or those of the publisher, the editors and the reviewers. Any product that may be evaluated in this article, or claim that may be made by its manufacturer, is not guaranteed or endorsed by the publisher.

Supplementary material

The Supplementary Material for this article can be found online at: https://www.frontiersin.org/articles/10.3389/fphar.2022.1039416/full#supplementary-material

References

Adjei, A. A., Cohen, R. B., Franklin, W., Morris, C., Wilson, D., Molina, J. R., et al. (2008). Phase I pharmacokinetic and pharmacodynamic study of the oral, small-molecule mitogen-activated protein kinase kinase 1/2 inhibitor AZD6244 (ARRY-142886) in patients with advanced cancers. *J. Clin. Oncol.* 26 (13), 2139–2146. doi:10.1200/jco.2007.14.4956

Ascierto, P. A., McArthur, G. A., Dreno, B., Atkinson, V., Liszkay, G., Di Giacomo, A. M., et al. (2016). Cobimetinib combined with vemurafenib in advanced brafv600-mutant melanoma (coBRIM): Updated efficacy results from a randomised, double-blind, phase 3 trial. *Lancet. Oncol.* 17 (9), 1248–1260. doi:10.1016/s1470-2045(16)30122-x

Bendell, J. C., Javle, M., Bekaii-Saab, T. S., Finn, R. S., Wainberg, Z. A., Laheru, D. A., et al. (2017). A phase 1 dose-escalation and expansion study of binimetinib (MEK162), a potent and selective oral MEK1/2 inhibitor. *Br. J. Cancer* 116 (5), 575–583. doi:10.1038/bjc.2017.10

Carlino, M. S., Long, G. V., Kefford, R. F., and Rizos, H. (2015). Targeting oncogenic BRAF and aberrant MAPK activation in the treatment of cutaneous melanoma. *Crit. Rev. Oncol. Hematol.* 96 (3), 385–398. doi:10.1016/j.critrevonc.2015.08.021

Cheng, Y., and Tian, H. (2017). Current development status of MEK inhibitors. *Molecules* 22 (10), E1551. doi:10.3390/molecules22101551

Conforti, C., and Zalaudek, I. (2021). Epidemiology and risk factors of melanoma: A Review. *Dermatol. Pract. Concept.* 11, e2021161S. doi:10.5826/dpc.11S1a161S

Davis, L. E., Shalin, S. C., and Tackett, A. J. (2019). Current state of melanoma diagnosis and treatment. *Cancer Biol. Ther.* 20 (11), 1366–1379. doi:10.1080/15384047.2019.1640032

Del Vecchio, M., Ascierto, P. A., Mandala, M., Sileni, V. C., Maio, M., Di Guardo, L., et al. (2015). Vemurafenib in BRAFV600 mutated metastatic melanoma: A subanalysis of the Italian population of a global safety study. *Future Oncol.* 11 (9), 1355–1362. doi:10.2217/fon.15.55

Dummer, R., Schadendorf, D., Ascierto, P. A., Arance, A., Dutriaux, C., Di Giacomo, A. M., et al. (2017). Binimetinib versus dacarbazine in patients with advanced NRAS-mutant melanoma (NEMO): A multicentre, open-label, randomised, phase 3 trial. *Lancet. Oncol.* 18 (4), 435–445. doi:10.1016/s1470-2045(17)30180-8

Infante, J. R., Fecher, L. A., Falchook, G. S., Nallapareddy, S., Gordon, M. S., Becerra, C., et al. (2012). Safety, pharmacokinetic, pharmacodynamic, and efficacy data for the oral MEK inhibitor trametinib: A phase 1 dose-escalation trial. *Lancet. Oncol.* 13 (8), 773–781. doi:10.1016/s1470-2045(12)70270-x

Jenkins, R. W., and Fisher, D. E. (2021). Treatment of advanced melanoma in 2020 and beyond. *J. Invest. Dermatol.* 141 (1), 23–31. doi:10.1016/j.jid.2020.03.943

Kakadia, S., Yarlagadda, N., Awad, R., Kundranda, M., Niu, J., Naraev, B., et al. (2018). Mechanisms of resistance to BRAF and MEK inhibitors and clinical update of US Food and Drug Administration-approved targeted therapy in advanced melanoma. *Onco. Targets. Ther.* 11, 7095–7107. doi:10.2147/ott.S182721

Karimkhani, C., Green, A. C., NijsTen, T., Weinstock, M. A., Dellavalle, R. P., NaghaviM., et al. (2017). The global burden of melanoma: Results from the global burden of disease study 2015. *Br. J. Dermatol.* 177 (1), 134–140. doi:10.1111/bjd.15510

Luke, J. J., Flaherty, K. T., Ribas, A., and Long, G. V. (2017). Targeted agents and immunotherapies: Optimizing outcomes in melanoma. *Nat. Rev. Clin. Oncol.* 14 (8), 463–482. doi:10.1038/nrclinonc.2017.43

Olsen, C. M., Thompson, J. F., Pandeya, N., and Whiteman, D. C. (2020). Evaluation of sex-specific incidence of melanoma. *JAMA Dermatol.* 156 (5), 553–560. doi:10.1001/jamadermatol.2020.0470

Podlipnik, S., Carrera, C., Boada, A., Richarz, N., Marcoval, J., Ferreres, J. R., et al. (2020). Incidence of melanoma in catalonia, Spain, is rapidly increasing in the elderly population. A multicentric cohort study. *J. Clin. Med.* 9 (11), E3396. doi:10.3390/jcm9113396

Randic, T., Kozar, I., Margue, C., Utikal, J., and Kreis, S. (2021). NRAS mutant melanoma: Towards better therapies. *Cancer Treat. Rev.* 99, 102238. doi:10.1016/j.ctrv.2021.102238

Robert, C., Karaszewska, B., Schachter, J., Rutkowski, P., Mackiewicz, A., Stroiakovski, D., et al. (2015). Improved overall survival in melanoma with combined dabrafenib and trametinib. *N. Engl. J. Med.* 372 (1), 30–39. doi:10.1056/NEJMoa1412690

Rosen, L. S., LoRusso, P., Ma, W. W., Goldman, J. W., Weise, A., Colevas, A. D., et al. (2016). A first-in-human phase I study to evaluate the MEK1/2 inhibitor, cobimetinib, administered daily in patients with advanced solid tumors. *Invest. New Drugs* 34 (5), 604–613. doi:10.1007/s10637-016-0374-3

Schadendorf, D., Fisher, D. E., Garbe, C., Gershenwald, J. E., Grob, J. J., Halpern, A., et al. (2015). Melanoma. *Nat. Rev. Dis. Prim.* 1, 15003. doi:10.1038/nrdp.2015.3

Schadendorf, D., van Akkooi, A. C. J., Berking, C., Griewank, K. G., Gutzmer, R., Hauschild, A., et al. (2018). Melanoma. *Lancet* 392 (10151), 971–984. doi:10.1016/s0140-6736(18)31559-9

Skoulidis, F., Li, B. T., Dy, G. K., Price, T. J., Falchook, G. S., Wolf, J., et al. (2021). Sotorasib for lung cancers with KRAS p.G12C mutation. *N. Engl. J. Med.* 384 (25), 2371–2381. doi:10.1056/NEJMoa2103695

Solit, D. B., Garraway, L. A., Pratilas, C. A., Sawai, A., Getz, G., Basso, A., et al. (2006). BRAF mutation predicts sensitivity to MEK inhibition. *Nature* 439 (7074), 358–362. doi:10.1038/nature04304

Tsao, H., Atkins, M. B., and Sober, A. J. (2004). Management of cutaneous melanoma. *N. Engl. J. Med.* 351 (10), 998–1012. doi:10.1056/NEJMra041245

U.S. Food and Drug Administration Center For Drug Evaluation And Research (2015). Clinical Pharmacology and biopharmaceutics Review(S). Retrieved October 13, 2022, from Available at:https://www.accessdata.fda.gov/drugsatfda_docs/nda/2015/206192Orig1s000ClinPharmR.pdf.

Wu, Y., Wang, Y., Wang, L., Yin, P., Lin, Y., and Zhou, M. (2020). Burden of melanoma in China, 1990-2017: Findings from the 2017 global burden of disease study. *Int. J. Cancer* 147 (3), 692–701. doi:10.1002/ijc.32764

frontiers | Frontiers in Pharmacology

TYPE Review
PUBLISHED 12 December 2022
DOI 10.3389/fphar.2022.1090227

OPEN ACCESS

EDITED BY
Hai-long Piao,
Dalian Institute of Chemical Physics (CAS), China

REVIEWED BY
Huai-Qiang Ju,
Sun Yat-sen University, China
Junli Liu,
Shanghai Jiao Tong University, China
Wei Yang,
Southern Medical University, China

*CORRESPONDENCE
Guozhi Lin,
tyfylgz@163.com

SPECIALTY SECTION
This article was submitted to Pharmacology of Anti-Cancer Drugs, a section of the journal Frontiers in Pharmacology

RECEIVED 05 November 2022
ACCEPTED 28 November 2022
PUBLISHED 12 December 2022

CITATION
Li R, Dong F, Zhang L, Ni X and Lin G (2022), Role of adipocytokines in endometrial cancer progression. *Front. Pharmacol.* 13:1090227. doi: 10.3389/fphar.2022.1090227

Role of adipocytokines in endometrial cancer progression

Ran Li[1], Fang Dong[1], Ling Zhang[1], Xiuqin Ni[1] and Guozhi Lin[2]*

[1]School of Health Sciences, Jiangsu Food and Pharmaceutical Science College, Huaian, China, [2]Department of Obstetrics and Gynecology, Second Affiliated Hospital to Shandong First Medical University, Taian, China

Endometrial cancer is considered a significant barrier to increasing life expectancy and remains one of the most common malignant cancers among women in many countries worldwide. The increasing mortality rates are potentially proportional to the increasing obesity incidence. Adipose tissue secretes numerous adipocytokines, which may play important roles in endometrial cancer progression. In this scenario, we describe the role of adipocytokines in cell proliferation, cell invasion, cell adhesion, inflammation, angiogenesis, and anti-apoptotic action. A better understanding of the mechanisms of these adipocytokines may open up new therapeutic avenues for women with endometrial cancer. In the future, larger prospective studies focusing on adipocytokines and specific inhibitors should be directed at preventing the rapidly increasing prevalence of gynecological malignancies.

KEYWORDS

endometrial cancer, signalling pathway, adipokines, inflammatory cytokines, angiogenic factors

1 Introduction

Endometrial cancer is considered a significant barrier to increasing life expectancy with significantly increased incidence (Morice et al., 2016) and remains one of the most common malignant cancers among women in many countries worldwide, particularly in more developed countries (Oaknin et al., 2022). Worldwide, endometrial cancer, which is classified into two histological subtypes (type I and type II), ranks sixth in incidence among all female cancers (Morice et al., 2016; Sung et al., 2021). Data from the International Agency for Research on Cancer indicate that 417,367 new corpus uteri cancer cases and approximately 97,370 deaths occurred in 2020. According to the results of previous study, the highest incidence rate was noted in North America (21.1 per 100,000) and was approximately 10-fold greater than the lowest rate, which was observed in Middle Africa (2.3 per 100,000) (Sung et al., 2021).

However, the variation in mortality rates in different regions was not as obvious. The lowest mortality rate was observed in Northern Africa (0.7 per 100,000), and the highest was noted in Eastern Europe (3.7 per 100,000) (Sung et al., 2021). In China, the endometrial cancer incidence rate is approximately 7.74/100 000, and the mortality rate is approximately 1.60/100 000 (Sun et al., 2022). The increasing mortality rates are mainly associated with the increasing incidence of obesity, a leading cause of endometrial cancer (Ding et al., 2020; Larsson.et al., 2022; Moukarzel et al., 2022). In adjusted mixed

linear models, weight loss is strongly related to the levels of cancer-associated biologically active substances, including reduced interleukin-6 (IL-6) levels and increased adiponectin levels (Linkov et al., 2012).

As a major site for the secretion of protein signals, adipose tissues mainly comprise adipocytes. In addition, as a major endocrine gland, dysfunctional adipose tissue is involved in obesity-related tumorigenesis, which is correlated with its high degree of plasticity (Sakers et al., 2022) and the permissive microenvironment generated by aberrant inflammatory cytokines, adipokines, angiogenic factors, and aromatase (Hefetz-Sela and Scherer 2013). White adipose tissue (WAT), the most abundant adipose form, secretes numerous adipokines and cytokines to regulate whole-body metabolism. Moreover, WAT inflammation, which increases the expression of proinflammatory and proneoplastic genes, is associated with endometrial cancer (Moukarzel et al., 2022). Additionally, it has become helpful to evaluate biomarkers in relation to cancer risk (Linkov et al., 2018).

2 Article types

Review.

3 Manuscript formatting

3.1 Role of adipokines in endometrial cancer progression

Adipokines, a diverse group of biologically active substances, are characterized by adipose tissue secretion (Trayhurn and Wood 2004). The levels of various adipokines, such as leptin (Madeddu et al., 2022), visfatin (Wang et al., 2019), galectin (Boutas et al., 2021), resistin (Ozgor et al., 2019), adiponectin (Ellis et al., 2020), and vaspin (Erdogan et al., 2013), are increased or decreased in endometrial cancer and significantly correlated with cancer progression (Ray et al., 2022).

3.1.1 Leptin

Leptin is a 16 kDa cytokine-like hormone encoded by the obesity gene on chromosome 7q31.3, which was first discovered in 1994 (Zhang et al., 1994). The mature leptin protein consists of 146 amino acids and is mainly secreted from white adipose tissue (Zhang et al., 1994). Women with genotype AG of SNP -2548 G/A of leptin are less likely to be at risk for endometrial cancer given that the heterozygote AG is less frequently observed in endometrial cancer patients (Bienkiewicz et al., 2017). Leptin acts on the hypothalamic regions by binding to leptin receptors (Ob-R), which exist in six isoforms with different lengths and C-terminal sequences (Baumann et al., 1996). The AG polymorphic variant of SNP LEP-R c.668A>G (p. Gln223Arg, rs1137101) in the leptin receptor is less frequently observed and considered a protective factor in women with endometrial cancer (Bienkiewicz et al., 2021). By analyzing data from tissue samples and whole blood, overexpression of leptin and its receptors was implicated in endometrial cancer both at the mRNA and protein levels (Boron et al., 2021). In endometrial cancer tissues, Ob-Ra is considered the most common form influencing biological outcomes, not Ob-Rb, which has the same extracellular domain (Yuan et al., 2004). Expression of the long leptin receptor isoform is approximately 5-fold higher in neoplastic tissue compared with normal tissue (Mantzos et al., 2011).

Leptin is involved in endometrial cancer by controlling energy homeostasis and increasing glycolytic capacity. Exposure to leptin could alter endometrial cancer cell morphology. The higher the leptin concentration, the greater the surface roughness (Dabrus et al., 2020). A positive correlation was noted between endometrial cancer and elevated serum leptin levels (Petridou et al., 2002; Tessitore et al., 2004). The incidence rate increased with increasing body mass index (BMI) in endometrial cancer patients (Cymbaluk et al., 2008). The cancer risk of postmenopausal women with the highest tertile of circulating leptin levels was almost three times that noted for women with the lowest tertile (Dallal et al., 2013). In addition, overexpression of leptin and its receptors was observed (Boron et al., 2021). These observations indicated that leptin and its receptors may be potential targets for intervention in the pathophysiology. Furthermore, useful cancer treatment strategies could be designed based on these findings (Boron et al., 2021).

To understand the potential molecular mechanisms of leptin, several studies have been conducted (Bogusiewicz et al., 2006; Carino et al., 2008; Zhou et al., 2015; Daley-Brown et al., 2019). These findings indicated that leptin, a known mitogenic, inflammatory, and angiogenic factor promoted the development of endometrial cancer mainly through the activation of classical biological signalling pathways.

Leptin receptors, including both long and short receptors, can bind to janus-activated kinases and transduce certain signals (Hegyi et al., 2004). Leptin induces two key cell-growth signalling pathways (extracellular signal-regulated kinase (ERK) (Carino et al., 2008) and the serine/threonine kinase (AKT) (Carino et al., 2008)) after rapidly activating the janus-activated kinase (JAK)/signal transducers and activators of transcription (STAT) pathway (Hegyi et al., 2004) (Figure 1). The addition of tyrphostin AG490 abolished leptin-induced proliferation by blocking ERK and AKT phosphorylation (Sharma et al., 2006). Furthermore, the increased phosphorylation of ERK1/2 and leptin-induced stimulation of proliferation were observed upon treatment with 100 ng/ml leptin (Gong et al., 2007). Leptin triggers the phosphatidylinositol3-kinase (PI3K)/AKT pathway by activating the leptin receptor, which is correlated with cell proliferation and invasiveness (Bogusiewicz et al., 2006).

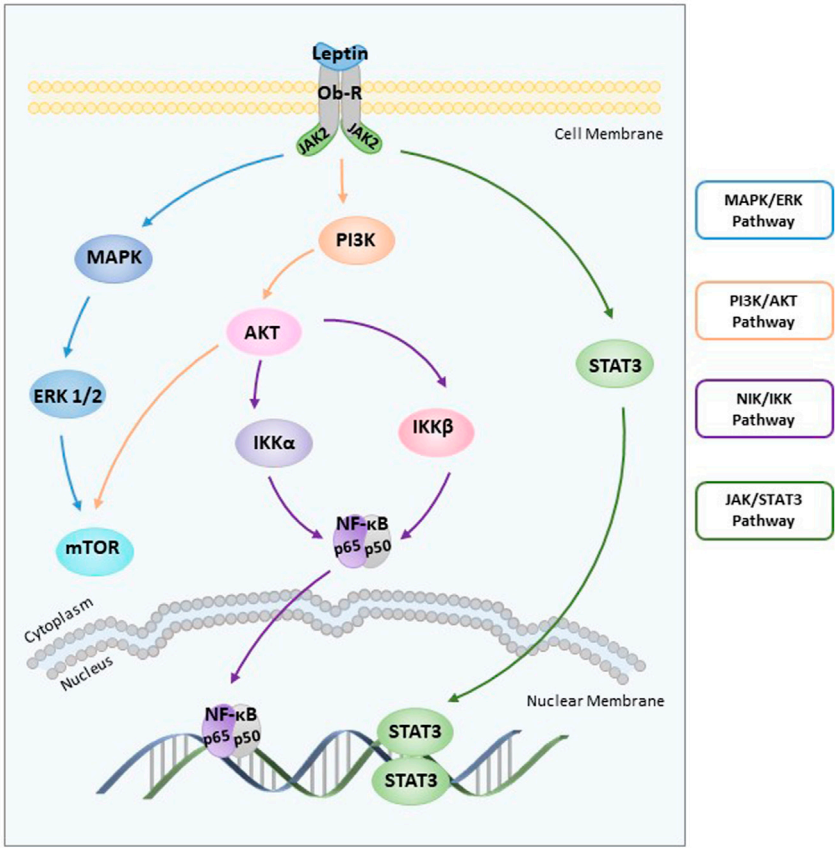

FIGURE 1
Role of leptin in endometrial cancer. Leptin induces two key cell-growth signalling pathways (ERK and AKT) after rapidly activating the JAK/STAT3 pathway. Leptin-induced NF-κB activation inhibits cancer cell apoptosis through the NIK/IKK signalling pathway. ERK: extracellular signal-regulated kinase; AKT: the serine/threonine kinase; JAK: janus-activated kinase; STAT3: signal transducers and activators of transcription 3; NIK: nuclear factor-kappa B inducing kinase; IKK: IKB kinase.

Another pathway involved in cancer progression is nuclear factor-kappaB inducing kinase (NIK)/IKB kinase (IKK), and leptin-induced NIK/IKK phosphorylation inhibits cancer cell apoptosis in carcinoma cells (Zhou et al., 2015) (Figure 1). First discovered in 1986, NF-κB is essentially involved in driving immune and inflammatory responses (Sen and Baltimore 1986). The NF-κB family includes five members and mediates DNA contact by forming homo or heterodimers (May and Ghosh 1997; Caamano and Hunter 2002). The IκB family of proteins, which includes four members, binds to the NF-κB family of proteins to inhibit the activity of transcription factors (Hoesel and Schmid 2013). Nuclear positivity for subunits of NF-κB as well as cytoplasmic staining for three IκB family members was assessed in 57 endometrial carcinoma cases by immunohistochemical evaluation. These data suggest that NF-κB/IκB may be involved in endometrial carcinoma cell proliferation and apoptosis (Pallares et al., 2004). Furthermore, leptin inhibits apoptosis of cancer cells by stimulating phosphorylation of IκBα, IκB kinase α (IKKα), IκB kinase β (IKKβ), and NIK in a dose-dependent manner (Zhou et al., 2015).

Leptin is involved in endometrial carcinoma cell mitosis, and leptin-mediated effects on endometrial cancer cell cycle progression are concentration-dependent. Leptin reduces the fraction of G0/G1-phase cells and increases S-phase cells by stimulating cyclin D1, a significant cell cycle regulator. Leptin-induced cyclin D1 overexpression increases STAT3-DNA and cAMP-response element binding protein (CREB)-DNA binding activity and recruitment (Catalano et al., 2009).

A positive correlation between overexpression of leptin and hypoxia-inducible factor 1 alpha (HIF-1α), an indicator of tissue hypoxia consisting of two subunits, was clearly observed in endometrial cancer tissues (Koda et al., 2007). Furthermore, leptin overexpression was stimulated through HIF-1α interaction with the leptin gene promotor in hypoxic adipocytes (Grosfeld et al., 2002). Among 48 human endometrioid adenocarcinoma patients, the number of patients positive for STAT3, HIF-1, leptin, and ObR was 36,

38, 29 and 15, respectively. It was clearly demonstrated that leptin induced HIF-1α through STAT3 in response to hypoxia (Wincewicz et al., 2008).

Leptin stimulates cell proliferation by increasing cyclooxygenase-2 (COX-2) protein expression through the JAK2/STAT3, MAPK/ERK, and PI3K/AKT signalling pathways (Gao et al., 2009). COX-2, a rate-limiting enzyme, is of considerable functional importance (Tsujii et al., 1998). The findings of basic *in vivo* and *in vitro* studies suggest that COX-2 overexpression is associated with increased susceptibility to endometrial cancer (Chen and Liao 2009; Ma et al., 2015). Increased COX-2 expression was found in higher-grade tumours. Several studies have indicated that functional activation of COX-2 is mediated by JAK2/STAT3 (Peng-Fei et al., 2021), MAPK/ERK (Adderley and Fitzgerald 1999), and PI3K/AKT (Rodriguez-Barbero et al., 2006) signalling pathways. After being treated with inhibitors (AG490, U0126, LY294002, and NS398) respectively, stimulated endometrial cancer cell proliferation and increased COX-2 protein expression induced by leptin were abolished (Gao et al., 2009). Therefore, COX-2 is also considered a significant biomarker for endometrial cancer diagnosis and prognosis (Oplawski et al., 2020).

Leptin-induced aromatase P450 (P450arom) overexpression increases oestrogen formation to promote endometrial cancer progression. P450arom, a key enzyme, is involved in the conversion of androstenedione to oestrogens (Noble et al., 1996). Excessive P450arom activity and transcript levels were found in endometrial cancer tissues. Higher P450arom mRNA and protein expression as well as oestradiol concentrations were observed in endometrial carcinoma cells treated with 100 ng/ml leptin, indicating a strong correlation between leptin and P450arom (Liu et al., 2013).

3.1.2 Adiponectin

Adiponectin, a type of insulin-sensitizing adipokine, is secreted predominantly by WAT (Scherer et al., 1995; Hu et al., 1996; Maeda et al., 1996; Nakano et al., 1996). In addition, recent studies have indicated that adipose-derived stem cell (ASC) is an important source of intracellular adiponectin (Ciortea et al., 2018). In human plasma, Acrp30, a type of full-length adiponectin which consists of 247–amino acid protein is the main adiponectin form found in circulation (Scherer et al., 1995). In a large case–control study, three SNPs in the ADIPOQ gene (rs3774262, rs1063539, rs12629945) were identified that potentially correlated with energy intake (Chen et al., 2012). Structurally, the adiponectin receptor has two isoforms, both of which include an internal N and an external C-terminus region (Yamauchi et al., 2003). AdipoR1 is ubiquitously expressed but has a higher affinity for globular adiponectin. However, AdipoR2 exhibits intermediate affinity for both globular and full-length adiponectin (Goldstein and Scalia 2004; Kadowaki and Yamauchi 2005). Analysis of endometrial tissues showed that both adiponectin receptors were expressed throughout the menstrual cycle and were especially present at higher levels in the mid-luteal phase (Takemura et al., 2006). Similar to leptin, adiponectin is also correlated with obesity. Higher levels of abdominal fat were found in the endometrial cancer group, and plasma adiponectin level was in a negative linear correlation with the abdominal fat level. (Mihu et al., 2013). Of note, significantly lower adiponectin levels were implicated in endometrial cancer patients (Rzepka-Gorska et al., 2008). Additionally, the abnormal expression of adiponectin receptors was observed in several insulin resistance-related tumours, such as breast cancer (Mocino-Rodriguez et al., 2017; Cicekdal et al., 2020), prostate cancer (Kaklamani et al., 2011; Huang et al., 2021), ovarian cancer (Jin et al., 2016), and endometrial cancer (Petridou et al., 2003; Soliman et al., 2006; Barb et al., 2007). In addition, adiponectin suppresses endometrial cancer proliferation by acting through AdipoRs, which were expressed in both tissue samples and cell lines (Moon et al., 2011). Positive staining was observed in low-grade adenocarcinoma, whereas negative staining was noted in high-grade adenocarcinoma. These results indicate that lower AdipoR expression was strongly correlated with higher histological grade in endometrioid adenocarcinoma (Yamauchi et al., 2012). Data from a study including 60 patients indicated that AdipoR1 levels are related to myometrial invasion (Yunusova et al., 2015). Moreover, another study indicated that the expression of AdipoR-1, not AdipoR-2, exerts suppressive effects on cancer cell proliferation, adhesion, and growth in a group of endometrial carcinoma patients (Yabushita et al., 2014).

Adiponectin directly reduced the viability of normal human endometrial stromal cells without any change in AdipoR1 and AdipoR2 levels (Bohlouli et al., 2013). Moreover, numerous findings showed that serum adiponectin levels were reduced in endometrial cancer patients compared with individuals with no history of endometrial cancer (Soliman et al., 2006; Cust et al., 2007; Ma et al., 2013; Zeng et al., 2015; Ellis et al., 2020). The expression levels of adiponectin and vaspin, which are considered anti-inflammatory molecules, are inversely proportional to endometrial cancer risk even after controlling for potential confounders (Erdogan et al., 2013). In particular, a linear dose-response relationship indicated that the risk was reduced by 3% for every 1 μg/ml increase in adiponectin (Lin et al., 2015). Furthermore, among women younger than 65 years, the odds ratios derived from three different models by multiple logistic regression indicated that the risk was reduced by 50% for a 1 SD increase in adiponectin (Petridou et al., 2003). Additionally, adiponectin concentrations were progressively reduced from grade 1 (19.04 μg/ml) to grade 2 (13.48 μg/ml), and finally grade 3 tumours (12.86 μg/ml). A significant difference was noted between grade 1 and grade 3 tumours but not between grade 1 and grade 2 tumours (Rzepka-Gorska et al., 2008).

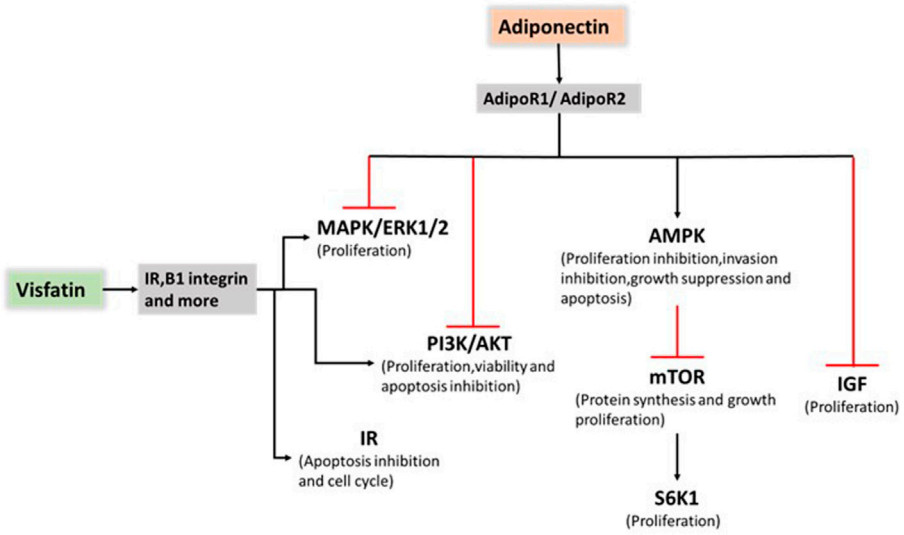

FIGURE 2
Role of adiponectin and visfatin in endometrial cancer progression. Adiponectin exerts an antiproliferative effect on endometrial cancer by stimulating AMPK pathway activation and suppressing PI3K/AKT, MAPK/ERK1/2 and IGF pathway activation. Visfatin promoted cancer progression mainly through PI3K/AKT, and MAPK/ERK1/2 pathway activation and IR. AMP: 5 adenosine monophosphate; AMPK: AMP-activated protein kinase; PI3K: phosphatidylinositol 3-kinase; AKT: the serine/threonine kinase; MAPK: mitogen-activated protein kinase; ERK1/2: extracellular signal-regulated kinases 1 and 2; IGF: insulin-like growth factor; IR: insulin resistance.

Leptin-to-adiponectin ratios (L/A ratios) may be more informative in studies of the risk of endometrial cancer among postmenopausal women (Dallal et al., 2013). Higher L/A ratios were strongly related to endometrial cancer progression even after controlling for the factors of diabetes mellitus and age. The OR of the L/A ratio [6.0 (95% CI: 3.2–11.9)] was higher than those of leptin alone [3.2 (95% CI: 1.8–5.8)] or adiponectin alone [0.5 (95% CI: 0.3–0.9)], suggesting that L/A ratios in individuals may better indicate cancer growth and proliferation (Ashizawa et al., 2010).

Adiponectin exerts an antiproliferative effect on endometrial cancer by increasing the number of G1/G0-phase cells and decreasing the number of S-phase cells. The reduction in cell counts in the HEC-1-A and RL95-2 cell lines reached approximately 30% and 20%, respectively, upon treatment with 40 mg/ml adiponectin. Furthermore, cyclin D1 and cyclin E2 expression was reduced, and 5 adenosine monophosphate-activated protein kinase (AMPK) was rapidly activated within 30 min in human endometrial cancer cell lines (Cong et al., 2007). Moon, H. S et al. (Moon et al., 2011) showed for the first time that adiponectin upregulated the tumour suppressor gene liver kinase B1 (LKB1), an adaptor molecule required for AMPK activation, to stimulate the AMPK/S6 axis. In addition, Wu et al. (Wu et al., 2012) demonstrated that Acrp30 effectively reduced leptin-induced STAT3 phosphorylation by stimulating the MAPK pathway in aggressive SPEC-2 endometrial cancer cells. After Ishikawa cells were treated with 10 μg/ml adiponectin, AMPK phosphorylation was rapidly activated and reached a maximum at 30 min. A 50% reduction in activated ERK and a 40% reduction in AKT expression were observed. Moreover, compound C inhibited adiponectin-induced ERK and AKT phosphorylation, demonstrating that ERK and AKT are downstream targets of AMPK. In addition, 10 μg/ml adiponectin treatment also caused significant reductions in cyclin D1 mRNA (49%), cyclin D1 protein (62%), B-cell lymphoma-2 (Bcl-2) mRNA (45%) and Bcl-2 protein (36%). This result suggested that adiponectin induced mitochondrial dysfunction by decreasing the Bcl-2/bcl-2-associated x (Bax) ratio (Zhang et al., 2015). Cai et al. (Cai et al., 2018) showed that AMPK phosphorylation was significantly induced by adiponectin, whereas mTOR and ribosomal protein S6 kinase-1 protein phosphorylation was inhibited. A considerably reduced proliferation inhibition ratio and enhanced cell migration were found in the inhibitor + adiponectin group than in the adiponectin group without the addition of an inhibitor. Adiponectin may inhibit cell proliferation and migration through the AMPK/(mTOR)/(S6K1) signalling pathway in patients with malignancies (Figure 2).

However, contrary to the previous role of adiponectin in suppressing cancer progression, several studies have showed that adiponectin contributes to an increased risk of liver cancer (Aleksandrova et al., 2014). Moreover, a study involving in exploring the relation between cancer and adiponectin underlying the obesity paradox, has showed that exogenous adiponectin significantly inhibited cell apoptosis by up-

regulating p-AMPK and Bcl-xL levels in renal cell carcinoma (Ito et al., 2017). This conclusion was consistent with the results of the later study conducted by Lee et al. (Lee et al., 2020). The study conducted in Hong Kong, including 5658 participants, indicated an interesting adiponectin paradox. They demonstrated that higher adiponectin concentrations might be harmful, and positively correlated with the incidence and deaths of cancer in type 2 diabetes (Lee et al., 2020). As the role of adiponectin still remains controversial in various cancers, further studies should be directed to exploring the complex mechanism.

3.1.3 Visfatin

Visfatin, a 52 kDa protein (Fukuhara et al., 2005), plays a significant role in cell growth (Zhang et al., 2011) and insulin resistance (Fukuhara et al., 2005). Recently, accumulating evidence has suggested that visfatin may be a complementary diagnostic and prognostic marker for malignancies, especially those that are strongly related to dysfunctional adipose tissue, such as breast cancer (Rajput et al., 2022), colorectal cancer (Zhao et al., 2020), and endometrial cancer (Mu et al., 2012). Tian et al. (Tian et al., 2020) reported that visfatin protein expression was upregulated by the PI3K/AKT and MAPK/ERK signalling pathways in polycystic ovary syndrome (PCOS) patients with endometrial cancer.

Tian et al. (Tian et al., 2013) suggested that serum visfatin levels were significantly higher in endometrial cancer patients compared with other groups. Furthermore, visfatin expression was measured in tissue samples. Visfatin tissue expression increased gradually from normal proliferative or secretory endometrium (58.1%) and hyperplastic endometrium (66.7%) to endometrial cancer (80.5%). Moreover, visfatin expression was significantly related to serum levels in 50 endometrial cancer patients. High serum visfatin levels represent a key factor correlated with deep myometrial invasion and poor survival (Tian et al., 2013). Visfatin promotes cancer progression mainly through PI3K/AKT and MAPK/ERK1/2 activation as well as insulin resistance (IR) (Figure 2). In 2014, Nergiz Avcioglu et al. (Nergiz Avcioglu et al., 2015) indicated three possible mechanisms (obesity, increased lipolysis, and insulin resistance) to explain the increased serum visfatin levels in endometrial cancer (Nergiz Avcioglu et al., 2015). A study focusing on the molecular mechanisms showed that visfatin exerts pro-proliferative and anti-apoptotic effects by stimulating cell proliferation and increasing the S-phase fraction of cells.

The expression of visfatin and its substrates was upregulated in the context of IR, and maximal levels were noted at 30 min. Increased C-MYC and cyclin D1 expressions as well as decreased caspase-3 expression were also observed with visfatin treatment. To confirm the effect of the PI3K/AKT and MAPK/ERK signalling pathways, Ishikawa cells were treated with 400 ng/ml visfatin. Larger G1 and S-phase fractions were found in Ishikawa cells pretreated with the inhibitor (Wang et al., 2016). Similar results are presented by Cymbaluk-Ploska et al. (Cymbaluk-Ploska et al., 2018). The visfatin concentration was 15.9 ng/ml for the endometrial cancer group and 9.5 ng/ml for the other. Furthermore, a slightly higher visfatin concentration was noted for cases with lower histological differentiation (22.2 and 31.8 ng/ml) compared with well-differentiated cases (17.3 and 22.2 ng/ml). The visfatin level was inversely proportional to the overall survival (OS) of patients (Cymbaluk-Ploska et al., 2018). A retrospective case–control study showed that the visfatin-adiponectin ratio in 53 endometrial cancer patients was significantly higher than that in the control group (Wang et al., 2019).

3.1.4 Galectin

It is clear that galectins are integrated into the physiological and pathological systems of individuals with a wide range of biological functions (Liu et al., 2002). To date, 11 identified different subtypes have been classified into three subgroups according to structure (prototype, tandem repeat-type, and chimeric-type) (Chou et al., 2018). Among them, four forms (galectin-1, galectin-3, galectin-7, and galectin-9) have been closely linked to gynecological cancer cell biology and immunology (Chetry et al., 2018). Furthermore, multiple studies have indicated that galectin-1, a homodimeric protein involved in angiogenesis (Thijssen and Griffioen 2014) and cross-linking receptors (Hernandez et al., 2006), and galectin-3, a chimaera-type protein associated with cancer metastasis (Fortuna-Costa et al., 2014) and inflammatory regulation (Henderson and Sethi 2009), are mainly involved in endometrial cancer. Galectin-1 expression was observed in endometrioid endometrial adenocarcinoma (EA) tissue (Zinovkin et al., 2019). Higher galectin-1 expression suggested a poorer prognosis (Sun and Dai 2020). In addition, galectin-1 immunoreaction was positively proportional to endometrial cancer grade, increasing from G1 to G3 (Mylonas et al., 2007). The microcystic, elongated and fragmented (MELF) pattern was inversely proportional to endometrial cancer patient survival (Stewart et al., 2009; Zinovkin et al., 2017). The median level of galectin-1 expression among 49 subjects was obviously higher (78.6%) in the positive group. The statistically significant differences analyzed by the Mann–Whitney test additionally indicated that this marker may be of considerable functional importance in the OS of patients (Zinovkin et al., 2019).

Galectin-1 and galectin-3 immunoperoxidase staining of the uterine carcinoma specimens obtained from Duke University Medical Center was performed and statistically analyzed. Lower scores of galectin-1 expression were found in normal endometrium (scores from 0 to 2), whereas higher scores were found in endometrial carcinomas (scores from 1 to 3). In contrast, galectin-3 expression was significantly decreased in endometrial cancer (van den Brule et al., 1996). This conclusion was consistent with the results of a later study

conducted in the Middle East. This finding demonstrated that galectin-3 may play a role in the suppression of cancer progression. Galectin-3 immunoreactivity progressively decreased from normal samples (80%) to endometrial carcinoma (55%), indicating poor prognoses (Al-Maghrabi et al., 2017). Interestingly, deeper invasion of the myometrium was found in cancer cells with only cytoplasmic immunoreactivity (van den Brule et al., 1996). The extent, intensity, and immunohistochemical reactivity of epithelial and stromal galectin-3 expression were reduced in the cancer group. The percentage of the cases with lymph node metastasis negative for galectin-3 expression (64%) was increased almost four-fold compared with cases without lymph node metastasis (18%). This investigation suggests that galectin-3 may be involved in the pathogenesis of endometrial carcinomas and lymph node metastasis (Ege et al., 2011).

However, contradictory results from a study involving 144 patients showed that increased galectin 3 expression was observed in patients with lymphovascular space invasion (Cymbaluk-Ploska., et al., 2020). The mean scores progressively increased from normal endometria (2.58) and atypical hyperplasia (4.77) to clear cell carcinoma (6.71), and significant differences were noted among the various conditions. Based on these findings, Brustmann et al. (Brustmann et al., 2003), assumed that galectin-3 expression was essential to maintain a transformed phenotype in endometrial carcinoma (Brustmann et al., 2003). To investigate the effect of galectin-3 on the endometrial cell cycle and adhesion, multiple analysis methods were used. After seventy-two hours of galectin-3 siRNA transfection, galectin-3 mRNA and protein expression were reduced by 70%–90% in RL95-2 cells. A decrease in S-phase cells and an increase in G1-phase cells were observed. Thus, galectin-3 may be involved in promoting cell adhesion and increasing integrin expression (Lei et al., 2007). Additionally, considering the fact that the environment composed of numerous adipokines and cytokines that promote tumour growth, the different conclusions may be clarified by method sensitivity, case differences, treatment differences, and different sizes of samples. To better understand the effect of galectin-3 and related biological signalling pathways on tumour size, growth, characteristics, and malignancy in endometrial cancers, more studies, such as longitudinal studies and large-scale studies, are needed.

3.2 Role of adipose-secreted inflammatory cytokines in endometrial cancer progression

Inflammatory cytokines, such as interleukin-1β (IL-1β), interleukin-6 (IL-6), and interleukin-8 (IL-8), can modify the immunological network in the endometrium. The primary sources of inflammatory cytokines mainly include inflammatory cells, adipocytes, and cancer cells. Among them, IL-1β and IL-6 are secreted by adipocytes through endocrine and paracrine secretion and are correlated with a modified adipocyte phenotype (Dirat et al., 2011). Inflammatory cytokines are the key factors that explain the difference in the immune microenvironment between normal and malignant endometria. Therefore, understanding the role of inflammatory cytokines in proinflammatory and protumorigenic effects on endometrial cancer progression is crucial.

IL-1β, IL-6, and IL-8, which exhibit a wide range of complex functions, have been extensively examined. Notably, IL-1 is ubiquitously expressed in endometrial tissues (Van Le et al., 1991). However, data from a clinical study revealed a significant increase in IL-8 concentrations, not IL-Iβ and IL-6, which were too low to detect (Chopra et al., 1997). Furthermore, later experiments clearly demonstrated that leptin significantly increased the levels of IL-1 and interleukin-1 receptor tI (IL-1R tI) in a dose-dependent manner. Based on experiments using a kinase inhibitor, the results indicated that leptin-mediated activation of the JAK2/STAT3, PI3K/AKT1, and mTOR signalling pathways was associated with an increase in IL-1β levels in primary endometrial epithelial cells. In contrast, leptin induced IL-1R tI in all endometrial epithelial cells through leptin canonical signalling pathways that generally include JAK2/STAT3, MAPK/ERK1/2, and mTOR without PI3K/AKT1 involvement (Carino et al., 2008).

Adiponectin also stimulated AMPK phosphorylation and suppressed the secretion of IL-6 and IL-8 induced by IL-1β in human endometrial stromal cells (ESCs), suggesting the effect of adiponectin on regulating energy supply and anti-inflammatory function (Takemura et al., 2006).

When assessing endometrial cancer cells using cell invasion assays and statistical analysis, Lipsey et al. (Lipsey et al., 2016) found that Notch, IL-1, and leptin crosstalk outcome (NILCO) was more highly expressed in type II endometrial cancer, the more aggressive form, not type I. Moreover, leptin-induced invasion of endometrial carcinoma cells was significantly reduced in the presence of an inhibitor (Daley-Brown et al., 2017). Remarkably, the levels of Notch receptors, ligands, and targeted molecules were at least a twofold increase compared to basal culture conditions without leptin treatment. After DAPT and anti-IL-1R tI antibodies were added, the results showed that leptin-induced migration of malignancies was abrogated. The role of leptin was more prominent in the more malignant phenotype, such as the more aggressive and poorly differentiated An3CA endometrial cancer cell line. Leptin-induced NILCO molecules in endometrial cancer affect cell proliferation, aggressiveness, and chemoresistance (Daley-Brown et al., 2019). Taken together, these studies indicated the complex crosstalk among Notch, IL-1, and leptin as well as the involvement of IL-1 in inducing inflammatory progression and upregulating leptin expression in endometrial cancer (Figure 3).

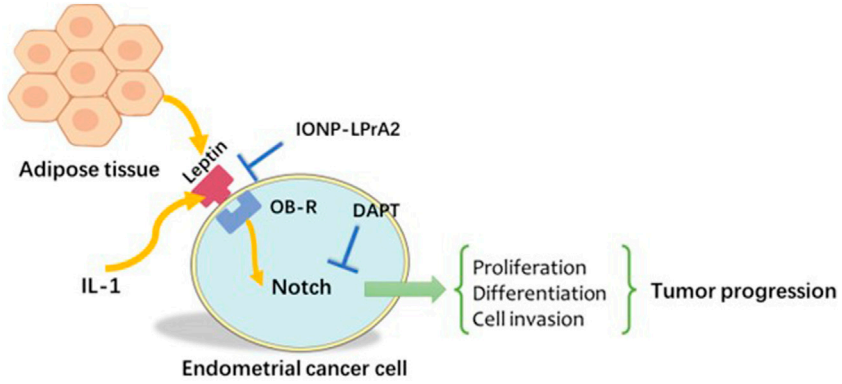

FIGURE 3
Notch, IL-1, and leptin crosstalk outcome (NILCO). Leptin induced Notch receptor, ligand, and targeted molecule expression. The inhibition of Notch and IL-1 signalling *in vitro* reduced leptin-induced invasion. IL-1: Interleukin-1.

3.3 Role of adipose-secreted angiogenic factors in endometrial cancer progression

Adipose-secreted angiogenic factors, such as vascular endothelial growth factor (VEGF) and fibroblast growth Factor 21 (FGF21), play significant roles in stimulating angiogenesis and forming the proangiogenic microenvironment. Potential therapeutic implications targeting VEGF and FGF21 may open up new avenues for endometrial cancer women with cancer cell metastasis.

VEGF, a multiple proangiogenic factor observed across endometrioid endometrial adenocarcinoma (EA) cells in different stages, was correlated with abnormal vasculature formation, insulin sensitivity, and adipocyte death (Sun et al., 2012; Goel and Mercurio 2013). Moderate VEGF expression was positively correlated with EA progression as well as an elongated and fragmented (MELF) pattern. However, this parameter was inversely proportional to the number of survival days (Zinovkin et al., 2019). A preliminary study suggested that leptin significantly increased the levels of VEGF and vascular endothelial growth factor receptor 2 (VEGFR2) through the MAPK/ERK1/2 and mTOR signalling pathways (Carino et al., 2008). In addition, overexpression of VEGF and its receptors in uterine tissue appeared to be affected by cotreatment (leptin and oestradiol) probably through the ERK1/2 and STAT3 pathways (Shetty et al., 2020). Interestingly, additional experiments clearly showed that leptin-induced angiogenesis was probably attributed to activating VEGFR-Notch signalling crosstalk in overweight cancer patients with increased expression of VEGF, VEGFR-2, and Notch (Lanier et al., 2016).

Fibroblast growth Factor 21 (FGF21) belongs to the sixth subfamily of FGFs and mainly modulates the storage of carbohydrates (Beenken and Mohammadi 2009). Based on comparative analysis, high FGF21 concentrations were positively related to high leptin levels. Taken together, the results showed that FGF21 concentrations were higher in poorly and moderately differentiated tumours compared with highly differentiated tumours. In addition, the area under the receiver operator characteristic curve (AUC) for FGF21 was 0.81, indicating that FGF21 was a promising diagnostic biomarker with good sensitivity and specificity through FGFR 2 and the PI3K/AKT and mTOR signalling pathways (Cymbaluk-Ploska et al., 2020).

3.4 Role of other adipocytokines in endometrial cancer progression

On review of the recent studies, other identified adipocytokines, including plasminogen activator inhibitor-1 (PAI-1) (Wang et al., 2021), and fatty acid-binding protein 4 (FABP4) (Wu et al., 2021), also play important roles in regulating various physiological processes. Of note, these adipocytokines have considerable consequences for promoting the proliferation and migration of endometrial cancer cells and may be possible targets for the therapy.

PAI-1, a promising prognostic factor involving in selective degradation of extracellular matrix components (Andreasen et al., 1997; Fredstorp-Lidebring et al., 2001), has been found to be associated with neovascularization, invasion, and migration in breast (Schmitt et al., 2010), prostate (Almasi et al., 2011), colorectal (Markl et al., 2017), ovarian (Zhang et al., 2013), and endometrial cancers (Tecimer et al., 2001). Women with PAI-1 rs1799889 4G/4G genotype are more likely to be at risk for endometrial cancer and the susceptibility to cancer may be associated with the 4G allele. (Su et al., 2011; Xu et al., 2012). Compared to normal endometrium, concentrations of PAI-1 in cytosols of endometrial cancer were significantly higher (Kohler et al., 1997; Osmak et al., 2001). In addition, expression of PAI-1 was regulated by estrogen and progesterone, and appeared negatively correlated with estrogen and progesterone receptor levels (Fujimoto et al., 1996; Steiner et al., 2008). The potential of sex steroids-

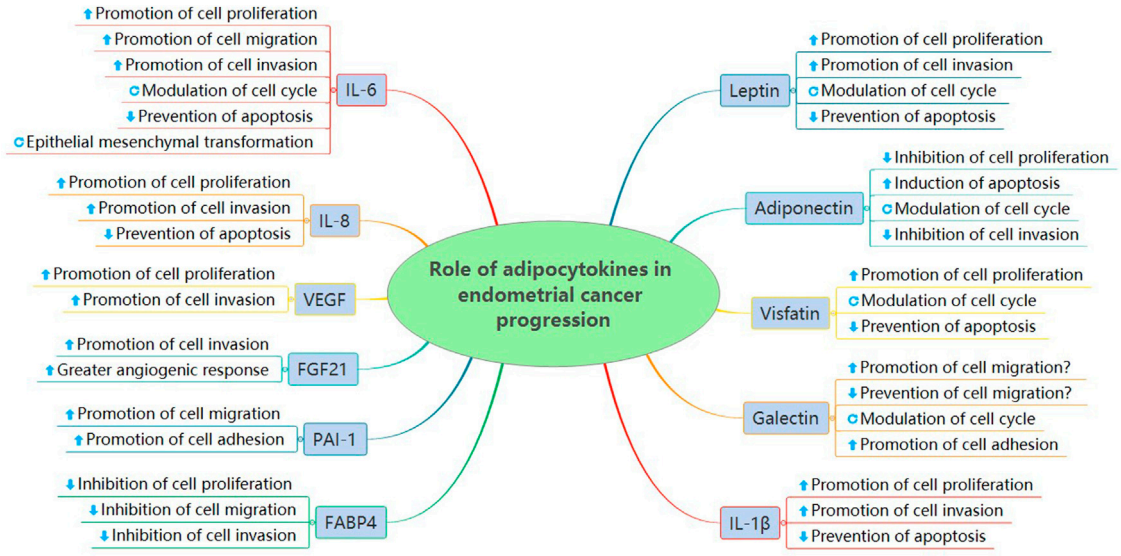

FIGURE 4
Role of adipocytokines in endometrial cancer progression.

dependent metastasis plays significant roles in cancer progression (Gotte et al., 2010; Fujimoto and Sato 2011). Previous studies showed that PAI-1 was positively correlated with cancer stage, but negatively correlated with relapse free time and OS of patients (Tecimer et al., 2001; Steiner et al., 2008). As one of the most abundant adipocytokines in adipose stromal cells (ASCs), PAI-1 could diminish transforming growth factor β (TGF-β)-mediated tumor suppressor activity through the TGF-β/SMAD pathway (Lin et al., 2020).

FABP4, belonging to the fatty acid binding proteins (FABPs) family, has a central role in tumour metastasis and endothelial migration by regulating metabolic and inflammatory pathways (Hotamisligil and Bernlohr 2015). As a marker involved in adipocyte differentiation (Bernlohr et al., 1984), FABP4 promotes the progression of feminine cancers, such as ovarian cancer, and cervical cancer (Gharpure et al., 2018; Jin et al., 2018). However, a recent study showed that FABP4 might play a possible suppressive role in endometrial cancer cell proliferation, migration, and invasion through the PI3K/AKT pathway (Wu et al., 2021). These studies have showed that the effects FABP4 exerts on cancers may be related to tumor type and signaling pathways. To further explore the decreased expression of FABP4 in endometrial cancer, more researches are required.

3.5 Possible role of adipocytokines in the treatment of endometrial cancer

Adipocytokines, including adipokines, inflammatory cytokines, and angiogenic factors, are significant biomarkers in various cancers, particularly endometrial cancer. To date, among the identified adipocytokines, some have been found to be good prognostic factors with a wide range of biological functions, including suppression of cell proliferation, induction of apoptosis, and reduced cell invasion. However, other adipocytokines, such as leptin, galectin, and visfatin, are considered poor prognostic factors associated with the promotion of cell proliferation, inhibition of apoptosis, and increased cell invasion (Figure 4). Leptin and adiponectin are the two main adipocytokines involved in most studies in endometrial cancer. However, studies on the potential molecular mechanisms of other adipocytokines, such as resistin, galectin, and visfatin, are limited. Particularly, contradictory results have been reported from different studies on galectin-3 concentrations and expression in endometrial cancers. The main inflammatory pathways predominantly reported include the MAPK/ERK1/2, JAK/STAT3, PI3K/AKT/mTOR, Notch, IR, IGF, AMPK/ERK, and AKT signalling pathways. When using specific inhibitors, endometrial cancer cell proliferation, invasion, and migration were reduced.

Based on the roles of significant adipocytokines and specific inhibitors, the use of targeted treatments in cancers has been studied in various experiments. Metformin, a potential anti-cancer drug, could induce cell cycle arrest and apoptosis through the AMPK and mTOR signalling pathways (Jalving et al., 2010). Furthermore, compared to metformin (Met) alone, metformin and silibinin (Sil) in magnetic PLGA/PEG nanoparticles (NPs) kill lung cancer cells more rapidly by reducing the expression of leptin and its receptor (Salmani Javan et al., 2022). Thiazolidinediones (TZDs) (rosiglitazone, pioglitazone) are also reported to increase adiponectin levels and decrease leptin, tumor necrosis factor-α (TNF-α), and IL-6 levels through modulatory mechanisms (Garikapati et al., 2019; Biondo et al., 2020). Moreover, TZDs have played important roles in

preventing progression of hepatocellular carcinoma (HCC) (Arvind et al., 2021), colon cancer (Yoon et al., 2020), and lung cancer (Konieczna et al., 2015). Atorvastatin reduces cardiovascular mortality by increasing levels of adiponectin, which is involved in insulin resistance (Koh et al., 2005; Ando et al., 2008). Atorvastatin has been reported to be used as a kind of important therapy in oesophageal adenocarcinoma by suppressing leptin-induced activation of cdc42 and AKT (Beales and Ogunwobi 2021).

Furthermore, recent studies have showed that mild obesity (BMI≥ 25.0,≤ 29.9) is correlated to an improved immunotherapy response (Li and Kalantar-Zadeh 2013; Li et al., 2017). The cancers who have mild obesity are more likely to reach a balance between pro- and anti-inflammatory cytokines (Assumpcao et al., 2022). Compared with poor response to chemotherapy in obese patients (Horowitz and Wright 2015), immunotherapy may be a more favorable therapeutic approach for the obesity (Waldman et al., 2020). The dysregulation of the secretion of adipocytokines, which involves in T cell modulation, macrophage polarization, and binding of adipocyte PD-L1 to anti-PD-L1 antibodies, affects immune checkpoint inhibitor therapy (Assumpcao et al., 2022). By using checkpoint inhibitor (anti–CTLA-4 mAb), Murphy et al. (Murphy et al., 2018) have found that leptin was a contributor to the failure of tumor immunotherapy. It implicated the potential role of leptin in the efficacy of immunotherapy.

4 Conclusion

Adipocytokines, regulating various physiological and pathological processes, play crucial roles in endometrial cancer progression. Larger prospective studies focusing on adipocytokines and specific inhibitors, particularly immune checkpoint inhibitor therapy, should be directed at preventing the rapidly increasing prevalence of gynecological malignancies.

Author contributions

Study concepts: GL and XN. Study design: RL and LZ. Manuscript preparation: RL and FD. Manuscript editing: RL, LZ, and GL. Manuscript review: RL, LZ, FD, XN, and GL.

Funding

This work was supported by the National Natural Science Foundation of China (81200011).

Conflict of interest

The authors declare that the research was conducted in the absence of any commercial or financial relationships that could be construed as a potential conflict of interest.

Publisher's note

References

Adderley, S. R., and Fitzgerald, D. J. (1999). Oxidative damage of cardiomyocytes is limited by extracellular regulated kinases 1/2-mediated induction of cyclooxygenase-2. *J. Biol. Chem.* 274, 5038–5046. doi:10.1074/jbc.274.8.5038

Al-Maghrabi, J., Abdelrahman, A. S., Ghabrah, T., Butt, N. S., Al-Maghrabi, B., and Khabaz, M. N. (2017). Immunohistochemical expression of galectin-3 is significantly associated with grade, stage and differentiation of endometrial carcinomas. *Pathol. Res. Pract.* 213, 348–352. doi:10.1016/j.prp.2017.01.012

Aleksandrova, K., Boeing, H., Nothlings, U., Jenab, M., Fedirko, V., Kaaks, R., et al. (2014). Inflammatory and metabolic biomarkers and risk of liver and biliary tract cancer. *Hepatology* 60, 858–871. doi:10.1002/hep.27016

Almasi, C. E., Brasso, K., Iversen, P., Pappot, H., Hoyer-Hansen, G., Dano, K., et al. (2011). Prognostic and predictive value of intact and cleaved forms of the urokinase plasminogen activator receptor in metastatic prostate cancer. *Prostate* 71, 899–907. doi:10.1002/pros.21306

Ando, H., Sugimoto, K., Yanagihara, H., Tsuruoka, S., Saito, T., Takamura, T., et al. (2008). Effects of atorvastatin and pravastatin on glucose tolerance, adipokine levels and inflammatory markers in hypercholesterolaemic patients. *Clin. Exp. Pharmacol. Physiol.* 35, 1012–1017. doi:10.1111/j.1440-1681.2008.04945.x

Andreasen, P. A., Kjoller, L., Christensen, L., and Duffy, M. J. (1997). The urokinase-type plasminogen activator system in cancer metastasis: A review. *Int. J. Cancer* 72, 1–22. doi:10.1002/(sici)1097-0215(19970703)72:1<1::aid-ijc1>3.0.co;2-z

Arvind, A., Memel, Z. N., Philpotts, L. L., Zheng, H., Corey, K. E., and Simon, T. G. (2021). Thiazolidinediones, alpha-glucosidase inhibitors, meglitinides, sulfonylureas, and hepatocellular carcinoma risk: A meta-analysis. *Metabolism.* 120, 154780. doi:10.1016/j.metabol.2021.154780

Ashizawa, N., Yahata, T., Quan, J., Adachi, S., Yoshihara, K., and Tanaka, K. (2010). Serum leptin-adiponectin ratio and endometrial cancer risk in postmenopausal female subjects. *Gynecol. Oncol.* 119, 65–69. doi:10.1016/j.ygyno.2010.07.007

Assumpcao, J. A. F., Pasquarelli-do-Nascimento, G., Duarte, M. S. V., Bonamino, M. H., and Magalhaes, K. G. (2022). The ambiguous role of obesity in oncology by promoting cancer but boosting antitumor immunotherapy. *J. Biomed. Sci.* 29, 12. doi:10.1186/s12929-022-00796-0

Barb, D., Williams, C. J., Neuwirth, A. K., and Mantzoros, C. S. (2007). Adiponectin in relation to malignancies: A review of existing basic research and clinical evidence. *Am. J. Clin. Nutr.* 86, s858–s866. doi:10.1093/ajcn/86.3.858S

Baumann, H., Morella, K. K., White, D. W., Dembski, M., Bailon, P. S., Kim, H., et al. (1996). The full-length leptin receptor has signaling capabilities of interleukin 6-type cytokine receptors. *Proc. Natl. Acad. Sci. U. S. A.* 93, 8374–8378. doi:10.1073/pnas.93.16.8374

Beales, I. L. P., and Ogunwobi, O. O. (2021). Leptin activates Akt in oesophageal cancer cells via multiple atorvastatin-sensitive small GTPases. *Mol. Cell. Biochem.* 476, 2307–2316. doi:10.1007/s11010-021-04067-8

Beenken, A., and Mohammadi, M. (2009). The FGF family: Biology, pathophysiology and therapy. *Nat. Rev. Drug Discov.* 8, 235–253. doi:10.1038/nrd2792

Bernlohr, D. A., Angus, C. W., Lane, M. D., Bolanowski, M. A., and Kelly, T. J., Jr. (1984). Expression of specific mRNAs during adipose differentiation: Identification of an mRNA encoding a homologue of myelin P2 protein. *Proc. Natl. Acad. Sci. U. S. A.* 81, 5468–5472. doi:10.1073/pnas.81.17.5468

Bienkiewicz, J., Romanowicz, H., Malinowski, A., and Smolarz, B. (2017). Association of Single Nucleotide Polymorphism -2548 G/A (rs12112075) of leptin gene with endometrial cancer and uterine leiomyomas. *Eur. J. Obstet. Gynecol. Reprod. Biol.* 218, 113–118. doi:10.1016/j.ejogrb.2017.09.022

Bienkiewicz, J., Romanowicz, H., Wilczynski, M., Jablonski, G., Stepowicz, A., Oblekowska, A., et al. (2021). Association of Single Nucleotide Polymorphism LEP-R c.668A>G (p.Gln223Arg, rs1137101) of leptin receptor gene with endometrial cancer. *BMC Cancer* 21, 925. doi:10.1186/s12885-021-08620-y

Biondo, L. A., Teixeira, A. A. S., Ferreira K, O. S., and Neto, J. C. R. (2020). Pharmacological strategies for insulin sensitivity in obesity and cancer: Thiazolidinediones and metformin. *Curr. Pharm. Des.* 26, 932–945. doi:10.2174/1381612826666200122124116

Bogusiewicz, M., Semczuk, A., Gogacz, M., Skomra, D., Jakowicki, J. A., and Rechberger, T. (2006). Lack of correlation between leptin receptor expression and PI3-K/Akt signaling pathway proteins immunostaining in endometrioid-type endometrial carcinomas. *Cancer Lett.* 238, 61–68. doi:10.1016/j.canlet.2005.06.028

Bohlouli, S., Khazaei, M., Teshfam, M., and Hassanpour, H. (2013). Adiponectin effect on the viability of human endometrial stromal cells and mRNA expression of adiponectin receptors. *Int. J. Fertil. Steril.* 7, 43–48.

Boron, D., Nowakowski, R., Grabarek, B. O., Zmarzly, N., and Oplawski, M. (2021). Expression pattern of leptin and its receptors in endometrioid endometrial cancer. *J. Clin. Med.* 10, 2787. doi:10.3390/jcm10132787

Boutas, I., Kontogeorgi, A., Dimitrakakis, C., and Kalantaridou, S. N. (2021). The expression of galectin-3 in endometrial cancer: A systematic review of the literature. *Mol. Biol. Rep.* 48, 5699–5705. doi:10.1007/s11033-021-06536-1

Brustmann, H., Riss, D., and Naude, S. (2003). Galectin-3 expression in normal, hyperplastic, and neoplastic endometrial tissues. *Pathol. Res. Pract.* 199, 151–158. doi:10.1078/0344-0338-00368

Caamano, J., and Hunter, C. A. (2002). NF-kappaB family of transcription factors: Central regulators of innate and adaptive immune functions. *Clin. Microbiol. Rev.* 15, 414–429. doi:10.1128/cmr.15.3.414-429.2002

Cai, Z. F., Deng, L., Wang, M. M., Zhang, J. Q., and Li, L. (2018). [Effect of AMPK/mTOR/S6K1 pathways and the insulin-sensitizing effect for adiponectin in endometrial cancer cells]. *Zhonghua Fu Chan Ke Za Zhi* 53, 554–560. doi:10.3760/cma.j.issn.0529-567x.2018.08.008

Carino, C., Olawaiye, A. B., Cherfils, S., Serikawa, T., Lynch, M. P., Rueda, B. R., et al. (2008). Leptin regulation of proangiogenic molecules in benign and cancerous endometrial cells. *Int. J. Cancer* 123, 2782–2790. doi:10.1002/ijc.23887

Catalano, S., Giordano, C., Rizza, P., Gu, G., Barone, I., Bonofiglio, D., et al. (2009). Evidence that leptin through STAT and CREB signaling enhances cyclin D1 expression and promotes human endometrial cancer proliferation. *J. Cell. Physiol.* 218, 490–500. doi:10.1002/jcp.21622

Chen, J. Y., and Liao, Q. P. (2009). [Expression and function of cyclooxygenase-2 in endometrial carcinoma]. *Beijing Da Xue Xue Bao Yi Xue Ban.* 41, 657–663.

Chen, X., Xiang, Y. B., Long, J. R., Cai, H., Cai, Q., Cheng, J., et al. (2012). Genetic polymorphisms in obesity-related genes and endometrial cancer risk. *Cancer* 118, 3356–3364. doi:10.1002/cncr.26552

Chetry, M., Thapa, S., Hu, X., Song, Y., Zhang, J., Zhu, H., et al. (2018). The role of galectins in tumor progression, treatment and prognosis of gynecological cancers. *J. Cancer* 9, 4742–4755. doi:10.7150/jca.23628

Chopra, V., Dinh, T. V., and Hannigan, E. V. (1997). Serum levels of interleukins, growth factors and angiogenin in patients with endometrial cancer. *J. Cancer Res. Clin. Oncol.* 123, 167–172. doi:10.1007/BF01214669

Chou, F. C., Chen, H. Y., Kuo, C. C., and Sytwu, H. K. (2018). Role of galectins in tumors and in clinical immunotherapy. *Int. J. Mol. Sci.* 19, 430. doi:10.3390/ijms19020430

Cicekdal, M. B., Kazan, B. T., Tuna, B. G., Ozorhan, U., Ekici, I. D., Zhu, F., et al. (2020). Effects of two types of calorie restriction on methylation levels of adiponectin receptor 1 (AdipoR1) and leptin receptor overlapping transcript (leprot) in a MMTV-TGF-alpha breast cancer mouse model. *Br. J. Nutr.* 123, 1079. doi:10.1017/S0007114520000471

Ciortea, R., Susman, S., Malutan, A. M., Berceanu, C., Mocan-Hognogi, R. F., Bucuri, C. E., et al. (2018). Mesenchymal stem cells derived from adipose tissue and Ishikawa cells co-culture highlight the role of adiponectin in endometrial cancer pathogenesis. *Rom. J. Morphol. Embryol.* 59, 1165–1172.

Cong, L., Gasser, J., Zhao, J., Yang, B., Li, F., and Zhao, A. Z. (2007). Human adiponectin inhibits cell growth and induces apoptosis in human endometrial carcinoma cells, HEC-1-A and RL95 2. *Endocr. Relat. Cancer* 14, 713–720. doi:10.1677/ERC-07-0065

Cust, A. E., Kaaks, R., Friedenreich, C., Bonnet, F., Laville, M., Lukanova, A., et al. (2007). Plasma adiponectin levels and endometrial cancer risk in pre- and postmenopausal women. *J. Clin. Endocrinol. Metab.* 92, 255–263. doi:10.1210/jc.2006-1371

Cymbaluk, A., Chudecka-Głaz, A., and Rzepka-Gorska, I. (2008). Leptin levels in serum depending on Body Mass Index in patients with endometrial hyperplasia and cancer. *Eur. J. Obstet. Gynecol. Reprod. Biol.* 136, 74–77. doi:10.1016/j.ejogrb.2006.08.012

Cymbaluk-Ploska, A., Chudecka-Glaz, A., Pius-Sadowska, E., Sompolska-Rzechula, A., Machalinski, B., and Menkiszak, J. (2018). Circulating serum level of visfatin in patients with endometrial cancer. *Biomed. Res. Int.* 2018, 8576179. doi:10.1155/2018/8576179

Cymbaluk-Ploska, A., Gargulinska, P., Chudecka-Glaz, A., Kwiatkowski, S., Pius-Sadowska, E., and Machalinski, B. (2020). The suitability of FGF21 and FGF23 as new biomarkers in endometrial cancer patients. *Diagnostics* 10, 414. doi:10.3390/diagnostics10060414

Cymbaluk-Ploska, A., Gargulinska, P., Kwiatkowski, S., Pius-Sadowska, E., and Machalinski, B. (2020). Could galectin 3 Be a good prognostic factor in endometrial cancer?. *Diagnostics*, 10, 635. doi:10.3390/diagnostics10090635

Dabrus, D., Kielbasinski, R., Grabarek, B. O., and Boron, D. (2020). Evaluation of the impact of cisplatin on variances in the expression pattern of leptin-related genes in endometrial cancer cells. *Int. J. Mol. Sci.* 21, 4135. doi:10.3390/ijms21114135

Daley-Brown, D., Harbuzariu, A., Kurian, A. A., Oprea-Ilies, G., and Gonzalez-Perez, R. R. (2019). Leptin-induced Notch and IL-1 signaling crosstalk in endometrial adenocarcinoma is associated with invasiveness and chemoresistance. *World J. Clin. Oncol.* 10, 222–233. doi:10.5306/wjco.v10.i6.222

Daley-Brown, D., Oprea-Iles, G., Vann, K. T., Lanier, V., Lee, R., Candelaria, P. V., et al. (2017). Type II endometrial cancer overexpresses NILCO: A preliminary evaluation. *Dis. Markers* 2017, 8248175. doi:10.1155/2017/8248175

Dallal, C. M., Brinton, L. A., Bauer, D. C., Buist, D. S., Cauley, J. A., Hue, T. F., et al. (2013). Obesity-related hormones and endometrial cancer among postmenopausal women: A nested case-control study within the B~FIT cohort. *Endocr. Relat. Cancer* 20, 151–160. doi:10.1530/ERC-12-0229

Ding, S., Madu, C. O., and Lu, Y. (2020). The impact of hormonal imbalances associated with obesity on the incidence of endometrial cancer in postmenopausal women. *J. Cancer* 11, 5456–5465. doi:10.7150/jca.47580

Dirat, B., Bochet, L., Dabek, M., Daviaud, D., Dauvillier, S., Majed, B., et al. (2011). Cancer-associated adipocytes exhibit an activated phenotype and contribute to breast cancer invasion. *Cancer Res.* 71, 2455–2465. doi:10.1158/0008-5472.CAN-10-3323

Ege, C. B., Akbulut, M., Zekioglu, O., and Ozdemir, N. (2011). Investigation of galectin-3 and heparanase in endometrioid and serous carcinomas of the endometrium and correlation with known predictors of survival. *Arch. Gynecol. Obstet.* 284, 1231–1239. doi:10.1007/s00404-010-1766-9

Ellis, P. E., Barron, G. A., and Bermano, G. (2020). Adipocytokines and their relationship to endometrial cancer risk: A systematic review and meta-analysis. *Gynecol. Oncol.* 158, 507–516. doi:10.1016/j.ygyno.2020.05.033

Erdogan, S., Sezer, S., Baser, E., Gun-Eryilmaz, O., Gungor, T., Uysal, S., et al. (2013). Evaluating vaspin and adiponectin in postmenopausal women with endometrial cancer. *Endocr. Relat. Cancer* 20, 669–675. doi:10.1530/ERC-13-0280

Fortuna-Costa, A., Gomes, A. M., Kozlowski, E. O., Stelling, M. P., and Pavao, M. S. (2014). Extracellular galectin-3 in tumor progression and metastasis. *Front. Oncol.* 4, 138. doi:10.3389/fonc.2014.00138

Fredstorp-Lidebring, M., Bendahl, P. O., Brunner, N., Casslen, B., Hogberg, T., Langstrom-Einarsson, E., et al. (2001). Urokinase plasminogen activator and its inhibitor, PAI-1, in association with progression-free survival in early stage endometrial cancer. *Eur. J. Cancer* 37, 2339–2348. doi:10.1016/s0959-8049(01)00306-9

Fujimoto, J., Hori, M., Ichigo, S., and Tamaya, T. (1996). Sex steroids regulate the expression of plasminogen activator inhibitor-1 (PAI-1) and its mRNA in uterine endometrial cancer cell line Ishikawa. *J. Steroid Biochem. Mol. Biol.* 59, 1–8. doi:10.1016/s0960-0760(96)00084-2

Fujimoto, J., and Sato, E. (2011). Sex steroids in uterine endometrial cancers. *Horm. Mol. Biol. Clin. Investig.* 5, 143–151. doi:10.1515/HMBCI.2010.049

Fukuhara, A., Matsuda, M., Nishizawa, M., Segawa, K., Tanaka, M., Kishimoto, K., et al. (2005). Visfatin: A protein secreted by visceral fat that mimics the effects of insulin. *Science* 307, 426–430. doi:10.1126/science.1097243

Gao, J., Tian, J., Lv, Y., Shi, F., Kong, F., Shi, H., et al. (2009). Leptin induces functional activation of cyclooxygenase-2 through JAK2/STAT3, MAPK/ERK, and PI3K/AKT pathways in human endometrial cancer cells. *Cancer Sci.* 100, 389–395. doi:10.1111/j.1349-7006.2008.01053.x

Garikapati, K. K., Ammu, Vvvrk, Krishnamurthy, P. T., Chintamaneni, P. K., and Pindiprolu., S. (2019). Possible role of thiazolidinedione in the management of type-II endometrial cancer. *Med. Hypotheses* 126, 78–81. doi:10.1016/j.mehy.2019.03.014

Gharpure, K. M., Pradeep, S., Sans, M., Rupaimoole, R., Ivan, C., Wu, S. Y., et al. (2018). FABP4 as a key determinant of metastatic potential of ovarian cancer. *Nat. Commun.* 9, 2923. doi:10.1038/s41467-018-04987-y

Goel, H. L., and Mercurio, A. M. (2013). VEGF targets the tumour cell. *Nat. Rev. Cancer* 13, 871–882. doi:10.1038/nrc3627

Goldstein, B. J., and Scalia, R. (2004). Adiponectin: A novel adipokine linking adipocytes and vascular function. *J. Clin. Endocrinol. Metab.* 89, 2563–2568. doi:10.1210/jc.2004-0518

Gong, C., Liu, Y., Xiao, W., Yin, J., Wang, D. H., and Sheng, H. (2007). The role of ERK1/2 in leptin promoting the proliferation of human endometrial cancer cell line Ishikawa. *Ai Zheng* 26, 1211–1214.

Gotte, M., Mohr, C., Koo, C. Y., Stock, C., Vaske, A. K., Viola, M., et al. (2010). miR-145-dependent targeting of junctional adhesion molecule A and modulation of fascin expression are associated with reduced breast cancer cell motility and invasiveness. *Oncogene* 29, 6569–6580. doi:10.1038/onc.2010.386

Grosfeld, A., Andre, J., Hauguel-De Mouzon, S., Berra, E., Pouyssegur, J., and Guerre-Millo, M. (2002). Hypoxia-inducible factor 1 transactivates the human leptin gene promoter. *J. Biol. Chem.* 277, 42953–42957. doi:10.1074/jbc.M206775200

Hefetz-Sela, S., and Scherer, P. E. (2013). Adipocytes: Impact on tumor growth and potential sites for therapeutic intervention. *Pharmacol. Ther.* 138, 197–210. doi:10.1016/j.pharmthera.2013.01.008

Hegyi, K., Fulop, K., Kovacs, K., Toth, S., and Falus, A. (2004). Leptin-induced signal transduction pathways. *Cell Biol. Int.* 28, 159–169. doi:10.1016/j.cellbi.2003.12.003

Henderson, N. C., and Sethi, T. (2009). The regulation of inflammation by galectin-3. *Immunol. Rev.* 230, 160–171. doi:10.1111/j.1600-065X.2009.00794.x

Hernandez, J. D., Nguyen, J. T., He, J., Wang, W., Ardman, B., Green, J. M., et al. (2006). Galectin-1 binds different CD43 glycoforms to cluster CD43 and regulate T cell death. *J. Immunol.* 177, 5328–5336. doi:10.4049/jimmunol.177.8.5328

Hoesel, B., and Schmid, J. A. (2013). The complexity of NF-κB signaling in inflammation and cancer. *Mol. Cancer* 12, 86. doi:10.1186/1476-4598-12-86

Horowitz, N. S., and Wright, A. A. (2015). Impact of obesity on chemotherapy management and outcomes in women with gynecologic malignancies. *Gynecol. Oncol.* 138, 201–206. doi:10.1016/j.ygyno.2015.04.002

Hotamisligil, G. S., and Bernlohr, D. A. (2015). Metabolic functions of FABPs-mechanisms and therapeutic implications. *Nat. Rev. Endocrinol.* 11, 592–605. doi:10.1038/nrendo.2015.122

Hu, E., Liang, P., and Spiegelman, B. M. (1996). AdipoQ is a novel adipose-specific gene dysregulated in obesity. *J. Biol. Chem.* 271, 10697–10703. doi:10.1074/jbc.271.18.10697

Huang, Q., Peng, L., Sun, Y., Huang, J., Han, T., Li, Y., et al. (2021). miR-593-3p promotes proliferation and invasion in prostate cancer cells by targeting ADIPOR1. *Onco. Targets. Ther.* 14, 3729–3737. doi:10.2147/OTT.S310198

Ito, R., Narita, S., Huang, M., Nara, T., Numakura, K., Takayama, K., et al. (2017). The impact of obesity and adiponectin signaling in patients with renal cell carcinoma: A potential mechanism for the "obesity paradox". *PLoS One* 12, e0171615. doi:10.1371/journal.pone.0171615

Jalving, M., Gietema, J. A., Lefrandt, J. D., de Jong, S., Reyners, A. K., Gans, R. O., et al. (2010). Metformin: Taking away the candy for cancer? *Eur. J. Cancer* 46, 2369–2380. doi:10.1016/j.ejca.2010.06.012

Jin, J. H., Kim, H. J., Kim, C. Y., Kim, Y. H., Ju, W., and Kim, S. C. (2016). Association of plasma adiponectin and leptin levels with the development and progression of ovarian cancer. *Obstet. Gynecol. Sci.* 59, 279–285. doi:10.5468/ogs.2016.59.4.279

Jin, J., Zhang, Z., Zhang, S., Chen, X., Chen, Z., Hu, P., et al. (2018). Fatty acid binding protein 4 promotes epithelial-mesenchymal transition in cervical squamous cell carcinoma through AKT/GSK3β/Snail signaling pathway. *Mol. Cell. Endocrinol.* 461, 155–164. doi:10.1016/j.mce.2017.09.005

Kadowaki, T., and Yamauchi, T. (2005). Adiponectin and adiponectin receptors. *Endocr. Rev.* 26, 439–451. doi:10.1210/er.2005-0005

Kaklamani, V., Yi, N., Zhang, K., Sadim, M., Offit, K., Oddoux, C., et al. (2011). Polymorphisms of ADIPOQ and ADIPOR1 and prostate cancer risk. *Metabolism.* 60, 1234–1243. doi:10.1016/j.metabol.2011.01.005

Koda, M., Sulkowska, M., Wincewicz, A., Kanczuga-Koda, L., Musiatowicz, B., Szymanska, M., et al. (2007). Expression of leptin, leptin receptor, and hypoxia-inducible factor 1 alpha in human endometrial cancer. *Ann. N. Y. Acad. Sci.* 1095, 90–98. doi:10.1196/annals.1397.013

Koh, K. K., Han, S. H., and Quon, M. J. (2005). Inflammatory markers and the metabolic syndrome: Insights from therapeutic interventions. *J. Am. Coll. Cardiol.* 46, 1978–1985. doi:10.1016/j.jacc.2005.06.082

Kohler, U., Hiller, K., Martin, R., Langanke, D., Naumann, G., Bilek, K., et al. (1997). Tumor-associated proteolytic factors uPA and PAI-1 in endometrial carcinoma. *Gynecol. Oncol.* 66, 268–274. doi:10.1006/gyno.1997.4751

Konieczna, A., Novakova, V., Medalova, J., Erceg, S., and Klabusay, M. (2015). Thiazolidinediones regulate the level of ABC transporters expression on lung cancer cells. *Klin. Onkol.* 28, 431–438. doi:10.14735/amko2015431

Lanier, V., Gillespie, C., Leffers, M., Daley-Brown, D., Milner, J., Lipsey, C., et al. (2016). Leptin-induced transphosphorylation of vascular endothelial growth factor receptor increases Notch and stimulates endothelial cell angiogenic transformation. *Int. J. Biochem. Cell Biol.* 79, 139–150. doi:10.1016/j.biocel.2016.08.023

Larsson, S. C., Spyrou, N., and Mantzoros, C. S. (2022). Body fatness associations with cancer: Evidence from recent epidemiological studies and future directions. *Metabolism.* 137, 155326. doi:10.1016/j.metabol.2022.155326

Lee, C. H., Lui, D. T. W., Cheung, C. Y. Y., Fong, C. H. Y., Yuen, M. M. A., Chow, W. S., et al. (2020). Response to letter to the editor: "Higher circulating adiponectin concentrations predict incident cancer in type 2 diabetes - the adiponectin paradox". *J. Clin. Endocrinol. Metab.* 105, dgaa386. doi:10.1210/clinem/dgaa386

Lei, C., Zhang, W., Sun, X., Du, G., Wang, L., and Liu, Y. (2007). Effects of galectin-3 inhibition on endometrial cell cycle and adhesion. *Front. Med. China* 1, 390–397. doi:10.1007/s11684-007-0076-5

Li, L., and Kalantar-Zadeh, K. (2013). Obesity that makes kidney cancer more likely but helps fight it more strongly. *J. Natl. Cancer Inst.* 105, 1848–1849. doi:10.1093/jnci/djt348

Li, S., Wang, Z., Huang, J., Fan, J., Du, H., Liu, L., et al. (2017). Systematic review of prognostic roles of body mass index for patients undergoing lung cancer surgery: Does the obesity paradox really exist? *Eur. J. Cardiothorac. Surg.* 51, 817–828. doi:10.1093/ejcts/ezw386

Lin, L. L., Kost, E. R., Lin, C. L., Valente, P., Wang, C. M., Kolonin, M. G., et al. (2020). PAI-1-Dependent inactivation of SMAD4-modulated junction and adhesion complex in obese endometrial cancer. *Cell Rep.* 33, 108253. doi:10.1016/j.celrep.2020.108253

Lin, T., Zhao, X., and Kong, W. M. (2015). Association between adiponectin levels and endometrial carcinoma risk: Evidence from a dose-response meta-analysis. *BMJ Open* 5, e008541. doi:10.1136/bmjopen-2015-008541

Linkov, F., Goughnour, S. L., Adambekov, S., Lokshin, A., Kelley, J. L., Sukumvanich, P., et al. (2018). Inflammatory biomarker in adipose stem cells of women with endometrial cancer. *Biomark. Med.* 12, 945–952. doi:10.2217/bmm-2017-0355

Linkov, F., Maxwell, G. L., Felix, A. S., Lin, Y., Lenzner, D., Bovbjerg, D. H., et al. (2012). Longitudinal evaluation of cancer-associated biomarkers before and after weight loss in RENEW study participants: Implications for cancer risk reduction. *Gynecol. Oncol.* 125, 114–119. doi:10.1016/j.ygyno.2011.12.439

Lipsey, C. C., Harbuzariu, A., Daley-Brown, D., and Gonzalez-Perez, R. R. (2016). Oncogenic role of leptin and Notch interleukin-1 leptin crosstalk outcome in cancer. *World J. Methodol.* 6, 43–55. doi:10.5662/wjm.v6.i1.43

Liu, F. T., Patterson, R. J., and Wang, J. L. (2002). Intracellular functions of galectins. *Biochim. Biophys. Acta* 1572, 263–273. doi:10.1016/s0304-4165(02)00313-6

Liu, L., Wang, L., Zheng, J., and Tang, G. (2013). Leptin promotes human endometrial carcinoma cell proliferation by enhancing aromatase (P450arom) expression and estradiol formation. *Eur. J. Obstet. Gynecol. Reprod. Biol.* 170, 198–201. doi:10.1016/j.ejogrb.2013.04.004

Ma, X., Hui, Y., Lin, L., Wu, Y., Zhang, X., and Liu, P. (2015). Clinical significance of COX-2, GLUT-1 and VEGF expressions in endometrial cancer tissues. *Pak. J. Med. Sci.* 31, 280–284. doi:10.12669/pjms.312.6604

Ma, Y., Liu, Z., Zhang, Y., and Lu, B. (2013). Serum leptin, adiponectin and endometrial cancer risk in Chinese women. *J. Gynecol. Oncol.* 24, 336–341. doi:10.3802/jgo.2013.24.4.336

Madeddu, C., Sanna, E., Gramignano, G., Tanca, L., Cherchi, M. C., Mola, B., et al. (2022). Correlation of leptin, proinflammatory cytokines and oxidative stress with tumor size and disease stage of endometrioid (type I) endometrial cancer and review

of the underlying mechanisms. *Cancers (Basel)* 14, 268. doi:10.3390/cancers14020268

Maeda, K., Okubo, K., Shimomura, I., Funahashi, T., Matsuzawa, Y., and Matsubara, K. (1996). cDNA cloning and expression of a novel adipose specific collagen-like factor, apM1 (AdiPose Most abundant Gene transcript 1). *Biochem. Biophys. Res. Commun.* 221, 286–289. doi:10.1006/bbrc.1996.0587

Mantzos, F., Vanakara, P., Samara, S., Wozniak, G., Kollia, P., Messinis, I., et al. (2011). Leptin receptor expression in neoplastic and normal ovarian and endometrial tissue. *Eur. J. Gynaecol. Oncol.* 32, 84–86.

Markl, B., Hardt, J., Franz, S., Schaller, T., Schenkirsch, G., Kriening, B., et al. (2017). Tumor budding, uPA, and PAI-1 in colorectal cancer: Update of a prospective study. *Gastroenterol. Res. Pract.* 2017, 6504960. doi:10.1155/2017/6504960

May, M. J., and Ghosh, S. (1997). Rel/NF-kappa B and I kappa B proteins: An overview. *Semin. Cancer Biol.* 8, 63–73. doi:10.1006/scbi.1997.0057

Mihu, D., Ciortea, R., and Mihu, C. M. (2013). Abdominal adiposity through adipocyte secretion products, a risk factor for endometrial cancer. *Gynecol. Endocrinol.* 29, 448–451. doi:10.3109/09513590.2012.752452

Mocino-Rodriguez, M. D., Santillan-Benitez, J. G., Dozal-Dominguez, D. S., Hernandez-Navarro, M. D., Flores-Merino, M. V., Sandoval-Cabrera, A., et al. (2017). Expression of AdipoR1 and AdipoR2 receptors as leptin-breast cancer regulation mechanisms. *Dis. Markers* 2017, 4862016. doi:10.1155/2017/4862016

Moon, H. S., Chamberland, J. P., Aronis, K., Tseleni-Balafouta, S., and Mantzoros, C. S. (2011). Direct role of adiponectin and adiponectin receptors in endometrial cancer: *In vitro* and *ex vivo* studies in humans. *Mol. Cancer Ther.* 10, 2234–2243. doi:10.1158/1535-7163.MCT-11-0545

Morice, P., Leary, A., Creutzberg, C., Abu-Rustum, N., and Darai, E. (2016). Endometrial cancer. *Lancet* 387, 1094–1108. doi:10.1016/S0140-6736(15)00130-0

Moukarzel, L. A., Ferrando, L., Stylianou, A., Lobaugh, S., Wu, M., Nobre, S. P., et al. (2022). Impact of obesity and white adipose tissue inflammation on the omental microenvironment in endometrial cancer. *Cancer* 128, 3297–3309. doi:10.1002/cncr.34356

Mu, N., Zhu, Y., Wang, Y., Zhang, H., and Xue, F. (2012). Insulin resistance: A significant risk factor of endometrial cancer. *Gynecol. Oncol.* 125, 751–757. doi:10.1016/j.ygyno.2012.03.032

Murphy, K. A., James, B. R., Sjaastad, F. V., Kucaba, T. A., Kim, H., Brincks, E. L., et al. (2018). Cutting edge: Elevated leptin during diet-induced obesity reduces the efficacy of tumor immunotherapy. *J. Immunol.* 201, 1837–1841. doi:10.4049/jimmunol.1701738

Mylonas, I., Mayr, D., Walzel, H., Shabani, N., Dian, D., Kuhn, C., et al. (2007). Mucin 1, thomsen-friedenreich expression and galectin-1 binding in endometrioid adenocarcinoma: An immunohistochemical analysis. *Anticancer Res.* 27, 1975–1980.

Nakano, Y., Tobe, T., Choi-Miura, N. H., Mazda, T., and Tomita, M. (1996). Isolation and characterization of GBP28, a novel gelatin-binding protein purified from human plasma. *J. Biochem.* 120, 803–812. doi:10.1093/oxfordjournals.jbchem.a021483

Nergiz Avcioglu, S., Altinkaya, S. O., Kucuk, M., Yuksel, H., Omurlu, I. K., and Yanik, S. (2015). Visfatin concentrations in patients with endometrial cancer. *Gynecol. Endocrinol.* 31, 202–207. doi:10.3109/09513590.2014.975687

Noble, L. S., Simpson, E. R., Johns, A., and Bulun, S. E. (1996). Aromatase expression in endometriosis. *J. Clin. Endocrinol. Metab.* 81, 174–179. doi:10.1210/jcem.81.1.8550748

Oaknin, A., Bosse, T. J., Creutzberg, C. L., Giornelli, G., Harter, P., Joly, F., et al.Esmo Guidelines Committee (2022). Electronic address: clinicalguidelines@esmo.orgEndometrial cancer: ESMO clinical practice guideline for diagnosis, treatment and follow-up. *Ann. Oncol.* 33, 860–877. doi:10.1016/j.annonc.2022.05.009

Oplawski, M., Dziobek, K., Zmarzly, N., Grabarek, B. O., Kielbasinski, R., Kieszkowski, P., et al. (2020). Variances in the level of COX-2 and iNOS in different grades of endometrial cancer. *Curr. Pharm. Biotechnol.* 21, 52–59. doi:10.2174/1389201020666190918104105

Osmak, M., Babic, D., Abramic, M., Milicic, D., Vrhovec, I., and Skrk, J. (2001). Plasminogen activator inhibitor type 2: Potential prognostic factor for endometrial carcinomas. *Neoplasma* 48, 462–467.

Ozgor, B. Y., Iyibozkurt, C., Bastu, E., Berkman, S., Yalcin, O., Cakmakoglu, B., et al. (2019). Investigation of resistin 420 and 62 gene polymorphism in patients with endometrial cancer. *Taiwan. J. Obstet. Gynecol.* 58, 164–167. doi:10.1016/j.tjog.2018.11.030

Pallares, J., Martinez-Guitarte, J. L., Dolcet, X., Llobet, D., Rue, M., Palacios, J., et al. (2004). Abnormalities in the NF-kappaB family and related proteins in endometrial carcinoma. *J. Pathol.* 204, 569–577. doi:10.1002/path.1666

Peng-Fei, H., Ru Na, A., Hui, C., Hong-Yu, W., and Jin-Shan, C. (2021). Activation of alpha7 nicotinic acetylcholine receptor protects bovine endometrial tissue against LPS-induced inflammatory injury via JAK2/STAT3 pathway and COX-2 derived prostaglandin E(2). *Eur. J. Pharmacol.* 900, 174067. doi:10.1016/j.ejphar.2021.174067

Petridou, E., Belechri, M., Dessypris, N., Koukoulomatis, P., Diakomanolis, E., Spanos, E., et al. (2002). Leptin and body mass index in relation to endometrial cancer risk. *Ann. Nutr. Metab.* 46, 147–151. doi:10.1159/000063081

Petridou, E., Mantzoros, C., Dessypris, N., Koukoulomatis, P., Addy, C., Voulgaris, Z., et al. (2003). Plasma adiponectin concentrations in relation to endometrial cancer: A case-control study in Greece. *J. Clin. Endocrinol. Metab.* 88, 993–997. doi:10.1210/jc.2002-021209

Rajput, P. K., Sharma, J. R., and Yadav, U. C. S. (2022). Cellular and molecular insights into the roles of visfatin in breast cancer cells plasticity programs. *Life Sci.* 304, 120706. doi:10.1016/j.lfs.2022.120706

Ray, I., Meira, L. B., Michael, A., and Ellis, P. E. (2022). Adipocytokines and disease progression in endometrial cancer: A systematic review. *Cancer Metastasis Rev.* 41, 211–242. doi:10.1007/s10555-021-10002-6

Rodriguez-Barbero, A., Dorado, F., Velasco, S., Pandiella, A., Banas, B., and Lopez-Novoa, J. M. (2006). TGF-beta1 induces COX-2 expression and PGE2 synthesis through MAPK and PI3K pathways in human mesangial cells. *Kidney Int.* 70, 901–909. doi:10.1038/sj.ki.5001626

Rzepka-Gorska, I., Bedner, R., Cymbaluk-Ploska, A., and Chudecka-Glaz, A. (2008). Serum adiponectin in relation to endometrial cancer and endometrial hyperplasia with atypia in obese women. *Eur. J. Gynaecol. Oncol.* 29, 594–597.

Sakers, A., De Siqueira, M. K., Seale, P., and Villanueva, C. J. (2022). Adipose-tissue plasticity in health and disease. *Cell* 185, 419–446. doi:10.1016/j.cell.2021.12.016

Salmani Javan, E., Lotfi, F., Jafari-Gharabaghlou, D., Mousazadeh, H., Dadashpour, M., and Zarghami, N. (2022). Development of a magnetic nanostructure for Co-delivery of metformin and silibinin on growth of lung cancer cells: Possible action through leptin gene and its receptor regulation. *Asian pac. J. Cancer Prev.* 23, 519–527. doi:10.31557/APJCP.2022.23.2.519

Scherer, P. E., Williams, S., Fogliano, M., Baldini, G., and Lodish, H. F. (1995). A novel serum protein similar to C1q, produced exclusively in adipocytes. *J. Biol. Chem.* 270, 26746–26749. doi:10.1074/jbc.270.45.26746

Schmitt, M., Mengele, K., Napieralski, R., Magdolen, V., Reuning, U., Gkazepis, A., et al. (2010). Clinical utility of level-of-evidence-1 disease forecast cancer biomarkers uPA and its inhibitor PAI-1. *Expert Rev. Mol. diagn.* 10, 1051–1067. doi:10.1586/erm.10.71

Sen, R., and Baltimore, D. (1986). Multiple nuclear factors interact with the immunoglobulin enhancer sequences. *Cell* 46, 705–716. doi:10.1016/0092-8674(86)90346-6

Sharma, D., Saxena, N. K., Vertino, P. M., and Anania, F. A. (2006). Leptin promotes the proliferative response and invasiveness in human endometrial cancer cells by activating multiple signal-transduction pathways. *Endocr. Relat. Cancer* 13, 629–640. doi:10.1677/erc.1.01169

Shetty, A., Venkatesh, T., Tsutsumi, R., and Suresh, P. S. (2020). Gene expression changes and promoter methylation with the combined effects of estradiol and leptin in uterine tissue of the ovariectomized mice model of menopause. *Mol. Biol. Rep.* 47, 151–168. doi:10.1007/s11033-019-05116-8

Soliman, P. T., Wu, D., Tortolero-Luna, G., Schmeler, K. M., Slomovitz, B. M., Bray, M. S., et al. (2006). Association between adiponectin, insulin resistance, and endometrial cancer. *Cancer* 106, 2376–2381. doi:10.1002/cncr.21866

Steiner, E., Pollow, K., Hasenclever, D., Schormann, W., Hermes, M., Schmidt, M., et al. (2008). Role of urokinase-type plasminogen activator (uPA) and plasminogen activator inhibitor type 1 (PAI-1) for prognosis in endometrial cancer. *Gynecol. Oncol.* 108, 569–576. doi:10.1016/j.ygyno.2007.11.025

Stewart, C. J., Brennan, B. A., Leung, Y. C., and Little, L. (2009). MELF pattern invasion in endometrial carcinoma: Association with low grade, myoinvasive endometrioid tumours, focal mucinous differentiation and vascular invasion. *Pathology* 41, 454–459. doi:10.1080/00313020903041135

Su, C. K., Yeh, K. T., Yeh, C. B., Wang, P. H., Ho, E. S., Chou, M. C., et al. (2011). Genetic polymorphism of the plasminogen activator inhibitor-1 is associated with an increased risk of endometrial cancer. *J. Surg. Oncol.* 104, 755–759. doi:10.1002/jso.22035

Sun, K., Wernstedt Asterholm, I., Kusminski, C. M., Bueno, A. C., Wang, Z. V., Pollard, J. W., et al. (2012). Dichotomous effects of VEGF-A on adipose tissue dysfunction. *Proc. Natl. Acad. Sci. U. S. A.* 109, 5874–5879. doi:10.1073/pnas.1200447109

Sun, K. X., Zheng, R. S., Zuo, J., Zhang, S. W., Zeng, H. M., Wang, S. M., et al. (2022). [The incidence and mortality of endometrial cancer in China, 2015.

Zhonghua Yi Xue Za Zhi 102, 1987–1992. doi:10.3760/cma.j.cn112137-20211029-02403

Sun, X. F., and Dai, S. Y. (2020). The significance of galectin-1 and galectin-9 expression in endometrial carcinoma. *Gynecol. Obstet. Invest.* 85, 34–40. doi:10.1159/000502787

Sung, H., Ferlay, J., Siegel, R. L., Laversanne, M., Soerjomataram, I., Jemal, A., et al. (2021). Global cancer statistics 2020: GLOBOCAN estimates of incidence and mortality worldwide for 36 cancers in 185 countries. *Ca. Cancer J. Clin.* 71, 209–249. doi:10.3322/caac.21660

Takemura, Y., Osuga, Y., Yamauchi, T., Kobayashi, M., Harada, M., Hirata, T., et al. (2006). Expression of adiponectin receptors and its possible implication in the human endometrium. *Endocrinology* 147, 3203–3210. doi:10.1210/en.2005-1510

Tecimer, C., Doering, D. L., Goldsmith, L. J., Meyer, J. S., Abdulhay, G., and Wittliff, J. L. (2001). Clinical relevance of urokinase-type plasminogen activator, its receptor, and its inhibitor type 1 in endometrial cancer. *Gynecol. Oncol.* 80, 48–55. doi:10.1006/gyno.2000.6015

Tessitore, L., Vizio, B., Pesola, D., Cecchini, F., Mussa, A., Argiles, J. M., et al. (2004). Adipocyte expression and circulating levels of leptin increase in both gynaecological and breast cancer patients. *Int. J. Oncol.* 24, 1529–1535.

Thijssen, V. L., and Griffioen, A. W. (2014). Galectin-1 and -9 in angiogenesis: A sweet couple. *Glycobiology* 24, 915–920. doi:10.1093/glycob/cwu048

Tian, W., Zhang, H., Zhang, Y., Wang, Y., Zhang, Y., Xue, F., et al. (2020). High level of visfatin and the activation of Akt and ERK1/2 signaling pathways are associated with endometrium malignant transformation in polycystic ovary syndrome. *Gynecol. Endocrinol.* 36, 156–161. doi:10.1080/09513590.2019.1650340

Tian, W., Zhu, Y., Wang, Y., Teng, F., Zhang, H., Liu, G., et al. (2013). Visfatin, a potential biomarker and prognostic factor for endometrial cancer. *Gynecol. Oncol.* 129, 505–512. doi:10.1016/j.ygyno.2013.02.022

Trayhurn, P., and Wood, I. S. (2004). Adipokines: Inflammation and the pleiotropic role of white adipose tissue. *Br. J. Nutr.* 92, 347–355. doi:10.1079/bjn20041213

Tsujii, M., Kawano, S., Tsuji, S., Sawaoka, H., Hori, M., and DuBois, R. N. (1998). Cyclooxygenase regulates angiogenesis induced by colon cancer cells. *Cell* 93, 705–716. doi:10.1016/s0092-8674(00)81433-6

van den Brule, F. A., Buicu, C., Berchuck, A., Bast, R. C., Deprez, M., Liu, F. T., et al. (1996). Expression of the 67-kD laminin receptor, galectin-1, and galectin-3 in advanced human uterine adenocarcinoma. *Hum. Pathol.* 27, 1185–1191. doi:10.1016/s0046-8177(96)90313-5

Van Le, L., Haskill, S., Jaffe, G. J., and Fowler, W. C., Jr. (1991). Expression of interleukin-1 and interleukin-1 receptor antagonists in endometrial cancer. *Gynecol. Oncol.* 42, 161–164. doi:10.1016/0090-8258(91)90338-6

Waldman, A. D., Fritz, J. M., and Lenardo, M. J. (2020). A guide to cancer immunotherapy: from T cell basic science to clinical practice. *Nat. Rev. Immunol.* 20, 651–668. doi:10.1038/s41577-020-0306-5

Wang, J., Peng, Y., Guo, H., and Li, C. (2021). PAI-1 polymorphisms have significant associations with cancer risk, especially feminine cancer. *Technol. Cancer Res. Treat.* 20, 15330338211037813. doi:10.1177/15330338211037813

Wang, Y., Gao, C., Zhang, Y., Gao, J., Teng, F., Tian, W., et al. (2016). Visfatin stimulates endometrial cancer cell proliferation via activation of PI3K/Akt and MAPK/ERK1/2 signalling pathways. *Gynecol. Oncol.* 143, 168–178. doi:10.1016/j.ygyno.2016.07.109

Wang, Z., Gao, S., Sun, C., Li, J., Gao, W., and Yu, L. (2019). Clinical significance of serum adiponectin and visfatin levels in endometrial cancer. *Int. J. Gynaecol. Obstet.* 145, 34–39. doi:10.1002/ijgo.12772

Wincewicz, A., Koda, M., Sulkowska, M., Kanczuga-Koda, L., and Sulkowski, S. (2008). Comparison of STAT3 with HIF-1alpha, Ob and ObR expressions in human endometrioid adenocarcinomas. *Tissue Cell* 40, 405–410. doi:10.1016/j.tice.2008.04.004

Wu, X., Yan, Q., Zhang, Z., Du, G., and Wan, X. (2012). Acrp30 inhibits leptin-induced metastasis by downregulating the JAK/STAT3 pathway via AMPK activation in aggressive SPEC-2 endometrial cancer cells. *Oncol. Rep.* 27, 1488–1496. doi:10.3892/or.2012.1670

Wu, Z., Jeong, J. H., Ren, C., Yang, L., Ding, L., Li, F., et al. (2021). Fatty acid-binding protein 4 (FABP4) suppresses proliferation and migration of endometrial cancer cells via PI3K/akt pathway. *Onco. Targets. Ther.* 14, 3929–3942. doi:10.2147/OTT.S311792

Xu, X., Xie, Y., Lin, Y., Xu, X., Zhu, Y., Mao, Y., et al. (2012). PAI-1 promoter 4G/5G polymorphism (rs1799768) contributes to tumor susceptibility: Evidence from meta-analysis. *Exp. Ther. Med.* 4, 1127–1133. doi:10.3892/etm.2012.734

Yabushita, H., Iwasaki, K., Obayashi, Y., and Wakatsuki, A. (2014). Clinicopathological roles of adiponectin and leptin receptors in endometrial carcinoma. *Oncol. Lett.* 7, 1109–1117. doi:10.3892/ol.2014.1846

Yamauchi, N., Takazawa, Y., Maeda, D., Hibiya, T., Tanaka, M., Iwabu, M., et al. (2012). Expression levels of adiponectin receptors are decreased in human endometrial adenocarcinoma tissues. *Int. J. Gynecol. Pathol.* 31, 352–357. doi:10.1097/PGP.0b013e3182469583

Yamauchi, T., Kamon, J., Ito, Y., Tsuchida, A., Yokomizo, T., Kita, S., et al. (2003). Cloning of adiponectin receptors that mediate antidiabetic metabolic effects. *Nature* 423, 762–769. doi:10.1038/nature01705

Yoon, J. K., Byeon, H. E., Ko, S. A., Park, B. N., An, Y. S., Lee, H. Y., et al. (2020). Cell cycle synchronisation using thiazolidinediones affects cellular glucose metabolism and enhances the therapeutic effect of 2-deoxyglucose in colon cancer. *Sci. Rep.* 10, 4713. doi:10.1038/s41598-020-61661-4

Yuan, S. S., Tsai, K. B., Chung, Y. F., Chan, T. F., Yeh, Y. T., Tsai, L. Y., et al. (2004). Aberrant expression and possible involvement of the leptin receptor in endometrial cancer. *Gynecol. Oncol.* 92, 769–775. doi:10.1016/j.ygyno.2003.11.043

Yunusova, N. V., Kondakova, I. V., Kolomiets, L. A., Afanasiev, S. G., Chernyshova, A. L., Shatokhina, O. V., et al. (2015). [Serum adipokines and their receptors in endometrial and colon cancer patients: Relationship with tumor invasion and metastasis]. *Vopr. Onkol.* 61, 619–623.

Zeng, F., Shi, J., Long, Y., Tian, H., Li, X., Zhao, A. Z., et al. (2015). Adiponectin and endometrial cancer: A systematic review and meta-analysis. *Cell. Physiol. biochem.* 36, 1670–1678. doi:10.1159/000430327

Zhang, L. Q., Heruth, D. P., and Ye, S. Q. (2011). Nicotinamide phosphoribosyltransferase in human diseases. *J. Bioanal. Biomed.* 3, 13–25. doi:10.4172/1948-593X.1000038

Zhang, L., Wen, K., Han, X., Liu, R., and Qu, Q. (2015). Adiponectin mediates antiproliferative and apoptotic responses in endometrial carcinoma by the AdipoRs/AMPK pathway. *Gynecol. Oncol.* 137, 311–320. doi:10.1016/j.ygyno.2015.02.012

Zhang, W., Ling, D., Tan, J., Zhang, J., and Li, L. (2013). Expression of urokinase plasminogen activator and plasminogen activator inhibitor type-1 in ovarian cancer and its clinical significance. *Oncol. Rep.* 29, 637–645. doi:10.3892/or.2012.2148

Zhang, Y., Proenca, R., Maffei, M., Barone, M., Leopold, L., and Friedman, J. M. (1994). Positional cloning of the mouse obese gene and its human homologue. *Nature* 372, 425–432. doi:10.1038/372425a0

Zhao, Q., Li, J. Y., Zhang, J., Long, Y. X., Li, Y. J., Guo, X. D., et al. (2020). Role of visfatin in promoting proliferation and invasion of colorectal cancer cells by downregulating SDF-1/CXCR4-mediated miR-140-3p expression. *Eur. Rev. Med. Pharmacol. Sci.* 24, 5367–5377. doi:10.26355/eurrev_202005_21320

Zhou, X., Li, H., Chai, Y., and Liu, Z. (2015). Leptin inhibits the apoptosis of endometrial carcinoma cells through activation of the nuclear factor κB-inducing kinase/i?b kinase pathway. *Int. J. Gynecol. Cancer* 25, 770–778. doi:10.1097/IGC.0000000000000440

Zinovkin, D. A., Achinovich, S. L., Zubritskiy, M. G., Whatmore, J. L., and Pranjol, M. Z. I. (2019). High expression of galectin-1, VEGF and increased microvessel density are associated with MELF pattern in stage I-iii endometrioid endometrial adenocarcinoma. *J. Pathol. Transl. Med.* 53, 280–288. doi:10.4132/jptm.2019.05.13

Zinovkin, D. A., Pranjol, M. Z. I., Petrenyov, D. R., Nadyrov, E. A., and Savchenko, O. G. (2017). The potential roles of MELF-pattern, microvessel density, and VEGF expression in survival of patients with endometrioid endometrial carcinoma: A morphometrical and immunohistochemical analysis of 100 cases. *J. Pathol. Transl. Med.* 51, 456–462. doi:10.4132/jptm.2017.07.19

frontiers | Frontiers in Pharmacology

TYPE Review
PUBLISHED 16 December 2022
DOI 10.3389/fphar.2022.1009952

OPEN ACCESS

EDITED BY
Hai-Long Piao,
Dalian Institute of Chemical Physics (CAS), China

REVIEWED BY
Zhiyang Li,
Nanjing Drum Tower Hospital, China
Bilikere S. Dwarakanath,
Sri Ramachandra Institute of Higher Education and Research, India

*CORRESPONDENCE
Gang Huang,
huanggang@sumhs.edu.cn
Hao Yang,
yangh@sumhs.edu.cn

SPECIALTY SECTION
This article was submitted to Pharmacology of Anti-Cancer Drugs, a section of the journal Frontiers in Pharmacology

RECEIVED 02 August 2022
ACCEPTED 07 December 2022
PUBLISHED 16 December 2022

CITATION
Yang H, Wang J and Huang G (2022), Small extracellular vesicles in metabolic remodeling of tumor cells: Cargos and translational application.
Front. Pharmacol. 13:1009952.
doi: 10.3389/fphar.2022.1009952

Small extracellular vesicles in metabolic remodeling of tumor cells: Cargos and translational application

Hao Yang[1]*, Jingyi Wang[2] and Gang Huang[1,2]*

[1]Shanghai Key Laboratory of Molecular Imaging, Jiading District Central Hospital Affiliated Shanghai University of Medicine and Health Sciences, Shanghai, China, [2]Department of Nuclear Medicine, Shanghai Chest Hospital, Shanghai Jiao Tong University, Shanghai, China

Warburg effect is characterized by excessive consumption of glucose by the tumor cells under both aerobic and hypoxic conditions. This metabolic reprogramming allows the tumor cells to adapt to the unique microenvironment and proliferate rapidly, and also promotes tumor metastasis and therapy resistance. Metabolic reprogramming of tumor cells is driven by the aberrant expression and activity of metabolic enzymes, which results in the accumulation of oncometabolites, and the hyperactivation of intracellular growth signals. Recent studies suggest that tumor-associated metabolic remodeling also depends on intercellular communication within the tumor microenvironment (TME). Small extracellular vesicles (sEVs), also known as exosomes, are smaller than 200 nm in diameter and are formed by the fusion of multivesicular bodies with the plasma membrane. The sEVs are instrumental in transporting cargoes such as proteins, nucleic acids or metabolites between the tumor, stromal and immune cells of the TME, and are thus involved in reprogramming the glucose metabolism of recipient cells. In this review, we have summarized the biogenesis and functions of sEVs and metabolic cargos, and the mechanisms through they drive the Warburg effect. Furthermore, the potential applications of targeting sEV-mediated metabolic pathways in tumor liquid biopsy, imaging diagnosis and drug development have also been discussed.

KEYWORDS

small extracellular vesicles, exosomes, warburg effect, tumor metabolism, liquid biopsy, glycolysis, drug development

1 Introduction

Tumor cells can rapidly utilize glucose through "aerobic glycolysis" and produce high levels of lactate—a phenomenon known as the Warburg effect. Hanahan and Weinberg characterized this metabolic reprogramming of tumor cells as one of the hallmarks of cancer, and a potential therapeutic target (Hanahan and Weinberg, 2011; Hanahan, 2022). The Warburg effect is primarily driven by the aberrant expression of key metabolic enzymes, production of oncometabolites, and overactivation of growth signals (Vander

Heiden et al., 2009; Liberti and Locasale, 2016; Poff et al., 2019). The key enzymes of glycolysis, including hexokinase 2 (HK2), 6-phosphofructo-2-kinase/fructose-2,6-bisphosphatase-3 (PFKFB3) and pyruvate kinase M2 (PKM2), promote the conversion of glucose to lactate instead of pyruvate in the tumor cells, which in turn impairs mitochondrial oxidative phosphorylation (Minchenko et al., 2002; Yang et al., 2014; Xu and Herschman, 2019). Furthermore, glucose 6-phosphate dehydrogenase (G6PD) produces ribose and NADPH in the tumor cells through the pentose phosphate pathway (PPP) as a source of energy for tumor growth (Jiang et al., 2011; Deng et al., 2021). Therefore, understanding the complex mechanisms underlying glucose uptake and metabolism by tumors, and the role of the tumor microenvironment (TME), can improve diagnostic accuracy and aid in drug development.

According to the classification criteria of the International Society for Extracellular Vesicles (ISEV), small extracellular vesicles (sEVs) or exosomes measure less than 200 nm in diameter, and are formed by the fusion of multivesicular bodies with the plasma membrane. They are typically secreted by tumor cells and other cells in the TME into various body fluids (Théry et al., 2018; Armacki et al., 2020; Möller and Lobb, 2020; Wu et al., 2021). The sEVs contain a large number of functional proteins, nucleic acid fragments (including DNA, mRNA or non-coding RNA) and other biologically active substances from the parent cells, and thus mediate transport and information exchange between cells. Most tumor cells release higher amounts of sEVs compared to normal cells. The tumor-derived sEVs promote angiogenesis, induce chemoresistance and differentiation of stromal cells in the TME, and regulate immune responses and the pre-metastatic microenvironment (Li and Nabet, 2019; Mashouri et al., 2019; Yousefi et al., 2020). Studies show that the sEVs in TME can also regulate tumor metabolism by directly delivering metabolic enzymes, metabolites or other factors to the recipient cells (Zhao et al., 2016; Wang et al., 2020b). Furthermore, these metabolically reprogrammed sEVs also modulate glucose uptake by tumor cells and other TME components, including stromal cells, immune cells and fibroblasts (Zhao et al., 2016; Yan et al., 2018; Rai et al., 2019; Morrissey et al., 2021). In this review, we have summarized the mechanisms through which the sEVs mediate the crosstalk between tumor cells and the TME, and propose possible applications of targeting sEV-related metabolic pathways for precise diagnosis and effective treatment of tumors.

2 Sorting of metabolic cargoes into sEVs and secretion

Tumor-specific sEVs can directly trigger the Warburg effect by transporting metabolites, enzymes, and the regulatory proteins and RNAs throughout the TME. The different intracellular components are loaded into sEVs through distinct sorting mechanisms (Figure 1). The biogenesis of sEVs is initiated following the inward budding of the membranes of multivesicular bodies (MVBs) to form intraluminal vesicles (ILVs). The mature MVBs fuse either with the plasma membrane and are expelled as sEVs, or with the lysosomes and are broken down (Anand et al., 2019). Rab GTPases act as the molecular switches that control ILV formation and transport within MVBs. The protein cargo is first sorted into the ILVs by tetraspanins and the endosomal sorting complex required for transport (ESCRT). VAMP2, VAMP3, VAMP7 and VAMP8 on the surface of MVBs form a SNARE complex with SNAP-23 on the plasma membrane, which releases the ILVs as sEVs (Clancy et al., 2019; Kumar et al., 2020; Zhang et al., 2021b). Pyruvate kinase M2 (PKM2) is co-sorted into the sEVs with the SNARE complex by phosphorylating SANP-23. In addition, the intra-vesicular PKM2 also promotes the exocytosis of sEVs from tumor cells (Wei et al., 2017; Fan et al., 2022). Lipids such as phospholipids and cholesterol are sorted into the sEVs by forming lipid rafts that are incorporated into sEV membranes (Zebrowska et al., 2019; Kumar and Deep, 2020). The sorting mechanism of other metabolites, including sugars, amino acids, nucleotides or vitamins, are not completely understood.

The mechanism underlying exosomal sorting of RNAs has been partially revealed (Liu et al., 2021). The RNA-binding Y-box protein I (YBX1) and Lupus La protein are required for loading miR-223 and miR-122 into sEVs, and is dependent on the high affinity of miRNAs for these RNA-binding proteins (Shurtleff et al., 2016; Temoche-Diaz et al., 2019). In fact, miRNAs that are sorted into sEVs possess similar motifs, and are enriched in the vesicles by specific RNA-binding proteins (Garcia-Martin et al., 2022b). For long RNAs such as mRNAs or lncRNAs, hnRNP A2B1 is responsible for binding to the corresponding motifs and sorting them into sEVs (O'Grady et al., 2022). The exact mechanism through which circRNAs are sorted into sEVs is still being explored, and studies suggest that it is likely accomplished through a miRNA binding-dependent manner or *via* direct interaction with RNA-binding proteins (Bao et al., 2016; Xu et al., 2020).

3 sEVs as drivers of Warburg effect

As already mentioned, the sEVs derived from tumor cells and TME components (fibroblasts, epithelial cells, macrophages, NK cells and other immune cells) reprogram glucose metabolism in tumor tissues by transporting proteins (metabolic enzymes, membrane proteins and other growth signaling proteins), nucleic acids (miRNAs, lncRNAs, circRNAs and mRNAs) and metabolites. The resulting dysregulation in metabolic pathways promote tumor progression, metastasis, and therapy resistance (Göran Ronquist, 2019; Zhang et al., 2021a). The contents of sEVs that regulate the Warburg effect are listed in Table 1.

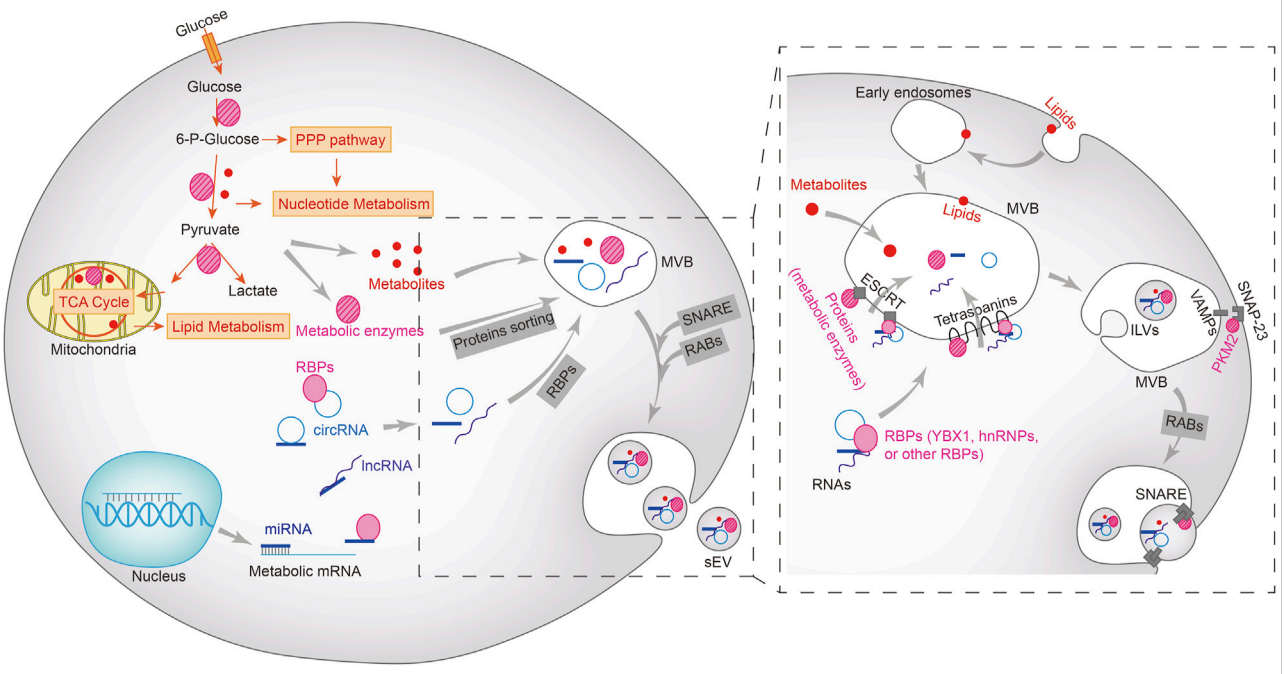

FIGURE 1
Metabolic cargoes in sEVs and their packaging, sorting and biogenesis. Metabolic enzymes and other regulatory proteins, metabolites, miRNAs, lncRNAs, and circRNAs are sorted into multivesicular bodies (MVBs) in different ways and subsequently excretes from the cells *via* the vesicle secretion pathways. Lipids (including phospholipids, sphingolipids, or triglycerides) on the plasma membrane enter MVBs *via* the early endosomes, but the sorting mechanism of other metabolites remains unclear. Proteins, including metabolic enzymes as well as RNA-bound RNA binding proteins (RBPs) enter the MVBs through ESCRT-dependent or independent mechanisms. The intraluminal vesicles (ILVs) in MVBs bind to the plasma membrane to form SNARE complex, which facilitates the extracellular release of sEV.

3.1 Metabolic enzymes in sEV

The hypoxic environment within solid tumors is a major inducer of Warburg Effect. Ovarian cancer cell-derived sEVs load higher levels of hexokinase (HK), UDP-glucuronosyltransferase, 6-phosphogluconolactonase and CTP synthase 1, which are the key enzymes in glucose, phospholipid and nucleic acid metabolism, when exposed to hypoxic conditions (Alharbi et al., 2021). These sEVs loaded with metabolic enzymes are critical for the development of platinum resistance in ovarian cancer. In a previous study, we showed that cisplatin-resistant non-small cell lung cancer (NSCLC) cells transmitted drug resistance to sensitive cells by secreting PKM2-loaded exosomes in response to hypoxic stimulation (Wang et al., 2021). Thus, inhibiting glucose metabolism could potentially reduce sEV-mediated chemoresistance in cancer cells. For example, pancreatic cancer cells with autophagy blockade exhibited low glucose uptake and expressed low levels of ATP-binding cassette sub-family G member 2 (ABCG2) in the secreted exosomes, which restored gemcitabine sensitivity (Bhattacharya et al., 2014). Although oxidative phosphorylation is attenuated in tumor cells, some enzymes of the Krebs cycle are also released within sEVs. We previously observed that exosomal release of cytoplasmic IDH1 promoted 5FU resistance in colorectal cancer cells (Yang et al., 2021). In addition to chemoresistance, exosomal metabolic enzymes can also enhance other malignant features such as invasion, metastasis, angiogenesis and immune escape. For example, exosomal angiopoietin-like protein 7 (ANGPTL7) secreted by the human ovarian cancer cells can promote tumor angiogenesis by regulating glucose and lipid metabolism, and oxidative stress (Parri et al., 2014). Several studies in recent years have established the presence of metabolic enzymes in sEVs and their impact on oncogenic signaling networks. Retinoblastoma-derived exosomes are enriched in multiple metabolic enzymes, including enolase 3 (ENO3), galactokinase-1 (GALK1), asparagine synthase (ASNS) and saccharopine dehydrogenase (SCCPDH) (Galardi et al., 2020). Taken together, transmission of metabolic enzymes *via* sEVs affects tumor progression through metabolic or non-metabolic signaling pathways.

3.2 Metabolites in sEV

Tumor or TME-derived sEVs can modulate tumor progression by transporting specific metabolites to distant

TABLE 1 sEV cargoes and mechanisms involved in the regulation of the Warburg effect.

Cargo type	sEV cargos	Cells of origin	Target	Biological behavior or application	Reference
Protein	HK1/2/3	Hypoxic ovarian cancer	Glycolysis	Carboplatin resistance	Alharbi et al. (2021)
	PKM2	Hypoxic NSCLC, gastric cancer	Glycolysis	Cisplatin resistance	Wang et al. (2021), Dai et al. (2022), Wu et al. (2022), Zhou et al. (2022)
	ITGB4	TNBC	Glycolysis	Growth and metastasis	Sung et al. (2020)
	HMGB-1, PD-L1	Lung adenocarcinoma	Glycolysis, nitric oxide metabolism	Suppressive immunity of macrophages	Morrissey et al. (2021), Wei et al. (2021)
	LMP1	Nasopharyngeal carcinoma	Glycolysis, Oxidative phosphorylation	CAF formation, radioresistance	Aga et al. (2014), Wu et al. (2020)
	ALDOA, GAPDH, LDHA/B, PGK1, PKM1/2	HPV-driven oropharyngeal cancer	Glycolysis	Tumor diagnosis	Tang et al. (2021)
	IDH1	Colorectal cancer	NADPH metabolism	5FU resistance	Yang et al. (2021)
	ENO3, GALK1, ASNS, SCCPDH	Retinoblastoma	Glucose metabolism	Intravitreal tumor metastasis	Galardi et al. (2020)
	ANGPTL7	Ovarian cancer	Glucose and lipid metabolism	Angiogenesis	Parri et al. (2014)
	ABCG2	Pancreatic cancer	Glucose uptake	Gemcitabine resistance	Bhattacharya et al. (2014), Giovannetti et al. (2017)
miRNA	miR-122	Breast cancer	PKM2, Glycolysis	Brain/lung metastases	Fong et al. (2015), Li et al. (2019)
	miR-451	Gastric cancer	AMPK/mTOR	T cell immunity	Liu et al. (2018), Li et al. (2021)
	miR-543	Epithelial ovarian cancer	Proteoglycan pathway	Tumor proliferation	Zhang et al. (2022)
LncRNA	MALAT1	NSCLC	Glycolysis	Tumor proliferation	Zhang et al. (2017), Wang et al. (2020a)
	TUG1	CAF	Glycolysis	Lung metastases of liver cancer	Lu et al. (2022)
	HISLA	Tumor-associated macrophages	Glycolysis	HIF-1α	Chen et al. (2019)
CircRNA	circ_0005963	Colorectal cancer	PKM2, Glycolysis	Oxaliplatin resistance	Wang et al. (2020c)
	circ-RNF121	Colorectal cancer	Glycolysis	Invasion and metastasis	Jiang et al. (2021)
	circ_0008928	NSCLC	HK2, Glycolysis	Cisplatin resistance	Shi et al. (2021)
	circ_0072083	Glioma cells	Glycolysis	TMZ resistance	Ding et al. (2021)
	circCCT3	Liver cancer related CAF	HK2, Glycolysis	Tumor proliferation	Lv et al. (2020)
	circARHGAP10	NSCLC	Glycolysis	Tumor proliferation	Fang et al. (2022)
Metabolites	Lactate, acetate, stearic acid, palmitic acid, amino acid	Prostate and pancreatic cancer related -CAF	Central carbon metabolism	Kras-dependent tumor growth	Zhao et al. (2016)
	Phosphatidylcholine	Mouse colon cancer cells	Lipid metabolisim	Insulin signaling resistance	Kumar et al. (2021)
	Linoleic acid	Lung adenocarcinoma	Glycolysis, nitric oxide metabolism	Suppressive immunity of macrophages	Morrissey et al. (2021)

tissues, immune cells, *etc.* For instance, colon cancer cells expressing CD63, CD9 and A33 are known to deliver exosomal phosphatidylcholine to liver tissues *via* the portal vein (Kumar et al., 2021). Furthermore, lung adenocarcinoma-derived exosomes are enriched in linoleic acid (LA) compared to those derived from normal lung epithelial cells, and promote

tumor metastasis by reprogramming macrophage glycolysis and PD-L1-dependent immunosuppression (Morrissey et al., 2021). Metabolomics have been used to identify the species, content and signaling pathways of metabolites in sEVs and other vesicles. Metabolite analysis of CAF-derived exosomes by gas chromatography-mass spectrometer (GC-MS) and ultra-high performance liquid chromatography (UPLC) revealed high levels of intermediates produced during glucose metabolism (such as citric acid and pyruvate), lipids (stearic and palmitic) and most amino acids (Zhao et al., 2016). However, the exact functions of these exosomal metabolites in tumor progression remains to be explored.

3.3 Nucleic acids regulate tumor metabolism *via* sEV

Exosomal nucleic acids, especially non-coding RNAs, are established diagnostic biomarkers of various tumors. Non-coding RNAs can promote or impede the Warburg effect by targeting specific metabolic enzymes or regulatory genes. For example, colorectal cancer cell-derived exosomal circ-RNF121 enhanced glycolysis and reduced ATP/ADP production in the tumor cells (Jiang et al., 2021). Furthermore, circ-0008928 is highly expressed in NSCLC cell-derived sEVs, and confers cisplatin resistance by acting as a "sponge" for miR-488, which enhances HK2 activity and glycolysis (Shi et al., 2021). NSCLC cells also secrete the lncRNA MALAT1 *via* sEVs, which is known to promote lactate dehydrogenase A (LDHA) expression and glycolysis (Wang et al., 2020a). Oxaliplatin-resistant colorectal cancer cells can transmit chemoresistance to the sensitive cells through exosomal circ-0005963, which sponges miR-122 and upregulates PKM2 (Wang et al., 2020c). Exosomal RNA-mediated decrease in glucose uptake in the normal tissues also contributes to tumor development. For instance, breast cancer cell-derived exosomal miR-122 drives brain/lung metastasis by downregulating PKM2 and inhibiting glucose uptake in distant non-tumor tissues (Fong et al., 2015). In addition to tumor cells, the stromal and immune cells of the TME also secrete sEVs that reprogram tumor metabolism. There is evidence that exosomal lncRNA TUG1 secreted by cancer-associated fibroblasts (CAFs) in HCC tissues increases LDH activity and lactate production in the tumor cells (Lu et al., 2022).

Interestingly, the metabolic reprograming induced by exosomal components exert a positive feedback by increasing cargo loading into the sEVs. For example, exosomal circ_0072083 derived from temozolomide (TMZ)-resistant glioma cells activates glycolysis and increases the levels of glucose transporter 1 (GLUT1), LDHA and PKM2, which further induce the expression of the circRNA and amplify TMZ resistance (Ding et al., 2021). Furthermore, the dissemination of sEVs in the TME also depends on the extracellular glucose status. Under energy-deficient low-glucose conditions, gastric cancer-derived exosomal miR-451 is more inclined to polarize T cells to the immunosuppressive Th17 cells, which leads to poor prognosis (Liu et al., 2018). In fact, tumor-derived sEVs can also trigger metabolic disorders, as exemplified by the interaction of pancreatic cancer and diabetes (Sah et al., 2019). Pancreatic cancer cell-derived exosomes delivered miR-19a to islet β cells and disrupted normal insulin secretion (Pang et al., 2021; Su et al., 2022), and reprogramed enteroendocrine cell function *via* multiple exosomal miRNAs (Zhang et al., 2018). Thus, TME-derived sEV RNA reprograms tumor glucose metabolism and creates favorable conditions for tumor cell growth and metastasis, while the sEV RNA cargo secreted by metabolically abnormal tumor cells also enhances the malignant potential.

3.4 Resident proteins in sEV

The sEVs derived from different tissues may express similar marker proteins, including CD9, CD63, CD81 or TSG101, which are used for their identification. However, most of these ubiquitous resident proteins of sEVs, most of which are membrane proteins, show differential expression across cell types during proteomics examination (Kowal et al., 2016; Rai et al., 2021; Garcia-Martin et al., 2022a). Some resident exosomal proteins are transferred to recipient cells, wherein they reprogram glucose metabolism. For example, nasopharyngeal carcinoma cell-derived sEVs can transform normal fibroblasts to a tumor-promoting phenotype by delivering latent membrane protein 1 (LMP1), which enhances glycolysis and inhibits mitochondrial oxidative phosphorylation *via* activation of the NF-κB pathway (Wu et al., 2020). Integrin beta 4 (ITGB4) is highly expressed on triple-negative breast cancer (TNBC) cells and their derived exosomes, and promotes glycolysis in CAFs through mitophagy (Sung et al., 2020). High mobility group box-1 (HMGB-1) is highly expressed in lung adenocarcinoma exosomes and promotes glycolysis in the tumor macrophages by upregulating PD-L1 expression (Morrissey et al., 2021). The 78 kDa glucose-regulated protein (GRP78) is translocated from the endoplasmic reticulum to the plasma membrane, and released *via* exosomes (Li et al., 2016; Gonzalez-Gronow et al., 2021). High expression of exosomal GRP78 in colorectal and breast tumors is associated with increased glycolysis and metastasis (Zheng et al., 2019; Li et al., 2022). Therefore, proteins that are differentially expressed in the tumor-derived exosomes relative to that secreted by normal cells should be considered as potential as biomarkers. Overall, tumor cell-derived sEV-resident proteins act as "villain messengers" by promoting malignant behaviors such as invasion, metastasis and immunosuppression through metabolic reprograming.

4 Application of targeting metabolic sEVs

Given their unique protein profiles, sEVs are promising biomarkers for early, non-invasive tumor detection, and for monitoring therapy (Liang et al., 2021). Tumor-derived exosomal protein or RNA cargoes can be easily detected in liquid biopsies for rapid diagnostic and prognostic evaluation. Furthermore, inhibitors of sEV secretion or the loaded cargos potential drug candidates for tumor therapy. In addition, *in vivo* imaging of sEVs can be used as a surrogate for tracking tumor progression and therapeutic efficacy.

4.1 Metabolic biomarkers for liquid biopsy

Proteomic mass spectrometry analysis of salivary exosomes from human papillomavirus (HPV)-driven oropharyngeal cancer patients revealed significantly elevated aldolase, glyceraldehyde dehydrogenase-3-phosphate dehydrogenase (GAPDH), LDHA/B, phosphoglycerate kinase 1 (PGK1) and PKM1/2 (Tang et al., 2021). Compared to healthy volunteers, serum-derived exosomal circARHGAP10 was upregulated in NSCLC patients, and associated with increased the expression of GLUT1 and LDH, which are drivers of NSCLC progression (Fang et al., 2022). Furthermore, presence of serum-derived exosomes with low levels of miR-543 in patients with epithelial ovarian cancer indicates favorable prognosis since downregulation of this miRNA inhibits glucose uptake by tumor cells (Zhang et al., 2022). Cancer stem cells (CSCs) drive tumor initiation, drug resistance and metastasis, and are the primary cause of tumor recurrence. Metabolomics analysis of CSCs-enriched primary melanoma tissues and serum-derived exosomes from melanoma patients revealed aberrant expression of multiple metabolites (Palacios-Ferrer et al., 2021). Thus, exosomal metabolites in liquid biopsies are ideal markers of tumor diagnosis, therapeutic efficacy and prognosis.

4.2 Therapeutic agents targeting metabolic regulators

Some small molecule drugs and natural compounds can inhibit tumor-associated sEV secretion or metabolic pathways, and are thus potential candidates for tumor therapy. The AMPK inhibitor compound C and the c-Jun inhibitor SP600125 blocked the delivery of exosomes from the TNBC cells into CAFs, which inhibited glycolysis and tumor cell proliferation (Sung et al., 2020). The sEV-mediated immunosuppression is partly attributed to the metabolic reprogramming of TME, and drugs targeting sEV-related tumor immunity are suitable for tumor therapy, such as immune checkpoint inhibitors (Marshall and Djamgoz, 2018; Bader et al., 2020; Yang et al., 2020). As already described, tumor cell-derived exosomes increased glucose uptake and PD-L1 expression in CAFs in an NF-kB-dependent manner, which was inhibited by the glycolysis inhibitor 2-deoxyglucose. Furthermore, tumor sEVs also inhibited oxidative phosphorylation in tumor-associated macrophages by upregulating NOS2 expression, and administration of the NOS2 inhibitor S-ethylisothiourea hydrobromide restored oxygen utilization (Kuruppu et al., 2014; Morrissey et al., 2021). In addition, coptisine disrupted the secretion of exosomal circCCT3 from CAFs and reduced the expression of HK2 in liver cancer cells (Lv et al., 2020), which has potential therapeutic value. The natural compound oleanolic acid reduced the secretion of exosomes from TMZ-resistant glioma cells, and shikonin inhibited resistant cells-derived exosomal circ_0072083 levels and the Warburg effect (Ding et al., 2021). These compounds have potential sensitizing effects on TMZ treatment of glioma. Therapeutic agents targeting sEV-related communications have also been shown to multidrug resistance -associated protein (MRP) -mediated resistance. The calmodulin-dependent protein kinase inhibitor KN-93 was used to reverse MSC sEV-mediated 5-FU resistance in gastric cancer (Ji et al., 2015). Mechanistically, these sEVs enhanced the expression of MRP and P-glycoprotein by regulating miR-301b and ERK kinase pathways (Ji et al., 2015; Zhu et al., 2022), which are inducers of glucose metabolism and malignant tumorigenesis (Asl et al., 2021; Jandova and Wondrak, 2021). However, the limitation lies in the lack of the effect of sEV from other TME components (other than MSC) on MRP and chemotherapy resistance. More studies are needed to explore the mechanism of chemotherapy resistance of metabolic sEV in order to develop therapeutic agents with relevant targets.

4.3 Metabolic imaging of sEVs in nuclear medicine

Due to the sentinel role of exosomes in early TME shaping and formation of the pre-metastatic niche, *in vivo* sEV imaging can be helpful for early tumor monitoring. At present, sEV imaging mainly focuses on tracking the fluorescently-labeled sEVs. For example, plasma membrane-specific fluorescent dyes such as DIR and PKH26 are commonly used to label exosomes and track them at the cellular level (Pužar Dominkuš et al., 2018; Sun et al., 2019; Kumar et al., 2021). Nuclear imaging, including ^{18}F-deoxyglucose (FDG)-positron emission tomography/computed tomography (PET/CT), is currently the main diagnostic method for evaluating tumor glucose uptake and metabolic activity, and offers the possibility for isotopic labeling and imaging of exosomes. Engineered exosomes labeled with radioisotopes (including ^{99m}Tc, ^{111}I, ^{125}I, ^{131}I, ^{64}Cu, ^{68}Ga) have achieved non-invasive PET or SPECT detection in animal models, and show promise for clinical translation (Morishita et al., 2015; Gangadaran et al.,

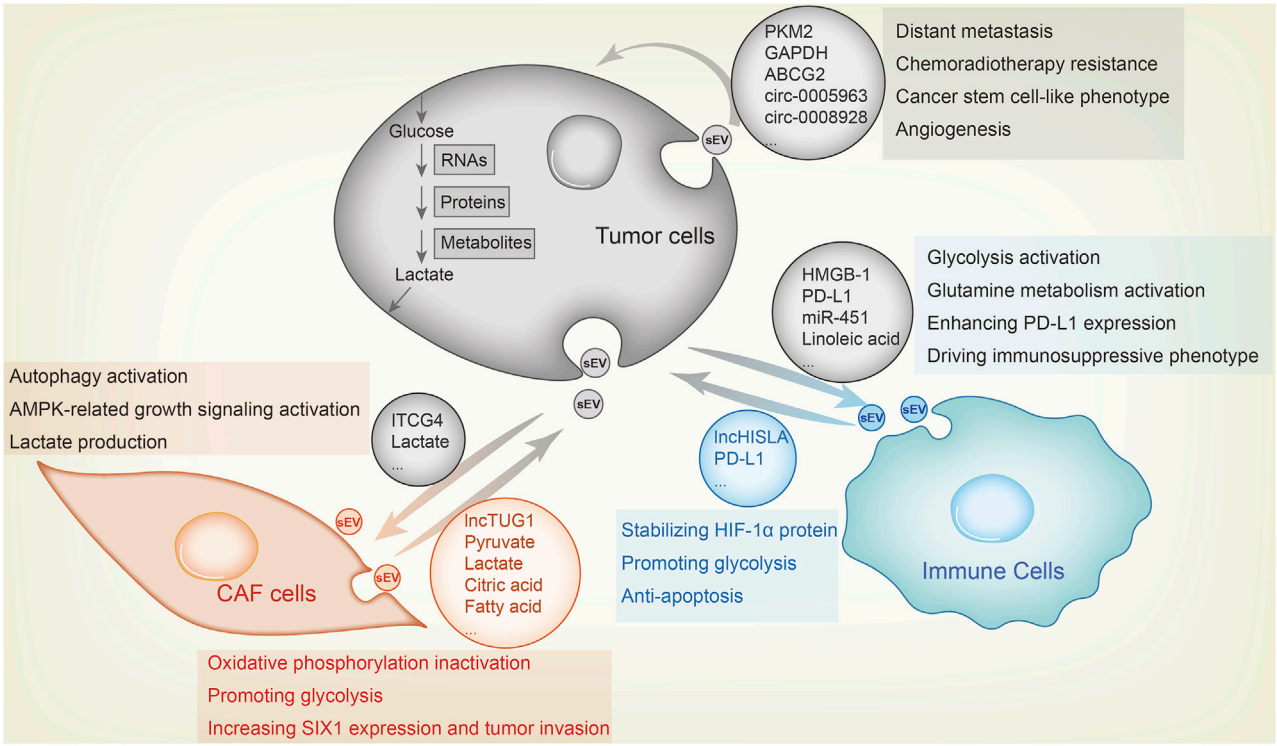

FIGURE 2
Metabolic sEV exchange between tumor cells and other components in the TME. The uptake of tumor-derived sEVs by CAFs or immune cells facilitates tumor growth, whereas tumor cell fusion of metabolic sEVs in TME leads to its malignant transformation. For example, CAFs-derived sEV lncRNA TUG1 delivers to liver cancer cells, increasing SIX1 expression and promoting glycolysis and tumor invasion. CAFs-derived sEVs inhibit oxidative phosphorylation and activates glycolysis by delivering lactate, pyruvate, citric acid, fatty acids and amino acids to pancreatic cancer cells. As feedback, breast cancer cells sEVs carry ITGB4 proteins that can be transmitted to CAFs, inducing autophagy, AMPK activation and lactate production in CAFs, which contribute to tumor invasion. As for the effect of sEV on immune cells, lung cancer-derived sEV HMGB1, PD-L1 and linoleic acid enhance glycolysis, glutamine metabolism and PD-L1 expression in macrophages and T cells through NF-κB signaling, endowing these immune cells with an immunosuppressive phenotype. MiR-451 in sEV of gastric cancer transmits to T cells and enhances their infiltration, causing them to differentiate to Th17 cells and forming malignant transformation of tumor microenvironment. Macrophages also secrete sEVs, which enhance aerobic glycolysis and anti-apoptosis of breast cancer cells by delivering lncRNA HISLA and stabilizing HIF-1α protein. Among tumor cells, highly metastatic cells, chemotherapy or radiotherapy resistant cells and cancer stem cell-like cells transfer sEV to sensitive cells to confer corresponding malignant phenotype.

2018; Rashid et al., 2019; Jung et al., 2020; Lázaro-Ibáñez et al., 2021).

Radio-labeled exosomes have excellent intra-tumoral homing ability and biosafety (Shi et al., 2019). FDG-PET imaging has been used to assess the function of exosomes in Alzheimer's disease development since glucose metabolism in the affected tissues correlates with the secretion of plasma-specific exosomes (Coumans et al., 2017; Chanteloup et al., 2019). In addition, FDG-PET imaging has also demonstrated the activation of glucose metabolism in breast tumor cells through EVs uptake (Kang et al., 2021). Furthermore, the enriched miRNA levels in plasma EVs from Hodgkin lymphoma patients matched the FDG PET imaging results, suggesting that EVs can be used for metabolic tracing in tumor patients (van Eijndhoven et al., 2016). In an *in vitro* study, ^{13}C isotope-labeled glucose was used to evaluate the effect of CAF-derived exosomes on the metabolites of glycolysis (Zhao et al., 2016). Although isotopic tracing of exosomes can be used for tumor imaging, very few studies have reported direct radiolabeling of metabolites in EVs for *in vivo* imaging.

5 Conclusion and perspectives

The Warburg effect is manifested as overactive glycolysis and aberrant activity of metabolic enzymes, and is instrumental for the rapid proliferation, invasiveness, drug resistance and immune escape of tumor cells. Extracellular vesicles (EVs) mediate intercellular communication in the TME, and the sEVs or exosomes have been studied the most. In this review, we outlined the mechanisms through which proteins, RNAs and metabolites are sorted into the sEVs within cells, as well as the

pathways regulated by the exosomal cargo to remodel tumor metabolism and promote tumor progression (Figure 2). Furthermore, we have also discussed the diagnostic and therapeutic potential of tumor-derived sEVs.

Analysis of exosomal protein mass spectrometry and sequencing data form EV databases such as ExoCarta, exoRBase or Vesiclepedia have also indicated that the resident metabolic enzymes or RNAs may be involved in regulating tumor metabolism (Kalra et al., 2012; Keerthikumar et al., 2016; Lai et al., 2021). Therefore, more sEV cargoes and functions may be discovered in the future, and provide new insights into tumor metabolic remodeling. Although some carbohydrate-metabolizing enzymes (such as HK2, ENO3 and PKM2) delivered *via* sEVs are known to remodel the TME, given the opposing functions of glycolytic and mitochondrial metabolic enzymes in the Warburg effect, it remains to be ascertained whether these enzymes exert different functions when sorted into sEVs and in the recipient cells. In addition, since tetraspanins may potentially regulate nutrient metabolism in tumor cells, their use as a biomarker of sEV protein cargo also needs to be considered (Wang et al., 2019; Najy et al., 2021).

The diagnostic, therapeutic and imaging applications of tumor-derived sEVs has gained considerable attention in recent years. Tumor patient-derived sEVs containing metabolic enzymes or miRNAs are diagnostic biomarkers, which opens up the possibility of developing rapid sEV isolation and microfluidic chip analysis of the cargo. ^{18}F-deoxyglucose (FDG) is routinely used as a tracer for the radiometabolic imaging of tumors during diagnosis and treatment evaluation (Jacobson and Chen, 2013; Yang et al., 2017; Sheikhbahaei et al., 2020). However, the clinical utility is somewhat limited. For example, FDG PET/CT is prone to inflammatory interference in cervical cancer, resulting in low diagnostic specificity (Dejanovic et al., 2021). In addition, tumors such as hepatocellular carcinoma (HCC) have a lower capacity for FDG uptake (Li et al., 2018). Therefore, isotope probes targeting tumor-specific sEVs offer more possibilities for the diagnosis of heterogeneous tumors than FDG. Although sEVs can be labeled with fluorophores or isotopes for *in vivo* tumor imaging, the metabolic components of sEVs cannot be directly labeled as yet. The development of metabolic enzyme-targeted probes or radionuclide-labeled metabolites will be a significant progress in tumor imaging and clinical decision-making. Finally, more therapeutic or engineered agents targeting the metabolic cargo in sEVs need to be developed as drug delivery systems. In conclusion, targeting metabolic sEVs will play an important role in tumor diagnosis and therapy.

Author contributions

Preparing the original manuscripts, HY and JW; writing and revising manuscripts, HY, JW, and GH. All authors have read and agreed to the published version of the manuscript.

Funding

This study was supported by grants from the National Natural Science Foundation of China (Grant Nos 82127807 and 81903065) and construction project of Shanghai Key Laboratory of Molecular Imaging (18DZ2260400).

Conflict of interest

The authors declare that the research was conducted in the absence of any commercial or financial relationships that could be construed as a potential conflict of interest.

Publisher's note

References

Aga, M., Bentz, G. L., Raffa, S., Torrisi, M. R., Kondo, S., Wakisaka, N., et al. (2014). Exosomal HIF1α supports invasive potential of nasopharyngeal carcinoma-associated LMP1-positive exosomes. *Oncogene* 33 (37), 4613–4622. doi:10.1038/onc.2014.66

Alharbi, M., Lai, A., Sharma, S., Kalita-de Croft, P., Godbole, N., Campos, A., et al. (2021). Extracellular vesicle transmission of chemoresistance to ovarian cancer cells is associated with hypoxia-induced expression of glycolytic pathway proteins, and prediction of epithelial ovarian cancer disease recurrence. *Cancers (Basel)* 13 (14), 3388. doi:10.3390/cancers13143388

Anand, S., Samuel, M., Kumar, S., and Mathivanan, S. (2019). Ticket to a bubble ride: Cargo sorting into exosomes and extracellular vesicles. *Biochim. Biophys. Acta. Proteins Proteom.* 1867 (12), 140203. doi:10.1016/j.bbapap.2019.02.005

Armacki, M., Polaschek, S., Waldenmaier, M., Morawe, M., Ruhland, C., Schmid, R., et al. (2020). Protein kinase D1, reduced in human pancreatic tumors, increases secretion of small extracellular vesicles from cancer cells that promote metastasis to lung in mice. *Gastroenterology* 159 (3), 10191019–10191035. doi:10.1053/j.gastro.2020.05.052

Asl, E. R., Amini, M., Najafi, S., Mansoori, B., Mokhtarzadeh, A., Mohammadi, A., et al. (2021). Interplay between MAPK/ERK signaling pathway and MicroRNAs: A crucial mechanism regulating cancer cell metabolism and tumor progression. *Life Sci.* 278, 119499. doi:10.1016/j.lfs.2021.119499

Bader, J. E., Voss, K., and Rathmell, J. C. (2020). Targeting metabolism to improve the tumor microenvironment for cancer immunotherapy. *Mol. Cell* 78 (6), 1019–1033. doi:10.1016/j.molcel.2020.05.034

Bao, C., Lyu, D., and Huang, S. (2016). Circular RNA expands its territory. *Mol. Cell. Oncol.* 3 (2), e1084443. doi:10.1080/23723556.2015.1084443

Bhattacharya, S., Pal, K., Sharma, A. K., Dutta, S. K., Lau, J. S., Yan, I. K., et al. (2014). GAIP interacting protein C-terminus regulates autophagy and exosome

biogenesis of pancreatic cancer through metabolic pathways. *PLoS One* 9 (12), e114409. doi:10.1371/journal.pone.0114409

Chanteloup, G., Cordonnier, M., Moreno-Ramos, T., Pytel, V., Matías-Guiu, J., Gobbo, J., et al. (2019). Exosomal HSP70 for monitoring of frontotemporal dementia and alzheimer's disease: Clinical and FDG-PET correlation. *J. Alzheimers Dis.* 71 (4), 1263–1269. doi:10.3233/jad-190545

Chen, F., Chen, J., Yang, L., Liu, J., Zhang, X., Zhang, Y., et al. (2019). Extracellular vesicle-packaged HIF-1α-stabilizing lncRNA from tumour-associated macrophages regulates aerobic glycolysis of breast cancer cells. *Nat. Cell Biol.* 21 (4), 498–510. doi:10.1038/s41556-019-0299-0

Clancy, J. W., Zhang, Y., Sheehan, C., and D'Souza-Schorey, C. (2019). An ARF6-Exportin-5 axis delivers pre-miRNA cargo to tumour microvesicles. *Nat. Cell Biol.* 21 (7), 856–866. doi:10.1038/s41556-019-0345-y

Coumans, F. A. W., Brisson, A. R., Buzas, E. I., Dignat-George, F., Drees, E. E. E., El-Andaloussi, S., et al. (2017). Methodological guidelines to study extracellular vesicles. *Circ. Res.* 120 (10), 1632–1648. doi:10.1161/circresaha.117.309417

Dai, Y., Liu, Y., Li, J., Jin, M., Yang, H., and Huang, G. (2022). Shikonin inhibited glycolysis and sensitized cisplatin treatment in non-small cell lung cancer cells via the exosomal pyruvate kinase M2 pathway. *Bioengineered* 13 (5), 13906–13918. doi:10.1080/21655979.2022.2086378

Dejanovic, D., Hansen, N. L., and Loft, A. (2021). PET/CT variants and pitfalls in gynecological cancers. *Semin. Nucl. Med.* 51 (6), 593–610. doi:10.1053/j.semnuclmed.2021.06.006

Deng, P., Li, K., Gu, F., Zhang, T., Zhao, W., Sun, M., et al. (2021). LINC00242/miR-1-3p/G6PD axis regulates Warburg effect and affects gastric cancer proliferation and apoptosis. *Mol. Med.* 27 (1), 9. doi:10.1186/s10020-020-00259-y

Ding, C., Yi, X., Chen, X., Wu, Z., You, H., Chen, X., et al. (2021). Warburg effect-promoted exosomal circ_0072083 releasing up-regulates NANGO expression through multiple pathways and enhances temozolomide resistance in glioma. *J. Exp. Clin. Cancer Res.* 40 (1), 164. doi:10.1186/s13046-021-01942-6

Fan, M., Sun, W., Gu, X., Lu, S., Shen, Q., Liu, X., et al. (2022). The critical role of STAT3 in biogenesis of tumor-derived exosomes with potency of inducing cancer cachexia *in vitro* and *in vivo*. *Oncogene* 41 (7), 1050–1062. doi:10.1038/s41388-021-02151-3

Fang, K., Chen, X., Qiu, F., Xu, J., Xiong, H., and Zhang, Z. (2022). Serum-derived exosomes-mediated circular RNA ARHGAP10 modulates the progression of non-small cell lung cancer through the miR-638/FAM83F Axis. *Cancer biother. Radiopharm.* 37 (2), 96–110. doi:10.1089/cbr.2019.3534

Fong, M. Y., Zhou, W., Liu, L., Alontaga, A. Y., Chandra, M., Ashby, J., et al. (2015). Breast-cancer-secreted miR-122 reprograms glucose metabolism in premetastatic niche to promote metastasis. *Nat. Cell Biol.* 17 (2), 183–194. doi:10.1038/ncb3094

Galardi, A., Colletti, M., Lavarello, C., Di Paolo, V., Mascio, P., Russo, I., et al. (2020). Proteomic profiling of retinoblastoma-derived exosomes reveals potential biomarkers of vitreous seeding. *Cancers (Basel)* 12 (6), 1555. doi:10.3390/cancers12061555

Gangadaran, P., Hong, C. M., Oh, J. M., Rajendran, R. L., Kalimuthu, S., Son, S. H., et al. (2018). *In vivo* non-invasive imaging of radio-labeled exosome-mimetics derived from red blood cells in mice. *Front. Pharmacol.* 9, 817. doi:10.3389/fphar.2018.00817

Garcia-Martin, R., Brandao, B. B., Thomou, T., Altindis, E., and Kahn, C. R. (2022a). Tissue differences in the exosomal/small extracellular vesicle proteome and their potential as indicators of altered tissue metabolism. *Cell Rep.* 38 (3), 110277. doi:10.1016/j.celrep.2021.110277

Garcia-Martin, R., Wang, G., Brandão, B. B., Zanotto, T. M., Shah, S., Kumar Patel, S., et al. (2022b). MicroRNA sequence codes for small extracellular vesicle release and cellular retention. *Nature* 601 (7893), 446–451. doi:10.1038/s41586-021-04234-3

Giovannetti, E., van der Borden, C. L., Frampton, A. E., Ali, A., Firuzi, O., and Peters, G. J. (2017). Never let it go: Stopping key mechanisms underlying metastasis to fight pancreatic cancer. *Semin. Cancer Biol.* 44, 43–59. doi:10.1016/j.semcancer.2017.04.006

Gonzalez-Gronow, M., Gopal, U., Austin, R. C., and Pizzo, S. V. (2021). Glucose-regulated protein (GRP78) is an important cell surface receptor for viral invasion, cancers, and neurological disorders. *IUBMB Life* 73 (6), 843–854. doi:10.1002/iub.2502

Göran Ronquist, K. (2019). Extracellular vesicles and energy metabolism. *Clin. Chim. Acta.* 488, 116–121. doi:10.1016/j.cca.2018.10.044

Hanahan, D. (2022). Hallmarks of cancer: New dimensions. *Cancer Discov.* 12 (1), 31–46. doi:10.1158/2159-8290.cd-21-1059

Hanahan, D., and Weinberg, R. A. (2011). Hallmarks of cancer: The next generation. *Cell* 144 (5), 646–674. doi:10.1016/j.cell.2011.02.013

Jacobson, O., and Chen, X. (2013). Interrogating tumor metabolism and tumor microenvironments using molecular positron emission tomography imaging. Theranostic approaches to improve therapeutics. *Pharmacol. Rev.* 65 (4), 1214–1256. doi:10.1124/pr.113.007625

Jandova, J., and Wondrak, G. T. (2021). Genomic GLO1 deletion modulates TXNIP expression, glucose metabolism, and redox homeostasis while accelerating human A375 malignant melanoma tumor growth. *Redox Biol.* 39, 101838. doi:10.1016/j.redox.2020.101838

Ji, R., Zhang, B., Zhang, X., Xue, J., Yuan, X., Yan, Y., et al. (2015). Exosomes derived from human mesenchymal stem cells confer drug resistance in gastric cancer. *Cell Cycle* 14 (15), 2473–2483. doi:10.1080/15384101.2015.1005530

Jiang, P., Du, W., Wang, X., Mancuso, A., Gao, X., Wu, M., et al. (2011). p53 regulates biosynthesis through direct inactivation of glucose-6-phosphate dehydrogenase. *Nat. Cell Biol.* 13 (3), 310–316. doi:10.1038/ncb2172

Jiang, Z., Hu, H., Hu, W., Hou, Z., Liu, W., Yu, Z., et al. (2021). Circ-RNF121 regulates tumor progression and glucose metabolism by miR-1224-5p/FOXM1 axis in colorectal cancer. *Cancer Cell Int.* 21 (1), 596. doi:10.1186/s12935-021-02290-3

Jung, K. O., Kim, Y.-H., Chung, S.-J., Lee, C.-H., Rhee, S., Pratx, G., et al. (2020). Identification of lymphatic and hematogenous routes of rapidly labeled radioactive and fluorescent exosomes through highly sensitive multimodal imaging. *Int. J. Mol. Sci.* 21 (21), 7850. doi:10.3390/ijms21217850

Kalra, H., Simpson, R. J., Ji, H., Aikawa, E., Altevogt, P., Askenase, P., et al. (2012). Vesiclepedia: A compendium for extracellular vesicles with continuous community annotation. *PLoS Biol.* 10 (12), e1001450. doi:10.1371/journal.pbio.1001450

Kang, S. Y., Lee, E. J., Byun, J. W., Han, D., Choi, Y., Hwang, D. W., et al. (2021). Extracellular vesicles induce an aggressive phenotype in luminal breast cancer cells via PKM2 phosphorylation. *Front. Oncol.* 11, 785450. doi:10.3389/fonc.2021.785450

Keerthikumar, S., Chisanga, D., Ariyaratne, D., Al Saffar, H., Anand, S., Zhao, K., et al. (2016). ExoCarta: A web-based compendium of exosomal cargo. *J. Mol. Biol.* 428 (4), 688–692. doi:10.1016/j.jmb.2015.09.019

Kowal, J., Arras, G., Colombo, M., Jouve, M., Morath, J. P., Primdal-Bengtson, B., et al. (2016). Proteomic comparison defines novel markers to characterize heterogeneous populations of extracellular vesicle subtypes. *Proc. Natl. Acad. Sci. U. S. A.* 113(8), E968–E977. doi: doi:doi:10.1073/pnas.1521230113

Kumar, A., and Deep, G. (2020). Hypoxia in tumor microenvironment regulates exosome biogenesis: Molecular mechanisms and translational opportunities. *Cancer Lett.* 479, 23–30. doi:10.1016/j.canlet.2020.03.017

Kumar, A., Sundaram, K., Mu, J., Dryden, G. W., Sriwastva, M. K., Lei, C., et al. (2021). High-fat diet-induced upregulation of exosomal phosphatidylcholine contributes to insulin resistance. *Nat. Commun.* 12 (1), 213. doi:10.1038/s41467-020-20500-w

Kumar, R., Tang, Q., Müller, S. A., Gao, P., Mahlstedt, D., Zampagni, S., et al. (2020). Fibroblast growth factor 2-mediated regulation of neuronal exosome release depends on VAMP3/cellubrevin in hippocampal neurons. *Adv. Sci.* 7 (6), 1902372. doi:10.1002/advs.201902372

Kuruppu, S., Rajapakse, N. W., Dunstan, R. A., and Smith, A. I. (2014). Nitric oxide inhibits the production of soluble endothelin converting enzyme-1. *Mol. Cell. Biochem.* 396 (1-2), 49–54. doi:10.1007/s11010-014-2141-0

Lai, H., Li, Y., Zhang, H., Hu, J., Liao, J., Su, Y., et al. (2021). exoRBase 2.0: an atlas of mRNA, lncRNA and circRNA in extracellular vesicles from human biofluids. *Nucleic Acids Res.* 50 (D1), D118–D128. doi:10.1093/nar/gkab1085

Lázaro-Ibáñez, E., Faruqu, F. N., Saleh, A. F., Silva, A. M., Tzu-Wen Wang, J., Rak, J., et al. (2021). Selection of fluorescent, bioluminescent, and radioactive tracers to accurately reflect extracellular vesicle biodistribution *in vivo*. *ACS Nano* 15 (2), 3212–3227. doi:10.1021/acsnano.0c09873

Li, B., Cao, Y., Sun, M., and Feng, H. (2021). Expression, regulation, and function of exosome-derived miRNAs in cancer progression and therapy. *FASEB J.* 35 (10), e21916. doi:10.1096/fj.202100294RR

Li, I., and Nabet, B. Y. (2019). Exosomes in the tumor microenvironment as mediators of cancer therapy resistance. *Mol. Cancer* 18 (1), 32. doi:10.1186/s12943-019-0975-5

Li, M., Zhao, X., Yong, H., Xu, J., Qu, P., Qiao, S., et al. (2022). Transketolase promotes colorectal cancer metastasis through regulating AKT phosphorylation. *Cell Death Dis.* 13 (2), 99. doi:10.1038/s41419-022-04575-5

Li, M., Zou, X., Xia, T., Wang, T., Liu, P., Zhou, X., et al. (2019). A five-miRNA panel in plasma was identified for breast cancer diagnosis. *Cancer Med.* 8 (16), 7006–7017. doi:10.1002/cam4.2572

Li, Y. C., Yang, C. S., Zhou, W. L., Li, H. S., Han, Y. J., Wang, Q. S., et al. (2018). Low glucose metabolism in hepatocellular carcinoma with GPC3 expression. *World J. Gastroenterol.* 24 (4), 494–503. doi:10.3748/wjg.v24.i4.494

Li, Z., Zhuang, M., Zhang, L., Zheng, X., Yang, P., and Li, Z. (2016). Acetylation modification regulates GRP78 secretion in colon cancer cells. *Sci. Rep.* 6, 30406. doi:10.1038/srep30406

Liang, Y., Lehrich, B. M., Zheng, S., and Lu, M. (2021). Emerging methods in biomarker identification for extracellular vesicle-based liquid biopsy. *J. Extracell. Vesicles* 10 (7), e12090. doi:10.1002/jev2.12090

Liberti, M. V., and Locasale, J. W. (2016). The Warburg effect: How does it benefit cancer cells? *Trends biochem. Sci.* 41 (3), 211–218. doi:10.1016/j.tibs.2015.12.001

Liu, F., Bu, Z., Zhao, F., and Xiao, D. (2018). Increased T-helper 17 cell differentiation mediated by exosome-mediated microRNA-451 redistribution in gastric cancer infiltrated T cells. *Cancer Sci.* 109 (1), 65–73. doi:10.1111/cas.13429

Liu, J., Ren, L., Li, S., Li, W., Zheng, X., Yang, Y., et al. (2021). The biology, function, and applications of exosomes in cancer. *Acta Pharm. Sin. B* 11 (9), 2783–2797. doi:10.1016/j.apsb.2021.01.001

Lu, L., Huang, J., Mo, J., Da, X., Li, Q., Fan, M., et al. (2022). Exosomal lncRNA TUG1 from cancer-associated fibroblasts promotes liver cancer cell migration, invasion, and glycolysis by regulating the miR-524-5p/SIX1 axis. *Cell. Mol. Biol. Lett.* 27 (1), 17. doi:10.1186/s11658-022-00309-9

Lv, B., Zhu, W., and Feng, C. (2020). Coptisine blocks secretion of exosomal circCCT3 from cancer-associated fibroblasts to reprogram glucose metabolism in hepatocellular carcinoma. *DNA Cell Biol.* 39, 2281–2288. doi:10.1089/dna.2020.6058

Marshall, H. T., and Djamgoz, M. B. A. (2018). Immuno-Oncology: Emerging targets and combination therapies. *Front. Oncol.* 8, 315. doi:10.3389/fonc.2018.00315

Mashouri, L., Yousefi, H., Aref, A. R., Ahadi, A. M., Molaei, F., and Alahari, S. K. (2019). Exosomes: Composition, biogenesis, and mechanisms in cancer metastasis and drug resistance. *Mol. Cancer* 18 (1), 75. doi:10.1186/s12943-019-0991-5

Minchenko, A., Leshchinsky, I., Opentanova, I., Sang, N., Srinivas, V., Armstead, V., et al. (2002). Hypoxia-inducible factor-1-mediated expression of the 6-phosphofructo-2-kinase/fructose-2, 6-bisphosphatase-3 (PFKFB3) gene. Its possible role in the Warburg effect. *J. Biol. Chem.* 277 (8), 6183–6187. doi:10.1074/jbc.M110978200

Möller, A., and Lobb, R. J. (2020). The evolving translational potential of small extracellular vesicles in cancer. *Nat. Rev. Cancer* 20 (12), 697–709. doi:10.1038/s41568-020-00299-w

Morishita, M., Takahashi, Y., Nishikawa, M., Sano, K., Kato, K., Yamashita, T., et al. (2015). Quantitative analysis of tissue distribution of the B16BL6-derived exosomes using a streptavidin-lactadherin fusion protein and iodine-125-labeled biotin derivative after intravenous injection in mice. *J. Pharm. Sci.* 104 (2), 705–713. doi:10.1002/jps.24251

Morrissey, S. M., Zhang, F., Ding, C., Montoya-Durango, D. E., Hu, X., Yang, C., et al. (2021). Tumor-derived exosomes drive immunosuppressive macrophages in a pre-metastatic niche through glycolytic dominant metabolic reprogramming. *Cell Metab.* 33 (10), 20402040–20402058.e10. doi:10.1016/j.cmet.2021.09.002

Najy, A. J., Jung, Y.-S., Kim, S., Fridman, R., and Kim, H.-R. C. (2021). Regulation of tumor metabolism and extracellular acidosis by the TIMP-10–CD63 Axis in breast carcinoma. *Cells* 10 (10), 2721. doi:10.3390/cells10102721

O'Grady, T., Njock, M. S., Lion, M., Bruyr, J., Mariavelle, E., Galvan, B., et al. (2022). Sorting and packaging of RNA into extracellular vesicles shape intracellular transcript levels. *BMC Biol.* 20 (1), 72. doi:10.1186/s12915-022-01277-4

Palacios-Ferrer, J. L., García-Ortega, M. B., Gallardo-Gómez, M., García, M., Díaz, C., Boulaiz, H., et al. (2021). Metabolomic profile of cancer stem cell-derived exosomes from patients with malignant melanoma. *Mol. Oncol.* 15 (2), 407–428. doi:10.1002/1878-0261.12823

Pang, W., Yao, W., Dai, X., Zhang, A., Hou, L., Wang, L., et al. (2021). Pancreatic cancer-derived exosomal microRNA-19a induces β-cell dysfunction by targeting ADCY1 and EPAC2. *Int. J. Biol. Sci.* 17 (13), 3622–3633. doi:10.7150/ijbs.56271

Parri, M., Pietrovito, L., Grandi, A., Campagnoli, S., De Camilli, E., Bianchini, F., et al. (2014). Angiopoietin-like 7, a novel pro-angiogenetic factor over-expressed in cancer. *Angiogenesis* 17 (4), 881–896. doi:10.1007/s10456-014-9435-4

Poff, A., Koutnik, A. P., Egan, K. M., Sahebjam, S., D'Agostino, D., and Kumar, N. B. (2019). Targeting the Warburg effect for cancer treatment: Ketogenic diets for management of glioma. *Semin. Cancer Biol.* 56, 135–148. doi:10.1016/j.semcancer.2017.12.011

Pužar Dominkuš, P., Stenovec, M., Sitar, S., Lasič, E., Zorec, R., Plemenitaš, A., et al. (2018). PKH26 labeling of extracellular vesicles: Characterization and cellular internalization of contaminating PKH26 nanoparticles. *Biochim. Biophys. Acta. Biomembr.* 1860 (6), 1350–1361. doi:10.1016/j.bbamem.2018.03.013

Rai, A., Fang, H., Claridge, B., Simpson, R. J., and Greening, D. W. (2021). Proteomic dissection of large extracellular vesicle surfaceome unravels interactive surface platform. *J. Extracell. Vesicles* 10 (13), e12164. doi:10.1002/jev2.12164

Rai, A., Greening, D. W., Chen, M., Xu, R., Ji, H., and Simpson, R. J. (2019). Exosomes derived from human primary and metastatic colorectal cancer cells contribute to functional heterogeneity of activated fibroblasts by reprogramming their proteome. *Proteomics* 19 (8), e1800148. doi:10.1002/pmic.201800148

Rashid, M. H., Borin, T. F., Ara, R., Angara, K., Cai, J., Achyut, B. R., et al. (2019). Differential *in vivo* biodistribution of (131)I-labeled exosomes from diverse cellular origins and its implication for theranostic application. *Nanomedicine* 21, 102072. doi:10.1016/j.nano.2019.102072

Sah, R. P., Sharma, A., Nagpal, S., Patlolla, S. H., Sharma, A., Kandlakunta, H., et al. (2019). Phases of metabolic and soft tissue changes in months preceding a diagnosis of pancreatic ductal adenocarcinoma. *Gastroenterology* 156 (6), 1742–1752. doi:10.1053/j.gastro.2019.01.039

Sheikhbahaei, S., Verde, F., Hales, R. K., Rowe, S. P., and Solnes, L. B. (2020). Imaging in therapy response assessment and surveillance of lung cancer: Evidenced-based review with focus on the utility of (18)F-FDG PET/CT. *Clin. Lung Cancer* 21 (6), 485–497. doi:10.1016/j.cllc.2020.06.020

Shi, Q., Ji, T., Ma, Z., Tan, Q., and Liang, J. (2021). Serum exosomes-based biomarker circ_0008928 regulates cisplatin sensitivity, tumor progression, and glycolysis metabolism by miR-488/HK2 Axis in cisplatin-resistant nonsmall cell lung carcinoma. *Cancer Biotherapy Radiopharm.* doi:10.1089/cbr.2020.4490

Shi, S., Li, T., Wen, X., Wu, S. Y., Xiong, C., Zhao, J., et al. (2019). Copper-64 labeled PEGylated exosomes for *in vivo* positron emission tomography and enhanced tumor retention. *Bioconjug. Chem.* 30 (10), 2675–2683. doi:10.1021/acs.bioconjchem.9b00587

Shurtleff, M. J., Temoche-Diaz, M. M., Karfilis, K. V., Ri, S., and Schekman, R. (2016). Y-box protein 1 is required to sort microRNAs into exosomes in cells and in a cell-free reaction. *Elife* 5, e19276. doi:10.7554/eLife.19276

Su, J., Pang, W., Zhang, A., Li, L., Yao, W., and Dai, X. (2022). Exosomal miR-19a decreases insulin production by targeting Neurod1 in pancreatic cancer associated diabetes. *Mol. Biol. Rep.* 49 (3), 1711–1720. doi:10.1007/s11033-021-06980-z

Sun, W., Li, Z., Zhou, X., Yang, G., and Yuan, L. (2019). Efficient exosome delivery in refractory tissues assisted by ultrasound-targeted microbubble destruction. *Drug Deliv.* 26 (1), 45–50. doi:10.1080/10717544.2018.1534898

Sung, J. S., Kang, C. W., Kang, S., Jang, Y., Chae, Y. C., Kim, B. G., et al. (2020). ITGB4-mediated metabolic reprogramming of cancer-associated fibroblasts. *Oncogene* 39 (3), 664–676. doi:10.1038/s41388-019-1014-0

Tang, K. D., Wan, Y., Zhang, X., Bozyk, N., Vasani, S., Kenny, L., et al. (2021). Proteomic alterations in salivary exosomes derived from human papillomavirus-driven oropharyngeal cancer. *Mol. Diagn. Ther.* 25 (4), 505–515. doi:10.1007/s40291-021-00538-2

Temoche-Diaz, M. M., Shurtleff, M. J., Nottingham, R. M., Yao, J., Fadadu, R. P., Lambowitz, A. M., et al. (2019). Distinct mechanisms of microRNA sorting into cancer cell-derived extracellular vesicle subtypes. *Elife* 8, e47544. doi:10.7554/eLife.47544

Théry, C., Witwer, K. W., Aikawa, E., Alcaraz, M. J., Anderson, J. D., Andriantsitohaina, R., et al. (2018). Minimal information for studies of extracellular vesicles 2018 (MISEV2018): A position statement of the international society for extracellular vesicles and update of the MISEV2014 guidelines. *J. Extracell. Vesicles* 7 (1), 1535750. doi:10.1080/20013078.2018.1535750

van Eijndhoven, M. A., Zijlstra, J. M., Groenewegen, N. J., Drees, E. E., van Niele, S., Baglio, S. R., et al. (2016). Plasma vesicle miRNAs for therapy response monitoring in Hodgkin lymphoma patients. *JCI Insight* 1 (19), e89631. doi:10.1172/jci.insight.89631

Vander Heiden, M. G., Cantley, L. C., and Thompson, C. B. (2009). Understanding the Warburg effect: The metabolic requirements of cell proliferation. *Science* 324 (5930), 1029–1033. doi:10.1126/science.1160809

Wang, D., Zhao, C., Xu, F., Zhang, A., Jin, M., Zhang, K., et al. (2021). Cisplatin-resistant NSCLC cells induced by hypoxia transmit resistance to sensitive cells through exosomal PKM2. *Theranostics* 11 (6), 2860–2875. doi:10.7150/thno.51797

Wang, S., Wang, T., Liu, D., and Kong, H. (2020a). LncRNA MALAT1 aggravates the progression of non-small cell lung cancer by stimulating the expression of COMMD8 via targeting miR-613. *Cancer Manag. Res.* 12, 10735–10747. doi:10.2147/cmar.s263538

Wang, V. M. Y., Ferreira, R. M. M., Almagro, J., Evan, T., Legrave, N., Zaw Thin, M., et al. (2019). CD9 identifies pancreatic cancer stem cells and modulates glutamine metabolism to fuel tumour growth. *Nat. Cell Biol.* 21 (11), 1425–1435. doi:10.1038/s41556-019-0407-1

Wang, W., Zhu, N., Yan, T., Shi, Y. N., Chen, J., Zhang, C. J., et al. (2020b). The crosstalk: Exosomes and lipid metabolism. *Cell Commun. Signal.* 18 (1), 119. doi:10.1186/s12964-020-00581-2

Wang, X., Zhang, H., Yang, H., Bai, M., Ning, T., Deng, T., et al. (2020c). Exosome-delivered circRNA promotes glycolysis to induce chemoresistance through the miR-122-PKM2 axis in colorectal cancer. *Mol. Oncol.* 14 (3), 539–555. doi:10.1002/1878-0261.12629

Wei, Y., Tang, X., Ren, Y., Yang, Y., Song, F., Fu, J., et al. (2021). An RNA–RNA crosstalk network involving HMGB1 and RICTOR facilitates hepatocellular carcinoma tumorigenesis by promoting glutamine metabolism and impedes immunotherapy by PD-L1+ exosomes activity. *Signal Transduct. Target. Ther.* 6 (1), 421. doi:10.1038/s41392-021-00801-2

Wei, Y., Wang, D., Jin, F., Bian, Z., Li, L., Liang, H., et al. (2017). Pyruvate kinase type M2 promotes tumour cell exosome release via phosphorylating synaptosome-associated protein 23. *Nat. Commun.* 8, 14041. doi:10.1038/ncomms14041

Wu, H., Fu, M., Liu, J., Chong, W., Fang, Z., Du, F., et al. (2021). The role and application of small extracellular vesicles in gastric cancer. *Mol. Cancer* 20 (1), 71. doi:10.1186/s12943-021-01365-z

Wu, J., Yuan, M., Shen, J., Chen, Y., Zhang, R., Chen, X., et al. (2022). Effect of modified Jianpi Yangzheng on regulating content of PKM2 in gastric cancer cells-derived exosomes. *Phytomedicine.* 103, 154229. doi:10.1016/j.phymed.2022.154229

Wu, X., Zhou, Z., Xu, S., Liao, C., Chen, X., Li, B., et al. (2020). Extracellular vesicle packaged LMP1-activated fibroblasts promote tumor progression via autophagy and stroma-tumor metabolism coupling. *Cancer Lett.* 478, 93–106. doi:10.1016/j.canlet.2020.03.004

Xu, S., and Herschman, H. R. (2019). A tumor agnostic therapeutic strategy for hexokinase 1-null/hexokinase 2-positive cancers. *Cancer Res.* 79 (23), 5907–5914. doi:10.1158/0008-5472.can-19-1789

Xu, Y., Kong, S., Qin, S., Shen, X., and Ju, S. (2020). Exosomal circRNAs: Sorting mechanisms, roles and clinical applications in tumors. *Front. Cell Dev. Biol.* 8, 581558. doi:10.3389/fcell.2020.581558

Yan, W., Wu, X., Zhou, W., Fong, M. Y., Cao, M., Liu, J., et al. (2018). Cancer-cell-secreted exosomal miR-105 promotes tumour growth through the MYC-dependent metabolic reprogramming of stromal cells. *Nat. Cell Biol.* 20 (5), 597–609. doi:10.1038/s41556-018-0083-6

Yang, H., Xie, S., Liang, B., Tang, Q., Liu, H., Wang, D., et al. (2021). Exosomal IDH1 increases the resistance of colorectal cancer cells to 5-Fluorouracil. *J. Cancer* 12 (16), 4862–4872. doi:10.7150/jca.58846

Yang, H. Y., Wu, C. Y., Powell, J. D., and Lu, K. L. (2020). Manipulation of metabolic pathways and its consequences for anti-tumor immunity: A clinical perspective. *Int. J. Mol. Sci.* 21 (11), 4030. doi:10.3390/ijms21114030

Yang, L., Xia, L., Wang, Y., He, S., Chen, H., Liang, S., et al. (2017). Development and external validation of nomograms to predict the risk of skeletal metastasis at the time of diagnosis and skeletal metastasis-free survival in nasopharyngeal carcinoma. *BMC Cancer* 17 (1), 628. doi:10.1186/s12885-017-3630-9

Yang, L., Xie, M., Yang, M., Yu, Y., Zhu, S., Hou, W., et al. (2014). PKM2 regulates the Warburg effect and promotes HMGB1 release in sepsis. *Nat. Commun.* 5, 4436. doi:10.1038/ncomms5436

Yousefi, H., Maheronnaghsh, M., Molaei, F., Mashouri, L., Reza Aref, A., Momeny, M., et al. (2020). Long noncoding RNAs and exosomal lncRNAs: Classification, and mechanisms in breast cancer metastasis and drug resistance. *Oncogene* 39 (5), 953–974. doi:10.1038/s41388-019-1040-y

Zebrowska, A., Skowronek, A., Wojakowska, A., Widlak, P., and Pietrowska, M. (2019). Metabolome of exosomes: Focus on vesicles released by cancer cells and present in human body fluids. *Int. J. Mol. Sci.* 20 (14), 3461. doi:10.3390/ijms20143461

Zhang, Q., Yang, X., and Liu, H. (2021a). Extracellular vesicles in cancer metabolism: Implications for cancer diagnosis and treatment. *Technol. Cancer Res. Treat.* 20, 15330338211037821. doi:10.1177/15330338211037821

Zhang, R., Xia, Y., Wang, Z., Zheng, J., Chen, Y., Li, X., et al. (2017). Serum long non coding RNA MALAT-1 protected by exosomes is up-regulated and promotes cell proliferation and migration in non-small cell lung cancer. *Biochem. Biophys. Res. Commun.* 490 (2), 406–414. doi:10.1016/j.bbrc.2017.06.055

Zhang, S., Pan, D., Zhang, S., Wu, Q., Zhen, L., Liu, S., et al. (2022). Exosomal miR-543 inhibits the proliferation of ovarian cancer by targeting IGF2. *J. Immunol. Res.* 2022, 2003739. doi:10.1155/2022/2003739

Zhang, Y., Huang, S., Li, P., Chen, Q., Li, Y., Zhou, Y., et al. (2018). Pancreatic cancer-derived exosomes suppress the production of GIP and GLP-1 from STC-1 cells *in vitro* by down-regulating the PCSK1/3. *Cancer Lett.* 431, 190–200. doi:10.1016/j.canlet.2018.05.027

Zhang, Y., Li, Y., Liu, P., Gong, D., Zhou, H., Li, W., et al. (2021b). Phosphatase Shp2 regulates biogenesis of small extracellular vesicles by dephosphorylating Syntenin. *J. Extracell. Vesicles* 10 (5), e12078. doi:10.1002/jev2.12078

Zhao, H., Yang, L., Baddour, J., Achreja, A., Bernard, V., Moss, T., et al. (2016). Tumor microenvironment derived exosomes pleiotropically modulate cancer cell metabolism. *Elife* 5, e10250. doi:10.7554/eLife.10250

Zheng, Y., Liu, P., Wang, N., Wang, S., Yang, B., Li, M., et al. (2019). Betulinic acid suppresses breast cancer metastasis by targeting GRP78-mediated glycolysis and ER stress apoptotic pathway. *Oxid. Med. Cell. Longev.* 2019, 8781690. doi:10.1155/2019/8781690

Zhou, S., Lan, Y., Li, Y., Li, Z., Pu, J., and Wei, L. (2022). Hypoxic tumor-derived exosomes induce M2 macrophage polarization via PKM2/AMPK to promote lung cancer progression. *Cell Transpl.* 31, 9636897221106998. doi:10.1177/09636897221106998

Zhu, T., Hu, Z., Wang, Z., Ding, H., Li, R., Wang, J., et al. (2022). microRNA-301b-3p from mesenchymal stem cells-derived extracellular vesicles inhibits TXNIP to promote multidrug resistance of gastric cancer cells. *Cell Biol. Toxicol.* doi:10.1007/s10565-021-09675-0

frontiers | Frontiers in Pharmacology

TYPE Original Research
PUBLISHED 09 February 2023
DOI 10.3389/fphar.2023.1088993

OPEN ACCESS

EDITED BY
Hai-long Piao,
Dalian Institute of Chemical Physics (CAS), China

REVIEWED BY
Qisheng Su,
Guangxi Medical University, China
Ning Li,
Wuhan University, China

*CORRESPONDENCE
Yangying Zhou,
zhouyy423@163.com
Hong Zhu,
zhuhong0719@126.com

SPECIALTY SECTION
This article was submitted to Pharmacology of Anti-Cancer Drugs, a section of the journal Frontiers in Pharmacology

RECEIVED 03 November 2022
ACCEPTED 31 January 2023
PUBLISHED 09 February 2023

CITATION
He F, Zeng P, Ma S, Yang X, Liu H, Liu Q, Zhou Y and Zhu H (2023), Identification and validation of a novel cuproptosis-related genes signature associated with prognosis, clinical implications and immunotherapy of hepatocellular carcinoma.
Front. Pharmacol. 14:1088993.
doi: 10.3389/fphar.2023.1088993

Identification and validation of a novel cuproptosis-related genes signature associated with prognosis, clinical implications and immunotherapy of hepatocellular carcinoma

Fengjiao He[1,2,3], Puhua Zeng[3], Sijing Ma[3], Ximing Yang[4], Huan Liu[1,2], Qiong Liu[1,2], Yangying Zhou[1,2]* and Hong Zhu[1,2]*

[1]Department of Oncology, Xiangya Hospital, Central South University, Changsha, China, [2]National Clinical Research Center for Geriatric Disorders, Xiangya Hospital, Central South University, Changsha, China, [3]Hunan Academy of Traditional Chinese Medicine Affiliated Hospital, Changsha, China, [4]Medical School, Hunan University of Chinese Medicine, Changsha, China

Background: Cuproptosis is a novel type of regulated cell death and is reported to promote tumor occurrence and progression. However, whether a cuproptosis-related signature has an impact on hepatocellular carcinoma (HCC) is still unclear.

Materials and methods: We analyzed the transcriptome data of HCC from The Cancer Genome Atlas (TCGA) and International Cancer Genome Consortium (ICGC) database, and searched for tumor types with different cuproptosis patterns through consistent clustering of cuproptosis genes. We then constructed a Cuproptosis-Related Genes (CRGs)-based risk signature through LASSO COX regression, and further analyzed its impact on the prognosis, clinical characteristics, immune cell infiltration, and drug sensitivity of HCC.

Results: We identified the expression changes of 10 cuproptosis-related genes in HCC, and all the patients can be divided into two subtypes with different prognosis by applying the consensus clustering algorithm. We then constructed a cuproptosis-related risk signature and identified five CRGs, which were highly correlated with prognosis and representative of this gene set, namely *G6PD*, *PRR11*, *KIF20A*, *EZH2*, and *CDCA8*. Patients in the low CRGs signature group had a favorable prognosis. We further validated the CRGs signature in ICGC cohorts and got consistent results. Besides, we also discovered that the CRGs signature was significantly associated with a variety of clinical characteristics, different immune landscapes and drug sensitivity. Moreover, we explored that the high CRGs signature group was more sensitive to immunotherapy.

Conclusion: Our integrative analysis demonstrated the potential molecular signature and clinical applications of CRGs in HCC. The model based on CRGs can precisely predict the survival outcomes of HCC, and help better guide risk stratification and treatment strategy for HCC patients.

KEYWORDS

hepatocellular carcinoma, cuproptosis-related genes, tumor microenvironment, drug sensitivity, prognosis model

1 Introduction

Hepatocellular Carcinoma (HCC) is one of the most common malignant tumors, and ranks the sixth most common and third mortality in all tumors worldwide by the World Health Organization (WHO) (Siegel et al., 2022)- (Ferlay et al., 2021). Although early-stage HCC can be cured by surgical treatment, enormous challenges remain in the treatment of advanced HCC, resulting in unfavorable prognosis, significant financial cost and high disease burden (Bandmann et al., 2015). Given the high morbidity and mortality of HCC, there is an urgent need to develop more effective prognostic models, and explore reliable prognostic factors, which is crucial for optimal individualized management and treatment.

Copper is an essential cofactor for all organisms, but copper is toxic if concentrations exceed a threshold maintained by evolutionarily conserved homeostatic mechanisms. However, how excess copper induces cell death is not known. The Broad institute currently uncovers a novel cell death mechanism, cuproptosis (Tsvetkov et al., 2022), which is distinct from the known apoptosis, necrosis, autophagy and iron death.

Cuproptosis is a form of copper-dependent and mitochondrial respiration-dependent, regulated cell death. Cuproptosis occurs by direct binding of copper to lipoylated components of the tricarboxylic acid (TCA) cycle (Beaino et al., 2014)- (Hatori et al., 2016), resulting in aberrant aggregation of lipoylated proteins and loss of ferroptosis proteins, leading to cell death by proteotoxic stress. Copper ions are involved in cell death as are iron ions, while the study from the Broad Institute demonstrates strategies to combat disease by pharmacologically inhibiting mitochondrial respiration (Tsvetkov et al., 2022). In addition, cancer cells are actively respiring and contain large amounts of lipoylated mitochondrial proteins. Copper ionophores could be used to destroy cancer cells, which opens up a new therapeutic direction for cancer. However, the metabolism of copper in liver diseases and the occurrence and development of HCC is still poorly understood. In the research stage. The evidence by Siddiqui et al., demonstrated that copper oxide nanoparticles have dose-dependent cytotoxicity and apoptotic effects on HepG2 cells (Siddiqui et al., 2013). Besides, copper contents were closely associated with liver cirrhosis and HCC, and serum levels of copper, like ceruloplasmin, may be used as a marker for the detection of HCC (Zhang et al., 1994). Recently, as reported, cuproptosis-related signature and the lncRNA profile linked with cuproptosis may bring new insights into the molecular pathways of the formation and progression of cancers, which were helpful to predict the prognosis and guiding treatment of cancer patients (Zhen et al., 2022)- (Zhang et al., 2022).

Emerging evidence also suggests crosstalk between curoprotosis and the tumor immune microenvironment (TME) (Lv et al., 2022)- (Li et al., 2022a). The tumor microenvironment plays a crucial role in cancer development and clinical outcomes (Wu and Dai, 2017). The TME includes cancer cells, immune cells, endothelial cells, inflammatory cells and fibroblasts, as well as extracellular components (growth factors, hormones, cytokines, etc.). Within the TME, interactions between cancer cells and immune cells regulate all links of tumor development, and tumor-infiltrating immune cells (TIICs) can also influence cancer progression (Lee and Cheah, 2019)- (Zhou et al., 2022a). Despite recent advances in immunotherapy for HCC, the prognosis of HCC remains heterogeneous, which suggests that the close connection between curoprotosis and the tumor immune microenvironment may play a crucial role in the development and progression of HCC. However, the role of cuprotosis-mediated gene patterns in HCC is unclear.

In this study, we comprehensively investigate the molecular alterations and clinical relevance of cuproptosis-related genes (CRGs) in HCC. We then constructed a cuproptosis-related risk signature and identified five CRGs for predicting survival outcomes and characterizing the immune landscape of HCC. Additionally, combined with clinicopathological features and treatment efficacy, the CRGs signature demonstrated great potential for precision and personalized therapy of HCC.

2 Materials and methods

2.1 Data download and preprocessing

Based on R package The Cancer Genome Atlas (TCGA) biolinks v1.16.0, the expression profile data (FPKM), genomic data (SNV and CNV) and clinical data of HCC were downloaded. Survival data were used from 2018 collated data (Liu et al., 2018). The TCGA HCC dataset (https://cancergenome.nih.gov/, version 27.0-fix, released on 9 November 2020) as training cohort, which included 269 HCC tumor samples and 50 tumor-adjacent normal tissues. In the meantime, the Liver Cancer-RIKEN-JP (LIRI-JP) of HCC transcriptome data (FPKM) and clinical survival data in the (International Cancer Genome Consortium) ICGC database (https://dcc.icgc.org/projects/LIRI-JP, version Release_28, processed on 27 March 2019) was used for the validation cohort, which contained 232 HCC cases. Above data, genes were removed when multiple ENSEMBL Identity Documents (ID) were encountered corresponding to the same SYMBOL. The batch effect between different datasets was corrected using the "sva" package of R software by adopting the "combat" algorithm. In addition, we filtered the genes that were expressed in less than 50% of the samples.

2.2 Difference analysis

Gene expression differences were calculated using DESeq2 through count expression profiles, and genes with an absolute value of Log2 Foldchange >1 and adjusted p values less than 0.05 were selected as differential genes. Multiple testing correction is based on the FDR method. Differential gene volcano plots were drawn by ggplot2 (3.3.6) and ggrepel (0.9.1) R packages, and significant cuproptosis-related genes were marked. The expression heatmap of Cuproptosis-related genes in HCC and normal tissues were plotted by the R package pheatmap (1.0.12).

2.3 Comparison of cuproptosis-related genes under different clinical

Based on the FPKM expression dataset of TCGA HCC and clinical feature data, we stratified the samples by TCGA molecular classification, alpha-fetoprotein value, bilirubin albumin maximum, fibrosis, grade, stage, age, gender, BMI, etc. We then calculated the expression differences of cuproptosis-related genes between groups by the Wilcoxon rank sum test. Boxplots were drawn using ggpubr (0.4.0) heatmaps were drawn using pheatmap (1.0.2).

2.4 Construction of protein interaction network

A PPI network was constructed based on ten cuproptosis-related genes using STRING (http://www.string-db.org/) (Szklarczyk et al., 2021), and Gene Ontology (GO) functional enrichment analysis was performed.

2.5 Gene correlation analysis

We extracted the expression values of cuproptosis genes or cuproptosis genes to immune checkpoints from the TCGA HCC FPKM data. We performed logarithmic transformation on the gene expression values, and calculated the correlation between the expression of the two genes by Pearson correlation analysis.

2.6 Identification of cuproptosis-associated tumor subtypes

Based on the TCGA dataset, we identified different subtypes based on the expression profile data of 10 cuproptosis-related genes, applying non-negative matrix decomposition and unsupervised consensus clustering analysis. We used the consensus cluster plus (4.5.1.902) and Non-negative matrix factorization (NMF) (0.24.0) packages to operate, and the consensus clustering used three clustering distances: Spearman, Pearson, as well as Euclidean. The clustering method was K-means clustering with l000 replicates to guarantee the stability of the classification. We selected consensus clustering (Euclidean distance) to determine the tumor cuproptosis subtype based on the idea that the survival *p*-value was minimally separated.

2.7 Functional enrichment analysis

GO and Kyoto Encyclopedia of Genes and Genomes (KEGG) pathway enrichment analyses were performed based on significantly differentially expressed genes and the R package cluster profiler (4.2.2), and results with FDR corrected *p*-values less than 0.05 were selected and the top few pathways were displayed using bubble plots (Li et al., 2022b). Construction of the cuproptosis-associated signature based on the two identified subtypes of cuproptosis tumors. In the transcriptome data of TCGA HCC, all gene expression values were divided into two groups according to the median value. Univariate Cox regression analysis was performed using the R package survival (3.3–1). Genes with a *p*-value less than 0.05 were filtered out, and cuproptosis-associated genes were further constructed by the R package glmnet (4.1–4) Lasso Cox regression to remove redundant genes, according to the following formula signature.

2.8 Survival analysis

In the TCGA database and ICGC validation dataset, median grouping was performed based on the calculated cuproptosis score, and the impact on prognosis was assessed by constructing Kaplan-Meier curves using the survival (3.3–1) R package and the log-rank test. ROC curve was plotted using the R package timer0c (0.4), and Cox regression (R package survival 3.3–1)) was performed to calculate hazard ratios (HR) for scoring groups and clinical characteristics.

2.9 Gene mutation and copy number variation analysis

The single nucleotide variation and copy number variation data of HCC The genes with mutation frequencies greater than 5% in the high and low copper death signature groups were then displayed using oncoPrint through the R package ComplexHeatmap (version 2.10.0), and the chi-square test was used to determine whether there was a significant difference between the two groups. The GenVisR (1.26.0) package defines low copy number variation with copy number < 1, and copy number > 3 as high fold variation, showing the copy number variation of the high and low groups.

2.10 Immune cell infiltration calculation

Using the R package IBOR (0.99.9) based on ESTIMATE (Aran et al., 2015), Microenvironment Cell Populations-counter (MCP-counter) (Giraldo et al., 2016), XCELL (Aran et al., 2017) and CIBERSORT (Newman et al., 2015)immune cell infiltration algorithms, the score of each immune cell in the HCC sample was calculated. The Wilcoxon rank test was used to compare the different levels of cuproptosis signature between the two groups with immune cell infiltration.

2.11 Drug sensitivity prediction

Based on Genomics of Drug Sensitivity in Cancer (GDSC) (Yang et al., 2013), Cancer Cell Line Encyclopedia (CCLE) (Barretina et al., 2012) and Cancer Therapeutics Response Portal (CTRP) (Basu et al., 2013) drug databases, we extracted cancer cell line expression data, calculated the cuproptosis fraction of each cell line, and grouped them based on the median gene expression. We then combined the genes expression with the Area Under the Curve (AUC) and Half maximal inhibitory concentration (IC50) data of multiple drugs in cell lines, and use Spearman's correlation to calculate the correlation with cuproptosis score, and further used the Wi1coxon test to compare the difference of AUC/IC50 between high and low cuproptosis groups in significantly related drugs.

2.12 Impact of immunotherapy response

Based on TCGA's HCC transcriptional data, we used the Tumor Immune Dysfunction and Exclusion (TIDE) tool (http://tide. dfci.harvard. edu/) (Jiang et al., 2018) to predict the immunotherapy response of the samples and compared the difference in scores between the responder and non-responder groups. The Wilcoxon rank test was used for a statistical test and the difference in the proportion of response and non-response between the two groups with high and low cuproptosis scores was compared.

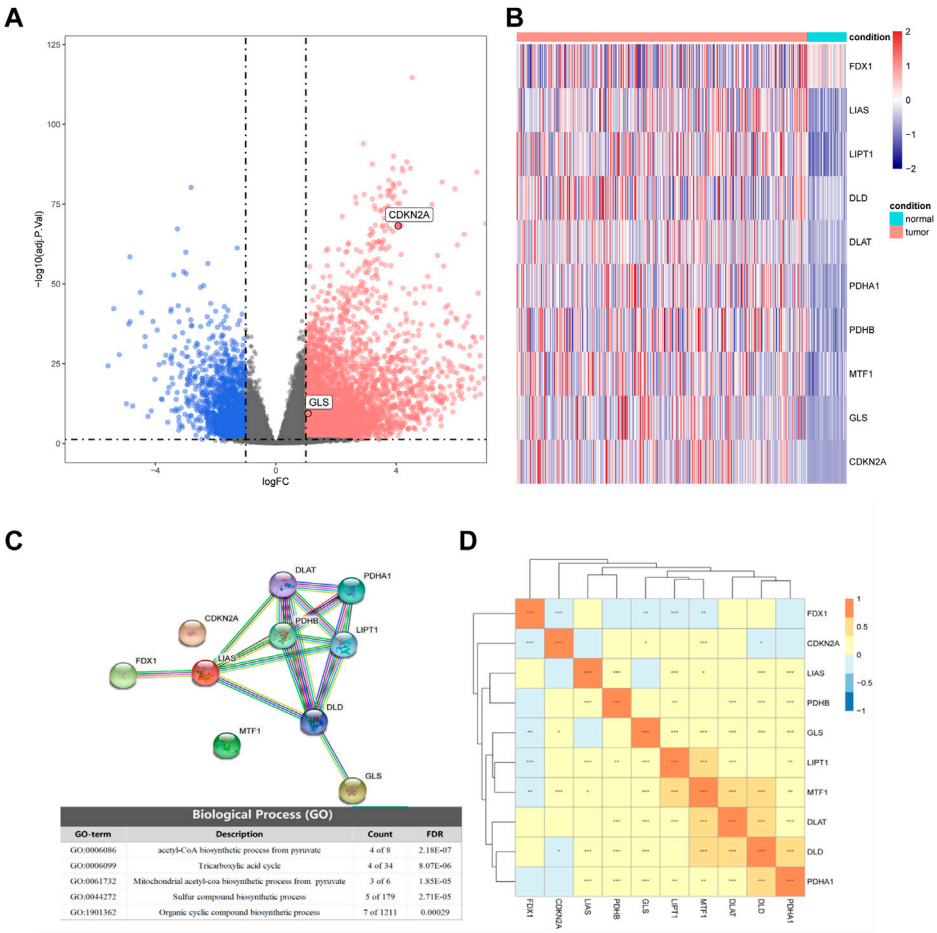

FIGURE 1
Differential expression of cuproptosis-related genes in hepatocellular carcinoma (HCC) and normal tissues. **(A)** Volcano plot of differential expression (blue represents downregulation in HCC, red represents upregulation in HCC, gray represents insignificant, and cuproptosis-related genes are marked in the figure). **(B)** The expression of 10 cuproptosis-related genes in HCC and normal tissues. **(C)** Partial results of protein-protein interactions (PPI) network map and gene ontology (GO) enrichment of 10 cuproptosis-related genes. **(D)** Heatmap of expression correlation of 10 cuproptosis-related genes in TCGA.

3 Results

3.1 The landscape of cuproptosis-related genes in HCC

Based on the TCGA transcriptome dataset, we performed differential gene analysis between HCC tumor and adjacent normal tissues, and explored 6,031 differential genes, of which 1,503 were downregulated and 4,528 were upregulated Figure 1A). We then plotted the heatmap by using the R to scale the FPKM of gene expression (Z-score). Among these differential genes, we discovered that CDKN2A and GLS were significantly upregulated in HCC among all the cuproptosis-related genes, and these two genes might contribute to the development of HCC (Figure 1B).

By analyzing the expression correlations of the 10 cuproptosis genes, we found that LIAS, LIPT1, DLD, DLAT, PDHA1, PDHB, MTF1, GLS, and CDKN2A showed positive correlations with other genes, while FDX1 was negatively correlated with the expression of other genes (Fig 1D). The protein-protein interaction (PPI) network of GO enrichment analysis revealed that the CRGs participated in compound biosynthesis and energy metabolism (Figure 1C).

We then compared the expression differences of CRGs among diverse clinical characteristics. We observed that different CRGs were differentially expressed in distinct signatures, such as *GLS* showing distinct expression differences in different age, Body Mass Index (BMI) subgroups, as well as different tumor stages (Figures 2A, C–E) Besides, *DLD* was significantly expressed at different α-fetoprotein levels (Figure 2B).

3.2 Identification and characterization of cuproptosis-related molecular subtypes in HCC

Firstly, we applied a consensus clustering algorithm to categorize the HCC patients based on the expression of 10 CRGs. The consistency coefficient was evaluated to determine the optimal clustering number (k value), and the results demonstrated that k = 2 was the best choice for dividing the cohort into two subgroups (Figures 3A, B). Based on the principal component analysis (PCA), the HCC patients were well separated into two categories (Figure 3C). We then discovered that *FDX1*, *LIPT1*, *MTF1*, *GLS*, and *CDKN2A* was

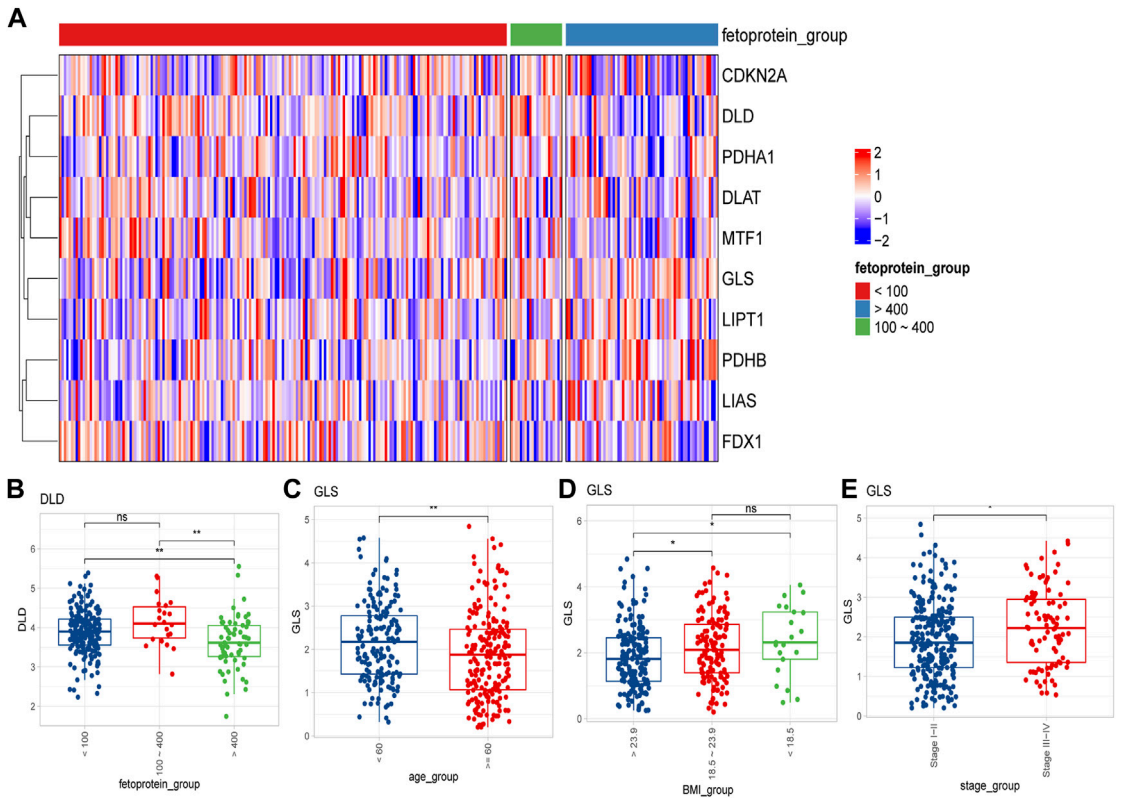

FIGURE 2
Differential expression of cuproptosis-related genes in different clinical feature groups. **(A)** Expression of 10 cuproptosis-related genes in different alpha-fetoprotein groups (<100 mg/dL, 100–400 mg/dL, >400 mg/dL); **(B)** *DLD* expression differences in different alpha-fetoprotein groups; **(C–E)** The difference of *GLS* expression in different age, BMI and different tumor stage groups (ns: p >0.05; *: p <0.05; **: p <0.01; ***: p <0.001).

significantly differentially expressed between the two groups (Figures 3D, E).

Furthermore, we analyzed the immune cell infiltration scores by using CIBERSORT, GSVA-cellreport, ESTIMATE, and MCP-counter algorithms. We found that Cluster-2 scored higher for stromal cells, while no significant differences were observed for immune scores and tumor purity (Figures 4A, B). We also discovered significant differences between Cluster-1 and Cluster-2 for distinct immune cell infiltration, such as T cells, B cells and macrophages (Figures 4C, D).

3.3 Construction and validation of cuproptosis-related genes signature

Based on the identified two subtypes of CRGs in HCC, we analyzed the differentially expressed genes (1,984 genes downregulated and 547 genes upregulated) between the two subtypes. We further performed GO and KEGG enrichment analysis for the differential genes, which were mainly enriched in pathways involved in cell proliferation (organelle fusion, nuclear division, etc.) and cell communication (neuroactive ligand, receptor interaction, etc.) (Figures 5A, B). Then, we performed LASSO and multivariate COX analysis on the two subtypes of differential genes, and obtained a five-gene signature model (*G6PD*, *PRR11*, *KIF20A*, *EZH2*, and *CDCA85*) (Figures 5C–E). The Kaplan-Meier analysis revealed that the CRGs signature was associated with patients' prognosis, and the patients in the high-risk group had an inferior overall survival (OS, $p < 0.0001$, Figure 6A). We further performed the time-dependent receiver operating characteristic (ROC) curve with the area under the curve (AUC). The AUC values of 6 months, 1-, 3-, and 5-year survival rates of prognostic subgroups were 0.718, 0.756, 0.714, and 0.707, respectively (Figure 6B). Meanwhile, we further validated the prognostic performance of the CRGs model in the LIRI-JP dataset. Similarly, we gained parallel results in the validation set, indicating an excellent predictive prognostic accuracy of the CRGs model for HCC patients. The AUC values of 6 months, 1-, 3-, and 5-year survival rates of prognostic subgroups were 0.778, 0.813, 0.749, and 0.797, respectively (Figures 6D, E). In addition, multivariate Cox regression showcased that the CRGs signature was an independent risk factor for HCC in both cohorts ($p < 0.0001$, Figures 6C, F).

3.4 Analysis of CRGs signature with clinical characteristics

To explore the CRGs risk model with clinical characteristics, we found that the CRGs signature was associated with multiple clinical features, including alpha-fetoprotein, histological grade, tumor stage, as well as TCGA molecular subtypes, etc. (Figures 7A–N). In the LIRI-JP dataset, we verified that the CRGs signature significantly correlated to the tumor stage (Figure 7O).

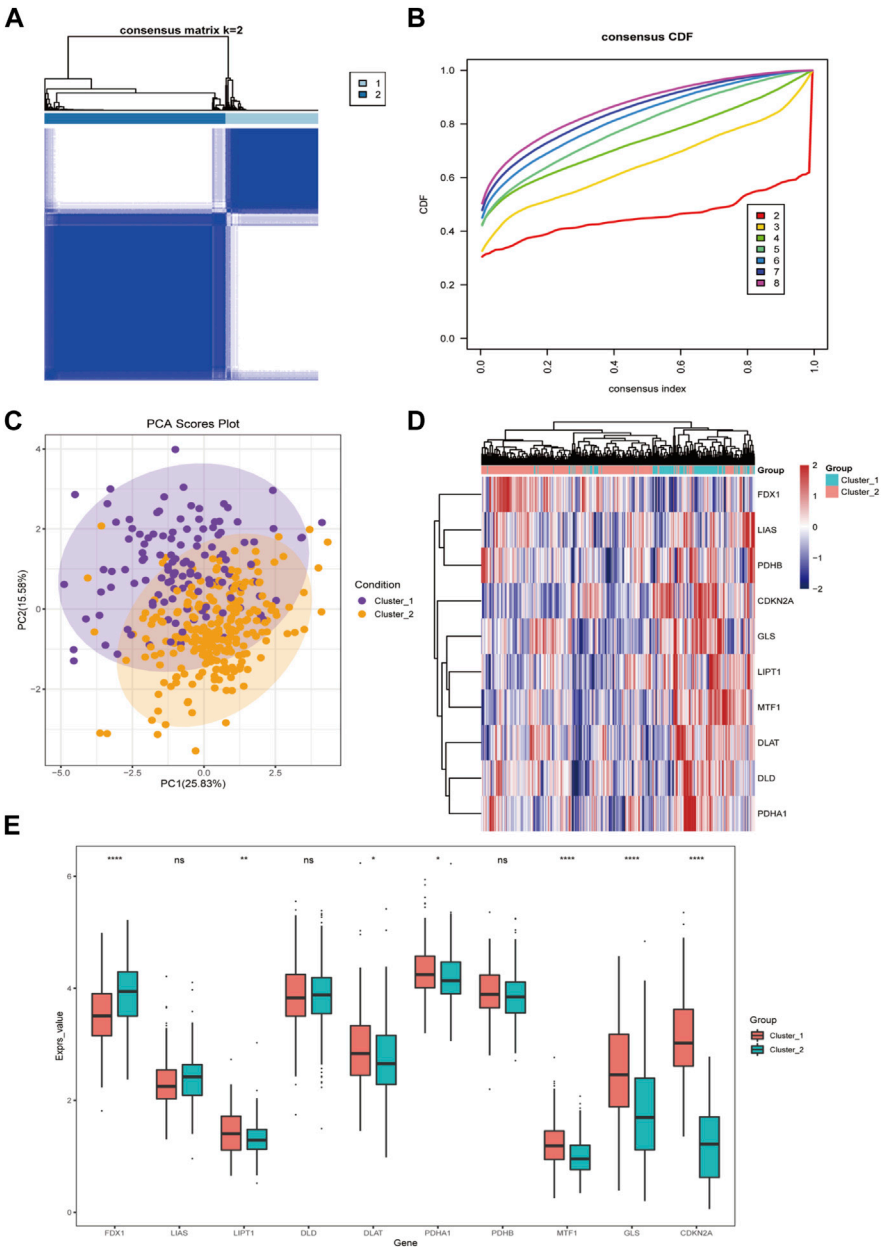

FIGURE 3
The cuproptosis-related genes divide hepatocellular carcinoma into two subtypes. **(A)** The sample squareness of the consistent clustering (number of classifications = 2); **(B)** The cumulative distribution map of the consistent clustering; **(C)** The principal component analysis graph of the two hepatocellular carcinoma subtypes; **(D)** The cuproptosis-related genes in the two categories Expression heatmap of hepatocellular carcinoma; **(E)** Boxplot of cuproptosis-related genes expression difference between two types of hepatocellular carcinoma (ns: $p > 0.05$; *: $p < 0.05$; **: $p < 0.01$; ***: $p < 0.001$; ****: $p < 0.0001$).

3.5 Characterization of molecular landscape, immunotherapeutic and druggable responses of cuproptosis-related genes signature

We analyzed the CRGs' genetic features based on the single nucleotide variants (SNV) and copy number variation (CNV) of HCC. We performed a chi-test in high and low CRGs groups with mutation frequency > 5%, and we observed no statistical significance between the two groups (Supplementary Figure S1A). We further characterized the high and low CRGs groups for copy number deletions and amplifications on chromosomes and also found no significant differences between the two groups (Supplementary Figure S1B). The GSVA enrichment analysis revealed that they differed significantly in the high and low CRGs groups, and the low CRGs group had more enriched pathways (Supplementary Figure S2).

Next, we explored the relationship between CRGs signature with drug sensitivity. We extracted cell line expression data based on GDSC, CCLE as well as CTRP databases, and combined them with the AUC/IC50 data for analysis. In the GDSC database, we discovered that the AUC was negatively correlated with CRGs signature for multiple drugs, such as 5-Fluorouracil, GDC0449 et al. (Figure 8A), and the AUC was significantly different between high and low CRGs

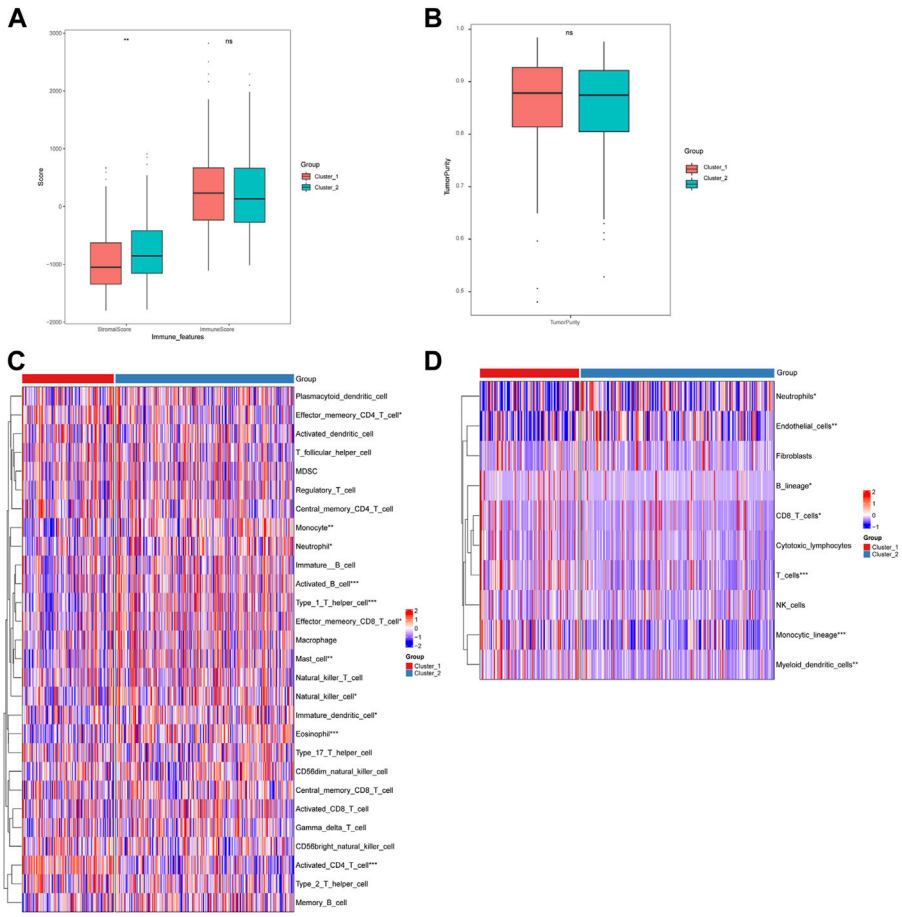

FIGURE 4
Differences in immune cell infiltration among hepatocellular carcinoma subtypes. **(A)** ESTIMATE algorithm calculates differences in stromal and immune scores between subtypes; **(B)** ESTIMATE algorithm calculates differences in tumor purity scores between subtypes; **(C)** GSVA-cell report algorithm calculates differences in immune cell infiltration between subtypes; **(D)** MCP-counter calculates differences in subtypes differences in immune cell infiltration (ns: p >0.05; *: p <0.05; **: p <0.01; ***: p <0.001; ****: p <0.0001).

groups (Figure 8B). We only discovered one drug AZD0530 with an IC50 positively correlated with CRGs signature in the CCLE database, and its IC50 was significantly different between high and low CRGs groups (Figures 8G, H). We also revealed that multiple drugs were associated with CRGs signatures in the CTRP database (Figures 8C–F).

In addition, we assessed the CRGs signature with the tumor microenvironment (TME). We evaluated the TME score, which included the stromal score, ESTIMATE score, and immune score between the two subtypes. We observed that there was no significant difference between the two groups in immune and ESTIMATE scores, while we discovered a higher stromal score in the low CRGs group (Figures 9A–C). The correlation analysis also revealed that the stromal score exhibited a significant negative correlation with the CRGs signature (Figures 9D–F). Moreover, multiple immune cell differences were differentially expressed between the two subtypes, such as T regulatory cells, macrophages, monocytes, etc. (Figure 9G). We then utilized TIDE for the immunotherapy response prediction, and we explored that the responders had higher CRGs scores and the high CRGs group also presented higher proportions of responding patients (Figures 10A, B). Furthermore, we found that there were significant correlations between immune checkpoints and CRGs (Figure 10C), and multiple immune checkpoints were differentially expressed between the two CRGs subgroups, such as CTLA4, LAG3, PDCD1 (PD-1), and CD274 (PD-L1) (Figure 10D), suggesting a potential role of the cuproptosis-related subtypes in immunotherapy.

4 Discussion

As one of the most severe malignancies in the world, current treatment strategies for HCC are rather limited (Llovet et al., 2016). In addition, the high heterogeneity of HCC and complicated risk factors make predicting prognosis much more difficult. Recent studies have shown that copper levels are significantly elevated in the serum and tumor tissue of cancer patients compared to healthy patients (Blockhuys et al., 2017)- (Ishida et al., 2013). Although dysregulation of copper homeostasis may trigger cytotoxicity, alterations in intracellular copper levels may affect cancer development and progression (Babak and Ahn, 2021). Recently, a new cell death pathway called cuproptosis has been noted, and it has been demonstrated that copper directly binds to lipoylated components of the tricarboxylic acid (TCA) cycle, leading to toxic protein stress, and ultimately cell death (Tsvetkov et al., 2022). Liver

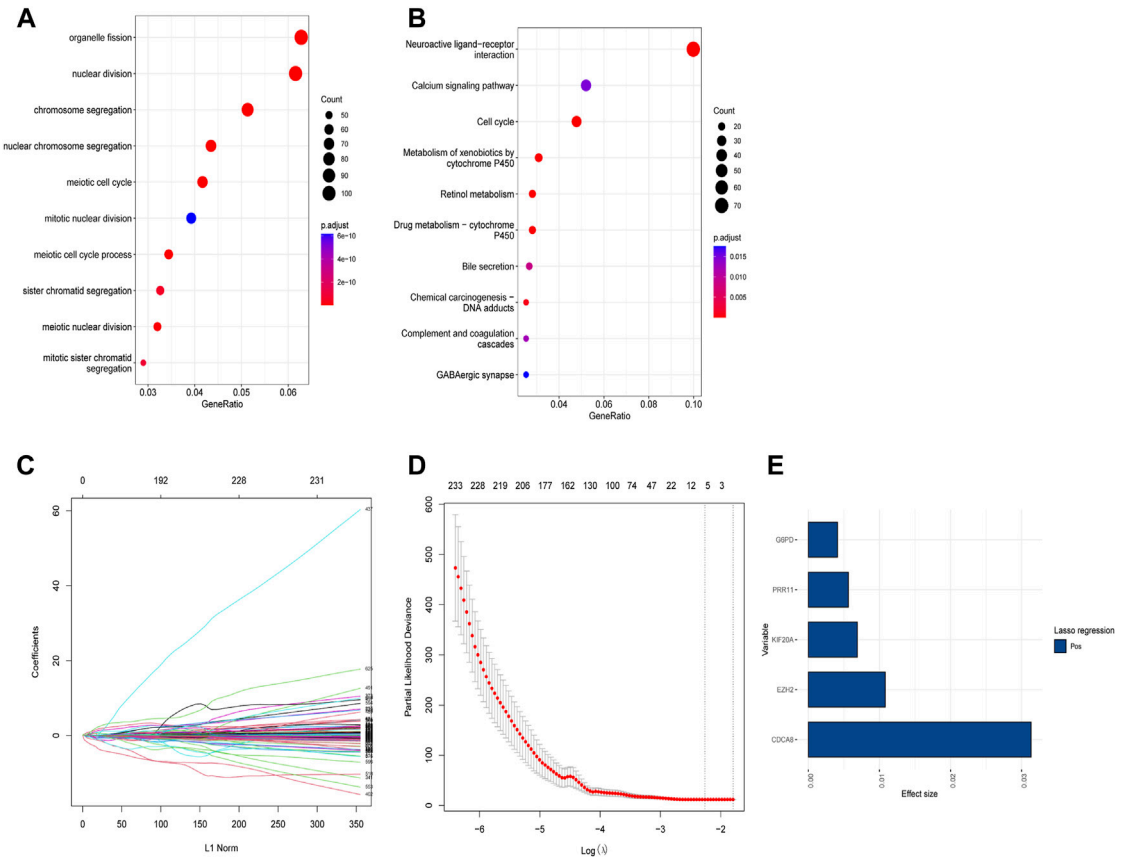

FIGURE 5
Functional analysis of different subtypes and the construction of cuproptosis-related genes (CRGs) signature in hepatocellular carcinoma. **(A)** Gene ontology (GO) enrichment analysis results in the two CRGs subtypes. **(B)** Kyoto Encyclopedia of Genes and Genomes (KEGG) enrichment analysis results in the two CRGs subtypes: **(C)** Lasso regression coefficients of each variable with L1 norm; **(D)** Lambda logarithm value in Lasso regression and the relationship with the error (the dotted line is the range that Lambda can choose); **(E)** The coefficient values of the Lasso regression screening variables.

cirrhosis, one of the crucial causes of HCC, showed copper accumulation compared to a healthy liver (Poznanski et al., 2021). Recent evidence demonstrated that increased levels of redox-active free copper might be associated with acute hepatitis and, ultimately, HCC (Koizumi et al., 1998). The above evidence indicates that copper levels play a role in HCC, which suggests that cuproptosis may be closely related to liver malignancy, so it is vital to explore the significance of CRGs in the development and prognosis of HCC.

Cuproptosis genes are widely perturbed in HCC. First, based on TCGA transcriptome datasets, we found that the CRGs of HCC and normal tissues were differentially expressed, and *GLS* (glutaminase) and *CDKN2A* were found to be significantly upregulated in HCC. *GLS* has been reported to be associated with several cancers (Masisi et al., 2020)- (Matés et al., 2019). *CDKN2A* is a tumor suppressor gene on chromosome 9p21.3 that plays a role in tumor proliferation suppression (Zhao et al., 2016). However, *CDKN2A* is upregulated in HCC and strongly associated with inferior prognosis (Luo et al., 2021). These two cuproptosis genes may play a vital role in the development of HCC. Next, a PPI network was constructed with 10 cuproptosis genes, and after GO enrichment analysis, the associated genes were enriched in several pathways, including compound biosynthesis and energy metabolism, such as pyruvate acetyl CoA biosynthesis, tricarboxylic acid cycle, mitochondrial acetyl CoA biosynthesis and organic cyclic compound biosynthesis, etc., suggesting that cuproposis activity was associated with multiple cancer-related pathways. By calculating the expression correlations of 10 CRGs, we found that *LIAS*, *LIPT1*, *DLD*, *DLAT*, *PDHA1*, *PDHB*, *MTF1*, *GLS*, and *CDKN2A* showed a positive correlation with other genes in HCC, while *FDX1* negatively correlated with multiple genes. Similar results have been reported in other types of cancer, for example, *CDKN2A* is upregulated in endometrial cancer and may contribute to its pathogenesis (Su et al., 2015). *PDHA1*, *PDHB*, *DLAT* and *DLD* act synergistically in the pyruvate dehydrogenase complex deficiency (Inui et al., 2022). Zhang et al. combined with bioinformatics tools have analyzed the expression and prognostic significance of *FDX1*, a key regulator of copper-induced death in HCC (Zhang et al., 1994). However, the expression and function of other CRGs in HCC are poorly understood and need further exploration.

Subtypes identification of cuproptosis genes was analyzed based on TCGA HCC transcriptome data. The HCC patients can be divided into two subtypes, and there were obvious expression differences between *FDX1* and *LIPT1* in the two subtypes. It has been reported that *FDX1*, a key regulator of cuproptosis, is downregulated in HCC and its high expression is associated with inferior prognosis in HCC patients (Zhang et al., 1994). Recent

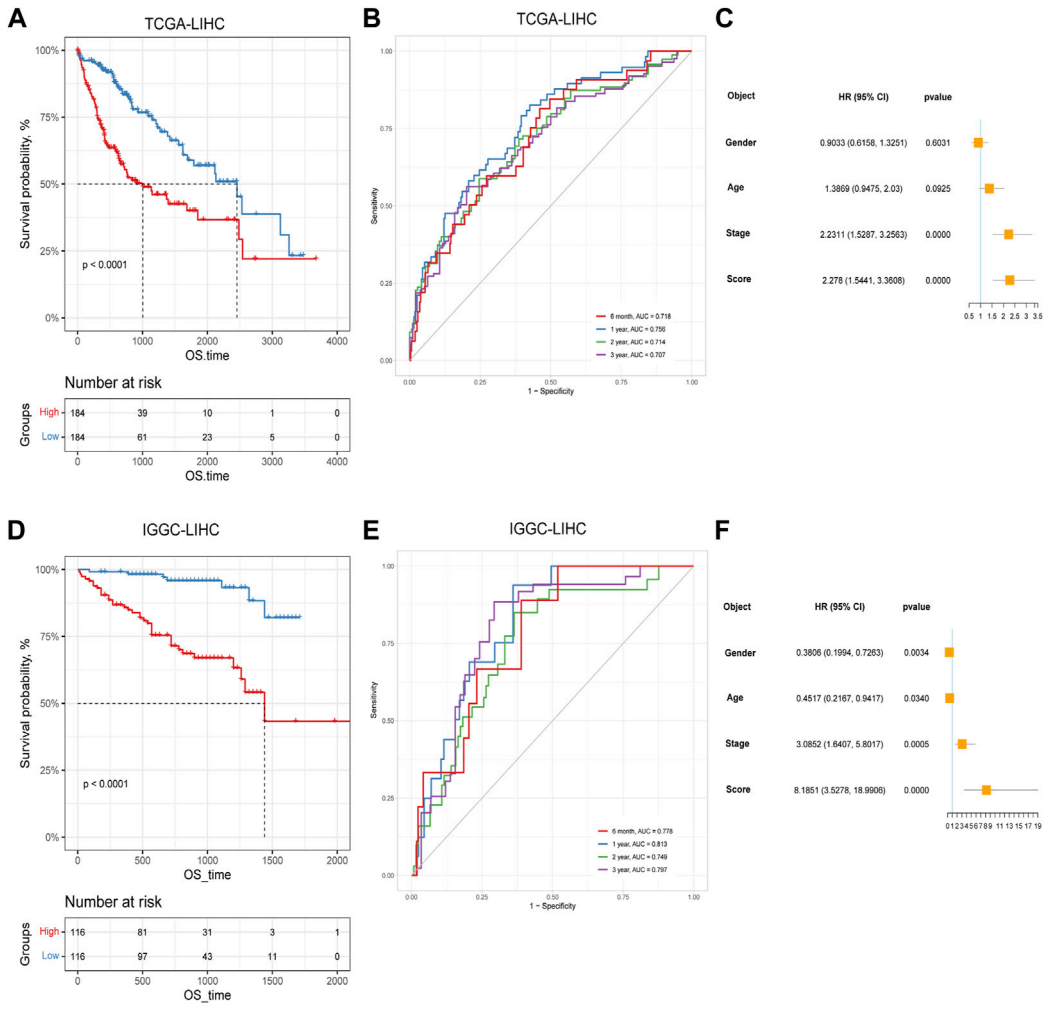

FIGURE 6
The prognostic effect of cuproptosis-related genes signatures in hepatocellular carcinoma. **(A)** Survival analysis of patients in TCGA cohort based on cuproptosis score; **(B)** Time-dependent receiver operating characteristic (ROC) curve of cuproptosis score in TCGA dataset; **(C)** Multivariate Cox analysis results in TCGA dataset; **(D)** Survival analysis of patients in LIRI-JP cohort based on cuproptosis score; **(E)** ROC curve of cuproptosis score in the LIRI-JP dataset; **(F)** Multivariate Cox analysis results in LIRI-JP dataset.

evidence suggests that *LIPT1* is involved in the lipoic acid metabolic pathway (Chen et al., 2018). The lipoic acid moiety can be transferred from one protein to another, affecting the tricarboxylic acid cycle. *LIPT1* expression is elevated in melanoma biopsies, and is an independent favorable prognostic indicator in melanoma patients (Liu et al., 2018). When calculating immune cell infiltration scores between subtypes, we found that two groups (including *FDX1*, *LIPT1*, *DLAT*, *PDHA1*, *MTF1*, *GLS*, and *CDKN2A*) were significant diversity in different immune cells (including T cells, B cells, and macrophages), suggesting that is a possible predictive value for prognosis. *LIPT1* expression was positively correlated with *PD-L1* expression and negatively associated with Treg cell infiltration. Melanoma patients with high *LIPT1* expression had longer overall survival than those with low *LIPT1* expression after receiving immunotherapy, suggesting the predictive value of *LIPT1* for prognosis (Lv et al., 2021).

The differential genes of the two subtypes of cuproptosis in HCC were identified along with GO and KEGG enrichment analysis, which revealed enrichment mainly in pathways involved in cell proliferation and cell communication. Univariate Cox regression was performed to select genes with significant *p*-values ($p < 0.05$), and five genes including G6PD, PRR11, KIF20A, EZH2, and CDCA8 were chosen to construct a cuproptosis-related signature after Lasso Cox regression. Glucose-6-phosphate dehydrogenase (G6PD) catalyzes a processive step in the oxidative pentose phosphate pathway to generate NADPH and nucleotide precursors, and G6PD depletion triggers TCA intermediates depletion. *In vivo*, G6PD impairment significantly inhibits KEAP1 mutant tumor growth (Ding et al., 2021). Additional studies have shown that G6PD promotes tumor growth by protecting cells from ROS (Hayes et al., 2020). PRR11 is a proline-rich protein that is encoded by the PRR11 gene. The PRR11 gene is located in the 17q23 amplified region. Copy regions of 17q23 are significantly enriched in brain tumors, lung, breast, and ovarian cancers (Zheng et al., 2017). The PRR11 is located in the 17q23 amplified region. Copy regions of 17q23 are significantly enriched in brain tumors, lung, breast, and ovarian cancers (Chen et al., 2015). It is highly expressed in malignant

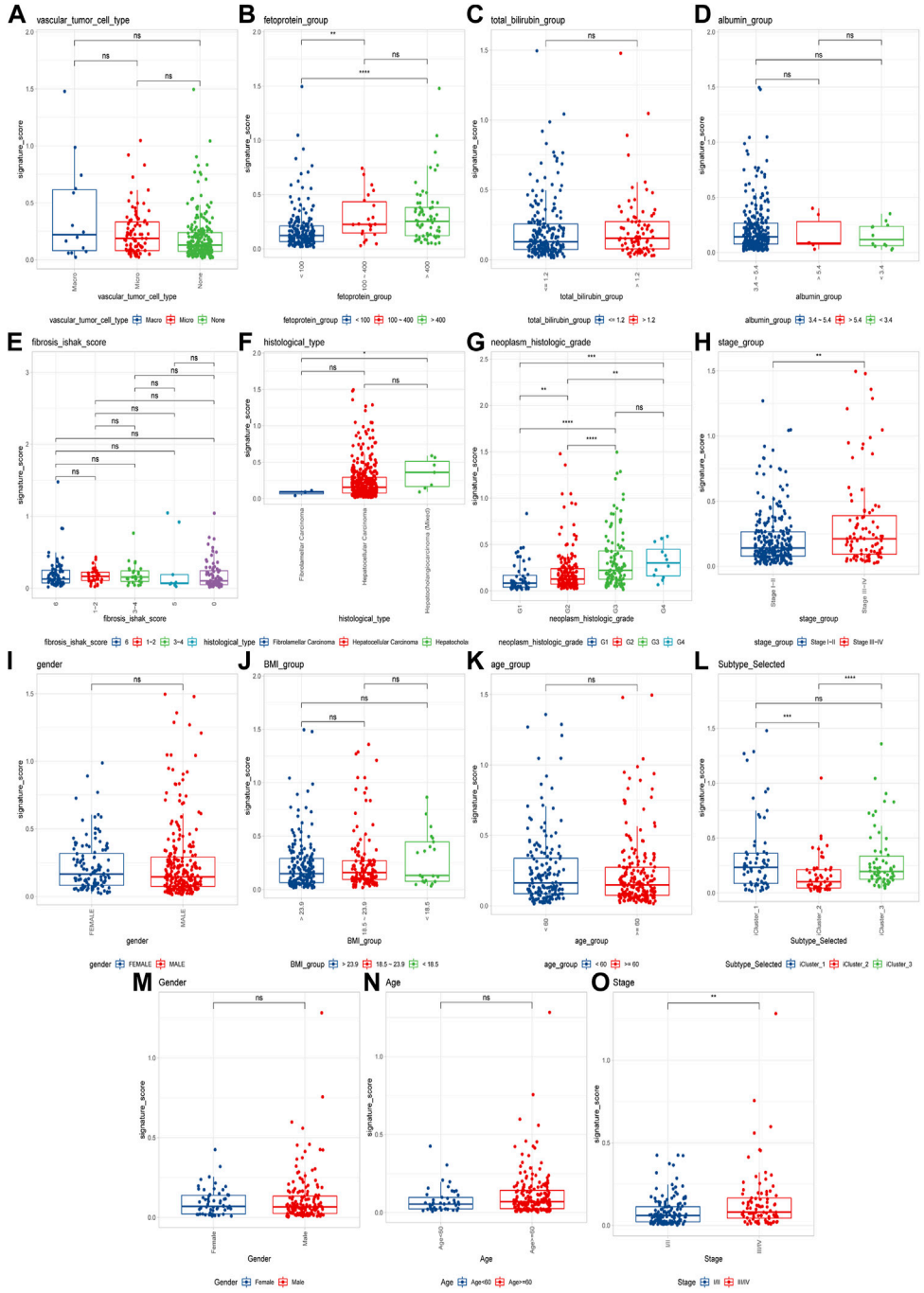

FIGURE 7
Cuproptosis-related genes signature correlates with clinical features. **(A–L)** Cuproptosis scores among different clinical features of hepatocellular carcinoma, including alpha-fetoprotein, total bilirubin, albumin, fibrosis score, histological type, histological grade, tumor stage, sex, BMI, age and molecular subtypes in TCGA cohort; **(M–O)** The differences of cuproptosis scores by gender, age, and tumor stage in the LIRI-JP cohort (ns: p >0.05; *: p <0.05; **: p <0.01; ***: p <0.001; ****: p <0.0001).

tumors, such as ovarian cancer and osteosarcoma tissues. Its expression level is associated with tumor size, Enneking stage, lymph node metastasis, and patient outcome (Li et al., 2021). Compared with normal hepatocytes, KIF20A expression was significantly upregulated in HCC HepG2 and Sk-hep1 cells, and silencing of KIF20A inhibited the proliferation of HCC cells and enhanced chemosensitivity and sorafenib sensitivity. Functional studies demonstrated that the knockout of KIF20A inhibited HCC cell proliferation (Wu et al., 2021). Upregulation of EZH2 expression in HCC is associated with unfavorable prognosis. The silence of EZH2 inhibits the HCC cell survival, migration and invasion, increased E-cadherin expression, and decreased N-cadherin and vimentin expression (Zhang et al., 2021). Cell division cycle associated 8 (CDCA8) is an essential component of the chromosome passenger complex (CPC). During mitosis, it is involved in the regulation of the dynamic localization of

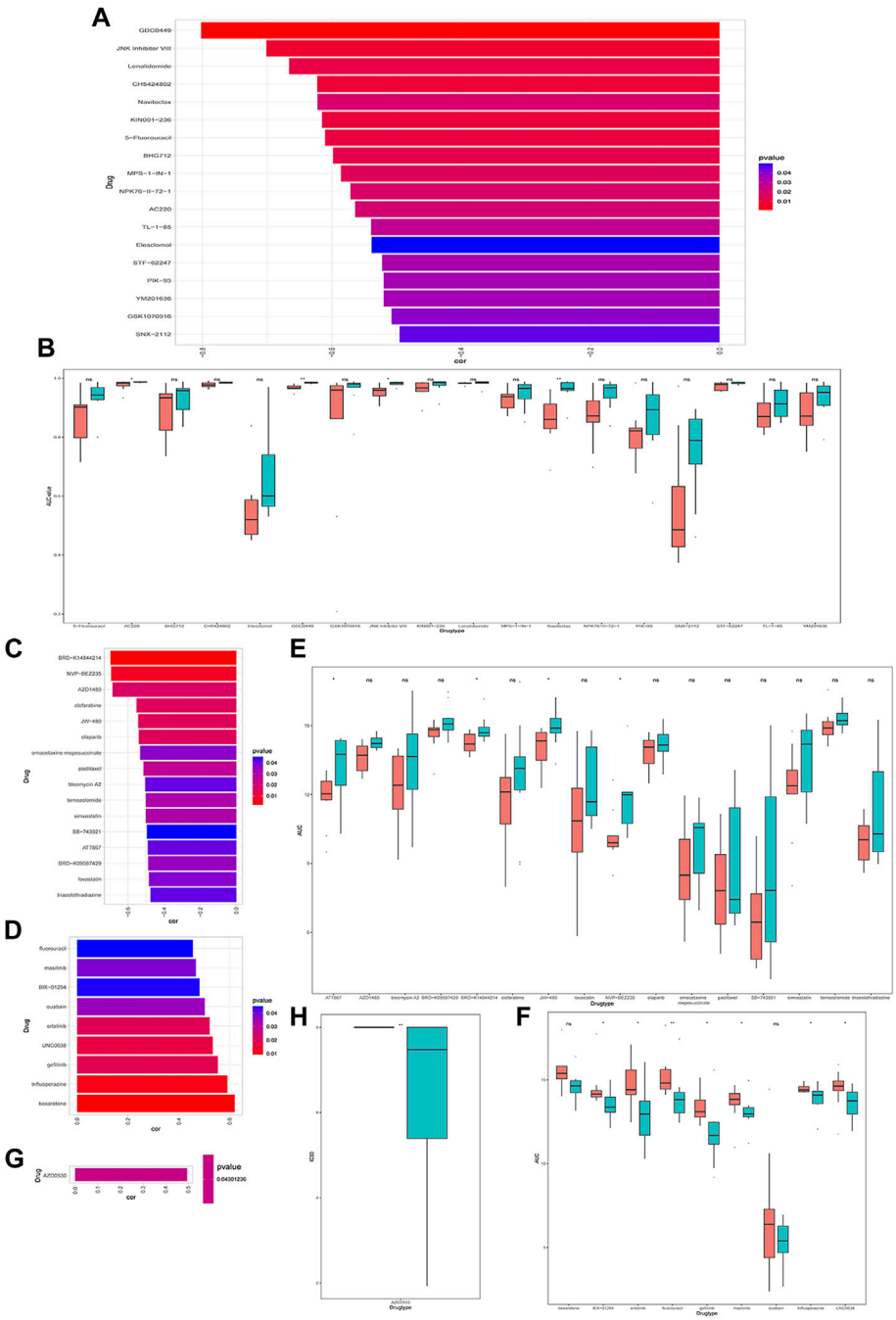

FIGURE 8
Drug sensitivity analysis of cuproptosis-related genes (CRGs)signature groups in Genomicsof Drug Sensitivity in Cancer (GDSC), Cancer Cell Line Encyclopedia (CCLE) and Cancer Therapeutics Response Portal (CTRP) databases. **(A)** Correlations between CRGs score and drug area under the curve (AUC) in GDSC ($p < 0.05$ was selected); **(B)** CRGs signature of each cell line under different drug treatments with significant negative correlation in GDSC database (* represents $p < 0.05$, ** represents $p < 0.01$, *** represents $p < 0.001$). **(C)** Correlations between CRGssignature and drug AUC in CTRP database ($p < 0.05$ and drug display with negative correlation were selected). **(D)** Correlations between CRGs signature and drug AUC in CTRP database (select $p < 0.05$ and positive correlated drugs); **(E)** The CRGs signature of each cell line under different drug treatments with significant negative correlations in CTRP database (ns: $p > 0.05$; *: $p < 0.05$); **(F)** The differences in theCRGs signature of each cell line under different drug treatments with significant positive correlation in CTRP (ns: $p > 0.05$; *: $p < 0.05$; **: $p < 0.01$); **(G)** The correlations between the CRGs signature in CCLE database and the IC50 of drugs ($p < 0.05$ and positive correlations were selected); **(H)** The differences in the CRGs signature of each cell line under different drug treatments with significant positive correlations in CCLE (*represents $p < 0.05$; *represents $p < 0.01$; **represents $p < 0.001$).

cells, and studies have suggested that CDCA8 can be used as a biomarker for the early diagnosis and prognosis prediction of HCC patients. In addition, CDCA8 may be an effective therapeutic target for HCC (Lv et al., 2021).

In addition, our study revealed diverse cuproptosis genes to be differentially expressed in distinct clinical features. For example, *GLS* was differentially expressed in distinct age stages, BMI groupings as well as different tumor stages, and *DLD* was differentially expressed in

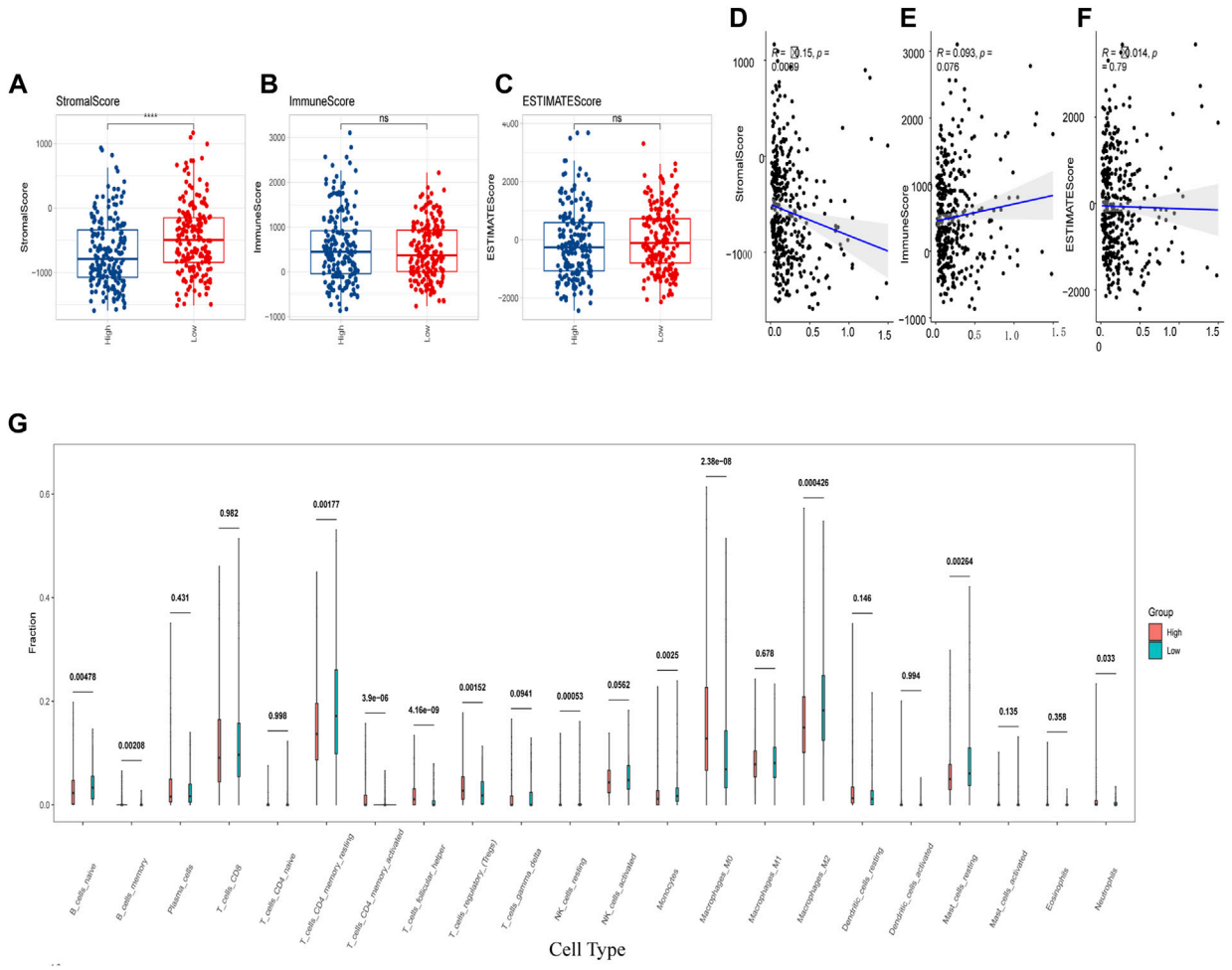

FIGURE 9
Cuproptosis-related genes (CRGs) signature was correlated with immune score and immune infiltrating cells. **(A–C)** Differences of matrix score **(A)**, immune score **(B)** and ESTIMATE score **(C)** between the two groups with high and low CRGs signature; **(D–F)** Correlations of CRGs signature and matrix score **(D)**, immune score **(E)** and ESTIMATE score **(F)**; **(G)** Differences in immune cell score between two CRGs groups with high and low CRGs signature (calculated by Cibersort) (ns: p >0.05; ****: p <0.0001).

alpha-fetoprotein levels. There were also significant expression differences among TCGA molecular classification, bilirubin, albumin maximum, fibrosis, grade, gender, and other clinical subgroups along with the 10 cuproptosis genes. It could be found that cuproptosis genes presented expression differences among different clinical features, suggesting the involvement of cuproptosis-related genes in the prognosis and development of HCC. To further explore the potential mechanism and the role of CRGs' prognostic value, we successfully established and validated CRGs signature, and analyzed the its prognostic values and clinical implications. Clustering and survival analysis by the median value of cuproptosis-associated signature revealed that signature was associated with HCC prognosis (p < 0.0001), and the areas under ROC curves were 0.718, 0.756, 0.714, 0.707 at 6 months, 1, 3, and 5 years, respectively. Meanwhile, we further validated its predictive accuracy in the LIRI-JP dataset of ICGC, and gained consistent results, and the areas under the ROC curves at 6 months, 1, 3, and 5 years were 0.778, 0.813, 0.749, 0.797, respectively. Survival analysis also suggested that the low CRGs signature was associated with a better prognosis (p < 0.0001). Besides, multivariate Cox regression showcased that the CRGs signature was an independent risk factor for HCC in both cohorts (p < 0.0001). Meanwhile, we revealed that significance was correlated with multiple clinical features including alpha-fetoprotein, histological grade, tumor stage as well as TCGA molecular subtypes in TCGA. In the LIRI-JP dataset, we verified that significance indeed showed a significant relationship with tumor stage. Therefore, our CRGs signature presented an excellent performance in predicting the prognosis of HCC patients, and provide new insights for the classification of HCC.

The hallmark enrichment score of tumors was calculated based on GSVA to evaluate the difference in hallmarks between the two CRGs groups, and we observed significant enrichments of multiple hallmark pathways in the low CRGs group compared with the high CRGs group. In the analysis of the tumor microenvironment, the stroma score in the high CRGs group was less significant than that in the low CRGs group, while the immune score and the estimated score were not statistically significant. Further analysis also revealed that the stromal score exhibited a significant negative correlation with the CRGs signature. The immune cell infiltration algorithm analysis also showcased multiple immune cell differences in the high and low

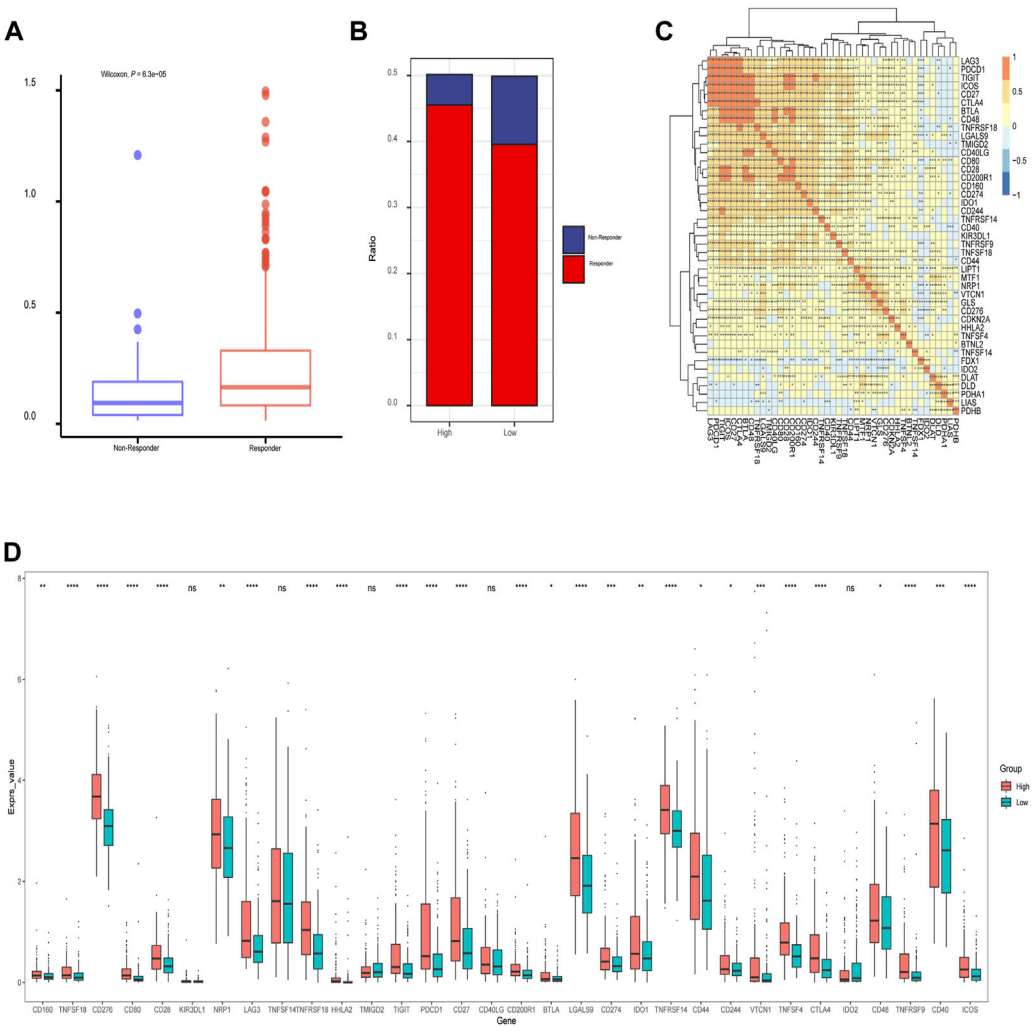

FIGURE 10
The relationship of immunotherapy responses and immune checkpoints in different cuproptosis-related genes (CRGs) signature groups. **(A)** Differences in CRGs signature of patients with different treatment outcomes (beneficial or non-beneficial) **(B)** the proportion of immunotherapy benefit and non-benefit between the two CRGs groups; **(C)** Heatmap of correlation analysis between CRGs groups and different immune checkpoints (*represents p <0.05; *represents p <0.01; **represents p <0.001; ***represents p <0.001); **(D)** Differences between the immune checkpoints and two CRGs groups (ns: p >0.05; *: p <0.05; **: p <0.01; ***: p <0.001; ****: p <0.0001).

CRGs groups. It has been reported that the expression of CDKN2A, GLS and LIPT1 is positively correlated with the abundance of CD8+T cells and neutrophils and CDKN2A expression positively correlated with the degree of tumor infiltration (Luo et al., 2021), which was in line with our study. It was also reported that in tumor-infiltrating cells, the levels of eosinophils, macrophages of M0 and M2 phenotypes, mast cell activation, and NK cell activation were positively correlated with the risk score in high-and low-risk groups (Li et al., 2022a). Additionally, we identified distinct immune checkpoint expression patterns in the two CRGs subgroups, which improved the effectiveness of immunotherapy in the era of personalized medicine in HCC.

Moreover, we further explored the drug sensitivity for the potential therapeutic possibilities of drugs in HCC. Our results showed that multiple drugs exhibiting a negative correlation between AUC and signature were found in the GDSC database, such as: 5-Fluorouracil, GDC044g et al., and the AUC was significantly different between high and low CRGs groups. Multiple drugs were also found to be correlated in the CTRP database, and the AUCs were obviously different between high and low CRGs groups. AZD0530, a drug with an IC50 positively correlated with CRGs signature in the CCLE, and its IC50 was significantly different between high and low CRGs groups.

In immune infiltration analysis, we observed a higher stromal score in the low CRGs group, the stromal score exhibited a significant negative correlation with the CRGs signature. Multiple immune cell differences were differentially expressed between the two CRGs subtypes, such as T regulatory cells, macrophages, monocytes, etc. We also discovered there was a significant association between immune checkpoints and CRGs, most notably *PDCD1* (PD-1), *TIGIT*, *CTLA4*, *ICOS*, *BTLA*, *CD28*, *LAG3*, and *CD27*. Previous studies demonstrated that the combination of immune checkpoint inhibitors (ICIs) and bevacizumab showed superiority over sorafenib in unresectable

HCC (Finn et al., 2020)- (Ren et al., 2021), which was consistent with the mechanism of immune checkpoints. *PDCD1* (PD-1) was strongly associated with tumor mutation burden (TMB), microsatellite instability (MSI), and immune cell infiltration, and it can be used as a prognostic marker in several cancer types (Miao et al., 2020). *LAG3* was the most promising immune checkpoint after PD-1 and CTLA-4, and higher *LAG3* and *FGL1* expression promoted tumor growth by suppressing the immune microenvironment (Shi et al., 2021). *CD27* played a critical role in T cell activation by providing costimulatory signals (Angelika and Anna, 2020). By grouping immunotherapy responses according to different CRGs signatures, we found that the high CRGs group had more sensitive to immunotherapy and presented higher proportions of responding patients. Besides, we found that multiple immune checkpoints were differentially expressed between the two CRGs subgroups, such as *CD276*, *CD80*, *CD28*, *CTLA4*, *LAG3*, *PDCD1* (PD-1), and *CD274* (PD-L1), indicating a potential role of the cuproptosis-related subtypes in immunotherapy. Zhou et al. (2022b) and Fu et al. (2022) also observed similar results to the current study, suggesting that CRGs were closely related to immune checkpoints. Bian et al., (Liao et al., 2022) also reported that in renal cancer, a prognostic risk score with CRGs expression signature exhibited good performance in predicting OS and PFS of patients and was significantly correlated with the level of immune infiltration and *PD-L1* expression, which was in consistent with our results. However, how cuproptosis or cuproptosis influencing drugs affect the function of anti-tumor immune cells remains unclear, and needs further exploration.

In the current work, we identified the signature of cuproptosis-related genes in HCC and developed a CRGs-based prognostic model, demonstrating a strong ability to predict the prognosis of HCC and assess treatment efficacy. Undoubtedly, our study still has certain shortcomings. Firstly, given the prognostic model was constructed and validated by utilizing data from public databases, further biological functional experiments were required to confirm our findings. Secondly, although a prognostic score focusing on the expression signatures of CRGs showed a favorable performance in predicting prognosis and clinical features in HCC, some vital clinical information was not available for analysis in the datasets, which would have impacted the prognosis and therapeutic effects of HCC. Finally, due to the limited sample size, a large-scale cohort study was crucial to evaluate the value of this model.

5 Conclusion

In summary, our integrative analysis depicted a molecular profile of CRGs and demonstrated its clinical implications in HCC. By establishing a CRGs-based prognosis model with the five hallmark genes (*G6PD*, *PRR11*, *KIF20A*, *EZH2*, and *CDCA8*), it brought prospective targets for determining the therapeutic efficacy of immunotherapy and targeted therapy, and accurately predicting the survival of HCC. The model based on CRGs helped better guide risk stratification and treatment strategy for HCC patients.

Data availability statement

The datasets presented in this study can be found in online repositories. The names of the repository/repositories and accession number(s) can be found in the article/Supplementary Material.

Author contributions

HZ contributed to the conception of the study. FH, QL, HL, and XY carried out literature retrieval and bioinformatics analysis, and prepared charts and manuscripts; YZ, SM, and PZ help with data collection, analysis and interpretation. YZ helped conceive the study and revised the manuscript. All authors contributed to the article and approved the submitted version.

Funding

This work was supported by the National Natural Science Foundation of China (81803787, 82203353), the Fellowship of China Postdoctoral Science Foundation (2022M723565), the Natural Science Foundation of Hunan Province (2022JJ40851), the Health Commission Foundation of Hunan Province (202202085327), and the Traditional Chinese Medicine Administration Foundation of Hunan Province (2021069).

Acknowledgments

We thank the TCGA and ICGC databases for the availability of the data.

Conflict of interest

The authors declare that the research was conducted in the absence of any commercial or financial relationships that could be construed as a potential conflict of interest.

Publisher's note

Supplementary material

The Supplementary Material for this article can be found online at: https://www.frontiersin.org/articles/10.3389/fphar.2023.1088993/full#supplementary-material

References

Angelika, M., and Anna, S. B. (2020). New emerging targets in cancer immunotherapy: CD27 (TNFRSF7). *ESMO Open* 4 (3), e000629. doi:10.1136/esmoopen-2019-000629

Aran, D., Hu, Z., and Atul, J. B. (2017). xCell: digitally portraying the tissue cellular heterogeneity landscape. *landscape* 18 (1), 220. doi:10.1186/s13059-017-1349-1

Aran, D., Sirota, M., and Atul, J. (2015). Systematic pan-cancer analysis of tumour purity. *Nat. Commun.* 6 (6), 8971. doi:10.1038/ncomms9971

Babak, M. V., and Ahn, D. (2021). Modulation of intracellular copper levels as the mechanism of action of anticancer copper complexes: Clinical relevance. *Biomedicines* 9, 852. doi:10.3390/biomedicines9080852

Bandmann, O., Weiss, K. H., and Kaler, S. G. (2015). Wilson's disease and other neurological copper disorders. *Lancet Neurol.* 14 (1), 103–113. doi:10.1016/S1474-4422(14)70190-5

Barretina, J., Caponigro, G., Stransky, N., Venkatesan, K., Margolin, A. A., Kim, S., et al. (2012). The Cancer Cell Line Encyclopedia enables predictive modelling of anticancer drug sensitivity. *Nature* 483 (7391), 603–607. doi:10.1038/nature11003

Basu, A., Nicole, E., BodycombeSchreiber, J. H. S. L., Cheah, J. H., Price, E. V., Liu, K., et al. (2013). An interactive resource to identify cancer genetic and lineage dependencies targeted by small molecules. *Cell.* 154 (5), 1151–1161. doi:10.1016/j.cell.2013.08.003

Beaino, W., Guo, Y., Chang, A. J., and Anderson, C. J. (2014). Roles of Atox1 and p53 in the traffi cking of copper-64 to tumor cell nuclei: Implications for cancer therapy. *J. Biol. Inorg. Chem.* 19 (3), 427–438. doi:10.1007/s00775-013-1087-0

Blockhuys, S., Celauro, E., Hildesjö, C., Feizi, A., Stål, O., Fierro-González, J. C., et al. (2017). Defining the human copper proteome and analysis of its expression variation in cancers. *Metallomics* 9, 112–123. doi:10.1039/c6mt00202a

Chen, B., Khodadoust, M. S., Liu, C. L., Newman, A. M., and Alizadeh, A. A. (2018). Profiling tumor infiltrating immune cells with CIBERSORT. *Methods Mol. Biol.* 1711, 243–259. doi:10.1007/978-1-4939-7493-1_12

Chen, Y., Cha, Z. S., Fang, W. Z., Qian, B. H., Yu, W. L., Li, W. F., et al. (2015). The prognostic potential and oncogenic effects of PRR11 expression in hilar cholangiocarcinoma. *Oncotarget* 6, 20419–20433. doi:10.18632/oncotarget.3983

Ding, H., Chen, Z., Papagiannakopoulos, T., Huang, S. M., Wu, W. L., LeBoeuf, S. E., et al. (2021). Activation oftheNRF2 antioxidant program sensitizes tumors to G6PD inhibition. *Sci. Adv.* 7, eabk1023–14. doi:10.1126/sciadv.abk1023

Ferlay, J., Siegel, R. L., Laversanne, M., Soerjomataram, I., and Jemal, A. (2021). Global cancer statistics 2020: GLOBOCAN estimates of incidence and mortality worldwide for 36 cancers in 185 countries. *CA Cancer J. Clin.* 71 (3), 209–249. doi:10.3322/caac.21660

Finn, R. S., Qin, S., Ikeda, M., Galle, P. R., Ducreux, M., Kim, T. Y., et al. (2020). Atezolizumab plus bevacizumab in unresectable hepatocellular carcinoma. *N. Engl. J. Med.* 382 (20), 1894–1905. doi:10.1056/NEJMoa1915745

Fu, J., Wang, S., Li, Z., Qin, W., Tong, Q., Liu, C., et al. (2022). Comprehensive multiomics analysis of cuproptosis-related gene characteristics in hepatocellular carcinoma. *Front. Genet.* 13, 942387. doi:10.3389/fgene.2022.942387

Giraldo, N. A., Lacroix, L., Buttard, B., Elarouci, N., and Petitprez, F. (2016). Estimating the population abundance of tissue-infiltrating immune and stromal cell populations using gene expression. *Genome Biol.* 17 (1), 218. doi:10.1186/s13059-016-1070-5

Hatori, Y., Yan, Y., Schmidt, K., Furukawa, E., Hasan, N. M., Yang, N., et al. (2016). Neuronal differentiation is associated with a redox-regulated increase of copper flow to the secretory pathway. *Nat. Commun.* 7, 10640. doi:10.1038/ncomms10640

Hayes, J. D., Dinkova-Kostova, A. T., and Tew, K. D. (2020). Oxidative stress in cancer. *Cancer Cell.* 38, 167c–197c. doi:10.1016/j.ccell.2020.06.001

Inui, T., Wada, Y., Shibuya, M., Arai-Ichinoi, N., Okubo, Y., Endo, W., et al. (2022). Intravenous ketogenic diet therapy for neonatal-onset pyruvate dehydrogenase complex deficiency. *Brain Dev.* 44 (3), 244–248. doi:10.1016/j.braindev.2021.11.005

Ishida, S., Andreux, P., Poitry-Yamate, C., Auwerx, J., and Hanahan, D. (2013). Bioavailable copper modulates oxidative phosphorylation and growth of tumors. *Proc. Natl. Acad. Sci. U. S. A.* 110, 19507–19512. doi:10.1073/pnas.1318431110

Jiang, P., Gu, S., Deng, P., Fu, J., Sahu, A., Hu, X., et al. (2018). Signatures of T cell dysfunction and exclusion predict cancer immunotherapy response. *Nat. Med.* 24 (10), 1550–1558. doi:10.1038/s41591-018-0136-1

Koizumi, M., Fujii, J., Suzuki, K., Inoue, T., Inoue, T., Gutteridge, J. M., et al. (1998). A marked increase in free copper levels in the plasma and liver of LEC rats: An animal model for wilson disease and liver cancer. *Free Radic. Res.* 28 (5), 441–450. doi:10.3109/10715769809066881

Lee, S. S., and Cheah, Y. K. (2019). The interplay between MicroRNAs and cellular components of tumour microenvironment (TME) on non-Small-Cell lung cancer (NSCLC) progression. *J. Immunol. Res.* 2019, 3046379. doi:10.1155/2019/3046379

Li, K., Yu, H., Zhao, C., and Li, J. (2021). Down-regulation of PRR11 affects the proliferation, migration and invasion of osteosarcoma by inhibiting the Wnt/β-catenin pathway. *J. Cancer* 12 (22), 6656–6664. doi:10.7150/jca.62491

Li, X., Kang, K., Peng, Y., Shen, L., Shen, L., and Zhou, Y. (2022). Comprehensive analysis of the expression profile and clinical implications of regulator of chromosome condensation 2 in pan-cancers. *Aging (Albany NY)* 14 (22), 9221–9242. doi:10.18632/aging.204403

Li, Y., Li, H., Zhang, Q., and Wei, S. (2022). The prognostic value and immune landscape of a cuproptosis-related lncRNA signature in head and neck squamous cell carcinoma. *Front. Genet.* 13 (13), 942785. doi:10.3389/fgene.2022.942785

Liao, P., Wang, W., Wang, W., Kryczek, I., Li, X., Bian, Y., et al. (2022). CD8(+) T cells and fatty acids orchestrate tumor ferroptosis and immunity via ACSL4. *Cancer Cell.* 40 (4), 365–378.e6. doi:10.1016/j.ccell.2022.02.003

Liu, J., Lichtenberg, T., Hoadley, K. A., Poisson, L. M., Lazar, A. J., Cherniack, A. D., et al. (2018). An integrated TCGA pan-cancer clinical data resource to drive high-quality survival outcome analytics. *Cell.* 173 (2), 400–416. doi:10.1016/j.cell.2018.02.052

Llovet, J. M., Zucman-Rossi, J., Pikarsky, E., Sangro, B., Schwartz, M., Sherman, M., et al. (2016). Hepatocellular carcinoma. *Nat. Rev. Dis. Prim.* 2, 16018. doi:10.1038/nrdp.2016.18

Luo, J. P., Wang, J., and Huang, J. H. (2021). CDKN2A is a prognostic biomarker and correlated with immune infiltrates in Hepatocellular Carcinoma. *Biosci. Rep.* 41 (10), BSR20211103. doi:10.1042/BSR20211103

Lv, H., Liu, X., Zeng, X., Liu, Y., Zhang, C., Zhang, Q., et al. (2021). Cell division cycle associated 8: A novel diagnostic and prognostic biomarker for hepatocellular carcinoma. *J. Cell. Mol. Med.* 25 (24), 11097–11112. doi:10.1111/jcmm.17032

Lv, H., Liu, X., Zeng, X., Liu, Y., Zhang, C., Zhang, Q., et al. (2022). Comprehensive analysis of cuproptosis-related genes in immune infiltration and prognosis in melanoma. *Front. Pharmacol.* 13 (13), 930041. doi:10.3389/fphar.2022.930041

Masisi, B. K., El Ansari, R., Alfarsi, L., Rakha, E. A., Green, A. R., and Craze, M. L. (2020). The role of glutaminase in cancer. *Histopathology* 76 (4), 498–508. doi:10.1111/his.14014

Matés, J. M., Campos-Sandoval, J. A., Santos-Jiménez, J. L., and Márquez, J. (2019). Dysregulation of glutaminase and glutamine synthetase in cancer. *Cancer Lett.* 467, 29–39. doi:10.1016/j.canlet.2019.09.011

Miao, Y., Wang, J., Li, Q., Quan, W., Wang, Y., Li, C., et al. (2020). Prognostic value and immunological role of PDCD1 gene in pan-cancer. *Source Int. Immuno- Pharmacol.* 89, 107080. doi:10.1016/j.intimp.2020.107080

Newman, A. M., Liu, C. L., Green, M. R., Alizadeh, A. A., Feng, W., Xu, Y., et al. (2015). Robust enumeration of cell subsets from tissue expression profiles. *Nat. Methods* 12 (5), 453–457. doi:10.1038/nmeth.3337

Poznanski, J., Soldacki, D., Czarkowska-Paczek, B., Bonna, A., Kornasiewicz, O., Krawczyk, M., et al. (2021). Cirrhotic liver of liver transplant recipients accumulate silver and Co-accumulate copper. *Int. J. Mol. Sci.* 22 (4), 1782. doi:10.3390/ijms22041782

Ren, Z., Xu, J., Bai, Y., Xu, A., Cang, S., Du, C., et al. (2021). Sintilimab plus a bevacizumab biosimilar (IBI305) versus sorafenib in unresectable hepatocellular carcinoma (ORIENT-32): A randomised, open-label, phase 2-3study. *Lancet Oncol.* 22 (7), 977–990. doi:10.1016/S1470-2045(21)00252-7

Shi, A. P., Tang, X. Y., Xiong, Y. L., Zheng, K. F., Liu, Y. J., Shi, X. G., et al. (2021). Immune checkpoint LAG3 and its ligand FGL1 in cancer. *Front. Immunol.* 12, 785091. doi:10.3389/fimmu.2021.785091

Siddiqui, M. A., Alhadlaq, H. A., Ahmad, J., Al-Khedhairy, A. A., Musarrat, J., and Ahamed, M. (2013). Copper oxide nanoparticles induced mitochondria mediated apoptosis in human hepatocarcinoma cells. *PloS One* 8 (8), e69534. doi:10.1371/journal.pone.0069534

Siegel, R. L., Miller, K. D., Fuchs, H. E., and Jemal, A. (2022). Cancer statistics, 2022. *Cancer J. Clin.* 72 (1), 7–33. doi:10.3322/caac.21708

Su, L., Wang, H., Miao, J., and Liang, Y. (2015). Clinicopathological significance and potential drug target of cdkn2a/p16 in endometrial carcinoma. *Sci. Rep.* 5, 13238. doi:10.1038/srep13238

Szklarczyk, D., Gable, A. L., Nastou, K. C., Lyon, D., Kirsch, R., Pyysalo, S., et al. (2021). The STRING database in 2021: Customizable protein-protein networks, and functional characterization of user-uploaded gene/measurement sets. *Nucleic. Acids. Res.* 49 (D1), D605–D612. doi:10.1093/nar/gkaa1074

Tsvetkov, P., Coy, S., Petrova, B., Dreishpoon, M., Verma, A., Abdusamad, M., et al. (2022). Copper induces cell death by targeting lipoylated TCA cycle proteins. *Science* 375 (6586), 1254–1261. doi:10.1126/science.abf0529

Wu, C., Qi, X., Qiu, Z., and Deng, G. (2021). Low expression of KIF20A suppresses cell proliferation, promotes chemosensitivity and is associated with better prognosis in HCC. *Aging (Albany NY)* 13 (18), 22148–22163. doi:10.18632/aging.203494

Wu, T., and Dai, Y. (2017). Tumor microenvironment and therapeutic response. *Cancer Lett.* 387, 61–68. doi:10.1016/j.canlet.2016.01.043

Yang, W., Soares, J., Greninger, P., Edelman, E. J., Lightfoot, H., Forbes, S., et al. (2013). Genomics of drug sensitivity in cancer (GDSC): A resource for therapeutic biomarker discovery in cancer cells. *Nucleic Acids Res.* 41, D955–D961. doi:10.1093/nar/gks1111

Zhang, G., Sun, J., and Zhang, X. (2022). A novel Cuproptosis-related LncRNA signature to predict prognosis in Hepatocellular Carcinoma. *Sci. Rep.* 12, 11325. doi:10.1038/s41598-022-15251-1

Zhang, K., Fang, T., Shao, Y., and Wu 3, Y. (2021). TGF-β-MTA1-SMAD7-SMAD3-SOX4-EZH2 signaling Axis promotes viability, migration, invasion and EMT of hepatocellular carcinoma cells. *Manag. Res.* 13, 7087–7099. doi:10.2147/cmar.s297765

Zhang, Y. J., Zhao, D. H., and Huang, C. X. (1994). The changes in copper contents and its clinical significance in patients with liver cirrhosis and hepatocarcinoma. *Zhonghua Nei Ke Za Zhi* 33 (2), 113–116.

Zhao, R., Choi, B. Y., Lee, M. H., Bode, A. M., and Dong, Z. (2016). Implications of genetic and epigenetic alterations of CDKN2A (p16(INK4a)) in cancer. *EBioMedicine* 8, 30–39. doi:10.1016/j.ebiom.2016.04.017

Zhen, Z., Zhang, Z., Liu, Y., Zhang, X., and Song, Z. (2022). Cuproptosis-related risk score predicts prognosis and characterizes the tumor microenvironment in hepatocellular carcinoma. *Front. Immunol.* 13 (13), 925618–925715. doi:10.3389/fimmu.2022.925618

Zheng, W., Zhu, G. W., Huang, Y. J., Hua, J., Yang, S. G., and Zhuang, J. F. (2017). PRR11 promotes growth and progress of colorectal cancer via epithelial-mesenchymal transition. *Int. J. Clin. Exp. Med.* 10, 13109–13122.

Zhou, Y., Li, X., Guo, L., Tao, Y., Zhou, L., and Tang, J. (2022). Identification and validation of a tyrosine metabolism-related prognostic prediction model and characterization of the tumor microenvironment infiltration in hepatocellular carcinoma. *Front. Immunol.* 13, 994259. doi:10.3389/fimmu.2022.994259

Zhou, Z., Zhou, Y., Liu, D., Yang, Q., Tang, M., and Liu, W. (2022). Prognostic and immune correlation evaluation of a novel cuproptosis-related genes signature in hepatocellular carcinoma. *Front. Pharmacol.* 13, 1074123. doi:10.3389/fphar.2022.1074123

frontiers | Frontiers in Pharmacology

TYPE Original Research
PUBLISHED 02 March 2023
DOI 10.3389/fphar.2023.1129709

OPEN ACCESS

EDITED BY
Hai-Long Piao,
Dalian Institute of Chemical Physics (CAS), China

REVIEWED BY
Yingcheng Wu,
Fudan University, China
Alessandro Rizzo,
University of Bologna, Italy

*CORRESPONDENCE
Zhong Chen,
chenz9806@163.com

†These authors have contributed equally to this work

SPECIALTY SECTION
This article was submitted to Pharmacology of Anti-Cancer Drugs, a section of the journal Frontiers in Pharmacology

RECEIVED 22 December 2022
ACCEPTED 20 February 2023
PUBLISHED 02 March 2023

CITATION
Song F, Lu C-L, Wang C-G, Hu C-W, Zhang Y, Wang T-L, Han L and Chen Z (2023), Uncovering the mechanism of Kang-ai injection for treating intrahepatic cholangiocarcinoma based on network pharmacology, molecular docking, and *in vitro* validation.
Front. Pharmacol. 14:1129709.
doi: 10.3389/fphar.2023.1129709

Uncovering the mechanism of Kang-ai injection for treating intrahepatic cholangiocarcinoma based on network pharmacology, molecular docking, and *in vitro* validation

Fei Song[1†], Chang-Liang Lu[1†], Cheng-Gui Wang[1], Chen-Wei Hu[1], Yu Zhang[1], Tian-Lun Wang[1], Lu Han[2] and Zhong Chen[1*]

[1]Department of Hepatobiliary Surgery, Affiliated Hospital of Nantong University, Medical School of Nantong University, Nantong, China, [2]Jiangsu Vocational College of Medicine, Yancheng, China

Objective: Kang-ai injection (KAI) has been a popular adjuvant treatment for solid tumors, but its anti-tumor mechanism in intrahepatic cholangiocarcinoma (ICC) remains poorly understood. This study applied a network pharmacology-based approach to unveil KAI's anti-tumor activity, key targets, and potential pharmacological mechanism in ICC by integrating molecular docking and *in vitro* validation.

Methods: The KAI-compound-target-ICC network was constructed to depict the connections between active KAI compounds and ICC-related targets based on the available data sources. The crucial ingredients, potential targets, and signaling pathways were screened using GO, KEGG enrichment analysis, and the PPI network. Molecular docking was performed to visualize the interactions between hub targets and components. *In vitro* experiments were carried out to validate the findings.

Results: Among the 87 active components of KAI and 80 KAI-ICC-related targets, bioinformatics analysis identified quercetin as a possible candidate. GO and KEGG enrichment analysis indicated that the PI3K-AKT signaling pathway might be essential in ICC pharmacotherapy. The PPI network and its sub-networks screened 10 core target genes, including AKT1 and IL1β. Molecular docking results showed stable binding between AKT1 and IL1β with KAI active ingredients. The *in vitro* experiments confirmed that KAI might suppress the

Abbreviation: ICC, intrahepatic cholangiocarcinoma; KAI, Kang-ai injection; CCK8, Cell Counting Kit-8; FBS, fetal bovine serum; IL1β, Interleukin-1 beta; BAX, Apoptosis regulator BAX; Cyclin D1, Cyclin-D1-binding protein 1; KEGG, Kyoto Encyclopedia of Genes and Genomes; MMP-9, matrix metallopeptidase 9; AKT1, RAC-alpha serine/threonine-protein kinase; GAPDH, glyceraldehyde 3-phosphate dehydrogenase; HIF1A, Hypoxia-inducible factor 1-alpha; HIF-2A, Hypoxia-inducible factor 2-alpha; TCMSP, Traditional Chinese Medicine Systems Pharmacology Database and Analysis Platform (http://lsp.nwu.edu.cn/tcmsp.php); TCMID, Traditional Chinese Medicines Integrated Database (http://www.megabionet.org/tcmid/); The Drug-Bank database, (https://www.drugbank.ca/); UniProt database, (http://www.uniprot.org/uploadlists/); OMIM, Online Mendelian Inheritance in Man (http://www.omim.org/); DisGeNET database, (https://www.disgenet.org/); GeneCardsSuite database platform, (https://www.genecards.org/); STRING database, (https://string-db.org/); RCSB PDB database, (http://www.rcsb.org/pdb/home/home.do); PubChem database, (https://pubchem.ncbi.nlm.nih.gov/).

proliferation of ICC cell lines by inhibiting the PI3K/AKT signaling pathway, consistent with the network pharmacology approach and molecular docking predictions.

Conclusion: The study sheds light on KAI's biological activity, potential targets, and molecular mechanisms in treating ICC and provides a promising strategy for understanding the scientific basis and therapeutic mechanisms of herbal treatments for ICC. This research has important implications for developing new, targeted therapies for ICC and highlights the importance of network pharmacology-based approaches in investigating complex herbal formulations.

KEYWORDS

Kang-ai injection, intrahepatic cholangiocarcinoma, network pharmacology, molecular docking, PI3K/Akt signaling pathway

Introduction

Intrahepatic cholangiocarcinoma (ICC) is a type of liver cancer that is second in prevalence only to hepatocellular carcinoma (HCC). It accounts for approximately 5%–10% of all primary liver cancers and has seen a rising incidence rate in recent years (Nuzzo et al., 2009; Sirica et al., 2009; Siegel et al., 2017). While surgery remains the preferred method for achieving a cure in patients with intrahepatic cholangiocarcinoma, a significant number of individuals cannot undergo this procedure at the time of diagnosis due to the advanced or inoperable nature of their disease. Timely diagnosis and systematic treatment are crucial for successful outcomes (Bridgewater et al., 2014; Kim et al., 2016). Despite undergoing surgical procedures such as local ablation or hepatic artery chemoembolization, some patients remain susceptible to postoperative recurrence (Wu et al., 2018). In recent years, targeted medications and immunotherapies have gained widespread recognition, leading to numerous clinical trials of targeted agents and immune checkpoint inhibitors (Rizzo et al., 2021; Viscardi et al., 2022). Nevertheless, as representatives of second-line ICB after sorafenib therapy failure, Nivolumab and Camrelizumab, among others, have shown unsatisfactory objective response rates (only about 15%) in recent large clinical trials (El-Khoueiry et al., 2017; Qin et al., 2020). Further investigation into potential anticancer drugs and techniques is imperative to change the current treatment paradigm for ICC.

Traditional Chinese Medicine (TCM) has been a cornerstone of health and wellness for millennia, embracing a holistic approach to promoting optimal balance, preventing ailments, and treating conditions. In particular, TCM holds great promise in managing complex conditions such as cancer tumors, immune disorders, and cardiovascular diseases (Xu et al., 2019). TCM can be considered a valuable resource and treasure trove for modern pharmaceutical development. As a hallmark of integrative oncology therapy in China, it plays a distinctive role in mitigating adverse effects, reducing the risk of recurrence, and enhancing the quality of life (Luo et al., 2021). On account of the advantages of TCM in tumor treatment, such as its multi-targeted approach and reduced drug resistance, the utilization of TCM in the treatment of intrahepatic cholangiocarcinoma has also achieved a commendable therapeutic outcome (Liu et al., 2019). However, TCM possesses the characteristic of multi-component and multi-targeted action, resulting in complex interactions among these targets, leading to an unclear molecular mechanism and a disconnect between basic research and clinical application. As a result, finding a solution to overcome this challenge has become an urgent concern in the development of TCM.

In response to the declining rates of drug discovery, mounting difficulties in research and development, and high rates of failure in phase II and III clinical trials, Hopkins introduced the concept of network pharmacology (Hopkins, 2007). For the first time, network pharmacology challenged the traditional approach of developing drugs with high selectivity for a single target and proposed a new model of drug action on biological networks, the "drug-multi-target-disease" approach (Kibble et al., 2015). Network pharmacology employs high-throughput omics data analysis, computer simulations, and network database searches to study the multi-target networks of diseases caused by the actions of compounds. This holistic and systematic model aligns with the comprehensive perspective of TCM, dialectical therapy, and prescription drugs. In recent years, numerous studies using network pharmacology have been conducted to examine the mechanisms of action of traditional Chinese medicine and to discover pharmacodynamic substances and active compounds (Guo et al., 2019; Liu et al., 2021).

Kang-ai Injection (KAI) is a traditional Chinese medicine that combines the properties of Astragalus, Ginseng, and sophora flavescens. It is famous for its beneficial effects, such as enhancing immune function, reducing side effects of chemotherapy, and improving chemotherapy sensitivity (Zhou et al., 2022). It is used to treat various types of cancer, including hepatocellular carcinoma, lung cancer, rectal cancer, and malignant lymphoma (Li et al., 2019; Sun et al., 2021; Zheng et al., 2022). Previous research on KAI had focused on its pharmacodynamic components, the pharmacological effects of its herbs, and clinical studies on its combination with chemotherapy drugs. However, the drug contains many active ingredients that can exert pharmacological effects through multiple targets and pathways. KAI's active components and exact molecular mechanism in treating intrahepatic cholangiocarcinoma remain largely enigmatic, necessitating further examination.

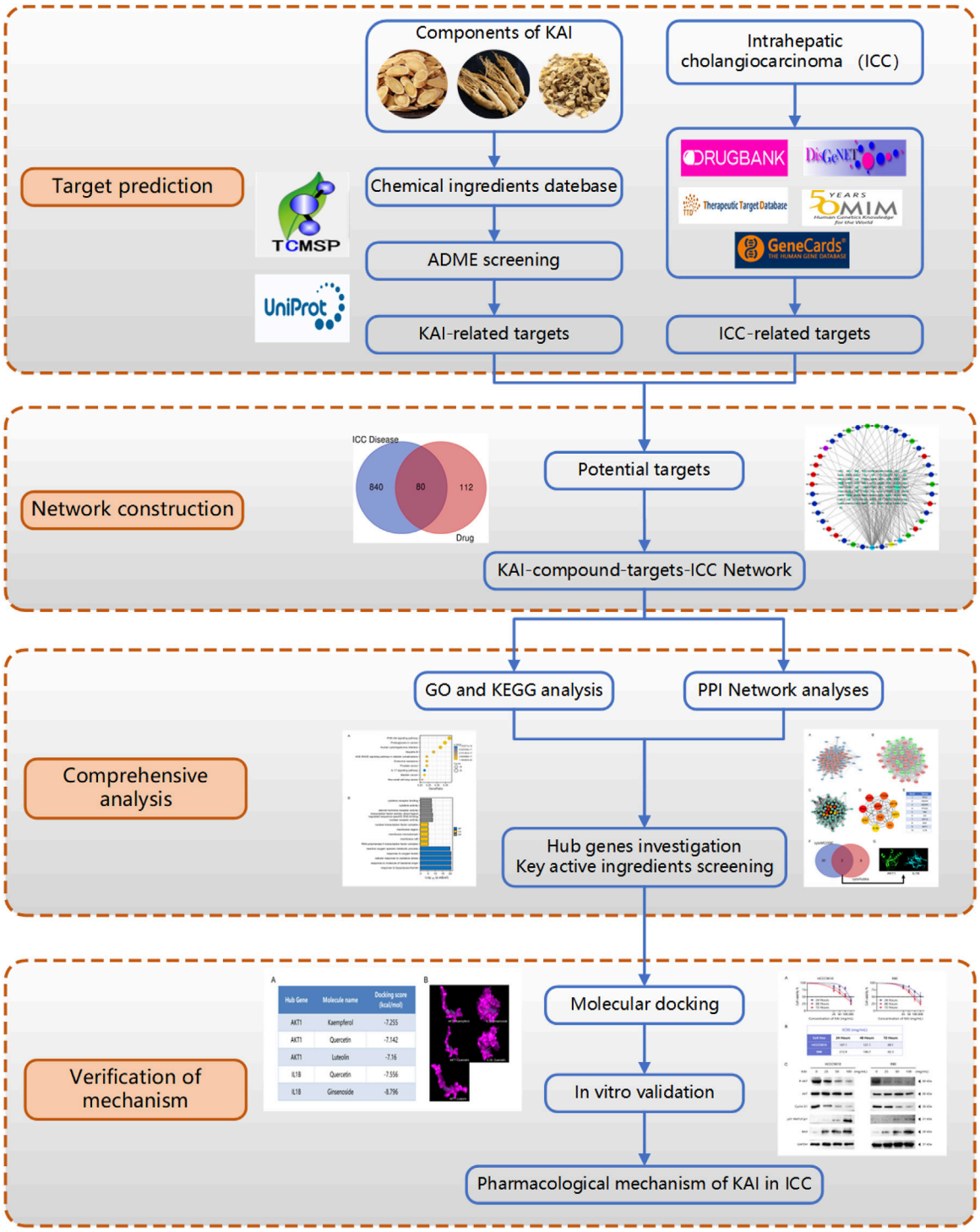

FIGURE 1
Flow diagram of the research on the mechanism of Kang-ai injection in intrahepatic cholangiocarcinoma.

This research utilized computer simulation, data analysis, and multiple database searches to predict KAI's primary active components and therapeutic targets. The predictions were then confirmed through molecular docking and *in vitro* cellular research (Figure 1). Concurrently, the target network of drug and disease interaction was established, which provided evidence for elucidating the mechanism of KAI in treating intrahepatic cholangiocarcinoma.

Materials and methods

Active ingredients and target collection of KAI

Chang-bai Shan Pharmaceutical Co., Ltd., supplied KAI (Jilin, China). Initially, we screened the active ingredients of Astragalus membranaceus, Ginseng, and Sophora flavescent in KAI through TCMSP, and set the oral bioavailability (OB) ≥ 30% and drug-like (DL) ≥ 0.18 as the active compound ADME screening conditions (Supplementary Table S1). These target proteins of the active drugs were matched with TCMID and the Drug-Bank database. Then, these target proteins are standardized into human species genes through UniProt database.

Acquisition of disease targets for intrahepatic cholangiocarcinoma

We screened targets related to intrahepatic cholangiocarcinoma by integrating information from OMIM, the Drug-Bank database, the DisGeNET database, and the GeneCardsSuite database platform.

Construction of protein-protein interaction network (PPI) and screening of hub gene

The targets of the active ingredients in KAI were mapped to coincide with the disease targets of intrahepatic cholangiocarcinoma to acquire the core target proteins for medication therapy. The STRING database was used to build the shared target-gene-protein interaction network; the protein interaction results were loaded into Cytoscape 3.7.2, and two algorithms were used to screen for critical genes. First, we used the cytoHubba function to perform a topological analysis of the network nodes to screen the top ten potential genes; then, we used the cytoMCODE function and the PPI network to screen the sub-networks and selected genes with scores above the median in the sub-network to intersect with the critical genes in the cytoHubba screen; finally, the Hub gene is screened according to the score (Chin et al., 2014; Ma et al., 2021).

Enrichment analysis of GO and KEGG pathway

The intersection targets of the KAI and ICC disease target network were analyzed for GO and KEGG pathway enrichment through the application of the biological information annotation database (DAVID). The GO analysis notes are divided into three parts, namely, molecular function (MF), cellular component (CC), and biological process (BP). The results were finally visualized by R software (Yu et al., 2012).

Molecular docking of active components of KAI with target protein

After searching the Uniprot database for the receptor protein encoded by the selected gene, we downloaded the crystal structure of the receptor protein in the RCSB PDB database and the 3D structure of the active ingredient of KAI in the PubChem database. ChemBio 3D software calculated the minimization energy and output 3D structure. The receptor protein was dehydrated using PyMOL 2.4.0 software, and it was hydrogenated and charge calculated by Autodock software. This receptor protein docking site's parameters were configured to incorporate the active pocket site for small molecule ligand binding. Ultimately, the receptor protein is docked to the active compound's small molecule ligand using Auto-dock Vina. Lesser the docking score, the more securely the ligand binds to the protein (Trott and Olson, 2010; Koebel et al., 2016; Nguyen et al., 2020).

TABLE 1 Antibodies for Westen blot assays.

Gene	Manufacturer	Dilution ratio
P-AKT	Cell Signaling Technology	1:800
AKT	Cell Signaling Technology	1:1,000
Bax	Cell Signaling Technology	1:1,000
Bcl-2	Cell Signaling Technology	1:1,000
Survivin	Cell Signaling Technology	1:800
GAPDH	Beyotime	1:1,000

P-AKT: Phospho-Akt (Ser473).

Cell proliferation

This study used HCC9810 (Shanghai Branch Cell Bank, China) and RBE (Tohoku University Cell Resource Center, Japan). Cell lines were incubated in RPMI 1640, with 10% FBS (Gibco) and antibiotics (penicillin 100 U/mL, streptomycin 100 mg/mL), at 37°C in an incubator containing 5% CO_2 (Song et al., 2021).

Utilizing CCK-8 (Dojindo, Kumamoto, Japan), the inhibitory impact of cell growth was detected. HCC9810 and RBE were cultured at a density of 5,000 cells per well in 96-well plates. They were incubated for 8 h before being treated for 24 h, 48 h, or 72 h, respectively, with or without KAI at the stated doses. The tumor cells were washed twice with PBS, treated with a 1:10 dilution of CCK-8 reagent, and incubated for two hours at 37°C. Each day, the absorbance of the cells at 450 nm was observed (Song et al., 2020).

Western blot

Cell lysates were collected using RIPA buffer containing 0.1% PMSF (BOSTER Biotechnology; Wuhan, China). SDS-PAGE performed separation on a 10% gradient gel. The separated proteins on the gel were transferred to a PVDF membrane of 0.45 μm (Chen et al., 2018). Refer to Table 1 for detailed antibody information.

Statistical analysis

Statistical analysis was performed using IBM SPSS 23.0 (SPSS, Chicago, IL) and GraphPad Prism 7 (GraphPad Software Inc., San

TABLE 2 The top 10 ingredients in the KAI-ICC network.

Mol ID	Degree	Molecule name
MOL000098	63	quercetin
MOL000006	33	luteolin
MOL000422	19	kaempferol
MOL000392	10	formononetin
MOL000378	9	7-O-methylisomucronulatol
MOL000417	8	Calycosin
MOL000358	8	isorhamnetin
MOL000456	8	beta-sitosterol
MOL000354	7	isorhamnetin
MOL000449	7	Stigmasterol

Diego, CA, United States). Continuous variables were expressed as mean ± SEM; comparisons between groups were made using Student *t*-test or Wilcoxon signed-rank test. The categorical data comparison was performed using the $\chi 2$ or Fisher's exact test. Statistical significance was set at $p < 0.05$. All experimental results were independently replicated three times (Hu et al., 2019).

Results

Screening active compounds and ICC-associated genes to identify potential ICC therapy targets

By using the TCMSP database, following the active compound ADME screening conditions, we obtained the active compound as a critical component in the drug: Astragalus membranaceus was screened for 20, Ginseng for 22, and Sophora flavescens for 45 active compounds; details are shown in Table 2. 192 drug target genes were obtained from the database (Figure 2A). Moreover, we screened 920 ICC-associated gene collections from the OMIM library, TTD database, DrugBank database, DisGeNET database, and GeneCardsSuite database platform for targets relevant to intrahepatic cholangiocarcinoma. We eventually got the set of potential target genes of ICC for drug therapy by mapping the crossover of drug target genes to disease-related genes (Figure 2B).

Critical gene AKT1 identified for drug therapy through network analysis

After discovering the compound-target disease-associated genes, we visualized the drug-active ingredient-target interaction network with 121 nodes and 264 edges using Cytoscape 3.7.2 (Figure 2C). Typically, multiple active compounds focus on a single gene, while a single compound can aim at multiple genes. We considered the degree of the node (Degree value), a crucial indicator to describe the node, to be represented by the number of nodes connected. As the substances with the higher degree values in this network, we discovered that quercetin (MOL000098) assumes the role of crucial compounds (Supplementary Table S1). The topology of network nodes was first analyzed using the cytoHubba function to screen the top ten potential genes (TP53, VEGFA, MMP9, PTGS2, TNF, IL6, HIF1A, EGF, AKT1, IL1β) by PPI protein interaction network analysis. AKT1 was ultimately chosen as our critical gene by the score after the genes were eventually intersected with the cytoMCODE functional screen (Figure 3).

KEGG and GO Enrichment Analysis Identifies Key Signaling Pathways in Drug Treatment of ICC

Through KEGG enrichment analysis, 80 target genes enrichment pathways were identified. Figure 4A displays the top ten KEGG signaling pathways with the highest enrichment. We found that PI3K-AKT pathway may play an essential role in the drug treatment of diseases. Potential BP, CC, and MF of 80 target genes were identified by GO enrichment analysis. The top 5 enriched pathways are shown in Figure 4B. The reactive oxygen species metabolic process in BP, the nuclear transcription factor complex in CC, and cytokine receptor binding and activity in MF all serve critical biological functions.

Validation of hub genes AKT1 and IL1β affinity to active components through molecular docking

We selected Hub genes (AKT1, IL1β) for molecular docking validation. Following identifying the docking components based on the target molecules, we got three active compounds against the AKT1 protein and two active compounds against IL1β from the compound-target interaction network for molecular docking. The affinity is judged by binding energy, less than 5.0 kcal/mol, indicating excellent affinity. According to the findings of molecular docking, the binding energies of the core target proteins AKT and IL1β with the active components of KAI are less than 5.0 kcal/mol, respectively (Figure 5A). The outcomes demonstrate that, as shown in Figure 5B, the active ingredients of KAI may easily access and stably bind the active pockets of AKT1 protein and IL1β protein.

KAI inhibits the proliferation of ICC cell lines by affecting PI3K/AKT pathway

The bioinformatics predictions suggest the crucial role of AKT1 as a target and the essential role of the PI3K/AKT Pathway in drug therapy for ICC. Thus, we used CCK-8 assay to detect the proliferation of ICC cell lines treated with different concentrations of KAI and found that it significantly inhibited the growth of tumor cells in a time- and dose-dependent manner (Figure 6A). Figure 6B displays the IC50 concentration values for the ICC cell lines.

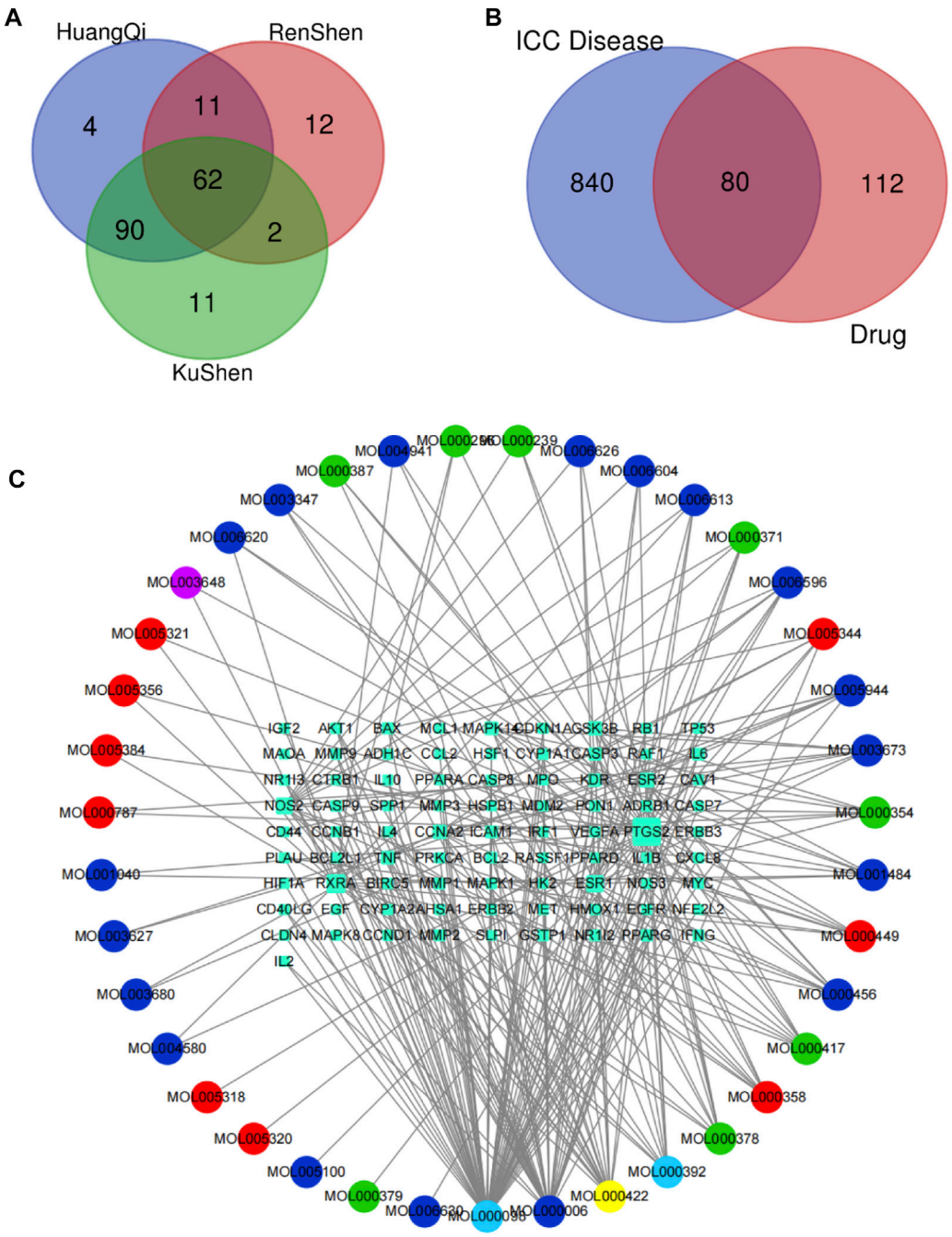

FIGURE 2
Screening of potential targets and construction of active ingredient-target networks. **(A)** The Vene diagram is composed of the target corresponding to the three main components of Astragalus, Ginseng, and Sophora flavescens. In the Vene diagram, Huangqi corresponds to Astragalus, Renshen corresponds to Ginseng, and Kushen corresponds to Sophora flavescens; **(B)** Identification of the drug-target disease-related genes by taking an intersection of drug-target genes and ICC−related genes; **(C)** The drug-targets interaction pharmacology network. The circle represents the small molecule active compound in KAI. Each color represents a traditional Chinese medicine ingredient, red represents the ingredient from Ginseng, green represents the ingredient from Astragalus membranaceus, blue represents the ingredient from Sophora flavescens, yellow represents the ingredient from Ginseng and Astragalus membranaceus, light blue represents the ingredient from astragalus membranaceus and sophora flavescens, and purple represents the ingredient from ginseng and sophora flavescens; squares represent drug-disease related target genes, node size represents the number of connections to surrounding nodes, and the lines between nodes represent interactions.

We used western blotting to evaluate the expression levels of PI3K/AKT signaling pathway. The results showed that the expression of P-AKT, p21 Waf1/Cip1, and BAX was significantly reduced, while proteins such as Cyclin D1 were downregulated after treatment of HCCC9810 and RBE with KAI (Figure 6C; Supplementary Figure S1). These findings imply that KAI suppressed ICC cell proliferation by inhibiting PI3K/AKT pathway (Figure 7).

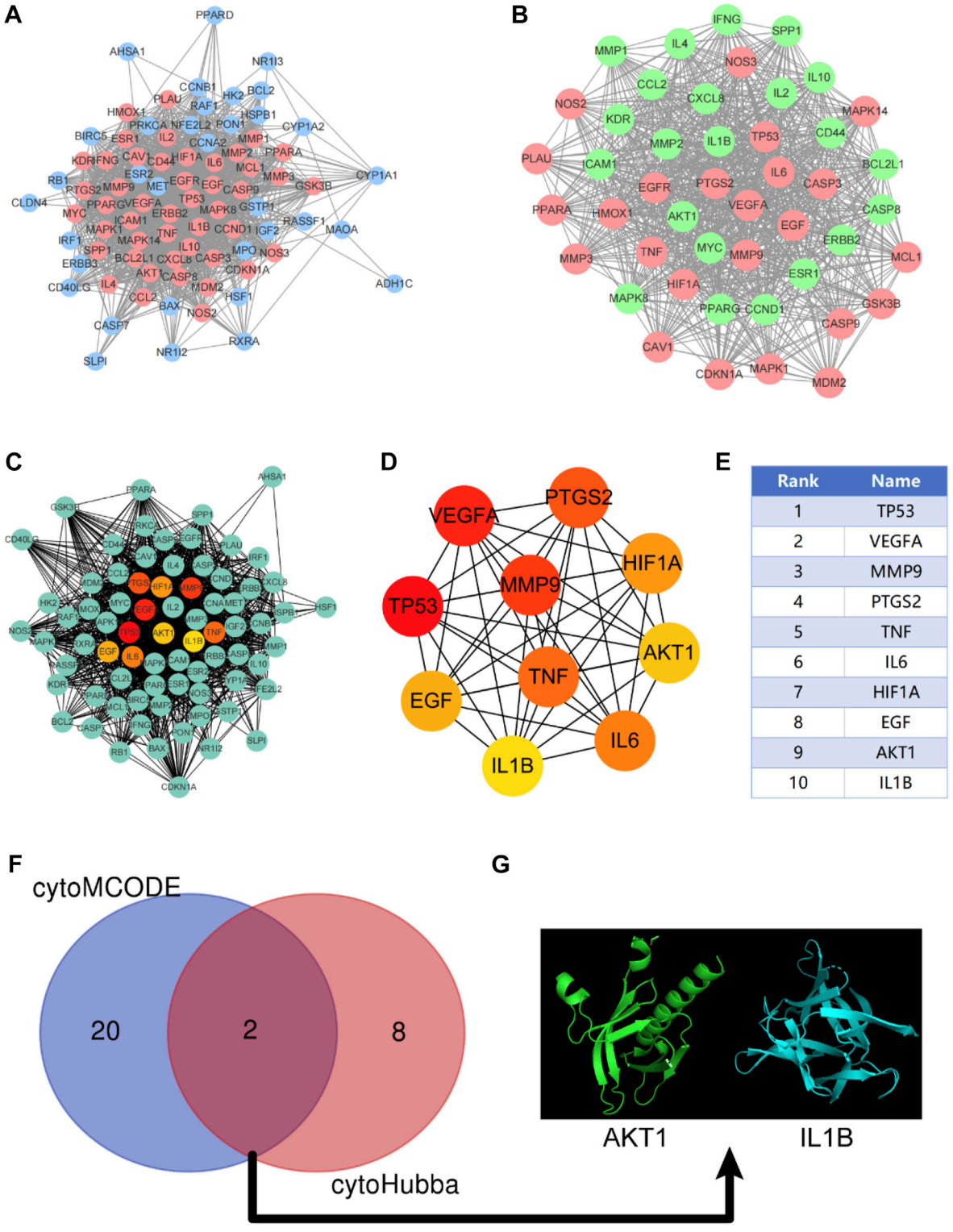

Rank	Name
1	TP53
2	VEGFA
3	MMP9
4	PTGS2
5	TNF
6	IL6
7	HIF1A
8	EGF
9	AKT1
10	IL1B

FIGURE 3
Construction of protein-protein interaction network (PPI) and screening of Hub gene. **(A)** PPI network constructed by KAI-ICC potential target, red represents the sub-network constructed by using the cytoMCODE function; **(B)** The sub-network constructed by cytoMCODE, in which green represents the selected genes in the sub-network with scores higher than the median; **(C–E)** The topology of network nodes is analyzed by using the cytoHubba algorithm to screen the top ten potential genes; **(F, G)** In the sub-network, select the genes with higher than median scores to intersect with the critical genes in the cytoHubba screening to obtain the hub genes.

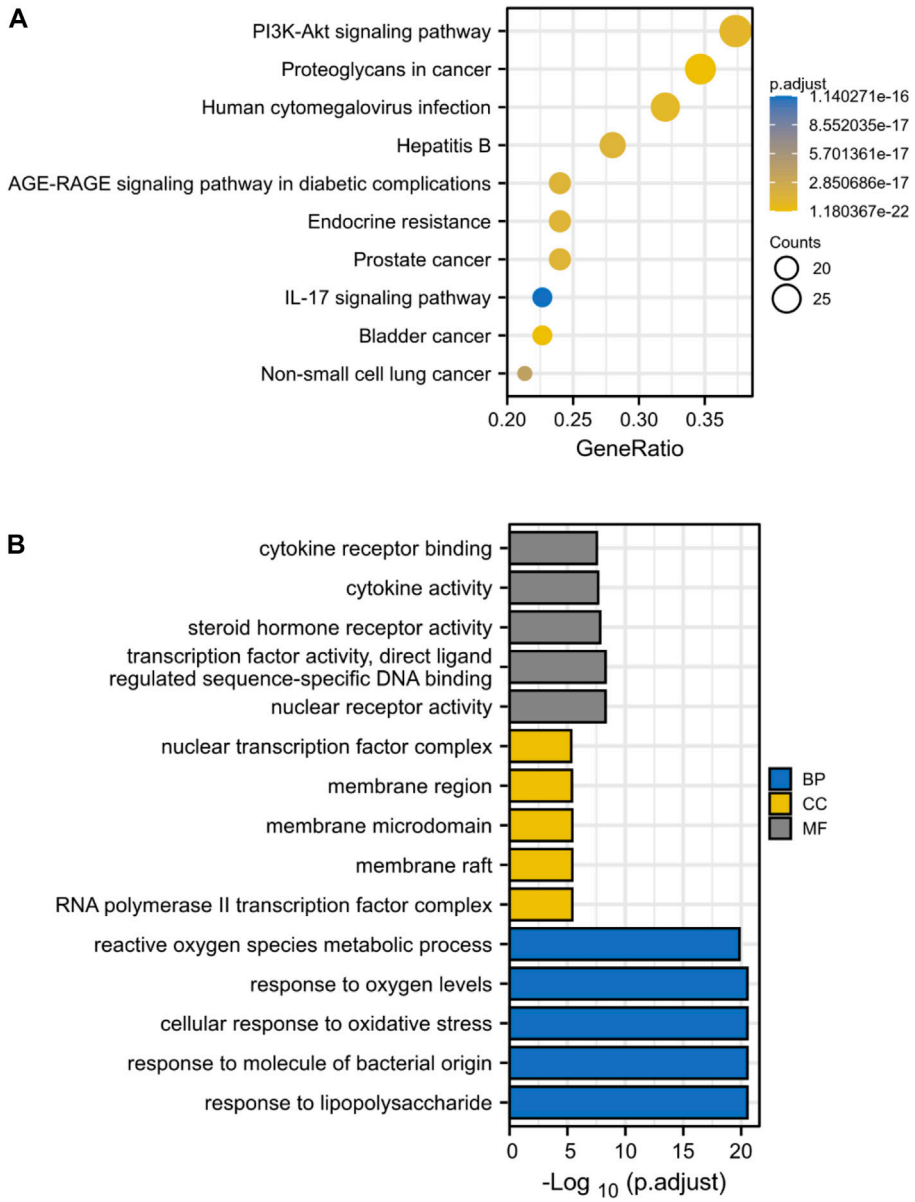

FIGURE 4
KEGG and GO Enrichment Analysis Identifies Key Signaling Pathways in Drug Treatment of ICC. **(A)** KEGG enrichment analysis, the size of each node indicates enriched counts, the abscissa represents the enriched gene ratio, and color means enriched adjusted *p*-value; **(B)** GO enrichment analysis, blue represents biological process enrichment analysis, yellow represents cell component enrichment analysis, and gray represents molecular function enrichment analysis.

Discussion

Intrahepatic cholangiocarcinoma is the most common type of primary liver malignancy after hepatocellular carcinoma. Due to its heterogeneity and aggressiveness, effective treatment has been lacking (Dong et al., 2018). TCM has a long history of success, particularly in treating challenging diseases such as major infectious diseases, immune inflammation, and malignant tumors. However, there is often more than one component of TCM, and the role of each component is often complex, which leads to the dilemma of unclear pharmacological mechanisms in the development of TCM. KAI, an injectable solution made using TCM theory, has demonstrated excellent therapeutic effects in clinical studies of several solid tumors, particularly hepatocellular cholangiocarcinoma.

Nevertheless, as the second largest tumor in primary liver cancer, ICC is far more malignant than HCC. There is a lack of research on the efficacy and mechanism of KAI in intrahepatic cholangiocarcinoma. In this research, we utilized network pharmacology and molecular docking to predict the potential targets and mechanisms of the effect of KAI in ICC. Concurrently, the drug's anti-tumor activity and pharmacological mechanism *in vitro* were verified using HCCC9810 and RBE, two intrahepatic bile duct-derived cell lines.

A

Hub Gene	Molecule name	Docking score (kcal/mol)
AKT1	Kaempferol	-7.255
AKT1	Quercetin	-7.142
AKT1	Luteolin	-7.16
IL1B	Quercetin	-7.556
IL1B	Ginsenoside	-8.796

B

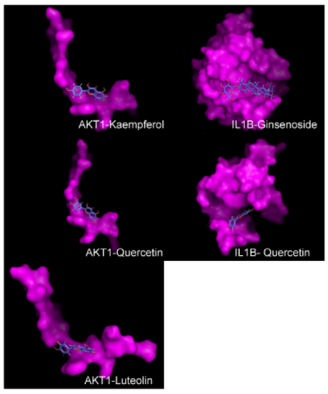

FIGURE 5
Molecular docking analysis of hub targets and corresponding active compounds. **(A)** Molecular docking score of hub target and corresponding active compound; **(B)** 3D conformational display of molecular docking between hub targets and corresponding active compound.

The main ingredients of KAI are Astragalus membranaceus, Ginseng, and Sophora flavescent, which are isolated from Chinese herbs (Zhang et al., 2018). About 87 active compounds were obtained from our ADME screening of three drugs for active compounds. The combined analysis of the topological isomerization of the drug-compound-target network revealed that the compound quercetin (MOL000098) might play a central role as the drug's active ingredient. Quercetin, a flavonoid compound, has demonstrated its inhibitory effects on tumor growth and invasion in various tumors (Tsou et al., 2016; Hu et al., 2017; Paller et al., 2018). Li S et al. showed that quercetin could enhance the synergistic effect of chemotherapeutic drugs on breast cancer cells while decreasing their toxic effects (Li et al., 2018). Quercetin also has anti-aging activity, and it can rejuvenate cells by regulating various cellular processes related to cell cycle, chromosome cohesion, and antioxidants (Geng et al., 2019). However, quercetin's poor water solubility and oral availability limit its application as an anti-tumor agent (Hu et al., 2017). In order to improve the bioavailability and stability of quercetin, Kaili Hu et al. phosphorylated quercetin hydroxyl groups to increase the aqueous solubility of hydrophobic drugs (Hu et al., 2017). KAI, as an injectable aqueous solvent, can very well avoid the poor oral utilization of quercetin. In addition, our molecular docking experiments revealed that quercetin, as the active compound, fitted well with the core target protein identified by the PPI protein interaction network (Figure 2C). Then we speculate that quercetin may be an essential active compound in KAI and play a subsequent biological function by combining with the core target protein.

KAI, one of the traditional injections of Chinese medicine, exhibits excellent anti-tumor activity and synergistic effects of chemotherapeutic drugs in various solid tumors (Cang et al., 2022; Pu et al., 2022). However, the possible mechanism of KAI in cancer therapy remains obscure. Pu Q et al. showed that KAI might inhibit cell death and modulate the cytotoxicity of chemotherapeutic agents in lung adenocarcinoma through cellular autophagy (Zhou et al., 2022). Our network pharmacology predictions and *in vitro* experiments both support the significant role played by the PI3K-AKT pathway in the mechanism of drug action in ICC (Figure 6). PI3K/AKT signal pathway is one of the primary growth regulation pathways in normal cells or cancer, in which AKT plays a vital role as the central node of the signal pathway (Kim et al., 2017; Zhang et al., 2017). PI3K/AKT signaling pathway regulates cell proliferation, cell cycle progression, and apoptosis through the phosphorylation of protein kinase B (also known as AKT) (Le et al., 2016). Western blot analysis showed that the expression of P-AKT1 in drug-treated ICC cells was reduced. Combining the molecular docking results of AKT1, we believe that AKT1, as a core target protein, changes its phosphorylation activity by binding with multiple active compounds of KAI.

In addition, our research also found that IL1β, another critical target molecule screened out, may also exert a potential role. As a cellular inflammatory factor secreted by various immune cells, such as macrophages, IL1β is often released together with proinflammatory factors after hepatocyte apoptosis, such as IL-6 and TNF-α (Guo et al., 2020). We speculate that KAI may affect the tumor immune microenvironment by releasing immune factors, which may provide synergy for future immune therapy. Among the genes screened using the cytoMCODE algorithm, we believe that TP53, VEGFA, MMP9, and HIF-1A, which rank first in the score, also play an essential role. TP53 encodes tumor suppressor p53, the most common mutated gene in human cancer (Boettcher et al., 2019). TP53, as a critical protein involved in multiple signal pathways, including Wnt and Akt, regulates cell proliferation and apoptosis (Chaudhary et al., 2018). Matrix metalloproteinase 9 (MMP9) is involved in the tumor cells' metastatic invasion as a downstream EMT transcription factor (Gujral et al., 2014; Aiello et al., 2018). Hypoxia is a significant driver of cancer invasion and metastasis, and HIF-1A and HIF-2A, as central regulators of the cellular response to hypoxia, play an essential role in this process (Liu et al., 2015; Vukovic et al., 2016). Overall, the pharmacological network of interaction between active components and targets reflects the characteristics of multi-components, multi-targets, and multi-pathways, which is consistent with the overall concept of TCM.

This study also has several limitations. Firstly, our study lacks further validation of the efficacy and safety of the drugs *in vivo*;

10.3389/fphar.2023.1129709

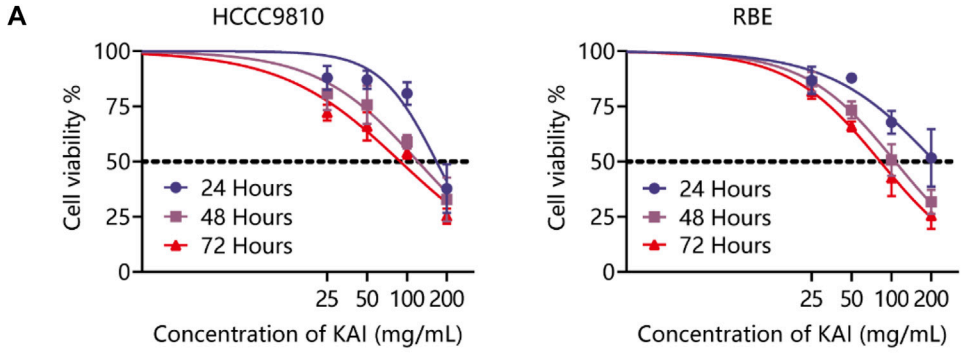

B

IC50 (mg/mL)			
Cell line	24 Hours	48 Hours	72 Hours
HCCC9810	167.1	121.1	89.1
RBE	212.9	106.7	82.3

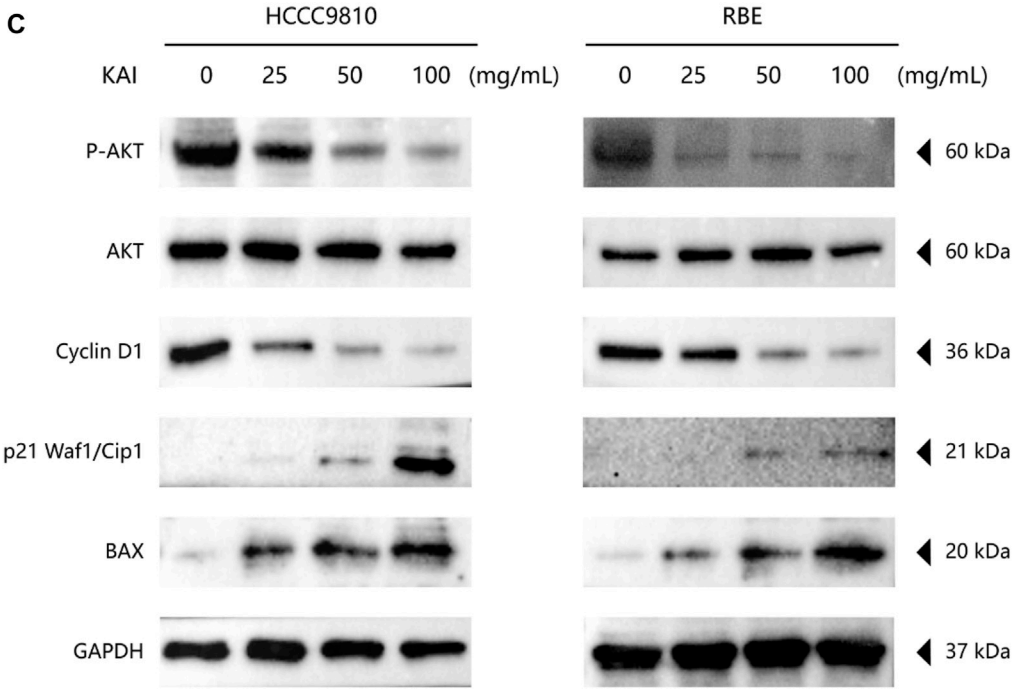

FIGURE 6
KAI inhibits the proliferation of ICC cell lines by affecting PI3K/AKT pathway. **(A, B)** HCCC9810 and RBE cells were treated with KAI at the indicated concentrations for 24 h, 48 h, or 72 h. Cell viability was measured using CCK8, and IC50 values were calculated; **(C)**. Western blot assay was used to detect the phosphate expression of AKT and the expression of AKT and its downstream proteins in ICC cells in different treatment groups.

secondly, this study lacks further verification of these phenotypes of immune infiltration, which may be of value for future anti-tumor collaboration with immunotherapy. Further data should be collected in our subsequent preclinical studies to verify anti-tumor activity, toxic effects, and adverse events.

In conclusion, our study demonstrated for the first time the anti-tumor efficacy of KAI in ICC, and its key components, target proteins, and signaling pathways were predicted using network pharmacology, molecular docking, and *in vitro* validation. It also revealed that the anti-tumor effect of KAI is mainly *via* inhibition of

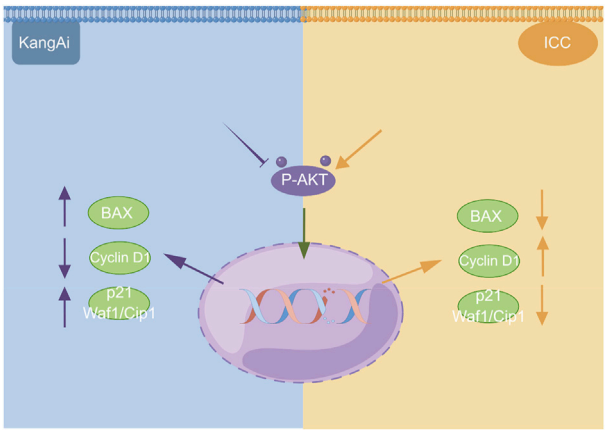

FIGURE 7
Schematic depiction of the underlying mechanism of KAI inhibiting tumor activity in ICC cells *via* the PI3K/AKT signaling pathway. This image was created with the help of the Fig-draw website, ID: ISRPYd1aa0.

AKT phosphorylation levels, thereby inhibiting PI3K/AKT signal, leading to changes in tumor cell proliferation of tumor cells.

Data availability statement

The datasets presented in this study can be found in online repositories. The names of the repository/repositories and accession number(s) can be found in the article/Supplementary Material.

Author contributions

FS performed the research and wrote the paper. FS, C-LL, and LH performed the network pharmacology and molecular docking analysis. C-LL and C-GW carried out the *in vitro* validation. C-WH and LH participated in the coordination of the research. C-WH, YZ, and T-LW performed the Westen blot analysis. FS and C-LL performed the statistical analysis. FS, ZC, and C-LL participated in the study design, and ZC edited the manuscript. All authors read and approved the final manuscript.

Funding

This study was supported by the National Natural Science Foundation of China grants (81871927 and 81070360), 2021 Changchun University of Chinese Medicine School-level Clinical Practice Teaching Reform Special Research Project (XJLCSJ202146), and the Nantong Hepatobiliary and Pancreatic Surgery Disease Research Center Construction Project (HS2015001).

Conflict of interest

The authors declare that the research was conducted in the absence of any commercial or financial relationships that could be construed as a potential conflict of interest.

Publisher's note

All claims expressed in this article are solely those of the authors and do not necessarily represent those of their affiliated organizations, or those of the publisher, the editors and the reviewers. Any product that may be evaluated in this article, or claim that may be made by its manufacturer, is not guaranteed or endorsed by the publisher.

Supplementary material

The Supplementary Material for this article can be found online at: https://www.frontiersin.org/articles/10.3389/fphar.2023.1129709/full#supplementary-material

SUPPLEMENTARY FIGURE S1
A Densitometry analysis was performed on three experiments representative of Figure 6C and expressed relative to GAPDH or the corresponding total protein as the internal control. All bar graphs depict the quantification of triplicate results with mean ± SD values. *P < 0.05; **P < 0.01; ***P < 0.001; ****P < 0.0001. (Image J 1.46r software; National Institutes of Health, Bethesda, MD).

SUPPLEMENTARY TABLE S1
Active components of KAI.

References

Aiello, N. M., Maddipati, R., Norgard, R. J., Balli, D., Li, J., Yuan, S., et al. (2018). EMT subtype influences epithelial plasticity and mode of cell migration. *Dev. Cell* 45 (6), 681–695.e4. doi:10.1016/j.devcel.2018.05.027

Boettcher, S., Miller, P. G., Sharma, R., McConkey, M., Leventhal, M., Krivtsov, A. V., et al. (2019). A dominant-negative effect drives selection of *TP53* missense mutations in myeloid malignancies. *Science* 365 (6453), 599–604. doi:10.1126/science.aax3649

Bridgewater, J., Galle, P. R., Khan, S. A., Llovet, J. M., Park, J. W., Patel, T., et al. (2014). Guidelines for the diagnosis and management of intrahepatic cholangiocarcinoma. *J. Hepatol.* 60 (6), 1268–1289. doi:10.1016/j.jhep.2014.01.021

Cang, S., Liu, R., Mu, K., Tang, Q., Cui, H., Bi, K., et al. (2022). Assessment of plasma amino acids, purines, tricarboxylic acid cycle metabolites, and lipids levels in NSCLC patients based on LC-MS/MS quantification. *J. Pharm. Biomed. Anal.* 221, 114990. doi:10.1016/j.jpba.2022.114990

Chaudhary, K., Poirion, O. B., Lu, L., and Garmire, L. X. (2018). Deep learning-based multi-omics integration robustly predicts survival in liver cancer. *Clin. Cancer Res.* 24 (6), 1248–1259. doi:10.1158/1078-0432.CCR-17-0853

Chen, X. X., Yin, Y., Cheng, J. W., Huang, A., Hu, B., Zhang, X., et al. (2018). BAP1 acts as a tumor suppressor in intrahepatic cholangiocarcinoma by modulating the ERK1/2 and JNK/c-Jun pathways. *Cell Death Dis.* 9 (10), 1036. doi:10.1038/s41419-018-1087-7

Chin, C. H., Chen, S. H., Wu, H. H., Ho, C. W., Ko, M. T., and Lin, C. Y. (2014). cytoHubba: identifying hub objects and sub-networks from complex interactome. *BMC Syst. Biol.* 8 (4), S11. doi:10.1186/1752-0509-8-S4-S11

Dong, L. Q., Shi, Y., Ma, L. J., Yang, L. X., Wang, X. Y., Zhang, S., et al. (2018). Spatial and temporal clonal evolution of intrahepatic cholangiocarcinoma. *J. Hepatol.* 69 (1), 89–98. doi:10.1016/j.jhep.2018.02.029

El-Khoueiry, A. B., Sangro, B., Yau, T., Crocenzi, T. S., Kudo, M., Hsu, C., et al. (2017). Nivolumab in patients with advanced hepatocellular carcinoma (CheckMate 040): An open-label, non-comparative, phase 1/2 dose escalation and expansion trial. *Lancet* 389 (10088), 2492–2502. doi:10.1016/S0140-6736(17)31046-2

Geng, L., Liu, Z., Zhang, W., Li, W., Wu, Z., Wang, W., et al. (2019). Chemical screen identifies a geroprotective role of quercetin in premature aging. *Protein Cell* 10 (6), 417–435. doi:10.1007/s13238-018-0567-y

Gujral, T. S., Chan, M., Peshkin, L., Sorger, P. K., Kirschner, M. W., and MacBeath, G. (2014). A noncanonical Frizzled2 pathway regulates epithelial-mesenchymal transition and metastasis. *Cell* 159 (4), 844–856. doi:10.1016/j.cell.2014.10.032

Guo, W., Huang, J., Wang, N., Tan, H. Y., Cheung, F., Chen, F., et al. (2019). Integrating network pharmacology and pharmacological evaluation for deciphering the action mechanism of herbal formula zuojin pill in suppressing hepatocellular carcinoma. *Front. Pharmacol.* 10, 1185. doi:10.3389/fphar.2019.01185

Guo, W. Z., Fang, H. B., Cao, S. L., Chen, S. Y., Li, J., Shi, J. H., et al. (2020). Six-transmembrane epithelial antigen of the prostate 3 deficiency in hepatocytes protects the liver against ischemia-reperfusion injury by suppressing transforming growth factor-β-activated kinase 1. *Hepatology* 71 (3), 1037–1054. doi:10.1002/hep.30882

Hopkins, A. L. (2007). Network pharmacology. *Nat. Biotechnol.* 25 (10), 1110–1111. doi:10.1038/nbt1007-1110

Hu, B., Cheng, J. W., Hu, J. W., Ma, X. L., Tang, W. G., et al. (2019). KPNA3 confers sorafenib resistance to advanced hepatocellular carcinoma via TWIST regulated epithelial-mesenchymal transition. *J. Cancer* 10 (17), 3914–3925. doi:10.7150/jca.31448

Hu, K., Miao, L., Goodwin, T. J., Li, J., Liu, Q., and Huang, L. (2017). Quercetin remodels the tumor microenvironment to improve the permeation, retention, and antitumor effects of nanoparticles. *ACS Nano* 11 (5), 4916–4925. doi:10.1021/acsnano.7b01522

Kibble, M., Saarinen, N., Tang, J., Wennerberg, K., Makela, S., and Aittokallio, T. (2015). Network pharmacology applications to map the unexplored target space and therapeutic potential of natural products. *Nat. Prod. Rep.* 32 (8), 1249–1266. doi:10.1039/c5np00005j

Kim, S. B., Dent, R., Im, S. A., Espie, M., Blau, S., Tan, A. R., et al. (2017). Ipatasertib plus paclitaxel versus placebo plus paclitaxel as first-line therapy for metastatic triple-negative breast cancer (LOTUS): A multicentre, randomised, double-blind, placebo-controlled, phase 2 trial. *Lancet Oncol.* 18 (10), 1360–1372. doi:10.1016/S1470-2045(17)30450-3

Kim, T., Kim, B. W., Wang, H. J., Lee, H. Y., Won, J. H., Kim, J., et al. (2016). Quantitative assessment of the portal pressure for the liver surgery using serological tests. *Ann. Surg.* 264 (2), 330–338. doi:10.1097/SLA.0000000000001460

Koebel, M. R., Schmadeke, G., Posner, R. G., and Sirimulla, S. (2016). AutoDock VinaXB: Implementation of XBSF, new empirical halogen bond scoring function, into AutoDock vina. *J. Cheminform* 8, 27. doi:10.1186/s13321-016-0139-1

Le, X., Antony, R., Razavi, P., Treacy, D. J., Luo, F., Ghandi, M., et al. (2016). Systematic functional characterization of resistance to PI3K inhibition in breast cancer. *Cancer Discov.* 6 (10), 1134–1147. doi:10.1158/2159-8290.CD-16-0305

Li, H., Ji, Y., Zhang, S., Gao, Z., Hu, C., Jiang, R., et al. (2019). Kangai injection combined with platinum-based chemotherapy for the treatment of stage III/IV non-small cell lung cancer: A meta-analysis and systematic review of 35 randomized controlled trials. *J. Cancer* 10 (21), 5283–5298. doi:10.7150/jca.31928

Li, S., Yuan, S., Zhao, Q., Wang, B., Wang, X., and Li, K. (2018). Quercetin enhances chemotherapeutic effect of doxorubicin against human breast cancer cells while reducing toxic side effects of it. *Biomed. Pharmacother.* 100, 441–447. doi:10.1016/j.biopha.2018.02.055

Liu, J., Liu, J., Tong, X., Peng, W., Wei, S., Sun, T., et al. (2021). Network pharmacology prediction and molecular docking-based strategy to discover the potential pharmacological mechanism of huai hua san against ulcerative colitis. *Drug Des. Devel Ther.* 15, 3255–3276. doi:10.2147/DDDT.S319786

Liu, X., Chen, Z., Xu, C., Leng, X., Cao, H., Ouyang, G., et al. (2015). Repression of hypoxia-inducible factor α signaling by Set7-mediated methylation. *Nucleic Acids Res.* 43 (10), 5081–5098. doi:10.1093/nar/gkv379

Liu, X., Li, M., Wang, X., Dang, Z., Yu, L., et al. (2019). Effects of adjuvant traditional Chinese medicine therapy on long-term survival in patients with hepatocellular carcinoma. *Phytomedicine* 62, 152930. doi:10.1016/j.phymed.2019.152930

Luo, X. Y., Wu, K. M., and He, X. X. (2021). Advances in drug development for hepatocellular carcinoma: Clinical trials and potential therapeutic targets. *J. Exp. Clin. Cancer Res.* 40 (1), 172. doi:10.1186/s13046-021-01968-w

Ma, H., He, Z., Chen, J., Zhang, X., and Song, P. (2021). Identifying of biomarkers associated with gastric cancer based on 11 topological analysis methods of CytoHubba. *Sci. Rep.* 11 (1), 1331. doi:10.1038/s41598-020-79235-9

Nguyen, N. T., Nguyen, T. H., Pham, T. N. H., Huy, N. T., Bay, M. V., Pham, M. Q., et al. (2020). Autodock vina adopts more accurate binding poses but Autodock4 forms better binding affinity. *J. Chem. Inf. Model* 60 (1), 204–211. doi:10.1021/acs.jcim.9b00778

Nuzzo, G., Giuliante, F., Ardito, F., and Giovannini, I. (2009). Intrahepatic cholangiocarcinoma. *Ann. Surg.* 249 (3), 541–542. doi:10.1097/SLA.0b013e31819aa76e

Paller, C. J., Zhou, X. C., Heath, E. I., Taplin, M. E., Mayer, T., Stein, M. N., et al. (2018). Muscadine grape skin extract (mpx) in men with biochemically recurrent prostate cancer: A randomized, multicenter, placebo-controlled clinical trial. *Clin. Cancer Res.* 24 (2), 306–315. doi:10.1158/1078-0432.CCR-17-1100

Pu, Q., Yu, L., Wang, X., Yan, H., Xie, Y., Jiang, Y., et al. (2022). Immunomodulatory effect of traditional Chinese medicine combined with systemic therapy on patients with liver cancer: A systemic review and network meta-analysis. *J. Cancer* 13 (11), 3280–3296. doi:10.7150/jca.74829

Qin, S., Ren, Z., Meng, Z., Chen, Z., Chai, X., Xiong, J., et al. (2020). Camrelizumab in patients with previously treated advanced hepatocellular carcinoma: A multicentre, open-label, parallel-group, randomised, phase 2 trial. *Lancet Oncol.* 21 (4), 571–580. doi:10.1016/S1470-2045(20)30011-5

Rizzo, A., Ricci, A. D., and Brandi, G. (2021). Durvalumab: An investigational anti-PD-L1 antibody for the treatment of biliary tract cancer. *Expert Opin. Investig. Drugs* 30 (4), 343–350. doi:10.1080/13543784.2021.1897102

Siegel, R. L., Miller, K. D., and Jemal, A. (2017). Cancer statistics, 2017. *CA Cancer J. Clin.* 67 (1), 7–30. doi:10.3322/caac.21387

Sirica, A. E., Dumur, C. I., Campbell, D. J., Almenara, J. A., Ogunwobi, O. O., and Dewitt, J. L. (2009). Intrahepatic cholangiocarcinoma progression: Prognostic factors and basic mechanisms. *Clin. Gastroenterol. Hepatol.* 7 (11), S68–S78. doi:10.1016/j.cgh.2009.08.023

Song, F., Chen, F. Y., Wu, S. Y., Hu, B., Liang, X. L., Yang, H. Q., et al. (2021). Mucin 1 promotes tumor progression through activating WNT/β-catenin signaling pathway in intrahepatic cholangiocarcinoma. *J. Cancer* 12 (23), 6937–6947. doi:10.7150/jca.63235

Song, F., Hu, B., Cheng, J. W., Sun, Y. F., Zhou, K. Q., Wang, P. X., et al. (2020). Anlotinib suppresses tumor progression via blocking the VEGFR2/PI3K/AKT cascade in intrahepatic cholangiocarcinoma. *Cell Death Dis.* 11 (7), 573. doi:10.1038/s41419-020-02749-7

Sun, C., Dong, F., Xiao, T., and Gao, W. (2021). Efficacy and safety of Chinese patent medicine (Kang-ai injection) as an adjuvant in the treatment of patients with hepatocellular carcinoma: A meta-analysis. *Pharm. Biol.* 59 (1), 472–483. doi:10.1080/13880209.2021.1915340

Trott, O., and Olson, A. J. (2010). AutoDock vina: Improving the speed and accuracy of docking with a new scoring function, efficient optimization, and multithreading. *J. Comput. Chem.* 31 (2), 455–461. doi:10.1002/jcc.21334

Tsou, L. K., Lara-Tejero, M., RoseFigura, J., Zhang, Z. J., Wang, Y. C., Yount, J. S., et al. (2016). Antibacterial flavonoids from medicinal plants covalently inactivate type III protein secretion substrates. *J. Am. Chem. Soc.* 138 (7), 2209–2218. doi:10.1021/jacs.5b11575

Viscardi, G., Tralongo, A. C., Massari, F., Lambertini, M., Mollica, V., Rizzo, A., et al. (2022). Comparative assessment of early mortality risk upon immune checkpoint inhibitors alone or in combination with other agents across solid malignancies: A systematic review and meta-analysis. *Eur. J. Cancer* 177, 175–185. doi:10.1016/j.ejca.2022.09.031

Vukovic, M., Sepulveda, C., Subramani, C., Guitart, A. V., Mohr, J., Allen, L., et al. (2016). Adult hematopoietic stem cells lacking Hif-1α self-renew normally. *Blood* 127 (23), 2841–2846. doi:10.1182/blood-2015-10-677138

Wu, R., Murali, R., Kabe, Y., French, S. W., Chiang, Y. M., Liu, S., et al. (2018). Baicalein targets GTPase-mediated autophagy to eliminate liver tumor-initiating stem cell-like cells resistant to mTORC1 inhibition. *Hepatology* 68 (5), 1726–1740. doi:10.1002/hep.30071

Xu, H. Y., Zhang, Y. Q., Liu, Z. M., Chen, T., Lv, C. Y., Tang, S. H., et al. (2019). Etcm: An encyclopaedia of traditional Chinese medicine. *Nucleic Acids Res.* 47 (D1), D976–D982. doi:10.1093/nar/gky987

Yu, G., Wang, L. G., Han, Y., and He, Q. Y. (2012). clusterProfiler: an R package for comparing biological themes among gene clusters. *OMICS* 16 (5), 284–287. doi:10.1089/omi.2011.0118

Zhang, D., Ni, M., Wu, J., Liu, S., Meng, Z., Tian, J., et al. (2018). The optimal Chinese herbal injections for use with radiotherapy to treat esophageal cancer: A systematic review and bayesian network meta-analysis. *Front. Pharmacol.* 9, 1470. doi:10.3389/fphar.2018.01470

Zhang, Y., Kwok-Shing Ng, P., Kucherlapati, M., Chen, F., Liu, Y., Tsang, Y. H., et al. (2017). A pan-cancer proteogenomic atlas of PI3K/AKT/mTOR pathway alterations. *Cancer Cell* 31 (6), 820–832.e3. doi:10.1016/j.ccell.2017.04.013

Zheng, B. B., Wang, Q., Yue, Y., Li, J., Li, X. J., and Wang, X. (2022). Network pharmacology and molecular docking validation to reveal the pharmacological mechanisms of kangai injection against colorectal cancer. *Biomed. Res. Int.* 2022, 3008842. doi:10.1155/2022/3008842

Zhou, H., Pan, P., Zhao, Q., Liu, W., Sun, Y., Wang, J., et al. (2022). Overcoming basal autophagy, kangai injection enhances cisplatin cytotoxicity by regulating FOXO3a-dependent autophagic cell death and apoptosis in human lung adenocarcinoma A549/DDP cells. *Biomed. Res. Int.* 2022, 6022981. doi:10.1155/2022/6022981

frontiers | Frontiers in Pharmacology

TYPE Review
PUBLISHED 08 March 2023
DOI 10.3389/fphar.2023.1130747

OPEN ACCESS

EDITED BY
Jongchan Kim,
Sogang University, Republic of Korea

REVIEWED BY
Jean-Marc A Lobaccaro,
Université Clermont Auvergne, France
Ana Fernanda Castillo,
University of Buenos Aires, Argentina

*CORRESPONDENCE
Yishu Wang,
wangys@jlu.edu.cn
Honglan Zhou,
hlzhou@jlu.edu.cn

SPECIALTY SECTION
This article was submitted to Pharmacology of Anti-Cancer Drugs, a section of the journal Frontiers in Pharmacology

RECEIVED 23 December 2022
ACCEPTED 22 February 2023
PUBLISHED 08 March 2023

CITATION
Li Y, Wu S, Zhao X, Hao S, Li F, Wang Y, Liu B, Zhang D, Wang Y and Zhou H (2023), Key events in cancer: Dysregulation of SREBPs.
Front. Pharmacol. 14:1130747.
doi: 10.3389/fphar.2023.1130747

Key events in cancer: Dysregulation of SREBPs

Yunkuo Li[1], Shouwang Wu[1], Xiaodong Zhao[1], Shiming Hao[1], Faping Li[1], Yuxiong Wang[1], Bin Liu[1], Difei Zhang[2], Yishu Wang[2]* and Honglan Zhou[1]*

[1]Department of Urology, The First Hospital of Jilin University, Changchun, China, [2]Key Laboratory of Pathobiology, Ministry of Education, Jilin University, Changchun, China

Lipid metabolism reprogramming is an important hallmark of tumor progression. Cancer cells require high levels of lipid synthesis and uptake not only to support their continued replication, invasion, metastasis, and survival but also to participate in the formation of biological membranes and signaling molecules. Sterol regulatory element binding proteins (SREBPs) are core transcription factors that control lipid metabolism and the expression of important genes for lipid synthesis and uptake. A growing number of studies have shown that SREBPs are significantly upregulated in human cancers and serve as intermediaries providing a mechanistic link between lipid metabolism reprogramming and malignancy. Different subcellular localizations, including endoplasmic reticulum, Golgi, and nucleus, play an indispensable role in regulating the cleavage maturation and activity of SREBPs. In this review, we focus on the relationship between aberrant regulation of SREBPs activity in three organelles and tumor progression. Because blocking the regulation of lipid synthesis by SREBPs has gradually become an important part of tumor therapy, this review also summarizes and analyzes several current mainstream strategies.

KEYWORDS

SREBPs, lipid metabolism, fatty acids, cholesterol, cancer therapy

Abbreviations: SREBPs, Sterol regulatory element binding proteins ER, endoplasmic reticulum SCAP, SREBP cleavage-activating protein INSIG, insulin-induced gene protein COPII, the Coat Protein complex II S1P, site 1 proteases S2P, site 2 proteases FAs, fatty acids FASN, fatty acid synthase ACC1, acetyl-CoA carboxylase 1 HCC, hepatocellular carcinoma 25-HC, 25-hydroxycholesterol SCD, stearoyl-CoA desaturase HCV, hepatitis C Virus ABCA1, ATP-binding cassette transporter A1 SOAT, sterol o-acyltransferase EPA, Eicosapentaenoic acid DHA, docosahexaenoic acid FFA4, free fatty acid receptor 4 LDLR, low-density lipoprotein receptor PKM2, pyruvate kinase M2 PTPRO, protein tyrosine phosphatase receptor type O YAP, Yes-associated protein AMPK, AMP-activated protein kinase PD-L1, programmed death 1 ligand 1 EMT, epithelial-mesenchymal transition HBXIP, Hepatitis B X-interacting protein LXR, liver X receptor IDH1, isocitrate dehydrogenase 1 FDXR, ferredoxin reductase TMEM33, ER transmembrane protein 33 SPRING/C12ORF49, SREBP-regulated gene DHT, dihydrotestosterone GP73, Golgi Protein 73 PCK1, phosphorylate cytosolic phosphoenolpyruvate carboxykinase 1 LPCAT1, lysophosphatidylcholine acyltransferase 1 LDs, lipid droplets HSP90, heat shock protein 90 PAQR3, progesterone and fat receptor 3 PPARγ, peroxisome-proliferator-activated receptor-gamma CREB, cAMP-response element binding protein RANKL, receptor activators for nuclear factor-κB ligand miRNAs, small non-coding RNAs lncRNAs, long noncoding RNAs PTN, pleiotrophin HIF, hypoxia-inducible factor EphA2, Ephrin-A3/Eph receptor A2 MALAT1, metastasis-associated lung adenocarcinoma transcript 1.

1 Introduction

Lipids, also known as fats, are classified into two types: lipoids (such as phospholipids, glycolipids, and sterols) and fats (such as triglycerides and sterols). Sterols mainly include cholesterol, sex hormones, and vitamin D (Cheng et al., 2018; Long et al., 2018). Lipids are widely distributed in cellular organelles and serve as important building blocks of all membranes. Additionally, lipids play a critical role as energy sources, signaling molecules, and secondary messengers (Snaebjornsson et al., 2020; Matsushita et al., 2021). As the availability of nutrients consistently changes with tumor progression, cancer cells in the tumor microenvironment use lipid metabolism to support their rapid proliferation, survival, migration, invasion, and metastasis (Bian et al., 2021).

Lipogenesis and lipid uptake is transcriptionally controlled by sterol regulatory element binding proteins (SREBPs) (Horton et al., 2002). There are two SREBP proteins in humans: SREBP1 encoded by the *SREBF1* gene and SREBP2 encoded by the *SREBF2* gene (Brown and Goldstein, 1997; Osborne and Espenshade, 2009). SREBP1 has two isoforms: SREBP1a and SREBP1c, produced through the use of alternative transcription start sites and the difference in the first exon (exon 1a and exon 1c) (Eberlé et al., 2004) that mainly regulate genes controlling fatty acid synthesis (Brown and Goldstein, 1997; Horton et al., 2002; Horton et al., 2003a; Osborne and Espenshade, 2009). SREBP2 regulates cholesterol biosynthesis gene expression (Brown and Goldstein, 1997; Horton et al., 2003a; Horton et al., 2003b). Inactive SREBPs reside in the endoplasmic reticulum (ER) membrane and interact with SREBP cleavage-activating protein (SCAP), a polytopic transmembrane protein (Gong et al., 2015) (Figure 1). The N-terminal domain of SCAP can combine with the insulin-induced gene protein (INSIG), forming an INSIG/SCAP/SREBP complex anchored to the ER (Yabe et al., 2002; Yang et al., 2002). When sterol levels decrease, SCAP dissociates from INSIG and mediates SREBPs into the Coat Protein complex II (COPII) vesicles, transporting the SCAP/SREBP complex from the ER to the Golgi. In the Golgi, SREBPs are sequentially cleaved by site 1 and 2 proteases (S1P and S2P), releasing their transcriptionally active N-terminal domains. After cleavage, mature SREBPs translocate to the nucleus and bind to SREs and E-boxes within target gene promoters (Nohturfft et al., 2000; Sun et al., 2007).

Cancer cells require high levels of lipid synthesis and uptake to support their continued replication. Highly expressed SREBPs play an important role in lipid reprogramming in a variety of cancers, including gastric cancer (Sun et al., 2020), colon cancer (Gao et al., 2019), breast cancer (Bao et al., 2016), glioblastoma (Han et al., 2020), prostate cancer (Ettinger et al., 2004; Huang et al., 2012), hepatocellular carcinoma (Yahagi et al., 2005; Li et al., 2014a; Heo et al., 2020), and thyroid cancer (Li et al., 2020; Huang et al., 2022). The activity of SREBPs is regulated by different mechanisms at different subcellular localizations, including the ER, Golgi, and nucleus. In this review, these three organelles serve as the main thread throughout the entire process of SREBP maturation and activity. In each organelle, we discuss the regulation of SREBPs by tumor cells through various signaling pathways, which further regulate tumor cell lipid uptake, lipid production (fatty acids (FAs) and cholesterol), and lipolysis to serve the tumor cells. Because blocking the activity of SREBPs has gradually become an important measure for cancer treatment, we summarize and analyze several current mainstream strategies at the end of the review.

2 Regulation of SREBPs in the ER

Normally, SREBPs are anchored to the ER in the form of an INSIG/SCAP/SREBP complex. SREBPs must undergo the following two stages to function: dissociation of the SCAP/SREBPs complex from INSIG in the ER and subsequent translocation to the Golgi. We reviewed many related studies on the regulation of SREBPs in the ER and found that four main factors affected these two stages: 1) classical regulation of sterols, 2) regulation of long-chain fatty acids, 3) dependent and independent mTOR signaling pathways, and 4) stability of INSIG/SCAP/SREBP complexes.

2.1 Regulation of sterols

Sterol fluctuations in the ER regulate SREBP activation (Figure 1). Decreased sterol levels facilitate the dissociation of SCAP from INSIGs and incorporation of SCAP/SREBP complexes into COPII-coated vesicles (Menendez and Lupu, 2007). Cholesterol disrupts the interaction between SCAP and COPII by binding to SCAP and retains SREBPs in the ER (Shimano and Sato, 2017). Cholesterol loading reduced the expression of SCAP and the translocation of SREBP1 to the nucleolus, as well as the expression of key rate-limiting enzymes (fatty acid synthase (FASN) and acetyl-CoA carboxylase 1 (ACC1)) in *de novo* fatty acid synthesis, inhibiting hepatocellular carcinoma (HCC) progression *in vivo* and *in vitro* (Zhao et al., 2019). 25-hydroxycholesterol (25-HC), an oxidized cholesterol, retains SREBPs in the ER stronger than cholesterol (Adams et al., 2004; Eberlé et al., 2004). Cancer cells are sensitive to sterols, and the expression of cholesterol and fatty acid biosynthesis genes (*SREBF1/2*, stearoyl-CoA desaturase (*SCD*), *FASN*) was inhibited by 25-HC in cancer cells, such as glioma, breast cancer, and prostate cancer cells (Williams et al., 2013). Similarly, 25-HC acts as an inhibitor of SREBPs and reduces hepatitis C Virus (HCV) replication in hepatoma cells. 25-HC and its synthesizing enzyme cholesterol 25-hydroxylase also inhibit HCV infection by inhibiting the maturation of SREBPs (Xiang et al., 2015). Changes in cholesterol transport and esterification can affect the activation of SREBPs and the occurrence and development of tumors. p53 can induce the transcription of cholesterol transporter ATP-binding cassette transporter A1 (ABCA1). Loss of p53 or ABCA1 ablation inhibited the retrograde transport of cholesterol from the plasma membrane to the ER, thereby promoting the maturation of SREBP2 and hepatocellular carcinoma in mice (Moon et al., 2019). ER-resident sterol o-acyltransferase (SOAT) reduces ER cholesterol levels by esterifying cholesterol to form cholesteryl esters and sequestering it into lipid droplets (Chang et al., 2006; Walther and Farese, 2009). Inhibition of SOAT resulted in ER cholesterol accumulation and decreased cholesterol esterification, thereby inhibiting SREBP1-regulated gene expression, glioblastoma growth, and prostate cancer cell invasion (Yue et al., 2014; Geng et al., 2016; Navarro-Imaz et al., 2019).

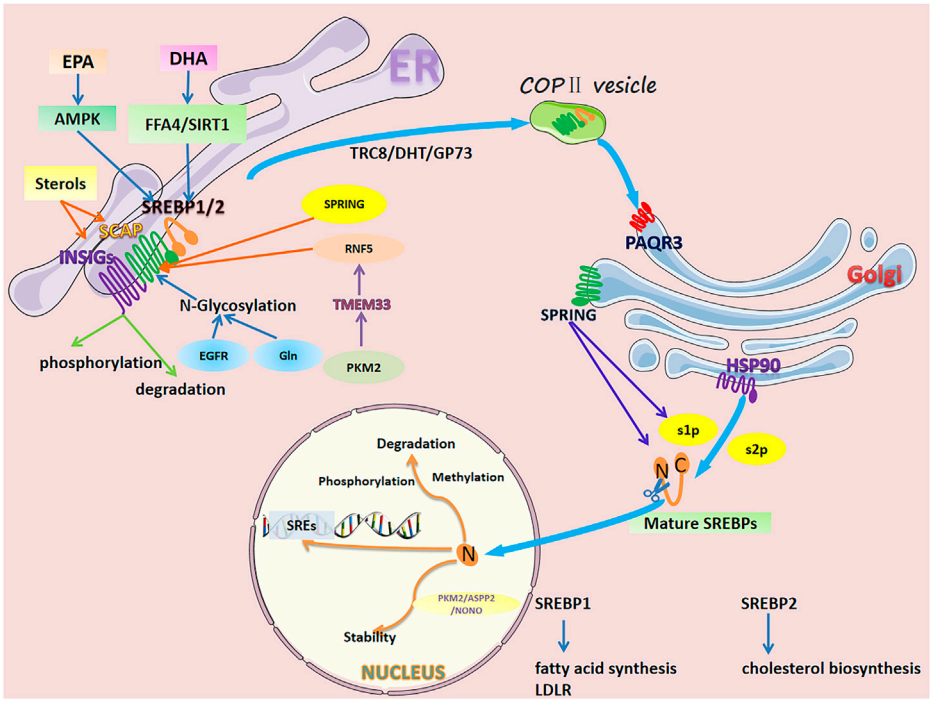

FIGURE 1
Regulation of SREBP1/2 in cancer cells. The activation process of SREBPs is as follows. Inactive SREBPs reside in the ER membrane and interact with SCAP. The N-terminal domain of SCAP combines with INSIG, forming an INSIG/SCAP/SREBP complex anchored to the ER. When sterol levels decrease, SCAP dissociates from INSIGs and mediates SREBPs into COPII vesicles, transporting the SCAP/SREBP complex from the ER to the golgi. In the golgi, SREBPs are sequentially cleaved by S1P and S2P, releasing their transcriptionally active N-terminal domains. After cleavage, mature SREBPs translocate to the nucleus and bind to SREs and E-boxes within target gene promoters. However, SREBPs are delicately and complexly regulated in individual organelles. In the ER, sterol levels directly affect the dissociation of SCAP from INSIGs. Long-chain polyunsaturated fatty acids (DHA and EPA) inhibit SREBPs at the mRNA and protein levels. N-glycosylation of SCAP, RNF5-induced degradation, SPRING-induced reduction, phosphorylation, and degradation of INSIGs all affect the transport of SREBPs to the golgi. In the golgi, PAQR3 promotes SCAP/SREBP localization and enhances the processing of SREBPs. HSP90 binds the SREBP-SCAP complex, stabilizing it and facilitating its transport from the ER to the golgi. SPRING, a necessary cofactor for the cleavage of SREBPs, directly affects the level of SREBP. In the nucleus, mature SREBPs undergo phosphorylation, methylation, and ubiquitination-related degradation. Additionally, protein-protein interactions affect their stability.

2.2 Regulation of long-chain fatty acids

Long-chain fatty acids characterized by a double bond on the third carbon atom (the hydroxycarboxylic acid chain counted from the methyl end) are called omega-3 polyunsaturated fatty acids (Calder, 2018). Omega-3 polyunsaturated fatty acids can inhibit SREBP1c in two ways: inhibition of nuclear abundance of SREBP1c and proteasome-mediated degradation of SREBP1c (Botolin et al., 2006; Scorletti and Byrne, 2013; Gnoni and Giudetti, 2016). Eicosapentaenoic acid [EPA; 20: 5(omega-3)] and docosahexaenoic acid [DHA; 22: 6(omega-3)] are ultra-long-chain highly unsaturated omega-3 fatty acids (Figure 1). Interestingly, DHA and EPA play an important role in inhibiting the proteolytic activation of SREBPs through an inhibitory mechanism distinct from sterols in cancer. In human breast cancer MCF-7 cells, DHA inhibits pAKT signaling, thereby inhibiting the precursor of SREBP1and its mature form expression and cancer cell proliferation (Huang et al., 2017). In liver cancer cells, DHA inhibits *SREBP1c* at the mRNA and protein levels; however, the inhibition of SREBP1c expression by DHA is related to free fatty acid receptor 4 (FFA4, a G protein-coupled receptor and target of DHA (Hirasawa et al., 2005)), and its inhibitory effect is attenuated by FFA4 knockdown (Kang et al., 2018). DHA protects against colon carcinogenesis by inhibiting insulin-induced activation of SREBP1 and cyclooxygenase-2 expression by upregulating SIRT1 (Song et al., 2014). DHA activation can activate SREBP2 in SW620 colon cancer cells. However, activated SREBP2 induces only a few target genes (low-density lipoprotein receptor (*LDLR*) and the first specific enzyme in cholesterol biosynthesis, *SQS/FDFT1*), and cholesterol biosynthesis remains reduced (Størvold et al., 2009). EPA, an agent that improves lipid metabolism (Carpentier et al., 2006), inhibits the development of steatohepatitis and HCC in Pten-deficient mice by increasing AMPKα1 and PPARα expression and decreasing SREBP1c expression (Ishii et al., 2009). In a human hepatoma cell line (HepG2), oxidized EPA inhibited the expression of SREBP1c and its downstream target genes more effectively than EPA (Nanthirudjanar et al., 2013). In addition to the regulatory effects of sterols and fatty acids, both ethanol and androgen can play a role in regulating SREBPs in cancer cells (Swinnen et al., 1997; You et al., 2002).

2.3 mTOR-dependent and mTOR-independent signaling pathways

Multiple signaling pathways, classified into mTOR-dependent or mTOR-independent mechanisms, can regulate the activation of

SREBPs in a lipid-independent manner in cancer (Figure 2). The most studied is the PI3K/AKT/mTOR/SREBP1 signaling pathway, which is often abnormally activated in tumor cells. In human melanoma cells, ganglioside GD3, expressed as a melanoma antigen, regulates the activity of SREBPs and cholesterol biosynthesis through the PI3K-AKT-mTORC1 signaling pathway. Interestingly, the presence of positive feedback to this signaling pathway through PI3K-AKT-mTORC1-enhanced SREBPs signaling further boosts Akt signaling in GD3-expressing human melanoma cells (Yamauchi et al., 2011). A new study revealed a novel mechanism of the PI3K/AKT/mTOR/SREBP1 signaling pathway that protects cancer cells by inhibiting ferroptosis (an iron-dependent form of cell death caused by the accumulation of phospholipid peroxides). Persistent activation of the PI3K/AKT/mTOR/SREBP1 signaling pathway mediates adipogenesis and renders cancer cells resistant to ferroptosis in PI3K-mutant breast cancer mice. SREBP1 inhibits ferroptosis in cancer cells by upregulating its transcriptional target SCD1 and producing monounsaturated fatty acids (Yi et al., 2020). Pyruvate kinase M2 (PKM2) is expressed at high levels in most cancers and catalyzes the last rate-limiting step in glycolysis. Downregulation of PKM2 reduces FASN expression and inhibits bladder cancer cell growth by significantly reducing the phosphorylation of both AKT and mTOR and inactivating the AKT/mTOR/SREBP1c signaling pathway (Tao et al., 2019). High expression of CD147, a transmembrane glycoprotein, is closely related to tumor growth, invasion, and angiogenesis (Su et al., 2009; Voigt et al., 2009). In HCC cells, the AKT/mTOR signaling pathway, activated by CD147, upregulates the expression of SREBP1c and its target genes *FASN* and *ACC* and promotes fatty acid synthesis. Concurrently, CD147 also inhibits fatty acid oxidation by inhibiting the fatty acid oxidation signaling pathways of p38 MAPK/PPARα/CPT1A and ACOX1, thereby reprogramming lipid metabolism and increasing cancer cell invasiveness (Li et al., 2015a). Protein tyrosine phosphatase receptor type O (PTPRO) suppresses tumors tumorigenesis and progression in several cancers. PTPRO, which has the opposite effect but a similar mechanism to CD147, inhibits the occurrence and metastasis of CRC by regulating two signaling pathways: AKT/mTOR/SREBP1/ACC1 and MAPK/PPARα/ACOX1 (Dai et al., 2022). The tumor microenvironment (TME) is considered a key factor in tumor progression and interaction with cancer cells (Quail and Joyce, 2013; Shi et al., 2017). Mesenchymal stem cells, an important component of the TME, increase the expression of cyclooxygenase 2 under hypoxic conditions, thereby increasing the secretion of prostaglandin E_2 (PGE_2). Hippo signaling pathway effector Yes-associated protein 1 (YAP), activated by PGE2, promotes hepatocellular carcinoma progression by upregulating the AKT/mTOR/SREBP1 signaling pathway (Liu et al., 2019). Interestingly, in non-tumorigenic MCF10A epithelial cells, YAP activates mTORC1/SREBP1 *via* serum and glucocorticoid-regulated kinase 1, rather than the AKT-mediated mTORC1/SREBP1 mechanism, which conflicts with the performance of hepatocellular carcinoma (Vaidyanathan et al., 2022). K-Ras activates the mTORC1/SREBPs (SREBP1 and SREBP2) signaling pathway and enhances the autonomous growth of breast cancer cells by activating Erk with minimal activation of Akt (Ricoult et al., 2016). Tumor necrosis factor-alpha inhibits the key regulator of energy homeostasis AMP-activated protein kinase (AMPK) and its downstream pathway mTOR/SREBP1, inducing lipid accumulation in human hepatoma HepG2 cells (Lv et al., 2015).

Cancer cells can also activate SREBP and support their increased lipid requirements for growth through an mTOR-independent mechanism. The relationship between upregulation of programmed death 1 ligand 1 (PD-L1) expression and epithelial-mesenchymal transition (EMT) plays a key role in the progression of multiple cancers (Alsuliman et al., 2015; Qiu et al., 2018). PD-L1 can directly induce EMT by upregulating SREBP1c in renal cell carcinoma, promoting cancer cell migration and invasion (Wang et al., 2015). Furthermore, PD-L1 activates SREBP1 *via* the PI3K/AKT signaling pathway, which can promote EMT and invasion of sorafenib-resistant HCC cells (Xu et al., 2020a). The expression of Hepatitis B X-interacting protein (HBXIP) in clinical breast cancer tissues positively correlates with the expression of FASN, contributing to abnormal lipid metabolism and the growth of cancer cells. Oncoprotein HBXIP directly interacts with liver X receptor-α (LXR) to co-activate and upregulate the transcription of SREBP1c and its target gene *FASN* (Zhao et al., 2016). Isocitrate dehydrogenase 1 (IDH1) is frequently mutated in human gliomas, especially the R132H mutation of IDH1 (Yan et al., 2009). $IDH1^{R132H}$ induces shunting of carbon from glycolysis to *de novo* synthesis of lipids and increases expression of *SREBPs* (mRNA levels of *1a*, *1c* and *2*). $IDH1^{R132H}$ is partially mediated by the SREBP1a signaling pathway and promotes glioma cell proliferation, growth, and migration (Zhu et al., 2013). SREBP1, upregulated by $IDH1^{R132H}$, enhances p21 expression (independent of the p53 signaling pathway) and inhibits phosphorylation of retinoblastoma protein, thereby slowing cell cycle progression in glioma cells (Miyata et al., 2013). Ferredoxin reductase (FDXR) and p53 work reciprocally and play key roles in iron homeostasis in tumors (Hwang et al., 2001; Liu and Chen, 2002; Zhang et al., 2017). Deficiency of p53 and FDXR activates SREBP1/2 and leads to increased cellular cholesterol and triglyceride levels by reducing ABCA1 expression. Meanwhile, deficiency of p53 and FDXR predisposes mice to spontaneous tumors, hepatic steatosis, and inflammation (Zhang et al., 2022).

2.4 Stability of INSIG/SCAP/SREBP complexes

Sterol and FA fluctuations and mTOR-dependent and -independent signaling pathways can regulate the INSIG/SCAP/SREBP complex in the ER. The N-terminal domain of SCAP can combine with INSIG1/2, forming an INSIG/SCAP/SREBP complex anchored to the ER. The relationship between INSIG/SCAP/SREBP is like that of an anchor, an anchor chain, and a ship. When the stability of INSIG/SCAP in cancer cells is affected, it also affects the "ship" heading to the Golgi for the next step of cutting activation (Figure 1). Under low sterol conditions, SCAP N-glycosylation mediated by glucose at three asparagine (N) positions N263, N590, and N641 *via* the SCAP protein is a prerequisite for SCAP/SREBP transport from the ER to the Golgi (Cheng et al., 2016). N-glycosylation of SCAP reduces its linkage to INSIG-1 and directs the transport of the SCAP/SREBP complex from the ER to

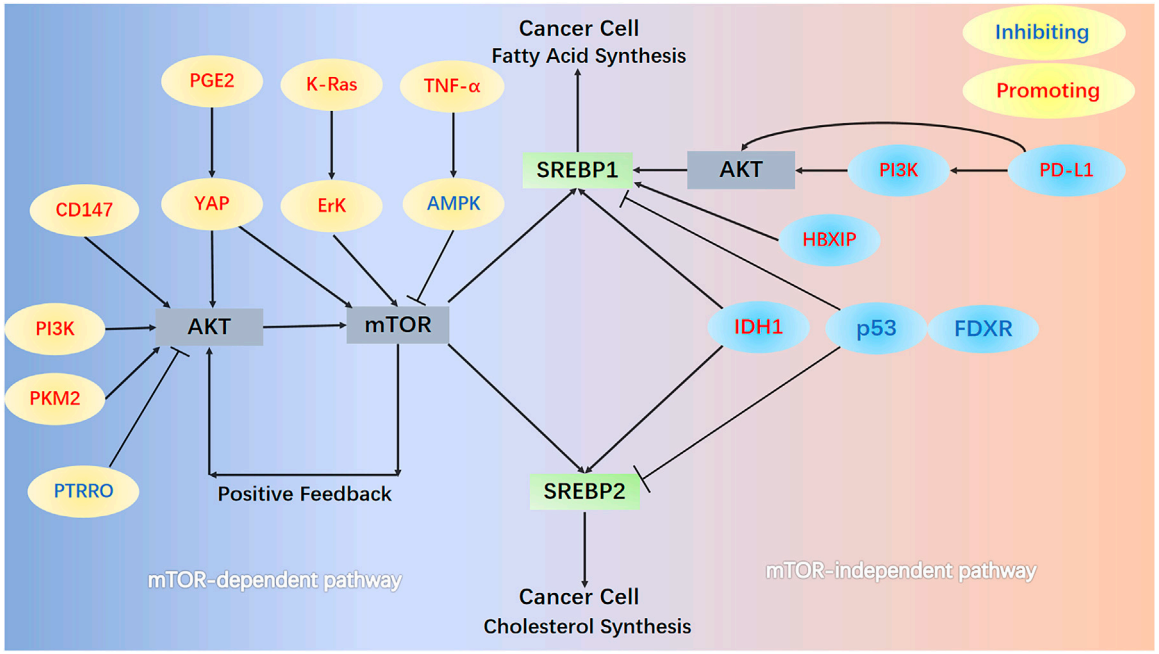

FIGURE 2
mTOR-dependent and mTOR-independent signaling pathways. In the mTOR-dependent signaling pathways, AKT/mTOR/SREBPs activate SREBPs in cancer cells. Numerous protein molecules can directly or indirectly (through AKT) act on mTOR, thereby regulating the activation of SREBPs. In the PI3K/AKT/mTOR/SREBP1 pathway, mTOR further enhances AKT signaling in melanoma cells through positive feedback. In the mTOR-independent pathway, HBXIP and PD-L1 act directly on SREBP1 and promote its activation. Mutation of the R132H site of IDH1, loss of p53, and FDXR all promote the activation of SREBP1 and SREBP2.

the Golgi (Guo, 2016). In glioblastoma, SREBP1, regulated by SCAP N-glycosylation, is highly activated (Guo et al., 2009a; Guo et al., 2009b; Guo et al., 2011; Cheng et al., 2015). EGFR signaling enhances SCAP N-glycosylation and protein levels by promoting glucose uptake, which triggers its dissociation from INSIG1. Dissociation of SCAP induces adipogenesis and glioblastoma growth through activation of SREBP1 (Cheng et al., 2015). Ammonia released from glutamine can also activate glucose-regulated N-glycosylated SCAP and dissociate from INSIG, leading to the translocation and activation of SREBP1, thereby promoting adipogenesis and tumor growth (Cheng et al., 2022). Degradation, reduction, or increase of SCAP affects the translocation and activation of SREBP. ER transmembrane protein 33 (TMEM33), a downstream effector of PKM2 upregulated upon loss of PKM2, regulates the activation of SREBPs. Upregulated TMEM33 recruits an E3 ligase, RNF5, and promotes the degradation of SCAP. Interestingly, depletion of PKM2 reduced breast cancer cell growth; however, systemic PKM2 knockdown accelerated tumor growth in allografts (Liu et al., 2021). SREBP-regulated gene (*SPRING/C12ORF49*), as a glycosylated Golgi-resident membrane protein, plays a decisive role in the SREBPs signaling pathway. In Hap1 and Hepa1-6 hepatoma cells, ablation of SPRING results in a reduction of SCAP and its mislocalization to the Golgi and decreases SREBPs signaling, independent of sterol status (Loregger et al., 2020). TRC8, encoding an E3-ubiquitin ligase and as an ER membrane-associated protein, is a putative tumor suppressor disrupted in a family of hereditary renal cell carcinomas (Gemmill et al., 2002). TRC8 is able to bind SREBP2 and SCAP to form the TRC8-SREBP2-SCAP complex, which blocks the interaction between SCAP and Sec24, one of the COPII proteins responsible for the transport of SREBP2 to the Golgi (Irisawa et al., 2009). The enhancement of SCAP-SREBPs interaction plays an important role in increasing the transport of SREBPs to the Golgi and the activation of SREBPs. High expression of dihydrotestosterone (DHT) or Golgi Protein 73 (GP73) can elevate SCAP-SREBP1 interaction and its trafficking to the Golgi, leading to increased nuclear SREBP1 and subsequent adipogenesis (Yang et al., 2017; Seidu et al., 2021). A more direct and increasingly interesting approach through pharmacological or genetic inhibition of SCAP can significantly inhibit tumor growth in various cancer models (Li et al., 2019; Liu et al., 2020; Lim et al., 2021). Strikingly, a recent study contradicts popular belief that suppressing SREBP by depletion of SCAP in the liver exacerbates liver carcinogenesis. This is due to inhibition of the SCAP/SREBP signaling pathway altering the fatty acid composition of phosphatidylcholine, resulting in ER stress and hepatocyte injury (Kawamura et al., 2022).

Phosphorylation, expression changes, and degradation of INSIGs all alter the translocation of ER-resident SREBPs to the Golgi. In human HCC cells, K-ras mutation and receptor tyrosine kinase activation can phosphorylate cytosolic phosphoenolpyruvate carboxykinase 1 (PCK1, as the gluconeogenesis rate-limiting enzyme) at Ser90 by activating AKT. Translocation of phosphorylated PCK1 to the ER, where it phosphorylates INSIG1 at Ser207 and INSIG2 at Ser151, uses GTP as a phosphate donor on the ER. This phosphorylation, in turn,

reduces the binding of INSIGs to sterols, thereby disrupting the interaction between INSIGs and SCAP and releasing the SCAP-SREBP complex for translocation to the Golgi. Ultimately, activation of SREBP proteins (SREBP1 or SREBP2) resulted in the *in vitro* proliferation of HCC cells and carcinogenesis in mice (Xu et al., 2020b). INSIG2 expression can be inhibited by insulin signaling and Akt activation by reducing *INSIG2* mRNA levels (Yecies et al., 2011). In esophageal squamous cell carcinoma, phospholipid biosynthesis/remodeling enzyme lysophosphatidylcholine acyltransferase 1 (LPCAT1) expression is high and positively correlated with SREBP1 expression in the nucleus of tumor tissue. LPCAT1 downregulates INSIG-1 expression by activating EGFR, thereby promoting SREBP1 translocation and cholesterol synthesis (Tao et al., 2021). Excess intracellular cholesterol is esterified by SOAT1 to form lipid droplets (LDs) for storage and to maintain ER cholesterol homeostasis. Inhibition of SOAT1 results in blockage of cholesterol esterification and LDs formation, allowing cholesterol accumulation in the ER. Cholesterol accumulation enhances SCAP and INSIG binding and leads to reduced adipogenesis and tumor suppression (Geng and Guo, 2017).

3 Regulation of SREBPs in the golgi

The translocation of the SCAP-SREBP complex from the ER to the Golgi can be triggered by the binding of COPII to SCAP (Figure 1). Membrane-bound S1P and S2P on the Golgi continuously cleave SREBPs and release their transcriptionally active N-terminal domains. Pharmacological inhibition of S1P blocks SREBP2 activation and Golgi complex ATF6 protein cleavage in human hepatoma cells, causing ER stress and contributing to apoptotic cell death (Lebeau et al., 2018). S1P may serve as a novel metabolic target, as its pharmacological inhibition impedes SREBP2 activation and cholesterol synthesis in glioblastoma (Caruana et al., 2017). Interestingly, pharmacological inhibition of S2P also inhibits the intramembrane proteolysis of ATF6 and SREBP1 (but not SREBP2). In castration-resistant prostate cancer and liposarcoma, it may serve as a new therapeutic target (Guan et al., 2011; Guan et al., 2012; Guan et al., 2015). SPRING, a cofactor that controls the maturation of S1P, localizes to the Golgi and is required for the cleavage of its substrates, including SREBPs. SPRING correlates with SREBP-regulated lipid metabolism-related genes. Loss of SPRING reduces mature (cleaved) SREBP levels, inhibits nuclear translocation of SREBPs, and reduces cancer cell proliferation in the absence of cholesterol. SPRING regulates SREBP processing because it interacts with the N-glycosylated form of MBTPS1 to catalyze the proteolytic cleavage of its substrate SREBPs. Notably, in the absence of MBTPS1 activity, the Golgi–ER cycle of SCAP is dysfunctional (Bayraktar et al., 2020; Xiao et al., 2021). Heat shock protein 90 (HSP90) binds the SREBP-SCAP complex, stabilizing it and promoting its transport from the ER to the Golgi. Deletion of HSP90β significantly reduces neutral lipid and cholesterol content by degrading mature SREBPs *via* the Akt-GSK3β-FBW7 signaling pathway (Zheng et al., 2019). Progesterone and fat receptor 3 (PAQR3), a Golgi-anchored membrane protein, plays an important role in tumor suppression by negatively regulating the Raf kinase and AKT signaling pathways (Feng et al., 2007; Xie et al., 2008; Zhang et al., 2010). The anchor protein of SCAP/SREBP in the ER and Golgi is INSIGs and PAQR3, respectively. PAQR3 promotes SCAP/SREBP localization in the Golgi and links it to the Golgi complex, enhancing SREBP processing and increasing cellular cholesterol levels (Xu et al., 2015a).

4 Regulation of SREBPs in the nucleus

SREBPs release their transcriptionally active N-terminal domains after cleavage in the Golgi. Mature (cleaved) SREBPs translocate to the nucleus as homodimers, subsequently binding to SREs and E-boxes within the promoters of target genes. In the nucleus, two factors are involved in the regulation of SREBPs and cancer: 1) The transcriptional regulation of SREBPs and 2) the function of SREBPs as transcription factors. Rapid degradation of the ubiquitin-proteasome signaling pathway and multiple chemical modifications (especially phosphorylation and methylation) are the greatest obstacles to nuclear SREBP activity as transcription factors. In addition, microRNAs (miRNAs) are key regulators of metabolism and play an important role in the regulation of SREBPs. Therefore, we summarize the associations of miRNAs, SREBPs, and cancer in a separate section.

4.1 Transcriptional control of SREBPs

There are two modes of transcriptional regulation of SREBPs. First, the *SREBF1* and *SREBF2* contain SREs in their promoters; these SREs mediate feed-forward transcriptional regulation (Sato et al., 1996; Amemiya-Kudo et al., 2002). Transcription of the genes encoding SREBP-1c is induced by insulin, which activates its promoter through SREs (Foretz et al., 1999; Dif et al., 2006). Feed-forward regulation of SREBPs also activates the expression of miR-33a and miR-33b encoded within introns of *SREBF1* and *SREBF2* (Brown et al., 2010; Najafi-Shoushtari et al., 2010), thereby suppressing the expression of ABCA1 and reducing efflux of newly synthesized cholesterol (Tall et al., 2008). Second, LXR-α and LXR-β mediate the transcriptional regulation of SREBPs by forming heterodimers with retinoic X receptors (RXR) (Repa et al., 2000). Ectopic overexpression of peroxisome-proliferator-activated receptor-gamma (PPARγ) co-activator-1alpha in the hepatoma line further enhances the abundance of *SREBP1c* mRNA in an LXR/RXR-dependent manner (Oberkofler et al., 2004).

In recent years, new mechanisms have been discovered for the transcriptional control of SREBPs in cancer. The *SREBP1a* promoter (−436 to −398 region) contains binding motifs for transcription factors C/EBP, which belong to a family of basic leucine zipper proteins (Qiao et al., 2013). Recent studies have shown that C/EBP-α and SREBP1 are significantly upregulated in human cancers, expanding a mechanistic link between altered lipid metabolism and malignancy (Guo et al., 2011; Li et al., 2012; Lee et al., 2017; Pang et al., 2021). Hepatitis B virus X protein (HBx) activates SREBP1a transcription *via* C/EBP-α, interacts with LXR-α in HCC cells, and recruits cAMP-response element binding protein (CREB) binding protein to the *SREBP1c* promoter (Na et al., 2009; Qiao et al., 2013). Breast cancer cells secrete several growth factors, including receptor activators for nuclear factor-κB ligand (RANKL),

which effectively promote osteoclast formation and activation, leading to excessive bone resorption (Blake et al., 2014; Bellanger et al., 2017). RANKL-induced CREB activation stimulates transcription and activation of SREBP2, which then translocates into the nucleus, promoting breast cancer metastasis and aggravating breast cancer-associated osteolysis (Jie et al., 2019).

4.2 Chemical modification and stability

Nuclear SREBPs are rapidly degraded by the ubiquitin-proteasome signaling pathway, suggesting that transcription of their target genes is tightly controlled by nuclear SREBP stability. Therefore, the chemical modification (especially phosphorylation and methylation) and stability of SREBPs in the nucleus are particularly important (Figure 1). Fbw7 interacts with the nuclear form of SREBP1a and phosphorylates it at T426 and S430 dependent on GSK3, resulting in enhanced ubiquitination and degradation (Sundqvist et al., 2005). In mitotic cells, the protein kinase Polo-like kinase 1 phosphorylates threonine residues at the docking site of nuclear SREBP1 with Fbw7, blocking the interaction between SREBP1 and Fbw7 and reducing nuclear SREBP1 Fbw7-dependent degradation (Bengoechea-Alonso and Ericsson, 2016). Protein arginine methyltransferase 5 induces arginine methylation (dimethylation of R321) of SREBP1a, preventing SREBP1a from being phosphorylated by GSK3β at S430 and dissociating from Fbw7, thereby evading degradation by the ubiquitin-proteasome signaling pathway. Methylation-stabilized SREBP1a increases lipid synthesis and accelerates cancer cell growth *in vivo* and *in vitro* (Liu et al., 2016). During mitosis, Cdk1 also mediates S439 phosphorylation of SREBP1, leading to increased stability of mature SREBP1 and supporting lipid synthesis (Bengoechea-Alonso and Ericsson, 2006). PKM2 interacts with nuclear SREBP1a and promotes Thr-59 phosphorylation of SREBP1a, which further enhances nuclear SREBP1a protein stability. Thr-59 phosphorylation of nuclear SREBP1a not only promotes the proliferation of hepatoma cells but also negatively correlates with overall survival in patients with hepatocellular carcinoma (Zhao et al., 2018). Interestingly, AMPK can interact with SREBP1c and SREBP2 and directly phosphorylate them at Ser372. In HepG2 hepatoma cells exposed to high glucose, SREBP1c nuclear translocation and lipid accumulation can be inhibited by Ser372 phosphorylation of SREBP1c (Li et al., 2011). The tumor suppressor ASPP2, as a p53 activator, can directly interact with nuclear SREBP2 and inhibit the transcriptional activity of its target genes, especially key enzymes of the mevalonate signaling pathway, leading to tumor growth in hepatocellular carcinoma (Liang et al., 2019). NONO binds to nuclear SREBP1a *via* residue Y267 and increases nuclear SREBP1a protein stability, thereby stimulating breast cancer cell proliferation and tumor growth *in vitro* and *in vivo* (Zhu et al., 2016). Thus, phosphorylation, methylation, ubiquitination, and protein-protein interactions all regulate the activity of nuclear SREBPs. The activity of nuclear SREBPs can also be regulated by controlling their localization and accumulation. Phosphatidic acid phosphatase LPIN1 promotes nuclear localization of mature SREBP1 by mTORC1-mediated phosphorylation and cytoplasmic retention, which in turn regulates *SREBP1* promoter activity and nuclear SREBP1 protein abundance (Peterson et al., 2011). In human HepG2 hepatoma cells, restriction of phosphatidylcholine (a major component of membranes) biosynthesis promotes nuclear SREBP1 accumulation and increases nuclear localization of SREBP1, leading to lipid droplet formation (Walker et al., 2011). Malic enzyme 2 promotes SREBP1 maturation and nuclear localization by inhibiting AMPK phosphorylation, which promotes preneuronal-mesenchymal transition in glioblastoma (Yang et al., 2021). Interestingly, nuclear accumulation of SREBP1 was blocked by the mTORC1 inhibitor rapamycin (Porstmann et al., 2008).

4.3 Regulation of SREBPs by microRNAs

miRNAs are small non-coding RNAs that are key regulators of metabolism and play an important role in regulating SREBPs in cancer (Figure 3). miR-122, the first miRNA associated with metabolic control, is mainly expressed in the liver (Rottiers and Näär, 2012). miR-122 has a clear and important role in up-regulating SREBPs through the following mechanism: INSIG1 restricts the cholesterol biosynthetic signaling pathway by anchoring the transcription factor SREBPs on the ER and causing degradation of the rate-limiting enzyme HMGCR in cholesterol biosynthesis (Iliopoulos et al., 2010; Shibata et al., 2013; Zhai et al., 2017). miR-122 regulates SREBPs activation by degrading SREBPs' anchor protein INSIG1, which regulates the expression of LH receptor mRNA binding protein, thereby mediating LH receptor mRNA levels (Menon et al., 2013; Menon et al., 2015; Menon et al., 2018). In Huh7 liver cancer cells, miR-122 regulates the use of polyadenylation sites in *INSIG1* mRNA and inhibits the translation of *INSIG1* isoform mRNA, thereby affecting the activation of SREBPs (Norman et al., 2017). In addition, miR-122 can be controlled by miR-370, further regulating the expression of SREBP1c and Cpt1α, thereby affecting the expression of other genes involved in lipid metabolism in HepG2 liver cancer cells (Iliopoulos et al., 2010). miR-29 inhibits the growth of glioblastoma cells *in vitro* after transfection (Xu et al., 2015b) and correlates with lipid metabolism signaling pathways in hepatoma and liver cells (Kurtz et al., 2014; Xu et al., 2016). EGFR signaling enhances miR-29 expression by upregulating the expression of SCAP/SREBP1, which transcriptionally activates a specific SRE motif in the *miR-29* promoter. Interestingly, miR-29 inversely represses SCAP and SREBP1 expression and drives glioblastoma growth by interacting with the 3′-UTR of SCAP and SREBP1 (Ru et al., 2016; Ru and Guo, 2017). TUT1, a nucleotidyl transferase and regulator of microRNA abundance, upregulates miRNA-24 and miRNA-29 to suppress the expression levels of PPARγ and SREBP1c and lipogenesis in osteosarcoma cells (Zhu et al., 2014).

The molecular link between miRNAs, SREBPs, and SIRT1 (an oncogene closely related to tumorigenesis (Yeung et al., 2004; Kuzmichev et al., 2005; Hida et al., 2007; Huffman et al., 2007)) in cancer is a topic of much focus. In glioma cells, miR-132 suppresses the expression of SIRT1, SREBP1c, and their downstream regulatory genes, reprogramming cholesterol production and adipogenesis. Overexpression of miR-132 can inhibit the proliferation, invasion, migration, and tumorigenicity of cancer cells and induce their apoptosis (Li et al., 2016). miR-449, a potent inducer of apoptosis, cell cycle arrest, and cell differentiation,

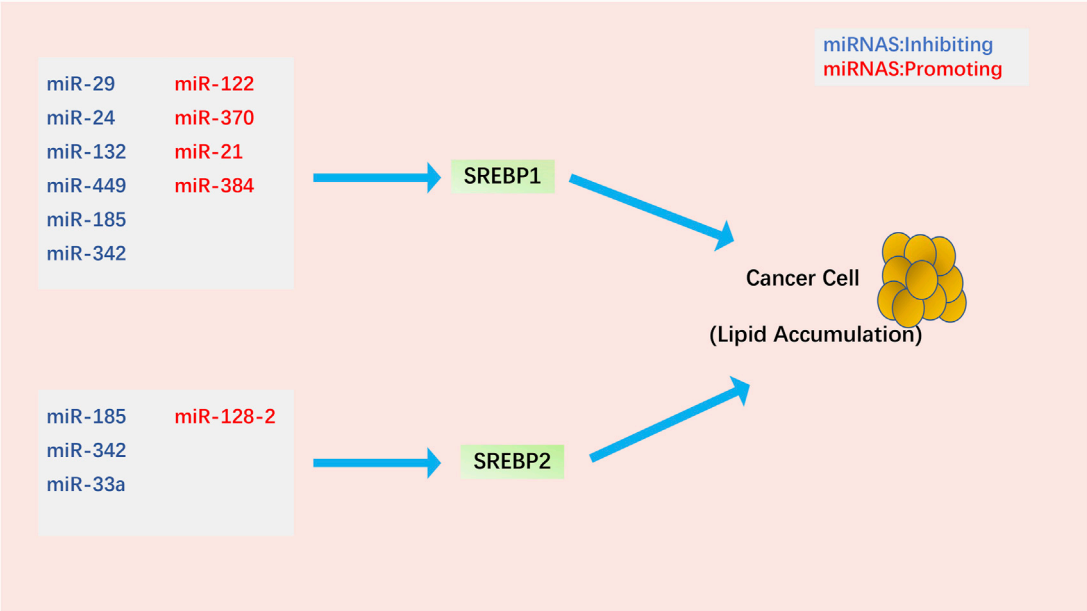

FIGURE 3
Regulation of SREBPs by miRNAs in cancer cells. Most miRNAs affect lipid accumulation in cancer cells by regulating SREBP1. Notably, miR-185 and miR-342 simultaneously inhibit the activation of SREBP1 and SREBP2.

is under-expressed in various cancers (Chen et al., 2012; Luo et al., 2013; Li et al., 2015b; Li et al., 2015c). miR-449 can inhibit SIRT1-SREBP signaling by reducing the expression of SIRT1, SREBP1c, and its downstream genes *FASN* and *HMGCR*, thereby controlling adipogenesis and cholesterol production in hepatoma cells. Restoration of miR-449 leads to liver tumorigenesis (Zhang et al., 2014). miRNA-128–2 (associated with apoptosis and cholesterol homeostasis) in HepG2, MCF7, and HEK293T cancer cell lines increases SREBP2 expression and decreases SREBP1 expression independent of SIRT1 status (Adlakha et al., 2013). In addition to the SIRT1-SREBP signaling pathway, microRNAs can also downregulate SREBPs in cancer cells through the following signaling pathways. miR-185 and miR-342 control lipogenesis and cholesterol synthesis in prostate cancer cells by inhibiting SREBP1 and SREBP2 expression and downregulating their target genes *FASN* and *HMGCR*. Upregulation of miR-185 and -342 induces caspase-dependent apoptosis in prostate cancer cells and regression of prostate tumors (Li et al., 2013). As one of the earliest discovered mammalian miRNAs, miR-21 is an oncogene in prostate cancer, and its expression level is associated with chemotherapy-resistant castration-resistant prostate cancer (Volinia et al., 2006; Si et al., 2007; Krichevsky and Gabriely, 2009; Wang et al., 2013). miR-21 acts as an oncogene during PCa progression by activating the IRS1/SREBP1 signaling pathway; knockdown of miR-21 can reduce IRS1/SREBP1 in mouse embryonic fibroblasts, mouse prostate tissue, and human PCa cells. Downregulated IRS1-SREBP1 signaling pathway inhibits its downstream targets, such as FASN and ACC, and inhibits prostate cancer progression (Kanagasabai et al., 2022). Long-term exposure to cisplatin develops chemoresistance, desensitizes non-small cell lung carcinoma (NSCLC) cells, and enhances SREBP1-mediated adipogenesis, affecting cancer prognosis. miR-497 induces cisplatin sensitivity in NSCLC cells *via* the SREBP-1/miR-497/SCAP/FASN signaling pathway (Tiong et al., 2022). miR-384 downregulates the oncogene pleiotrophin (PTN) in liver cancer cells by directly binding to 3′-UTR, whereas PTN, an oncogene, acts on liver cancer cells and promotes cell proliferation and adipogenesis through the function of the N-syndecan growth factor. N-syndecan promotes *de novo* lipogenesis in hepatoma cells through the PI3K/Akt/mTORC1/SREBP1c signaling pathway. In hepatocellular carcinoma, HBx inhibits miR-384, upregulating PTN and promoting the proliferation, metastasis, and adipogenesis of cancer cells (Bai et al., 2017). Finally, miR-33a not only cooperates with the SREBP2 cholesterol transcription factor to increase intracellular cholesterol levels (Gerin et al., 2010; Horie et al., 2010; Marquart et al., 2010; Najafi-Shoushtari et al., 2010; Rayner et al., 2010) but also works with miR-33b and their SREBP host gene products to regulate intracellular fatty acid and lipid levels (Gerin et al., 2010; Dávalos et al., 2011). Dysregulation of miR-33a levels may promote tumorigenesis by affecting cholesterol levels. Most studies have shown that miR-33a acts as a tumor suppressor in various cancer cells, inhibiting the proliferation and metastasis of cancer cells (Kuo et al., 2013; Zhang et al., 2015; Han et al., 2016; Karatas et al., 2017; Shan et al., 2017). However, whether miR-33a and miR-33b have extensive cooperation with SREBPs and specific mechanisms in the control of cholesterol and lipid homeostasis during the occurrence and development of cancer still needs further research. We found that most of the current studies on microRNAs and SREBPs are stuck on the effect of lipid accumulation in cancer cells. However, it is still not entirely clear whether the lipid accumulation induced by microRNAs through SREBPs has a direct link to cancer cell phenotype.

In addition to miRNAs, long noncoding RNAs (lncRNAs) also play an irreplaceable role, although the role of regulating SREBPs in cancer is less studied. Hypoxia, a frequent occurrence in solid tumors, is considered an adverse factor for patient prognosis (Vaupel and Mayer, 2007; Bertout et al., 2008). Hypoxia promotes the expression of unknown lncRNAs at the EFNA3 locus through hypoxia-inducible factor (HIF), leading to Ephrin-A3 protein accumulation. Ephrin-A3 expression leads to poor prognosis and increased risk of metastasis in patients with breast cancer (Gómez-Maldonado et al., 2015). Interestingly, HIF-1a directly upregulated EFNA3 expression and Ephrin-A3 accumulation under hypoxic conditions in HCC, similar to the above studies. The authors extended the role of Ephrin-A3 in metabolic reprogramming in a hypoxic microenvironment, reporting for the first time that the Ephrin-A3/Eph receptor A2 (EphA2) axis-promoted SREBP1 maturation and SREBP1-ACLY-mediated metabolic reprogramming are its important downstream signals (Husain et al., 2022). LncRNA metastasis-associated lung adenocarcinoma transcript 1 (MALAT1) is upregulated in many cancers (Gutschner et al., 2013; Hu et al., 2015; Goyal et al., 2021) and involved in the regulation of pre-mRNA splicing (Tripathi et al., 2010; Engreitz et al., 2014). In HCC cells, MALAT1 regulates the expression of genes involved in lipid metabolism, including *SREBF1* and *SCD*, through RNA splicing or transcription (Wang et al., 2021a).

5 Treatment in cancer

Given the important regulatory status of SREBPs in lipid metabolism and cancer growth, SREBPs have become potential targets, and the prevention and treatment of cancer can be achieved through small molecules or natural products. There are currently three main treatment strategies: 1) Targeting the translocation of SREBPs from the ER to the Golgi and the cleavage in the Golgi, intervening in the activation of SREBP1/SREBP2; 2) small molecules and natural substances targeting SREBP1 only; and 3) mevalonate signaling pathway inhibition targeting SREBP2 only.

5.1 Intervention in the activation of SREBP1/SREBP2

Fatostatin, a non-sterol diarylthiazole derivative, is a specific inhibitor of SREBP activation (Table 1). The important basis for its tumor suppressor effect is to bind to SCAP to inhibit the translocation of SREBP1/SREBP2 from the ER to the Golgi (Kamisuki et al., 2009; Li et al., 2014b; Shao et al., 2016). In prostate cancer, fatostatin inhibits cell proliferation, invasion, and migration of androgen-responsive or insensitive cancer cells. Fatostatin can also induce G2-M cell cycle arrest and induce apoptosis (Li et al., 2014b). Fatostatin inhibits prostate tumor growth and distant lymph node metastasis in mice by inhibiting the activation of SREBPs (Chen et al., 2018). Moreover, the combined use of fatostatin and docetaxel can inhibit the proliferation and apoptosis of prostate cancer cells (especially p53 mutants) to a greater extent than monotherapy (Li et al., 2015d). In endometrial cancer, fatostatin exhibits antitumor effects by inhibiting the SREBPs-regulated metabolic signaling pathways and inducing caspase-mediated apoptosis (Gao et al., 2018). Fatostatin inhibits endometrial cancer cell growth, proliferation, cell cycle, and apoptosis *in vitro* and has antitumor activity *in vivo* (Yao et al., 2020). In breast cancer, fatostatin inhibits cell cycle arrest and apoptosis, especially in estrogen receptor-positive cells. Interestingly, instead of inhibiting lipogenesis by inhibiting the activity of SREBPs, fatostatin caused lipid accumulation through ER stress (Brovkovych et al., 2018). In a variety of cancers, fatostatin inhibits cancer cell proliferation by inhibiting tubulin polymerization and mitosis in cancer cells and disrupting its mitotic microtubule spindle assembly (Gholkar et al., 2016). Betulin, a natural triterpenoid, specifically inhibits the maturation of SREBPs by enhancing the interaction of SCAP with INSIG (Tang et al., 2011). In hepatocellular carcinoma, betulin reduces the level of pro-inflammatory lipids and suppresses inflammation and ER stress by inhibiting the SREBPs signaling pathway, ultimately inhibiting the progression of liver cancer (Li et al., 2017). Betulin inhibits glucose metabolism in hepatocellular carcinoma and enhances the antitumor effect of sorafenib by inhibiting SREBP1 (Yin et al., 2019). In addition to inhibiting the translocation of SCAP/SREBP, inhibiting the Golgi cleavage of SREBPs is also a major therapeutic strategy to prevent their activation. Two important SREBP cleaving enzymes S1P and S2P in the Golgi can be inhibited by PF-429242 and nelfinavir, respectively. In renal cell carcinoma, PF-429242 potently inhibits cell proliferation, migration, and invasion and activates apoptosis by targeting S1P (Wang et al., 2021b). In hepatocellular carcinoma, PF-429242 inhibits viral assembly in infected cells by reducing LD formation, thereby blocking HCV establishment of infection in hepatoma cells (Blanchet et al., 2012; Olmstead et al., 2012). PF-429242 can also synergize with GSK_{343} (EZH2 inhibitor) in hepatocellular carcinoma, enhancing the anticancer activity of GSK_{343} (Yang et al., 2019). In glioblastoma, PF-429242 downregulates steroid, isoprenoid, and unsaturated fatty acid biosynthetic signaling pathways and upregulates pro-inflammatory genes to reduce cancer cell viability and promote apoptosis (Caruana et al., 2017). In liposarcoma, nelfinavir upregulates the precursors SREBP1 and ATF6 by inhibiting the cleavage of S2P, resulting in ER stress and induction of apoptosis (Guan et al., 2011). In prostate cancer, nelfinavir also reduces the proliferation of castration-resistant prostate cancer and promotes apoptosis through the accumulation of unprocessed SREBP1 and ATF6 (Guan et al., 2012; Guan et al., 2015). Notably, in these three nelfinavir reports, the authors used another S2P-specific inhibitor, 1,10-phenanthroline, and achieved similar effects to nelfinavir in cancer.

5.2 Small molecules and natural substances targeting SREBP1

Several classes of small molecules or new formulations have been reported as modulators of adipogenesis targeting SREBP1 in cancer

TABLE 1 Treatment in cancer.

Targets	Drugs	Cancer types	Mechanisms
SREBP1/SREBP2	Fatostatin	Prostate cancer	Inhibits cell proliferation, invasion, and migration of cancer cells and causes G2-M cell cycle arrest and induces apoptosis (Li et al., 2014b)
			Inhibits prostate tumor growth and distant lymph node metastasis in mice by inhibiting the activation of SREBPs (Chen et al., 2018)
			Combined use with docetaxel can inhibit the proliferation and apoptosis of prostate cancer cells (especially p53 mutants) to a greater extent (Li et al., 2015d)
		Endometrial cancer	Inhibits metabolic signaling pathways regulated by SREBPs and induces caspase-mediated apoptosis (Gao et al., 2018)
			Inhibits growth, proliferation, cell cycle, and apoptosis and has antitumor activity *in vivo* (Yao et al., 2020)
		Breast cancer	Causes cell cycle arrest and apoptosis by ER stress (Brovkovych et al., 2018)
		Multiple cancers	Inhibits tubulin polymerization and mitosis and perturbs its mitotic microtubule spindle assembly (Gholkar et al., 2016)
	Betulin	Hepatocellular carcinoma	Reduces the levels of pro-inflammatory lipids and suppresses inflammation and ER stress by inhibiting the translocation of SREBPs (Li et al., 2017)
			Inhibits glucose metabolism and enhances the antitumor effect of Sorafenib by inhibiting SREBP1 (Yin et al., 2019)
	PF-429242	Renal cell carcinoma	Inhibits cell proliferation, migration, and invasion, and activates apoptosis by targeting S1P (Wang et al., 2021b)
		Hepatocellular carcinoma	Inhibits viral assembly in infected cells by reducing LD formation, thereby blocking HCV establishment of infection (Blanchet et al., 2012; Olmstead et al., 2012)
			Synergizes with GSK_{343}, enhancing the anticancer activity of GSK_{343} (Yang et al., 2019)
		Glioblastoma	Downregulates steroid, isoprenoid, and unsaturated fatty acid biosynthetic signaling pathways and upregulates pro-inflammatory genes to reduce cancer cell viability and promote apoptosis (Caruana et al., 2017)
	Nelfinavir,1,10-phenanthroline	Liposarcoma	Upregulates the precursors SREBP1 and ATF6 by inhibiting the cleavage of S2P, resulting in ER stress and induction of apoptosis (Guan et al., 2011)
		Prostate cancer	Reduces the proliferation of castration-resistant prostate cancer and promotes apoptosis through the accumulation of unprocessed SREBP1 and ATF6 (Guan et al., 2012; Guan et al., 2015)

(Table 2). Apatinib, an inhibitor of VEGFR2, downregulates GPX4 expression by inhibiting SREBP1a, thereby inducing lipid peroxidation and ferroptosis in gastric cancer (Zhao et al., 2021). Mollugin, with anti-inflammatory and apoptotic effects, inhibits proliferation and induces apoptosis in HER2-overexpressing breast and ovarian cancers by regulating SREBP1c and its target gene *FASN* through the HER2/Akt signaling pathway (Do et al., 2013a). WY 14,643 and troglitazone, agonists of PPARα and PPARγ, respectively, inhibit SREBP1 activation through the upregulation of INSIG, ultimately reducing triacylglycerol synthesis in hepatoma cells (König et al., 2009). Azathioprine, an immunosuppressant, inhibits elevated lipid metabolism *via* the EGFR/AKT/SREBP1 signaling pathway and induces ER stress to induce apoptosis in glioblastoma cells (Nam et al., 2021). GW3965, a hepatic X receptor agonist, promotes glioblastoma cell death by inhibiting the EGFR/AKT/SREBP1/LDLR signaling pathway (Guo et al., 2011). Gefitinib induces downregulation of SREBP1 in non-small cell lung cancer treatment-sensitive cells, inhibits fatty acid synthesis, and alters the ratio of saturated to unsaturated phospholipids (Xu et al., 2021a). Metformin inhibits bladder cancer cell growth by controlling lipid synthesis *via* the Clusterin/SREBP1c/FASN axis (Deng et al., 2021). Proxalutamide, an AR antagonist, significantly inhibits prostate cancer cell proliferation and migration and induces apoptosis. Proxalutamide also inhibits the expression of ACL, ACC, FASN, and SREBP1 to reduce lipid droplet levels and triglyceride content in cancer cells (Gu et al., 2021). ASC-J9, as an AR degradation enhancer, inhibits the proliferation and invasion of prostate cancer cells through the AR/SREBP1/FASN

TABLE 2 Treatment in cancer.

Targets	Drugs	Cancer types	Mechanisms
SREBP1	Apatinib	Gastric cancer	Downregulates GPX4 expression by inhibiting SREBP1a, thereby inducing lipid peroxidation and ferroptosis (Zhao et al., 2021)
	Mollugin	Breast/ovarian cancers	Inhibits proliferation and induces apoptosis through the HER2/Akt/SREBP1c/FASN signaling pathway (Do et al., 2013a)
	WY 14,643 and troglitazone	Hepatocellular carcinoma	inhibit SREBP1 activation through the upregulation of INSIG, ultimately reducing triacylglycerol synthesis (König et al., 2009)
	Azathioprine	Glioblastoma	Inhibits elevated lipid metabolism *via* EGFR/AKT/SREBP1 signaling pathway and induces ER stress to induce apoptosis (Nam et al., 2021)
	GW3965	Glioblastoma	Promotes cell death by inhibiting the EGFR/AKT/SREBP1/LDLR signaling pathway (Guo et al., 2011)
	Gefitinib	Non-small cell lung cancer	Induces downregulation of SREBP1, and alters the ratio of saturated to unsaturated phospholipids (Xu et al., 2021a)
	Metformin	Bladder cancer	Inhibits cancer cell growth by controlling lipid synthesis *via* the Clusterin/SREBP1c/FASN axis (Deng et al., 2021)
	Proxalutamide	Prostate cancer	Inhibits proliferation, migration, and expression of ACL, ACC, FASN, and SREBP1 to reduce lipid droplet levels and triglyceride content (Gu et al., 2021)
	ASC-J9	Prostate cancer	Inhibits the proliferation and invasion of prostate cancer cells by the AR/SREBP1/FASN or API3K/Akt/SREBP1/FASN signaling pathways according to whether AR is positive or not (Wen et al., 2016)
	RA-XII	Colorectal cancer	Inhibits the growth and metastasis of colorectal tumors by reducing the expression of SREBP1 and its target genes (Wang et al., 2019)
	Berberin	Colon cancer	Mediates lipogenesis by inhibiting SCAP expression and SREBP1 activation, thereby inhibiting cell proliferation and colon cancer xenograft growth (Liu et al., 2020)
	Ginsenoside Rh2	Non-small cell lung cancer	Reverses cyclophosphamide-induced immunodeficiency by inhibiting the expression of SREBP1 and affecting the interaction of SREBP1 with FASN (Qian et al., 2019)
	Davallia formosana ethanol extract	Prostate cancer	Inhibits proliferation, migration, and invasion by inhibiting the expression of SREBP1 and FASN and reducing the expression of AR and PSA (Hsieh et al., 2020)
	Curcumin	Hepatocarcinoma	Reduces adipogenesis by activating the phosphorylation of AMPK to reduce the expression of SREBP1 and FASN and increases the expression of PPARα (Kang et al., 2013)
	Oleiferasaponin A_2	Hepatocarcinoma	Inhibits lipid accumulation by significantly down-regulating fatty acid synthesis genes and up-regulating fatty acid β-oxidation genes (Di et al., 2018)
	Piperine	Breast cancer	Reduces the expression of SREBP1 and FASN by inhibiting ERK1/2 signaling, and also inhibits the proliferation by activating caspase-3 and cleaving PARP (Do et al., 2013b)

and PI3K/Akt/SREBP1/FASN signaling pathways according to whether AR is positive or not (Wen et al., 2016).

Notably, natural substances can also modulate SREBP1 for the treatment of different cancers. The natural cyclic peptide RA-XII, isolated from Rubia yunnanensis, inhibits the growth and metastasis of colorectal tumors by reducing the expression of SREBP1 and its target genes (Wang et al., 2019). Berberin, extracted from the Rizoma coptidis, mediates lipogenesis by inhibiting SCAP expression and SREBP1 activation, thereby inhibiting colon cancer cell proliferation and colon cancer xenograft growth (Liu et al., 2020). Ginsenoside Rh2, an extract from ginseng, reverses cyclophosphamide-induced immunodeficiency in non-small cell lung cancer by inhibiting the expression of SREBP1 and its nuclear translocation and affecting the interaction of SREBP1 with FASN (Qian et al., 2019). Davallia formosana ethanol extract inhibits proliferation, migration, and invasion in prostate cancer cells by inhibiting the expression of SREBP1 and FASN and reducing the expression of AR and prostate-specific antigen (PSA) (Hsieh et al., 2020). Curcumin, the yellow pigment from turmeric, exhibits anti-cancer and antioxidant effects, especially in hepatocarcinoma. Curcumin can not only reduce adipogenesis in hepatoma cells by activating the phosphorylation of AMPK to reduce SREBP1 and the expression of FASN but also increase the expression of PPARα and increase its antioxidant effect (Kang

TABLE 3 Treatment in cancer.

Targets	Drugs	Cancer types	Mechanisms
SREBP2	AtorvastatinL	Breast cancer	Alter the expression of 50 genes with a shared cluster of 37 genes, including the Hippo, Notch, and Wnt signaling pathways, preventing the EMT process (Koohestanimobarhan et al., 2019)
	Ovastatin		
	Simvastatin		
	Lovastatin	Breast cancer	Signal through PPARγ and upregulate *PTEN* at the transcriptional level (Teresi et al., 2006)
	Simvastatin	Breast cancer	Contributes to breast cancer cell death by inducing inactivation of PI3K/Akt and MAPK/Erk signaling (Wang et al., 2016)
	Cerivastatin	Breast cancer	Inhibits the elevated levels of mevalonate produced by the transcriptional activity of SREBP2 and impedes the nuclear localization and transcription of YAP/TAZ (Piccolo et al., 2014; Sorrentino et al., 2014)
	Lovastatin	Osteosarcoma	Reduces the expression of CYR61 *via* SREBP2/miR-33a, which in turn inhibits osteosarcoma cell invasion (Huang et al., 2018)
	Fluvastatin	Thymic carcinoma	Inhibits HMGCR to suppresses cell proliferation, which might be mediated by inhibiting the production of geranylgeranyl-pyrophosphate (Hayashi et al., 2020)
	Fluvastatin	Non-small cell lung cancer	Alters Braf/MEK/ERK1/2 and Akt signaling pathways by inhibiting HMGCR, which can inhibit cell growth, induce apoptosis, and inhibit tumorigenesis in non-small cell lung cancer (Zhang et al., 2019)
	Simvastatin	Colorectal cancer	Suppresses PD-L1 expression and promotes antitumor immunity by inhibiting lncRNA SNHG29 expression and its mediated YAP activation (Ni et al., 2021)
	Simvastatin	Prostate cancer	Reduce cell proliferation and induce apoptosis mediated by phosphorylation downregulation of AKT/FOXO1 signaling pathway (Deng et al., 2019)
	Fluvastatin		
	Simvastatin	Prostate cancer	Overcome enzalutamide resistance by reducing AR by inhibiting the mTOR signaling pathway (Kong et al., 2018)
	Simvastatin	Pancreatic cancer	Inhibit invasion and growth and exhibit synergistic antitumor effects in ORP5-expressing pancreatic cancer cells (Ishikawa et al., 2010)
	Tricostatin A		
	Fluvastatin	Bladder cancer	Affect cholesterol biosynthesis to enhance archazolid B-induced cell killing (Hamm et al., 2014)
	Archazolid B		
	Atorvastatin	Cervical cancer	Retain the SCAP-SREBP complex in the ER by stabilizing the INSIG protein (Esquejo et al., 2021)
	Dipyridamole		
	Fluvastatin	Prostate cancer	Inhibit SREBP2 activation and promotes apoptosis in statin-insensitive prostate cancer cells (Longo et al., 2019)
	Dipyridamole		
	Simvastatin	Ovarian cancer	Significantly enhance the cytotoxicity and antitumor activity of statins against ovarian cancer cells (Casella et al., 2014)
	25-hydroxycholesterol		
	Pitavastatin	Oral and Esophageal Cancer	Suppresses AKT and ERK signaling to inhibit tumor growth alone, and significantly reduces tumor growth in cooperation with capmatinib (Xu et al., 2021b)
	Capmatinib		
	Simvastatin	Primary leukemia and lymphoma	Enhances the proapoptotic activity of venetoclax (B cell lymphoma-2 inhibitor) in primary leukemia and lymphoma cells but not normal peripheral blood mononuclear cells (Lee et al., 2018)
	Venetoclax		
	Lovastatin	Renal cell carcinoma	Increases glycolysis levels through regulated HSP90 expression levels, leading to lactate accumulation and acceleration of renal cell carcinoma development. The tumor-promoting effect of lovastatin is reversed by Shikonin (Huang et al., 2021)
	Shikonin		

et al., 2013). Oleiferasaponin A_2, isolated from the defatted seeds of Camellia oleifera, inhibits lipid accumulation in hepatoma cells by significantly down-regulating fatty acid synthesis genes (the genes encoding SREBP1c, FASN, ACC) and up-regulating fatty acid β-oxidation genes (the genes encoding PPARα, ACOX-1, CPT-1) (Di et al., 2018). Piperine, extracted from black pepper, significantly reduces the expression of SREBP1 and FASN by inhibiting ERK1/2 signaling and also inhibits the proliferation of HER2-overexpressing breast cancer cells by activating caspase-3 and cleaving PARP (Do et al., 2013b). Interestingly, physical exercise induces changes in lipid metabolism signaling pathways (decreased expression of CD36, SREBP1, and SCAP) and prostate cell apoptosis, suggesting that physical exercise may be a new therapeutic strategy for the treatment of prostate cancer (Teixeira et al., 2020).

5.3 Mevalonate signaling pathway inhibition targeting SREBP2

Cholesterol metabolism, a risk signal and driver of tumor growth, is controlled by SREBP2 over the expression of important cholesterol biosynthetic genes and is associated with prognosis in multiple cancers (Table 3). HMGCR (the rate-limiting enzyme for cholesterol synthesis) is a key target for inhibiting the SREBP2 signaling pathway for cancer therapy. Statins, the most classic HMGCR inhibitors, have become the cornerstone of therapy in cancer patients with high cholesterol levels and have also reduced cancer incidence and recurrence (Khurana et al., 2007; Singh et al., 2009; Tran et al., 2020). Statins are mainly divided into two types, fungal fermentation or chemical synthesis, including type 1, lovastatin, mevastatin, and simvastatin, and type 2, fluvastatin and atorvastatin (Xue et al., 2020). In breast cancer, atorvastatin, lovastatin, and simvastatin alter the expression of 50 genes with a shared cluster of 37 genes, including the Hippo, Notch, and Wnt signaling pathways, preventing the EMT process (Koohestanimobarhan et al., 2019). Lovastatin can signal through PPARγ (a breast cancer-associated tumor suppressor) and upregulate *PTEN* at the transcriptional level (Teresi et al., 2006). Simvastatin further contributes to breast cancer cell death by inducing the inactivation of PI3K/Akt and MAPK/Erk signaling (Wang et al., 2016). In breast cancer cells, elevated levels of mevalonate produced by SREBP2 transcriptional activity promote the activation of YAP/TAZ signaling, whereas cerivastatin inhibits this signaling pathway and hinders the nuclear localization and transcription of YAP/TAZ (Piccolo et al., 2014; Sorrentino et al., 2014). Lovastatin reduces the expression of CYR61 *via* SREBP2/miR-33a, which in turn inhibits osteosarcoma cell invasion (Huang et al., 2018). In thymic carcinoma, Fluvastatin inhibits HMGCR to suppresses cell proliferation, which might be mediated by inhibiting the production of geranylgeranyl-pyrophosphate (Hayashi et al., 2020). Fluvastatin alters Braf/MEK/ERK1/2 and Akt signaling pathways by inhibiting HMGCR, which can inhibit cell growth, induce apoptosis, and inhibit tumorigenesis in non-small cell lung cancer (Zhang et al., 2019). In colorectal cancer, simvastatin suppresses PD-L1 expression and promotes antitumor immunity by inhibiting lncRNA SNHG29 expression and its mediated YAP activation (Ni et al., 2021). Simvastatin and fluvastatin reduce cell proliferation and induce apoptosis mediated by phosphorylation downregulation of the AKT/FOXO1 signaling pathway in prostate cancer cells (Deng et al., 2019). In potential-resistant prostate cancer, reduction of AR by simvastatin *via* inhibition of the mTOR signaling pathway overcomes enzalutamide resistance (Kong et al., 2018). In addition to regulating multiple signaling pathways to affect tumors, statins can also synergize with multiple drugs. Simvastatin and tricostatin A, an HDAC inhibitor, inhibit invasion and growth and exhibit synergistic antitumor effects in ORP5-expressing pancreatic cancer cells. Combination therapy can inhibit the growth of cancer cells to a greater extent (Ishikawa et al., 2010). Archazolid B, a vacuolar H (+)-ATPase inhibitor, causes dramatic disturbance of cholesterol homeostasis, activation of SREBP2 and upregulation of the target gene *HMGCR*. The combination of archazolid B and fluvastatin affects cholesterol biosynthesis to enhance archazolid B-induced cell death (Hamm et al., 2014). Dipyridamole, a phosphodiesterase inhibitor, can retain the SCAP-SREBP complex in the ER by stabilizing the INSIG protein when acting alone, and when combined with atorvastatin can further enhance the inhibition of cervical cancer cell growth by atorvastatin (Esquejo et al., 2021). Dipyridamole inhibits fluvastatin-induced SREBP2 activation and enhances apoptosis in statin-insensitive prostate cancer cells (Longo et al., 2019). Combination treatment of 25-hydroxycholesterol with simvastatin significantly enhances statin cytotoxicity and antitumor activity in ovarian cancer cells (Casella et al., 2014). In Oral and Esophageal Cancer, pitavastatin suppresses AKT and ERK signaling in cells to inhibit tumor growth alone. Importantly, pitavastatin significantly reduces tumor growth in cooperation with capmatinib, a MET-specific inhibitor (Xu et al., 2021b). Simvastatin enhances the proapoptotic activity of venetoclax (B cell lymphoma-2 inhibitor) in primary leukemia and lymphoma cells but not normal peripheral blood mononuclear cells (Lee et al., 2018). Interestingly, Low serum cholesterol levels are positively associated with poorer survival outcomes in patients with renal cell carcinoma. Lovastatin fails to inhibit tumor progression, but instead increases glycolysis levels through regulated HSP90 expression levels, leading to lactate accumulation and acceleration of renal cell carcinoma development. However, Shikonin (a PKM2 inhibitor) can reverse the tumor-promoting effect of lovastatin (Huang et al., 2021).

6 Conclusion

In conclusion, with the reprogramming of lipid metabolism as an emerging hallmark of cancer, we need to deepen our understanding of the dysregulation of lipid metabolism in cancer. Intracellular oncogenic signal transduction, DNA, RNA, cytokines, growth factors, and tumor microenvironment can all regulate lipid metabolism in tumor cells. Aberrant lipid metabolism can also influence oncogenic signaling pathways in cancer cells. SREBPs, as core transcription factors in lipid metabolism, link oncogenic signal transduction with changes in lipid metabolism and play an important role in malignant tumors. Tumor cells voraciously upregulate SREBPs through different subcellular localizations, including the ER, Golgi, and nucleus, thereby further regulating the lipid uptake, lipid production (FAs and cholesterol), and lipid decomposition of tumor cells, serving the tumor cells themselves. In particular, numerous signaling molecules can regulate the transcription, expression, activation, stability, and binding of SREBPs, which can mediate downstream signaling pathways, leading to tumor proliferation, invasion, metastasis, apoptosis, epithelial-mesenchymal transition, and ER stress. An in-depth study of the specific regulatory mechanisms of SREBPs in tumors will provide

new and exciting therapeutic opportunities to eliminate cancer with the best efficacy and minimal side effects.

Author contributions

Conceptualisation: HZ, YiW, and YL; drafting of manuscript: SW and XZ; revising of manuscript: SH and FL; searching the literature: YuW and BL; designing the figures and tables: DZ.

Funding

This study was supported by grants from the National Natural Science Foundation of China (No. 82270785).

Conflict of interest

The authors declare that the research was conducted in the absence of any commercial or financial relationships that could be construed as a potential conflict of interest.

Publisher's note

All claims expressed in this article are solely those of the authors and do not necessarily represent those of their affiliated organizations, or those of the publisher, the editors and the reviewers. Any product that may be evaluated in this article, or claim that may be made by its manufacturer, is not guaranteed or endorsed by the publisher.

References

Adams, C. M., Reitz, J., De Brabander, J. K., Feramisco, J. D., Li, L., Brown, M. S., et al. (2004). Cholesterol and 25-hydroxycholesterol inhibit activation of SREBPs by different mechanisms, both involving SCAP and Insigs. *J. Biol. Chem.* 279, 52772–52780. doi:10.1074/jbc.M410302200

Adlakha, Y. K., Khanna, S., Singh, R., Singh, V. P., Agrawal, A., and Saini, N. (2013). Pro-apoptotic miRNA-128-2 modulates ABCA1, ABCG1 and RXRα expression and cholesterol homeostasis. *Cell Death Dis.* 4, e780. doi:10.1038/cddis.2013.301

Alsuliman, A., Colak, D., Al-Harazi, O., Fitwi, H., Tulbah, A., Al-Tweigeri, T., et al. (2015). Bidirectional crosstalk between PD-L1 expression and epithelial to mesenchymal transition: Significance in claudin-low breast cancer cells. *Mol. Cancer* 14, 149. doi:10.1186/s12943-015-0421-2

Amemiya-Kudo, M., Shimano, H., Hasty, A. H., Yahagi, N., Yoshikawa, T., Matsuzaka, T., et al. (2002). Transcriptional activities of nuclear SREBP-1a, -1c, and -2 to different target promoters of lipogenic and cholesterogenic genes. *J. Lipid Res.* 43, 1220–1235. doi:10.1194/jlr.m100417-jlr200

Bai, P. S., Xia, N., Sun, H., and Kong, Y. (2017). Pleiotrophin, a target of miR-384, promotes proliferation, metastasis and lipogenesis in HBV-related hepatocellular carcinoma. *J. Cell Mol. Med.* 21, 3023–3043. doi:10.1111/jcmm.13213

Bao, J., Zhu, L., Zhu, Q., Su, J., Liu, M., and Huang, W. (2016). SREBP-1 is an independent prognostic marker and promotes invasion and migration in breast cancer. *Oncol. Lett.* 12, 2409–2416. doi:10.3892/ol.2016.4988

Bayraktar, E. C., La, K., Karpman, K., Unlu, G., Ozerdem, C., Ritter, D. J., et al. (2020). Metabolic coessentiality mapping identifies C12orf49 as a regulator of SREBP processing and cholesterol metabolism. *Nat. Metab.* 2, 487–498. doi:10.1038/s42255-020-0206-9

Bellanger, A., Donini, C. F., Vendrell, J. A., Lavaud, J., Machuca-Gayet, I., Ruel, M., et al. (2017). The critical role of the ZNF217 oncogene in promoting breast cancer metastasis to the bone,. *J. Pathol.* 242, 73–89. doi:10.1002/path.4882

Bengoechea-Alonso, M. T., and Ericsson, J. (2006). Cdk1/cyclin B-mediated phosphorylation stabilizes SREBP1 during mitosis. *Cell Cycle* 5, 1708–1718. doi:10.4161/cc.5.15.3131

Bengoechea-Alonso, M. T., and Ericsson, J. (2016). The phosphorylation-dependent regulation of nuclear SREBP1 during mitosis links lipid metabolism and cell growth,. *Cell Cycle* 15, 2753–2765. doi:10.1080/15384101.2016.1220456

Bertout, J. A., Patel, S. A., and Simon, M. C. (2008). The impact of O2 availability on human cancer,. *Nat. Rev. Cancer* 8, 967–975. doi:10.1038/nrc2540

Bian, X., Liu, R., Meng, Y., Xing, D., Xu, D., and Lu, Z. (2021). Lipid metabolism and cancer. *J. Exp. Med.* 218. doi:10.1084/jem.20201606

Blake, M. L., Tometsko, M., Miller, R., Jones, J. C., and Dougall, W. C. (2014). RANK expression on breast cancer cells promotes skeletal metastasis. *Clin. Exp. Metastasis* 31, 233–245. doi:10.1007/s10585-013-9624-3

Blanchet, M., Seidah, N. G., and Labonté, P. (2012). SKI-1/S1P inhibition: A promising surrogate to statins to block hepatitis C virus replication. *Antivir. Res.* 95, 159–166. doi:10.1016/j.antiviral.2012.05.006

Botolin, D., Wang, Y., Christian, B., and Jump, D. B. (2006). Docosahexaneoic acid (22:6,n-3) regulates rat hepatocyte SREBP-1 nuclear abundance by Erk- and 26S proteasome-dependent pathways. *J. Lipid Res.* 47, 181–192. doi:10.1194/jlr.M500365-JLR200

Brovkovych, V., Izhar, Y., Danes, J. M., Dubrovskyi, O., Sakallioglu, I. T., Morrow, L. M., et al. (2018). Fatostatin induces pro- and anti-apoptotic lipid accumulation in breast cancer. *Oncogenesis* 7, 66. doi:10.1038/s41389-018-0076-0

Brown, M. S., and Goldstein, J. L. (1997). The SREBP pathway: Regulation of cholesterol metabolism by proteolysis of a membrane-bound transcription factor,. *Cell* 89, 331–340. doi:10.1016/s0092-8674(00)80213-5

Brown, M. S., Ye, J., and Goldstein, J. L. (2010). Medicine. HDL miR-ed down by SREBP introns. *Science* 328, 1495–1496. doi:10.1126/science.1192409

Calder, P. C. (2018). Very long-chain n-3 fatty acids and human health: Fact, fiction and the future. *Proc. Nutr. Soc.* 77, 52–72. doi:10.1017/S0029665117003950

Carpentier, Y. A., Portois, L., and Malaisse, W. J. (2006). n-3 fatty acids and the metabolic syndrome. *Am. J. Clin. Nutr.* 83, 1499S–1504s. doi:10.1093/ajcn/83.6.1499S

Caruana, B. T., Skoric, A., Brown, A. J., and Lutze-Mann, L. H. (2017). Site-1 protease, a novel metabolic target for glioblastoma. *Biochem. Biophys. Res. Commun.* 490, 760–766. doi:10.1016/j.bbrc.2017.06.114

Casella, C., Miller, D. H., Lynch, K., and Brodsky, A. S. (2014). Oxysterols synergize with statins by inhibiting SREBP-2 in ovarian cancer cells. *Gynecol. Oncol.* 135, 333–341. doi:10.1016/j.ygyno.2014.08.015

Chang, T. Y., Chang, C. C., Ohgami, N., and Yamauchi, Y. (2006). Cholesterol sensing, trafficking, and esterification. *Annu. Rev. Cell Dev. Biol.* 22, 129–157. doi:10.1146/annurev.cellbio.22.010305.104656

Chen, H., Lin, Y. W., Mao, Y. Q., Wu, J., Liu, Y. F., Zheng, X. Y., et al. (2012). MicroRNA-449a acts as a tumor suppressor in human bladder cancer through the regulation of pocket proteins. *Cancer Lett.* 320, 40–47. doi:10.1016/j.canlet.2012.01.027

Chen, M., Zhang, J., Sampieri, K., Clohessy, J. G., Mendez, L., Gonzalez-Billalabeitia, E., et al. (2018). An aberrant SREBP-dependent lipogenic program promotes metastatic prostate cancer. *Nat. Genet.* 50, 206–218. doi:10.1038/s41588-017-0027-2

Cheng, C., Geng, F., Cheng, X., and Guo, D. (2018). Lipid metabolism reprogramming and its potential targets in cancer. *Cancer Commun. (Lond)* 38, 27. doi:10.1186/s40880-018-0301-4

Cheng, C., Geng, F., Li, Z., Zhong, Y., Wang, H., Cheng, X., et al. (2022). Ammonia stimulates SCAP/Insig dissociation and SREBP-1 activation to promote lipogenesis and tumour growth. *Nat. Metab.* 4, 575–588. doi:10.1038/s42255-022-00568-y

Cheng, C., Guo, J. Y., Geng, F., Wu, X., Cheng, X., Li, Q., et al. (2016). Analysis of SCAP N-glycosylation and trafficking in human cells. *J. Vis. Exp.*, 54709. doi:10.3791/54709

Cheng, C., Ru, P., Geng, F., Liu, J., Yoo, J. Y., Wu, X., et al. (2015). Glucose-mediated N-glycosylation of SCAP is essential for SREBP-1 activation and tumor growth. *Cancer Cell* 28, 569–581. doi:10.1016/j.ccell.2015.09.021

Dai, W., Xiang, W., Han, L., Yuan, Z., Wang, R., Ma, Y., et al. (2022). PTPRO represses colorectal cancer tumorigenesis and progression by reprogramming fatty acid metabolism. *Cancer Commun. (Lond)* 42, 848–867. doi:10.1002/cac2.12341

Dávalos, A., Goedeke, L., Smibert, P., Ramírez, C. M., Warrier, N. P., Andreo, U., et al. (2011). miR-33a/b contribute to the regulation of fatty acid metabolism and insulin signaling. *Proc. Natl. Acad. Sci. U. S. A.* 108, 9232–9237. doi:10.1073/pnas.1102281108

Deng, J. L., Zhang, R., Zeng, Y., Zhu, Y. S., and Wang, G. (2019). Statins induce cell apoptosis through a modulation of AKT/FOXO1 pathway in prostate cancer cells. *Cancer Manag. Res.* 11, 7231–7242. doi:10.2147/CMAR.S212643

Deng, J., Peng, M., Zhou, S., Xiao, D., Hu, X., Xu, S., et al. (2021). Metformin targets Clusterin to control lipogenesis and inhibit the growth of bladder cancer cells through SREBP-1c/FASN axis. *Signal Transduct. Target Ther.* 6, 98. doi:10.1038/s41392-021-00493-8

Di, T. M., Yang, S. L., Du, F. Y., Zhao, L., Li, X. H., Xia, T., et al. (2018). Oleiferasaponin A_2, a novel saponin from Camellia oleifera abel. Seeds, inhibits lipid accumulation of HepG2 cells through regulating fatty acid metabolism. *Molecules* 23, 3296. doi:10.3390/molecules23123296

Dif, N., Euthine, V., Gonnet, E., Laville, M., Vidal, H., and Lefai, E. (2006). Insulin activates human sterol-regulatory-element-binding protein-1c (SREBP-1c) promoter through SRE motifs. *Biochem. J.* 400, 179–188. doi:10.1042/BJ20060499

Do, M. T., Hwang, Y. P., Kim, H. G., Na, M., and Jeong, H. G. (2013). Mollugin inhibits proliferation and induces apoptosis by suppressing fatty acid synthase in HER2-overexpressing cancer cells. *J. Cell Physiol.* 228, 1087–1097. doi:10.1002/jcp.24258

Do, M. T., Kim, H. G., Choi, J. H., Khanal, T., Park, B. H., Tran, T. P., et al. (2013). Antitumor efficacy of piperine in the treatment of human HER2-overexpressing breast cancer cells. *Food Chem.* 141, 2591–2599. doi:10.1016/j.foodchem.2013.04.125

Eberlé, D., Hegarty, B., Bossard, P., Ferré, P., and Foufelle, F. (2004). SREBP transcription factors: Master regulators of lipid homeostasis. *Biochimie* 86, 839–848. doi:10.1016/j.biochi.2004.09.018

Engreitz, J. M., Sirokman, K., McDonel, P., Shishkin, A. A., Surka, C., Russell, P., et al. (2014). RNA-RNA interactions enable specific targeting of noncoding RNAs to nascent Pre-mRNAs and chromatin sites. *Cell* 159, 188–199. doi:10.1016/j.cell.2014.08.018

Esquejo, R. M., Roqueta-Rivera, M., Shao, W., Phelan, P. E., Seneviratne, U., Am Ende, C. W., et al. (2021). Dipyridamole inhibits lipogenic gene expression by retaining SCAP-SREBP in the endoplasmic reticulum. *Cell Chem. Biol.* 28, 169–179.e7. doi:10.1016/j.chembiol.2020.10.003

Ettinger, S. L., Sobel, R., Whitmore, T. G., Akbari, M., Bradley, D. R., Gleave, M. E., et al. (2004). Dysregulation of sterol response element-binding proteins and downstream effectors in prostate cancer during progression to androgen independence. *Cancer Res.* 64, 2212–2221. doi:10.1158/0008-5472.can-2148-2

Feng, L., Xie, X., Ding, Q., Luo, X., He, J., Fan, F., et al. (2007). Spatial regulation of Raf kinase signaling by RKTG. *Proc. Natl. Acad. Sci. U. S. A.* 104, 14348–14353. doi:10.1073/pnas.0701298104

Foretz, M., Guichard, C., Ferré, P., and Foufelle, F. (1999). Sterol regulatory element binding protein-1c is a major mediator of insulin action on the hepatic expression of glucokinase and lipogenesis-related genes. *Proc. Natl. Acad. Sci. U. S. A.* 96, 12737–12742. doi:10.1073/pnas.96.22.12737

Gao, S., Shi, Z., Li, X., Li, W., Wang, Y., Liu, Z., et al. (2018). Fatostatin suppresses growth and enhances apoptosis by blocking SREBP-regulated metabolic pathways in endometrial carcinoma. *Oncol. Rep.* 39, 1919–1929. doi:10.3892/or.2018.6265

Gao, Y., Nan, X., Shi, X., Mu, X., Liu, B., Zhu, H., et al. (2019). SREBP1 promotes the invasion of colorectal cancer accompanied upregulation of MMP7 expression and NF-κB pathway activation. *BMC Cancer* 19, 685. doi:10.1186/s12885-019-5904-x

Gemmill, R. M., Bemis, L. T., Lee, J. P., Sozen, M. A., Baron, A., Zeng, C., et al. (2002). The TRC8 hereditary kidney cancer gene suppresses growth and functions with VHL in a common pathway,. *Oncogene* 21, 3507–3516. doi:10.1038/sj.onc.1205437

Geng, F., Cheng, X., Wu, X., Yoo, J. Y., Cheng, C., Guo, J. Y., et al. (2016). Inhibition of SOAT1 suppresses glioblastoma growth via blocking SREBP-1-mediated lipogenesis. *Clin. Cancer Res.* 22, 5337–5348. doi:10.1158/1078-0432.CCR-15-2973

Geng, F., and Guo, D. (2017). Lipid droplets, potential biomarker and metabolic target in glioblastoma. *Intern. Med. Rev.* 3. doi:10.18103/imr.v3i5.443

Gerin, I., Clerbaux, L. A., Haumont, O., Lanthier, N., Das, A. K., Burant, C. F., et al. (2010). Expression of miR-33 from an SREBP2 intron inhibits cholesterol export and fatty acid oxidation. *J. Biol. Chem.* 285, 33652–33661. doi:10.1074/jbc.M110.152090

Gholkar, A. A., Cheung, K., Williams, K. J., Lo, Y. C., Hamideh, S. A., Nnebe, C., et al. (2016). Fatostatin inhibits cancer cell proliferation by affecting mitotic microtubule spindle assembly and cell division. *J. Biol. Chem.* 291, 17001–17008. doi:10.1074/jbc.C116.737346

Gnoni, A., and Giudetti, A. M. (2016). Dietary long-chain unsaturated fatty acids acutely and differently reduce the activities of lipogenic enzymes and of citrate carrier in rat liver. *J. Physiol. Biochem.* 72, 485–494. doi:10.1007/s13105-016-0495-3

Gómez-Maldonado, L., Tiana, M., Roche, O., Prado-Cabrero, A., Jensen, L., Fernandez-Barral, A., et al. (2015). EFNA3 long noncoding RNAs induced by hypoxia promote metastatic dissemination. *Oncogene* 34, 2609–2620. doi:10.1038/onc.2014.200

Gong, X., Li, J., Shao, W., Wu, J., Qian, H., Ren, R., et al. (2015). Structure of the WD40 domain of SCAP from fission yeast reveals the molecular basis for SREBP recognition. *Cell Res.* 25, 401–411. doi:10.1038/cr.2015.32

Goyal, B., Yadav, S. R. M., Awasthee, N., Gupta, S., Kunnumakkara, A. B., and Gupta, S. C. (2021). Diagnostic, prognostic, and therapeutic significance of long non-coding RNA MALAT1 in cancer. *Biochim. Biophys. Acta Rev. Cancer* 1875, 188502. doi:10.1016/j.bbcan.2021.188502

Gu, Y., Xue, M., Wang, Q., Hong, X., Wang, X., Zhou, F., et al. (2021). Novel strategy of proxalutamide for the treatment of prostate cancer through coordinated blockade of lipogenesis and androgen receptor Axis. *Int. J. Mol. Sci.* 22, 13222. doi:10.3390/ijms222413222

Guan, M., Fousek, K., and Chow, W. A. (2012). Nelfinavir inhibits regulated intramembrane proteolysis of sterol regulatory element binding protein-1 and activating transcription factor 6 in castration-resistant prostate cancer. *Febs J.* 279, 2399–2411. doi:10.1111/j.1742-4658.2012.08619.x

Guan, M., Fousek, K., Jiang, C., Guo, S., Synold, T., Xi, B., et al. (2011). Nelfinavir induces liposarcoma apoptosis through inhibition of regulated intramembrane proteolysis of SREBP-1 and ATF6. *Clin. Cancer Res.* 17, 1796–1806. doi:10.1158/1078-0432.CCR-10-3216

Guan, M., Su, L., Yuan, Y. C., Li, H., and Chow, W. A. (2015). Nelfinavir and nelfinavir analogs block site-2 protease cleavage to inhibit castration-resistant prostate cancer. *Sci. Rep.* 5, 9698. doi:10.1038/srep09698

Guo, D., Hildebrandt, I. J., Prins, R. M., Soto, H., Mazzotta, M. M., Dang, J., et al. (2009). The AMPK agonist AICAR inhibits the growth of EGFRvIII-expressing glioblastomas by inhibiting lipogenesis,. *Proc. Natl. Acad. Sci. U. S. A.* 106, 12932–12937. doi:10.1073/pnas.0906606106

Guo, D., Prins, R. M., Dang, J., Kuga, D., Iwanami, A., Soto, H., et al. (2009). EGFR signaling through an Akt-SREBP-1-dependent, rapamycin-resistant pathway sensitizes glioblastomas to antilipogenic therapy. *Sci. Signal* 2, ra82. doi:10.1126/scisignal.2000446

Guo, D., Reinitz, F., Youssef, M., Hong, C., Nathanson, D., Akhavan, D., et al. (2011). An LXR agonist promotes glioblastoma cell death through inhibition of an EGFR/AKT/SREBP-1/LDLR-dependent pathway. *Cancer Discov.* 1, 442–456. doi:10.1158/2159-8290.CD-11-0102

Guo, D. (2016). SCAP links glucose to lipid metabolism in cancer cells. *Mol. Cell Oncol.* 3, e1132120. doi:10.1080/23723556.2015.1132120

Gutschner, T., Hämmerle, M., Eissmann, M., Hsu, J., Kim, Y., Hung, G., et al. (2013). The noncoding RNA MALAT1 is a critical regulator of the metastasis phenotype of lung cancer cells,. *Cancer Res.* 73, 1180–1189. doi:10.1158/0008-5472.CAN-12-2850

Hamm, R., Chen, Y. R., Seo, E. J., Zeino, M., Wu, C. F., Müller, R., et al. (2014). Induction of cholesterol biosynthesis by archazolid B in T24 bladder cancer cells. *Biochem. Pharmacol.* 91, 18–30. doi:10.1016/j.bcp.2014.06.018

Han, M., Wang, S., Yang, N., Wang, X., Zhao, W., Saed, H. S., et al. (2020). Therapeutic implications of altered cholesterol homeostasis mediated by loss of CYP46A1 in human glioblastoma. *EMBO Mol. Med.* 12, e10924. doi:10.15252/emmm.201910924

Han, S. Y., Han, H. B., Tian, X. Y., Sun, H., Xue, D., Zhao, C., et al. (2016). MicroRNA-33a-3p suppresses cell migration and invasion by directly targeting PBX3 in human hepatocellular carcinoma. *Oncotarget* 7, 42461–42473. doi:10.18632/oncotarget.9886

Hayashi, K., Nakazato, Y., Morito, N., Sagi, M., Fujita, T., Anzai, N., et al. (2020). Fluvastatin is effective against thymic carcinoma. *Life Sci.* 240, 117110. doi:10.1016/j.lfs.2019.117110

Heo, M. J., Kang, S. H., Kim, Y. S., Lee, J. M., Yu, J., Kim, H. R., et al. (2020). UBC12-mediated SREBP-1 neddylation worsens metastatic tumor prognosis. *Int. J. Cancer* 147, 2550–2563. doi:10.1002/ijc.33113

Hida, Y., Kubo, Y., Murao, K., and Arase, S. (2007). Strong expression of a longevity-related protein, SIRT1, in Bowen's disease. *Arch. Dermatol Res.* 299, 103–106. doi:10.1007/s00403-006-0725-6

Hirasawa, A., Tsumaya, K., Awaji, T., Katsuma, S., Adachi, T., Yamada, M., et al. (2005). Free fatty acids regulate gut incretin glucagon-like peptide-1 secretion through GPR120. *Nat. Med.* 11, 90–94. doi:10.1038/nm1168

Horie, T., Ono, K., Horiguchi, M., Nishi, H., Nakamura, T., Nagao, K., et al. (2010). MicroRNA-33 encoded by an intron of sterol regulatory element-binding protein 2 (Srebp2) regulates HDL *in vivo*. *Proc. Natl. Acad. Sci. U. S. A.* 107, 17321–17326. doi:10.1073/pnas.1008499107

Horton, J. D., Goldstein, J. L., and Brown, M. S. (2002). SREBPs: Activators of the complete program of cholesterol and fatty acid synthesis in the liver. *J. Clin. Invest.* 109, 1125–1131. doi:10.1172/JCI15593

Horton, J. D., Shah, N. A., Warrington, J. A., Anderson, N. N., Park, S. W., Brown, M. S., et al. (2003). Combined analysis of oligonucleotide microarray data from transgenic and knockout mice identifies direct SREBP target genes. *Proc. Natl. Acad. Sci. U. S. A.* 100, 12027–12032. doi:10.1073/pnas.1534923100

Horton, J. D., Shimomura, I., Ikemoto, S., Bashmakov, Y., and Hammer, R. E. (2003). Overexpression of sterol regulatory element-binding protein-1a in mouse adipose tissue produces adipocyte hypertrophy, increased fatty acid secretion, and fatty liver. *J. Biol. Chem.* 278, 36652–36660. doi:10.1074/jbc.M306540200

Hsieh, P. F., Jiang, W. P., Huang, S. Y., Basavaraj, P., Wu, J. B., Ho, H. Y., et al. (2020). Emerging therapeutic activity of Davallia formosana on prostate cancer cells through coordinated blockade of lipogenesis and androgen receptor expression. *Cancers (Basel)* 12, 914. doi:10.3390/cancers12040914

Hu, L., Wu, Y., Tan, D., Meng, H., Wang, K., Bai, Y., et al. (2015). Up-regulation of long noncoding RNA MALAT1 contributes to proliferation and metastasis in esophageal squamous cell carcinoma. *J. Exp. Clin. Cancer Res.* 34, 7. doi:10.1186/s13046-015-0123-z

Huang, J., Zhao, X., Li, X., Peng, J., Yang, W., and Mi, S. (2021). HMGCR inhibition stabilizes the glycolytic enzyme PKM2 to support the growth of renal cell carcinoma. *PLoS Biol.* 19, e3001197. doi:10.1371/journal.pbio.3001197

Huang, L. H., Chung, H. Y., and Su, H. M. (2017). Docosahexaenoic acid reduces sterol regulatory element binding protein-1 and fatty acid synthase expression and

inhibits cell proliferation by inhibiting pAkt signaling in a human breast cancer MCF-7 cell line. *BMC Cancer* 17, 890. doi:10.1186/s12885-017-3936-7

Huang, T. S., Lee, J. J., Huang, S. Y., and Cheng, S. P. (2022). Regulation of expression of sterol regulatory element-binding protein 1 in thyroid cancer cells. *Anticancer Res.* 42, 2487–2493. doi:10.21873/anticanres.15727

Huang, W. C., Li, X., Liu, J., Lin, J., and Chung, L. W. (2012). Activation of androgen receptor, lipogenesis, and oxidative stress converged by SREBP-1 is responsible for regulating growth and progression of prostate cancer cells. *Mol. Cancer Res.* 10, 133–142. doi:10.1158/1541-7786.MCR-11-0206

Huang, Y., Zhang, J., Shao, H., Liu, J., Jin, M., Chen, J., et al. (2018). miR-33a mediates the anti-tumor effect of lovastatin in osteosarcoma by targeting CYR61. *Cell Physiol. Biochem.* 51, 938–948. doi:10.1159/000495396

Huffman, D. M., Grizzle, W. E., Bamman, M. M., Kim, J. S., Eltoum, I. A., Elgavish, A., et al. (2007). SIRT1 is significantly elevated in mouse and human prostate cancer. *Cancer Res.* 67, 6612–6618. doi:10.1158/0008-5472.CAN-07-0085

Husain, A., Chiu, Y. T., Sze, K. M., Ho, D. W., Tsui, Y. M., Suarez, E. M. S., et al. (2022). Ephrin-A3/EphA2 axis regulates cellular metabolic plasticity to enhance cancer stemness in hypoxic hepatocellular carcinoma. *J. Hepatol.* 77, 383–396. doi:10.1016/j.jhep.2022.02.018

Hwang, P. M., Bunz, F., Yu, J., Rago, C., Chan, T. A., Murphy, M. P., et al. (2001). Ferredoxin reductase affects p53-dependent, 5-fluorouracil-induced apoptosis in colorectal cancer cells. *Nat. Med.* 7, 1111–1117. doi:10.1038/nm1001-1111

Iliopoulos, D., Drosatos, K., Hiyama, Y., Goldberg, I. J., and Zannis, V. I. (2010). MicroRNA-370 controls the expression of microRNA-122 and Cpt1alpha and affects lipid metabolism. *J. Lipid Res.* 51, 1513–1523. doi:10.1194/jlr.M004812

Irisawa, M., Inoue, J., Ozawa, N., Mori, K., and Sato, R. (2009). The sterol-sensing endoplasmic reticulum (ER) membrane protein TRC8 hampers ER to Golgi transport of sterol regulatory element-binding protein-2 (SREBP-2)/SREBP cleavage-activated protein and reduces SREBP-2 cleavage,. *J. Biol. Chem.* 284, 28995–29004. doi:10.1074/jbc.M109.041376

Ishii, H., Horie, Y., Ohshima, S., Anezaki, Y., Kinoshita, N., Dohmen, T., et al. (2009). Eicosapentaenoic acid ameliorates steatohepatitis and hepatocellular carcinoma in hepatocyte-specific Pten-deficient mice. *J. Hepatol.* 50, 562–571. doi:10.1016/j.jhep.2008.10.031

Ishikawa, S., Nagai, Y., Masuda, T., Koga, Y., Nakamura, T., Imamura, Y., et al. (2010). The role of oxysterol binding protein-related protein 5 in pancreatic cancer,. *Cancer Sci.* 101, 898–905. doi:10.1111/j.1349-7006.2009.01475.x

Jie, Z., Xie, Z., Xu, W., Zhao, X., Jin, G., Sun, X., et al. (2019). SREBP-2 aggravates breast cancer associated osteolysis by promoting osteoclastogenesis and breast cancer metastasis. *Biochim. Biophys. Acta Mol. Basis Dis.* 1865, 115–125. doi:10.1016/j.bbadis.2018.10.026

Kamisuki, S., Mao, Q., Abu-Elheiga, L., Gu, Z., Kugimiya, A., Kwon, Y., et al. (2009). A small molecule that blocks fat synthesis by inhibiting the activation of SREBP,. *Chem. Biol.* 16, 882–892. doi:10.1016/j.chembiol.2009.07.007

Kanagasabai, T., Li, G., Shen, T. H., Gladoun, N., Castillo-Martin, M., Celada, S. I., et al. (2022). MicroRNA-21 deficiency suppresses prostate cancer progression through downregulation of the IRS1-SREBP-1 signaling pathway. *Cancer Lett.* 525, 46–54. doi:10.1016/j.canlet.2021.09.041

Kang, O. H., Kim, S. B., Seo, Y. S., Joung, D. K., Mun, S. H., Choi, J. G., et al. (2013). Curcumin decreases oleic acid-induced lipid accumulation via AMPK phosphorylation in hepatocarcinoma cells. *Eur. Rev. Med. Pharmacol. Sci.* 17, 2578–2586.

Kang, S., Huang, J., Lee, B. K., Jung, Y. S., Im, E., Koh, J. M., et al. (2018). Omega-3 polyunsaturated fatty acids protect human hepatoma cells from developing steatosis through FFA4 (GPR120). *Biochim. Biophys. Acta Mol. Cell Biol. Lipids* 1863, 105–116. doi:10.1016/j.bbalip.2017.11.002

Karatas, O. F., Wang, J., Shao, L., Ozen, M., Zhang, Y., Creighton, C. J., et al. (2017). miR-33a is a tumor suppressor microRNA that is decreased in prostate cancer. *Oncotarget* 8, 60243–60256. doi:10.18632/oncotarget.19521

Kawamura, S., Matsushita, Y., Kurosaki, S., Tange, M., Fujiwara, N., Hayata, Y., et al. (2022). Inhibiting SCAP/SREBP exacerbates liver injury and carcinogenesis in murine nonalcoholic steatohepatitis. *J. Clin. Invest.* 132, e151895. doi:10.1172/JCI151895

Khurana, V., Bejjanki, H. R., Caldito, G., and Owens, M. W. (2007). Statins reduce the risk of lung cancer in humans: A large case-control study of US veterans. *Chest* 131, 1282–1288. doi:10.1378/chest.06-0931

Kong, Y., Cheng, L., Mao, F., Zhang, Z., Zhang, Y., Farah, E., et al. (2018). Inhibition of cholesterol biosynthesis overcomes enzalutamide resistance in castration-resistant prostate cancer (CRPC). *J. Biol. Chem.* 293, 14328–14341. doi:10.1074/jbc.RA118.004442

König, B., Koch, A., Spielmann, J., Hilgenfeld, C., Hirche, F., Stangl, G. I., et al. (2009). Activation of PPARalpha and PPARgamma reduces triacylglycerol synthesis in rat hepatoma cells by reduction of nuclear SREBP-1. *Eur. J. Pharmacol.* 605, 23–30. doi:10.1016/j.ejphar.2009.01.009

Koohestanimobarhan, S., Salami, S., Imeni, V., Mohammadi, Z., and Bayat, O. (2019). Lipophilic statins antagonistically alter the major epithelial-to-mesenchymal transition signaling pathways in breast cancer stem-like cells via inhibition of the mevalonate pathway. *J. Cell Biochem.* 120, 2515–2531. doi:10.1002/jcb.27544

Krichevsky, A. M., and Gabriely, G. (2009). miR-21: a small multi-faceted RNA. *J. Cell Mol. Med.* 13, 39–53. doi:10.1111/j.1582-4934.2008.00556.x

Kuo, P. L., Liao, S. H., Hung, J. Y., Huang, M. S., and Hsu, Y. L. (2013). MicroRNA-33a functions as a bone metastasis suppressor in lung cancer by targeting parathyroid hormone related protein. *Biochim. Biophys. Acta* 1830, 3756–3766. doi:10.1016/j.bbagen.2013.02.022

Kurtz, C. L., Peck, B. C., Fannin, E. E., Beysen, C., Miao, J., Landstreet, S. R., et al. (2014). MicroRNA-29 fine-tunes the expression of key FOXA2-activated lipid metabolism genes and is dysregulated in animal models of insulin resistance and diabetes. *Diabetes* 63, 3141–3148. doi:10.2337/db13-1015

Kuzmichev, A., Margueron, R., Vaquero, A., Preissner, T. S., Scher, M., Kirmizis, A., et al. (2005). Composition and histone substrates of polycomb repressive group complexes change during cellular differentiation. *Proc. Natl. Acad. Sci. U. S. A.* 102, 1859–1864. doi:10.1073/pnas.0409875102

Lebeau, P., Byun, J. H., Yousof, T., and Austin, R. C. (2018). Pharmacologic inhibition of S1P attenuates ATF6 expression, causes ER stress and contributes to apoptotic cell death. *Toxicol. Appl. Pharmacol.* 349, 1–7. doi:10.1016/j.taap.2018.04.020

Lee, J., Imm, J. Y., and Lee, S. H. (2017). β-Catenin mediates anti-adipogenic and anticancer effects of arctigenin in preadipocytes and breast cancer cells. *J. Agric. Food Chem.* 65, 2513–2520. doi:10.1021/acs.jafc.7b00112

Lee, J. S., Roberts, A., Juarez, D., Vo, T. T., Bhatt, S., Herzog, L. O., et al. (2018). Statins enhance efficacy of venetoclax in blood cancers. *Sci. Transl. Med.* 10, eaaq1240. doi:10.1126/scitranslmed.aaq1240

Li, A., Yao, L., Fang, Y., Yang, K., Jiang, W., Huang, W., et al. (2019). Specifically blocking the fatty acid synthesis to inhibit the malignant phenotype of bladder cancer. *Int. J. Biol. Sci.* 15, 1610–1617. doi:10.7150/ijbs.32518

Li, C., Peng, X., Lv, J., Zou, H., Liu, J., Zhang, K., et al. (2020). SREBP1 as a potential biomarker predicts levothyroxine efficacy of differentiated thyroid cancer. *Biomed. Pharmacother.* 123, 109791. doi:10.1016/j.biopha.2019.109791

Li, C., Yang, W., Zhang, J., Zheng, X., Yao, Y., Tu, K., et al. (2014). SREBP-1 has a prognostic role and contributes to invasion and metastasis in human hepatocellular carcinoma. *Int. J. Mol. Sci.* 15, 7124–7138. doi:10.3390/ijms15057124

Li, J., Huang, Q., Long, X., Zhang, J., Huang, X., Aa, J., et al. (2015). CD147 reprograms fatty acid metabolism in hepatocellular carcinoma cells through Akt/mTOR/SREBP1c and P38/PPARα pathways. *J. Hepatol.* 63, 1378–1389. doi:10.1016/j.jhep.2015.07.039

Li, J., Yuan, J., Yuan, X. R., Zhang, C., Li, H. Y., Zhao, J., et al. (2015). Induction effect of MicroRNA-449a on glioma cell proliferation and inhibition on glioma cell apoptosis by promoting PKCα. *Eur. Rev. Med. Pharmacol. Sci.* 19, 3587–3592.

Li, N., Zhou, Z. S., Shen, Y., Xu, J., Miao, H. H., Xiong, Y., et al. (2017). Inhibition of the sterol regulatory element-binding protein pathway suppresses hepatocellular carcinoma by repressing inflammation in mice. *Hepatology* 65, 1936–1947. doi:10.1002/hep.29018

Li, Q., Peng, J., Li, X., Leng, A., and Liu, T. (2015). miR-449a targets Flot2 and inhibits gastric cancer invasion by inhibiting TGF-β-mediated EMT. *Diagn Pathol.* 10, 202. doi:10.1186/s13000-015-0435-5

Li, W., Tai, Y., Zhou, J., Gu, W., Bai, Z., Zhou, T., et al. (2012). Repression of endometrial tumor growth by targeting SREBP1 and lipogenesis. *Cell Cycle* 11, 2348–2358. doi:10.4161/cc.20811

Li, X., Chen, Y. T., Hu, P., and Huang, W. C. (2014). Fatostatin displays high antitumor activity in prostate cancer by blocking SREBP-regulated metabolic pathways and androgen receptor signaling. *Mol. Cancer Ther.* 13, 855–866. doi:10.1158/1535-7163.MCT-13-0797

Li, X., Chen, Y. T., Josson, S., Mukhopadhyay, N. K., Kim, J., Freeman, M. R., et al. (2013). MicroRNA-185 and 342 inhibit tumorigenicity and induce apoptosis through blockade of the SREBP metabolic pathway in prostate cancer cells. *PLoS One* 8, e70987. doi:10.1371/journal.pone.0070987

Li, X., Wu, J. B., Chung, L. W., and Huang, W. C. (2015). Anti-cancer efficacy of SREBP inhibitor, alone or in combination with docetaxel, in prostate cancer harboring p53 mutations. *Oncotarget* 6, 41018–41032. doi:10.18632/oncotarget.5879

Li, Y., Xu, S., Mihaylova, M. M., Zheng, B., Hou, X., Jiang, B., et al. (2011). AMPK phosphorylates and inhibits SREBP activity to attenuate hepatic steatosis and atherosclerosis in diet-induced insulin-resistant mice. *Cell Metab.* 13, 376–388. doi:10.1016/j.cmet.2011.03.009

Li, Y., Zhang, J., He, J., Zhou, W., Xiang, G., and Xu, R. (2016). MicroRNA-132 cause apoptosis of glioma cells through blockade of the SREBP-1c metabolic pathway related to SIRT1. *Biomed. Pharmacother.* 78, 177–184. doi:10.1016/j.biopha.2016.01.022

Liang, B., Chen, R., Song, S., Wang, H., Sun, G., Yang, H., et al. (2019). ASPP2 inhibits tumor growth by repressing the mevalonate pathway in hepatocellular carcinoma. *Cell Death Dis.* 10, 830. doi:10.1038/s41419-019-2054-7

Lim, S. A., Wei, J., Nguyen, T. M., Shi, H., Su, W., Palacios, G., et al. (2021). Lipid signalling enforces functional specialization of T(reg) cells in tumours. *Nature* 591, 306–311. doi:10.1038/s41586-021-03235-6

Liu, F., Ma, M., Gao, A., Ma, F., Ma, G., Liu, P., et al. (2021). PKM2-TMEM33 axis regulates lipid homeostasis in cancer cells by controlling SCAP stability. *Embo J.* 40, e108065. doi:10.15252/embj.2021108065

Liu, G., and Chen, X. (2002). The ferredoxin reductase gene is regulated by the p53 family and sensitizes cells to oxidative stress-induced apoptosis,. *Oncogene* 21, 7195–7204. doi:10.1038/sj.onc.1205862

Liu, L., Zhao, X., Zhao, L., Li, J., Yang, H., Zhu, Z., et al. (2016). Arginine methylation of SREBP1a via PRMT5 promotes de novo lipogenesis and tumor growth. *Cancer Res.* 76, 1260–1272. doi:10.1158/0008-5472.CAN-15-1766

Liu, Y., Hua, W., Li, Y., Xian, X., Zhao, Z., Liu, C., et al. (2020). Berberine suppresses colon cancer cell proliferation by inhibiting the SCAP/SREBP-1 signaling pathway-mediated lipogenesis. *Biochem. Pharmacol.* 174, 113776. doi:10.1016/j.bcp.2019.113776

Liu, Y., Ren, H., Zhou, Y., Shang, L., Zhang, Y., Yang, F., et al. (2019). The hypoxia conditioned mesenchymal stem cells promote hepatocellular carcinoma progression through YAP mediated lipogenesis reprogramming,. *J. Exp. Clin. Cancer Res.* 38, 228. doi:10.1186/s13046-019-1219-7

Long, J., Zhang, C. J., Zhu, N., Du, K., Yin, Y. F., Tan, X., et al. (2018). Lipid metabolism and carcinogenesis, cancer development. *Am. J. Cancer Res.* 8, 778–791.

Longo, J., Mullen, P. J., Yu, R., van Leeuwen, J. E., Masoomian, M., Woon, D. T. S., et al. (2019). An actionable sterol-regulated feedback loop modulates statin sensitivity in prostate cancer. *Mol. Metab.* 25, 119–130. doi:10.1016/j.molmet.2019.04.003

Loregger, A., Raaben, M., Nieuwenhuis, J., Tan, J. M. E., Jae, L. T., van den Hengel, L. G., et al. (2020). Haploid genetic screens identify SPRING/C12ORF49 as a determinant of SREBP signaling and cholesterol metabolism. *Nat. Commun.* 11, 1128. doi:10.1038/s41467-020-14811-1

Luo, W., Huang, B., Li, Z., Li, H., Sun, L., Zhang, Q., et al. (2013). MicroRNA-449a is downregulated in non-small cell lung cancer and inhibits migration and invasion by targeting c-Met. *PLoS One* 8, e64759. doi:10.1371/journal.pone.0064759

Lv, Q., Zhen, Q., Liu, L., Gao, R., Yang, S., Zhou, H., et al. (2015). AMP-kinase pathway is involved in tumor necrosis factor alpha-induced lipid accumulation in human hepatoma cells. *Life Sci.* 131, 23–29. doi:10.1016/j.lfs.2015.03.003

Marquart, T. J., Allen, R. M., Ory, D. S., and Baldán, A. (2010). miR-33 links SREBP-2 induction to repression of sterol transporters. *Proc. Natl. Acad. Sci. U. S. A.* 107, 12228–12232. doi:10.1073/pnas.1005191107

Matsushita, Y., Nakagawa, H., and Koike, K. (2021). Lipid metabolism in oncology: Why it matters, how to research, and how to treat. *Cancers (Basel)* 13, 474. doi:10.3390/cancers13030474

Menendez, J. A., and Lupu, R. (2007). Fatty acid synthase and the lipogenic phenotype in cancer pathogenesis. *Nat. Rev. Cancer* 7, 763–777. doi:10.1038/nrc2222

Menon, B., Gulappa, T., and Menon, K. M. (2015). miR-122 regulates LH receptor expression by activating sterol response element binding protein in rat ovaries. *Endocrinology* 156, 3370–3380. doi:10.1210/en.2015-1121

Menon, B., Guo, X., Garcia, N., Gulappa, T., and Menon, K. M. J. (2018). miR-122 regulates LHR expression in rat granulosa cells by targeting Insig1 mRNA. *Endocrinology* 159, 2075–2082. doi:10.1210/en.2017-03270

Menon, B., Sinden, J., Franzo-Romain, M., Botta, R. B., and Menon, K. M. (2013). Regulation of LH receptor mRNA binding protein by miR-122 in rat ovaries. *Endocrinology* 154, 4826–4834. doi:10.1210/en.2013-1619

Miyata, S., Urabe, M., Gomi, A., Nagai, M., Yamaguchi, T., Tsukahara, T., et al. (2013). An R132H mutation in isocitrate dehydrogenase 1 enhances p21 expression and inhibits phosphorylation of retinoblastoma protein in glioma cells. *Neurol. Med. Chir. (Tokyo)* 53, 645–654. doi:10.2176/nmc.oa2012-0409

Moon, S. H., Huang, C. H., Houlihan, S. L., Regunath, K., Freed-Pastor, W. A., et al. (2019). p53 represses the mevalonate pathway to mediate tumor suppression. *Cell* 176, 564–580. doi:10.1016/j.cell.2018.11.011

Na, T. Y., Shin, Y. K., Roh, K. J., Kang, S. A., Hong, I., Oh, S. J., et al. (2009). Liver X receptor mediates Hepatitis B virus X protein-induced lipogenesis in Hepatitis B virus-associated hepatocellular carcinoma. *Hepatology* 49, 1122–1131. doi:10.1002/hep.22740

Najafi-Shoushtari, S. H., Kristo, F., Li, Y., Shioda, T., Cohen, D. E., Gerszten, R. E., et al. (2010). MicroRNA-33 and the SREBP host genes cooperate to control cholesterol homeostasis. *Science* 328, 1566–1569. doi:10.1126/science.1189123

Nam, H. J., Kim, Y. E., Moon, B. S., Kim, H. Y., Jung, D., Choi, S., et al. (2021). Azathioprine antagonizes aberrantly elevated lipid metabolism and induces apoptosis in glioblastoma. *iScience* 24, 102238. doi:10.1016/j.isci.2021.102238

Nanthirudjanar, T., Furumoto, H., Hirata, T., and Sugawara, T. (2013). Oxidized eicosapentaenoic acids more potently reduce LXRα-induced cellular triacylglycerol via suppression of SREBP-1c, PGC-1β and GPA than its intact form. *Lipids Health Dis.* 12, 73. doi:10.1186/1476-511X-12-73

Navarro-Imaz, H., Chico, Y., Rueda, Y., and Fresnedo, O. (2019). Channeling of newly synthesized fatty acids to cholesterol esterification limits triglyceride synthesis in SND1-overexpressing hepatoma cells. *Biochim. Biophys. Acta Mol. Cell Biol. Lipids* 1864, 137–146. doi:10.1016/j.bbalip.2018.11.004

Ni, W., Mo, H., Liu, Y., Xu, Y., Qin, C., Zhou, Y., et al. (2021). Targeting cholesterol biosynthesis promotes anti-tumor immunity by inhibiting long noncoding RNA SNHG29-mediated YAP activation. *Mol. Ther.* 29, 2995–3010. doi:10.1016/j.ymthe.2021.05.012

Nohturfft, A., Yabe, D., Goldstein, J. L., Brown, M. S., and Espenshade, P. J. (2000). Regulated step in cholesterol feedback localized to budding of SCAP from ER membranes. *Cell* 102, 315–323. doi:10.1016/s0092-8674(00)00037-4

Norman, K. L., Chen, T. C., Zeiner, G., and Sarnow, P. (2017). Precursor microRNA-122 inhibits synthesis of Insig1 isoform mRNA by modulating polyadenylation site usage. *Rna* 23, 1886–1893. doi:10.1261/rna.063099.117

Oberkofler, H., Schraml, E., Krempler, F., and Patsch, W. (2004). Restoration of sterol-regulatory-element-binding protein-1c gene expression in HepG2 cells by peroxisome-proliferator-activated receptor-gamma co-activator-1alpha. *Biochem. J.* 381, 357–363. doi:10.1042/BJ20040173

Olmstead, A. D., Knecht, W., Lazarov, I., Dixit, S. B., and Jean, F. (2012). Human subtilase SKI-1/S1P is a master regulator of the HCV Lifecycle and a potential host cell target for developing indirect-acting antiviral agents. *PLoS Pathog.* 8, e1002468. doi:10.1371/journal.ppat.1002468

Osborne, T. F., and Espenshade, P. J. (2009). Evolutionary conservation and adaptation in the mechanism that regulates SREBP action: What a long, strange tRIP it's been. *Genes Dev.* 23, 2578–2591. doi:10.1101/gad.1854309

Pang, B., Zhang, J., Zhang, X., Yuan, J., Shi, Y., and Qiao, L. (2021). Inhibition of lipogenesis and induction of apoptosis by valproic acid in prostate cancer cells via the C/EBPα/SREBP-1 pathway. *Acta Biochim. Biophys. Sin. (Shanghai)* 53, 354–364. doi:10.1093/abbs/gmab002

Peterson, T. R., Sengupta, S. S., Harris, T. E., Carmack, A. E., Kang, S. A., Balderas, E., et al. (2011). mTOR complex 1 regulates lipin 1 localization to control the SREBP pathway. *Cell* 146, 408–420. doi:10.1016/j.cell.2011.06.034

Piccolo, S., Dupont, S., and Cordenonsi, M. (2014). The biology of YAP/TAZ: Hippo signaling and beyond,. *Physiol. Rev.* 94, 1287–1312. doi:10.1152/physrev.00005.2014

Porstmann, T., Santos, C. R., Griffiths, B., Cully, M., Wu, M., Leevers, S., et al. (2008). SREBP activity is regulated by mTORC1 and contributes to Akt-dependent cell growth. *Cell Metab.* 8, 224–236. doi:10.1016/j.cmet.2008.07.007

Qian, Y., Huang, R., Li, S., Xie, R., Qian, B., Zhang, Z., et al. (2019). Ginsenoside Rh2 reverses cyclophosphamide-induced immune deficiency by regulating fatty acid metabolism. *J. Leukoc. Biol.* 106, 1089–1100. doi:10.1002/JLB.2A0419-117R

Qiao, L., Wu, Q., Lu, X., Zhou, Y., Fernández-Alvarez, A., Ye, L., et al. (2013). SREBP-1a activation by HBx and the effect on Hepatitis B virus enhancer II/core promoter. *Biochem. Biophys. Res. Commun.* 432, 643–649. doi:10.1016/j.bbrc.2013.02.030

Qiu, X. Y., Hu, D. X., Chen, W. Q., Chen, R. Q., Qian, S. R., Li, C. Y., et al. (2018). PD-L1 confers glioblastoma multiforme malignancy via Ras binding and Ras/Erk/EMT activation. *Biochim. Biophys. Acta Mol. Basis Dis.* 1864, 1754–1769. doi:10.1016/j.bbadis.2018.03.002

Quail, D. F., and Joyce, J. A. (2013). Microenvironmental regulation of tumor progression and metastasis. *Nat. Med.* 19, 1423–1437. doi:10.1038/nm.3394

Rayner, K. J., Suárez, Y., Dávalos, A., Parathath, S., Fitzgerald, M. L., Tamehiro, N., et al. (2010). MiR-33 contributes to the regulation of cholesterol homeostasis. *Science* 328, 1570–1573. doi:10.1126/science.1189862

Repa, J. J., Liang, G., Ou, J., Bashmakov, Y., Lobaccaro, J. M., Shimomura, I., et al. (2000). Regulation of mouse sterol regulatory element-binding protein-1c gene (SREBP-1c) by oxysterol receptors, LXRalpha and LXRbeta. *Genes Dev.* 14, 2819–2830. doi:10.1101/gad.844900

Ricoult, S. J., Yecies, J. L., Ben-Sahra, I., and Manning, B. D. (2016). Oncogenic PI3K and K-Ras stimulate de novo lipid synthesis through mTORC1 and SREBP. *Oncogene* 35, 1250–1260. doi:10.1038/onc.2015.179

Rottiers, V., and Näär, A. M. (2012). MicroRNAs in metabolism and metabolic disorders. *Nat. Rev. Mol. Cell Biol.* 13, 239–250. doi:10.1038/nrm3313

Ru, P., and Guo, D. (2017). microRNA-29 mediates a novel negative feedback loop to regulate SCAP/SREBP-1 and lipid metabolism. *RNA Dis.* 4, e1525. doi:10.14800/rd.1525

Ru, P., Hu, P., Geng, F., Mo, X., Cheng, C., Yoo, J. Y., et al. (2016). Feedback loop regulation of SCAP/SREBP-1 by miR-29 modulates EGFR signaling-driven glioblastoma growth. *Cell Rep.* 16, 1527–1535. doi:10.1016/j.celrep.2016.07.017

Sato, R., Inoue, J., Kawabe, Y., Kodama, T., Takano, T., and Maeda, M. (1996). Sterol-dependent transcriptional regulation of sterol regulatory element-binding protein-2. *J. Biol. Chem.* 271, 26461–26464. doi:10.1074/jbc.271.43.26461

Scorletti, E., and Byrne, C. D. (2013). Omega-3 fatty acids, hepatic lipid metabolism, and nonalcoholic fatty liver disease. *Annu. Rev. Nutr.* 33, 231–248. doi:10.1146/annurev-nutr-071812-161230

Seidu, T., McWhorter, P., Myer, J., Alamgir, R., Eregha, N., Bogle, D., et al. (2021). DHT causes liver steatosis via transcriptional regulation of SCAP in normal weight female mice. *J. Endocrinol.* 250, 49–65. doi:10.1530/JOE-21-0040

Shan, Y., Liu, Y., Zhao, L., Liu, B., Li, Y., and Jia, L. (2017). MicroRNA-33a and let-7e inhibit human colorectal cancer progression by targeting ST8SIA1. *Int. J. Biochem. Cell Biol.* 90, 48–58. doi:10.1016/j.biocel.2017.07.016

Shao, W., Machamer, C. E., and Espenshade, P. J. (2016). Fatostatin blocks ER exit of SCAP but inhibits cell growth in a SCAP-independent manner. *J. Lipid Res.* 57, 1564–1573. doi:10.1194/jlr.M069583

Shi, Y., Du, L., Lin, L., and Wang, Y. (2017). Tumour-associated mesenchymal stem/stromal cells: Emerging therapeutic targets. *Nat. Rev. Drug Discov.* 16, 35–52. doi:10.1038/nrd.2016.193

Shibata, C., Kishikawa, T., Otsuka, M., Ohno, M., Yoshikawa, T., Takata, A., et al. (2013). Inhibition of microRNA122 decreases SREBP1 expression by modulating suppressor of cytokine signaling 3 expression. *Biochem. Biophys. Res. Commun.* 438, 230–235. doi:10.1016/j.bbrc.2013.07.064

Shimano, H., and Sato, R. (2017). SREBP-Regulated lipid metabolism: Convergent physiology - divergent pathophysiology. *Nat. Rev. Endocrinol.* 13, 710–730. doi:10.1038/nrendo.2017.91

Si, M. L., Zhu, S., Wu, H., Lu, Z., Wu, F., and Mo, Y. Y. (2007). miR-21-mediated tumor growth. *Oncogene* 26, 2799–2803. doi:10.1038/sj.onc.1210083

Singh, H., Mahmud, S. M., Turner, D., Xue, L., Demers, A. A., and Bernstein, C. N. (2009). Long-term use of statins and risk of colorectal cancer: A population-based study. *Am. J. Gastroenterol.* 104, 3015–3023. doi:10.1038/ajg.2009.574

Snaebjornsson, M. T., Janaki-Raman, S., and Schulze, A. (2020). Greasing the wheels of the cancer machine: The role of lipid metabolism in cancer,. *Cell Metab.* 31, 62–76. doi:10.1016/j.cmet.2019.11.010

Song, N. Y., Na, H. K., Baek, J. H., and Surh, Y. J. (2014). Docosahexaenoic acid inhibits insulin-induced activation of sterol regulatory-element binding protein 1 and cyclooxygenase-2 expression through upregulation of SIRT1 in human colon epithelial cells. *Biochem. Pharmacol.* 92, 142–148. doi:10.1016/j.bcp.2014.08.030

Sorrentino, G., Ruggeri, N., Specchia, V., Cordenonsi, M., Mano, M., Dupont, S., et al. (2014). Metabolic control of YAP and TAZ by the mevalonate pathway. *Nat. Cell Biol.* 16, 357–366. doi:10.1038/ncb2936

Størvold, G. L., Fleten, K. G., Olsen, C. G., Follestad, T., Krokan, H. E., and Schønberg, S. A. (2009). Docosahexaenoic acid activates some SREBP-2 targets independent of cholesterol and ER stress in SW620 colon cancer cells. *Lipids* 44, 673–683. doi:10.1007/s11745-009-3324-4

Su, J., Chen, X., and Kanekura, T. (2009). A CD147-targeting siRNA inhibits the proliferation, invasiveness, and VEGF production of human malignant melanoma cells by down-regulating glycolysis,. *Cancer Lett.* 273, 140–147. doi:10.1016/j.canlet.2008.07.034

Sun, L. P., Seemann, J., Goldstein, J. L., and Brown, M. S. (2007). Sterol-regulated transport of SREBPs from endoplasmic reticulum to Golgi: Insig renders sorting signal in Scap inaccessible to COPII proteins. *Proc. Natl. Acad. Sci. U. S. A.* 104, 6519–6526. doi:10.1073/pnas.0700907104

Sun, Q., Yu, X., Peng, C., Liu, N., Chen, W., Xu, H., et al. (2020). Activation of SREBP-1c alters lipogenesis and promotes tumor growth and metastasis in gastric cancer. *Biomed. Pharmacother.* 128, 110274. doi:10.1016/j.biopha.2020.110274

Sundqvist, A., Bengoechea-Alonso, M. T., Ye, X., Lukiyanchuk, V., Jin, J., Harper, J. W., et al. (2005). Control of lipid metabolism by phosphorylation-dependent degradation of the SREBP family of transcription factors by SCF(Fbw7). *Cell Metab.* 1, 379–391. doi:10.1016/j.cmet.2005.04.010

Swinnen, J. V., Ulrix, W., Heyns, W., and Verhoeven, G. (1997). Coordinate regulation of lipogenic gene expression by androgens: Evidence for a cascade mechanism involving sterol regulatory element binding proteins. *Proc. Natl. Acad. Sci. U. S. A.* 94, 12975–12980. doi:10.1073/pnas.94.24.12975

Tall, A. R., Yvan-Charvet, L., Terasaka, N., Pagler, T., and Wang, N. (2008). HDL, ABC transporters, and cholesterol efflux: Implications for the treatment of atherosclerosis. *Cell Metab.* 7, 365–375. doi:10.1016/j.cmet.2008.03.001

Tang, J. J., Li, J. G., Qi, W., Qiu, W. W., Li, P. S., Li, B. L., et al. (2011). Inhibition of SREBP by a small molecule, betulin, improves hyperlipidemia and insulin resistance and reduces atherosclerotic plaques. *Cell Metab.* 13, 44–56. doi:10.1016/j.cmet.2010.12.004

Tao, M., Luo, J., Gu, T., Yu, X., Song, Z., Jun, Y., et al. (2021). LPCAT1 reprogramming cholesterol metabolism promotes the progression of esophageal squamous cell carcinoma. *Cell Death Dis.* 12, 845. doi:10.1038/s41419-021-04132-6

Tao, T., Su, Q., Xu, S., Deng, J., Zhou, S., Zhuang, Y., et al. (2019). Down-regulation of PKM2 decreases FASN expression in bladder cancer cells through AKT/mTOR/SREBP-1c axis. *J. Cell Physiol.* 234, 3088–3104. doi:10.1002/jcp.27129

Teixeira, G. R., Mendes, L. O., Veras, A. S. C., Thorpe, H. H. A., Fávaro, W. J., de Almeida Chuffa, L. G., et al. (2020). Physical resistance training-induced changes in lipids metabolism pathways and apoptosis in prostate. *Lipids Health Dis.* 19, 14. doi:10.1186/s12944-020-1195-0

Teresi, R. E., Shaiu, C. W., Chen, C. S., Chatterjee, V. K., Waite, K. A., and Eng, C. (2006). Increased PTEN expression due to transcriptional activation of PPARgamma by Lovastatin and Rosiglitazone. *Int. J. Cancer* 118, 2390–2398. doi:10.1002/ijc.21799

Tiong, T. Y., Weng, P. W., Wang, C. H., Setiawan, S. A., Yadav, V. K., Pikatan, N. W., et al. (2022). Targeting the SREBP-1/hsa-mir-497/SCAP/FASN oncometabolic Axis inhibits the cancer stem-like and chemoresistant phenotype of non-small cell lung carcinoma cells. *Int. J. Mol. Sci.* 23, 7283. doi:10.3390/ijms23137283

Tran, K. T., McMenamin Ú, C., Coleman, H. G., Cardwell, C. R., Murchie, P., Iversen, L., et al. (2020). Statin use and risk of liver cancer: Evidence from two population-based studies. *Int. J. Cancer* 146, 1250–1260. doi:10.1002/ijc.32426

Tripathi, V., Ellis, J. D., Shen, Z., Song, D. Y., Pan, Q., Watt, A. T., et al. (2010). The nuclear-retained noncoding RNA MALAT1 regulates alternative splicing by modulating SR splicing factor phosphorylation,. *Mol. Cell* 39, 925–938. doi:10.1016/j.molcel.2010.08.011

Vaidyanathan, S., Salmi, T. M., Sathiqu, R. M., McConville, M. J., Cox, A. G., and Brown, K. K. (2022). YAP regulates an SGK1/mTORC1/SREBP-dependent lipogenic program to support proliferation and tissue growth. *Dev. Cell* 57, 719–731.e8. doi:10.1016/j.devcel.2022.02.004

Vaupel, P., and Mayer, A. (2007). Hypoxia in cancer: Significance and impact on clinical outcome. *Cancer Metastasis Rev.* 26, 225–239. doi:10.1007/s10555-007-9055-1

Voigt, H., Vetter-Kauczok, C. S., Schrama, D., Hofmann, U. B., Becker, J. C., and Houben, R. (2009). CD147 impacts angiogenesis and metastasis formation. *Cancer Invest.* 27, 329–333. doi:10.1080/07357900802392675

Volinia, S., Calin, G. A., Liu, C. G., Ambs, S., Cimmino, A., Petrocca, F., et al. (2006). A microRNA expression signature of human solid tumors defines cancer gene targets,. *Proc. Natl. Acad. Sci. U. S. A.* 103, 2257–2261. doi:10.1073/pnas.0510565103

Walker, A. K., Jacobs, R. L., Watts, J. L., Rottiers, V., Jiang, K., Finnegan, D. M., et al. (2011). A conserved SREBP-1/phosphatidylcholine feedback circuit regulates lipogenesis in metazoans,. *Cell* 147, 840–852. doi:10.1016/j.cell.2011.09.045

Walther, T. C., and Farese, R. V., Jr (2009). The life of lipid droplets,. *Biochim. Biophys. Acta* 1791, 459–466. doi:10.1016/j.bbalip.2008.10.009

Wang, H., Zhang, Y., Guan, X., Li, X., Zhao, Z., Gao, Y., et al. (2021). An integrated transcriptomics and proteomics analysis implicates lncRNA MALAT1 in the regulation of lipid metabolism. *Mol. Cell Proteomics* 20, 100141. doi:10.1016/j.mcpro.2021.100141

Wang, P., Zhuang, L., Zhang, J., Fan, J., Luo, J., Chen, H., et al. (2013). The serum miR-21 level serves as a predictor for the chemosensitivity of advanced pancreatic cancer, and miR-21 expression confers chemoresistance by targeting FasL,. *Mol. Oncol.* 7, 334–345. doi:10.1016/j.molonc.2012.10.011

Wang, T. B., Geng, M., Jin, H., Tang, A. G., Sun, H., Zhou, L. Z., et al. (2021). SREBP1 site 1 protease inhibitor PF-429242 suppresses renal cell carcinoma cell growth. *Cell Death Dis.* 12, 717. doi:10.1038/s41419-021-03999-9

Wang, T., Seah, S., Loh, X., Chan, C. W., Hartman, M., Goh, B. C., et al. (2016). Simvastatin-induced breast cancer cell death and deactivation of PI3K/Akt and MAPK/ERK signalling are reversed by metabolic products of the mevalonate pathway. *Oncotarget* 7, 2532–2544. doi:10.18632/oncotarget.6304

Wang, Y., Guo, D., He, J., Song, L., Chen, H., Zhang, Z., et al. (2019). Inhibition of fatty acid synthesis arrests colorectal neoplasm growth and metastasis: Anti-cancer therapeutical effects of natural cyclopeptide RA-XII. *Biochem. Biophys. Res. Commun.* 512, 819–824. doi:10.1016/j.bbrc.2019.03.088

Wang, Y., Wang, H., Zhao, Q., Xia, Y., Hu, X., and Guo, J. (2015). PD-L1 induces epithelial-to-mesenchymal transition via activating SREBP-1c in renal cell carcinoma. *Med. Oncol.* 32, 212. doi:10.1007/s12032-015-0655-2

Wen, S., Niu, Y., Lee, S. O., Yeh, S., Shang, Z., Gao, H., et al. (2016). Targeting fatty acid synthase with ASC-J9 suppresses proliferation and invasion of prostate cancer cells. *Mol. Carcinog.* 55, 2278–2290. doi:10.1002/mc.22468

Williams, K. J., Argus, J. P., Zhu, Y., Wilks, M. Q., Marbois, B. N., York, A. G., et al. (2013). An essential requirement for the SCAP/SREBP signaling axis to protect cancer cells from lipotoxicity. *Cancer Res.* 73, 2850–2862. doi:10.1158/0008-5472.CAN-13-0382-T

Xiang, Y., Tang, J. J., Tao, W., Cao, X., Song, B. L., and Zhong, J. (2015). Identification of cholesterol 25-hydroxylase as a novel host restriction factor and a part of the primary innate immune responses against hepatitis C virus infection. *J. Virol.* 89, 6805–6816. doi:10.1128/JVI.00587-15

Xiao, J., Xiong, Y., Yang, L. T., Wang, J. Q., Zhou, Z. M., Dong, L. W., et al. (2021). POST1/C12ORF49 regulates the SREBP pathway by promoting site-1 protease maturation. *Protein Cell* 12, 279–296. doi:10.1007/s13238-020-00753-3

Xie, X., Zhang, Y., Jiang, Y., Liu, W., Ma, H., Wang, Z., et al. (2008). Suppressive function of RKTG on chemical carcinogen-induced skin carcinogenesis in mouse. *Carcinogenesis* 29, 1632–1638. doi:10.1093/carcin/bgn139

Xu, B., Muramatsu, T., and Inazawa, J. (2021). Suppression of MET signaling mediated by pitavastatin and capmatinib inhibits oral and esophageal cancer cell growth. *Mol. Cancer Res.* 19, 585–597. doi:10.1158/1541-7786.MCR-20-0688

Xu, C., Zhang, L., Wang, D., Jiang, S., Cao, D., Zhao, Z., et al. (2021). Lipidomics reveals that sustained SREBP-1-dependent lipogenesis is a key mediator of gefitinib-acquired resistance in EGFR-mutant lung cancer. *Cell Death Discov.* 7, 353. doi:10.1038/s41420-021-00744-1

Xu, D., Wang, Z., Xia, Y., Shao, F., Xia, W., Wei, Y., et al. (2020). The gluconeogenic enzyme PCK1 phosphorylates INSIG1/2 for lipogenesis,. *Nature* 580, 530–535. doi:10.1038/s41586-020-2183-2

Xu, D., Wang, Z., Zhang, Y., Jiang, W., Pan, Y., Song, B. L., et al. (2015). PAQR3 modulates cholesterol homeostasis by anchoring Scap/SREBP complex to the Golgi apparatus. *Nat. Commun.* 6, 8100. doi:10.1038/ncomms9100

Xu, G. L., Ni, C. F., Liang, H. S., Xu, Y. H., Wang, W. S., Shen, J., et al. (2020). Upregulation of PD-L1 expression promotes epithelial-to-mesenchymal transition in

sorafenib-resistant hepatocellular carcinoma cells. *Gastroenterol. Rep. (Oxf)* 8, 390–398. doi:10.1093/gastro/goaa049

Xu, H., Sun, J., Shi, C., Sun, C., Yu, L., Wen, Y., et al. (2015). miR-29s inhibit the malignant behavior of U87MG glioblastoma cell line by targeting DNMT3A and 3B. *Neurosci. Lett.* 590, 40–46. doi:10.1016/j.neulet.2015.01.060

Xu, P., Wu, M., Chen, H., Xu, J., Wu, M., Li, M., et al. (2016). Bioinformatics analysis of hepatitis C virus genotype 2a-induced human hepatocellular carcinoma in Huh7 cells. *Onco Targets Ther.* 9, 191–202. doi:10.2147/OTT.S91748

Xue, L., Qi, H., Zhang, H., Ding, L., Huang, Q., Zhao, D., et al. (2020). Targeting SREBP-2-regulated mevalonate metabolism for cancer therapy. *Front. Oncol.* 10, 1510. doi:10.3389/fonc.2020.01510

Yabe, D., Brown, M. S., and Goldstein, J. L. (2002). Insig-2, a second endoplasmic reticulum protein that binds SCAP and blocks export of sterol regulatory element-binding proteins. *Proc. Natl. Acad. Sci. U. S. A.* 99, 12753–12758. doi:10.1073/pnas.162488899

Yahagi, N., Shimano, H., Hasegawa, K., Ohashi, K., Matsuzaka, T., Najima, Y., et al. (2005). Co-ordinate activation of lipogenic enzymes in hepatocellular carcinoma. *Eur. J. Cancer* 41, 1316–1322. doi:10.1016/j.ejca.2004.12.037

Yamauchi, Y., Furukawa, K., Hamamura, K., and Furukawa, K. (2011). Positive feedback loop between PI3K-Akt-mTORC1 signaling and the lipogenic pathway boosts Akt signaling: Induction of the lipogenic pathway by a melanoma antigen. *Cancer Res.* 71, 4989–4997. doi:10.1158/0008-5472.CAN-10-4108

Yan, H., Parsons, D. W., Jin, G., McLendon, R., Rasheed, B. A., Yuan, W., et al. (2009). IDH1 and IDH2 mutations in gliomas. *N. Engl. J. Med.* 360, 765–773. doi:10.1056/NEJMoa0808710

Yang, M., Chen, X., Zhang, J., Xiong, E., Wang, Q., Fang, W., et al. (2021). ME2 promotes proneural-mesenchymal transition and lipogenesis in glioblastoma. *Front. Oncol.* 11, 715593. doi:10.3389/fonc.2021.715593

Yang, P. M., Hong, Y. H., Hsu, K. C., and Liu, T. P. (2019). p38α/S1P/SREBP2 activation by the SAM-competitive EZH2 inhibitor GSK343 limits its anticancer activity but creates a druggable vulnerability in hepatocellular carcinoma. *Am. J. Cancer Res.* 9, 2120–2139.

Yang, T., Espenshade, P. J., Wright, M. E., Yabe, D., Gong, Y., Aebersold, R., et al. (2002). Crucial step in cholesterol homeostasis: Sterols promote binding of SCAP to INSIG-1, a membrane protein that facilitates retention of SREBPs in ER. *Cell* 110, 489–500. doi:10.1016/s0092-8674(02)00872-3

Yang, X., Wu, F., Chen, J., Wang, C., Zhu, Y., Li, F., et al. (2017). GP73 regulates Hepatic Steatosis by enhancing SCAP-SREBPs interaction. *Sci. Rep.* 7, 14932. doi:10.1038/s41598-017-06500-9

Yao, L., Chen, S., and Li, W. (2020). Fatostatin inhibits the development of endometrial carcinoma in endometrial carcinoma cells and a xenograft model by targeting lipid metabolism. *Arch. Biochem. Biophys.* 684, 108327. doi:10.1016/j.abb.2020.108327

Yecies, J. L., Zhang, H. H., Menon, S., Liu, S., Yecies, D., Lipovsky, A. I., et al. (2011). Akt stimulates hepatic SREBP1c and lipogenesis through parallel mTORC1-dependent and independent pathways. *Cell Metab.* 14, 21–32. doi:10.1016/j.cmet.2011.06.002

Yeung, F., Hoberg, J. E., Ramsey, C. S., Keller, M. D., Jones, D. R., Frye, R. A., et al. (2004). Modulation of NF-kappaB-dependent transcription and cell survival by the SIRT1 deacetylase. *Embo J.* 23, 2369–2380. doi:10.1038/sj.emboj.7600244

Yi, J., Zhu, J., Wu, J., Thompson, C. B., and Jiang, X. (2020). Oncogenic activation of PI3K-AKT-mTOR signaling suppresses ferroptosis via SREBP-mediated lipogenesis. *Proc. Natl. Acad. Sci. U. S. A.* 117, 31189–31197. doi:10.1073/pnas.2017152117

Yin, F., Feng, F., Wang, L., Wang, X., Li, Z., and Cao, Y. (2019). SREBP-1 inhibitor Betulin enhances the antitumor effect of Sorafenib on hepatocellular carcinoma via restricting cellular glycolytic activity. *Cell Death Dis.* 10, 672. doi:10.1038/s41419-019-1884-7

You, M., Fischer, M., Deeg, M. A., and Crabb, D. W. (2002). Ethanol induces fatty acid synthesis pathways by activation of sterol regulatory element-binding protein (SREBP). *J. Biol. Chem.* 277, 29342–29347. doi:10.1074/jbc.M202411200

Yue, S., Li, J., Lee, S. Y., Lee, H. J., Shao, T., Song, B., et al. (2014). Cholesteryl ester accumulation induced by PTEN loss and PI3K/AKT activation underlies human prostate cancer aggressiveness. *Cell Metab.* 19, 393–406. doi:10.1016/j.cmet.2014.01.019

Zhai, X., Cheng, F., Ji, L., Zhu, X., Cao, Q., Zhang, Y., et al. (2017). Leptin reduces microRNA-122 level in hepatic stellate cells *in vitro* and *in vivo*. *Mol. Immunol.* 92, 68–75. doi:10.1016/j.molimm.2017.10.006

Zhang, C., Zhang, Y., Ding, W., Lin, Y., Huang, Z., and Luo, Q. (2015). MiR-33a suppresses breast cancer cell proliferation and metastasis by targeting ADAM9 and ROS1. *Protein Cell* 6, 881–889. doi:10.1007/s13238-015-0223-8

Zhang, H., Feng, Z., Huang, R., Xia, Z., Xiang, G., and Zhang, J. (2014). MicroRNA-449 suppresses proliferation of hepatoma cell lines through blockade lipid metabolic pathway related to SIRT1. *Int. J. Oncol.* 45, 2143–2152. doi:10.3892/ijo.2014.2596

Zhang, T., Bai, R., Wang, Q., Wang, K., Li, X., Liu, K., et al. (2019). Fluvastatin inhibits HMG-CoA reductase and prevents non-small cell lung carcinogenesis. *Cancer Prev. Res. (Phila)* 12, 837–848. doi:10.1158/1940-6207.CAPR-19-0211

Zhang, Y., Jiang, X., Qin, X., Ye, D., Yi, Z., Liu, M., et al. (2010). RKTG inhibits angiogenesis by suppressing MAPK-mediated autocrine VEGF signaling and is downregulated in clear-cell renal cell carcinoma. *Oncogene* 29, 5404–5415. doi:10.1038/onc.2010.270

Zhang, Y., Mohibi, S., Vasilatis, D. M., Chen, M., Zhang, J., and Chen, X. (2022). Ferredoxin reductase and p53 are necessary for lipid homeostasis and tumor suppression through the ABCA1-SREBP pathway. *Oncogene* 41, 1718–1726. doi:10.1038/s41388-021-02100-0

Zhang, Y., Qian, Y., Zhang, J., Yan, W., Jung, Y. S., Chen, M., et al. (2017). Ferredoxin reductase is critical for p53-dependent tumor suppression via iron regulatory protein 2. *Genes Dev.* 31, 1243–1256. doi:10.1101/gad.299388.117

Zhao, L., Peng, Y., He, S., Li, R., Wang, Z., Huang, J., et al. (2021). Apatinib induced ferroptosis by lipid peroxidation in gastric cancer. *Gastric Cancer* 24, 642–654. doi:10.1007/s10120-021-01159-8

Zhao, X., Zhao, L., Yang, H., Li, J., Min, X., Yang, F., et al. (2018). Pyruvate kinase M2 interacts with nuclear sterol regulatory element-binding protein 1a and thereby activates lipogenesis and cell proliferation in hepatocellular carcinoma. *J. Biol. Chem.* 293, 6623–6634. doi:10.1074/jbc.RA117.000100

Zhao, Y., Li, H., Zhang, Y., Li, L., Fang, R., Li, Y., et al. (2016). Oncoprotein HBXIP modulates abnormal lipid metabolism and growth of breast cancer cells by activating the LXRs/SREBP-1c/FAS signaling cascade. *Cancer Res.* 76, 4696–4707. doi:10.1158/0008-5472.CAN-15-1734

Zhao, Z., Zhong, L., He, K., Qiu, C., Li, Z., Zhao, L., et al. (2019). Cholesterol attenuated the progression of DEN-induced hepatocellular carcinoma via inhibiting SCAP mediated fatty acid de novo synthesis. *Biochem. Biophys. Res. Commun.* 509, 855–861. doi:10.1016/j.bbrc.2018.12.181

Zheng, Z. G., Zhang, X., Liu, X. X., Jin, X. X., Dai, L., Cheng, H. M., et al. (2019). Inhibition of HSP90β improves lipid disorders by promoting mature SREBPs degradation via the ubiquitin-proteasome system. *Theranostics* 9, 5769–5783. doi:10.7150/thno.36505

Zhu, D. Q., Lou, Y. F., He, Z. G., and Ji, M. (2014). Nucleotidyl transferase TUT1 inhibits lipogenesis in osteosarcoma cells through regulation of microRNA-24 and microRNA-29a. *Tumour Biol.* 35, 11829–11835. doi:10.1007/s13277-014-2395-x

Zhu, J., Cui, G., Chen, M., Xu, Q., Wang, X., Zhou, D., et al. (2013). Expression of R132H mutational IDH1 in human U87 glioblastoma cells affects the SREBP1a pathway and induces cellular proliferation. *J. Mol. Neurosci.* 50, 165–171. doi:10.1007/s12031-012-9890-6

Zhu, Z., Zhao, X., Zhao, L., Yang, H., Liu, L., Li, J., et al. (2016). p54(nrb)/NONO regulates lipid metabolism and breast cancer growth through SREBP-1A. *Oncogene* 35, 1399–1410. doi:10.1038/onc.2015.197

frontiers | Frontiers in Pharmacology

TYPE Original Research
PUBLISHED 05 May 2023
DOI 10.3389/fphar.2023.1093650

OPEN ACCESS

EDITED BY
Hai-long Piao,
Chinese Academy of Sciences (CAS), China

REVIEWED BY
Zhuo-Xun Wu,
St. John's University, United States
Qiuxu Teng,
St. John's University, United States

*CORRESPONDENCE
Qizhi Cao,
qizhicao@bzmc.edu.cn
Hua Li,
yilulihua626@sina.com

†These authors have contributed equally to this work

RECEIVED 09 November 2022
ACCEPTED 24 April 2023
PUBLISHED 05 May 2023

CITATION
Zhang H, Shangguan F, Zhang L, Ma N, Song S, Ma L, Liu C, Liu M, An J, Li H and Cao Q (2023), A novel mechanism of 6-methoxydihydroavicine in suppressing ovarian carcinoma by disrupting mitochondrial homeostasis and triggering ROS/ MAPK mediated apoptosis.
Front. Pharmacol. 14:1093650.
doi: 10.3389/fphar.2023.1093650

A novel mechanism of 6-methoxydihydroavicine in suppressing ovarian carcinoma by disrupting mitochondrial homeostasis and triggering ROS/ MAPK mediated apoptosis

Huachang Zhang[1†], Fugen Shangguan[2†], Lan Zhang[3†], Nengfang Ma[4], Shuling Song[5], Li Ma[1], Chuntong Liu[1], Mengke Liu[1], Jing An[6], Hua Li[3*] and Qizhi Cao[1*]

[1]Department of Immunology, School of Basic Medical Sciences, Binzhou Medical University, Yantai, Shandong, China, [2]Key Laboratory of Diagnosis and Treatment of Severe Hepato-Pancreatic Diseases of Zhejiang Province, The First Affiliated Hospital of Wenzhou Medical University, Wenzhou, China, [3]The Affiliated Taian City Central Hospital of Qingdao University, Taian, Shandong, China, [4]School of Life and Environmental Sciences, Wenzhou University, Wenzhou, China, [5]School of Gerontology, Binzhou Medical University, Yantai, Shandong, China, [6]Division of Infectious Diseases and Global Health, School of Medicine, University of California San Diego (UCSD), La Jolla, CA, United States

Introduction: Alkaloids derived from *M. cordata* (Papaveraceae family), have been found to display antineoplastic activity in several types of cancer. However, the antitumor effects and mechanisms of a new alkaloid extracted from the fruits of *M. cordata*, named 6-Methoxydihydroavicine (6-ME), remains unclear in the case of ovarian cancer (OC).

Methods: CCK-8 assay was employed to analyze the cell viabilities of OC cells. RTCA, and colony-formation assays were performed to measure OC cell growth. Alterations in apoptosis and ROS levels were detected by flow cytometry in accordance with the instructions of corresponding assay kits. A Seahorse XFe96 was executed conducted to confirm the effects of 6-ME on cellular bioenergetics. Western blot and q-RT-PCR were conducted to detect alterations in target proteins. The subcutaneous xenografted tumor model of OC was used to further validate the anti-tumor activity of 6-ME *in vivo*.

Results: Here, we reported for the first time that 6-ME inhibits OC cells growth *in vitro* and *in vivo*. Meanwhile, we found that 6-ME showed great antineoplastic activities by disrupting mitochondria homeostasis and promoting apoptosis in OC cells. Further investigation of the upstream signaling of apoptosis revealed that 6-ME-triggered apoptosis was induced by reactive oxygen species (ROS)-mediated mitogen-activated protein kinase (MAPK) activation and mitochondria dysfunction in OC cells. Furthermore, we found oxaloacetic acid (OAA), a crucial metabolite has been proved to be related to NADPH production, can block the cytotoxicity and accumulation of ROS caused by 6-ME in OC cells.

Discussion: In summary, our data show that 6-ME exhibits cytotoxicity to OC cells in a ROS-dependent manner by interrupting mitochondrial respiration homeostasis and inducing MAPK-mediated apoptosis. This evidence suggests that 6-ME is a promising remedy for OC intervention.

KEYWORDS

6-methoxydihydroavicine (6-ME), ovarian cancer (OC), mitochondria homeostasis, reactive oxygen species (ROS), MAPK, oxaloacetic acid (OAA) metabolism

1 Introduction

Ovarian cancer (OC), a common gynecological tumor with a high mortality rate, is the eighth leading cause of morbidity and mortality among women worldwide, with 313,959 cases and 207,252 deaths in 2020 (Sung et al., 2021). Nearly 90% of OC cases are epithelial ovarian cancer (EOC) histotypes, main including high-grade serous, low-grade serous, endometrioid, clear cell, and mucinous subtypes (Torre et al., 2018; Millstein et al., 2020). High-grade serous ovarian cancer (HGSOC) accounts for more than 65% of EOC cases and contributes to the high mortality rate of EOC (Torre et al., 2018). Due to the difficulties of early diagnosis of EOC, about 70% of patients are already advanced at the time of diagnosis, with a 5-year survival rate of less than 50% (Torre et al., 2018; Herrera et al., 2019; Schoutrop et al., 2022). Currently, chemotherapy is still the main strategy for OC treatment, but the side effects and resistance of chemotherapy drugs remain urgent issues to be solved (Lisio et al., 2019; Marchetti et al., 2021). Therefore, the exploitation of novel and safety antitumor remedies of natural origin is of great importance. Fortunately, a range of natural compounds, likes alkaloids, terpenes, and polyphenols, have been shown to have therapeutic potential for cancer (Atanasov et al., 2021). *Macleaya cordata (Willd.) R. Br.* (*M. cordata*), a traditional medicine belongs to the *Papaveraceae* family that has long been used in Asia, especially in China to treat myodynia, wound inflammation, and bee stings (Ali et al., 2021). Previous studies have indicated that *M. cordata* contains a variety of alkaloids, which are the basis for demonstrating its medical benefits (Guo et al., 2014). The explorations of the potential pharmacological functions of these alkaloids seem to be valuable, particularly in the context of tumor treatment. To date, several *M. cordata* alkaloids have been found to exhibit antitumor activity in different types of cancer. For example, the *M. cordata* alkaloids sanguinarine, chelerythrine, and berberine have shown promising antineoplastic properties in pancreatic cancer (Almeida et al., 2017; Zhu et al., 2019; Ali et al., 2021). Chelerythrine triggered apoptosis in gastric cancer by reducing the expression of Bcl-xL and Bcl-2 proteins (Zhengfu et al., 2012). Macleayins A exerted its anti-cervical cancer activity by inhibiting Wnt/β-Catenin-dependent proliferation and inducing apoptosis (Sai et al., 2021). Ethoxysanguinarinenon regulated the AMPK/mTOR pathway as an antitumor property (Si et al., 2019). Given this evidence, further investigation of safe and effective natural compounds from these alkaloids for cancer intervention is practical and worth pursuing.

Many chemotherapeutic drugs exhibit antitumor properties by initialing programmed cell death (PCD), which includes necroptosis (Su et al., 2016; Jing et al., 2018), pyroptosis (Wang et al., 2017; Wu et al., 2021), ferroptosis (Liang et al., 2019; Lei et al., 2022), and apoptosis (Tang et al., 2019; Shahar and Larisch, 2020). As the most well-understood and extensively researched type of PCD, apoptosis occurs with membrane blebbing, nuclear fragmentation, and cell shrinkage (Koren and Fuchs, 2021). Reactive oxygen species (ROS), which are always initialed by oxidative stimuli and some antitumor drugs, have been shown to be closely associated with apoptosis (Jacquemin et al., 2015; Holze et al., 2018; Li et al., 2020; Jiang et al., 2022). Noticeably, MAPK signaling, main including JNK/MAPK, ERK/MAPK, and p38/MAPK proteins, has been found to act as a bridge for ROS-induced apoptosis. Mao et al. showed that shikonin triggers ROS/JNK-dependent apoptosis in leukemia cells (Mao et al., 2008). Curcumin derivatives have consistently been found to active apoptosis in breast cancer via the ROS/YAP/JNK axis (Wang et al., 2019). Moreover, Lan et al. observed that deferoxamine induces esophageal cancer cell apoptosis through ROS/ERK-reliant mitochondrial dysfunction (Lan et al., 2018). Furthermore, the ERK/p38-MAPK axis has been linked to ROS-initialed apoptosis caused by liposomal honokiol in medulloblastoma cells (Li C et al., 2022). Conversely, the activation of ERK/MAPK may have anti-apoptosis effects in some circumstances (Dang et al., 2017; Lu et al., 2021; Xing et al., 2021). Recent studies have indicated that δ-Tocotrienol increases the sensitivity of OC cells to cisplatin by facilitating the ROS/JNK and ROS/p38 pathways (Fontana et al., 2021). Similarly, Zhu et al. found that escin exhibited promising anti-osteosarcoma property by activating ROS/p38-dependent apoptosis (Zhu et al., 2017). All these discoveries suggest the important and unique role of the MAPK axis in ROS-induce apoptosis.

In this study, we report a novel alkaloid, 6-ME, with excellent anti-OC activity, which has never been published before. We focus on elucidating the underlying mechanisms by which 6-ME exhibits its antitumor properties in OC cells.

2 Materials and methods

2.1 Cell lines and cell culture

The CAOV3 and SKOV3 were brought from the Cell Bank of the Chinese Academy of Sciences (Shanghai, China). CAOV3 and SKOV3 cell lines were cultured in DMEM medium and McCoy's 5A respectively, supplementing with 10% fetal bovine serum and penicillin-streptomycin. All cells were incubated in a humidified incubator with 5% CO_2 at 37°C.

2.2 Reagents and antibodies

Reagents are listed in Supplementary Table S1 while antibodies are shown in Supplementary Table S2.

2.3 Cell viability assessment

The inhibitory concentration (IC_{50}) of 6-ME was estimated by conducting CCK-8 assay in CAOV3 and SKOV3 cells according to the manufacturer's instructions. The cells were counted and seeded at 10,000 cells per well in 96-well cell culture plates and cultured overnight. They were then t treated with concentration gradients of 6-ME or DMSO for 24 h, followed by an additionally 3 h incubation with CCK-8 solution at 37°C. Afterward, the observance at OD_{450nm} was measured using Varioskan Flash (Thermo Scientific).

2.4 Measurement of cell proliferation by real time cellular analysis (RTCA)

RTCA assays were conducted to measure the anti-proliferation activity of 6-ME in OC cells following the manufacturer's protocol. The SKOV3 cells were counted and seeded at the density of 10,000 cells per well and cultured with the indicated concentrations of 6-ME at 37°C for several days. The data were then exported and graphed.

2.5 Colony formation assay

CAOV3 and SKOV3 cells were inoculated in 6-well cell culture plates at the density of 1,000/well and cultured under the presence or absence of different concentrations of 6-ME for 2 weeks. After washing three times with PBS, fixing for 30 min with 4% paraformaldehyde, and staining for 30 min with crystal violet, clonal colonies >40–50 cells/each were counted.

2.6 Western blot analysis

CAOV3 and SKOV3 cells were incubated with 6-ME alone or in combination with NAC or OAA for 24 h. These cells were then collected, incubated with appropriate cell lysis buffer on ice for 20 min, and centrifuged at 12, 000 rpm for 20 min at 4°C. After transferring the supernatants to a new 1.5 ml EP tube on ice, the protein concentration was determined using Pierce™ BCA Protein Assay kit (Thermo Fisher Scientific, 23,225) following the manufacturer's protocol. Subsequently, the protein concentration was adjusted to 1 μg/μL/sample with 5X DualColor Protein Loading Buffer (Fude Biological Technology, FD006) and heated at 95°C for 5 min in a Digital Dry Baths/Block Heaters (Thermo Fisher Scientific, 88870005). For western blot analysis, protein samples (20 μg/each) were loaded onto the SDS-PAGE gel, electrophoresed, and transferred onto 0.22 μM PVDF membranes. Afterblocking with 5% NON-Fat Powdered Milk (Solarbio Life Science, D8340) for 90 min, the membranes were incubated with the desired primary antibodies overnight at 4°C, washed with 1X TBS-T for 5 min at least three time, and incubated with corresponding secondary antibodies at room temperature for 90 min. Finally, these membranes were washed with 1X TBS-T for 10 min at least three times, visualized with the SuperSignal™ West Pico PLUS kit (Thermo Fisher Scientific, 34,580), and quantified using ImageJ software.

2.7 Cell apoptosis analysis

CAOV3 and SKOV3 cells were incubated with different concentrations of 6-ME for 12 h, then harvested, and stained with Annexin V-FITC/PI at room temperature for 20 min in darkness, and detected by flow cytometry.

2.8 Photograph of cell morphology

After culturing CAOV3 and SKOV3 cells with 6-ME for 24 h, cell morphologies were viewed under a LEICA DMI1 microscope and photographed using a LAS V4.12 digital camera (LEICA Corporation) with a ×10 eyepieces and ×20 objective.

2.9 Oxygen consumption rate (OCR) measurement

The XFe96 extracellular flux analyzer was employed to measure the alterations of OCR when OC cells were exposed to 6-ME alone or in combination with NAC or OAA. The OC cells (20,000 cells per well) were seed in specialized cell plates and cultured overnight at 37°C. Afterward, the cells were exposed to 6-ME alone or 6-ME combined with NAC or OAA for 4 h; they were then incubated for another 1 h with a base medium containing Glucose and Pyruvic acid sodium. Finally, three working solutions, including Oligomycin, FCCP, and Rotenone/Antimycin A, were added to the corresponding wells, and changes in OCR were detected using the XFe96 Extracellular Flux analyzer under specific procedures.

2.10 Extracellular acidification rate (ECAR) measurement

The XFe96 extracellular flux analyzer was employed to measure the alterations of ECAR when OC cells were exposed to 6-ME. The OC cells (20,000 cells per well) were seed in specialized cell plates and cultured overnight at 37°C. Afterward, the cells were exposed to 6-ME for 4 h; they were then incubated for another 1 h with a base medium containing Glutamine. Finally, three working solutions, including Glucose, Oligomycin, and 2-DG were added to the corresponding wells, and changes in ECAR were detected using the XFe96 Extracellular Flux analyzer under specific procedures.

2.11 FACS analysis for ROS

To examine the alteration of reactive oxygen species (ROS) in 6-ME -treated OC cells for 12 h, we stained the cells with dichloro-dihydro-fluorescein diacetate (DCFH-DA) and analyzed them using flow cytometry in accordance with manufacturer's protocol.

2.12 Measurement of MMP

To detect changes in mitochondrial membrane potential (MMP) in OC cells after 12 h treatment with 6-ME, we dyed the cells with JC-1 and analyzed them by flow cytometry according to the manufacturer's protocol.

10.3389/fphar.2023.1093650

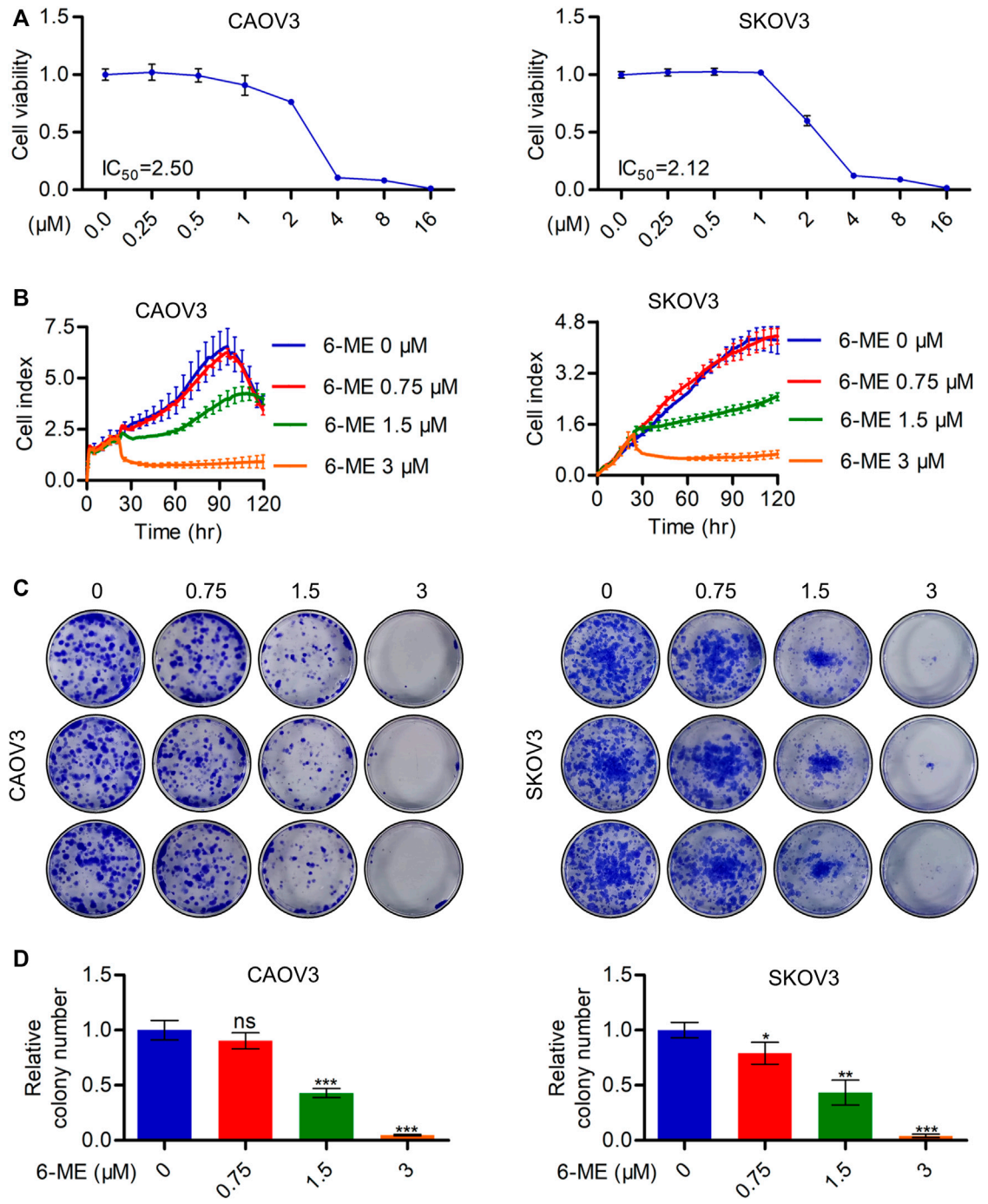

FIGURE 1
6-ME depresses *in vitro* OC cell growth. **(A)**. CCK-8 assays were used to analyze the inhibitory activities of 6-ME in OC cells. **(B)**. RTCA assays were performed to detect the ability of proliferation in OC cells. **(C)**. The clonogenic activities were confirmed by performing colony formation assays. **(D)**. The numbers of clonal colonies were counted and then analyzed, data was showed as mean ± SD.

2.13 Nude mouse tumor-bearing experiments

All animal studies were carried out in accordance with the protocol approved by the Animal Protection and Utilization Committee of Binzhou Medical University. Female BALB/c-nude mice were raised in an environment free of specific pathogens (SPF). In 5-week-old nude mice (n = 8), CAOV3 cells (5×10^6) were injected subcutaneously ventrally. The mice were separated into two groups of four

10.3389/fphar.2023.1093650

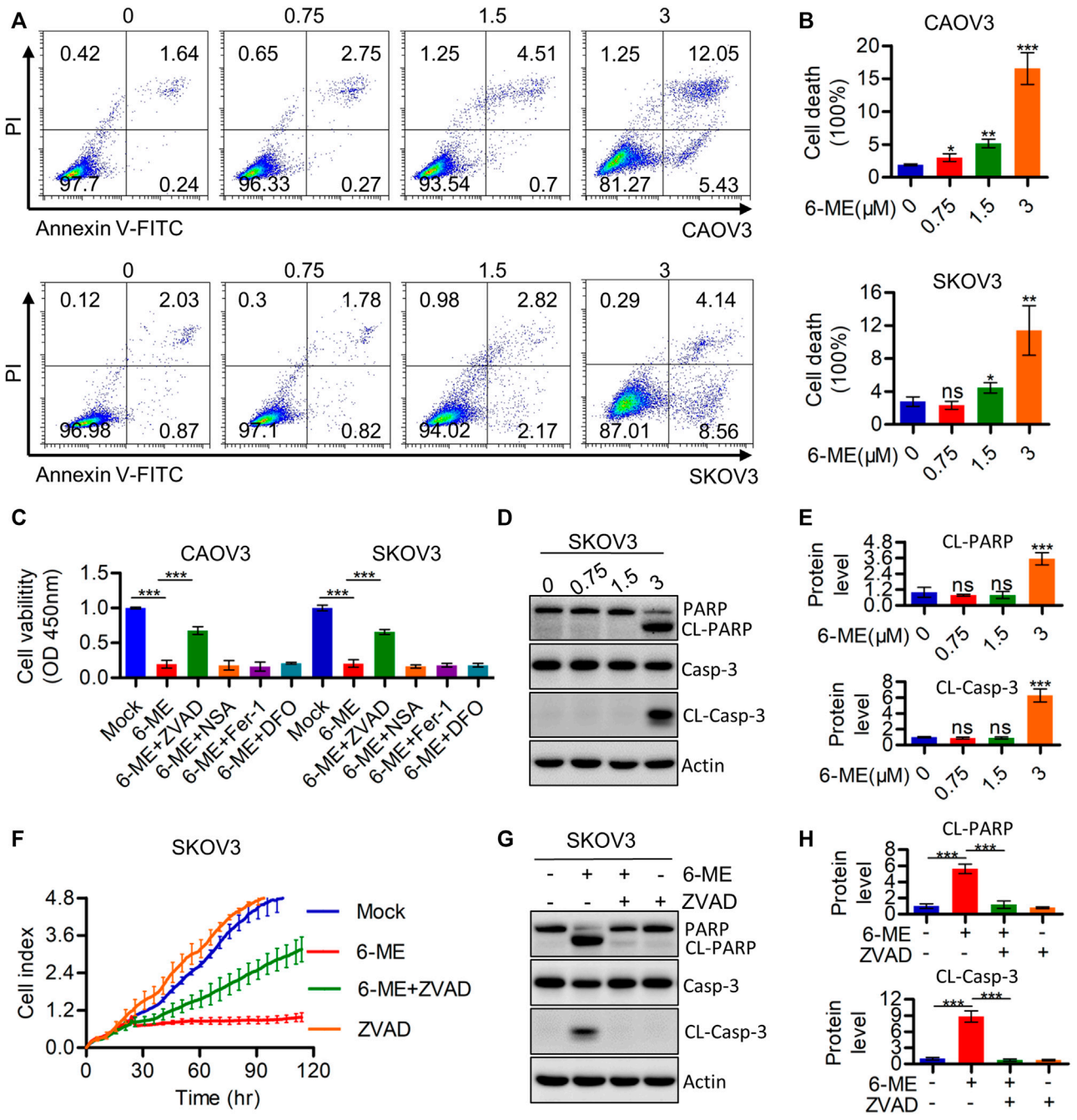

FIGURE 2
6-ME induces Caspase-mediated apoptosis in OC cells. **(A)**. The cell death was analyzed by flow cytometry in Annexin V-FITC/PI dyeing OC cells. **(B)**. The cell death rates were statistically analyzed and showed as mean ± SD. **(C)**. Cell viabities were measured after 6-ME treated alone or in combination with PCD inhibitors, data was showed as mean ± SD. **(D)**. Western blot were used to detect the activation of PARP and caspase-3, Actin was acted as a loading control. **(E)**. The cleavage of PARP and caspase-3 were quantified and statistically analyzed, data was showed as mean ± SD. **(F)**. RTCA assays were performed to detect the ability of proliferation in 6-ME exposed OC cells in the presence of ZVAD. **(G)**. Western blot were used to detect the activation of PARP and caspase-3 in 6-ME exposed OC cells in the presence of ZVAD, Actin was acted as a loading control. **(H)**. The cleavage of PARP and caspase-3 were quantified and statistically analyzed, data was showed as mean ± SD.

mice each when the tumor volume reached ~100 mm^3. 5% DMSO, 40% PEG300, 5% Tween80, 50% H_2O was used as the solvent of 6-ME. Mice in one group received an intraperitoneal injection of 6-ME (5 mg/kg), whereas mice in the control group received an injection of solvent. The tumor volume (mm^3) was calculated using the formula volume = length × (width) ^{2}/2 after the tumor size was determined using a vernier caliper. Every 2 days, weigh it. After 14 days, the mice were sacrificed and the tumors were photographed, dissected, and weighed.

2.14 Statistical analysis

All the statistical analyses were performed using SPSS16.0 statistical analysis software and GraphPad Prism 5. The data are shown as the mean ± SD of three independent replicate experiments. T-test was used to analyze the statistical difference between two independent groups and one-way ANOVA with the Tukey *post-hoc* test was used to analyze differences more than two groups for a single variable. p-value <0.05 was considered statistically significant.

3 Results

3.1 6-ME inhibits *in vitro* OC cell growth

The inhibitory activities of 6-ME on CAOV3 and SKOV3 cell survivals were initially detected using CCK-8 assays (Figure 1A). Subsequent RTCA assays revealed a significant decrease in the proliferation of OC cells after 6-ME exposure (Figure 1B). Reduction in the clonogenic activities in 6-ME-treated OC cells were further confirmed by performing colony formation assays (Figures 1C, D). These data indicate that 6-ME effectively represses the *in vitro* growth of OC cells.

3.2 6-ME triggers caspase-dependent apoptosis in OC cells

The cytotoxicity caused by 6-ME in OC cells was further investigated using flow cytometry. Annexin V-FITC/PI data showed that 6-ME significantly induced OC cell death when compared to DMSO vehicle control (Figures 2A, B). Subsequent measurements of cell viability after treatment with 6-ME alone or in combination with corresponding PCD inhibitors showed that the presence of the apoptosis inhibitor ZVAD, but not of other cell-death inhibitors, including necroptosis inhibitor NSA and ferroptosis inhibitors DFO or Fer-1, eliminated the cytotoxicity caused by 6–ME (Figure 2C). However, in 6-ME-exposed OC cells, we did not observe the appearance of balloon-like bubbles and cleavage of gasdermin family proteins (GSDMB, GSDMC, GSDMD, and GSDME), which are typical cell morphology of pyroptosis (Supplementary Figures S1A, B). Echoing the results of counteracting 6-ME-induced inhibition of cell proliferation (Figure 2F; Supplementary Figure S1C), treatment of OC cells with 6-ME in the presence or absence of Z-VAD halted the increase in 6-ME-mediated cleavages of PARP and caspase-3 (Figures 2D, E, G, H). These results show that 6-ME exerts its anti-OC properties by initializing caspase-dependent apoptosis.

3.3 6-ME impairs mitochondrial respiration and induces oxidative stress, but does not alter aerobic glycolysis in OC cells

It is well known that disruption of mitochondrial function can cause caspase-3-dependent apoptosis. Therefore, we hypothesized that the interruption of mitochondria homeostasis by 6-ME is a step in its response that causes cytotoxicity in OC cells. To corroborate this hypothesis, we analyzed the oxygen consumption rate (OCR) after 6-ME administration using the Seahorse XF96 bioenergy analyzer. 6-ME significantly inhibited not only the total OCR but also the maximal respiration of CAOV3 and SKOV3 cells (Figures 3A, B). Moreover, 6-ME exposure resulted in increased in ROS levels (Figure 3C) and inhibition of the key mitochondrial fusion proteins MFN1 and MFN2 (Figure 3D; Supplementary Figure S2A). To further explore the effects of 6-ME on aerobic glycolysis, a crucial resource of ATP and metabolic intermediates for tumor growth, we analyzed the extracellular acidification rate (ECAR) using the Seahorse XF96 bioenergy analyzer. Our results reveal that 6-ME is unable to alter the hemostasis of aerobic glycolysis in OC cells (Figures 3E, F). These findings suggest that 6-ME initializes mitochondrial dysfunction and oxidative stress in OC cells.

3.4 6-ME exhibits its anti-OC properties by triggering mitochondrial dysfunction through the promotion of ROS production, which can be eliminated by the antioxidant NAC

To further investigate the underlying mechanism by which 6-ME regulates mitochondrial imbalance, the effects of ROS on mitochondrial homeostasis were subsequently determined. Exploration of 6-ME treated alone or combination with ROS scavenger NAC uncovered that NAC markedly eliminated the decrease in overall OCR and maximal respiration (Figures 4A, B). Moreover, the 6-ME-induced inhibitions of MFN1 and MFN2 expressions were alleviated by the addition of NAC (Figures 4C, D). 6-ME-caused mitochondrial morphological abnormalities were also markedly attenuated by NAC, based on the results of Mitotracker staining (Figure 4E). Culturing OC cells with NAC clearly eliminated the effects of 6-ME on promoting ROS accumulation in the cells (Figure 4F). NAC also mitigated the inhibitory effects of 6-ME on OC cell viability and proliferation (Figures 4G, H). Overall, 6-ME-induced mitochondrial dysfunction is mediated by ROS accumulation, which leads to OC cell growth inhibition, while the antioxidant NAC significantly overcomes the 6-ME-induced mitochondrial impairment.

3.5 6-ME causes ROS/MAPK axis-dependent apoptosis in OC cells

Considering the important role of ROS in modulating MAPK signaling, Western blotting was further performed to detect alterations of crucial factors involved in the pathway in response to 6-ME treatment. JNK/MAPK and ERK/MAPK, but not p-p38, were activated in OC cells after 6-ME treatment (Figures 5A, B). Culturing OC cells with 6-ME alone or in combination with NAC confirmed that the addition of NAC obviously diminished the effects of 6-ME on MAPK axis activation (Figures 5C, D). Similarly, 6-ME-

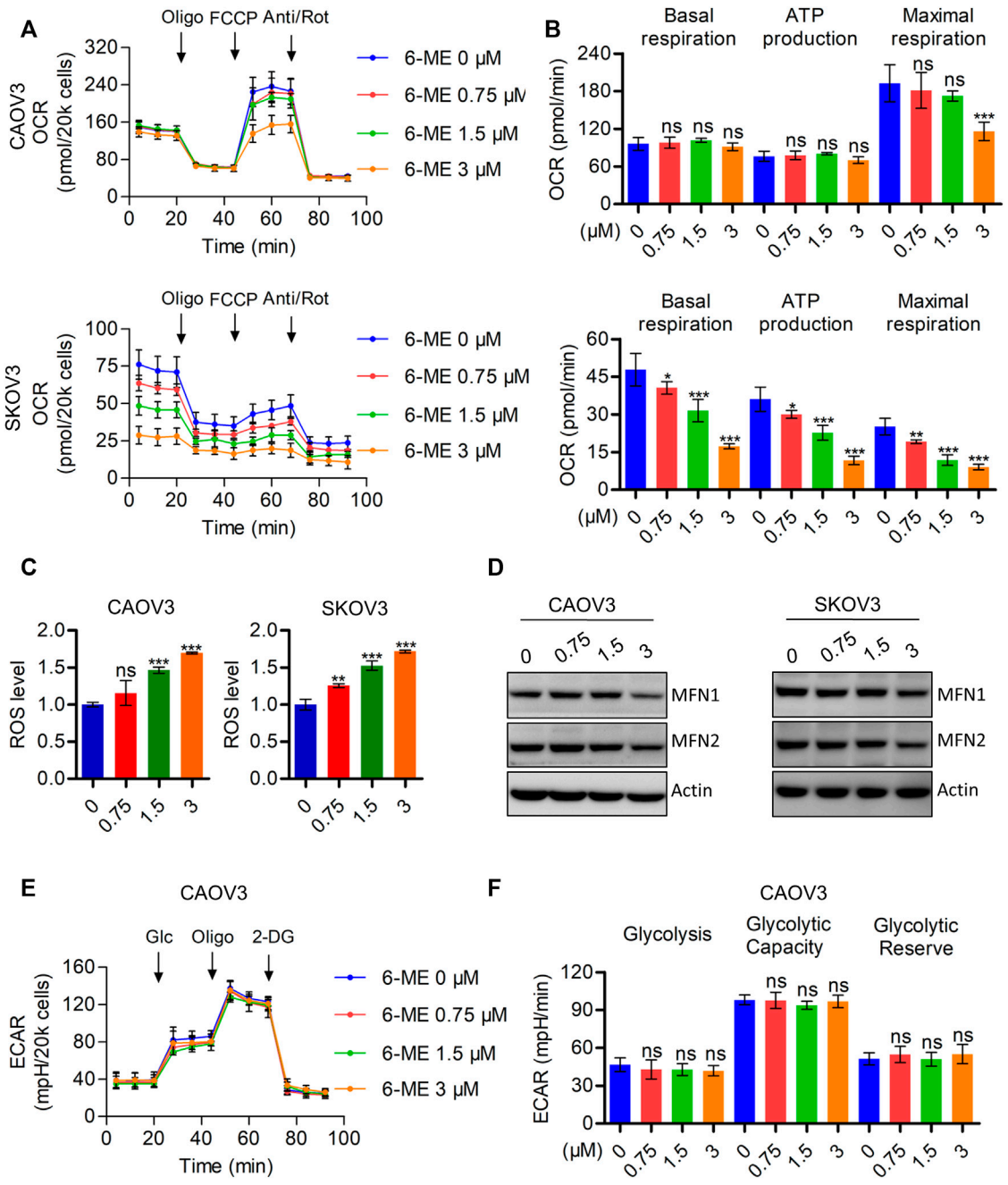

FIGURE 3
6-ME triggers ROS accumulation and mitochondrial dysfunction. **(A)**. The OCR was measured by Seahorse XF96 bioenergy analyzer after 6-ME addition. **(B)**. The data comes from OCR was analyzed and showed as basal respiration, ATP production, and maximal respiration, all data were showed as mean ± SD. **(C)**. ROS level was analyzed by flow cytometry in DCFH-DA staining OC cells and showed as mean ± SD. **(D)**. The alteration of MFN1 and MFN2 were confirmed by western blot, actin was acted as a loading control. **(E)**. The ECAR was measured by Seahorse XF96 bioenergy analyzer after 6-ME administration. **(F)**. The data comes from ECAR was analyzed and showed as glycolysis, glycolytic capacity, and glycolytic reserve, all data were showed as mean ± SD.

promoted cleavages of PARP and caspase-3 were mitigated by NAC (Figures 5E, F). Measurement of the apoptotic rates in OC cells cultured with 6-ME alone or in combination with NAC further revealed that the presence of NAC led to the reduction of 6-ME-induced cell death (Figures 5G, H). These observations imply that 6-ME exerts its cytotoxicity by initiating apoptosis, at least in part, through ROS-mediated MAPK activation.

3.6 6-ME may disrupt the metabolic homeostasis of OAA and thereby activating ROS production

This study demonstrated the indispensable roles of ROS in regulating cell death and mitochondrial dysfunction. Therefore, the regulatory mechanisms behind the 6-ME-induced increase in

10.3389/fphar.2023.1093650

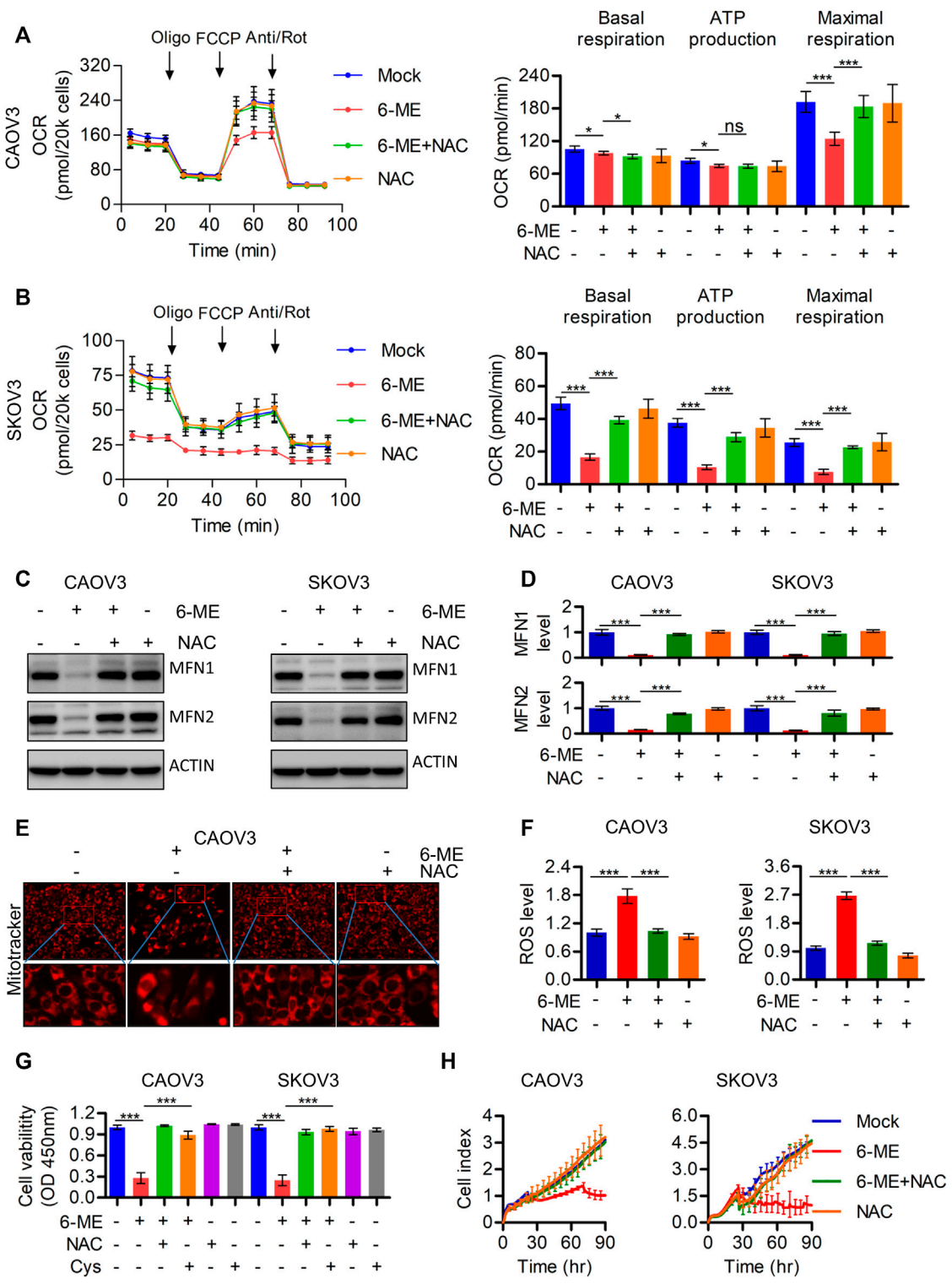

FIGURE 4
6-ME caused ROS activation leads to the dysfunction of mitochondria in OC cells. **(A,B)**. The OCR was measured by Seahorse XF96 bioenergy analyzer in 6-ME treated cell with or without NAC. **(C)**. The alteration of MFN1 and MFN2 were confirmed in 6-ME exposed OC cells in the presence of NAC by western blot, actin was acted as a loading control. **(D)**. The changes of MFN1 and MFN2 were quantified and statistically analyzed, data was showed as mean ± SD. **(E)**. 6-ME-caused mitochondrial morphological abnormalities were observed in Mitotracker dyed OC cells. **(F)**. ROS level was analyzed by flow cytometry in 6-ME treated OC cells after NAC addition and the data was showed as mean ± SD. **(G)**. The cell viabilities were analyzed in 6-ME exposed alone or combination of NAC or Cys and data was showed as mean ± SD. **(H)**. The cell proliferation abilities were analyzed in 6-ME exposed alone or combination of NAC and data was showed as mean ± SD.

10.3389/fphar.2023.1093650

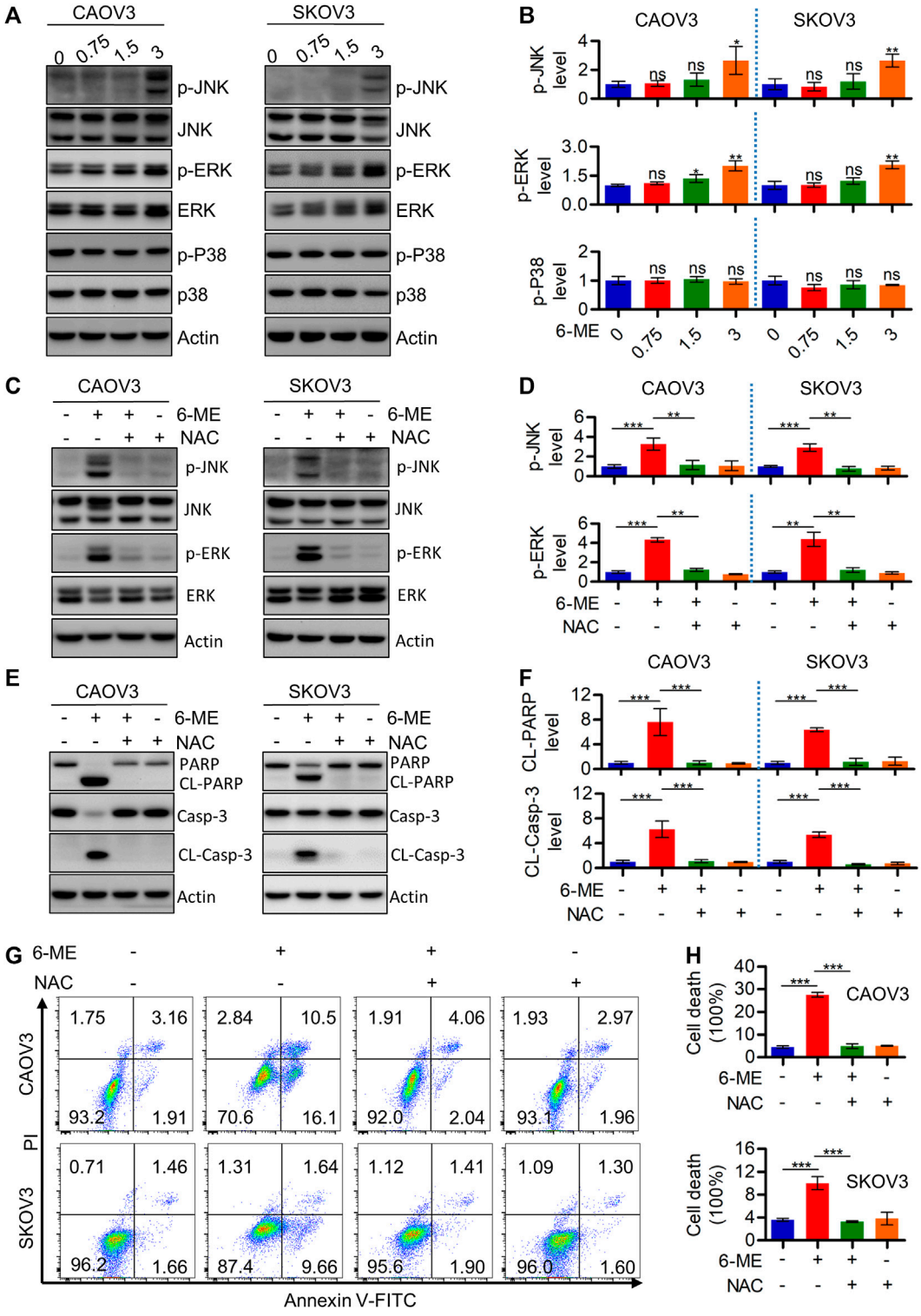

FIGURE 5
6-ME activates ROS/MAPK axis-dependent apoptosis in OC cells. **(A)**. Western blot was performed to detect the activation of JNK, ERK, and p38, the Actin was act as a loading control. **(B)**. The changes of these proteins were then quantified and analyzed, the data was showed as mean ± SD. **(C)**. Western blot was performed to detect the activation of JNK and ERK in 6-ME treated with or without NAC in OC cells, the Actin was act as a loading control. **(D)**. The changes of p-JNK and p-ERK were then quantified and analyzed, the data was showed as mean ± SD. **(E)**. Western blot was performed to detected the activation of PARP and caspase-3 in 6-ME treated with or without NAC in OC cells, the Actin was act as a loading control. **(F)**. The changes of PARP and caspase-3 were then quantified and analyzed, and the data was showed as mean ± SD. **(G)**. The cell death was analyzed by flow cytometry in Annexin V-FITC/PI dyeing and 6-ME cultured OC cells in the presence of NAC. **(H)**. The cell death rates were then statistically analyzed and showed as mean ± SD.

10.3389/fphar.2023.1093650

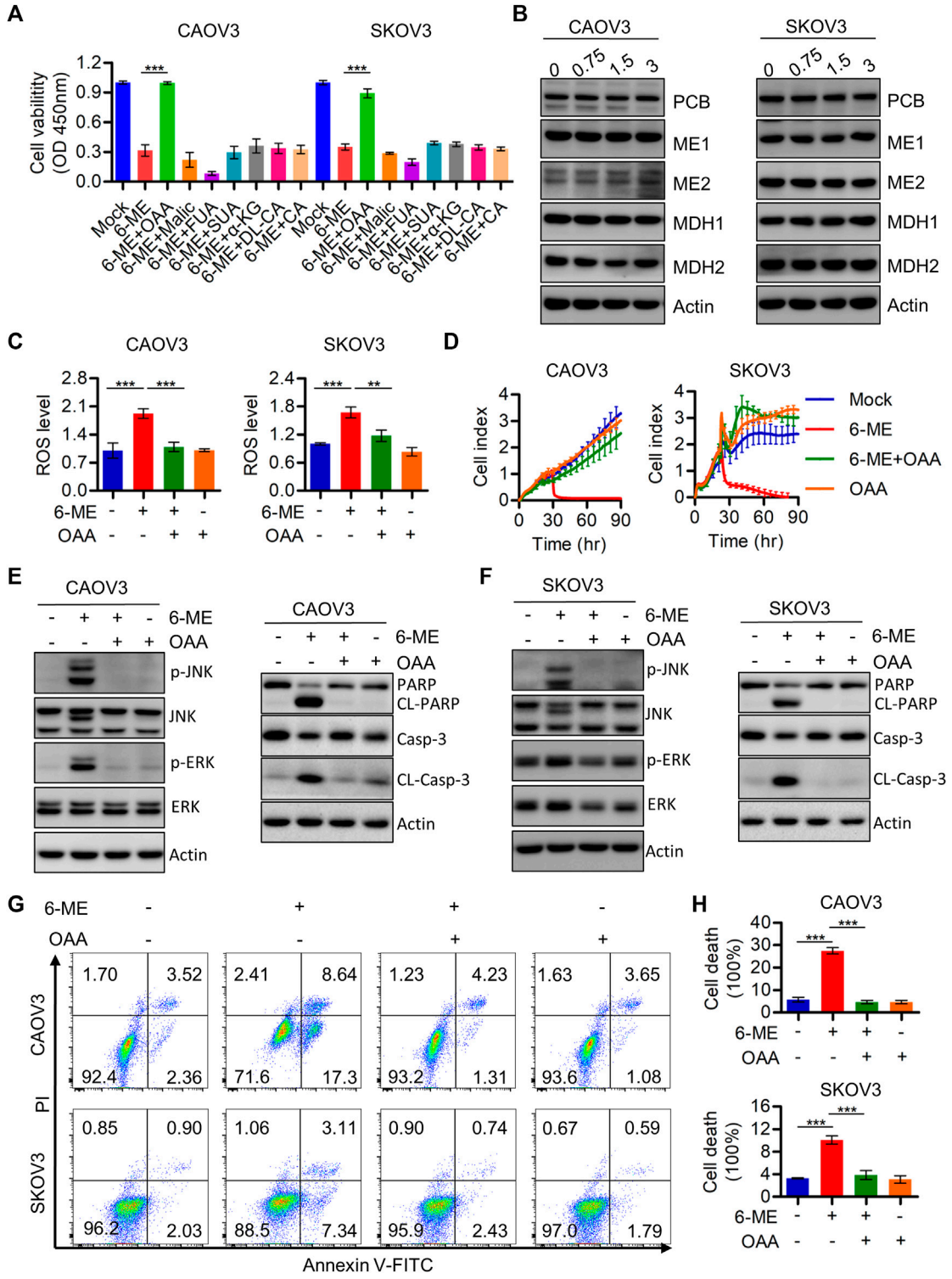

FIGURE 6
6-ME may disrupt the metabolic homeostasis of OAA and thereby activating ROS production. **(A)**. Cell viabilities were measured after 6-ME treated alone or in combination with TCA cycle metabolites, data was showed as mean ± SD. **(B)**. Western blot were used to detect the alteration of PCB, MDH1, MDH2, ME1 and ME2, Actin was acted as a loading control. **(C)**. ROS level was analyzed by flow cytometry in 6-ME treated OC cells after OAA addition and the data was showed as mean ± SD. **(D)**. The cell proliferation abilities were analyzed in 6-ME exposed alone or combination of OAA and data was showed as mean ± SD. **(E,F)**. Western blot was performed to detect the activation of JNK, ERK, PARP, and caspase-3 in 6-ME treated with or without OAA in OC cells, the Actin was act as a loading control. **(G)**. The cell death was analyzed by flow cytometry in Annexin V-FITC/PI dyeing and 6-ME cultured OC cells in the presence of OAA. **(H)**. The cell death rates were then statistically analyzed and showed as mean ± SD.

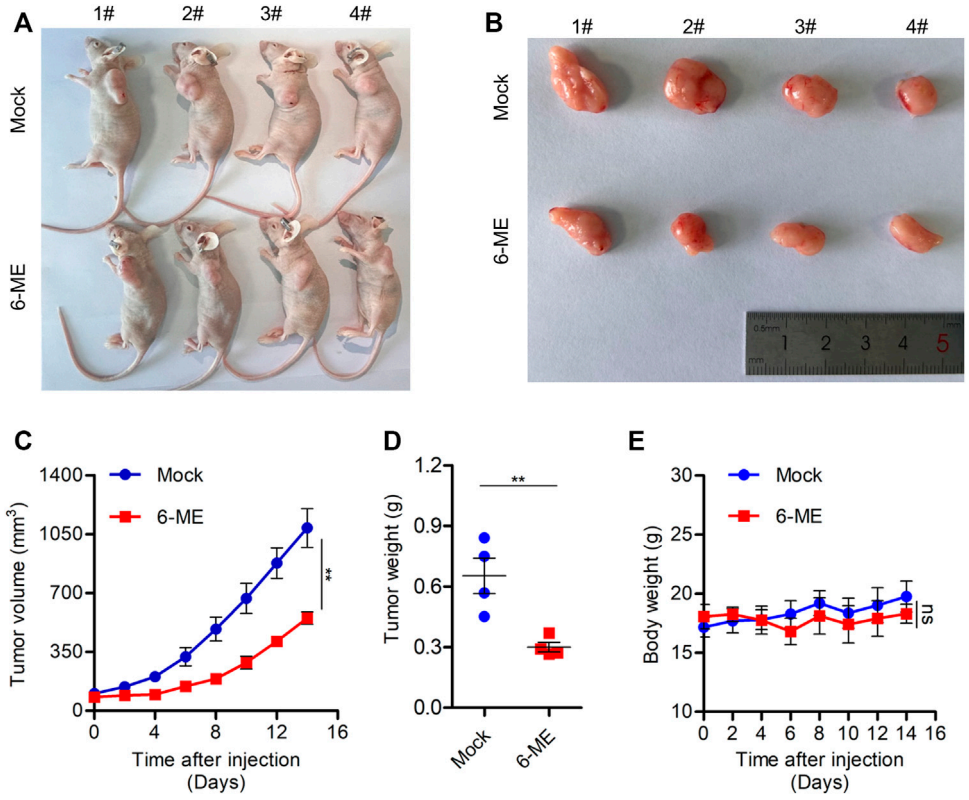

FIGURE 7
6-ME efficiently blocks OC growth *in vivo*. **(A)** Images of nude mice treated with 6-ME (5 mg/kg). **(B)** Corresponding tumor tissue pictures obtained after the nude mice were sacrificed. **(C)** Tumor growth in nude mice after treatment with 6-ME. **(D)** The tumor weight of OC treated with 6-ME was analyzed. **(E)** Volume changes of nude mice in two groups. The data showed as mean ± SD.

ROS production were further explored. It is worth mentioning that oxaloacetic acid (OAA), but not other crucial metabolites of the TCA cycle counteracted the cytotoxicity caused by 6-ME in OC cells (Figure 6A). Considering the important role of OAA in regulating NADPH production, we also speculated that 6-ME could modulate ROS generation by disrupting OAA metabolic homeostasis. The alterations of crucial enzymes involved in OAA metabolism were thus analyzed by Western blotting, which confirmed that the expression of PCB (pyruvate carboxylase), MDH1, MDH2, ME1, ME2, the key enzymes for OAA synthesis, unchanged after 6-ME treatment (Figure 6B). Interestingly, detection of ROS levels in 6-ME-exposed cells with or without OAA revealed that OAA mitigated the activation of ROS after 6-ME addition (Figure 6C). The addition of OAA also effectively reverted 6-ME-induced proliferation inhibition (Figure 6D), eliminated the 6-ME-mediated increase in phosphorylation of JNK and ERK and cleavages of PARP and caspase-3 (Figures 6E, F; Supplementary Figures S4A, B), and mitigated the influence of 6-ME-promoted apoptosis in OC cells (Figures 6G, H). These results indicate that 6-ME may contribute to increased ROS levels by disturbing OAA metabolism homeostasis, leading to ROS/MAPK-dependent apoptosis in OC cells.

3.7 6-ME depress *in vivo* OC cell growth in nude mouse

We used a tumor-bearing nude mouse model to further investigate the anti-tumor effect of 6-ME *in vivo*. 6-ME dramatically reduced tumor growth in tumor-bearing nude mice (Figures 7A, B), which is consistent with the experimental evidence of OC cells *in vitro*. In comparison to the control group, the 6-ME group's tumor volume and weight were much lower (Figures 7C, D). Since there was no discernible change in body weight between the two groups, 6-ME showed no physiologically harmful effects on mice (Figure 7E). These findings imply that 6-ME is a potentially effective anticancer medication for the treatment of ovarian carcinoma.

4 Discussion

The promising antitumor properties of alkaloids and others extracts from *M. cordata* have been demonstrated in different cancer types (Zhengfu et al., 2012; Guo et al., 2014; Almeida et al., 2017; Si et al., 2019; Zhu et al., 2019; Ali et al., 2021; Sai et al., 2021). Notably,

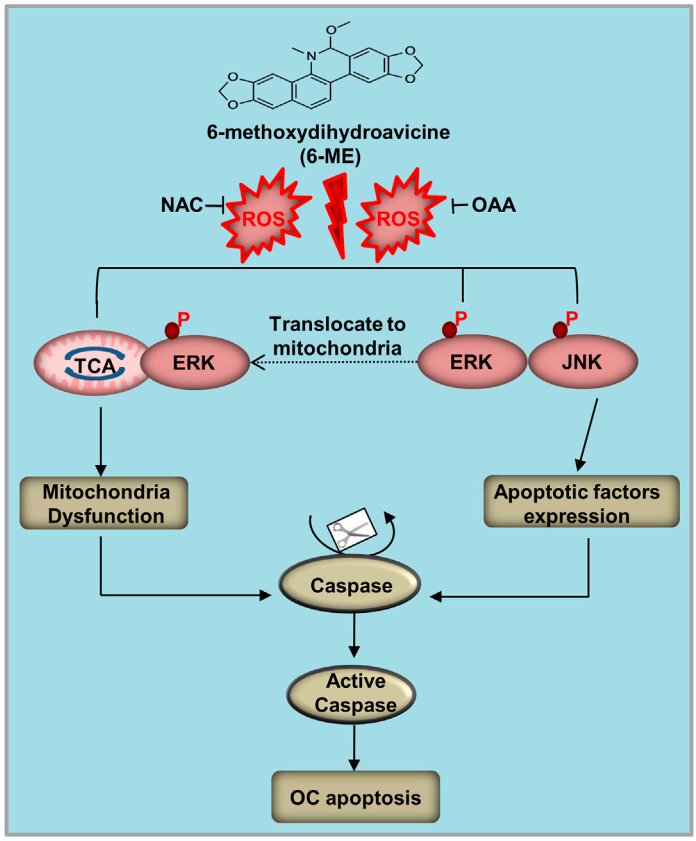

FIGURE 8
Mechanistic model of 6-ME induces OC cell apoptosis and mitochondrial dysfunction. 6-ME caused disruption of OAA metabolism and led to the accumulation of ROS. Subsequently, 6-ME caused ROS-facilitated JNK-ERK/MAPK activation and disruption of mitochondrial hemostasis, thus driving OC cell apoptosis.

our recent study has confirmed that 6-ME can induce mitochondrial dysfunction and ROS/RIPK1-dependent pyroptosis that hinder pancreatic cancer progression (Ma et al., 2022). However, it remains unclear whether 6-ME possess a potential against OC and what the underlying mechanisms of its action might be. In the present study, we reported a novel anti-OC pathway in which 6-ME disrupts mitochondrial hemostasis and causes ROS/MAPK axis-dependent apoptosis. These findings indicate that 6-ME is a promising natural compound worthy of further investigation for OC intervention.

PCD, which primarily includes apoptosis, pyroptosis, necroptosis, and ferroptosis, has been employed in therapeutic strategies to kill cancer cells and/or hinder their progression (Koren and Fuchs, 2021). We employed corresponding PCD inhibitors to confirm the specific type of PCD in OC cells induced by 6-ME. The cell viability data showed that only the apoptosis inhibitor ZVAD, but not the other PCD inhibitors, can antagonize 6-ME-induced PCD (Figure 2C). Considering the cross talk between apoptosis and pyroptosis (Koren and Fuchs, 2021), we conducted further investigations to verify these processes. Western blotting results indicated that 6-ME could not to lead to increase in cleavages of GSDMB, GSDMC, GSDMD, and GSDME (Supplementary Figure S1B), which are crucial biochemical indexes of cellular pyroptosis. Also, no balloon-like bubbles were observed in 6-ME-exposed OC cells (Supplementary Figure S1A), which is the classical cell morphology of pyroptosis (Shi et al., 2017). Therefore, we confirm that 6-ME exerts its cytotoxicity by inducing OC cell apoptosis rather than GSDMX-mediated pyroptosis. Cleavages of PARP and caspase-3, two crucial factors of apoptosis, were initiated by 6-ME and inhibited upon the addition of ZVAD in OC cells (Figures 2G, H). The 6-ME-induced cytotoxicity was also mitigated by the presence of ZVAD, based on the viability data of OC cells treated with 6-ME alone or in combination with ZVAD (Figure 2F; Supplementary Figure S1C). Based on these results, we conclude that 6-ME triggers OC cell apoptosis, which is a different mode of cell death from the one previously reported in the 6-ME-induced pyroptosis of pancreatic cancer (Ma et al., 2022).

It is well known that avoidance and resistance to apoptosis are hallmarks of tumors, to fight cancer, we can use strategies that target them (Hanahan and Weinberg, 2011). In the past, many studies have demonstrated that targeting mitochondria-mediated apoptosis can be a candidate therapeutic option for cancer

treatment (Burke, 2017). Our experimental results are consistent with this evidence by suggesting that 6-ME may exhibit cytotoxicity by modulating mitochondrial homeostasis and apoptosis in OC cells (Ma et al., 2019; Song et al., 2019; Temel et al., 2020). We found that 6-ME can dramatically inhibit mitochondrial respiration along with maximal respiration (Figures 3A, B). Furthermore, flow cytometry results revealed that 6-ME can remarkably trigger ROS production in OC cells (Figure 3C), providing that ROS is an important signal transduction that occurs in mitochondria-mediated apoptosis (Jacquemin et al., 2015; Li et al., 2019; Cao et al., 2020). Further investigations of the underlying mechanisms found that NAC, a potent ROS scavenger, can diminish the disruption of mitochondria and the activation of apoptosis caused by 6-ME when comparing OC cells exposed to 6-ME alone or in combination with NAC (Figures 4A, B; Figures 5G, H). This indicates that 6-ME may promote ROS-dependent mitochondrial dysfunction, thereby leading to the activation of OC cell apoptosis. Notably, ROS can further trigger the activation of some downstream pro-apoptotic signal pathways, such as the MAPK axis. MAPK has been reported as an important cellular signal transduction molecule that may act as a bridge between ROS and apoptosis in several cancer types (Mao et al., 2008; Dang et al., 2017; Zhu et al., 2017; Lan et al., 2018; Wang et al., 2019; Fontana et al., 2021; Lu et al., 2021; Xing et al., 2021; Li S et al., 2022). Similarly, in our study, we found that 6-ME-caused the activation of JNK/MAPK and ERK/MAPK in OC cells (Figures 5A, B). Moreover, the increase in phosphorylation of JNK/MAPK and ERK/MAPK, as well as increased cleavages of PARP and caspase 3 induced by 6-ME, can be eliminated by the addition of NAC (Figures 5C–F). Consistent with this, the 6-ME cause apoptosis was also blocked by NAC (Figures 5G, H). In particular, we observed an increase in 6-ME-induced phosphorylation of ERK/MAPK in the mitochondrial fraction (Supplementary Figure S3C), where they may behave as apoptotic inducers by causing mitochondrial dysfunction (Lan et al., 2018; Li C et al., 2022). These findings imply that 6-ME can induce the activation of JNK-ERK/MAPK to trigger subsequent apoptosis in OC cells.

Mitochondria are one of the main sources of cellular ROS production, and mitochondrial disruption can often occur during cancer development and treatment (Choucair et al., 2022; Dakik et al., 2022; Liu et al., 2022). We speculated that 6-ME-induced OC cell apoptosis is due to its involvement in triggering signals for ROS production and accumulation. To investigate this hypothesis, we cultured OC cells with 6-ME in the presence or absence of OAA (a crucial metabolite of the TCA cycle), which has been demonstrated to modulate the homeostasis of mitochondrial function (Desideri et al., 2015; Martinez-Reyes and Chandel, 2020). We thus confirmed that OAA, rather than other metabolites, can eliminate the cytotoxicity caused by 6-ME in OC cells (Figure 6A), which was consistent with our latest results regarding the effects of 6-ME and OAA on pancreatic cancer (Ma et al., 2022). The deficiency of OAA has been verified to contribute to the impairment of the balance of NADPH generation, which leads to the accumulation of ROS (Son et al., 2013; Abrego et al., 2017). Our subsequent studies further proved that the addition of OAA significantly impeded 6-ME-induced ROS accumulation (Figure 6C), JNK/MAPK and ERK/MAPK activation (Figures 6E, F), and increased apoptosis in OC cells (Figures 6G, H). Importantly, 6-ME has been reported that has the potential to bind to the regulatory center of enzymatic activity of PCB, which has been demonstrated to be the key enzyme supplying OAA to the TCA cycle (Ma et al., 2022). Meanwhile, we did not observe changes in PCB expression in 6-ME-treated OC cells by western blot (Figure 5B), suggesting that 6-ME may bind to PCB and then inhibit its activity rather than expression. The mechanism behind this process remains unclear and requires further investigation. Overall, 6-ME may modulate ROS production by directly binding to PCB and thereby hindering its activity.

In this study, we proposed a mechanistic model by which 6-ME inhibits cell growth and promotes apoptosis of OC cells *in vitro* and *in vivo* (Figure 8). 6-ME modulated PCB activity, which then caused disruption of OAA metabolism and led to the accumulation of ROS. Subsequently, 6-ME caused ROS-facilitated JNK-ERK/MAPK activation and disruption of mitochondrial hemostasis, thus driving OC cell apoptosis. These findings uncover novel mechanisms for the antineoplastic property of 6-ME in OC cells, supporting its potential as a natural drug for OC intervention. A 6-ME-based treatment approach may also offer significant benefits to patients with other tumors.

Data availability statement

The original contributions presented in the study are included in the article/Supplementary Material, further inquiries can be directed to the corresponding authors.

Ethics statement

The animal study was reviewed and approved by the Animal Protection and Utilization Committee of Binzhou Medical University.

Author contributions

HL and QC conceived the study. HZ, FS, LZ, NM, LM, and CL performed laboratory work. HZ, FS, LZ, ML, and SS conducted data analysis. HZ and FS are responsible for writing the first draft of the article and revised by HL and QC. JA checked and improved our writing.

Funding

This work has been supported by the National Natural Science Foundation of China (Nos. 81672757 and 82200109), the Shandong Provincial Natural Science Foundation Joint Fund (ZR2021LZY024), the Youth Innovation and Technology Support Program in Colleges and Universities of Shandong Province (No. 2022KJ090), the Project of Zhejiang Provincial Naturel Science Foundation of China (LQ23H310006), and grants from the Science and Technology Bureau of Wenzhou (Y20220171).

Conflict of interest

The authors declare that the research was conducted in the absence of any commercial or financial relationships that could be construed as a potential conflict of interest.

Publisher's note

All claims expressed in this article are solely those of the authors and do not necessarily represent those of their affiliated organizations, or those of the publisher, the editors and the reviewers. Any product that may be evaluated in this article, or claim that may be made by its manufacturer, is not guaranteed or endorsed by the publisher.

Supplementary material

The Supplementary Material for this article can be found online at: https://www.frontiersin.org/articles/10.3389/fphar.2023.1093650/full#supplementary-material

References

Abrego, J., Gunda, V., Vernucci, E., Shukla, S. K., King, R. J., Dasgupta, A., et al. (2017). GOT1-mediated anaplerotic glutamine metabolism regulates chronic acidosis stress in pancreatic cancer cells. *Cancer Lett.* 400, 37–46. doi:10.1016/j.canlet.2017.04.029

Ali, I., Li, J., Cui, L., Zhao, H., He, Q., and Wang, D. (2021). Efficient extraction and purification of benzo[c]phenanthridine alkaloids from Macleaya cordata (Willd) R. Br. by combination of ultrahigh pressure extraction and pH-zone-refining counter-current chromatography with anti-breast cancer activity *in vitro*. *Phytochem. Anal.* 32 (3), 423–432. doi:10.1002/pca.2990

Almeida, I. V., Fernandes, L. M., Biazi, B. I., and Vicentini, V. (2017). Evaluation of the anticancer activities of the plant alkaloids sanguinarine and chelerythrine in human breast adenocarcinoma cells. *Anticancer Agents Med. Chem.* 17 (11), 1586–1592. doi:10.2174/1871520617666170213115132

Atanasov, A. G., Zotchev, S. B., Dirsch, V. M., and Supuran, C. T. (2021). Natural products in drug discovery: Advances and opportunities. *Nat. Rev. Drug Discov.* 20 (3), 200–216. doi:10.1038/s41573-020-00114-z

Burke, P. J. (2017). Mitochondria, bioenergetics and apoptosis in cancer. *Trends Cancer* 3 (12), 857–870. doi:10.1016/j.trecan.2017.10.006

Cao, Y., Wang, J., Tian, H., and Fu, G. H. (2020). Mitochondrial ROS accumulation inhibiting JAK2/STAT3 pathway is a critical modulator of CYT997-induced autophagy and apoptosis in gastric cancer. *J. Exp. Clin. Cancer Res.* 39 (1), 119. doi:10.1186/s13046-020-01621-y

Choucair, H., Rahman, M. K., Umashankar, B., Al-Zubaidi, Y., Bourget, K., Chen, Y., et al. (2022). The aryl-ureido fatty acid CTU activates endoplasmic reticulum stress and PERK/NOXA-mediated apoptosis in tumor cells by a dual mitochondrial-targeting mechanism. *Cancer Lett.* 526, 131–141. doi:10.1016/j.canlet.2021.11.022

Dakik, H., El, D. M., Bourgeais, J., Kouzi, F., Herault, O., Gouilleux, F., et al. (2022). Diphenyleneiodonium triggers cell death of acute myeloid leukemia cells by blocking the mitochondrial respiratory chain, and synergizes with cytarabine. *Cancers (Basel)* 14 (10), 2485. doi:10.3390/cancers14102485

Dang, J. H., Jin, Z. J., Liu, X. J., Hu, D., Wang, J., Luo, Y., et al. (2017). Metformin in combination with cisplatin inhibits cell viability and induces apoptosis of human ovarian cancer cells by inactivating ERK 1/2. *Oncol. Lett.* 14 (6), 7557–7564. doi:10.3892/ol.2017.7176

Desideri, E., Vegliante, R., and Ciriolo, M. R. (2015). Mitochondrial dysfunctions in cancer: Genetic defects and oncogenic signaling impinging on TCA cycle activity. *Cancer Lett.* 356 (2), 217–223. doi:10.1016/j.canlet.2014.02.023

Fontana, F., Marzagalli, M., Raimondi, M., Zuco, V., Zaffaroni, N., and Limonta, P. (2021). δ-Tocotrienol sensitizes and re-sensitizes ovarian cancer cells to cisplatin via induction of G1 phase cell cycle arrest and ROS/MAPK-mediated apoptosis. *Cell Prolif.* 54 (11), e13111. doi:10.1111/cpr.13111

Guo, Z. Q., Guo, Q., Zhu, Z. X., Zhang, S. Y., Li, C., Chai, X. Y., et al. (2014). Chemical constituents from a Tibetan medicine Meconopsis horridula. *Zhongguo Zhong Yao Za Zhi* 39 (7), 1152–1156. doi:10.4268/cjcmm20140702

Hanahan, D., and Weinberg, R. A. (2011). Hallmarks of cancer: The next generation. *Cell* 144 (5), 646–674. doi:10.1016/j.cell.2011.02.013

Herrera, F. G., Irving, M., Kandalaft, L. E., and Coukos, G. (2019). Rational combinations of immunotherapy with radiotherapy in ovarian cancer. *Lancet Oncol.* 20 (8), e417–e433. doi:10.1016/S1470-2045(19)30401-2

Holze, C., Michaudel, C., Mackowiak, C., Haas, D. A., Benda, C., Hubel, P., et al. (2018). Oxeiptosis, a ROS-induced caspase-independent apoptosis-like cell-death pathway. *Nat. Immunol.* 19 (2), 130–140. doi:10.1038/s41590-017-0013-y

Jacquemin, G., Margiotta, D., Kasahara, A., Bassoy, E. Y., Walch, M., Thiery, J., et al. (2015). Granzyme B-induced mitochondrial ROS are required for apoptosis. *Cell Death Differ.* 22 (5), 862–874. doi:10.1038/cdd.2014.180

Jiang, B., Zhang, J., Zhao, G., Liu, M., Hu, J., Lin, F., et al. (2022). Filamentous GLS1 promotes ROS-induced apoptosis upon glutamine deprivation via insufficient asparagine synthesis. *Mol. Cell.* 82 (10), 1821–1835.e6. doi:10.1016/j.molcel.2022.03.016

Jing, L., Song, F., Liu, Z., Li, J., Wu, B., Fu, Z., et al. (2018). MLKL-PITPα signaling-mediated necroptosis contributes to cisplatin-triggered cell death in lung cancer A549 cells. *Cancer Lett.* 414, 136–146. doi:10.1016/j.canlet.2017.10.047

Koren, E., and Fuchs, Y. (2021). Modes of regulated cell death in cancer. *Cancer Discov.* 11 (2), 245–265. doi:10.1158/2159-8290.CD-20-0789

Lan, L., Wei, W., Zheng, Y., Niu, L., Chen, X., Huang, D., et al. (2018). Deferoxamine suppresses esophageal squamous cell carcinoma cell growth via ERK1/2 mediated mitochondrial dysfunction. *Cancer Lett.* 432, 132–143. doi:10.1016/j.canlet.2018.06.012

Lei, G., Zhuang, L., and Gan, B. (2022). Targeting ferroptosis as a vulnerability in cancer. *Nat. Rev. Cancer*. 22 (7), 381–396. doi:10.1038/s41568-022-00459-0

Li, C., Ma, D., Chen, Y., Liu, W., Jin, F., and Bo, L. (2022). Selective inhibition of JNK located on mitochondria protects against mitochondrial dysfunction and cell death caused by endoplasmic reticulum stress in mice with LPSinduced ALI/ARDS. *Int. J. Mol. Med.* 49 (6), 85. doi:10.3892/ijmm.2022.5141

Li, S., Chen, J., Fan, Y., Wang, C., Wang, C., Zheng, X., et al. (2022). Liposomal Honokiol induces ROS-mediated apoptosis via regulation of ERK/p38-MAPK signaling and autophagic inhibition in human medulloblastoma. *Signal Transduct. Target Ther.* 7 (1), 49. doi:10.1038/s41392-021-00869-w

Li, X., Fang, F., Gao, Y., Tang, G., Xu, W., Wang, Y., et al. (2019). ROS induced by KillerRed targeting mitochondria (mtKR) enhances apoptosis caused by radiation via cyt c/caspase-3 pathway. *Oxid. Med. Cell. Longev.* 2019, 4528616. doi:10.1155/2019/4528616

Li, X., Wang, Y., Chen, Y., Zhou, P., Wei, K., Wang, H., et al. (2020). Hierarchically constructed selenium-doped bone-mimetic nanoparticles promote ROS-mediated autophagy and apoptosis for bone tumor inhibition. *Biomaterials* 257, 120253. doi:10.1016/j.biomaterials.2020.120253

Liang, C., Zhang, X., Yang, M., and Dong, X. (2019). Recent progress in ferroptosis inducers for cancer therapy. *Adv. Mat.* 31 (51), e1904197. doi:10.1002/adma.201904197

Lisio, M. A., Fu, L., Goyeneche, A., Gao, Z. H., and Telleria, C. (2019). High-grade serous ovarian cancer: Basic Sciences, clinical and therapeutic standpoints. *Int. J. Mol. Sci.* 20 (4), 952. doi:10.3390/ijms20040952

Liu, Y., Wang, X., Zhu, W., Sui, Z., Wei, X., Zhang, Y., et al. (2022). TRPML1-induced autophagy inhibition triggers mitochondrial mediated apoptosis. *Cancer Lett.* 541, 215752. doi:10.1016/j.canlet.2022.215752

Lu, D., Sun, J., Zheng, J., Zheng, L., Xue, W., Li, C., et al. (2021). Shenxiong glucose injection inhibits H2O2-induced H9c2 cell apoptosis by activating the ERK signaling pathway. *Biomed. Pharmacother.* 143, 112114. doi:10.1016/j.biopha.2021.112114

Ma, L., Wei, J., Wan, J., Wang, W., Wang, L., Yuan, Y., et al. (2019). Low glucose and metformin-induced apoptosis of human ovarian cancer cells is connected to ASK1 via mitochondrial and endoplasmic reticulum stress-associated pathways. *J. Exp. Clin. Cancer Res.* 38 (1), 77. doi:10.1186/s13046-019-1090-6

Ma, N., Shangguan, F., Zhou, H., Huang, H., Lei, J., An, J., et al. (2022). 6-methoxydihydroavicine the alkaloid extracted from Macleaya cordata (Willd) R Br (Papaveraceae) triggers RIPK1/Caspase-dependent cell death in pancreatic cancer cells through the disruption of oxaloacetic acid metabolism and accumulation of reactive oxygen species. *Phytomedicine* 102, 154164. doi:10.1016/j.phymed.2022.154164

Mao, X., Yu, C. R., Li, W. H., and Li, W. X. (2008). Induction of apoptosis by shikonin through a ROS/JNK-mediated process in Bcr/Abl-positive chronic myelogenous leukemia (CML) cells. *Cell Res.* 18 (8), 879–888. doi:10.1038/cr.2008.86

Marchetti, C., De Felice, F., Romito, A., Iacobelli, V., Sassu, C. M., Corrado, G., et al. (2021). Chemotherapy resistance in epithelial ovarian cancer: Mechanisms and emerging treatments. *Semin. Cancer Biol.* 77, 144–166. doi:10.1016/j.semcancer.2021.08.011

Martinez-Reyes, I., and Chandel, N. S. (2020). Mitochondrial TCA cycle metabolites control physiology and disease. *Nat. Commun.* 11 (1), 102. doi:10.1038/s41467-019-13668-3

Millstein, J., Budden, T., Goode, E. L., Anglesio, M. S., Talhouk, A., Intermaggio, M. P., et al. (2020). Prognostic gene expression signature for high-grade serous ovarian cancer. *Ann. Oncol.* 31 (9), 1240–1250. doi:10.1016/j.annonc.2020.05.019

Sai, C., Qin, W., Meng, J., Gao, L. N., Huang, L., Zhang, Z., et al. (2021). Macleayins A from *macleaya* promotes cell apoptosis through wnt/β-catenin signaling pathway and inhibits proliferation, migration, and invasion in cervical cancer HeLa cells. *Front. Pharmacol.* 12, 668348. doi:10.3389/fphar.2021.668348

Schoutrop, E., Moyano-Galceran, L., Lheureux, S., Mattsson, J., Lehti, K., Dahlstrand, H., et al. (2022). Molecular, cellular and systemic aspects of epithelial ovarian cancer and its tumor microenvironment. *Semin. Cancer Biol.* 86, 207–223. doi:10.1016/j.semcancer.2022.03.027

Shahar, N., and Larisch, S. (2020). Inhibiting the inhibitors: Targeting anti-apoptotic proteins in cancer and therapy resistance. *Drug Resist Updat* 52, 100712. doi:10.1016/j.drup.2020.100712

Shi, J., Gao, W., and Shao, F. (2017). Pyroptosis: Gasdermin-Mediated programmed necrotic cell death. *Trends biochem. Sci.* 42 (4), 245–254. doi:10.1016/j.tibs.2016.10.004

Si, Y., Wang, J., Liu, X., Zhou, T., Xiang, Y., Zhang, T., et al. (2019). Ethoxysanguinarine, a novel direct activator of AMP-activated protein kinase, induces autophagy and exhibits therapeutic potential in breast cancer cells. *Front. Pharmacol.* 10, 1503. doi:10.3389/fphar.2019.01503

Son, J., Lyssiotis, C. A., Ying, H., Wang, X., Hua, S., Ligorio, M., et al. (2013). Glutamine supports pancreatic cancer growth through a KRAS-regulated metabolic pathway. *Nature* 496 (7443), 101–105. doi:10.1038/nature12040

Song, X., Liu, L., Chang, M., Geng, X., Wang, X., Wang, W., et al. (2019). NEO212 induces mitochondrial apoptosis and impairs autophagy flux in ovarian cancer. *J. Exp. Clin. Cancer Res.* 38 (1), 239. doi:10.1186/s13046-019-1249-1

Su, Z., Yang, Z., Xie, L., Dewitt, J. P., and Chen, Y. (2016). Cancer therapy in the necroptosis era. *Cell Death Differ.* 23 (5), 748–756. doi:10.1038/cdd.2016.8

Sung, H., Ferlay, J., Siegel, R. L., Laversanne, M., Soerjomataram, I., Jemal, A., et al. (2021). Global cancer statistics 2020: GLOBOCAN estimates of incidence and mortality worldwide for 36 cancers in 185 countries. *CA Cancer J. Clin.* 71 (3), 209–249. doi:10.3322/caac.21660

Tang, J. Y., Ou-Yang, F., Hou, M. F., Huang, H. W., Wang, H. R., Li, K. T., et al. (2019). Oxidative stress-modulating drugs have preferential anticancer effects - involving the regulation of apoptosis, DNA damage, endoplasmic reticulum stress, autophagy, metabolism, and migration. *Semin. Cancer Biol.* 58, 109–117. doi:10.1016/j.semcancer.2018.08.010

Temel, S. G., Giray, A., Karakas, B., Gul, O., Kozanoglu, I., Celik, H., et al. (2020). RAB25 confers resistance to chemotherapy by altering mitochondrial apoptosis signaling in ovarian cancer cells. *Apoptosis* 25 (11-12), 799–816. doi:10.1007/s10495-020-01635-z

Torre, L. A., Trabert, B., Desantis, C. E., Miller, K. D., Samimi, G., Runowicz, C. D., et al. (2018). Ovarian cancer statistics, 2018. *CA Cancer J. Clin.* 68 (4), 284–296. doi:10.3322/caac.21456

Wang, L., Wang, C., Tao, Z., Zhao, L., Zhu, Z., Wu, W., et al. (2019). Curcumin derivative WZ35 inhibits tumor cell growth via ROS-YAP-JNK signaling pathway in breast cancer. *J. Exp. Clin. Cancer Res.* 38 (1), 460. doi:10.1186/s13046-019-1424-4

Wang, Y., Gao, W., Shi, X., Ding, J., Liu, W., He, H., et al. (2017). Chemotherapy drugs induce pyroptosis through caspase-3 cleavage of a gasdermin. *Nature* 547 (7661), 99–103. doi:10.1038/nature22393

Wu, D., Wang, S., Yu, G., and Chen, X. (2021). Cell death mediated by the pyroptosis pathway with the aid of nanotechnology: Prospects for cancer therapy. *Angew. Chem. Int. Ed. Engl.* 60 (15), 8018–8034. doi:10.1002/anie.202010281

Xing, Z., Wang, X., Liu, J., Liu, G., Zhang, M., Feng, K., et al. (2021). Effects of ulinastatin on proliferation and apoptosis of breast cancer cells by inhibiting the ERK signaling pathway. *Biomed. Res. Int.* 2021, 9999268. doi:10.1155/2021/9999268

Zhengfu, Z., Ying, G., Lingwei, Z., Jianbin, Z., and Xionghui, W. (2012). Chelerythrine chloride from Macleaya cordata induces growth inhibition and apoptosis in human gastric cancer BGC-823 cells. *Acta Pharm. Sin. B* 2 (5), 464–471. doi:10.1016/j.apsb.2011.12.013

Zhu, J., Yu, W., Liu, B., Wang, Y., Shao, J., Wang, J., et al. (2017). Escin induces caspase-dependent apoptosis and autophagy through the ROS/p38 MAPK signalling pathway in human osteosarcoma cells *in vitro* and *in vivo*. *Cell Death Dis.* 8 (10), e3113. doi:10.1038/cddis.2017.488

Zhu, M., Cui, Y., Yang, L., Yang, T., Wang, H., Zhang, D., et al. (2019). Ephrin type-B receptor 4 affinity chromatography: An effective and rapid method studying the active compounds targeting Ephrin type-B receptor 4. *J. Chromatogr. A* 1586, 82–90. doi:10.1016/j.chroma.2018.12.005

frontiers | Frontiers in Pharmacology

TYPE Original Research
PUBLISHED 15 June 2023
DOI 10.3389/fphar.2023.1098915

OPEN ACCESS

EDITED BY
Hai-long Piao,
Chinese Academy of Sciences (CAS), China

REVIEWED BY
Han-Li Huang,
Taipei Medical University, Taiwan
Biqiang Zhu,
Huazhong University of Science and Technology, China

*CORRESPONDENCE
Wen-Bo Meng,
mengwb@lzu.edu.cn
Jian-Jun Chen,
chenjj@lzu.edu.cn
Kun Gao,
npchem@lzu.edu.cn

†These authors have contributed equally to this work

RECEIVED 15 November 2022
ACCEPTED 31 May 2023
PUBLISHED 15 June 2023

CITATION
Zhang C, Yang H-Y, Gao L, Bai M-Z, Fu W-K, Huang C-F, Mi N-N, Ma H-D, Lu Y-W, Jiang N-Z, Tian L, Cai T, Lin Y-Y, Zheng X-X, Gao K, Chen J-J and Meng W-B (2023), Lanatoside C decelerates proliferation and induces apoptosis through inhibition of STAT3 and ROS-mediated mitochondrial membrane potential transformation in cholangiocarcinoma.
Front. Pharmacol. 14:1098915.
doi: 10.3389/fphar.2023.1098915

Lanatoside C decelerates proliferation and induces apoptosis through inhibition of STAT3 and ROS-mediated mitochondrial membrane potential transformation in cholangiocarcinoma

Chao Zhang[1,2†], Hong-Ying Yang[3†], Long Gao[1,4†], Ming-Zhen Bai[1,4†], Wen-Kang Fu[1,4], Chong-Fei Huang[1,4], Ning-Ning Mi[1,4], Hai-Dong Ma[1,4], Ya-Wen Lu[1,4], Ning-Zu Jiang[1,4], Liang Tian[1,4], Teng Cai[1,4], Yan-Yan Lin[1,4], Xing-Xing Zheng[5], Kun Gao[3]*, Jian-Jun Chen[3]* and Wen-Bo Meng[1,4]*

[1]The First Clinical Medical College, Lanzhou University, Lanzhou, Gansu, China, [2]Department of Orthopedics, The First Hospital of Lanzhou University, Lanzhou, Gansu, China, [3]State Key Laboratory of Applied Organic Chemistry, College of Chemistry and Chemical Engineering, Lanzhou University, Lanzhou, China, [4]Department of General Surgery, The First Hospital of Lanzhou University, Lanzhou, Gansu, China, [5]Department of Ophthalmology, The Second Hospital of Lanzhou University, Lanzhou, Gansu, China

Introduction: The incidence of cholangiocarcinoma (CCA) has increased worldwide in recent years. Given the poor prognosis associated with the current management approach of CCA, new therapeutic agents are warranted to improve the prognosis of this patient population.

Methods: In this study, we extracted five cardiac glycosides (CGs) from natural plants: digoxin, lanatoside A, lanatoside C, lanatoside B, and gitoxin. Follow-up experiments were performed to assess the effect of these five extracts on cholangiocarcinoma cells and compounds with the best efficacy were selected. Lanatoside C (Lan C) was selected as the most potent natural extract for subsequent experiments. We explored the potential mechanism underlying the anticancer activity of Lan C on cholangiocarcinoma cells by flow cytometry, western blot, immunofluorescence, transcriptomics sequencing, network pharmacology and *in vivo* experiments.

Results: We found that Lan C time-dependently inhibited the growth and induced apoptosis of HuCCT-1 and TFK-1 cholangiocarcinoma cells. Besides Lan C increased the reactive oxygen species (ROS) content in cholangiocarcinoma cells, decreased the mitochondrial membrane potential (MMP) and resulted in apoptosis. Besides, Lan C downregulated the protein expression of STAT3, leading to decreased expression of Bcl-2 and Bcl-xl, increased expression of Bax, activation of caspase-3, and initiation of apoptosis. N-acetyl-L-cysteine (NAC) pretreatment reversed the effect of Lan C. *In vivo*, we found that Lan C inhibited the growth of cholangiocarcinoma xenografts without toxic effects on normal

cells. Tumor immunohistochemistry showed that nude mice transplanted with human cholangiocarcinoma cells treated with Lan C exhibited decreased STAT3 expression and increased caspase-9 and caspase-3 expression in tumors, consistent with the *in vitro* results.

Conclusion: In summary, our results substantiates that cardiac glycosides have strong anti-CCA effects. Interestingly the biological activity of Lan C provides a new anticancer candidate for the treatment of cholangiocarcinoma.

KEYWORDS

Lanatoside C, cholangiocarcinoma, reactive oxygen species, mitochondrial membrane potential, stat3, apoptosis

Background

Cholangiocarcinoma (CCA) is an epithelial tumor occurring in the intrahepatic or extrahepatic bile duct with bile duct cell differentiation, anatomically divided into intrahepatic cholangiocarcinoma (iCCA), periportal cholangiocarcinoma (pCCA) and distal cholangiocarcinoma (dCCA) (Razumilava and Gores, 2014). Each subtype is associated with different risk factors, molecular pathogenesis, treatment options and prognosis (Kelley et al., 2020). Current evidence suggests that pCCA has a poor prognosis, with a median survival of fewer than 2 years for patients with advanced disease (Rizvi and Gores, 2013). For the three anatomical subtypes, surgical resection and liver transplantation represent the mainstay of treatment (Rodrigues et al., 2021). However, the median 5-year survival rate after CCA resection is only 30%. Liver transplantation as represents a treatment modality indicated only for iCCA and pCCA. According to an international multicenter study, the 5-year survival rate of liver transplantation was 65% for very early-stage iCCA (tumor size less than 2 cm) compared to 45% for the advanced group (tumor size greater than 2 cm). Despite these encouraging results, most patients presented with advanced-stage disease at diagnosis (Mazzaferro et al., 2020). Standard systemic chemotherapy with gemcitabine and cisplatin is indicated is indicated for patients who are not surgical resection or liver transplantation candidates. However, the median survival for this combination chemotherapy regimen is only 11.7 months (Sato et al., 2020). Moreover, no specific targeted molecular therapies have hitherto been approved for CCA. The poor efficacy of conventional chemotherapeutic compounds and the development of their resistance, has boosted interest traditional compounds and their extracts. The antitumor activity of gentian biosides against 10 lung cancer cells was evaluated by *in vitro* experiments. They found that gentian glycosides inhibited tumor cell proliferation and induced apoptosis by regulating the Bax/Caspase-9/Caspase-3 cell pathway (Chen et al., 2017). Besides, it has been established that curculigo saponin I inhibits the proliferation of osteosarcoma cells by inactivating the Wnt/β-catenin pathway, blocks the cell cycle in the G2/M phase, induces apoptosis and inhibits the invasion and migration of osteosarcoma cells (Chang et al., 2017). Besides, curcumol reportedly plays an anticancer effect on cholangiocarcinoma cells by downregulating CDKL3 (Zhang et al., 2018). In addition, a recent study revealed that radix astragali extract is cytotoxic and inhibits cholangiocarcinoma cell proliferation (Wang et al., 2020). An increasing body of evidence from recently published literature suggests that cardiac glycosides are selectively cytotoxic to cancer cells, which has generated interest in their use as anticancer molecules (Hu et al., 2018; Reddy et al., 2019).

It is widely acknowledged that cardiac glycosides are found in *D. lanata* Ehrh (Kreis, 2017). Currently, the pharmaceutical industry still relies on natural resources, and cardiac glycosides of digitalis origin remain a source of cardiac compounds for clinical practice. For example, the cardiac glycosides digoxin and digitalis toxin for the treating congestive heart failure and arrhythmias can be isolated from the leaves of this plant. Compared to other plants of the genus trichoderma, *Digitalis lanata* has a higher content of cardiac glycosides (Ehle et al., 2011). Cardiac glycosides are compounds of natural origin with steroid and glycone fractions in their structure. Interestingly cardiac glycoside analogs can inhibit subunits of the prevalent transmembrane protein Na+/K + - ATPase (Yan and Shapiro, 2016). Overwhelming evidence substantiates that CGs could block lung cancer cells at G0/G1 phase in a dose-dependent manner, thereby inhibiting cancer cell proliferation (Kaushik et al., 2017). A study revealed that targeting FXYD2 by cardiac glycosides could potently block tumor growth in ovarian clear cell carcinoma (Hsu et al., 2016). In another study, cardiac glycosides induced mitotic arrest and apoptosis in colorectal cancer HT-29 cells through HIF-1α and NF-κB-mediated downregulation of Plk1 expression (Xie et al., 2013). Studies on the anti-cancer effects of cardiac glycosides have substantiated that these compounds have heterogeneous effects on different tumors, and their possible mechanisms of action are different (Pratt et al., 2018; Rasheduzzaman et al., 2019). However, the effects of these compounds on CCA have rarely reported in the literature. Therefore, this study was conducted to investigate the inhibitory effects of cardiac glycosides on CCA and the underlying mechanisms in the quest, to find new candidate compounds for the treatment of cholangiocarcinoma.

Herein, we explored the anticancer effects of Lan C on CCA. We revealed that Lan C could inhibit proliferation and induce apoptosis of CCA cells. Besides, we investigated the potential mechanisms of the cytotoxic effects of Lan C and identified the regulatory role of ROS in the apoptotic process. Overall, the present study provides preliminary evidence that Lan C induces apoptosis in CCA cells by affecting ROS expression, thereby regulating changes in mitochondrial membrane potential.

Methods

Reagents and cell culture

Compounds (Y1-Y5) were dissolved in dimethyl sulfoxide and stored at −20°C. N-acetyl-L-cysteine (NAC) was purchased from Sigma (St.Louis, MO, United States). Antibodies, including anti-GAPDH, m-IgGκ BP-HRP and mouse anti-rabbit IgG-HRP, were purchased from Santa Cruz Biotechnology (Santa Cruz, CA, United States). Antibodies, including anti-Bcl-2, anti-Bcl-xl, anti-Bax, anti-caspase-3, anti-cleaved-PARP and anti-STAT3, were purchased from Cell Signaling Technology (Danvers, MA, United States). Antibodies, including anti-caspase-9, were purchased from Abcam (Cambridge, MA, United States). FITC Annexin V apoptosis Detection Kit I and Propidium Iodide (PI) were purchased from BD Pharmingen (Franklin Lakes, NJ, United States). Human cholangiocarcinoma cell line HuCCT-1 was purchased from Shanghai Fu Heng Biological, and TFK-1 was purchased from Creative Bioarray in the United States. HuCCT-1 is a well-established intrahepatic cholangiocarcinoma cell line, that causes iCCA, while TFK-1 is an extrahepatic cholangiocarcinoma cell line, that causes pCCA and dCCA. The cells were maintained in RPMI-1640 medium containing 10% fetal bovine serum (FBS) at 37 °C in a humidified incubator with a 5% CO_2 atmosphere. The NMR spectra were recorded on a Bruker AVANCE NEO-600 spectrometer. Semipreparative HPLC was carried out on a Waters 1,525 with a reversed-phase C18 (150 × 10 mm, 10 μm) column and Waters 2,998 photodiode array detector. Microporous resins, Sephadex LH-20, and silica gel for crude extract or fractions were purchased from Qingdao Marine Chemical Inc.

Extraction and isolation of compounds Y1-Y5

The leaves of *D. lanata* were collected in September 2016 at Wuhu City, Anhui Province, P. R. China. The plant was authenticated by Dr. Jian-Yin Li from the School of Pharmacy, Lanzhou University. A voucher specimen (accession number: 20160912) was deposited at the School of State Key Laboratory of Applied Organic Chemistry, College of Chemistry and Chemical Engineering, Lanzhou University. The dried leaves of *D. lanata* (15 kg) were extracted with methanol, concentrated under reduced pressure and vacuum dried. The extract (3.5 kg) was partitioned with EtOAc (420 g). Subsequently, the EtOAc fraction was separated with D101 macroporous resin column chromatography and eluted with H_2O/MeOH system (100:0, 70:30, 50:50,20:80, 0:100 v/v) to give four fractions (Fr.A–Fr.D). Fr.D (80% MeOH/H_2O) underwent silica gel column chromatography (CH_2Cl_2/MeOH (20:1 to 1:1, v/v)) to yield Fr.D1-Fr.D4. Sephadex LH-20 was used to separate Fr.D1–Fr.D4. Compounds Y2 (Lanatoside A, 2.3 g), Y3 (Lanatoside C, 3.5 g) and Y4 (Lanatoside B, 900 mg) were obtained from Fr.D4 by recrystallization at the mixed solution of CH_2Cl_2/MeOH. The supernate of Fr.D4 was purified by semipreparative HPLC to obtain compound Y1 (digoxin, 300 mg). Compound Y5 (gitoxin, 850 mg) was crystallized in a solution of CH_2Cl_2/MeOH at fraction Fr.D3.

Toxicity testing

We first determined the structures of five compounds and then treated two cholangiocarcinoma cell lines with these five compounds: HuCCT-1, an intrahepatic cholangiocarcinoma cell line, and TFK-1, an extrahepatic cholangiocarcinoma cell line.

The compounds were diluted to different concentrations and their inhibition rates were determined by CCK-8 method. The concentration of the compound was taken as the abscissa and the inhibition rate as the ordinate. The concentration of a compound with a inhibition rate of 50% is indicated by IC50. The lower the IC50 value, the stronger the inhibitory effect of the compound on tumor cells. Therefore, ideal compounds were selected based on IC50 for follow-up studies. When this compound was selected, wound healing and transwell assays were performed to further verify its effect. At the same time, CCK-8 assay was performed on human intrahepatic bile duct epithelial cell (HIBEpiC) to observe the toxic effects of the selected compounds on normal cells.

Live-cell imaging

HuCCT-1 and TFK-1 cells were separated into control and experimental groups. The experimental group was treated with Lan C and incubated in a live cell imager for 48 h. The cell growth was observed at 0, 12, 24, and 48 h to assess the effect of Lan C on cholangiocarcinoma cells.

Cell apoptosis and cycle analysis by flow cytometry

Cholangiocarcinoma cells were treated with Lan C for 48 h; then, the cells were harvested and washed twice with PBS on ice. The washed cell samples were resuspended in 500 μL of binding buffer, and Annexin V and propidium iodide (PI) were double-stained in the binding buffer for 30 min by FACSCalibur flow cytometer to observe cell apoptosis and cycle change. In some experiments, cells were pretreated with 5 mM NAC for 2 h prior to exposure to Lan C, and changes in apoptosis of two types of cholangiocarcinoma cells were analyzed at this time. In addition, we also observed the effect of Lan C on HIBEpiC apoptosis.

Tunel cell apoptosis analysis

The adherent cholangiocarcinoma cells were cultured for 24 h, and the culture medium containing Lan C was added to the experimental group. After an additional 48 h of incubation, the medium was discarded, washed once with PBS, and fixed with 4% paraformaldehyde for 30 min. After washing once with PBS, PBS containing 0.3% Triton X-100 was added and incubated for 5 min at room temperature. They were washed twice with PBS. 50 μL of TUNEL assay solution was added to the samples and incubated at 37°C for 60 min in the dark. Cells were washed three times with PBS. Nuclei were counterstained with DAPI working solution and incubated at room temperature in the dark for

5 min. Cells were washed three times with PBS. The slides were sealed with an anti-fluorescence quenching blocking solution and observed under a fluorescence microscope.

Transcriptomics sequencing and data analysis

Human cholangiocarcinoma cells HuCCT-1 were cultured to the logarithmic growth phase and divided into control and experimental groups. Three samples from each group were prepared for the experiment. The experimental group was cultured in a medium containing Lan C (dissolved in DMSO) for 48 h, the control group was cultured for 48 h in a medium containing the same concentration of DMSO. The adherent cells were trypsinized, centrifuged and suspended in PBS, centrifuged again, and the cell precipitate was collected. 1 mL of Trizol lysate was added to the cell precipitate, cells were gently blown evenly, then blown into the EP tube and sealed. The cells were transported in dry ice for sequencing. After rRNA was extracted, the sequencing library was prepared according to Illumina TruSeq RNA sample preparation guidelines (Illumina, San Diego, California, United States). Once the double-stranded cDNA was synthesized, the index connector was connected. After size selection using Agencurt AMPure XP (Beckman), Qubit 2.0 Fluorometer with Qubit dsDNA HS Analysis Kit (Invitrogen, Eugene, OR, United States) and Agilent Bioanalyzer Quantitative and qualitative library (Agilent Technologies, Santa Clara, CA, United States), submit the sample to Illumina HiSeq X-10 (Illumina, San Diego, CA, US) for double-ended sequencing. Quality control and filtering of fastq data were performed using fastq (Chen et al., 2018). Paired-end reads were then mapped to GRCh38 human reference genome using via the Hisat2 tool (version 2.1.1) (Kim et al., 2015). Using the DESeq package (Anders and Huber, 2013) (version 1.8.3) of R software (version 4.1.0), the transcriptome sequencing results were subjected to differential expression analysis according to criteria: |log2 (FoldChange)| > 1 and significant p-value < 0.05. To clarify the potential biological significance of the differential genes, we used the topGO package (version 2.24.0) to perform GO enrichment analysis. GO analysis was used to preliminarily understand the cellular localization, molecular functions and enriched biological processes of the differentially expressed genes. Gene function was based on the following categories: Molecular Function (MF), Cellular Component (CC) and Biological Process (BP). In addition, KEGG signal pathway enrichment analysis provides a better understandind of the biological function of genes, signal transduction pathways, *etc.* The genes were blasted onto the KEGG pathways database using the KAAS webserver (Moriya et al., 2007). Significantly enriched pathways were identified with a p-value <0.05.

Network pharmacology

The target genes of Lan C were predicted using SwissTargetPrediction and Comparative Toxicogenomics Database (CTD). The intersection of the target genes and the differentially expressed genes of transcriptome sequencing was obtained. Next, we performed protein-protein interaction network analysis on the intersected genes using the STRING database to analyze the hub genes in the network. Next, the candidate target protein was selected for molecular docking. We downloaded the 2D structures of compounds from the PubChem database (https://pubchem.ncbi.nlm.nih.gov/) and imported them into Chem3D software to minimize energy (MM2 force field) and converted them into 3D structures. Next, using AutoDock tools 1.5.6, the obtained 3D structures were modified by the addition of hydrogens and protonation. We retrieved the 3D structure of the protein from the Protein Data Bank (PDB) (http://www.rcsb.org/), and imported it into the software Pymol and modified it by removing water molecules, co-crystallized ligand and ions. Subsequently, missing hydrogens and Kollman partial charges were added, non-polar hydrogens were merged to their corresponding carbons. AutoDock tools 1.5.6 was used to construct mating pockets of docking. When constructing the mating box, the spacing (angstrom) was set to 1, the center was set on the macromolecule, and the number of points on the x-, y-, and z-dimension were set to make the protein completely covered by the mating box. Autodock tools was used to preprocess the 3D structures of targets and small molecules, Autodock Vina was utilized for docking, and Pymol software was used to visualize the docking results.

Western blot

Cholangiocarcinoma cells treated with Lan C for 48 h were homogenized in a protein lysis buffer, centrifuged at 12,000 g for 10 min at 4°C to remove debris, and the protein concentration of the whole cell extract was determined using the Bradford protein assay (Bio-Rad, CA, United States). Equal amounts of lysed proteins were separated by SDS-polyacrylamide gel electrophoresis and electroblotted on polyvinylidene fluoride membranes. The membranes were blocked with 5% nonfat milk for 2 h at room temperature in TBST, followed by incubation with specific primary antibodies (including rabbit anti-Bcl-xl (1: 1,000,CST, United States), rabbit anti-Bax (1: 1,000, CST, United States), mouse anti-Bcl-2 (1: 1,000,CST, United States), rabbit anti-caspase-3 (1: 1,000,CST, United States), mouse anti-STAT3 (1: 1,000,CST, United States), rabbit anti-p-STAT3 (1: 1,000,CST, United States) and mouse anti-caspase-9 (1: 500, Abcam, United States), rabbit anti-Cleaved PARP (1:1,000,CST, United States), mouse anti-GAPDH (1:5,000, Proteintech, United States)) in TBST overnight at 4°C. After 3 washes with TBST, the cells were incubated with secondary antibody [HRP-conjugated anti-rabbit or anti-mouse IgG (1: 3,000, CST, United States)] for 1 h, and immunoreactive bands were visualized using an ECL kit, and detected by the ChemiDoc MP Imaging System (Bio-Rad, California, United States). The band intensity of proteins was quantified using ImageJ software (National Institutes of Health, MD, United States), and the relative protein expression was normalized to GAPDH expression. In some experiments, cells were pretreated with 5 mM NAC for 2 h before exposure to Lan C, and the expression

of the above proteins in two types of cholangiocarcinoma cells was verified by this method.

Measurement of reactive oxygen species production

Cells were plated in 6-well plates overnight in a complete medium, and then treated with Lan C-containing medium for 48 h. Cells were stained with 10 μM DCFH-DA (Beyotime, Shanghai, China) for 30 min at 37°C in the dark. Cells were collected and analyzed for fluorescence by immunofluorescence and flow cytometry. In some experiments, cells were pretreated with 5 mM NAC for 2 h prior to exposure to Lan C and analyzed for trends in ROS.

Mitochondrial membrane potential assay

The changes of JC-1 in cells were detected by flow cytometry to reflect the changes in mitochondrial membrane potential. Cells were plated in 6-well plates overnight in a complete medium. It was then treated with Lan C-containing medium for 48 h. Cells were stained with 10 μM DCFH-DA (Beyotime, Shanghai, China) for 30 min at 37°C in the dark. Cells were collected and analyzed by immunofluorescence and flow cytometry assays. In some experiments, cells were pretreated with 5 mM NAC for 2 h prior to exposure to Lan C and changes in mitochondrial membrane potential were verified by analysis of JC-1.

In Vivo antitumor studies

In vivo experiments were performed using athymic nude mice (Balb/c nu, 4–5 weeks, male). All experimental animal protocols were approved by the Ethics Committee of the First Hospital of Lanzhou University. The experimental animals were randomly divided into control group, NAC + Lan C group, and Lan C group, with 6 nude mice in each group. Animals were housed at constant room temperature on a 12-h light/12-h dark cycle and fed standard water and rodent chow. The right forelimb of the mouse was injected subcutaneously with HuCCT-1 cells (5×10^6 cells, 100 μL serum-free RPMI-1640. When the tumor reached 5 mm^3, the control group was given gavage with 100 μL PBS/d, the Lan C group was given gavage with 40 mg/kg/d and volume of 100 μL, and the NAC + Lan C group was given gavage with 100 mg/kg/d of NAC 2 h before Lan C, the content of DMSO in the three groups was the same. The length (L) and width (W) of the tumor were measured weekly, and the volume of the tumor was calculated ($V = 0.5 \times L \times W^2$). After the experiment, the animals were sacrificed with excess pentobarbital sodium, the tumors were removed and weighed.

Immunohistochemical

Briefly, the tumor specimens from three groups of mice were fixed in a 4% formaldehyde solution, dehydrated, transparent, and embedded in paraffin for further assay. Paraffin-embedded tissue was cut into 4 μm-thick sections. The sections were first dewaxed, hydrated, and antigenically repaired. Then, the sections were incubated in 3% H_2O_2 for 15 min at 37°C to inhibit endogenous peroxidase. Next, the sections were blocked using 10% goat serum at room temperature for 30 min, then incubated with the primary antibody overnight at 4°C. Primary antibodies included rabbit anti-caspase-3 (1:100, CST, United States), mouse anti-STAT3 (1: 500, CST, United States), and mouse anti-caspase-9 (1: 100, Abcam, United States). On the second day, the sections were incubated with the secondary antibody for 30 min, and then incubated with DAB and hematoxylin. Finally, tissue sections were photographed for analysis.

Statistical analysis

The data were presented as the means ± standard deviations (SD). The Student's t-test was used to analyze the differences between the two groups. Comparison among three or more groups was conducted using a one-way analysis of variance (ANOVA) followed by Tukey test. A two-side p-value <0.05 was considered statistically significant. All *in vitro* experiments were repeated three times.

Results

Extraction and structural formula of compounds

After isolation and purification, we isolated five compounds from *D. lanata*: Y1-Y5, and were identified as digoxin (Y1), lanatoside A (Y2), lanatoside C (Y3), lanatoside B (Y4) and gitoxin (Y5), (Figure 1). Their structures were elucidated by comparing their NMR spectral data with the literature (Lehtola et al., 1981; Ren et al., 2020) (Supplementary Figure S1, Supplementary Table S1). The IC50 value of Lan C in HIBEpiC was significantly higher than that in the two bile duct cancer cells, suggesting that Lan C is safe (Supplementary Figure S2).

Lan C inhibits the proliferation of cholangiocarcinoma cells and has strong anticancer activity

The results of the CCK-8 assay showed that five compounds were cytotoxic action to the HuCCT-1 and TFK-1 (Figures 2A, B). Based on the results of IC_{50}, Lan C was finally selected as an ideal compound for subsequent studies. Wound healing and transwell assay confirmed that the viability of HuCCT1 and TFK-1 cells decreased significantly after Lan C treatment (Figures 2C–G). However, the cytotoxic effect on HIBEpiC cell was less (Supplementary Figure S3). The live cell imaging assay showed that the increase of cholangiocarcinoma cells in the experimental group was significantly inhibited compared with the control group. Representative images of HuCCT-1 and TFK-1 cells at 0, 12, 24, and 48 h were acquired in Cytation 5 (Supplementary Figures S4A–D). Our work reveals that Lan C has strong anti-cholangiocarcinoma activity.

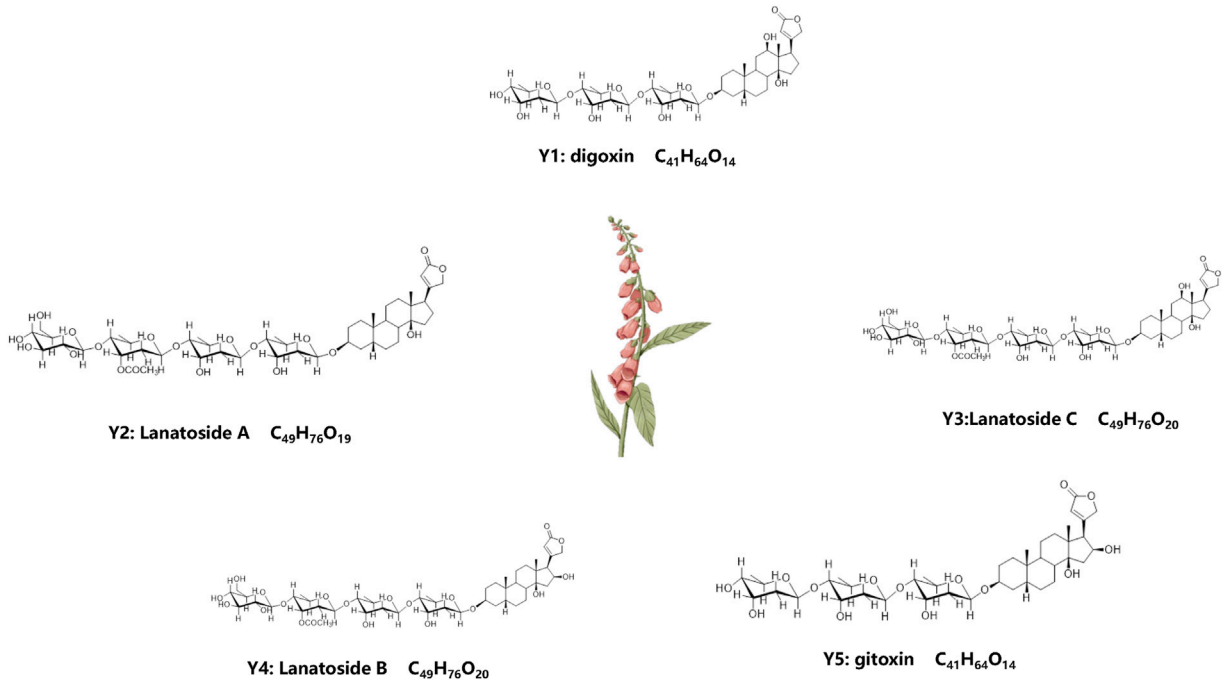

FIGURE 1
Molecular formula and chemical structure of 5 compounds extracted from plant D. lanata. Y1: Digoxin, Y2: Lanatoside A, Y3: Lanatoside C, Y4: Lanatoside B, Y5: Gitoxin.

Lanatoside C induced cholangiocarcinoma cell cycle arrest and apoptosis

Given that cell proliferation depends on cell cycle progression, we therefore investigated the cell cycle phase distribution in Lan C treated HuCCT-1 and TFK-1 cells. Significantly increase in S/G2 phase proportion was observed in cells treated with Lan C compared with control group (Figures 3A–C). Quantitative results showed that Lan C blocked HuCCT-1 and TFK-1 cell cycle progression in S/G2 phase (Figures 3B–D). Usually the anti-proliferation activity was correlated with cell apoptotic response. After 48 h of Lan C treatment, increase in the proportion of apoptosis was observed in both HuCCT-1 and TFK-1 cells (Figures 3E–G). This was also confirmed by quantitative results (Figures 3F–H). Interestingly, these results were significantly inhibited when cells were pretreated with 5 mM NAC for 2 h before exposure to Lan C, confirming ROS involvement in the pro-apoptotic effect of Lan C (Supplementary Figure S5). In addition, we also found that the pro-apoptotic effect of Lan C on HIBEpiC was significantly lower than that on cholangiocarcinoma cells (Supplementary Figure S6). To further demonstrate the promoting effect of Lan C on apoptosis of HuCCT-1 and TFK-1 cells, we performed TUNEL experiments to reveal the apoptosis-inducing effect of Lan C (Figures 3I, J). Taken together, these results suggest that Lan C exhibits significant anticancer activity by inhibiting proliferation and inducing apoptosis of cholangiocarcinoma cells, but has no significant toxic effect on HIBEpiC.

Transcriptomics and network pharmacology analysis revealed that lan C targets STAT3

Transcriptomics and network pharmacology analysis revealed that Lan C targeted STAT3. Utilizing high-throughput transcriptomics sequencing, a total of 8,859 differentially expressed genes (DEGs) were obtained by volcano plot (Figure 4A). We performed functional enrichment analysis to explore the pathways associated with DEGs. The results showed that DEGs were mainly enriched to 2735 GO terms (top 10 of GO terms shown in Figure 4B) and 90 KEGG pathways (top 20 shown in Figure 4C). We obtained 42 target genes of Lan C utilized Comparative Toxicogenomics Database (https://ctdbase.org/) and SwissTargetPrediction (http://www.swisstargetprediction.ch/) database. A Venn diagram showing the intersection of the 25 genes from the two datasets (Figure 4D). We used the STRING database (https://cn.string-db.org/) to explore the protein-protein interaction (Figure 4E) and the top 15 ranked proteins were presented (Figure 4F). We also plotted heatmap of those genes using ggplot2 package (Figure 4G). STAT3 was obtained by PPI network analysis and verified further. Finally, we performed compound Lanatoside C and STAT3 molecular docking, the binding affinity for target protein was −10.1 (Figure 4H). These results were strongly demonstrated in subsequent Western blotting analysis. Lan C inhibited STAT3 expression, which favored the downregulation of Bcl-2 and Bcl-xl and increased the expression of Bax. Meanwhile, the decrease in mitochondrial membrane potential activated caspase-9 and caspase-3. Ultimately, Lan C promoted apoptosis in cholangiocarcinoma cells (Figures 5A–C).

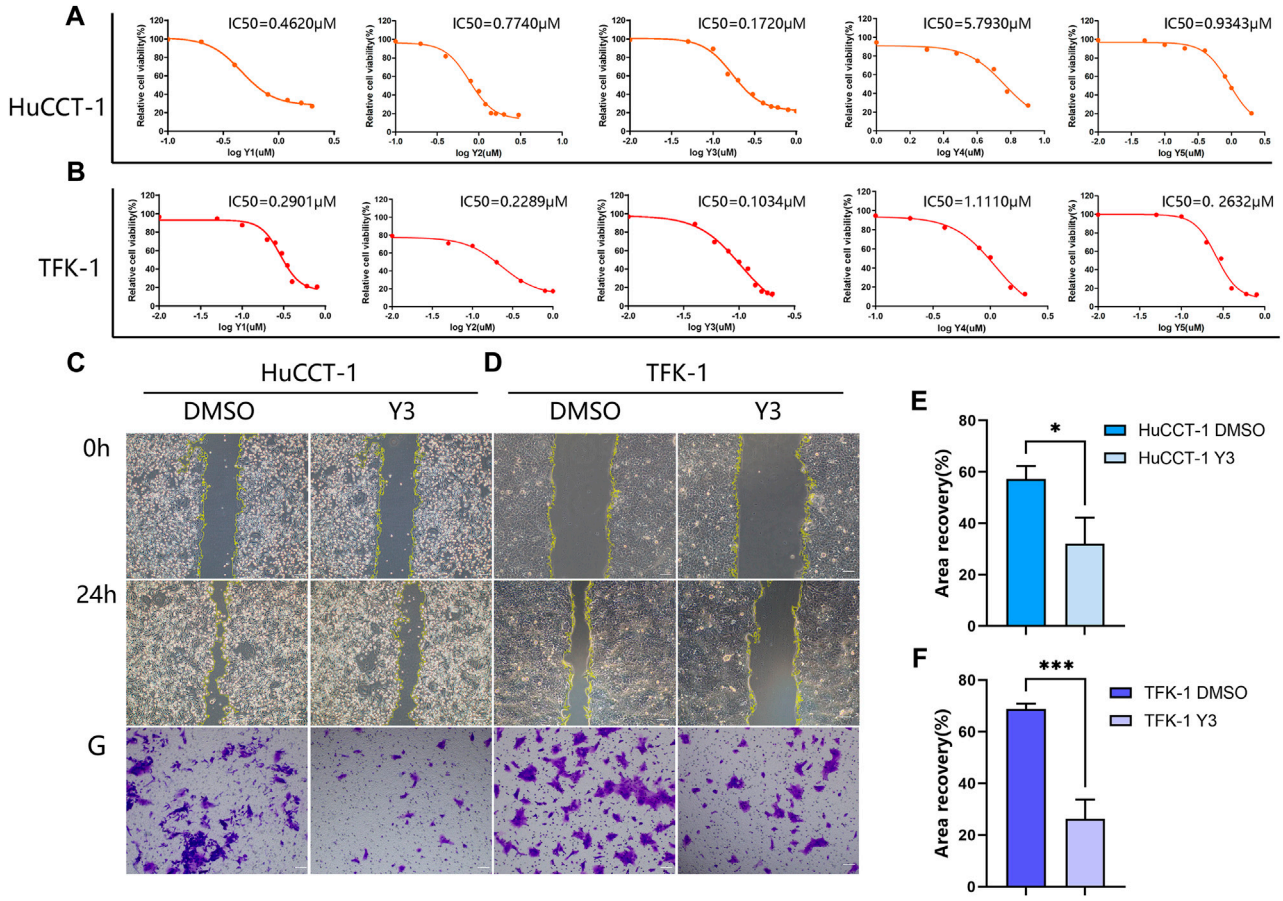

FIGURE 2
Lan C inhibited the proliferation of CCA. **(A, B)** The IC_{50} values of five drugs (Y1-Y5) in HuCCT-1 and TFK-1 cell lines. **(C, E)** Representative images of wound healing after 24 h of Y3 treatment in HuCCT-1 cell, the therapeutic concentration of Y3 was 0.1720 μM. **(D, F)** Representative images of wound healing after 24 h of Y3 treatment in TFK-1 cell, the therapeutic concentration of Y3 was 0.1034uM. **(G)** Representative images of transwell assay after 24 h of Y3 treatment in HuCCT-1 and TFK-1 cell. *Represents *p*-value less than 0.05, ***Represents *p*-value less than 0.001. Scale bars, 100 μm.

Lan C induces oxidative stress in cholangiocarcinoma cells

Current evidence suggests that elevated intracellular reactive oxygen species (ROS) disrupt the integrity of mitochondria, resulting in an intrinsic apoptotic caspase cascade (Rizwan et al., 2020). ROS can act as second messengers, amplifying extracellular signals and delivering them to mitochondria (Yan and Zhao, 2020). Accordingly, we measured ROS levels in cholangiocarcinoma cells treated with Lan C by immunofluorescence. The experimental results confirmed that Lan C treatment resulted in increased ROS levels in HuCCT-1 and TFK-1 cells (Figures 5D, E). NAC is an inhibitor of ROS and can effectively inhibit the effect of ROS (Saxena et al., 2019). This was confirmed by flow cytometry, pretreatment of cells with NAC significantly reversed Lan C induced increase in ROS levels. Removal of ROS significantly attenuated Lan C induced growth inhibition of HuCCT-1 and TFK-1 cells (Figures 6A–D). These results suggest that ROS generation is a key regulator of Lan C induced apoptosis in cholangiocarcinoma cells.

Changes in mitochondrial membrane potential (MMP) are involved in Lan C induced apoptosis in cholangiocarcinoma cells

We analyzed the effect of MMP in CCA cells treated with Lan C by detecting the changes of JC-I in CCA cells. Immunofluorescence analysis showed that JC-1 was present in the mitochondria of HuCCT-1 and TFK-1 cells as a polymer with bright red fluorescence. In contrast, CCA cells treated with Lan C exhibited decreased mitochondrial membrane potential, and JC-1 was not present in the mitochondrial matrix as a polymer. Green fluorescence in the cytoplasm was significantly enhanced, substantiating that the mitochondrial membrane potential was involved in the apoptosis of CCA cells (Figures 5F, G). Flow cytometry and their quantitative data also confirmed that the amount of JC-1 monomers was significantly increased in HuCCT-1 and TFK-1 cells treated with Lan C. Interestingly, NAC pretreated cells significantly reversed this outcome (Figures 6E–H).

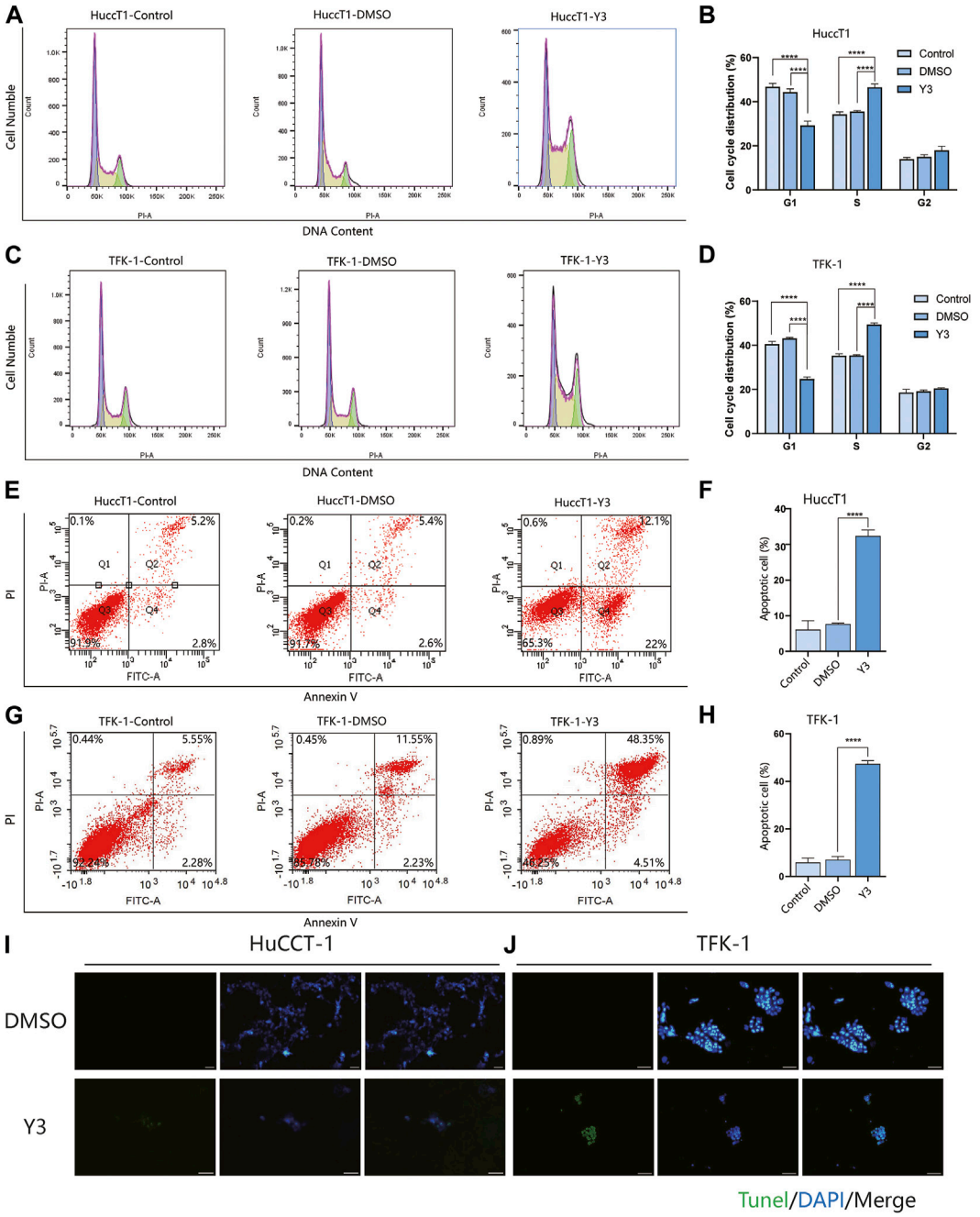

FIGURE 3
Y3 suppresses cell growth and induces apoptosis in CCA cells. **(A, B)** HuCCT-1 cells were treated with Y3 for 48h, and cell cycle distribution was determined by flow cytometry. **(C, D)** TFK-1 cells were treated with Y3 for 48h, and cell cycle distribution was determined by flow cytometry. **(E, F)** The HuCCT-1 cell line was treated with Y3 for 48h, percentage of cell apoptosis was determined by Annexin-V/PI staining and flow cytometry. **(G, H)** The TFK-1 cell line was treated with Y3 for 48h, percentage of cell apoptosis was determined by Annexin-V/PI staining and flow cytometry. **(I, J)** HuCCT-1 and TFK-1 cells were treated with Y3 for 48h, and the changes in apoptosis were detected by TUNEL assay. In the figure, the therapeutic concentration of Y3 for HuCCT-1 cell line was 0.1720uM, and that for TFK-1 cell line was 0.1034uM. ****Represents *p*-value less than 0.0001. Scale bars, 20 μm.

Lan C induced mitochondrial membrane potential is dependent on ROS production in cholangiocarcinoma cells

Our previous studies have demonstrated that Lan C induces apoptosis in CCA cells leading to an increase in intracellular ROS and a decrease in MMP. Nevertheless, it remains unclear whether there is a relationship between ROS and MMP levels. Current evidence suggests that the decrease in mitochondrial membrane potential may be related to intracellular electron leakage resulting in ROS generatio (Odagiri et al., 2009). In a subsequent experiment, we investigated the effect of the ROS inhibitor NAC on Lan C induced

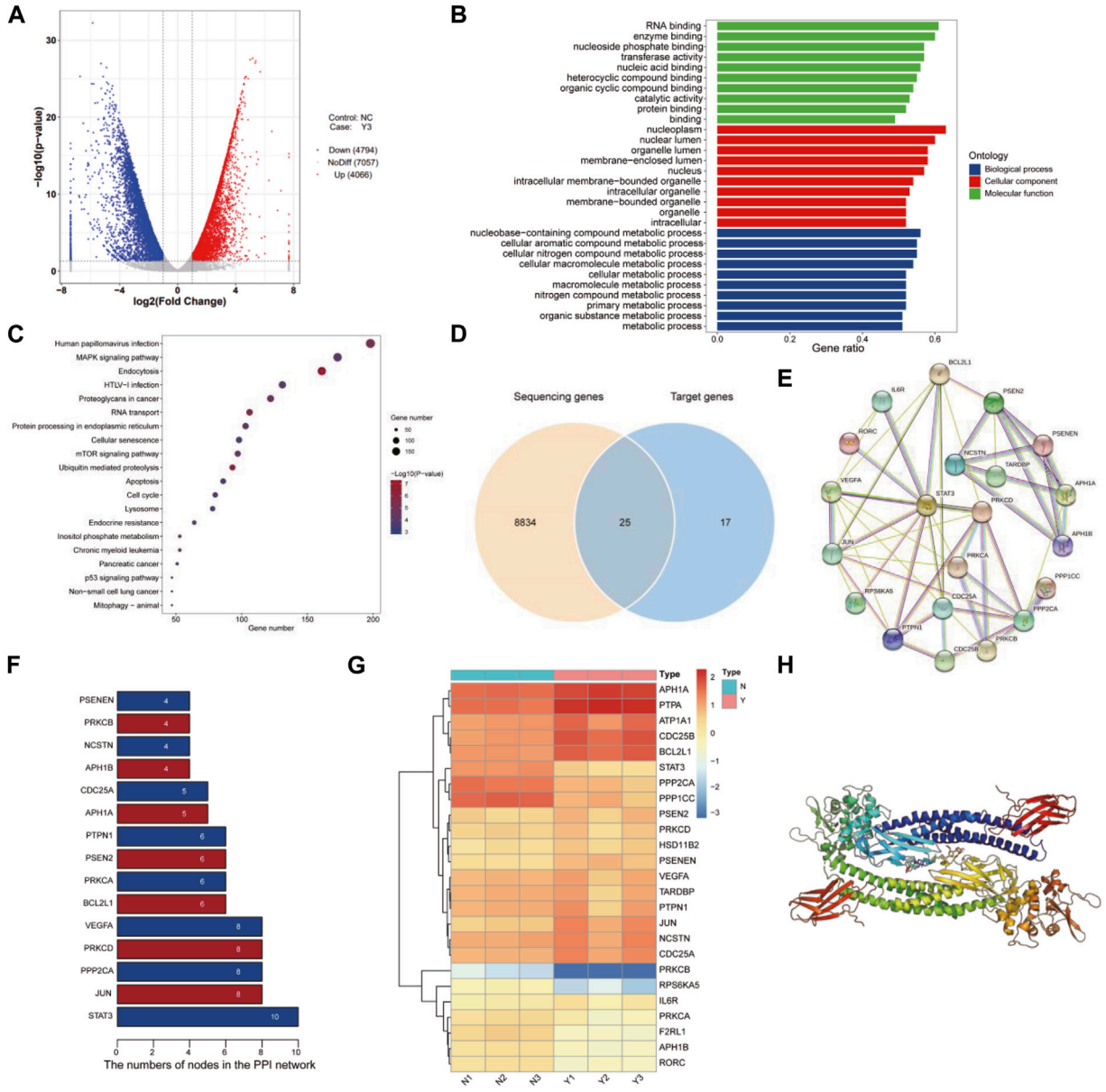

FIGURE 4
Transcriptomic and network pharmacology analyses. **(A)** Volcano plot of differentially expressed genes. **(B)** GO enrichment analysis of differentially expressed genes. **(C)** KEGG enrichment analysis of differentially expressed genes. **(D)** Venn diagram of differentially expressed genes and compound target genes. **(E)** Protein interaction network analysis of intersecting genes. **(F)** Protein interaction network node degree statistics. **(G)** Heat map of intersection genes. The colors of the tiles in the heat map represent the measured expression value of genes, a three color scale is used with steelblue indicating low expression values, yellow indicating intermediately expressed genes, and brown representing highly expressed genes. **(H)** Compound Lanatoside C and STAT3 molecular docking.

apoptosis in cholangiocarcinoma cells by Western blotting. After NAC pretreatment, STAT3 expression was not downregulated in cholangiocarcinoma cells, the expression of p-STAT3 was significantly increased compared with Y3 group, and caspase-3, caspase-9, cleaved PARP expression were significantly inhibited (Figures 5H–J). The same results were confirmed by immunofluorescence (Figures 6I, J). These results suggest that ROS production may be an upstream regulator of Lan C induced changes in mitochondrial membrane potential, ultimately leading to apoptosis in CCA cells.

Lan C inhibits the growth of HuCCT-1 xenograft tumors *in Vivo*

To investigate the effect of Lan C on tumor growth *in vivo*, we used a subcutaneously transplanted HuCCT-1 cell model from immunodeficient mice and performed subsequent experiments using gavage. A 40 mg/kg dose of Lan C significantly reduced the volume and weight of HuCCT-1 tumors compared to controls. Importantly, 42 days of Lan C treatment was well tolerated and did not result in significant weight loss (Figures 7A–C; Supplementary

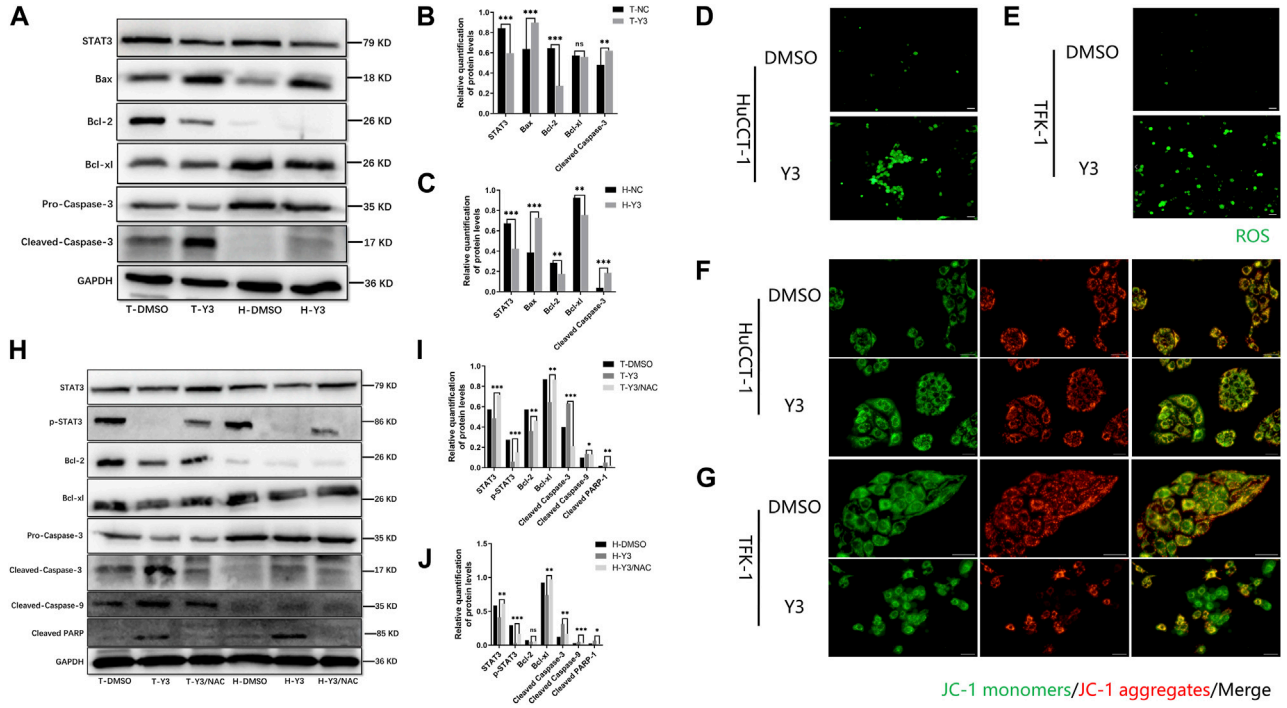

FIGURE 5
Y3 induces apoptosis by inhibiting STAT3 and ROS-mediated mitochondrial membrane potential transformation. WB and immunofluorescence results. **(A–C)** Western blotting analysis of the expression of STAT3 and apoptotic protein Caspase-3, Bax, Bcl-2 and Bcl-xl in HuCCT-1 and TFK-1 cells after 48 h treatment with Y3. GAPDH served as the loading control. **(D, E)** Fluorescence imaging was used to evaluate ROS generation in HuCCT-1 cell and TFK-1 cell after 48 h treatment with Y3. **(F, G)** HuCCT-1 and TFK-1 cells treated with Y3 were stained using JC-1 dye and examined using fluorescence microscopic analysis, green represents JC-1 monomers, red represents JC-1 aggregates, yellow represents merge images. **(H–J)** Western blotting analysis of the expression of STAT3, p-STAT3 and apoptosis related protein in HuCCT-1 cell and TFK-1 cell after treatment with Y3 or Y3+NAC. In the figure, the therapeutic concentration of Y3 for HuCCT-1 cell line was 0.1720uM, and that for TFK-1 cell line was 0.1034uM. *Represents *p*-value less than 0.05, **Represents *p*-value less than 0.01, ***Represents *p*-value less than 0.001, ns represent *p*-value greater than 0.05. Scale bars, 20 μm.

Figure S7). The size of the tumor in nude mice given NAC + Lan C intragastric administration was between the control group and the experimental group, indicating that NAC also inhibited the effect of ROS *in vivo*. Furthermore, we assessed the expression levels of major proteins associated with apoptosis in tumors using immunohistochemical assays. We found that Lan C induced a significant increase in caspase-9 and caspase-3 activity and a significant decrease in STAT3 expression in tumor tissues, consistent with the results *in vitro* experiments (Figures 7D–F).

Lan C inhibits STAT3 expression and promotes apoptosis in cholangiocarcinoma cells mediated by ROS

We treated HuCCT-1 and TFK-1 cells with Lan C and then detected the expression of STAT3 by Western blot. We found that STAT3 expression was significantly reduced in HuCCT-1 and TFK-1 cells after Lan C treatment. In the present study, we observed that downregulation of STAT3 expression resulted in decreased Bcl-2 and Bcl-xl expression, increased Bax expression, activation of caspase-9, cleaved PARP and caspase-3, and the apoptotic cascade was initiated in HuCCT-1 and TFK-1 cells. In addition, pretreatment of HuCCT-1 and TFK-1 cells by NAC reversed the effect of Lan C on STAT3 and downstream apoptosis-related proteins. These results suggest that Lan C may promote apoptosis of cholangiocarcinoma cells by increasing ROS content while inducing a decrease in STAT3 expression (Figure 8). Taken together, these results suggest that Lan C can not only activate caspase-9 and caspase-3 by inducing an increase in ROS, leading to a decrease in mitochondrial membrane potential, but also inhibit STAT3 expression, resulting in a downregulation of Bcl-2 and Bcl-xl expression and an increase in Bax expression, thus promoting apoptosis in cholangiocarcinoma cells. The above results were also confirmed *in vivo*.

Discussion

Cardiac glycosides comprise a large family of naturally derived compounds, such as Lan C, digoxin, digitalis toxin and ouabain, which share a common structural parent. Their core structure consists of a steroidal structure, widely thought to be responsible for the pharmacodynamic activity of these

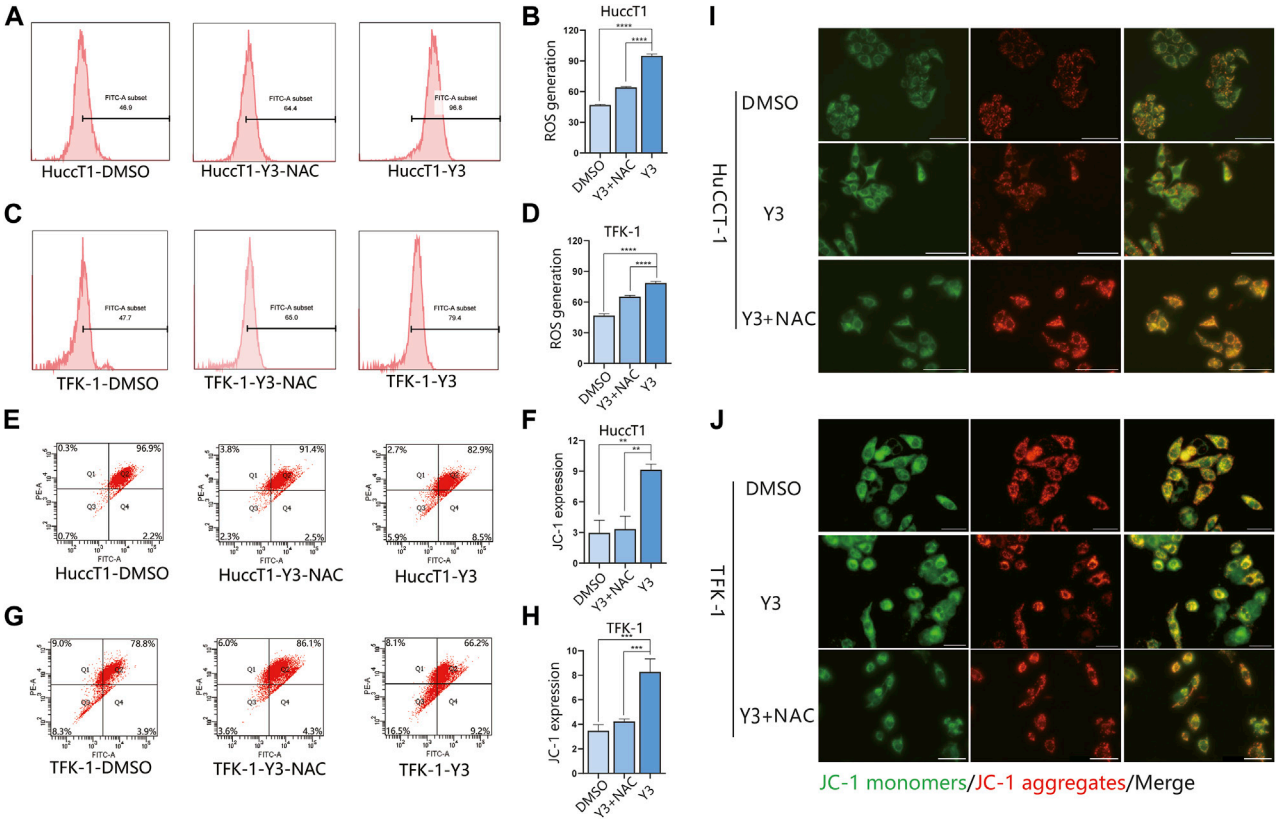

FIGURE 6
Y3 induces apoptosis by inhibiting STAT3 and ROS-mediated mitochondrial membrane potential transformation. Flow cytometry and immunofluorescence results. **(A, B)** HuCCT-1 cell lines were treated with Y3 or Y3+ NAC, and the changes of ROS were determined by flow cytometry. **(C, D)** TFK-1 cell lines were treated with Y3 or Y3+NAC, and the changes of ROS were determined by flow cytometry **(E, F)** HuCCT-1 cells were treated with Y3 or Y3+NAC, Annexin V/PI staining and flow cytometry were used to detect the changes of JC-1. **(G, H)** TFK-1 cells were treated with Y3 or Y3+NAC, Annexin V/PI staining and flow cytometry were used to detect the changes of JC-1. **(I, J)** HuCCT-1 and TFK-1 cells treated with Y3 or Y3+NAC were stained with JC-1 dye, green represents JC-1 monomers, red represents JC-1 aggregates, yellow represents merged images. In the figure, the therapeutic concentration of Y3 for HuCCT-1 cell line was 0.1720uM, and that for TFK-1 cell line was 0.1034uM. **Represents *p*-value less than 0.01. ***Represents *p*-value less than 0.001. ****Represents *p*-value less than 0.0001. Scale bars, 20 μm.

compounds (Whayne, 2018). Lan C and digoxin are closely related structurally, as digoxin can be obtained from the hydrolysis of the acetyl and glucose fractions from Lan C. The main pharmacological effect of cardiac glycosides, which are still widely used in clinical practice, is to inhibit cell membrane Na^+/K^+-ATPase and indirectly enhance myocardial contractility (Hood et al., 2014; Alpert, 2021). Recent studies have shown that several cardiac glycosides exert anticancer activity through different mechanisms, such as the SRC/EGFR/RAS/ERK signaling pathway, p21, NF-κB, AP-1, topoisomerase, and HIF-1 (Biggar et al., 2011; Biggar, 2012; Liu et al., 2020). These results suggest that cardiac glycosides has huge prospects for clinical application as an anticancer drug. In the present study, we explored the antitumor activity of Lan C in CCA and confirmed that Lan C has strong pro-apoptotic activity mediated by two pathways. On the one hand, increased intracellular ROS can induce a decrease in mitochondrial membrane potential, activating the mitochondrial apoptotic pathway. On the other hand, increased ROS inhibits the pro-oncogenic effect of STAT3, which leads to a decrease in Bcl-2 and Bcl-cl levels and an increase in Bax expression, ultimately causing apoptosis in CCA. Taken together, our findings suggest that ROS is an important target for treatment.

The sodium pump is the target of cardiac glycosides, which have long been used in the treatment of heart failure (Katz, 1985). Recent studies have found that sodium pump expression is higher in colon, prostate, pancreatic, lung and breast cancers. Regardless of the tissue origin, the higher the level of sodium pump expression, the more sensitive the cells were to prednisolone treatment (Bagrov et al., 2002; Silva et al., 2021; Cheung and Vousden, 2022). In the present study, Lan C yielded a strong pro-apoptotic effect on cholangiocarcinoma cells, which strongly suggests the high expression of sodium pump is elevated in cholangiocarcinoma cells. It has been reported that cardiac glycosides can induce Src activation and increase ROS production by reducing Na^+/K^+-ATPase activity (Xie and Cai, 2003). Moreover, excess ROS can disrupt the antioxidant defense of cells, alter the mitochondrial genome, increase protein oxidation, and lead to mitochondrial damage (Durmaz et al., 2016). Our study confirmed that Lan C could elevate ROS in

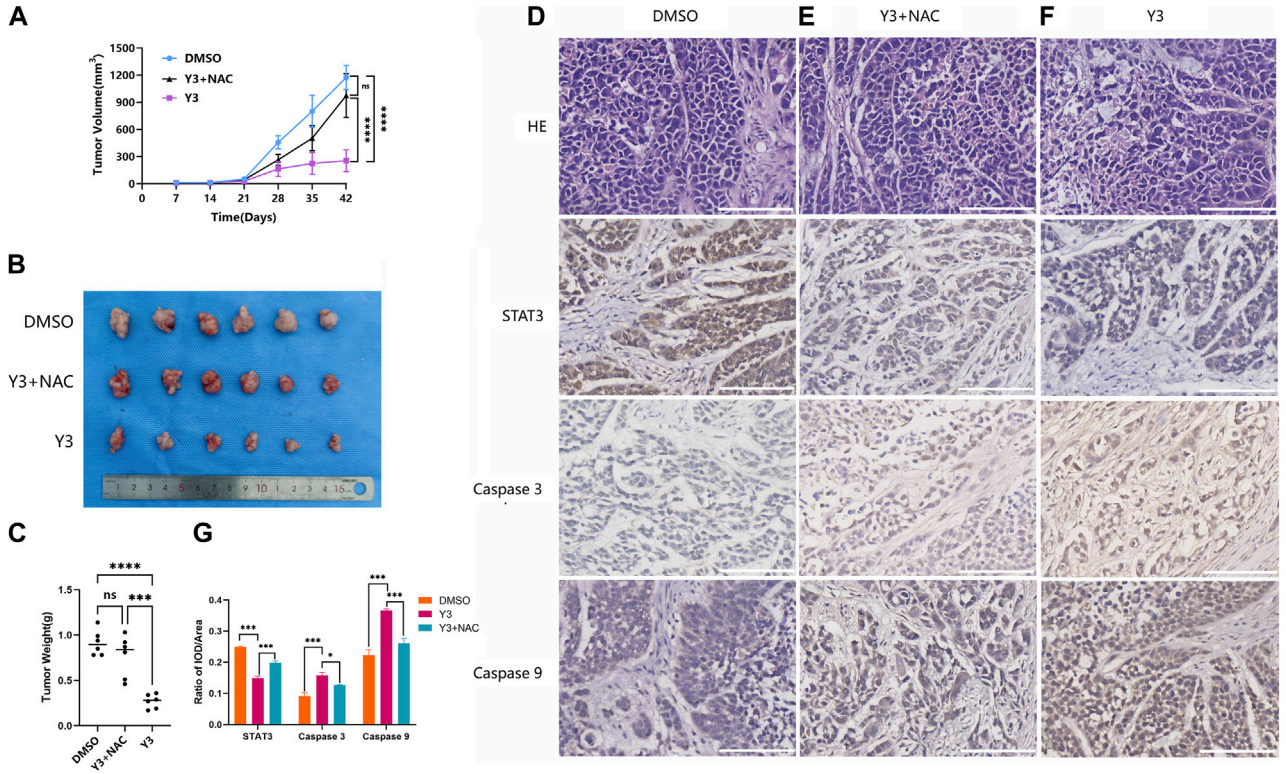

FIGURE 7
Y3 inhibited CCA progression *in vivo*. **(A)** Tumor volume in three groups of xenografted mice. Circle represents mice treated with 100ul PBS/d, square represents mice treated with Y3 40 mg/kg/d and volume of 100ul, the triangle represents mice treated with NAC + Y3, and 100 mg/kg/d NAC was given by gavage 2 h before Y3 **(B)** Xenograft tumors in the three groups. **(C)** The weight of the three groups of xenograft tumors. **(D–F)** HE staining and immunohistochemical images of STAT3, Caspase-3 and Caspase-9 in the three groups. **(G)** Immunohistochemical statistical results of STAT3, Caspase-3 and Caspase-9 in three groups. *Represents *p*-value less than 0.05, ***Represents *p*-value less than 0.001, ****Represents *p*-value less than 0.0001, ns represent *p*-value greater than 0.05. Scale bars, 100 μm.

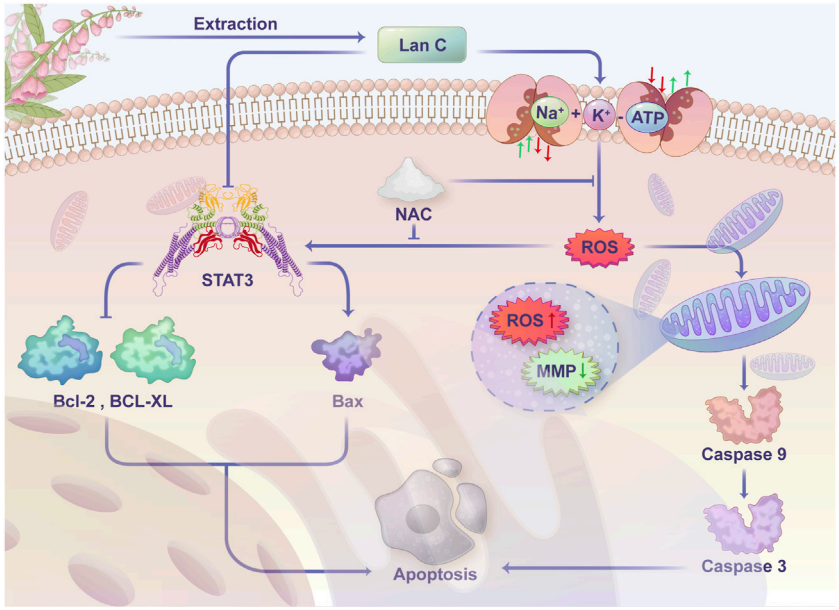

FIGURE 8
Schematic representation of the proposed anti-cancer effect of Lanatoside C on CCA cells.

cholangiocarcinoma cells, thus causing mitochondrial dysfunction. Interestingly, ROS may act as a second messenger to transmit extracellular signals inside the cells during this process.

Redox reactions are related to energy metabolism redox and are indispensable for life itself. It is widely acknowledged that ROS generation and elimination systems actively maintain the intracellular redox state, mediate redox signaling and regulate cellular functions (Rigoulet et al., 2011; Shadel and Horvath, 2015). Current evidence suggests that reactive oxygen species play a subtle role in regulating various aspects of cellular function, targeting and modifying the function, localization and activity of widely distributed proteins in a strictly regulated and reversible manner. For example, activating a large number of cell surface receptors increases intracellular hydrogen peroxide levels, thereby mediating downstream effects in a second messenger-like manner (Shi et al., 2017; Moloney and Cotter, 2018; Srinivas et al., 2019).

Mitochondria represent the main site of ROS production and the target of ROS (Zorov et al., 2014). Under specific pathological conditions, the accumulation of excessive ROS can disrupt intracellular homeostasis, leading to oxidative stress and mitochondrial dysfunction, which can damage the mitochondrial lipid membrane, leading to alterations in the mitochondrial membrane potential and apoptosis (Wang et al., 2018). In the present study, the action of Lan C on cholangiocarcinoma cells increased intracellular ROS production and inhibited the pro-oncogenic function of the transcription factor STAT3. ROS acts as the target molecule for the anti-cancer effect of Lan C. When the intracellular content of ROS increases, Bax protein may be recruited to the mitochondrial surface to form pore channels and promote the apoptosis of cholangiocarcinoma cells. In addition, ROS levels in mitochondria increased rapidly, resulting in a decrease in mitochondrial membrane potential, which activated Caspase-9, cleaved PARP and Caspase-3 and promoted apoptosis in CCA. This phenomenon was reversed by NAC, an inhibitor of ROS, reversing the switching effect of ROS.

Mitochondrial function is a key indicator of cellular health and can be assessed by monitoring changes in mitochondrial membrane potential (MMP) (Demine et al., 2019). Mitochondrial dysfunction has been associated with various diseases, such as cancer, cardiovascular disease, diabetes and neurodegenerative diseases (Bock and Tait, 2020). Many compounds can reduce MMP by interfering with multiple macromolecules in mitochondria, affecting mitochondrial function (Battogtokh et al., 2018). JC-1 has been extensively used to evaluate MMP over the years. In the present study, we used JC-1 staining to detect changes in mitochondrial membrane potential in cholangiocarcinoma cells after treated with Lan C. After cholangiocarcinoma cells were treated with Lan C action, a change from red to green fluorescence was observed under fluorescence staining. The ratio of JC-1 polymer/JC-1 monomer was significantly decreased, indicating that Lan C could cause membrane depolarization, resulting in decreased MMP. Flow cytometry also confirmed that Lan C caused loss of mitochondrial membrane potential in CCA cells, which resulted in apoptosis. Blockade of ROS production by NAC completely reversed Lan C-induced changes in mitochondrial membrane potential and apoptosis, suggesting that the Lan C-induced decrease in mitochondrial membrane potential and apoptosis were dependent on ROS production.

The signal transducer and activator of transcription (STAT) is a family of transcription factors, of which STAT3 is associated with signaling from cell surface receptors to the nucleus and has been a research hot in recent years (Haghikia et al., 2014; Zou et al., 2020). Various cancers, including cholangiocarcinoma, frequently exhibit STAT3 activation (Fathi et al., 2018). Accordingly, compounds that can dysregulate STAT3 activation have huge therapeutic potential, and blocking the STAT3 signaling pathway may lead to cancer cell growth inhibition and apoptosis. In our study, sequencing and network pharmacology analysis suggested that STAT3 represents a poteneially important target of Lan C action on cholangiocarcinoma cells, confirmed in subsequent WB and *in vivo* experiments. Lan C caused a decrease in the protein expression of STAT3 in cholangiocarcinoma cells, which inhibited the classical STAT3 pro-cancer pathway and led to apoptosis of cancer cells. In the same experimental group, the change of p-STAT3 was consistent with that of STAT3, suggesting that Lan C may play a pro-apoptotic role by inhibiting the phosphorylation of STAT3. In contrast, NAC pretreatment reversed this change, suggesting that this effect is also associated with ROS. Thus, our study reveals a unique approach to target STAT3 via ROS-induced anticancer compounds, providing a promising avenue for treating cholangiocarcinoma.

Herein, we aimed to elucidate the molecular mechanism underlying the anticancer effect of Lan C in cholangiocarcinoma. We found that Lan C caused an increase in intracellular ROS content, which in turn caused a decrease in the mitochondrial membrane potential of cholangiocarcinoma cells and eventually led to apoptosis. Lan C also downregulated the protein expression of STAT3 through ROS, increased the expression of Bax, decreased Bcl-2 and Bcl-xl levels, and activated caspase-9, cleaved PARP and caspase-3, which initiated apoptosis. These results suggest that Lan C may be a new anti-cholangiocarcinoma compound. However, our study has some limitations. First, the molecular mechanism of lanc's antitumor effect needs further investigation. Besides, little is currently known about the interactions between ROS and STAT3. Based on the strong oxidative properties of ROS, we speculate that this characteristic may be critical in affecting STAT3 function. Indeed, further research is warranted before clinical translation.

Conclusion

In conclusion, our results provide hitherto undocumented evidence of the mechanism of action of Lan C in cholangiocarcinoma. We demonstrated that Lan C inhibits the growth of cholangiocarcinoma cells and promotes their apoptosis by increasing ROS production, decreasing mitochondrial membrane potential and inhibiting the pro-oncogenic effect of STAT3. Overall our results suggest that Lan C could be acandidate compounds for cholangiocarcinoma.

Data availability statement

The datasets presented in this study can be found in online repositories. The names of the repository/repositories and

accession number(s) can be found in the article/Supplementary Material.

Ethics statement

The animal study was reviewed and approved by The Human Research Ethics Committee of the First Hospital of Lanzhou University (LDYYLL2022-419).

Author contributions

W-BM, J-JC, and KG designed the experiments. CZ, H-YY, LG, and M-ZB performed the experiments and collected the data. CZ, W-KF, C-FH and N-NM et. Analyzed and interpreted the data. CZ and H-YY wrote the article. All authors contributed to the article and approved the submitted version.

Funding

This work was supported by Grant(s) from the National Natural Science Foundation of China (82060551 to W-BM, 81973193 to J-JC, 22177044 to KG), Lanzhou Science and Technology Development Guiding Plan Project (2020-ZD-79 to CZ), Foundation of Lanzhou University: Izuyxcx-2022-157, The Health Industry Scientific Research Program of Gansu Province (GSWSKY 2020-11 to Y-YL).

Conflict of interest

The authors declare that the research was conducted in the absence of any commercial or financial relationships that could be construed as a potential conflict of interest.

Publisher's note

All claims expressed in this article are solely those of the authors and do not necessarily represent those of their affiliated organizations, or those of the publisher, the editors and the reviewers. Any product that may be evaluated in this article, or claim that may be made by its manufacturer, is not guaranteed or endorsed by the publisher.

Supplementary material

The Supplementary Material for this article can be found online at: https://www.frontiersin.org/articles/10.3389/fphar.2023.1098915/full#supplementary-material

SUPPLEMENTARY FIGURE S1
NMR spectrum of compounds Y1-Y5.

SUPPLEMENTARY FIGURE S2
The IC50 value of Y3 in human intrahepatic bile duct epithelial cell line (HIBEpiC) is 0.2124 μM/L.

SUPPLEMENTARY FIGURE S3
Cytotoxic effects of Lan C on HuCCT-1 cells and HIBEpiC cells.

SUPPLEMENTARY FIGURE S4
Live cell imaging assay. **(A, B)** The cell number of HuCCT-1 and TFK-1 cells treated with Y3 for 48 h were monitored using Cytation 5. **(C, D)** Representative images acquired in Cytation 5 of HuCCT-1 and TFK-1 cells at 0, 12, 24, and 48 h.

SUPPLEMENTARY FIGURE S5
The HuCCT-1 and TFK-1 cells line were treated with Y3 or NAC + Y3 for 48 h, percentage of cell apoptosis was determined by Annexin-V/PI staining and flow cytometry.

SUPPLEMENTARY FIGURE S6
The HIBEpiC cell line was treated with Y3 or NAC + Y3 for 48 h, percentage of cell apoptosis was determined by Annexin-V/PI staining and flow cytometry.

SUPPLEMENTARY FIGURE S7
Weight of tumor xenografts mice treated with PBS, Y3 and NAC + Y3.

References

Alpert, J. S. (2021). Is digitalis therapy still viable? Foxglove therapy makes a comeback. *Am. J. Med.* 134, 1–2. doi:10.1016/j.amjmed.2020.09.001

Anders, S., and Huber, W. J. E. (2013). *Differential expression of RNA-Seq data at the gene level – the DESeq package*. Germany: EMBL.

Bagrov, A. Y., Bagrov, Y. Y., Fedorova, O. V., Kashkin, V. A., Patkina, N. A., and Zvartau, E. E. (2002). Endogenous digitalis-like ligands of the sodium pump: Possible involvement in mood control and ethanol addiction. *Eur. Neuropsychopharmacol. J. Eur. Coll. Neuropsychopharmacol.* 12, 1–12. doi:10.1016/s0924-977x(01)00127-4

Battogtokh, G., Choi, Y. S., Kang, D. S., Park, S. J., Shim, M. S., Huh, K. M., et al. (2018). Mitochondria-targeting drug conjugates for cytotoxic, anti-oxidizing and sensing purposes: Current strategies and future perspectives. *Acta Pharm. Sin. B* 8, 862–880. doi:10.1016/j.apsb.2018.05.006

Biggar, R. J. (2012). Molecular pathways: Digoxin use and estrogen-sensitive cancers--risks and possible therapeutic implications. *Clin. Cancer Res. Official J. Am. Assoc. Cancer Res.* 18, 2133–2137. doi:10.1158/1078-0432.CCR-11-1389

Biggar, R. J., Wohlfahrt, J., Oudin, A., Hjuler, T., and Melbye, M. (2011). Digoxin use and the risk of breast cancer in women. *J. Clin. Oncol. Official J. Am. Soc. Clin. Oncol.* 29, 2165–2170. doi:10.1200/JCO.2010.32.8146

Bock, F. J., and Tait, S. W. G. (2020). Mitochondria as multifaceted regulators of cell death. *Nat. Rev. Mol. Cell Biol.* 21, 85–100. doi:10.1038/s41580-019-0173-8

Chang, J., Li, Y., Wang, X., Hu, S., Wang, H., Shi, Q., et al. (2017). Polyphyllin I suppresses human osteosarcoma growth by inactivation of Wnt/β-catenin pathway *in vitro* and *in vivo*. *Sci. Rep.* 7, 7605. doi:10.1038/s41598-017-07194-9

Chen, G., Zhou, D., Li, X.-Z., Jiang, Z., Tan, C., Wei, X.-Y., et al. (2017). A natural chalcone induces apoptosis in lung cancer cells: 3D-QSAR, docking and an *in vivo*/vitro assay. *Sci. Rep.* 7, 10729. doi:10.1038/s41598-017-11369-9

Chen, S., Zhou, Y., Chen, Y., and Gu, J. (2018). fastp: an ultra-fast all-in-one FASTQ preprocessor. *Bioinformatics* 34, i884–i890. doi:10.1093/bioinformatics/bty560

Cheung, E. C., and Vousden, K. H. (2022). The role of ROS in tumour development and progression. *Nat. Rev. Cancer* 22, 280–297. doi:10.1038/s41568-021-00435-0

Demine, S., Renard, P., and Arnould, T. (2019). Mitochondrial uncoupling: A key controller of biological processes in physiology and diseases. *Cells* 8, 795. doi:10.3390/cells8080795

Durmaz, I., Guven, E. B., Ersahin, T., Ozturk, M., Calis, I., and Cetin-Atalay, R. (2016). Liver cancer cells are sensitive to Lanatoside C induced cell death independent of their PTEN status. *Phytomedicine Int. J. Phytotherapy Phytopharm.* 23, 42–51. doi:10.1016/j.phymed.2015.11.012

Ehle, M., Patel, C., and Giugliano, R. P. (2011). Digoxin: Clinical highlights: A review of digoxin and its use in contemporary medicine. *Crit. Pathw. Cardiol.* 10, 93–98. doi:10.1097/HPC.0b013e318221e7dd

Fathi, N., Rashidi, G., Khodadadi, A., Shahi, S., and Sharifi, S. (2018). STAT3 and apoptosis challenges in cancer. *Int. J. Biol. Macromol.* 117, 993–1001. doi:10.1016/j.ijbiomac.2018.05.121

Haghikia, A., Ricke-Hoch, M., Stapel, B., Gorst, I., and Hilfiker-Kleiner, D. (2014). STAT3, a key regulator of cell-to-cell communication in the heart. *Cardiovasc. Res.* 102, 281–289. doi:10.1093/cvr/cvu034

Hood, W. B., Dans, A. L., Guyatt, G. H., Jaeschke, R., and Mcmurray, J. J. V. (2014). Digitalis for treatment of heart failure in patients in sinus rhythm. *Cochrane Database Syst. Rev.* 2014, CD002901. doi:10.1002/14651858.CD002901.pub3

Hsu, I. L., Chou, C.-Y., Wu, Y.-Y., Wu, J.-E., Liang, C.-H., Tsai, Y.-T., et al. (2016). Targeting FXYD2 by cardiac glycosides potently blocks tumor growth in ovarian clear cell carcinoma. *Oncotarget* 7, 62925–62938. doi:10.18632/oncotarget.7497

Hu, Y., Yu, K., Wang, G., Zhang, D., Shi, C., Ding, Y., et al. (2018). Lanatoside C inhibits cell proliferation and induces apoptosis through attenuating Wnt/β-catenin/c-Myc signaling pathway in human gastric cancer cell. *Biochem. Pharmacol.* 150, 280–292. doi:10.1016/j.bcp.2018.02.023

Katz, A. M. (1985). Effects of digitalis on cell biochemistry: Sodium pump inhibition. *J. Am. Coll. Cardiol.* 5, 16A–21A. doi:10.1016/s0735-1097(85)80459-9

Kaushik, V., Yakisich, J. S., Azad, N., Kulkarni, Y., Venkatadri, R., Wright, C., et al. (2017). Anti-tumor effects of cardiac glycosides on human lung cancer cells and lung tumorspheres. *J. Cell. Physiology* 232, 2497–2507. doi:10.1002/jcp.25611

Kelley, R. K., Bridgewater, J., Gores, G. J., and Zhu, A. X. (2020). Systemic therapies for intrahepatic cholangiocarcinoma. *J. Hepatology* 72, 353–363. doi:10.1016/j.jhep.2019.10.009

Kim, D., Langmead, B., and Salzberg, S. L. (2015). Hisat: A fast spliced aligner with low memory requirements. *Nat. Methods* 12, 357–360. doi:10.1038/nmeth.3317

Kreis, W. (2017). The foxgloves (digitalis) revisited. *Planta Medica* 83, 962–976. doi:10.1055/s-0043-111240

Lehtola, T., Huhtikangas, A., Hiltunen, R., and V Schantz, M. (1981). Radioimmunoassay of digoxigenin glycosides in digitalis lanata. *Planta Medica* 42, 250–254. doi:10.1055/s-2007-971635

Liu, S.-H., Yu, J., Creeden, J. F., Sutton, J. M., Markowiak, S., Sanchez, R., et al. (2020). Repurposing metformin, simvastatin and digoxin as a combination for targeted therapy for pancreatic ductal adenocarcinoma. *Cancer Lett.* 491, 97–107. doi:10.1016/j.canlet.2020.08.002

Mazzaferro, V., Gorgen, A., Roayaie, S., Droz Dit Busset, M., and Sapisochin, G. (2020). Liver resection and transplantation for intrahepatic cholangiocarcinoma. *J. Hepatology* 72, 364–377. doi:10.1016/j.jhep.2019.11.020

Moloney, J. N., and Cotter, T. G. (2018). ROS signalling in the biology of cancer. *Seminars Cell and Dev. Biol.* 80, 50–64. doi:10.1016/j.semcdb.2017.05.023

Moriya, Y., Itoh, M., Okuda, S., Yoshizawa, A. C., and Kanehisa, M. (2007). Kaas: An automatic genome annotation and pathway reconstruction server. *Nucleic Acids Res.* 35, W182–W185. doi:10.1093/nar/gkm321

Odagiri, K., Katoh, H., Kawashima, H., Tanaka, T., Ohtani, H., Saotome, M., et al. (2009). Local control of mitochondrial membrane potential, permeability transition pore and reactive oxygen species by calcium and calmodulin in rat ventricular myocytes. *J. Mol. Cell. Cardiol.* 46, 989–997. doi:10.1016/j.yjmcc.2008.12.022

Pratt, R. D., Brickman, C. R., Cottrill, C. L., Shapiro, J. I., and Liu, J. (2018). The Na/K-ATPase signaling: From specific ligands to general reactive oxygen species. *Int. J. Mol. Sci.* 19, 2600. doi:10.3390/ijms19092600

Rasheduzzaman, M., Yin, H., and Park, S.-Y. (2019). Cardiac glycoside sensitized hepatocellular carcinoma cells to TRAIL via ROS generation, p38MAPK, mitochondrial transition, and autophagy mediation. *Mol. Carcinog.* 58, 2040–2051. doi:10.1002/mc.23096

Razumilava, N., and Gores, G. J. (2014). Cholangiocarcinoma. *Lancet (London, Engl.* 383, 2168–2179. doi:10.1016/S0140-6736(13)61903-0

Reddy, D., Kumavath, R., Ghosh, P., and Barh, D. (2019). Lanatoside C induces G2/M cell cycle arrest and suppresses cancer cell growth by attenuating MAPK, Wnt, JAK-STAT, and PI3K/AKT/mTOR signaling pathways. *Biomolecules* 9, 792. doi:10.3390/biom9120792

Ren, Y., Ribas, H. T., Heath, K., Wu, S., Ren, J., Shriwas, P., et al. (2020). Na+/K+-ATPase-Targeted cytotoxicity of (+)-Digoxin and several semisynthetic derivatives. *J. Nat. Prod.* 83, 638–648. doi:10.1021/acs.jnatprod.9b01060

Rigoulet, M., Yoboue, E. D., and Devin, A. (2011). Mitochondrial ROS generation and its regulation: Mechanisms involved in H(2)O(2) signaling. *Antioxidants Redox Signal.* 14, 459–468. doi:10.1089/ars.2010.3363

Rizvi, S., and Gores, G. J. (2013). Pathogenesis, diagnosis, and management of cholangiocarcinoma. *Gastroenterology* 145, 1215–1229. doi:10.1053/j.gastro.2013.10.013

Rizwan, H., Pal, S., Sabnam, S., and Pal, A. (2020). High glucose augments ROS generation regulates mitochondrial dysfunction and apoptosis via stress signalling cascades in keratinocytes. *Life Sci.* 241, 117148. doi:10.1016/j.lfs.2019.117148

Rodrigues, P. M., Olaizola, P., Paiva, N. A., Olaizola, I., Agirre-Lizaso, A., Landa, A., et al. (2021). Pathogenesis of cholangiocarcinoma. *Annu. Rev. Pathology* 16, 433–463. doi:10.1146/annurev-pathol-030220-020455

Sato, K., Glaser, S., Alvaro, D., Meng, F., Francis, H., and Alpini, G. (2020). Cholangiocarcinoma: Novel therapeutic targets. *Expert Opin. Ther. Targets* 24, 345–357. doi:10.1080/14728222.2020.1733528

Saxena, S., Vekaria, H., Sullivan, P. G., and Seifert, A. W. (2019). Connective tissue fibroblasts from highly regenerative mammals are refractory to ROS-induced cellular senescence. *Nat. Commun.* 10, 4400. doi:10.1038/s41467-019-12398-w

Shadel, G. S., and Horvath, T. L. (2015). Mitochondrial ROS signaling in organismal homeostasis. *Cell* 163, 560–569. doi:10.1016/j.cell.2015.10.001

Shi, X., Li, W., Liu, H., Yin, D., and Zhao, J. (2017). The ROS/NF-κB/NR4A2 pathway is involved in H2O2 induced apoptosis of resident cardiac stem cells via autophagy. *Oncotarget* 8, 77634–77648. doi:10.18632/oncotarget.20747

Silva, C. I. D., Gonçalves-De-Albuquerque, C. F., Moraes, B. P. T. D., Garcia, D. G., and Burth, P. (2021). Na/K-ATPase: Their role in cell adhesion and migration in cancer. *Biochimie* 185, 1–8. doi:10.1016/j.biochi.2021.03.002

Srinivas, U. S., Tan, B. W. Q., Vellayappan, B. A., and Jeyasekharan, A. D. (2019). ROS and the DNA damage response in cancer. *Redox Biol.* 25, 101084. doi:10.1016/j.redox.2018.101084

Wang, Y., Branicky, R., Noë, A., and Hekimi, S. (2018). Superoxide dismutases: Dual roles in controlling ROS damage and regulating ROS signaling. *J. Cell Biol.* 217, 1915–1928. doi:10.1083/jcb.201708007

Wang, Y., Dong, B., Xue, W., Feng, Y., Yang, C., Liu, P., et al. (2020). Anticancer effect of radix astragali on cholangiocarcinoma *in vitro* and its mechanism via network pharmacology. *Med. Sci. Monit. Int. Med. J. Exp. Clin. Res.* 26, e921162. doi:10.12659/MSM.921162

Whayne, T. F. (2018). Clinical use of digitalis: A state of the art review. *Am. J. Cardiovasc. Drugs Drugs, Devices, Other Interventions* 18, 427–440. doi:10.1007/s40256-018-0292-1

Xie, C.-M., Liu, X.-Y., Yu, S., and Cheng, C. H. K. (2013). Cardiac glycosides block cancer growth through HIF-1α- and NF-κB-mediated Plk1. *Carcinogenesis* 34, 1870–1880. doi:10.1093/carcin/bgt136

Xie, Z., and Cai, T. (2003). Na+-K+--ATPase-mediated signal transduction: From protein interaction to cellular function. *Mol. Interv.* 3, 157–168. doi:10.1124/mi.3.3.157

Yan, T., and Zhao, Y. (2020). Acetaldehyde induces phosphorylation of dynamin-related protein 1 and mitochondrial dysfunction via elevating intracellular ROS and Ca2+ levels. *Redox Biol.* 28, 101381. doi:10.1016/j.redox.2019.101381

Yan, Y., and Shapiro, J. I. (2016). The physiological and clinical importance of sodium potassium ATPase in cardiovascular diseases. *Curr. Opin. Pharmacol.* 27, 43–49. doi:10.1016/j.coph.2016.01.009

Zhang, J., Su, G., Tang, Z., Wang, L., Fu, W., Zhao, S., et al. (2018). Curcumol exerts anticancer effect in cholangiocarcinoma cells via down-regulating CDKL3. *Front. Physiology* 9, 234. doi:10.3389/fphys.2018.00234

Zorov, D. B., Juhaszova, M., and Sollott, S. J. (2014). Mitochondrial reactive oxygen species (ROS) and ROS-induced ROS release. *Physiol. Rev.* 94, 909–950. doi:10.1152/physrev.00026.2013

Zou, S., Tong, Q., Liu, B., Huang, W., Tian, Y., and Fu, X. (2020). Targeting STAT3 in cancer immunotherapy. *Mol. Cancer* 19, 145. doi:10.1186/s12943-020-01258-7

frontiers | Frontiers in Pharmacology

TYPE Original Research
PUBLISHED 01 September 2023
DOI 10.3389/fphar.2023.1135898

OPEN ACCESS

EDITED BY
Olivier Feron,
Université catholique de Louvain, Belgium

REVIEWED BY
Udhaya Kumar. S,
Baylor College of Medicine, United States
Young Hoon Son,
Emory University, United States
Hassan Bardania,
Yasuj University of Medical Sciences, Iran

*CORRESPONDENCE
Manzoor Ahmad Mir,
drmanzoor@kashmiruniversity.ac.in

†These authors have contributed equally to this work

RECEIVED 02 January 2023
ACCEPTED 09 August 2023
PUBLISHED 01 September 2023

CITATION
Mir WR, Bhat BA, Kumar A, Dhiman R, Alkhanani M, Almilaibary A, Dar MY, Ganie SA and Mir MA (2023), Network pharmacology combined with molecular docking and *in vitro* verification reveals the therapeutic potential of *Delphinium roylei* munz constituents on breast carcinoma.
Front. Pharmacol. 14:1135898.
doi: 10.3389/fphar.2023.1135898

Network pharmacology combined with molecular docking and *in vitro* verification reveals the therapeutic potential of *Delphinium roylei* munz constituents on breast carcinoma

Wajahat Rashid Mir[1†], Basharat Ahmad Bhat[1†], Ashish Kumar[2], Rohan Dhiman[2], Mustfa Alkhanani[3], Abdullah Almilaibary[4], Mohd Younis Dar[5], Showkat Ahmad Ganie[6] and Manzoor Ahmad Mir[1*]

[1]Department of Bio-Resources, School of Biological Sciences, University of Kashmir, Srinagar, Jammu and Kashmir, India, [2]Department of Life Science, National Institute of Technology, Rourkela, Odisha, India, [3]Department of Family and Community Medicine, Faculty of Medicine, Al Baha University, Al Bahah, Saudi Arabia, [4]Department of Biology, College of Science, Hafr Al Batin University of Hafr Al-Batin, Hafar Al Batin, Saudi Arabia, [5]Regional Research Institute of Unani Medicine (RRIUM), University of Kashmir, Srinagar, Jammu and Kashmir, India, [6]Department of Clinical Biochemistry, School of Biological Sciences, University of Kashmir, Srinagar, Jammu and Kashmir, India

Delphinium roylei Munz is an indigenous medicinal plant to India where its activity against cancer has not been previously investigated, and its specific interactions of bioactive compounds with vulnerable breast cancer drug targets remain largely unknown. Therefore, in the current study, we aimed to evaluate the anti-breast cancer activity of different extracts of *D. roylei* against breast cancer and deciphering the molecular mechanism by Network Pharmacology combined with Molecular Docking and *in vitro* verification. The experimental plant was extracted with various organic solvents according to their polarity index. Phytocompounds were identified by High resolution-liquid chromatography-mass spectrometry (HR-LC/MS) technique, and SwissADME programme evaluated their physicochemical properties. Next, target(s) associated with the obtained bioactives or breast cancer-related targets were retrieved by public databases, and the Venn diagram selected the overlapping targets. The networks between overlapping targets and bioactive were visualized, constructed, and analyzed by STRING programme and Cytoscape software. Finally, we implemented a molecular docking test (MDT) using AutoDock Vina to explore key target(s) and compound(s). HR-LC/MS detected hundreds of phytocompounds, and few were accepted by Lipinski's rules after virtual

Abbreviations: AKT1; RAC-alpha serine/threonine-protein kinase, HR-LC/MS; High Resolution Liquid Chromatography Mass Spectrometry, STRING; Search Tool for the Retrieval of Interacting Genes/Proteins, CDKs; Cyclin Dependent Kinases, RCSB; Research Collaboratory for Structural Bioinformatics, PDB; Protein Data Bank, LGA; Lamarckian Genetic Algorithm, MD; Molecular Dynamic Simulation, RMSD; Root Mean Square Deviation, RMSF; Root Mean Square Fluctuation, OPLS; Optimized Potentials for Liquid Simulations, RG; Radius of Gyration, SASA; Solvent Accessible Surface Area, DPPH; 2,2-diphenyl-1-picrylhydrazyl, MTT; (3-(4,5-Dimethylthiazol-2-yl)-2,5-Diphenyltetrazolium Bromide), GO; Gene ontology, KEGG; (Kyoto Encyclopaedia of Genes and Genomes).

screening and therefore classified as drug-like compounds (DLCs). A total of 464 potential target genes were attained for the nine quantitative phytocompounds and using Gene Cards, OMIM and DisGeNET platforms, 12063 disease targets linked to breast cancer were retrieved. With Kyoto Encyclopaedia of Genes and Genomes (KEGG) pathway enrichment, a total of 20 signalling pathways were manifested, and a hub signalling pathway (PI3K-Akt signalling pathway), a key target (Akt1), and a key compound (8-Hydroxycoumarin) were selected among the 20 signalling pathways via molecular docking studies. The molecular docking investigation revealed that among the nine phytoconstituents, 8-hydroxycoumarin showed the best binding energy (−9.2 kcal/mol) with the Akt1 breast cancer target. 8-hydroxycoumarin followed all the ADME property prediction using SwissADME, and 100 nanoseconds (ns) MD simulations of 8-hydroxycoumarin complexes with Akt1 were found to be stable. Furthermore, *D. roylei* extracts also showed significant antioxidant and anticancer activity through *in vitro* studies. Our findings indicated for the first time that *D. roylei* extracts could be used in the treatment of BC.

KEYWORDS

***Delphinium roylei*, breast cancer, HR/LC-MS, 8-hydroxycoumarin, anticancer activity, network pharmacology, molecular docking and MD simulations**

Introduction

Breast cancer (BC) is the most commonly diagnosed cancer worldwide, and its burden has been rising over the past decades (Pistelli et al., 2021; Pospelova et al., 2022). Having replaced lung cancer as the most commonly diagnosed cancer globally, breast cancer today accounts for 1 in 8 cancer diagnoses and a total of 2.3 million new cases in both sexes combined (Sung et al., 2021). Representing a quarter of all cancer cases in females, it was by far the most commonly diagnosed cancer in women in 2020, and its burden has been growing in many parts of the world, particularly in transitioning countries (Heer et al., 2020). An estimated 685,000 women died from breast cancer in 2020, corresponding to 16% or 1 in every 6 cancer deaths in women (Deo et al., 2022). The discovery of new cancer treatments is still regarded as an active research area despite the great advance in the area of chemotherapy. Medicinal plants are regarded as a renewable source of bioactive compounds that can be exploited in the treatment of various ailments including cancer (Tariq et al., 2021; Mir et al., 2022a; Mir et al., 2022b). Phytochemicals play an important role in the initiation, development, and advancement of carcinogenesis, as well as in suppressing or reversing the early stages of cancer or the invading potential of premalignant cells and also regulate cell proliferation and apoptosis signalling pathways in transformed cells (George et al., 2021; Bhat et al., 2022a; Bhat et al., 2022b).

Delphinium roylei Munz. is an important medicinal herb of the Delphinium genus. The ethnomedicinal uses of this plant include treating the liver and persistent lower back discomfort (Sharma and Singh, 1989; Kumar and Hamal, 2011). Diterpenoid alkaloid and flavanols, which constitute most of the compounds isolated from Delphinium plants, have been tested for various biological activities, such as effects on cholinesterase inhibition, antimicrobial, antineoplastic, insecticidal, anti-inflammatory, and anticancer activities (Yin et al., 2021). Delphinidin is a type of anthocyanin isolated from genus *Delphinium*, which has anticancer, anti-inflammatory, and anti-angiogenic properties. Recent *in-vitro* studies showed that delphinidin can inhibit the invasion of HER-2-positive MDA-MB-453 breast cancer cell line, with low cytotoxicity on normal breast cells (Wu et al., 2021) and ovarian cancer cells (Lim et al., 2017) and can also induce autophagy in breast cancer cells (Chen et al., 2018).

Due to the complex nature of plant extracts and their chemical constituents, it is difficult to understand the molecular mechanism by which they act on certain molecular targets due to the synergistic effects of their chemical constituents and the fact that they could interact with many targets simultaneously. In recent years, network pharmacological analysis has been effectively applied for prediction of the protein targets and the related disease pathways of plant active constituents.

Network pharmacology, based on system biology, includes network database retrieval, virtual computing, and high throughput omics data analysis. This approach breaks the ancient limitation of one drug–one biological target research and is applied mainly to explaining effective mechanisms, active ingredient screening, and pathogenesis research (Yu et al., 2021).

The versatile approach of molecular docking, which is based on the theory of ligand-receptor interactions, is widely used in drug discovery to understand how compounds bind with their molecular targets (Tiwari and Singh, 2022; Saifi et al., 2023).

Here, in the present study, we carried out a HR/LC-MS analysis to identify the phytoconstituents present in the *D. roylei* and screened to find drug-likeness compounds by ADMET analysis. Secondly, we used network pharmacology to predict the potential effective components, corresponding target genes, and pathways of phytocompounds of *D. roylei* against breast cancer. Lastly, we explore the molecular mechanism of the most potent bioactive constituent of *D. roylei* and a hub therapeutic target to alleviate the breast cancer based on molecular docking, molecular dynamic (MD) simulation and *in vitro* experimental analysis.

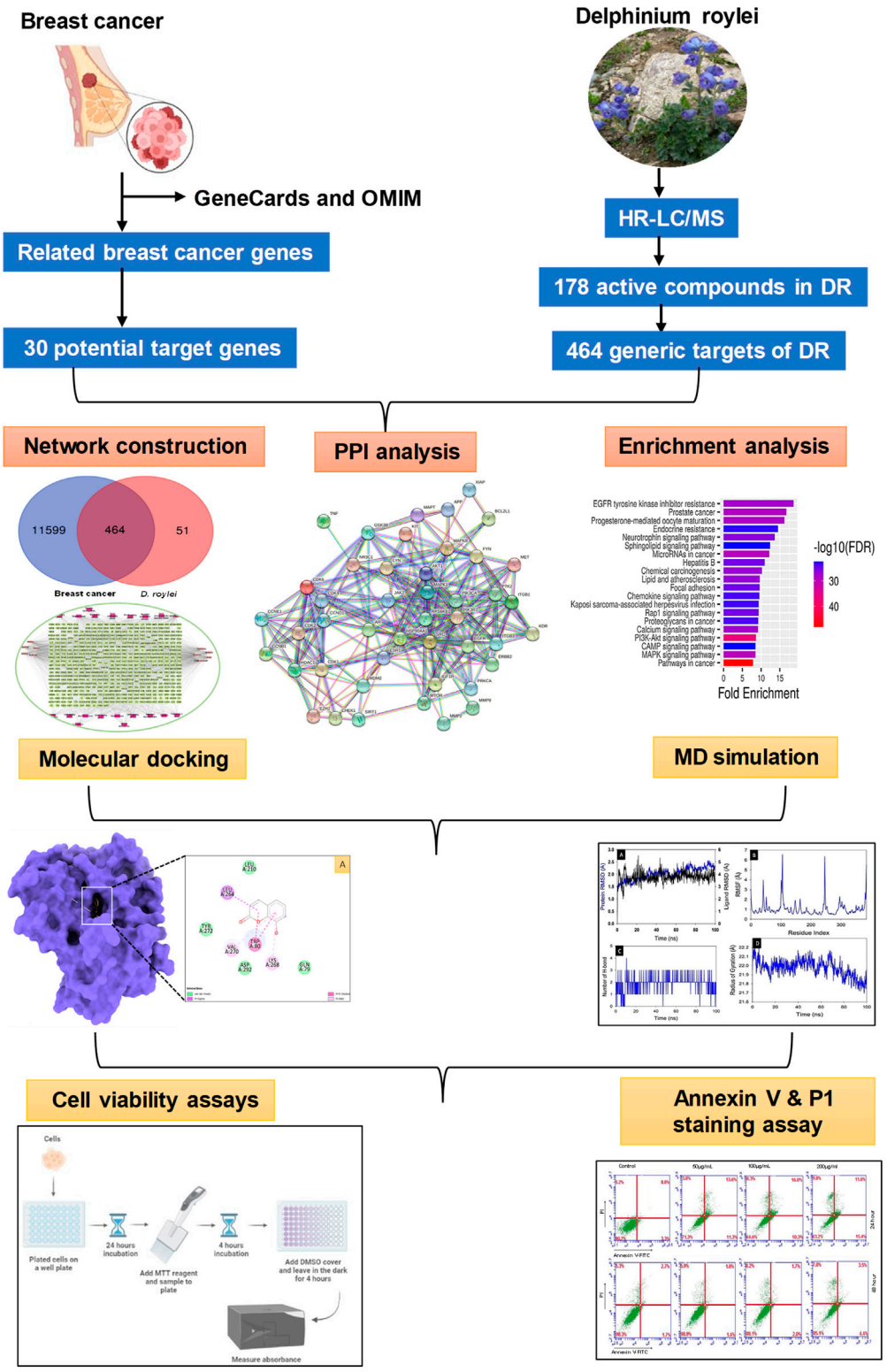

GRAPHICAL ABSTRACT
The graphical abstract illustrates a multidisciplinary approach to uncover the therapeutic promise of Delphinium roylei Munz, a medicinal plant, against breast carcinoma.

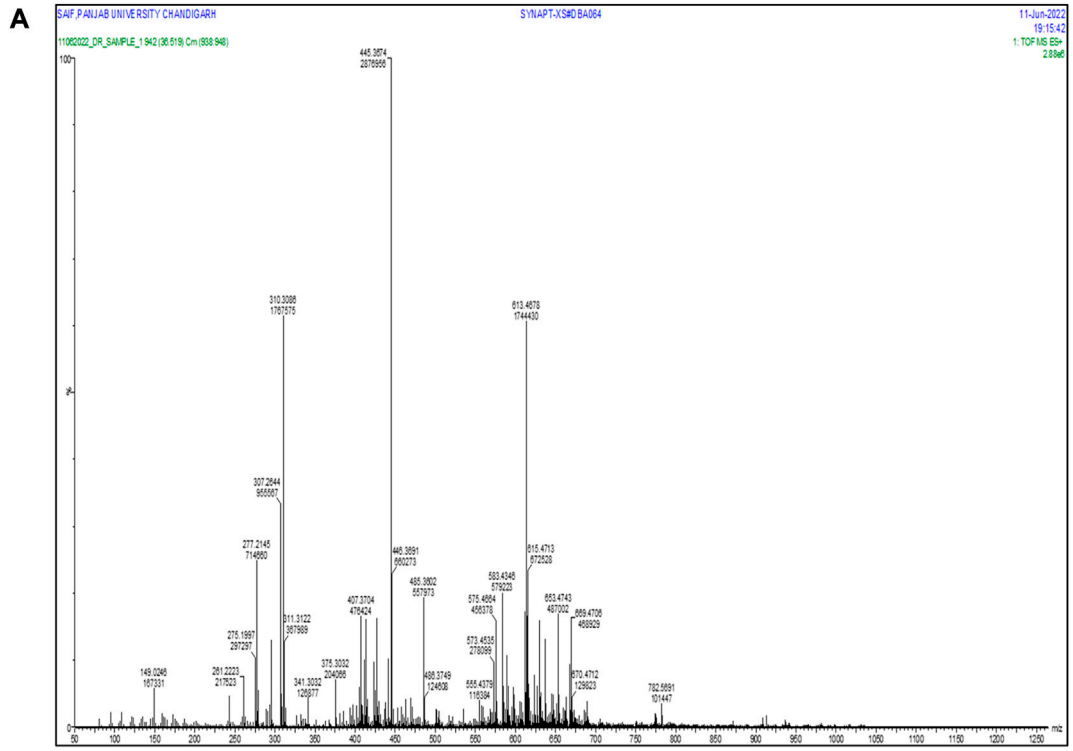

FIGURE 1
(Continued).

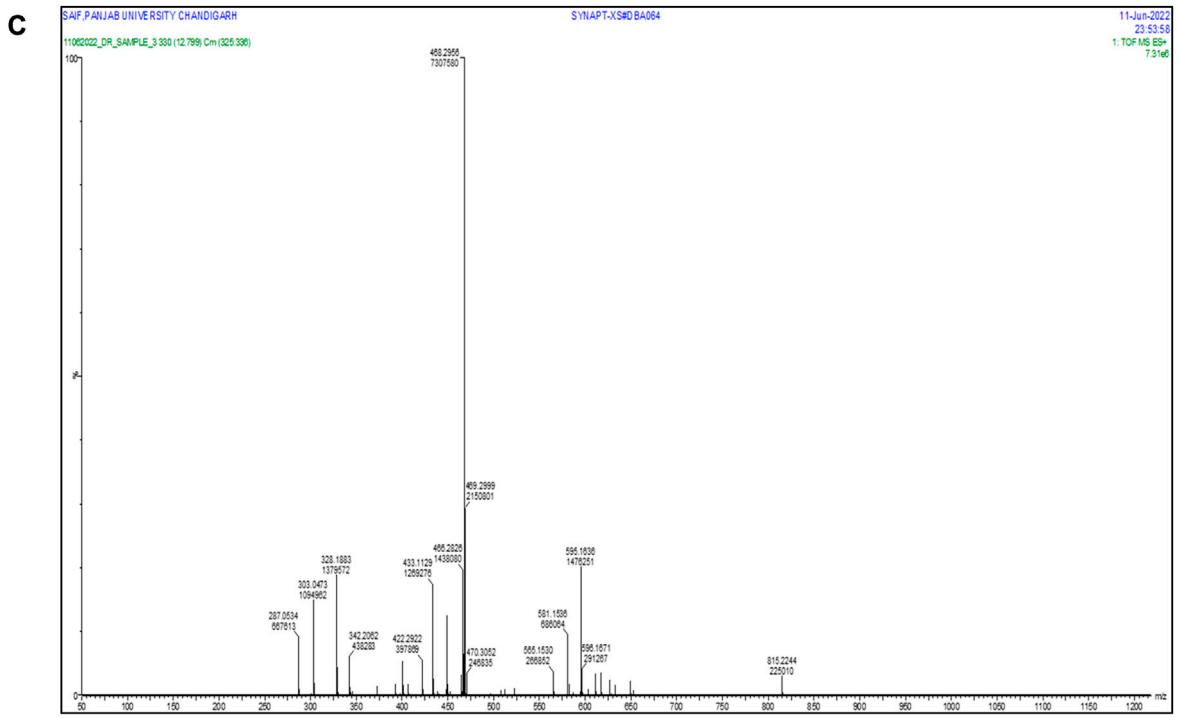

HR-LC/MS chromatogram of Ethyl acetate extract in positive mode of *D. roylei*

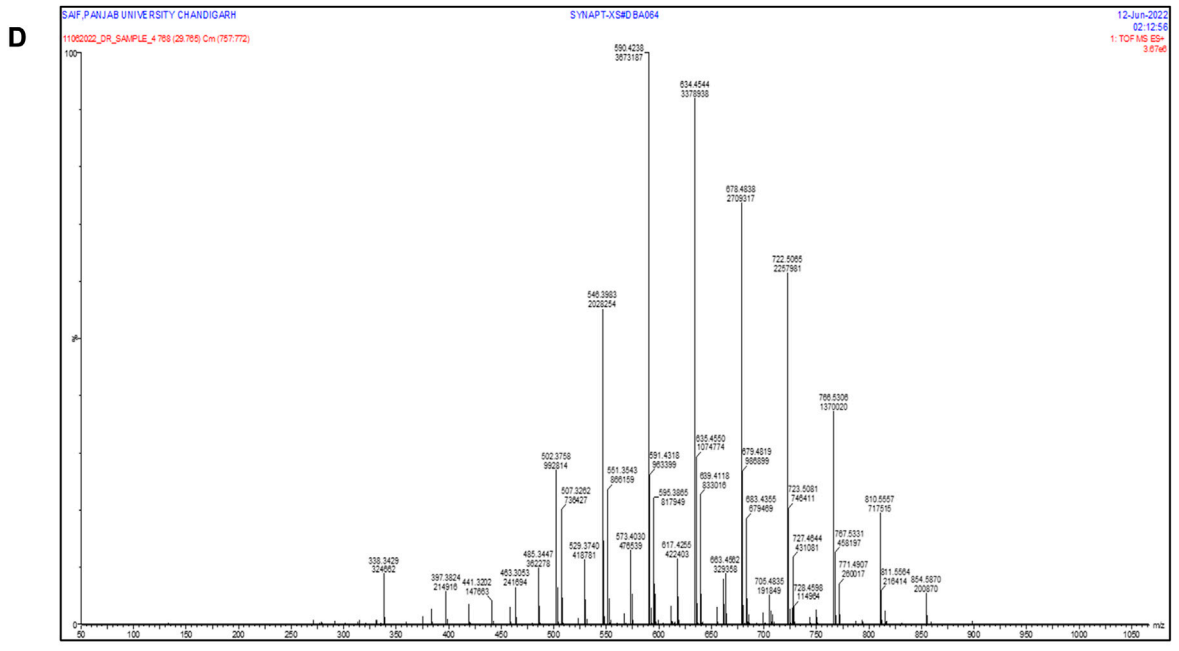

HR-LC/MS chromatogram of Petroleum ether extract in positive mode of *D. roylei*.

FIGURE 1
(Continued). **(A)**. HR-LC/MS chromatogram of methanolic extract in positive mode of *D. roylei* **(B)** HR-LC/MS chromatogram of ethanolic extract in positive mode of *D. roylei* **(C)** HR-LC/MS chromatogram of Ethyl acetate extract in positive mode of *D. roylei* **(D)** HR-LC/MS chromatogram of Petroleum ether extract in positive mode of *D. roylei*.

TABLE 1 List of selected phytocompounds detected in *D. roylei* by HR-LC/MS.

S. No	Compound name	Molecular formula	PubChem ID	Molecular weight
1	8-hydroxycoumarin	C_9H_6O3	122783	162.14
2	Delsoline	$C_{25}H_{41}NO_7$	441727	467.6
3	Royleinine	$C_{24}H_{39}NO_5$	101076550	421.6
4	Delsemine B	$C_{37}H_{53}N_3O_{10}$	101341025	699.8
5	Herniarin	$C_{10}H_8O_3$	10748	176.17
6	Aloesin	$C_{19}H_{22}O_9$	160190	394.4
7	Talatisamine	$C_{24}H_{39}NO_5$	159891	421.6
8	Narwedine	$C_{17}H_{19}NO_3$	10356588	285.34
9	Scoparone	$C_{11}H_{10}O_4$	8,417	206.19
10	Piperine	$C_{17}H_{19}NO_3$	638024	285.34

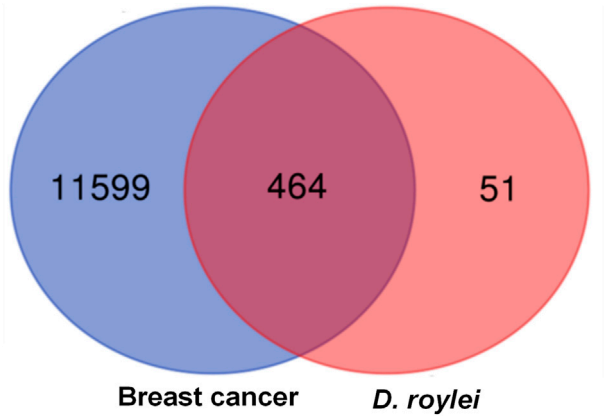

FIGURE 2
Venn diagram represents common target genes for compound prescription and disease. The size denotes the number of the target genes, the blue circle symbolizes the target genes of breast cancer, the red circle represents the target genes of 10 quantitative components in HR/LC-MS, and the coincident part depicts the common target genes.

Materials and methods

Collection of plant material

The root parts of the *Delphinium roylei* plant were taken from high-altitude areas of Kashmir Himalaya. The collected samples were identified and confirmed by Akhtar Hussain Malik, Taxonomist, Department of Botany, the University of Kashmir, with voucher specimen No.2954-(KASH).

Extraction

Various solvents such as methanol, ethanol, ethyl acetate, and petroleum ether were selected as extraction solvents according to their polarity index to obtain plant extract using the Soxhlet equipment technique. About 200 g of the *D. roylei* plant material was powdered using a mechanical grinder after being cleaned with deionized water, dried in the shade for 15 days, pulverized with a mechanical grinder, and placed in an airtight container. The extracts were concentrated using a rotating vacuum evaporator after being filtered using Whatman no. 1 filter paper. They were then kept at 4°C for further use.

High resolution-liquid chromatography-mass spectrometry (HR/LC-MS)

The HR/LC-MS analysis of the ethanolic extract was carried out by a UHPLC-PDA-Detector Mass Spectrophotometer (HR/LC-MS 1290 Infinity UHPLC System), Agilent Technologies®, Santa Clara, CA, USA (Noumi et al., 2020). It consisted of a HiP sampler, binary gradient solvent pump, column compartment, and Quadrupole Time of Flight Mass Spectrometer (MS Q-TOF) with a dual Agilent Jet Stream Electrospray (AJS ES) ion source. A total of 1% formic acid was used as a solvent in deionized water (solvent A) and acetonitrile (solvent B). The flow rate of 0.350 mL/min was used, while MS detection was performed in MS Q-TOF. Compounds were identified via their mass spectra and their unique mass fragmentation patterns. Compound Discoverer 2.1, ChemSpider, and PubChem were the main tools for identifying the phytochemical constituents.

Network pharmacology-based analysis

Eight 8) compounds were identified according to UPLC-MS/MS analysis and were subjected to network pharmacology-based analysis. The identification of the target genes linked to the selected constituents was performed using the database STITCH DB (http://stitch.embl.de/,ver.5.0) and the obtained results were utilized for construction of compound-target (C-T) network using Cytoscape 3.5.1. Cytoscape combined score of interactions was adopted for judging the importance of nodes in each given network. Information about functional annotation and the pathways that were highly associated with the target proteins were retrieved

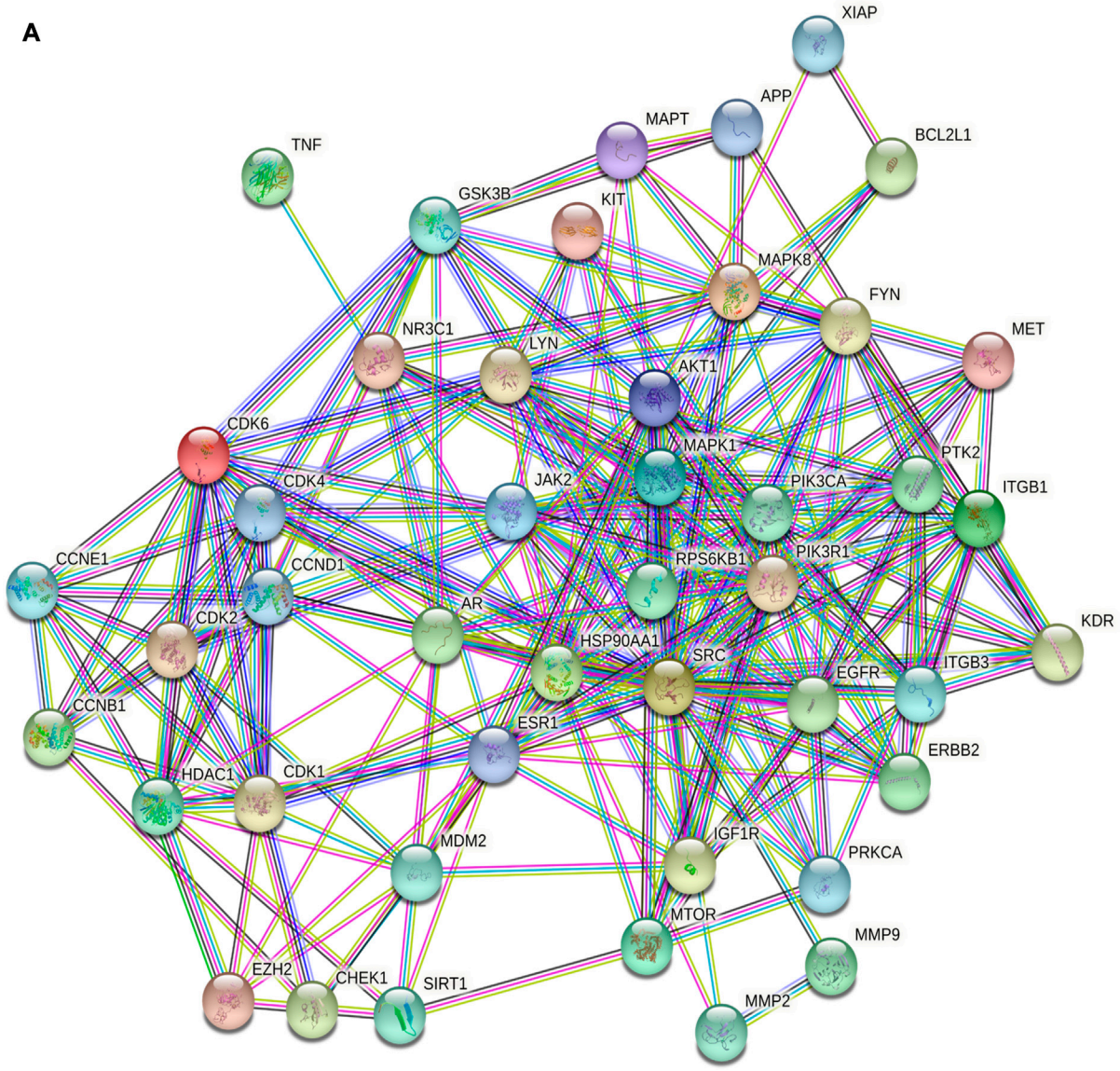

FIGURE 3
(Continued).

from DAVID ver. 6.8 (Database for Annotation, Visualization and Integrated Discovery) and the Kyoto Encyclopedia of Genes and Genomes (KEGG) pathways. Relevant pathways with p-values <0.05 were selected. Target-pathway and constituent-Pathway networks were constructed to visualize the interactions between compounds, targets and cancer-related pathways.

In-silico drug-likeness and toxicity predictions

In silico drug-likeness and toxicity of top hit compounds in the database based on were carried out using the SwissADME web browser (http://www.swissdme.com) (Daina et al., 2017). Drug-likeness and toxicity filtering was based on Lipinski's rule of five (Lipinski, 2004). For example, constituents with predicted oral bioavailability (OB) ≥30 were considered active. Constituents that satisfied less than three criteria were considered inactive.

Molecular docking

The ligand molecule (8-hydroxycoumarin) are retrieved in the form of 3D Standard Data Format from the PubChem database (3D SDF) (Bolton et al., 2011). The ligand was then converted from 3D SDF to Protein Data Bank (PDB) format using Avogadro software. The crystal structures of breast cancer target proteins (Akt1, SRC, EGFR, IL6, HSP90AA and ESR1) were retrieved from the Protein Data Bank. Biovia Discovery studio was used to eliminate undesirable bindings, ligand molecules, water molecules, and other contaminants from the macromolecule. After that polar hydrogens were added to the protein throughout the preparation process for improved interactions, followed

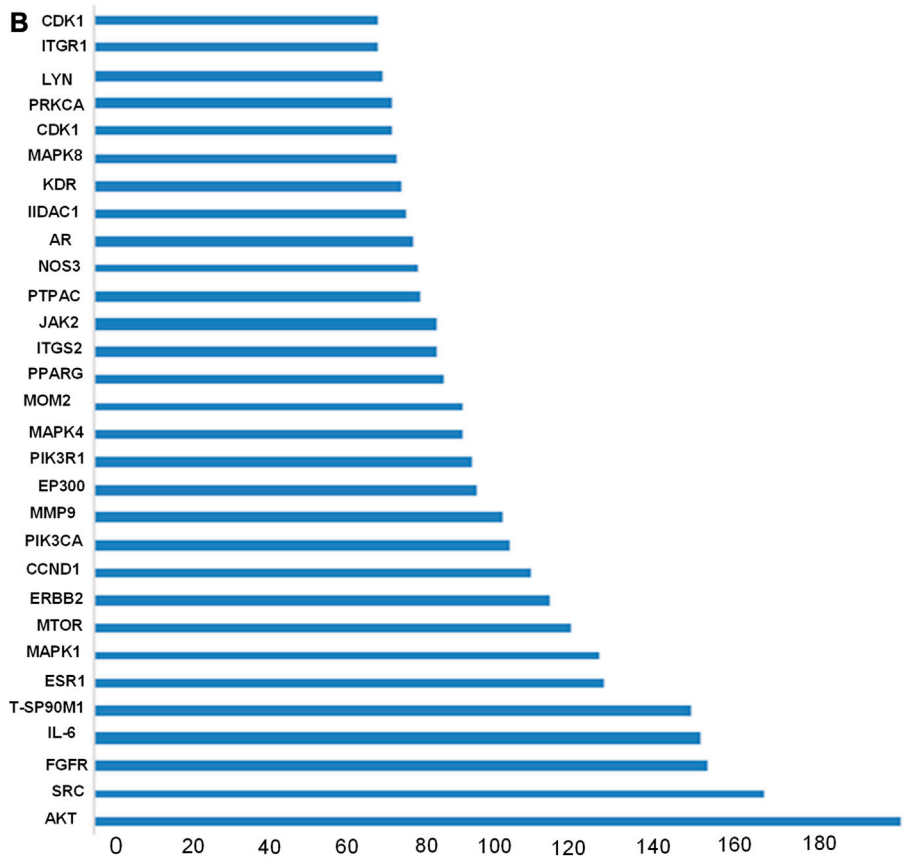

FIGURE 3
(Continued). The common target genes network interaction results **(A)** PPI network of the common target genes. The nodes represent target genes; the stuffing of the nodes represents the 3D structure of target genes; the edges represent target genes-target genes associations; the colors of the edges represent different interactions; cyan and purple represent known interactions; green, red, and blue-purple represent predicted interactions; chartreuse, black, and light blue represent others.

by Kollman charges and other modifications. Molecular docking studies were performed between the target proteins of breast cancer and compounds of the selected plant using AutoDock version 4.2.1 (Trott and Olson, 2010). All other parameters were left at their default values. the grid box was generated centered at X = 14.09, Y = 15.47, Z = 15.48 with dimensions X:3.53, Y:0.58, Z: 12.41. The Lamarckian Genetic Algorithm (LGA) was used for docking studies on the protein and ligand complexes (Fuhrmann et al., 2010). The RMSD clustering maps were developed after the docking process was complete by re-clustering with the clustering tolerances of 1, 0.5, and 0.25 to identify the best cluster with the most populations and lowest energy score.

Molecular dynamics (MD) simulation study

MD simulations were performed using the Desmond 2020.1 from Schrodinger, LLC (Chow et al., 2008; Release, 2017) on the dock complex of Akt1 and 8-hydroxycoumarin ligand. This system used the OPLS4. force field (Mazurek et al., 2021) and an explicit solvent model containing TIP3P water molecules in a period boundary salvation box of 10 Å × 10 Å x 10 Å dimensions. The system was initially equilibrated to retrain over the protein-ligand complexes using an NVT ensemble for 10 ns. Following the preceding phase, an NPT ensemble was used to carry out the brief run of minimization and equilibration for 12 ns. The NPT ensemble was assembled using the Nose–Hoover chain coupling method and operated at 27°C for 1.0 ps under a pressure of 1 bar for the duration of the investigation. The time step was 2 fs. The Martyna–Tuckerman–Klein barostat method with a 02 ps relaxation time was adopted for pressure regulation. The radius for coulomb interactions was set at 9 nm, and long-range electrostatic interactions were calculated using Ewald's particle mesh approach. With each trajectory, the bonded forces were estimated using the RESPA integrator for the time step of 2 fs. Root mean square fluctuation (RMSF), root mean square deviation (RMSD), solvent accessible surface area (SAS Area), and radius of gyration (Rg) were estimated to monitor the stability of molecular docking simulations (Rapaport and Rapaport, 2004).

In vitro antioxidant activity

1, 1-diphenyl-2-picrylhydrazyl radical scavenging activity

The capacity of the D. roylei extracts to scavenge the DPPH radicals were assessed by using the Gyamfi et al. method with slight

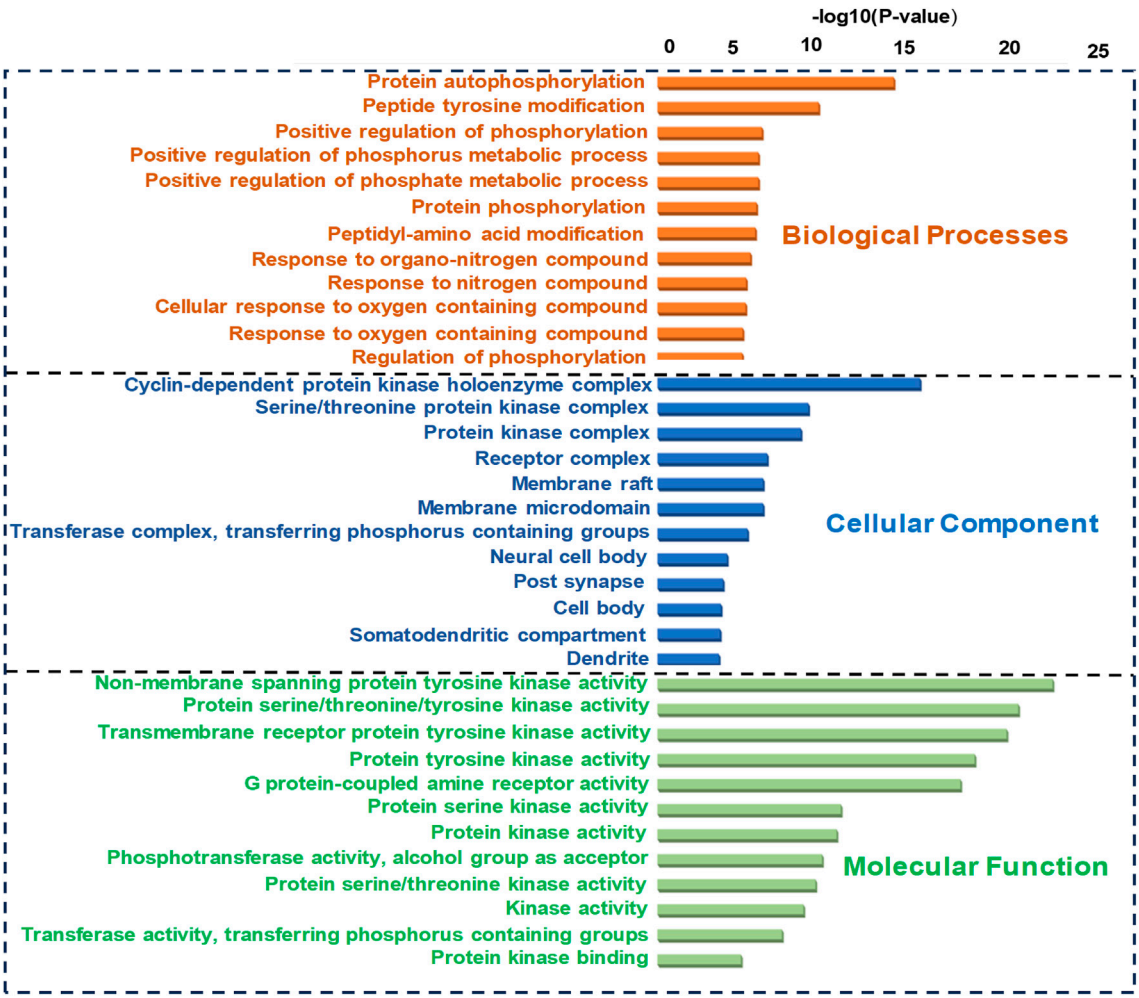

FIGURE 4
GO (Biological process, molecular function, and cellular component) analysis (top 20). The node length represents the number of target genes enriched, and the node color from blue to red represents the *p*-value from large to small.

modification (Obi et al., 2022). 0.5 mL of a test extract aliquot at various concentrations of 20–160 µg/mL in methanol was dissolved with 0.5 mL of a 100 mM DPPH solution. The resulting absorbance was measured at 517 nm after a 30-min incubation period in complete darkness and at room temperature. The following formula was used to compute the percentage inhibition:

$$\text{Percentage inhibition: } \left(\text{Absorbance}_{\text{conrol}} - \text{Absorbance}_{\text{sample}}\right) \text{x } 100 \Big/ \text{absorbance}_{\text{control}}$$

Hydroxyl radical scavenging activity

Hydroxyl radical scavenging activity was determined by Elizabeth and Rao with a bit of modification (Nwakaego et al., 2019). The assay measures the 2-deoxyribose breakdown product by condensing it with Thiobarbituric acid. Hydroxyl radicals are produced by the Fenton reaction, which includes a ferric ions-EDTA-ascorbic acid-H_2O_2system. The reaction mixture contains these above components and different plant extract concentrations (10–80 µg/mL). 0.5 mL of the reaction mixture was dissolved in 1 mL of 2.8 percent of TCA after 1-h incubation at 37°C, then 1 mL of 1 percent aqueous TBA was poured, and the mixture was then incubated for 15 min at 90°C to develop the color. The absorbance was calculated at 532 nm. Butylated hydroxytoluene (BHT) was used as standard.

$$\text{Scavenging effect: } \left(\text{Absorbance}_{\text{conrol}} - \text{Absorbance}_{\text{sample}}\right) \text{x } 100 \Big/ \text{absorbance}_{\text{control}}$$

Reducing power

The assay was carried out using Oyaizu's method (Zhang et al., 2021). This method estimated the reduction of Fe_3^+-Fe_2^+ by measuring the absorbance of Pearl's Prussian blue complex. This procedure relies on the stoichiometric reduction of (Fe_3^+) ferricyanide relative to antioxidants. Various concentrations of the plant extracts (1–200 µg/mL) were added to 2.5 mL of 1% potassium ferricyanide [K_3Fe $(CN)_6$] and 2.5 mL of 0.2 M phosphate buffer with a pH of 6.6. Then 2.5 mL of 10% trichloroacetic acid was added to the mixture after 20 min of incubation at 50°C, and the mixture was then centrifuged at

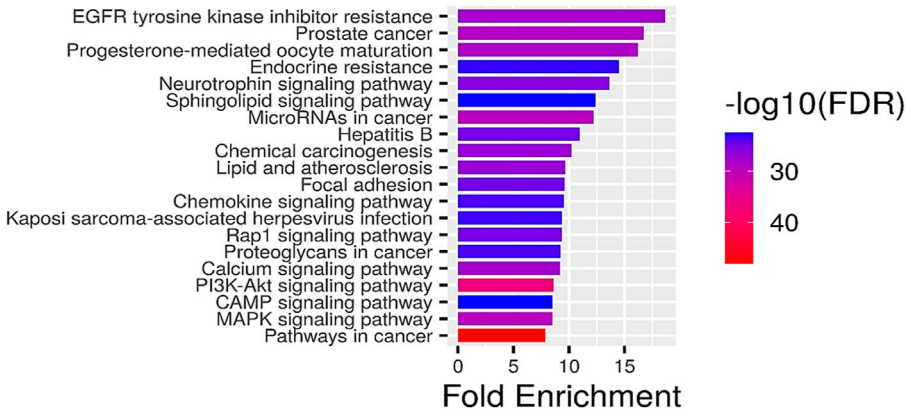

FIGURE 5
KEGG pathway enrichment analysis (top 20). The node size represents the number of target genes enriched, and the node color from blue to red represents the *p*-value from large to small.

TABLE 2 Pathway enrichment analysis (top 20).

Pathway	nGenes	Enrichment FDR
Pathways in cancer	85	9.57052E-49
PI3K-Akt signalling pathway	62	2.08477E-37
MAPK signaling pathway	51	2.01947E-30
MicroRNAs in cancer	40	3.70614E-30
Prostate cancer	33	7.6318E-30
Progesterone-mediated oocyte maturation	33	2.03033E-29
EGFR tyrosine kinase inhibitor resistance	30	6.62478E-29
Calcium signaling pathway	45	1.22381E-28
Chemical carcinogenesis	41	5.63792E-28
Lipid and atherosclerosis	42	1.26925E-27
Neurotrophin signaling pathway	33	6.99563E-27
Rap1 signaling pathway	40	7.78613E-26
Hepatitis B	36	7.98124E-26
Focal adhesion	39	1.19652E-25
Proteoglycans in cancer	38	2.05389E-24
Chemokine signaling pathway	37	2.8697E-24
Kaposi sarcoma-associated herpesvirus infection	37	4.83818E-24
Endocrine resistance	28	8.41165E-24
Sphingolipid signaling pathway	30	2.65785E-23
CAMP signaling pathway	38	3.29632E-23

3,000 rpm for 10 min. The upper layer (2.5 mL) was dissolved in 2.5 mL of distilled water and 0.5 mL of 0.1% $FeCl_3$, and the absorbance was determined at 700 nm. Rutin was taken as a positive antioxidant, and the reducing power was calculated according to the absorbance values.

Superoxide radical scavenging activity

This assay was based on the extract's capacity to reduce formazan production by scavenging the radicals produced by the riboflavin-NBT system (Jaganathan et al., 2018). The reaction mixture consists of 20 µg riboflavin, 50 mM phosphate buffer with a pH of 7.6, 0.1 mg/3mL NBT,

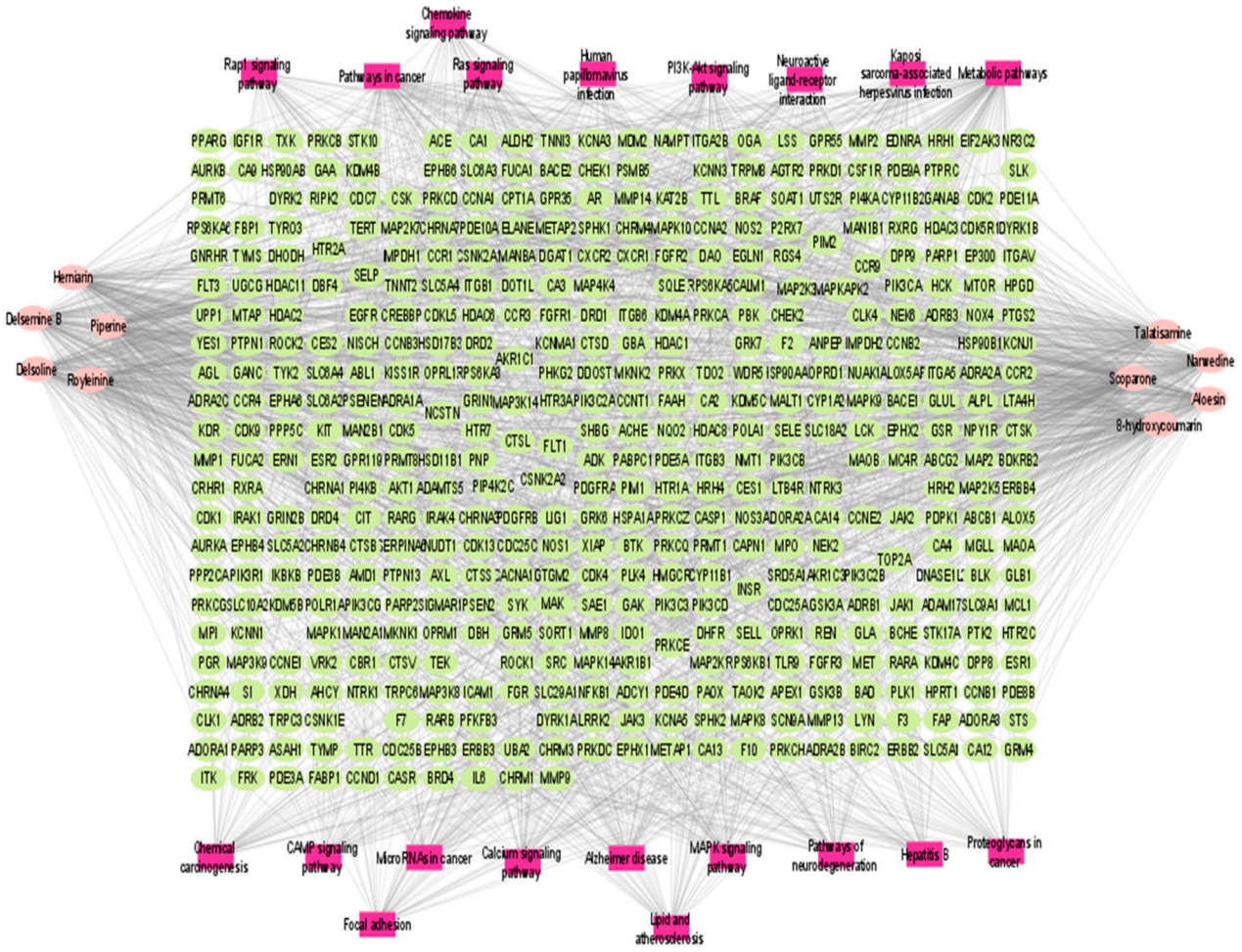

FIGURE 6
Compound prescription-active component-disease-target gene. The node colors represent different groups: purple represents the components, and blue represents target genes. Component node size represents the degree; low to high degree represents the node size from small to large.

and 12 mM EDTA. The reaction was initiated by illuminating the above reaction mixture with various concentrations of plant extracts (10–80 μg/mL) for 90 s. Then the absorbance was estimated at 590 nm. BHT was used standard antioxidant. The %age of scavenging of superoxide anion s was calculated using the equation.

$$\text{Percentage Inhibition: } (1 - A_S/A_C)\,x100$$

Where A_S is the absorbance of the test sample, and A_C is the absorbance of the control used.

In vitro anticancer activity

Cell culture

MCF-7, MDA-MB-231, and MDA-MB-468 cell lines were purchased from the National Centre for Cell Science (NCCS) in Pune. Prof. Annapoorni Rangarajan, IISC, Bangalore, kindly supplied the 4T1 cell line. Cells were grown in high glucose media DMEM using 10% FBS and 1% penicillin/streptomycin. The cells were cultured in a CO2 incubator (5%) at 37°C.

Cytotoxicity assay

The MTT (3-(4,5-Dimethylthiazol-2-yl)-2,5-diphenyltetrazolium bromide) assay was utilized to determine the cell cytotoxicity (Rezadoost et al., 2019). Breast cancer cells were seeded in 96 well plates with the cell number of 3×10^3 cells in each well and allowed to adhere overnight. To prepare the stock solution, From the stock solution 10 mg/mL, various concentrations (12.5–400 μg/mL) of various extracts of *Delphinium roylei* were obtained in fresh media. Then the breast cancer cells (MCF-7, MDA-MB-231, MDA-MB-468 and 4T1) were treated with extracts of *Delphinium roylei* for 72 h and the plate system was placed into the incubator. MTT solution was applied to every well after incubation. The plate was kept in the incubator at 37° C for 4 h under dim lighting. The supernatant was removed after 4 h, and 100 μL of DMSO was added to the purple formazan to dilute it. The ELISA plate reader was used to read the plate at 595 nm. The percentage of cell cytotoxicity was determined using an optical density.

$$\text{Percentage Cell viability} = (\text{OD of test sample}/\text{OD of control}) \times 100$$

TABLE 3 Interaction network details of 21 active components.

Component	Degree	Target genes
8-hydroxycoumarin	112	*CCNB3 CDK2 CCNE2 CDK9 CCND1 CDK5R1 DAO CA12 CA9 CA2 MPI EGFR GPR35 AKR1B1 PDGFRB FLT4 IGF1R INSR AURKB PTK2 PLK1 CSNK2A1 CA4 PLK4 TEK AKT1 BACE1 MAP3K8 EPHB4 HSPA1A NUAK1 SQLE FGR LYN METAP2 SRC GSR CYP1A2 ERBB2 GSK3B MAOA ADORA1 PSMB5 IDO1 TDO2 CA1 ESR1 CA14 DBH NFKB1 BRAF CA3 KDR HSD17B3 AURKA MET ACHE CA13 KAT2B XDH PARP1 F2 ADRA2A ADRA2C ADRA2B HTR2A NISCH ADRA1A HTR1A SLC6A3 PDPK1 CDK1 CDK5 ALDH2 GSK3A PRKCG PRKCD PRKCA PRKCB PRKCZ PRKCE PRKCH NQO2 RPS6KA3 MAP2 TYMS GRM4 KCNA3 GRK6 ESR2 CLK1 CCNA1 CCNT1 CDK1 CDK2 CDK4 CDK5 TNNT2 CCNA2 CCNB1 CCNE1 TNNI3 CCNB2 TNNC1 CA6 CA5B CA5A CA7 GPR84 CHRM5 NQO1 HTR2B*
Delsoline	104	*CDK2 CCNE2 GBA AGL UGCG GAA SI GLB1 GANAB FUCA1 FUCA2 GANC GLA KCNJ1 MTAP MAN2B1 CHRM1 EGFR BACE1 CCR1 CA2 PNP PIK3CA MAN2A1 ADRB1 SLC5A2 ADRB2 HRH1 CCR3 SLC5A4 OPRL1 MMP8 PDE5A PDE11A PDE10A CDC25B METAP2 CTSD HTR2A AMD1 FLT3 UTS2R ADRB3 SLC5A1 IKBKB SPHK1 TOP2A SPHK2 CCR9 OGA ANPEP MAPK9 MANBA CHRNA4 SCN9A HSP90AB1 FLT1 KIT KDR CHRM3 HPRT1 LRRK2 ADCY1 CDC25A LSS SRC NOS1 NOS3 CDC25C TTR PRKCQ UPP1 TLR9 RPS6KB1 CACNA1G AURKA ACE ADORA1 ADORA3 HDAC1 HRH4 TTL CASR DRD1 DPP8 ALOX5 MMP13 MMP1 MAP2K7 NUDT1 IRAK4 CCNA1 CDK2 CCNA2 CCNE1 GBA2 MGAM SLC47A2 HTR4 YARS CHRM2 TRPV3 HTR2B DPP7*
Royleinine	101	*GRIN1 CHRM1 GBA CHRM3 AGL KCNJ1 BACE1 PNP PDE5A PDE11A PDE10A FUCA1 CHRNA4 UGCG GAA LRRK2 HTR1A ADRB2 ADRB1 ADRB3 KCNA5 GANAB SLC18A2 CDC25B OPRL1 MTAP MAN1B1 MAN2A1 PABPC1 NOS1 NOS3 BRD4 SLC5A4 CTSD SLC5A1 CREBBP DRD1 NMT1 SLC6A4 UTS2R SI SPHK1 SLC6A2 NR3C2 PGR CCR1 SPHK2 SLC5A2 CA2 DRD4 TTL CCR3 TOP2A CCR2 DPP8 CSF1R XIAP P2RX7 BIRC2 EIF2AK3 ALOX5 NUDT1 CHRM4 PARP1 ERBB2 MAPK8 MAPK9 CACNA1G FAP HTR3A SERPINA6 TERT ROCK2 SHBG IL6 JAK1 ADAM17 PIK3CA GLUL FABP1 CASR GSK3B CDK2 PRMT6 PRMT8 IDO1 PRMT1 SRC GSR GRIN2B CHRM2 GBA2 SLC47A2 HTR4 DPP7 TRPV3 DUSP3 HTR1D MGAM HTR1F GPBAR1*
Delsemine B	104	*CCNE2 F3 PIK3CA CHRNA7 MTOR SLC10A2 IMPDH1 IMPDH2 PDE10A PIK3CD PIK3CB PIK3CG PIK3CA CA2 PDE8B SLC6A3 PIM1 PIM2 EGFR POLA1 MAP3K14 MMP2 CSF1R GNRHR CCR1 ADORA2A DHFR PIK3C2A PIK3C3 SYK MAP3K9 FGR PIK3C2B CCR4 ERBB2 SLC5A2 FGFR3 FGFR1 FGFR2 NAMPT CDK4 SLC5A1 SLC9A1 ADK ABL1 FLT3 BLK DYRK1A PHKG2 LCK MAPK14 SRC MMP13 ERBB4 MMP9 HCK IRAK1 MET MMP14 STK10 MAPK9 SLK MKNK2 FRK GAK TXK DYRK2 STK17A EPHA6 MMP8 MKNK1 AXL RPS6KA6 CSNK1E MAP2K5 RIPK2 DYRK1B CIT EPHB6 ERBB3 MAP2K1 AKT1 TYRO3 SELP MAP4K4 F10 PRKDC DDOST ALOX5AP PPP2CA DOT1L F7 KIT YES1 CDK2 F7 PIK3R1 CCNE1 PIM3 PDE6A HIPK4 SBK1 PHKG1 CSNK1D*
Herniarin	102	*CDK2 CA1 CA12 CA14 CA9 CA4 CA13 EGFR MAOA CA2 AKR1C3 AKR1C1 CA3 KCNA3 SRD5A1 XDH MAOB CBR1 ACHE PARP1 CYP1A2 MET GSK3B AURKA APEX1 GPR35 PTK2 PLK4 MAP3K8 HSPA1A SQLE FGR LYN ALOX5 AURKB PARP2 IGF1R AHCY EP300 KAT2B NOS1 NOS2 NOS3 SRC KDR ADORA1 ADORA2A ESR2 MCL1 ADAMTS5 PTPRC NQO2 MAPK10 RGS4 JAK1 JAK2 TYK2 CDC7 NUDT1 MAP3K14 AKR1B1 KDM4C PDGFRB CES1 MAPK8 CTSK CES2 DYRK2 DYRK1B ADORA3 HSD11B1 GRM4 CAPN1 HMGCR BACE1 HRH2 MGLL MKNK1 SYK TGM2 GRM5 CLK4 RPS6KA5 RPS6KB1 PIM2 PBK BTK NTRK3 PRKX MAP4K4 PDE5A CCNA1 CCNA2 CA7 CA6 CA5A CA5B MCHR1 ADRA1D MIF ADORA2B PIM3*
Aloesin	108	*CDK9 CCNA2 CCND1 ITGB1 ITGAV ITGA2B ITGAV SAE1 AKR1B1 SLC29A1 CA12 MMP9 MMP2 ESR1 ESR2 HDAC6 IGF1R AURKB SRC PTK2 KDR PLK1 HDAC8 HDAC1 MET NEK2 AKT1 NEK6 NUAK1 NOS2 MMP13 CA2 CA4 EGLN1 BACE1 NQO2 HSP90AB1 SORT1 NOX4 DNASE1L3 IKBKB PTPN1 HDAC3 HDAC2 ADORA2A ABCB1 DHODH LIG1 CXCR2 CALM1 HSP90AA1 FBP1 KCNMA1 ERN1 CA1 CA9 HSP90B1 PRKCG PRKCB PRKCZ CDC7 ADRA2C ALOX5 CXCR1 SLC5A1 CBR1 SLC5A2 MCL1 LTB4R SELL SELP PPARG STS SIGMAR1 DRD2 BAD OPRM1 OPRK1 ABCG2 LRRK2 GRK7 TAOK2 MAK CDKL5 VRK2 PIP4K2C CDK13 CSF1R ABL1 CCNT1 CDK2 CDK4 ITGA5 ITGB3 ITGB6 UBA2 CA7 HDAC10 DUSP3 PTGES CA6 VEGFA PSMG3 BCL2 HTR2B HIPK4 ICK*
Talatisamine	101	*GRIN1 CHRM1 PABPC1 CHRM3 AGL GBA BACE1 KCNJ1 SIGMAR1 PNP PDE5A PDE11A PDE10A UGCG GAA MTAP UTS2R CTSD KCNA5 MAN1B1 MAN2A1 LRRK2 CA2 FUCA1 CCR3 ADRB1 CCR1 SPHK2 XIAP BIRC2 PIK3CA P2RX7 DRD1 REN ADRB2 SRC ADRB3 CDC25B HTR7 TOP2A BRD4 FLT3 PDE9A CREBBP TERT NOS1 CACNA1G NOS3 SI NMT1 PRKCB NPY1R ERBB2 PRKCQ MANBA SLC5A4 DRD4 PRKDC PRMT6 CSF1R PRMT8 MKNK2 MKNK1 PRMT1 HTR3A PIM1 PIM2 GANAB PARP1 TTL MAPK8 CHEK2 CDK2 MAPK9 CHEK1 SLC5A2 HSP90AB1 MMP8 CASR NR3C2 PGR ABL1 KIT YES1 ALOX5 LCK MAPK14 CSK GRIN2B CHRM2 HTR4 GBA2 SLC47A2 DPP7 DUSP3 HTR1D PDE1C TRPV3 MGAM HTR1F MAPK11*
Narwedine	105	*CDK1 DBF4 CHRNA3 ROCK2 ACHE OPRM1 OPRD1 BCHE OPRK1 BDKRB2 SLC6A2 SLC6A4 SLC6A3 MAOB DRD4 PAOX MC4R CHRM4 CHRM3 NOS2 CHRNA4 KDM5C MPO KDM4B KDM5B PARP2 JAK3 CHEK2 JAK1 JAK2 ROCK2 PDE10A CHRNA1 PIM1 PIM2 CHEK1 KDM4A ROCK1 POLR1A HTR3A HTR2C HTR1A MAPK8 PRKCD PRKCE PRKD1 RPS6KA5 PRKX PRMT6 IMPDH2 PRMT8 PRMT1 CSNK2A1 CSNK2A2 PRKCQ HTR7 AURKB RPS6KB1 AURKA ADORA1 MALT1 LTA4H DPP8 DPP9 KISS1R WDR5 MAOA CDC25C SYK SIGMAR1 MAPK1 HRH2 PNP KCNA5 NOS1 FAP CDC7 PBK CSF1R PRKCA ESR2 MAP2K1 ADRA2B HRH4 PARP3 EGFR TERT KCNJ1 HRH1 GSK3B MMP13 MMP9 CCNB1 CDC7 CHRNB4 ROCK1 CHRM5 DPP7 ADRA1D PIM3 HTR1F HTR2B HTR1D CHRNB2*
Scoparone	102	*CDK2 CA12 CA9 CA13 CA14 CA1 CA4 XDH CA2 EGFR ALOX5 SRD5A1 CA3 CBR1 SRC MAOA AKR1B1 AKR1C1 GSK3B MAOB ESR2 KCNA3 PTGS2 IGF1R KDR AURKA ERBB2 PDE5A ADAMTS5 PDE3A PDE3B BACE1 GPR35 SQLE FGR LYN PARP1 PARP2 MAPK8 MPO AURKB TYMP GRM4 CDC7 KCNN1 KCNN3 CTSK CTSS CTSL PDGFRB FLT4 INSR TEK EPHB4 MAP2K3 BTK IKBKB MAPK10 CES1 ROCK2 CES2 EPHB3 SYK CLK4 RPS6KA5 RPS6KB1 PIM2 PBK NTRK3 PRKX MAP4K4 PLK1 JAK2 PTPRC TYK2 BRAF HSP90AA1 DYRK1B NQO2 KDM4C MET MAPK14 TGM2 PTPN13 METAP1 ICAM1 SELE CASP1 MAP3K14 APEX1 MCL1 NUAK1 MAPKAPK2 JAK1 CCNA1 CCNA2 CA7 CA6 CA5B CA5A KCNN2 PIM3*
Piperine	110	*PSEN2 CDK2 DBF4 CCNA2 CCNE1 PDGFRA ROCK2 MAOB SIGMAR1 SOAT1 ITK KDM5C KDM4A KDM4C EPHX2 PRKCQ FLT3 SRC JAK2 ADORA2A CSF1R CPT1A FAAH NTRK1 ASAH1 IMPDH2 PDE4D PARP1 CDC7 TRPM8 IRAK4 DGAT1 AURKB ADAMTS5 CDK1 AURKA EDNRA ALPL ACHE ABL1 PFKFB3 STS PDE10A LCK PI4KA SLC5A1 TRPC6 TRPC3 HDAC11 DRD2 NAMPT ADORA3 IDO1 MDM2 GPR119 PPP5C AR EPHX1 PGR ROCK2 GPR55 PDE5A CTSV CTSL RPS6KA3 F10 ADORA1 RPS6KB1 TOP2A ELANE GRM5 CTSB LRRK2 CYP11B1 RARG RARB RARA PDE3A CYP11B2 PDE3B PI4KB CDK5 RXRA RXRG HPGD AGTR2 CRHR1 IKBKB BACE2 CCNA1 CDC7 CDK2 PDGFRB PSENEN ROCK1 CCNA2 NCSTN KDM4E ACACB KDM4D QPCT NAAA SLC6A9 PDE7A HDAC10 SCN2A SCN10A ADORA2B APH1A*

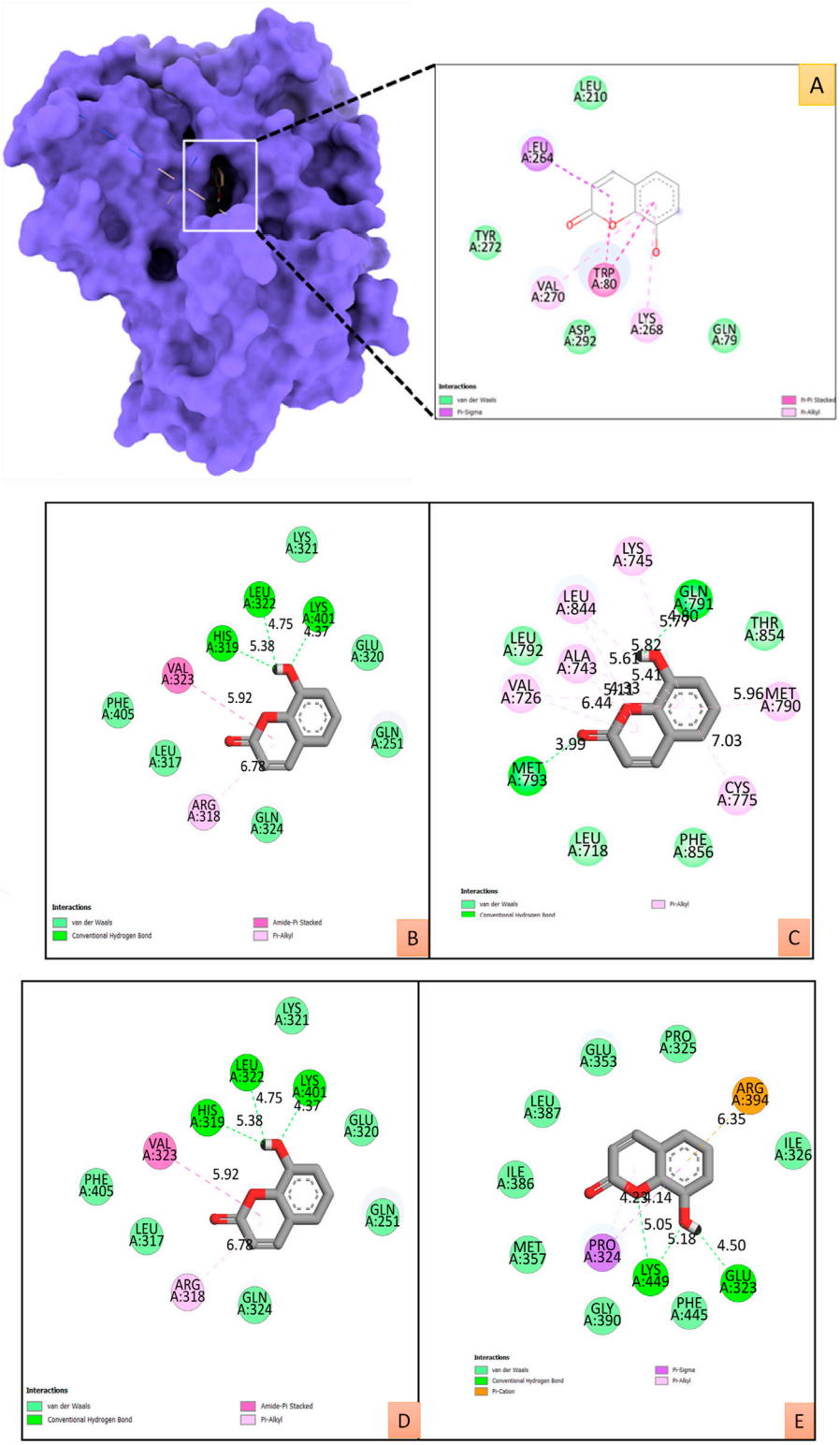

FIGURE 7
(A). The surface view of the best pose of the Akt1 (PDB ID:4EKL) +8-Hydroxycoumarin complex displays the surface view on the left panel and the 2D interaction profile of the ligand with binding cavity residues. **B-E:** 2D and 3D interactions of 8-Hydroxycoumarin with various target proteins **(B).** SRC (PDB ID:2H8H), **(C).** EGFR (PDB ID: 6DUK), **(D).** IL-6 (PDB ID:1P9M), **(E).** ESR-1 (PDB ID: 1GWQ) with respective amino acids respectively.

TABLE 4 Binding energy obtained from the docking calculations of bioactive phytoconstituents with target proteins.

S. No.	Compound name	Akt1 Energy score (kcal/mol)	SRC Energy score (kcal/mol)	EGFR Energy score (kcal/mol)	IL-6 Energy score (kcal/mol)	Hsp90aa1 Energy score (kcal/mol)	ESR-1 Energy score (kcal/mol)
1	8-hydroxycoumarin	−9.2	−5.30	−5.74	−4.06	−5.42	−5.75
2	Delsoline	−6.8	−7.4	−6.3	−5.9	−5.8	−7.2
3	Royleinine	−7.5	−8.1	−7.4	−6.1	−6.3	−6.7
4	Delsemine B	−9	−8.7	−8.2	−7.3	−7.2	−8.2
5	Herniarin	−7.4	−6.6	−5.9	−5.9	−5.5	−6.6
6	Aloesin	−8.1	−7.7	−8.9	−6.9	−6.8	−7.4
7	Talatisamine	−7.5	−7.3	−6.6	−6	−6.2	−7
8	Narwedine	−8.5	−7.1	−7.6	−7	−6.5	−8.6
9	Scoparone	−7.5	−6.5	−6.1	−5.9	−5.3	−6.8
10	Piperine	−9	−8.4	−7.6	−6.7	−7.4	−8

TABLE 5 Drug-likeness prediction of *D. roylei* phytoconstituents by ADMET evaluation using SwissADME Software.

Compound Name	MW	HBA	HBD	RB	TPSA (Å^2)	Lipinski's Rule	GI absorption	BBB	Solubility	ADMET Screening
8-hydroxycoumarin	162.14	3	1	0	50.44	Yes	High	Yes	soluble	Yes
Delsoline	467.6	8	3	6	100.85	Yes	High	No	Very soluble	Yes
Royleinine	421.6	6	2	4	71.39	No	High	No	soluble	Yes
Delsemine B	699.8	11	4	14	179.39	No	Low	No	soluble	No
Herniarin	176.17	3	0	1	39.44	No	High	Yes	soluble	Yes
Aloesin	394.4	9	5	4	157.66	Yes	Low	No	soluble	Yes
Talatisamine	421.6	6	2	5	71.39	No	High	No	soluble	Yes
Narwedine	285.34	4	0	1	38.77	Yes	High	Yes	soluble	Yes
Scoparone	206.19	4	0	2	48.67	Yes	High	Yes	soluble	Yes
Piperine	284.34	3	0	4	38.77	Yes	High	Yes	soluble	Yes

MW: molecular weight, HBA: hydrogen bond acceptors, HBD: hydrogen bond donors, RB: rotatory bonds, GI: gastrointestinal absorption, BBB: blood brain barrier.

Annexin V/PI apoptosis detection

We used a BD Biosciences Annexin V apoptosis detection kit to examine the mechanism behind the anticancer effect of D. roylei ethyl acetate extract. MDA-MB-231 was treated with acetate extract for 24 and 48 h. As instructed by the manufacturer, adherent and free-floating cells were all collected and stained with the fluorescent dyes FITC-Annexin V and PI. Flow cytometry was performed at the Department of Biotechnology, National Institute of Technology, Rourkela, Odisha, India, on a BD Accuri™ C6 flow cytometer (Mehraj et al., 2022)

Results

Quantification of chemical components of HR/LC-MS

In our previous investigation, 168 phytocompounds were tentatively identified using the chromatography-mass spectrometry (LC/MS) approach in both negative and positive ionization modes (Mir et al., 2022b). A few more compounds were identified by performing the advanced technique like HR-LC/MS) and chromatograms in TOF MS ES + shown in (Figures 1A–D). Figure S1 demonstrates the total ion chromatogram (TIC) of the studied plant's methanolic, ethanolic, ethyl acetate, and petroleum ether extracts. The examples of a few phytoconstituents identified through HR-LC/MS are 8-hydroxycoumarin, Delsoline, Royleinine, Delsemine B, Herniarin, Aloesin, Talatisamine, Narwedine, Scoparone, and Piperine in *D. roylei* extracts by contrasting their output mass data and retention time relatives to external standards with a reference database and already published data using different software's. Some identified phytocompounds from chromatograms that possess important pharmacological properties are listed in Table 1. These nine compounds were subjected to network pharmacology, *in silico* docking, and MD simulations analysis. These phytocompounds were identified as

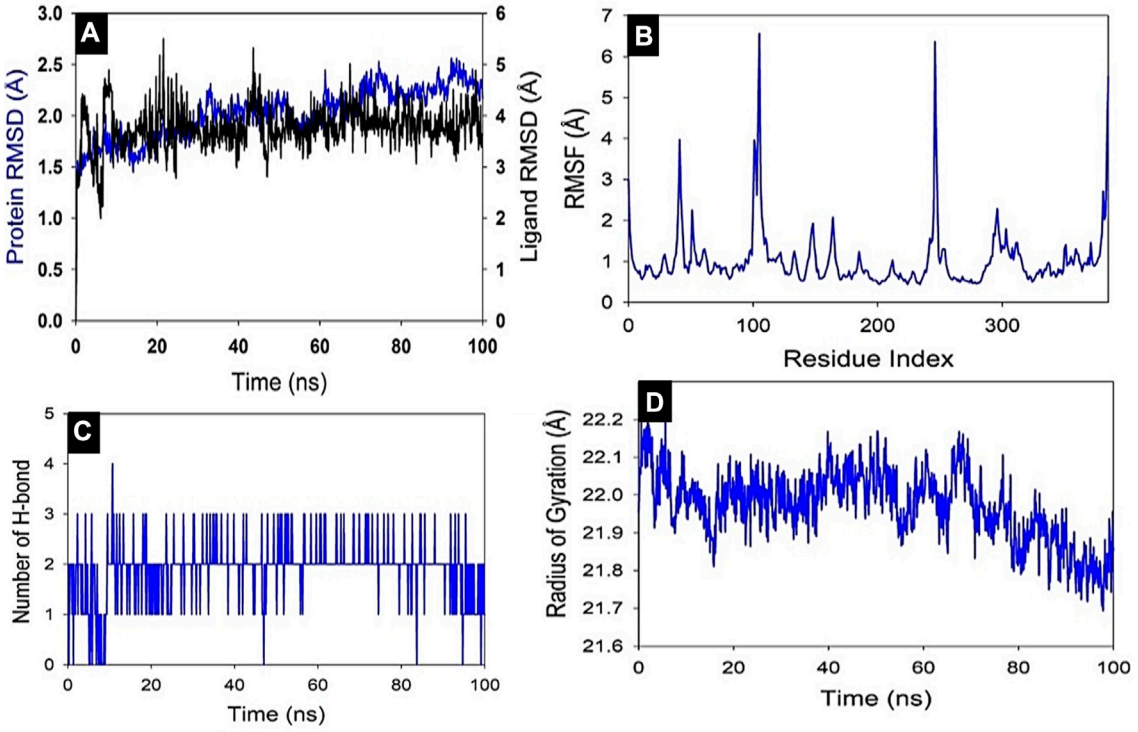

FIGURE 8
MD simulation analysis of 100 ns trajectories of **(A)** Cα backbone of Akt1 bound to 8-Hydroxycoumarin ligand, **(B)** RMSF of Cα backbone of Akt1 bound to 8-Hydroxycoumarin-ligand **(C)** Radius of gyration (Rg) of Cα backbone of Akt1 bound to 8-Hydroxycoumarin **(D)** Formation of hydrogen bonds in Akt1 bound to 8-Hydroxycoumarin.

TABLE 6 Binding free energy components for the Akt1+8-hydoxycoumarin calculated by MM-GBSA.

Energies (kcal/mol)	AKT1 + 8-hydroxycoumarin
ΔG_{bind}	−52.23 ± 5.12
ΔG_{bind}Lipo	−12.23 ± 2.19
ΔG_{bind}vdW	−41.12 ± 1.08
ΔG_{bind}Coulomb	−27.41 ± 2.29
$\Delta G_{bind}H_{bond}$	−3.13 ± 1.32
ΔG_{bind}SolvGB	35.41 ± 1.57
ΔG_{bind}Covalent	5.91 ± 2.61

chemical markers and listed as potential candidates for further network pharmacology analysis.

Network pharmacology

Target gene screening and interaction network construction

Total of 514 potential target genes were obtained for the 10 quantitative components of HR/LC-MS (shown in Figure 2). Meanwhile, 12063 disease target genes associated with breast cancer were retrieved using GeneCards, OMIM and DisGeNET platforms. 464 shared common target genes were identified between the quantitative components of HR/LC-MS and breast cancer. All 10 components in *D. roylei*, namely, 8-hydroxycoumarin, Delsoline, Royleinine, Delsemine B, Herniarin, Aloesin, Talatisamine, Narwedine, Scoparone, Piperine in *D. roylei* were targeted for further analysis. The common target genes PPI diagram indicated that there were 464 nodes and 6,035 edges in PPI (Figure 3A). The frequency of occurrence of the top 30 common target genes was shown in Figure 3B. Akt1, SRC, EGFR, IL6, HSP90AA, and other target genes exhibited a high frequency of protein interaction, which may be the node protein of the whole network. The results showed that the selected components of *D. roylei* had a high binding activity with these target proteins and could be used as the potential target genes of HR/LC-MS for treating breast cancer.

Screening of key pathways of HR-LC/MS for treating breast cancer

GO analysis of the common target genes showed that the biological process was mainly involved in Protein autophosphorylation, peptidyl-tyrosine modification, and pos. neg. of phosphorylation (Figure 4) and also given as S-2 to S-4. The molecular functions non-membrane spanning protein tyrosine kinase activity and protein serine/threonine/tyrosine kinase activity were leading. The cyclin-dependent protein kinase holoenzyme complex and protein-kinase complex were observed in the cellular component. KEGG pathway enrichment analysis of the aforementioned common target genes is shown in Figure 5 and

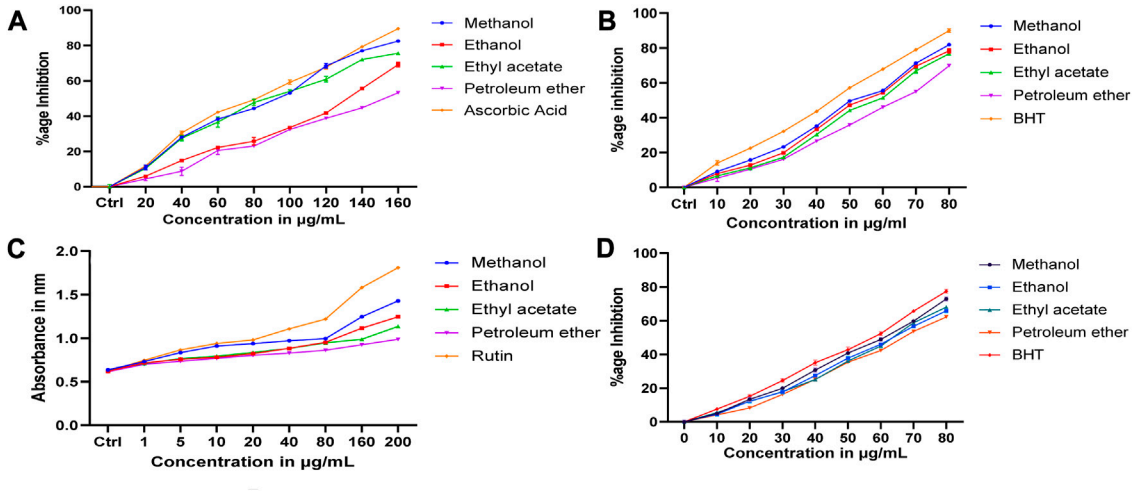

FIGURE 9
Antioxidant results of *D. roylei* **(A)**. DPPH radical scavenging assay **(B)**. Hydroxyl radical scavenging assay **(C)**. Reducing power assay, and **(D)**. Superoxide radical scavenging assay.

also given as S-5. After the exclusion of broad pathways, the top 20 signalling pathways are listed in Table 2. This suggested that the effect of HR-LC/MS for treating breast cancer may act on multiple pathways, as well as complex interactions among these pathways.

Compound prescription-active component-disease target gene-pathway interaction network

Compound prescription-active component-disease-target gene-pathway interaction network finding is shown in Figure 6. The network contained 474 nodes (464 target genes, 10 active components. Besides, the interaction network results of 10 active compounds are shown in Table 3. The degree of 8-hydroxycoumarin, Delsoline, Royleinine, Delsemine B, Herniarin, Aloesin, Talatisamine, Narwedine, Scoparone, and Piperine were 112, 104, 101, 104, 102, 108, 101, 105, 102 and 110 respectively. The results above show that quality markers in LC-MS may act on the whole biological network system rather than on a single target gene.

Molecular docking studies

All the binding energy scores are calculated from the best cluster (95%) that falls within the lowest RMSD 0.25 Å. With the lowest binding energy (ΔG–9.2 kcal/mol) and inhibitory concentration, Ki (1.14 µM), 8-hydroxycoumarin showed a considerable binding affinity for the Akt1 (Figure 7A). During the interaction of the ligand 8-hydroxycoumarin, Trp80 is involved in pi-pi stacking, and Lys268 and Val270 residues are involved in pi-alkyl interaction at the binding cavity of the protein. Besides hydrogen bonding, Leu264 is involved in pi-sigma interaction, and the rest residues are van der Waal's interactions by amino acid residues formed weak non-bonded interaction with the ligand (Figure 7A and right panel). Molecular docking studies were performed to verify the affinity of target protein(s) and bioactive phytocompounds. The 3D interactions of 8-Hydroxycoumarin with various target proteins; SRC, EGFR, IL-6, Hsp90aa1 and ESR-1 and 2D structure of 8-Hydroxycoumarin interacted with respective amino acids respectively are shown in Figures 7B–F. Table 4 depicts the docking and scores of the *D. roylei* compounds; 8-hydroxycoumarin, Delsoline, Royleinine, Delsemine B, Herniarin, Aloesin, Talatisamine, Narwedine, Scoparone, and Piperine against the active sites of the identified protein targets, Akt1, SRC, EGFR, IL-6, Hsp90aa1and ESR-1 performed using the AutoDock Vina software.

Drug-likeness prediction of *D. roylei* phytoconstituents

The compounds retrieved from PubChem were assessed for Lipinski's Rule of 5, with drug-likeliness properties. Furthermore, ADMET evaluation was applied and was selected for molecular docking to determine the binding affinity with protein at the active site. Almost all the nine phytoconstituents accept Lipinski's rule with few limitations, as shown in Table 5.

Molecular dynamic (MD) simulation study

Studies using molecular dynamics and simulation (MD) were conducted to determine the convergence and stability of the Akt1+8-Hydroxycoumarin complex. Comparing the root mean square deviation (RMSD) values, the simulation of 100 ns showed stable conformation. The RMSD of the Cα-backbone of Akt1 bound to 8-Hydroxycoumarin showed a deviation of 2.1 Å (Figure 8A), while the ligand showed an RMSD deviation of 3.8.0 Å. Stable RMSD plots indicate good convergence and stable conformations throughout the simulation. As a result, it may be inferred that 8-Hydroxycoumarin bound with Akt1 is quite stable in complex due to the ligand's increased affinity. The plot for root mean square fluctuations (RMSF) indicates the residual fluctuations due to conformational variations in different secondary structures. Here RMSF plot displayed fluctuating residues while high fluctuations were observed among 50–60, 110–130, and 240–260 residual positions (Figure 8B). The highest fluctuating peaks comprised of 3.8 Å to 6.7–6.8 Å, might be due to higher ordered flexibility conforming into loops (Figure 2B). Therefore, the protein Akt1 has significant flexibility to conform to specific secondary structures to accommodate the ligand. The radius of gyration (Rg)

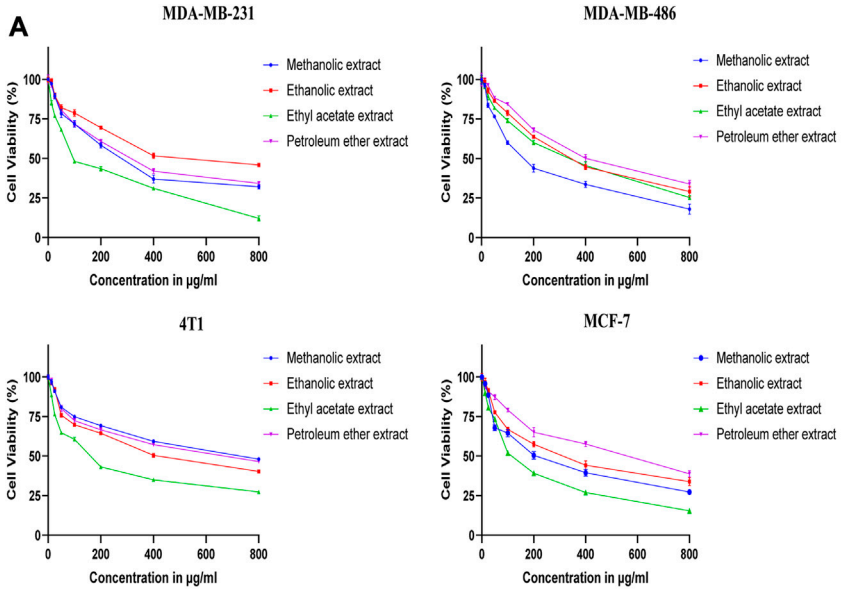

Cell viability of *D. roylei* extracts against various breast cancer cell lines.

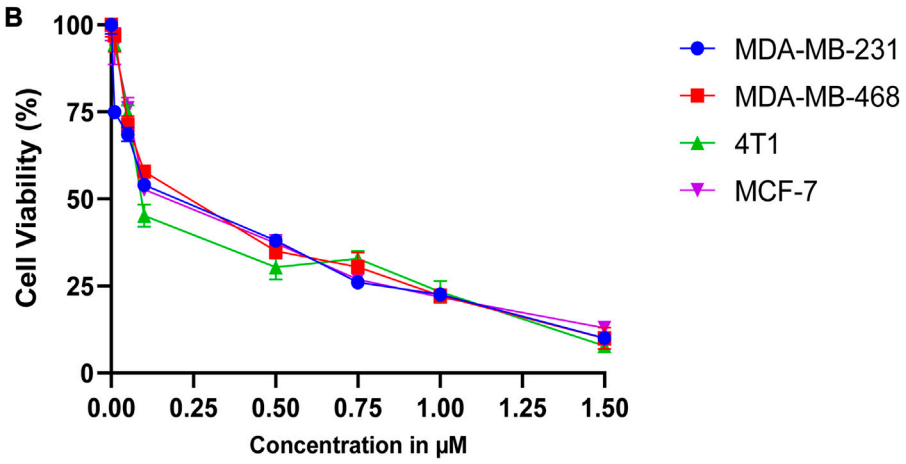

Cell viability of positive control (Doxorubicin) against various breast cancer cell lines.

FIGURE 10
(A). Cell viability of *D. roylei* extracts against various breast cancer cell lines. **(B)** Cell viability of positive control (Doxorubicin) against various breast cancer cell lines.

TABLE 7 IC_{50} values in µg/mL of various extracts of *D. roylei* against different breast cancer cell lines.

Extracts	MDA-MB-231	MDA-MB-268	4T1	MCF-7
Methanolic extract	274.1	166.3	689.4	213.4
Ethanolic extract	549.3	335.5	420.7	299.3
Ethyl acetate extract	116.5	296.1	157.9	125.5
Petroleum ether extract	317.1	415.5	598.9	498.6
Doxorubicin standard	0.1311	0.1875	0.1433	0.1822

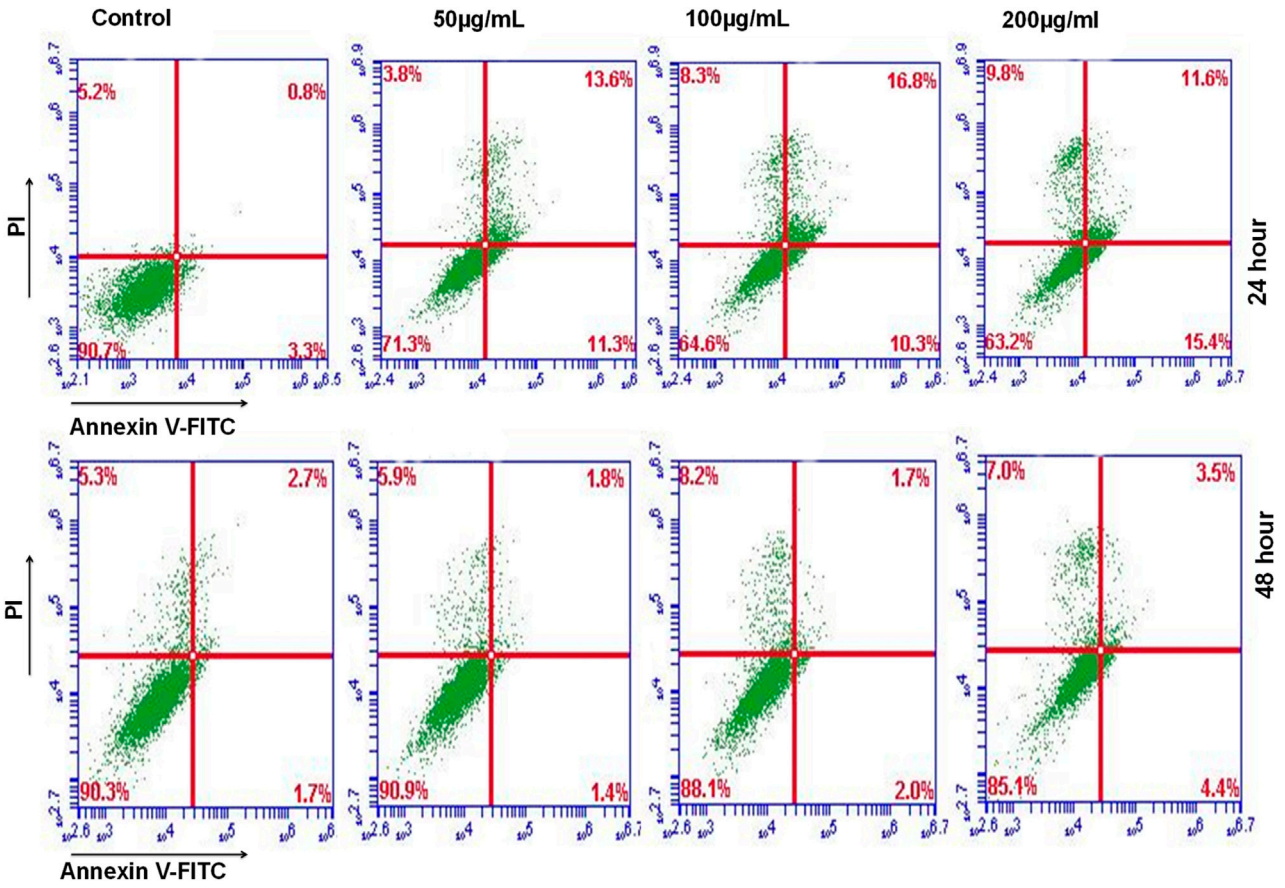

FIGURE 11
Annexin V & P1 staining showed increased apoptotic cells in plates treated with the ethyl acetate extract of *D. roylei* after 24 h or 48 h periods.

quantifies how compact a protein is with a ligand molecule (Miu et al., 2008). In this investigation, the Akt1 Cα -backbone linked to 8-hydroxycourmarin demonstrated a stable radius of gyration (Rg) values between 22.1 and 21.8 Å, hence there are no sudden changes in radius of gyration as shown in (Figure 8D). This steady values of Rg suggest that despite the structural changes caused by the compounds, the protein remains folded. Significant stable gyration (Rg) suggests that the protein is oriented in a highly compact manner when it is attached to a ligand. The quantity of hydrogen bonds between the ligand and protein indicates the complex's interaction's complex stability and depth. During the 100 ns of the simulation, there were significant numbers of hydrogen bonds between Akt1 and 8-hydroxycourmarin (Figure 8C). Between Akt1 and 8-hydroxycourmarin-ligand, the average number of hydrogen bonds is two. The overall analysis of Rg indicates that the binding of the various ligands causes the corresponding proteins to become less flexible and more compact.

Molecular mechanics generalized born surface area (MM-GBSA) calculations

Utilizing the MD simulation trajectory, the binding free energy and other contributing energy in the form of MM-GBSA is determined for Akt1 bound to 8-Hydroxycoumarin complexes. The results (Table 6) suggested that the maximum contribution to ΔGbind in the stability of the simulated complexes was due to ΔG_{bind}Coulomb, ΔG_{bind}vdW, ΔG_{bind}Hbond, and ΔG_{bind}Lipo, while ΔG_{bind}Covalent and ΔG_{bind}SolvGB contributed to the instability of the corresponding complex. Akt1 bound to 8-Hydroxycoumarin complex has significantly higher binding free energies dGbind = −52.23 ± 5.12 kcal/mol (Table 6). These results supported the potential of AKT1 bound to 8-Hydroxycoumarin having a high affinity of binding to the protein, efficiency in binding to the selected protein, and the ability to form stable protein-ligand complexes (Balasubramaniam et al., 2021).

In vitro antioxidant activity

DPPH assay

All the extracts showed different levels of DPPH radical scavenging activity over the range of 20–160 μg/mL concentration, as shown in Figure 9A. The methanolic extract exhibited the strongest DPPH radical scavenging activity compared to other extracts. The extract's radical scavenging activity was effective in the order Methanolic > ethanol > Ethyl acetate > Petroleum ether. A maximum of 82.46% ± 0.2% radical scavenging potential was observed at 200 μg/mL of methanolic extract used, whereas for ascorbic acid, the scavenging activity was 89.57% ± 0.25%. A minimum of 66.35% ± 0.32% scavenging potential was observed at

200 µg/mL of petroleum ether extract. Standards and all the extracts showed a dose-dependent inhibition of the DPPH radicals.

Hydroxyl radical scavenging assay

In this assay, results showed that the methanolic extract of *D. roylei* had the highest potential to scavenge hydroxyl radicals than the ethanolic extracts, ethyl acetate, and petroleum ether, as shown in Figure 9B. At a concentration of 80 µg/mL, the methanolic, ethyl acetate, ethanolic, and petroleum ether extract showed the maximum scavenging effect of 81.92% ± 0.49%, 78.72% ± 0.8%, 73% ± 0.7% and 69.88% ± 0.55% inhibition on hydroxyl radicals. Butylated hydroxytoluene (BHT) taken as a control had shown a more scavenging effect (90.07% ± 1%) than plant extracts.

Reducing power assay

As illustrated in Figure 9C, Fe_3^+ was transformed to Fe_2^+ in the presence of *D. roylei* extract and the reference compound Rutin to measure the reductive capability. The reducing power increased with an increase in the concentration of plant extracts. The methanolic extract of *D. roylei* showed significant reducing power when compared with standard Rutin. The reducing power demonstrated by the methanolic extract of the plant was 1.429 ± 0.005 at the concentration of 200 µg/ml as compared to 1.811 ± 0.0035 shown by standard Rutin at the same concentration. Ethanolic, ethyl acetate, and petroleum ether extracts showed less reducing power (1.246 ± 0.0025, 1.136 ± 003, and 0.987 ± 0.005, respectively) compared to methanolic extracts at 200 µg/mL concentration.

Superoxide radical scavenging (SARS) assay

All the test extracts exhibited effective O_2^{-*} scavenging activity in a concentration-dependent manner (10–80 µg/mL), as shown in Figure 9D. The highest activity (Scavenging effect of 72.91 ± 0.76 was shown by methanolic extracts of *D. roylei* at a concentration of 80 µg/mL, followed by ethyl acetate, ethanolic, and petroleum ether extracts with a scavenging effect of 68.125% ± 0.45%, 65.84% ± 0.41% and 62.27% ± 0.5% respectively, which is least as compared to methanolic extract and standard Rutin. Standard Rutin showed the highest scavenging potential of 77.46% ± 0.7% showed the highest potential at 80 µg/mL concentration as compared to all four extracts of the plant.

In vitro anticancer activity

MTT results

Figures 10A,B shows the cell viability (%) of various breast cancer cell lines; MDA-MB-231, MCF-7, MDA-MB-468, and 4T1 when treated with different concentrations of methanolic, ethanolic, ethyl acetate, and petroleum ether extracts of *D. roylei* and doxorubicin drug. The IC50 values of four different extracts and positive control against various breast cancer cell lines are shown in Table 7. The ethyl acetate extract of the plant showed a maximum cytotoxic effect on MDA-MB-231 with an IC_{50} value of 116.7 µg/mL, followed by methanolic, petroleum ether, and ethanolic extract with IC_{50} values of 274.1, 317.1, and 549.3 µg/mL respectively. The Methanolic extract of the plant showed maximum reduction in the growth of MD-MB-468 breast cancer cell line with the lowest IC_{50} value of 166.3 µg/mL, followed by ethyl acetate, ethanolic, and petroleum ether extract with IC_{50} values of 296.1, 335.5 and 415.5 µg/mL respectively. The ethyl acetate extract showed maximum anti-proliferative potential against the 4T1 cell line with an IC_{50} value of 157.9 µg/mL. The ethanolic, petroleum ether and methanolic extracts have shown less anti-proliferative potential against 4T1with IC_{50} values of 420.7, 598.9, and 689.4 µg/mL, respectively. The ethyl acetate extract is highly specific to MCF-7 cell lines with an IC_{50} value of 125.5 µg/mL, followed by methanolic, ethanolic, and petroleum ether extracts with IC_{50} values of 213, 299.3, and 498.6 µg/mL, respectively. The IC_{50} values of standard doxorubicin are shown in Table 4. Hence ethyl acetate extract of *D. roylei* showed the highest anticancer activity against the MDA-MB-231, MCF-7 and 4T1 cell lines compared to the other three extracts.

Furthermore, we utilized Annexin V and PI staining to assess the apoptosis induction potential of ethyl acetate extract of *D. roylei*. MDA-MB-231 cells were treated for 24 and 48 h, followed by staining with Annexin V and PI. Flow cytometry analysis revealed that plant extract induction tumour cell death via induction of apoptosis and apoptosis enhanced significantly upon higher concentration are shown in Figure 11.

Discussion

In the current study, many secondary metabolites were identified using HR-LC/MS of *D. roylei,* out of which few phytocompounds were selected to propose a possible mechanism against breast cancer treatment using network pharmacology, molecular docking, molecular dynamic simulation and *in vitro* studies. The network pharmacology analysis suggested that the therapeutic efficacy of the *D. roylei* phytoconstituents against breast cancer was mainly associated with 20 signalling pathways, 30 potential target genes, and 10 bioactives. Through the network pharmacology, we identified the most significant protein (Akt1) associated with the occurrence and development of cancer and a bioactive 8-hydroxycoumarin (8-hydroxychromen-2-one) from the *D. roylei*. We identified a hub signaling pathway (PI3K-Akt signaling pathway, indicating the lowest rich factor among 20 signaling pathways. Akt1 kinase is a protein made according to instructions from the Akt1 gene (Lv et al., 2020). This protein is present in many different cell types throughout the body and plays a crucial role in numerous signaling pathways. For instance, Akt1 kinase is vital in controlling cell survival, apoptosis, proliferation, and differentiation (Jafari et al., 2019). Recent research has demonstrated that the PI3K/Akt signalling pathways, which play a role in the above-mentioned processes, are frequently disrupted in various human malignancies (Xu et al., 2019). This pathway is crucial for tumor growth and potential responsiveness to cancer treatments.

Many new targeted agents have been created, especially to target P13K/Akt-related targets. Therefore, having a better understanding of the PI3K/Akt signaling pathway may help to enhance the oncologist's accuracy of prediction as to response to treatment.

Based on the degree value of compounds in the network, we obtained the 8-hydroxycoumarin compound as the most active

ingredient of *D. roylei*. Previous studies have revealed that 7-and 4-hydroxycoumarin and its derivatives have numerous therapeutic benefits (Gaber et al., 2021). These are employed as drug intermediates and as antitumor drugs, anti-inflammatory, anti-HIV, antimicrobial, anti-coagulant, antioxidant, and anti-viral agents (Gaber et al., 2021). However, the degree of other compounds was also high, indicating that quality markers may affect the entire biological network system instead of only one target gene.

Furthermore, the KEGG pathway enrichment analysis of 30 targets suggested that 20 top signaling pathways were involved in breast cancer occurrence and development. This indicated that the effect of phytocompounds acts on multiple pathways for treating breast cancer and complex interactions among these pathways. Based on the frequency of each gene in the compound-gene network, Akt1 showed the highest frequency of protein interaction, followed by SRC, MAPK3, EGFR, IL-6, HSP90AA1, ESR-1, and other target genes.

Furthermore, an *in silico* docking analysis of the nine most prevalent compounds was carried out against the 30 potential targets using AutoDock version 4.2.6 software (Morris et al., 2008). All tested compounds showed promising results against Akt1 protein based on docking scores. Among the all, 8-hydroxycoumarin bioactive showed the highest energy score with Akt1. 8-hydroxycoumarin fits comfortably into the binding sites on Akt1 protein and interacts favourably with critical amino acid residues (Figure 7). During the interaction of the ligand 8-hydroxycoumarin, Trp80 is involved in pi-pi stacking, and Lys268 and Val270 residues are involved in pi-alkyl interaction at the binding cavity of the protein. Besides hydrogen bonding, Leu264 is involved in pi-sigma interaction, and the rest residues are van der Waal's interactions by amino acid residues formed weak non-bonded interaction with the ligand (Figure 7A and right panel). All the binding energy scores are determined from the best cluster (95 percent) that falls within the lowest RMSD 0.25Å. Therefore, it can be inferred from the molecular docking studies that 8-hydroxycoumarin has a high affinity for the protein Akt1.

Also, the stability of the representative Akt1 and 8-hydroxycoumarin complex was further explored using molecular dynamics simulations. The RMSD plots show that the MD results showed stable patterns throughout the entire simulation run (Figures 8A,B). The RMSF graphs show that Akt1 has high flexibility to accommodate the ligand at the binding pocket. The Rg plots demonstrate that the protein stayed compact throughout the simulation. According to the average results observed, the protein backbone was compact. To understand how the residues behaved throughout the simulation run, the fluctuations of the residues were analyzed. After ligand binding, the target's surface area that was accessible to solvent decreased.

Additionally, our research aimed to find the antioxidant and anticancer potential of *D. roylei* active extracts by *in-vitro* approach. In this investigation, DPPH radical scavenging, Hydroxyl scavenging effect, reducing power, and superoxide radical anion scavenging have shown the antioxidant potential of *D. roylei* extracts and were observed to be significant when compared to positive controls such as Ascorbic acid, BHT, Rutin, and BHT respectively. These observations are in accordance with the previous studies on the antioxidant potential of *Delphinium malabaricum* extracts that the DPPH radical scavenging assay has investigated and the Ferric reducing antioxidant power (FRAP) assay (Lotfaliani et al., 2021)

Further, the petroleum ether, ethyl acetate, methanol, and ethanolic extracts were subjected to cytotoxicity assay against various breast cancer cell lines. The results shown in Figure 10 demonstrated that ethyl acetate extract of *D. roylei* showed the highest anticancer activity against the 4T1, MCF-7, MD-MB-468, and MDA-MB-231 breast cell lines as compared to the other three extracts. As a result, the phytoconstituents found in plant extracts might have a greater propensity to suppress the proliferation of cancer cells. *D. roylei* extracts had relatively lower IC_{50} values against breast cancer cell lines, which may be due to phytocomponents with stronger binding affinities or altering proteins or pathways implicated in tumor development. It can be observed that the ethyl acetate extract had the highest content of the compounds verifying the above-given conclusions about these compounds being the key constituents responsible for the cytotoxic activity of the studied plant. Previous studies by (Yin et al., 2020) revealed that Siwanine E, Uraphine, Delpheline, Delcorinine, Nordhagenine A, Delbrunine, and Delbrunine from *D. honanense* and *D. chrysotrichum* exhibited anticancer potential against MCF-7 and cells with IC_{50} values of 9.62–35.32 μM. Flow cytometry analysis revealed that plant extract induction tumor cell death via induction of apoptosis and apoptosis enhanced significantly upon higher concentration are shown in Figure 11.

Conclusion

In the present study, we explored the potential mechanisms of phytocompounds present in *D. roylei* in suppressing breast cancer by network pharmacology-based analysis in combination with chemical profiling, molecular docking, MD simulation, and *in vitro* studies. HR-LC/MS identified some important phytoconstituents followed by network pharmacology analysis which revealed that 8-hydroxycoumarin, Delsoline, Royleinine, Delsemine B, Herniarin, Aloesin, Talatisamine, Narwedine, Scoparone, and Piperine were the main constituents related to breast cancer targets while Akt1, SRC, EGFR, IL-6, Hsp-90AA1, and ESR-1 were the main breast cancer-related molecular targets. 20 cancer-related pathways were identified where neuroactive ligand-receptor interaction was the most enriched with the highest number of observed genes and lowest false discovery rate, followed by non-small-cell lung cancer. Molecular docking studies showed that 8-hydroxycoumarin possessed the highest binding energies towards all the target proteins, followed by other compounds against studied targets. Furthermore, *in vitro* studies showed that ethyl acetate extract possess the highest anticancer activity and methanolic extract showed significant antioxidant activity compared to other extracts in the studied plant. The study provided a comprehensive understanding of the suggested mechanism of action of *Delphinium roylei* that may have potential use in breast cancer treatment.

Data availability statement

The original contributions presented in the study are included in the article/Supplementary Material, further inquiries can be directed to the corresponding author.

Author contributions

MM conceived and designed the study; WM and BB performed the study and wrote the manuscript; AK, RD, MA, AA, MD, and SG analyzed the data. All authors contributed to the article and approved the submitted version.

Funding

This work was funded by the Jammu Kashmir Science Technology & Innovation Council Department of Science and Technology JKST&IC India with grant No. JKST&IC/SRE/885-87 to MM.

Conflict of interest

The authors declare that the research was conducted in the absence of any commercial or financial relationships that could be construed as a potential conflict of interest.

Publisher's note

All claims expressed in this article are solely those of the authors and do not necessarily represent those of their affiliated organizations, or those of the publisher, the editors and the reviewers. Any product that may be evaluated in this article, or claim that may be made by its manufacturer, is not guaranteed or endorsed by the publisher.

References

Balasubramaniam, M., Lakkaniga, N. R., Dera, A. A., Fayi, M. A., Abohashrh, M., Ahmad, I., et al. (2021). FCX-146, a potent allosteric inhibitor of Akt kinase in cancer cells: lead optimization of the second-generation arylidene indanone scaffold. *Biotechnol. Appl. Biochem.* 68, 82–91. doi:10.1002/bab.1896

Bhat, B. A., Almilaibary, A., Mir, R. A., Aljarallah, B. M., Mir, W. R., Ahmad, F., et al. (2022a). Natural therapeutics in aid of treating alzheimer's disease: a green gateway toward ending quest for treating neurological disorders. *Front. Neurosci.* 16, 884345. doi:10.3389/fnins.2022.884345

Bhat, B. A., Mir, W. R., Sheikh, B. A., Alkanani, M., and Mir, M. A. (2022b). Metabolite fingerprinting of phytoconstituents from Fritillaria cirrhosa D. Don and molecular docking analysis of bioactive peonidin with microbial drug target proteins. *Sci. Rep.* 12, 7296. doi:10.1038/s41598-022-10796-7

Bolton, E. E., Chen, J., Kim, S., Han, L., He, S., Shi, W., et al. (2011). PubChem3D: a new resource for scientists. *J. cheminformatics* 3, 32–15. doi:10.1186/1758-2946-3-32

Chen, J., Zhu, Y., Zhang, W., Peng, X., Zhou, J., Li, F., et al. (2018). Delphinidin induced protective autophagy via mTOR pathway suppression and AMPK pathway activation in HER-2 positive breast cancer cells. *BMC cancer* 18, 342–413. doi:10.1186/s12885-018-4231-y

Chow, E., Rendleman, C. A., Bowers, K. J., Dror, R. O., Hughes, D. H., Gullingsrud, J., et al. (2008). *Desmond performance on a cluster of multicore processors*. Report DESRES/TR–2008-01. New York: DE Shaw Research Technical.

Daina, A., Michielin, O., and Zoete, V. (2017). SwissADME: a free web tool to evaluate pharmacokinetics, drug-likeness and medicinal chemistry friendliness of small molecules. *Sci. Rep.* 7, 42717–42813. doi:10.1038/srep42717

Deo, S. V. S., Sharma, J., and Kumar, S. (2022). GLOBOCAN 2020 report on global cancer burden: challenges and opportunities for surgical oncologists. *Ann. Surg. Oncol.* 29, 6497–6500. doi:10.1245/s10434-022-12151-6

Fuhrmann, J., Rurainski, A., Lenhof, H. P., and Neumann, D. (2010). A new Lamarckian genetic algorithm for flexible ligand-receptor docking. *J. Comput. Chem.* 31, 1911–1918. doi:10.1002/jcc.21478

Gaber, A., Alsanie, W. F., Alhomrani, M., Alamri, A. S., El-Deen, I. M., and Refat, M. S. (2021). Synthesis and characterization of some new coumarin derivatives as probable breast anticancer MCF-7 drugs. *Crystals* 11, 565. doi:10.3390/cryst11050565

George, B. P., Chandran, R., and Abrahamse, H. (2021). Role of phytochemicals in cancer chemoprevention: insights. *Antioxidants* 10, 1455. doi:10.3390/antiox10091455

Heer, E., Harper, A., Escandor, N., Sung, H., McCormack, V., and Fidler-Benaoudia, M. M. (2020). Global burden and trends in premenopausal and postmenopausal breast cancer: a population-based study. *Lancet Glob. Health* 8, e1027–e1037. doi:10.1016/S2214-109X(20)30215-1

Jafari, M., Ghadami, E., Dadkhah, T., and Akhavan-Niaki, H. (2019). PI3k/AKT signaling pathway: erythropoiesis and beyond. *J. Cell. physiology* 234, 2373–2385. doi:10.1002/jcp.27262

Jaganathan, P., Rajan, M., Sathyanarayanan, S., Murugaiyan, I., Jeyalakshmi, G. S. S., and Thangaraj, P. (2018). *17 antioxidant potential. Medicinal plants: promising future for health and new drugs*, 317.

Kumar, S., and Hamal, I. A. (2011). *Herbal remedies used against arthritis in Kishtwar high altitude National Park*. India: NISCAIR-CSIR.

Lim, W-C., Kim, H., Kim, Y-J., Park, S-H., Song, J-H., Lee, K. H., et al. (2017). Delphinidin inhibits BDNF-induced migration and invasion in SKOV3 ovarian cancer cells. *Bioorg. Med. Chem. Lett.* 27, 5337–5343. doi:10.1016/j.bmcl.2017.09.024

Lipinski, C. A. (2004). Lead-and drug-like compounds: the rule-of-five revolution. *Drug Discov. today Technol.* 1, 337–341. doi:10.1016/j.ddtec.2004.11.007

Lotfaliani, M., Ayatollahi, S. A., Kobarfard, F., Pour, P. M., and Mohammadi Pour, P. (2021). Chemistry, biological activities and toxic effects of alkaloidal constituents of genus Delphinium-A mini review. *J. Herbmed Pharmacol.* 10, 486–499. doi:10.34172/jhp.2021.56

Lv, P., Gao, P., Tian, G., Yang, Y., Mo, F., Wang, Z-H., et al. (2020). Osteocyte-derived exosomes induced by mechanical strain promote human periodontal ligament stem cell proliferation and osteogenic differentiation via the miR-181b-5p/PTEN/AKT signaling pathway. *Stem Cell Res. Ther.* 11, 295–315. doi:10.1186/s13287-020-01815-3

Mazurek, A. H., Szeleszczuk, Ł., and Gubica, T. (2021). Application of molecular dynamics simulations in the analysis of cyclodextrin complexes. *Int. J. Mol. Sci.* 22, 9422. doi:10.3390/ijms22179422

Mehraj, U., Mir, I. A., ul Hassan, M., Mir, N. A., and Mir, M. A. (2022). *Adapalene synergistically with doxorubicin promotes apoptosis of TNBC Cells by hyperactivation of the ERK1/2 pathway through ROS induction*. Preprint.

Mir, W. R., Bhat, B. A., Almilaibary, A., Asdaq, S. M. B., and Mir, M. A. (2022a). Evaluation of the *in vitro* antimicrobial activities of Delphinium roylei: an insight from molecular docking and MD-simulation studies. *Med. Chem.* 18, 1109–1121. doi:10.2174/1573406418666220429093956

Mir, W. R., Bhat, B. A., Rather, M. A., Muzamil, S., Almilaibary, A., Alkhanani, M., et al. (2022b). Molecular docking analysis and evaluation of the antimicrobial properties of the constituents of Geranium wallichianum D. Don ex Sweet from Kashmir Himalaya. *Sci. Rep.* 12, 12547. doi:10.1038/s41598-022-16102-9

Miu, L., Bogatyreva, N. S., and Galzitskaia, O. V. (2008). Radius of gyration is indicator of compactness of protein structure. *Mol. Biol.* 42, 701–706.

Morris, G. M., Huey, R., and Olson, A. J. (2008). Using autodock for ligand-receptor docking. *Curr. Protoc. Bioinforma.* 24, Unit 8.14–14. doi:10.1002/0471250953.bi0814s24

Noumi, E., Snoussi, M., Anouar, E. H., Alreshidi, M., Veettil, V. N., Elkahoui, S., et al. (2020). HR-LCMS-based metabolite profiling, antioxidant, and anticancer properties of teucrium polium L. Methanolic extract: computational and *in vitro* study. *Antioxidants* 9, 1089. doi:10.3390/antiox9111089

Nwakaego, N. L., Chibuike, O. K., Chukwugekwu, E. M., Marylyn, A. C., Ngozi, E. I., and Chukwunonye, E. R. (2019). *In vitro* antioxidant and free radical scavenging potential of methanolic extracts of Uvaria chamae leaves and roots. *Int. J. Pharm. Pharm. Sci.* 11, 67–71. doi:10.22159/ijpps.2019v11i1.29330

Obi, K. N., Onyeike, E. N., and Anacletus, F. C. (2022). Studies on *in vitro* Radical Scavenging Potentials of Methanol Leaf Extract of Ficus sur and its Fractions. *Free Radicals Antioxidants* 12, 15–21. doi:10.5530/fra.2022.1.3

Pistelli, M., Natalucci, V., Scortichini, L., Agostinelli, V., Lenci, E., Crocetti, S., et al. (2021). The impact of lifestyle interventions in high-risk early breast cancer patients: a modeling approach from a single institution experience. *Cancers* 13, 5539. doi:10.3390/cancers13215539

Pospelova, M., Krasnikova, V., Fionik, O., Alekseeva, T., Samochernykh, K., Ivanova, N., et al. (2022). Adhesion molecules ICAM-1 and PECAM-1 as potential biomarkers of central nervous system damage in women breast cancer survivors. *Pathophysiology* 29, 52–65. doi:10.3390/pathophysiology29010006

Rapaport, D. C., and Rapaport, D. C. R. (2004). *The art of molecular dynamics simulation*. Cambridge: Cambridge University Press.

Release, S. (2017). *3: desmond molecular dynamics system*. New York, NY: DE Shaw research, Maestro-Desmond Interoperability Tools, Schrödinger.

Rezadoost, M. H., Kumleh, H. H., and Ghasempour, A. (2019). Cytotoxicity and apoptosis induction in breast cancer, skin cancer and glioblastoma cells by plant extracts. *Mol. Biol. Rep.* 46, 5131–5142. doi:10.1007/s11033-019-04970-w

Saifi, I., Bhat, B. A., Hamdani, S. S., Bhat, U. Y., Lobato-Tapia, C. A., Mir, M. A., et al. (2023). Artificial intelligence and cheminformatics tools: a contribution to the drug development and chemical science. *J. Biomol. Struct. Dyn.* 2023, 1–19. doi:10.1080/07391102.2023.2234039

Sharma, P. K., and Singh, V. (1989). Ethnobotanical studies in northwest and Trans-Himalaya. V. Ethno-veterinary medicinal plants used in Jammu and Kashmir, India. *J. Ethnopharmacol.* 27, 63–70. doi:10.1016/0378-8741(89)90078-0

Sung, H., Ferlay, J., Siegel, R. L., Laversanne, M., Soerjomataram, I., Jemal, A., et al. (2021). Global cancer statistics 2020: gLOBOCAN estimates of incidence and mortality worldwide for 36 cancers in 185 countries. *CA a cancer J. Clin.* 71, 209–249. doi:10.3322/caac.21660

Tariq, L., Bhat, B. A., Hamdani, S. S., and Mir, R. A. (2021). Phytochemistry, pharmacology and toxicity of medicinal plants. *Med. Aromatic Plants Healthc. Industrial Appl.* 2021, 217–240.

Tiwari, A., and Singh, S. (2022). "Computational approaches in drug designing," in *Bioinformatics* (Amsterdam, Netherlands: Elsevier), 207–217.

Trott, O., and Olson, A. J. (2010). AutoDock Vina: improving the speed and accuracy of docking with a new scoring function, efficient optimization, and multithreading. *J. Comput. Chem.* 31, 455–461. doi:10.1002/jcc.21334

Wu, A., Zhu, Y., Han, B., Peng, J., Deng, X., Chen, W., et al. (2021). Delphinidin induces cell cycle arrest and apoptosis in HER-2 positive breast cancer cell lines by regulating the NF-κB and MAPK signaling pathways. *Oncol. Lett.* 22, 832–911. doi:10.3892/ol.2021.13093

Xu, X., Yu, Y., Zong, K., Lv, P., and Gu, Y. (2019). Up-regulation of IGF2BP2 by multiple mechanisms in pancreatic cancer promotes cancer proliferation by activating the PI3K/Akt signaling pathway. *J. Exp. Clin. Cancer Res.* 38, 497–514. doi:10.1186/s13046-019-1470-y

Yin, T., Cai, L., and Ding, Z. (2020). An overview of the chemical constituents from the genus Delphinium reported in the last four decades. *RSC Adv.* 10, 13669–13686. doi:10.1039/d0ra00813c

Yin, T., Zhang, H., Zhang, W., and Jiang, Z. (2021). Chemistry and biological activities of hetisine-type diterpenoid alkaloids. *RSC Adv.* 11, 36023–36033. doi:10.1039/d1ra07173d

Yu, S., Gao, W., Zeng, P., Chen, C., Zhang, Z., Liu, Z., et al. (2021). Exploring the effect of Gupi Xiaoji Prescription on hepatitis B virus-related liver cancer through network pharmacology and *in vitro* experiments. *Biomed. Pharmacother.* 139, 111612. doi:10.1016/j.biopha.2021.111612

Zhang, K., Xie, Y., Noble, B. B., Monteiro, M. J., Lutkenhaus, J. L., Oyaizu, K., et al. (2021). Unravelling kinetic and mass transport effects on two-electron storage in radical polymer batteries. *J. Mater. Chem. A* 9, 13071–13079. doi:10.1039/d1ta03449a

Frontiers in Pharmacology

Explores the interactions between chemicals and living beings

The most cited journal in its field, which advances access to pharmacological discoveries to prevent and treat human disease.

Discover the latest Research Topics

See more →

Frontiers

Avenue du Tribunal-Fédéral 34
1005 Lausanne, Switzerland
frontiersin.org

Contact us

+41 (0)21 510 17 00
frontiersin.org/about/contact